V. Vishal · T. N. Singh
Editors

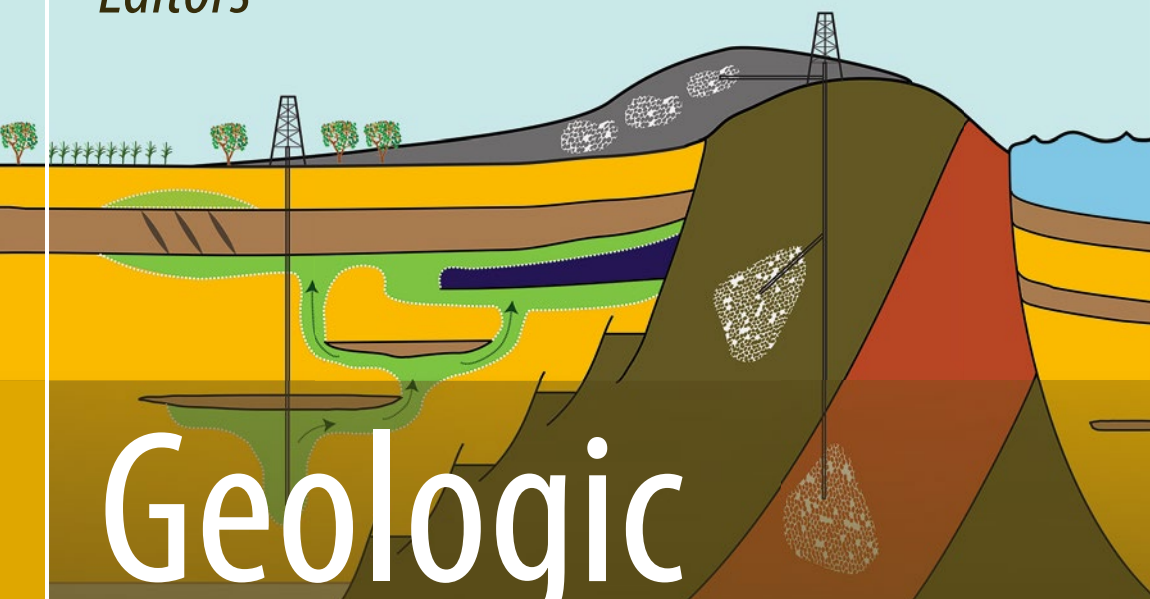

Geologic Carbon Sequestration

Understanding Reservoir Behavior

Springer

Geologic Carbon Sequestration

V. Vishal • T.N. Singh
Editors

Geologic Carbon Sequestration

Understanding Reservoir Behavior

Springer

Editors
V. Vishal
Department of Earth Sciences
Indian Institute of Technology Bombay
Mumbai, India

T.N. Singh
Department of Earth Sciences
Indian Institute of Technology Bombay
Mumbai, India

ISBN 978-3-319-27017-3 ISBN 978-3-319-27019-7 (eBook)
DOI 10.1007/978-3-319-27019-7

Library of Congress Control Number: 2016932893

Cover figure: with courtesy of Dennis Bird and Pablo García del Real, Department of Geological Sciences, Stanford University, California, USA

Printed on acid-free paper

This Springer imprint is published by Springer Nature
The registered company is Springer International Publishing AG Switzerland

Foreword

I congratulate the editors for a thorough review of the literature, as well as for their identification of gaps in the existing knowledge in the domain of geologic sequestration. Their contributions have helped bring out this fine volume. I take this opportunity to commend the contributions made by Prof. V. Vishal and Prof. T.N. Singh in the field of carbon storage.

This book is unique in its presentation of geologic sequestration. It briefly introduces the concepts of carbon capture, utilization, and storage (CCUS) in its first chapter and systematically progresses into the potential geological sinks in subsequent chapters. The subdivision of the book into various sections helps the readers to identify the reservoir type of particular interest. Expert authors in each category of CO_2 storage sites have contributed to the book. While detailed chapters on CO_2 storage in deep saline aquifers and depleted hydrocarbon reserves give useful information, the authors have also described the risks associated under various scenarios in the concluding section of the book.

Global climate change is an important problem of this century, and expert organizations suggest that with the goal of arresting global warming instabilities, further investigation on carbon storage is most important. Several books have been written in the last decade in this area where storage contribution was minimal compared to the other aspects such as capture and transport. The uniqueness of this book lies in its specialized subject matter with focus on the individual category of carbon storage reservoirs.

It is a challenge to bring out important recent developments in this field, a feat that could have only been achieved by contributions from authorities from across the globe. The editors and authors together have meticulously built the chapters to form sections, which come together logically to form this complete volume. The

knowledge within this text fills a void that should satisfy both scientific and the industrial communities alike. I have found the book to be systematic in its presentation, well edited, and of supreme relevance to all who believe in the future of carbon sequestration to combat an increase in atmospheric CO_2 concentration.

Jawaharlal Nehru Centre
for Advanced Scientific Research
Bangalore, India

C.N.R. Rao, F.R.S.

Preface

With rising concerns about increasing concentration of CO_2 in the atmosphere, which is often held responsible for global warming phenomena, methods to restrict CO_2 release are one of the grand challenges of this century. The growing interest in understanding the reservoirs used for geological carbon sequestration has prompted the editing of this exclusive book volume with contributions from eminent subject experts from more than ten countries. The book discusses and emphasizes the details of individual storage types, covering recent advances in the science and technology of carbon storage. The topic is of immense interest to geoscientists, reservoir engineers, environmentalists, and all researchers working on methodologies for atmospheric CO_2 reduction.

The seven sections in the book comprise a total of 15 chapters and deal with the characterization of storage sites, CO_2 storage in deep saline aquifers, coal mines, depleted/producing oil and gas reservoirs, and other sites such as fractured igneous rocks and ocean floor. Finally the assessment of risks associated with geological storage is treated. While the book introduces fundamental understanding of reservoirs, in the case studies detailed applications at different sites are presented. The idea behind editing this book volume was to emphasize the characteristics of the different reservoir types. The book is an immediate need for all researchers, scientists, students, and the industry for understanding the individual carbon storage site types. Other book volumes on carbon capture, utilization and storage (CCUS) attempt to cover the entire process of CCUS, but the topic of geologic sequestration is not discussed in detail. This book focuses on the recent trends and information on different storage rock types, ranging from deep saline aquifers to coal to basaltic formations.

We thank all authors who contributed such excellent chapters to this book. Thanks are due to all technical reviewers who devoted their valuable time and offered their expertise. We express sincere appreciation to the publishing team for their dedication and efficient work which is reflected in the final shape of the book. We believe that this book will bring the knowledge and understanding to the

forefront that is needed in characterizing and understanding the concepts of CO_2 reservoirs from different perspectives.

Mumbai, India V. Vishal
Mumbai, India T.N. Singh

Contents

Part I
Introduction

Carbon Capture, Transport and Geologic Storage: A Brief Introduction

Nikhil Jain, Akash Srivastava, and T.N. Singh

Abstract Carbon capture and storage can simply be defined as capturing of waste CO_2 from industrial sources at various stages (ex. pre-, post- combustion etc.), transporting it to a storage site (through pipelines etc.) and then depositing it underground so that the CO_2 will not re-enter the atmosphere for a geologically significant long time. Because of the low prices of fossil fuels and lesser statutory restrictions in developing countries (which are primarily dependent on this form of energy), aided by slow development and high cost of alternative energy projects, the CO_2 emission into the atmosphere has been ever increasing. The long lasting effects of such high levels of CO_2 in atmosphere can portray an image of an impending catastrophe but a better approach would be to avoid those and look into the solutions to minimize the CO_2 levels in atmosphere. This introductory chapter offers an insight into the technologies and the techniques that have been developed for carbon capture followed by transporting methods (and their problems) and ends with discussing the various storage technologies.

1 Introduction

Global growth in demand of energy linked with an extended dependence on fossil fuel as an energy resource has contributed to a substantial rise in the atmospheric levels of carbon dioxide (CO_2). To make conditions worse, this step-up has been giving no indications of slowing down. As of now, renewables provide us 13 % of our energy, which could rise to 30 % by 2030. However, the fact still remains that fossil fuels will continue to serve as the primary source of energy in the coming decades. According to the International Energy Agency, there has been an estimation that energy demand may foresee a hike by 45 % between now and 2030, if no

N. Jain (✉) • A. Srivastava
Department of Mining Engineering, Indian Institute of Technology (BHU), Varanasi, India
e-mail: nikhilchhajar@gmail.com

T.N. Singh
Department of Earth Sciences, Indian Institute of Technology Bombay, Mumbai, India
e-mail: tnsingh@iitb.ac.in

V. Vishal, T.N. Singh (eds.), *Geologic Carbon Sequestration*,
DOI 10.1007/978-3-319-27019-7_1

remedial actions are taken to harness it [1]. As also reported by International Energy Agency's (IEA's) World Energy Outlook 2007, there will be a transformation of growth in energy related to CO_2 emissions by 2030 as proposed to a rising 57 % [2]. With rising worry about the likely climate changes on account of assemblage of greenhouse gases (GHGs) in the atmosphere has led to multiple studies of the phenomenon, focused on inventories of emissions, climate change models and other physical processes [3, 4]. For slackening and ceasing emissions, transformational alterations will be required in the energy sector, both in the way the world generates and consumes energy.

Carbon capture and storage (CCS) is a technology that comprises capture of carbon from industrial and power plants and its storage which facilities its isolation from the atmosphere for a large period of time. The possible storage methods include storage in coal beds (which can't be mined), geological formations (including the likes of depleted oil and gas fields), and deep saline reservoirs [5]. This storage of CO_2 that occurs is mentioned as Geosequestration or geologic storage [6]. The utilization of CO_2 for enhanced oil recovery (EOR) is an instance of geological storage or geosequestration. There are other storage sites in addition to geosequestration, for storing CO_2, for example, oceans where there is injection onto the deep seafloor or by the direct discharge into ocean water column, followed by the fixation of CO_2 by inorganic carbonates. As recently researched there is a greater potential for using forestry as a means to sequester carbon for reduction of growth of emissions from India. An early estimate had suggested that over a period of a decade, with strong afforestation programs, around 17 % of energy emissions could be offset [7].

Countries like China and India with high population are heavily dependent on coal for generation of energy, thereby reporting a substantial rise in the quantity of coal-fired plants being constructed. As concurred by the UNFCC meeting (Copenhagen, 2009), following a settlement at the global level, CCS must be viewed as a vital technology in the quest for achieving carbon level reductions at the global level. Special and conclusive efforts need to be made so as to motivate the placement and operation of CCS in the developing world [8].

2 Fossil Fuels

In this developing world, where the coal reserves are still far greater when compared to oil and gas and hence, on an average 2 coal-based power stations are being constructed in a week, fossil fuels will continue to serve as a primary energy source for major parts of the world for this century.

As demonstrated in Fig. 1 by International Energy Agency (IEA), fossil fuels fulfill more than 80 % of the primary energy needs; remaining portions are made up of atomic- and hydro-electricity, and renewable energy (like wind and solar energy, geothermal energy and biomass). Countries like United Kingdom which are having

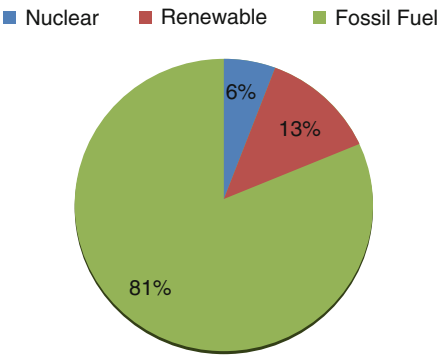

Fig. 1 World total primary energy supply [1]

nuclear power and renewable energy sources also have large coal deposits. These deposits might serve as a suitable security in the future as an energy source.

3 Carbon Capture

The abatement in anthropogenic CO_2 emissions (i.e. human activity generated CO_2) into the atmosphere can be accomplished through a number of measures. As brought to light by Professor Yoichi Kaya of the University of Tokyo, these measures find their reflectance as:

$$CO_2{}^{\uparrow} = \text{POP} * \frac{GDP}{POP} * \frac{BTU}{GDP} * \frac{CO_2{}^{\uparrow\uparrow}}{BTU} - CO_2{}^{\downarrow} \tag{1}$$

where $CO_2{}^{\uparrow}$ is the overall CO_2 being released into the atmosphere, POP reflects the population level, GDP/POP is per capita gross domestic product (can be considered as a measure of standard of living), BTU/GDP is energy consumption per unit of GDP (reflects degree of energy intensity); $CO_2{}^{\uparrow\uparrow}$/BTU is the quantity of carbon dioxide released per unit of energy consumed (reflects degree of carbon intensity); $CO_2{}^{\downarrow}$is the quantity of carbon dioxide stored or isolated in biosphere & geosphere sinks [9].

Given the current scenario, what can be easily incurred is that population decrease is not a realistic option. Thus, one would have to include that the CO_2 going into the atmosphere through human activities will have to be curtailed. This can be realized by:

I. Decrease in energy intensity
II. Decrease in carbon intensity (implying consumption of carbon-free fuel)
III. Increasing CO_2 sequestration levels

Options (I) and (II) focus on energy efficiency and pivoting to non-fossil fuel energy for example hydrogen, non-renewable energy. However, involved in the

parameters of learning rate of these technologies, the economics & its justification and also the risks, an immediate shift can be ruled out. A gradual implementation and continuous thorough research is however the need of the hour. Moreover, the current power infrastructure will need changes to incorporate non-renewable energy sources at a fast pace. Thus, we have to focus on third option which is capturing and storing the carbon dioxide produced from fossil fueled power plants. The objective is to develop cheaper technologies to capture carbon at the source and sequester as the world gradually moves towards non –renewable energy sources. The pace and the balance in terms of economics and development are crucial; else it can have major repercussions on the world economy. Though capture and sequestration is a mid-term solution but its requirement given the current levels of GHGs production and its potential repercussions is immediate. Overall, among all the industries generating and emitting CO_2, power plants running on fossil fuels account for the largest amount of CO_2 emissions (which is numerically 33–40 % of the aggregate) [10].

Capturing CO_2 from flue gas streams at these point sources is quintessential for the sequestration of CO_2 from the environment and to the carbon management processes.

Following are 3 technical pathways which may be followed for CO_2 capture from power plants based on coal: post-combustion capture, oxy-combustion and pre-combustion capture. Some key elements in establishing the suitability of the capture system are –

(i) CO_2 levels in the gas stream
(ii) Gas stream pressure
(iii) Type of fuel

3.1 Post- Combustion Capture

Post-combustion capture involves the treatment of the flue gas produced by combustion for the removal of carbon dioxide. A plausible method to achieve this involves the use of chemical absorption, example, monoethanolamine absorption. This practice has been extensively deployed in natural gas industry for more than 50 years now. It produces a comparatively pure CO_2 stream. In terms of size and cost of the absorber required, it would be comparable to that of a SO_2 scrubber. However, the absorber would consume about $1/4^{th}$ to $1/3^{rd}$ of the net steam produced by the plant. Hence, it will decrease its generating capacity by a similar amount [11]. This is so because the today's power plants utilize air (approximately 80 % N_2) for combustion, producing a flue gas which, at atmospheric pressure, has CO_2 concentration levels ranging between 4 and 14 %. Hence, thermodynamically speaking, the driving force for carbon dioxide's capture from flue gas is very less, with partial pressure of carbon dioxide going below 0.15 atm. Some major hurdles include (but not limited to) high input capital, large equipment size and major

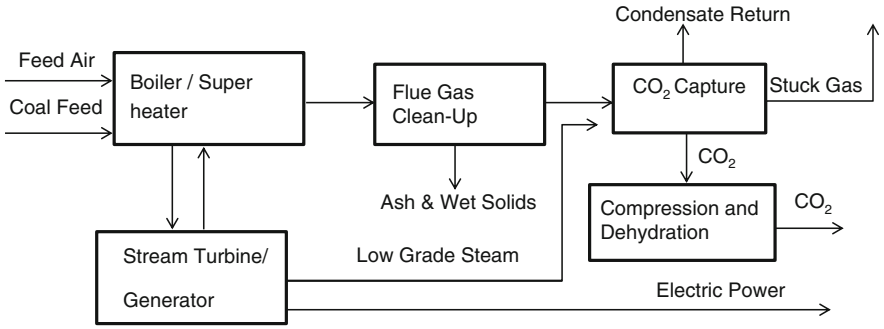

Fig. 2 Post-combustion capture from a pulverized coal-fired power plant, after [12]

design challenges due to temperature of flue gas etc. A process flow diagram has been provided (Fig. 2).

3.2 Oxy-Fuel Combustion

Oxy-fuel combustion is based on the combustion of fossil fuels in an O_2 rich environment instead of air. The environment here comprises of nearly pure oxygen which is mixed with recycled exhaust gas. Under these conditions of combustion, the formation of nitrogen oxides is almost nullified. Hence, the gas which leaves the combustion zone is primarily made up of CO_2 (almost 90 % after SO_2 removal) which make it easier to separate and remove it. As shown in the process flow diagram (Fig. 3), boiler is supplied with oxygen from air separation unit and recycled flue air. The gas stream, post combustion, can then be cleaned of PM, nitrogen oxides, and sulfur.

Following the condensing operations, the flue gas can be subjected to direct compression since it has a high enough CO_2 concentration. Though, to bring the purity levels of compressed flue gas in line with the compressed CO_2, it may have to be subjected to further cleaning of co-constituents [13].

The mainstay of oxyfuel combustion is comparatively easier separation of CO_2 than other techniques, with other positives like no solvent, smaller physical size with a potential to retrofit on existing plants (given that the boilers are reconstructed). Its drawbacks include the very low SOx levels required on leaving burners; requirement of the materials resistant to greater temperature ranges [14]. Forthcoming advances may improve the higher-temperature operations while also decrease the energy associated costs for separation of O_2 from air.

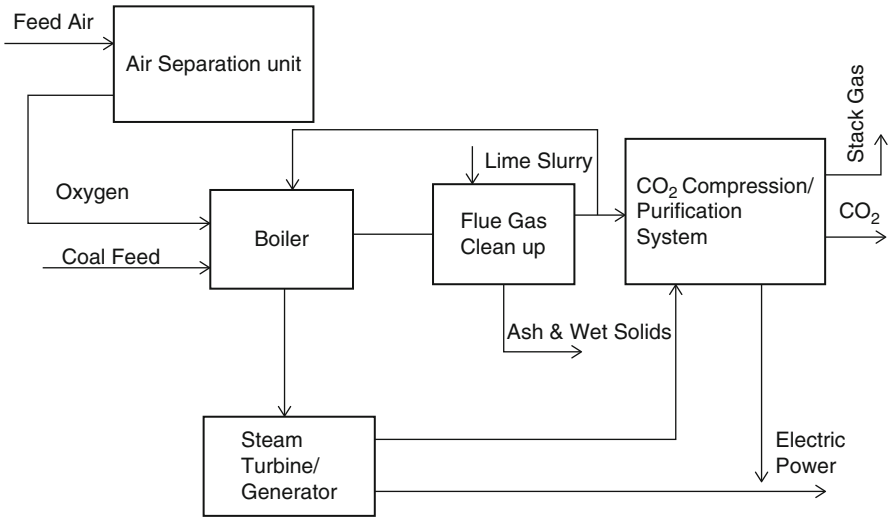

Fig. 3 Oxy-fuel combustion with capture, after [12]

3.3 Pre- Combustion Carbon Capture

Pre-combustion capture of CO_2 involves reaction of fuel with oxygen/air/steam, to produce primarily CO and H_2 (as shown in Fig. 4). Any kind of fossil fuel can be gasified (subject to primary combustion or reformation) with sub-stoichiometric quantities of O_2 (and generally small amounts of steam) at high pressures (around 30–70 atmospheres) to give a 'synthesis gas'. This gas is primarily a mixture of CO and H_2. To the synthesized gas, steam is then added, following which the mixture is passed through a series of catalyst beds. The objective is to approach equilibrium through the 'water–gas shift' reaction:

$$CO + H_2O \leftrightarrow CO_2 + H_2 \tag{2}$$

Under the water–gas shift reaction, steam addition and reduction of the temperature can promote conversion of CO into CO_2 [15].

Using above mentioned process, CO_2 capture has already been proven to function at the mega ton per year scale. The challenge here lies in appropriating the right reliability levels for all components for total continuous integration. In spite of the challenges, pre-combustion capture is still potentially a cheaper option as compared to post-combustion capture. IGCC (Integrated gasification combined cycle) power plants based on pre-combustion capture are far more efficient in comparison to pulverized coal-fired plants. These, hence, would be the choice for the new plants [16].

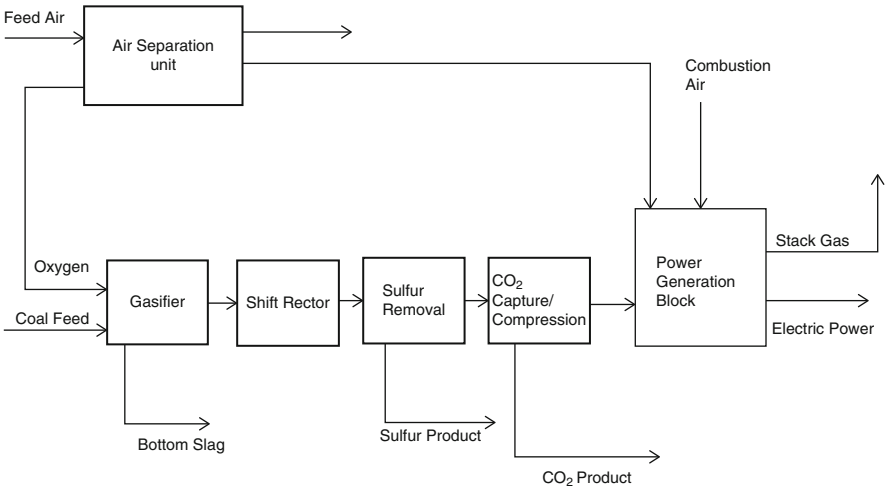

Fig. 4 Pre-combustion capture on an IGCC power plant, after [12]

3.4 Chemical Looping Combustion Process

Chemical looping combustion (CLC), as a process deploys inherent CO_2 capture. It deploys unmixed combustion employing a dual fluidized bed system. CLC is based on circulation of solid oxygen carrier (metal oxide, represented by Me_xO_y, where Me is denoted as metal) between separated sections in which intermediate oxidation and reduction reactions are performed [17]. Small particles of metal oxide serve as suitable oxygen carriers. Examples include Fe_2O_3, NiO, CuO or MN_2O_3. Figure 5 depicts a basic CLC system.

$$O_2 + 2Me \rightarrow 2MeO \tag{3}$$

$$C_nH_{2m} + (2n + m)MeO \rightarrow nCO_2 + mH_2O + (2n + m)Me \tag{4}$$

Chemical looping combustion (CLC) relies on using 2 or more reactions for achieving oxidation of the hydrocarbon-based fuels (as given above). In its most basic form, a metal (serving as oxygen carrying specie) is firstly oxidized in air to form an oxide. This oxide is subsequently reduced in a second reaction using a hydrocarbon (functioning as reducer). CLC has multiple advantages over conventional combustion. The exhaust gas steam from the air reactor is harmless since it primarily consists of N_2. Moreover, thermal formation of NOx should not be there since oxygen carrier's regeneration occurs without flame and at moderate temperature levels. In it, CO_2 and H_2O are the primary constituents of the fuel reactor's exhaust gas. CO_2 separation can be achieved through a condenser. It serves as a major advantage by avoiding the high energy penalties necessary in traditional amine-scrubbing process for capturing of CO_2. This leads to lesser operational cost. Actual operation of CLC with gaseous fuels was demonstrated in 2003 and later

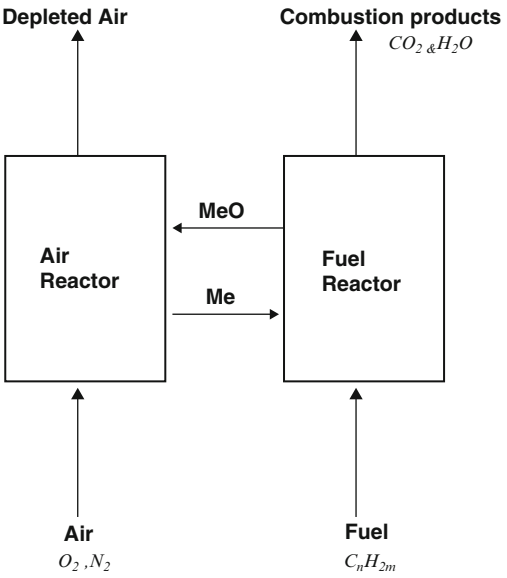

Fig. 5 Schematic diagram of chemical looping combustion system, after [18]

with solid fuels in 2006 [19, 20]. Net operational experience in running pilots of capacity 0.3–120 kW is of more than 4000 h. However, no large scale demonstrations have been made.

There are various capture technologies whose potentials are discussed in given Table 1.

4 Transport

The captured CO_2 is transported for storage at a suitable site by a pipeline or ship. As of now, CO_2 is already being transported by road tanker, ship or through pipeline for commercial purposes. While methods that have been mentioned are practical, however, the shear amount of CO_2 to be transported from capture site will probably require development of local and regional infrastructure for proper transport. If CO_2 is dry ($<$10 ppm of H_2O), conventional carbon steel can be deployed. This practice will reduce the transportation cost greatly while also remove the risk associated with hydrate crystallization. CO_2 feed-in might be contaminated with N_2, O_2, H_2S, and/or SO_3, depending on the type of plant and capture system deployed. For a CO_2 mixture with impurities, the operational pressure required so as to avoid dew-point condensation into liquids increases (from approximately 73 bars in pure CO_2 to about 90 bars in CO_2 having impurities). Obviously, in order to shun the costs of over compression, a purity standard for pipelines will be required [14].

Table 1 Potential of various capture technologies [9]

Post combustion	Pre-combustion	Oxy fuel combustion
Relevant technology w.r.t. a large number of existing coal-fired plants	Normally higher CO_2 concentration levels compared to post combustion capture	Very high CO_2 concentration in flue gas
High capture levels require higher circulation volume	CO_2 separation facilitated by higher driving force	Combustors would be fairly conventional
CO_2 is produced at lower pressure in comparison to requirements of sequestration	Fuel processing is needed	Requirement of large cryogenic oxygen production levels may result in cost escalation
Option of retrofit technology	Compression costs/loads can be potentially reduced	Requirement of recycling large quantities of flue gas for avoiding excessively high temperatures of combustion
Energy losses might be reduced by improved solvents	Lower efficiency and cost penalties compared to post-combustion capture, for coal plants	Option of recycling CO_2 to the compressor for providing expansion medium, instead of air
Possibilities for huge cost savings	Barriers exist in commercial application	Potential in less energy intensive,cutting-edge O_2 separation membranes
–	Extensive supporting systems requirements	Option of retrofit and repowering technology.

5 Carbon Storage

To address climate change by keeping greenhouse gas (GHG) out of atmosphere, underground storage of CO_2 emissions produced by human activity will be of immense help, as it is a tested and old technology-. Even numerous oil and gas industries have deployed enhanced oil recovery (EOR) for utilizing CO_2. With the presence of many geological systems all around the world, it is capable of holding back centuries' worth of CO_2 captured from industrial treatments. Though the storage of gases in geological ways, occurring naturally have been safely used by industry from past few decades, but there lies challenges in providing satisfactory explanation to the public.

Various key standards are essentially implemented to the storage method: (a) the storage period should be lengthy, preferably hundreds to thousands of years; (b) the storage cost, letting in the cost of transportation from the source to the storage site, should be belittled; (c) the danger of accidents should be extinguished; (d) the environmental impact should be kept minimum; (e) the storage method should not breach any national or international laws and regulations

The figured worldwide capacities for storage of CO_2 in the various media, as listed in Table 2. As a comparison to the storage capacities, we note that current global anthropogenic emissions amount to close to 7 gigatons of carbon (GtC) per year (1 GtC = 1 billion metric tons of carbon equivalent = 3.7 Gt CO_2).

Table 2 The universal capacity of possible CO_2 storage reservoirs [6]

Ocean and land-based sites unitedly hold enormous capacity for storage of CO_2[a]. The world's oceans have by far the largest ocean storage capacities	
Sequestration option	**Worldwide capacity[b]**
Ocean	1000–10,000+GtC
Deep Saline formations	100–10,000 GtC
Depleted oil and gas reservoirs	100–1000 GtC
Coal seams	10–1000 GtC
Terrestrial	10–100 GtC
Utilization	Currently <0.1 GtC/year

[a]Worldwide total anthropogenic carbon emissions are ~ 7GtC per year (1 GtC = 1 billion tons of carbon equivalent)
[b]Orders of magnitude estimates

5.1 Geologic Storage

Geological sinks for CO_2 comprise depleted oil and gas reservoirs, enhanced oil recovery, unminable coal seams, and deep porous formations [21]. Unitedly, these can contain hundreds to thousands of gigatons of carbon (GtC), and the technology to inject CO_2 into the ground is well proven. CO_2 is stored in geologic formations by a number of dissimilar trapping mechanisms, with the exact mechanism depending on the formation type.

5.2 Depleted Oil and Gas Reservoirs

Although a relatively new idea in the context of climate change moderation, injecting CO_2 into depleted oil and gas fields has been rehearsed for many years. The prime purpose of these injections was the discarding off of "acid gas," a mixture of CO_2, H_2S and other byproducts of oil and gas exploitation and refining. Basically, acid gas injection schemes take out CO_2 and H_2S from the oil or gas stream brought forth, compress and transport the gases via pipeline to an injection well, and re-inject the gases into a different formation for disposal. Proponents of acid gas injection postulate that these schemes affect in less environmental impact than substitutes for treating and disposing unwanted gases, where mostly CO_2 constitutes up to 90 % of total injected volume. In past, depleted and producing reservoirs have demonstrated to be very reliable containers of both hydrocarbons and acid gases over time.

5.3 Enhanced Oil Recovery (EOR)

Being a developed technology, EOR is implemented in carbon dioxide injection into geological formations. On commercial or research levels, in the year 2000, 84 projects were operational, worldwide, of which USA accounts for 72 projects, mostly located in the Permian Basin. Together, these projects produced 200,772 barrels (bbl) of oil per day, a small but meaningful fraction (0.3 %) of the 67.2 million bbl per day total of world-wide oil production that year. ONGC has formulated a plan for usage of CO_2 that is stripped from offshore sour gas at its Hazira facility for EOR at its onshore Ankleswar oil field, 70 km away. Roughly 1200 tonnes of CO_2 will be captured and transported to the oil field on a daily basis (440,000 tonnes of CO_2/year) [22].

In majority of CO_2-EOR projects, a lot of CO_2 injected into the oil reservoir is temporarily stored because the withdrawing of an EOR project usually demands for the "blowing down" of the reservoir pressure to tap oil recovery, thus resulting in the release of CO_2, with a small but substantial amount of the injected CO_2 staying dissolved in the immobile oil.

5.4 Unminable Coal Seams

Desolated or wasteful seams are another likely storage site where CO_2 spread-out through the pore structure or coal and is physically absorbed to it. This process is alike to the way of activation of carbon aids in the removal of impurities from air or water. The uncovered coal surface has a preferred chemical attraction for adsorption of CO_2 than for methane with a ratio of 2:1, which favors its usage in EOR. Thus CO_2 can be used to increase the recovery of coal bed methane (CBM), which may be very cost effective or even cost free, as the additional methane removal can countervail the cost of CO_2 storage operation. The total worldwide potential for CBM is guessed at around 2 trillion scm, with about 7.1 billion tons of linked CO_2 storage potential.

The structure of coal is represented by a dual-porosity arrangement consisting of microporous (coal matrix) and macroporous network (cleat network). The gas is trapped in adsorbed form in the microporosity and in free-state in the macroporosity with the microporous share over 90 %. The complete mechanism of gas production in the coal bed upon depressurization of the reservoir is as follows: molecules desorb from the matrix → molecules diffuse through the microporous network → molecules join the free gas in the cleats and exhibit laminar flow through the cleats to the production well. The transport phenomena for coal bed geosequestration is the vice versa of the above, ending in gas adsorption in the micropores [20]. During this phenomenon, coal matrix experiences shrinkage and swelling as a consequence of adsorption and desorption affecting the permeability of the reservoir directly or in the worst case, physical integrity compromise of the reservoir [5, 23]. The

storage mechanisms provide the basis for the efficiency of extraction which is determined by the transport mechanisms within the rock. Significant changes in the structure of coal take place as a consequence of coal-fluid interaction due to physico-chemical and thermodynamic reactions within coal, with added effects of change in the characteristics of carbon dioxide [24–26].

The coal seam geosequestration (with/without ECBM) literature consisting of various studies ranging from experimental to analytical and numerical modeling, have been conducted in the past covering the physical aspects like fluid flow in coal, fluid existence in the adsorbed form, matrix deformation of the porous media, effect of shrinkage/swelling, flow permeability, existence of fluid in its different phases etc. in context to coals worldwide. A novel alternative to the basic method of coal bed methane recovery by depressurization of the reservoir by water removal is by the injection of gases having higher adsorptive affinity to CH_4 to release the hydrocarbon fuel and is referred to as enhanced coal bed methane (ECBM) recovery.

5.5 Carbon Sequestration in Soil

The process by which atmospheric carbon dioxide can be fixed into soil such that it is held there in a comparatively permanent form, i.e. the term ‘sequestration’ which implies a combination of both capture and storage, is called carbon sequestration.

An inorganic carbon cycle in soil, where carbon dioxide is dissolved in rainwater resulting in the formation of carbonic acid which on reaction with basic cations, makes secondary carbonates, or with calcium–magnesium silicate minerals during the weathering process to liberate basic cations then that precipitate as carbonates [27]. However, such treatments are extremely slow and are only probably to be of significance in the saline and sodic (alkaline) soils discovered in arid and semi-arid zones [28]. In comparison to inorganic carbon cycle, organic ones hold greater significance, whereby atmospheric carbon dioxide is settled by photosynthesis into plants by making organic compounds, most of which are cellulose, hemi-cellulose and lignin, though with additional protein, lipids and other complex compounds.

5.6 Carbon Dioxide Sequestration by Mineral Carbonation

As intimated by mineral carbonation of carbon sequestration, the process is defined as the natural weathering of rocks, aiding in the decrement of CO_2 concentration in the atmosphere in the past, after creation of earth. This so-called ‘mineral CO_2 sequestration’ alternative was earlier suggested by Seifritz [29]. The first elaborated study develops from Lackner et al. [30]. The primary advantage of the process is that the produced mineral carbonates are end products of geologic

processes and are recognized to be stable over geological time periods (millions of years) [31].

A brief definition of the mineralization storage can be recited as the injection of CO_2 or CO_2 dissolved water into divalent cation based alkaline and alkaline-earth metal minerals (Ca^{2+}, $Mg^{2+}$and Fe^{2+}) at optimum reaction conditions to from chemically stable carbonates such as calcite ($CaCO_3$), dolomite ($CaMg(CO_3)_2$), magnesite ($MgCO_3$), siderite ($FeCO_3$) and Mg–Fe carbonate solid solutions [32, 33]. A typical reaction involved during mineral carbonation can be seen as follows [34]:

$$\text{Metal oxide} + CO_2 \rightarrow \text{Metal carbonate} + \text{Heat} \tag{5}$$

Process layouts of different types have been suggested for mineral CO_2 sequestration. Three main types of processes can be classified as:

1. In-situ: Combined mineral CO_2 sequestration in underground along with geological storage of CO_2.
2. Ex-situ: Happens above ground as industrial process. There exists a possible further subdivision between end-of-pipe technology and integrated technology within the process.

5.7 Deep Saline Aquifers and Ocean Storage

Compared to other storage options such as depleted hydrocarbon reservoirs, coal seams etc., deep saline aquifers provide more feasible storage space for prospective CO_2 sequestration, up to 10,000 Gt worldwide [35]. The trapping mechanisms that secure the CO_2 molecules in the aquifers are as follows: Hydrodynamic trapping, residual trapping, pore-scale trapping, solubility trapping and mineral trapping [36]. The convective currents owing to the density and concentration gradient in the brine pockets effectively contribute to the storage dynamics. The multiphase flow dynamics, geochemical interactions, geomechanical attributes, porosity and permeability etc. are the important parameters that determine the impact of CO_2 migration with respect to brine [37]. Injections began in 1990s in Canada, when there was a necessity to dispose of acid-gas i.e. mixtures of H_2S and CO_2 from sour gas wells [38]. Thereafter, successful commercial projects were established at Sleipner field (Norwegian region of North Sea), Snøhvit (offshore Norway) and In Salah (Algeria) and about 15 Mt of CO_2 have been successfully injected between 1996 and 2007 [39]. Other pilot scale and commercial projects have been planned at Gorgon (Australia), Nagaoka (Japan), Ketzin (Germany), the projects by the DOE's Regional Carbon Sequestration Partnership (RCSP) etc.

Till now, the largest potentiality shown as sink for anthropogenic CO_2 are represented by oceans, holding already an estimated 40,000 GtC (billion metric tons of carbon) in comparison to atmospheric CO_2 content of 750 GtC and 2200 GtC in the terrestrial biosphere. Besides surface layer, unsaturation with respect to

CO_2 lies in deeper waters of ocean. As per estimation even double the atmospheric concentration of anthropogenic CO_2, would bring about changes in concentration by hardly 2 %, if injected into deep Ocean and also lower its pH by less than 0.15 units. In order to realize about ocean storage of CO_2, basic understanding of properties of CO_2 and seawater needs to be clarified.

For efficient and economic transport of CO_2, its discharge mode is preferable in its liquid phase. It is discharged at a depth greater than 3000 m in order to prevent it from rising up and getting mixed back into atmosphere. At such depth due to high pressure (>44.4 atm) and low temperature (<10 °C), CO_2 becomes a dense hydrate. With two primary methods of injection of CO_2 into ocean based on depth of injection, it is found that in shallower depth (1500–3000 m), injection is done from a bottom mounted pipe and at greater depths (>3000 m), a "deep lake" phenomena is witnessed. Also, researches are going on for seeking secondary alternatives of injection of CO_2 as bicarbonate ions in solution. This would be incorrect if stated that sea water would not be acidified by injection of CO_2. But processes prevail to reduce the magnitude of impact, e.g. dispersal of the injected CO_2 by an array of diffusers, or addition of pulverized limestone to the injected CO_2 in order that carbonic acid gets buffered [40–44].

6 Assessment of Environmental Impacts and Research and Development Growth

Persistent need lies for advancement in research into possible consequences and measurement of CO_2 and co-mobilized substances, for development, validation and deployment of related technologies on site with estimated cost. Technologies comprise (1) Site characterization measuring methods; (2) Technology and methods for detection and monitoring of leak and rating of possible impacts on the ecosystem, and (3) tools of modeling for forecasting behavior of system and impacts on specific targets. Dimension and magnitude of impacts that might lead from the likely leakage of CO_2, which needs to be evaluated and they will be dependent on the storage site and potential targets. The wide division will be amongst marine / sub-seabed and terrestrial sites; each will require their own judgment methods and technology.

Eventually there will be involvement of public and specifically local interest groups upon request, in the process and information will be conveyed about likely risks. To obtain confidence of public in the technology, there lies a dire need of a former communication about EIA with them.

The transport and storage of CO_2 by normalized technologies and scientific methods is considered a necessity for preparation of CCS on a widespread basis. This is nothing but investigation into the fate of CO_2 in the subsurface and its effect on quality of groundwater and local ecosystems on the off chance of leakage, for both settings, terrestrial and marine, with evolved monitoring methods for specific

issues, as if remote sensing techniques for former spotting and broad scale rating of likely environmental impacts from storage of CO_2 and substructure growth.

References

1. International Energy Agency Key world energy Statistics (2009) http://www.iea.org/textbase/nppdf/free/2009/key_stats_2009.pdf. Accessed Feb 2015
2. International Energy Agency World Energy Outlook (2007) https://www.iea.org/publications/freepublications/publication/weo-2007 full.html. Accessed Feb 2015
3. Mongia N, Bhatia R, Sathaye J, Mongia P (1991) Cost of reducing CO 2 emissions from India: imperatives for international transfer of resources and technologies. Energy Policy 19 (10):978–986
4. Morthorst PE, Grohnheit PE (1992) UNEP greenhouse gas abatement costing studies. Risoe National Lab., Roskilde (Denmark). Systems Analysis
5. Vishal V, Ranjith PG, Singh TN (2013) CO_2 permeability of Indian bituminous coals: implications for carbon sequestration. Int J Coal Geol 105:36–47
6. Herzog H, Golomb D (2004) Carbon capture and storage from fossil fuel use. Encycl Energy 1:1–11
7. Sathaye J, Norgaard R, Makundi W (1993) A conceptual framework for the evaluation of cost-effectiveness of projects to reduce ghg emissions and sequester carbon. LBL-33859, Lawrence Berkeley Laboratory, Berkeley, CA, USA
8. White CM, Strazisar BR, Granite EJ, Hoffman JS, Pennline HW (2003) Separation and capture of CO_2 from large stationary sources and sequestration in geological formations—coalbeds and deep saline aquifers. J Air Waste Manag Assoc 53(6):645–715
9. Olajire AA (2010) CO 2 capture and separation technologies for end-of-pipe applications–a review. Energy 35(6):2610–2628
10. Stewart C, Hessami MA (2005) A study of methods of carbon dioxide capture and sequestration—the sustainability of a photosynthetic bioreactor approach. Energy Convers Manag 46(3):403–420
11. Yang H, Xu Z, Fan M, Gupta R, Slimane RB, Bland AE, Wright I (2008) Progress in carbon dioxide separation and capture: a review. J Environ Sci 20(1):14–27
12. Katzer J, Ansolabehere S, Beer J, Deutch J, Ellerman AD, Friedmann SJ, Steinfeld E (2007) The future of coal: options for a carbon-constrained world. Massachusetts Institute of Technology, MA, USA
13. Forbes SM, Verma P, Curry TE, Friedmann SJ, Wade SM (2008) Guidelines for carbon dioxide capture, transport and storage. World Resources Institute, Washington, DC, USA
14. Haszeldine RS (2009) Carbon capture and storage: how green can black be? Science 325 (5948):1647–1652
15. Gibbins J, Chalmers H (2008) Carbon capture and storage. Energy Policy 36(12):4317–4322
16. Rochon E, Kuper J, Bjureby E, Johnston P, Oakleym R, Santillo D, Goerne GV (2008) False hope: why carbon capture and storage won't save the climate. Greenpeace International, Amsterdam, Netherlands.
17. Richter HJ, Knoche KF (1983) Reversibility of combustion processes. In: Gaggioli RA (ed) Efficiency and costing, second law analysis of process, ACS Symposium Series 235. American Chemical Society, Washington, DC, pp 71–85
18. Bao L, Trachtenberg MC (2005) Modeling CO_2-facilitated transport across a diethanolamine liquid membrane. Chem Eng Sci 60(24):6868–6875
19. Lyngfelt A (2004) A new combustion technology. Greenhouse Gas Issues 73:2–3
20. Vishal V, Ranjith PG, Pradhan SP, Singh TN (2013) Permeability of sub-critical carbon dioxide in naturally fractured Indian bituminous coal at a range of down-hole stress conditions. Eng Geol 167:148–156

21. Lyngfelt A (2007) Chemical looping combustion of solid fuels. Greenhouse Gas Issues 87:9
22. Shackley S, Verma P (2008) Tackling CO_2 reduction in India through use of CO_2 capture and storage (CCS): prospects and challenges. Energy Policy 36(9):3554–3561
23. Vishal V, Singh L, Pradhan SP, Singh TN, Ranjith PG (2013) Numerical modeling of Gondwana coal seams in India as coalbed methane reservoirs substituted for carbon dioxide sequestration. Energy 49:384–394
24. Vishal V, Ranjith PG, Singh TN (2015) An experimental investigation on behaviour of coal under fluid saturation, using acoustic emission. J Nat Gas Sci Eng 22:428–436
25. Vishal V, Singh TN, Ranjith PG (2015) Influence of sorption time in CO_2-ECBM process in Indian coals using coupled numerical simulation. Fuel 139:51–58
26. Vishal V, Singh TN (2015) A laboratory investigation of permeability of coal to supercritical CO_2. Geotech Geol Eng 33:1009–1016
27. Lal R (2008) Soil carbon stocks under present and future climate with specific reference to European ecoregions. Nutr Cycl Agroecosyst 81(2):113–127
28. Lal R, Follett RF, Kimble JM (2003) Achieving soil carbon sequestration in the United States: a challenge to the policy makers. Soil Sci 168(12):827–845
29. Seifritz W (1990) CO_2 disposal by means of silicates. Nature 345:486
30. Lackner KS, Wendt CH, Butt DP, Joyce EL, Sharp DH (1995) Carbon dioxide disposal in carbonate minerals. Energy 20(11):1153–1170
31. GHG I (2000) CO_2 storage as carbonate minerals. CSMA Consultants Ltd, Cheltenham. PH3/17
32. Oelkers EH, Gislason SR, Matter J (2008) Mineral carbonation of CO_2. Elements 4 (5):333–337
33. Gislason SR, Wolff-Boenisch D, Stefansson A, Oelkers EH, Gunnlaugsson E, Sigurdardottir H, Fridriksson T (2010) Mineral sequestration of carbon dioxide in basalt: a pre-injection overview of the CarbFix project. Int J Greenhouse Gas Control 4(3):537–545
34. Sanna A, Uibu M, Caramanna G, Kuusik R, Maroto-Valer MM (2014) A review of mineral carbonation technologies to sequester CO_2. Chem Soc Rev 43(23):8049–8080
35. Bachu S (2003) Screening and ranking of sedimentary basins for sequestration of CO_2 in geological media in response to climate change. Environ Geol 44(3):277–289
36. Pruess K (2003) Numerical simulation of leakage from a geologic disposal reservoir for CO_2, with transitions between super-and sub-critical conditions. Lawrence Berkeley National Laboratory, Berkeley, CA, United States.
37. Bandilla KW, Celia MA, Birkholzer JT, Cihan A, Leister EC (2015) Multiphase modeling of geologic carbon sequestration in saline aquifers. Groundwater 53(3):362–377
38. Bachu S, Gunter WD (2004) Overview of acid-gas injection operations in western Canada. In: Proceedings of the 7th international conference on greenhouse gas control technologies, Edmonton, AB, Canada,Vol 1, p 5–9
39. Michael K, Golab A, Shulakova V, Ennis-King J, Allinson G, Sharma S, Aiken T (2010) Geological storage of CO_2 in saline aquifers—a review of the experience from existing storage operations. Int J Greenhouse Gas Control 4(4):659–667
40. Herzog H, Drake E, Tester J, Rosenthal R (1993) A research needs assessment for the capture, utilization, and disposal of carbon dioxide from fossil fuel-fired power plants. Report to the US Department of Energy, Grant No. DEFG02-92ER30194. AOOO, from MIT Energy Laboratory, MA, USA
41. Herzog H, Drake E, Adams E (1997) CO_2 capture, reuse, and storage technologies for mitigating global climate change: a white paper. MIT Energy Laboratory, MA, USA
42. Reichle D, Houghton J, Kane B, Ekmann J (1999) Carbon sequestration research and development (No. DOE/SC/FE-1). National Lab/National Energy Technology Lab/National Energy Technology Lab, Oak Ridge/Pittsburgh/Morgantown, USA
43. Herzog HJ (2001) Peer reviewed: what future for carbon capture and sequestration? Environ Sci Technol 35(7):148A–153A
44. Williams D, Durie B, McMullan P, Paulson C, Smith A (2001) Greenhouse gas control technologies. In: Proceedings from the fifth international conference (GHGT-5). CSIRO Publishing, Clayton, Victoria, Australia

Part II
Geological Characterisation of Storage Sites

Algorithms for CO_2 Storage Capacity Estimation: Review and Case Study

Barbara Cantucci, Mauro Buttinelli, Monia Procesi, Alessandra Sciarra, and Mario Anselmi

Abstract The estimation of CO_2 storage capacity in deep geologic formations is a pre-requisite for an efficient and safe application of Carbon Capture and Storage (CCS). The evaluation of storage resources for CO_2 geological sequestration is a challenging task and has been tackled using several static algorithms and dynamic methods, on a variety of scales ranging from country to site-specific. The purpose of this study is to present an up-to-date as well as an overall review of the storage capacity algorithms for oil and gas reservoirs, coal seams, and deep saline aquifers, including some worldwide estimation examples. Moreover, a practical application at local scale was also performed for an Italian deep reservoir located in the Po Plain (Northern Italy). The effective storage capacities were obtained applying the commonly established static methods, using both the theoretical and the geocellular volume of the reservoir. Although a conservative approach, this study demonstrates that the selected structure has favorable characteristics for CO_2 geological storage and has the capacity to host the most part of the Po Plain CO_2 emissions for several decades.

1 Introduction

Carbon Capture and Storage (CCS) consists of separating CO_2 from other industrial flue gases and storing it in suitable geological reservoirs at supercritical conditions (31.1 °C and 7.38 M Pa) [1]. Possible options for storing CO_2 in geological formations include deep oil and/or natural gas reservoirs, unmineable coal seams and deep saline aquifers. Once injected into a reservoir, the CO_2 can be retained at depth through several processes [1]: (*i*) confined by a structural or stratigraphic traps as a free, buoyant supercritical fluid (structural/stratigraphic trapping); (*ii*) retained in the pore space by capillary forces at irreducible gas saturation (residual trapping); *(iii)* dissolved into formation water and/or crude oil (solubility trapping); (*iv*) incorporated into newly-formed minerals as a result of water-CO_2-rock inter-

B. Cantucci (✉) • M. Buttinelli • M. Procesi • A. Sciarra • M. Anselmi
Istituto Nazionale di Geofisica e Vulcanologia, Via di Vigna Murata 605, 00143 Rome, Italy
e-mail: barbara.cantucci@ingv.it

V. Vishal, T.N. Singh (eds.), *Geologic Carbon Sequestration*,
DOI 10.1007/978-3-319-27019-7_2

actions in the hosting reservoir (mineral trapping); (*v*) adsorbed on coal seams. These processes can act at different temporal scale, ranging from instantaneous to tens of thousands of years. In the evaluation of site suitability for CO_2 storage, the estimation of storage capacity is a critical issue in terms of economic feasibility and safety. Various methods for assessing the CO_2 storage capacities have been applied worldwide [2–16]. However, none of these methodologies have been accepted as a standard one, since they operate at different scales (from country to site-specific), adopting different terminologies, various trapping mechanisms and boundary conditions, rather than showing highly variable and sometimes conflicting results [13]. A summary of commonly used CO_2 storage assessment methods for different reservoirs typology is shown in Table 1. In 2007, the Carbon Sequestration Leadership Forum (CSLF) and the United States Department of Energy's (USDOE) developed consistent methodologies for CO_2 storage capacity estimations in hydrocarbon reservoirs, coal beds and saline aquifers [2, 3, 7]. These two approaches are widely used even if the definition of a standard is still debated. The CO_2 capacity estimation methods can be roughly divided in static and dynamic methods. The static methods are based on volumetric approaches by using algorithms, whereas the dynamic methods are based on both analytical and numerical simulations to predict the injected gas behavior within the reservoir over the time. To properly carry out subsurface evaluations, it is necessary to define the boundary conditions of a reservoir. In open systems, native fluid can be laterally or vertically displaced away from the injection area making pore space available for CO_2 [2, 3, 10, 17–22]. In closed or semi-closed systems, the movement of fluids is restricted within the formation impermeable boundaries [8, 23–25] and CO_2 capacity is mainly due to the compressibility of brine and hosting rocks [8, 23, 26], thereby leading to an increase in the system pressure. The major parts of storage capacity algorithms include the storage efficiency factor (*E*), i.e. the parameter which defines the fraction of the total pore volume that can be filled by CO_2 [10, 27]. The efficiency factor depends on:

(*i*) physical characteristics of the reservoir; (*ii*) boundary conditions of formation; (*iii*) typology of injection; and (*iv*) maximum allowed pressure [27]. The values of E are generally comprised between 1 and 4 % [3], but they can vary from <1 to >10 % [27], since every approach suggests its own range values depending on the combination of factors listed above.

The purpose of this study is to present an up-to-date overall review of the storage capacity algorithms, including some worldwide capacity estimation examples and a storage capacity assessment at local-scale for a potentially suitable reservoir in Northern Italy. The case study was performed on a reservoir in the Po Plain, selected among previously defined CCS suitable areas [28, 29]. Although an important seismic sequence occurred in the Po Plain during the 2012, this study shows that the selected reservoir is set in relatively stable tectonic environment. In addition the existence of hydrocarbon fields in the Po Plain might indicate that the influence of earthquakes on the stability of the reservoirs should be limited. Some static algorithms were applied to evaluate the CO_2 storage capacity of the selected reservoir. The estimates focused on CO_2 storage in saline aquifers since available underground data for the selected reservoir didn't report any hydrocarbons presence.

Table 1 Summary of different CO_2 storage capacity estimation methods commonly used

Reservoir	Method	Trap	Equation	Storage efficiency
Oil	CSLF	Structural/ stratigraphic	$G_t = \rho_{CO_2}\left[\frac{R_f\ \mathrm{OGIP}}{\mathrm{B_f}} - V_{iw} + V_{pw}\right]$	$C = C_m\ C_b C_h C_w\ C_a$
Gas			$G_t = \rho_{CO_2} R_f (1 - F_{IG})\ \mathrm{OGIP}\left[\frac{P_s Z_r T_r}{P_r Z_s T_s}\right]$	
Oil and gas			$G_t = \rho_{CO_2}\left[R_f\ A\ h\ \varphi\ (1 - S_w) - V_{wi} + V_{wp}\right]$	
Oil and gas	USDOE	Structural/ stratigraphic	$G_e = A\ H\ \varphi_e (1 - S_w) B_f \rho_{CO_2\ std}\ E$	Based on CO_2-EOR or EGR experience
Gas	IEA	Structural/ stratigraphic	$G_e = URR gas_{std} B_f \rho_{CO_2}\ E$	EGR derived values
Coal	CSLF	Structural/ stratigraphic	$G_e = \rho_{CO_2 std}\ IGIP\ R_f\ C'$,	Not defined
	USDOE	Structural/ stratigraphic	$G_e = Ah\ C\ \rho_{CO_2 std}\ E$	$E = \left(E_{An/At} \times E_{Hn/Hg}\right) E_A E_V E_G E_D$
	Zhao et al. [16]	Adsorption, solubility and displacement	$G_t = \left(\frac{0.1 \times Ah\rho_{coal} G_c R_f\ ER\ \rho_{CO_2 std}}{10^6}\right) + [Ah\varphi\ (1 - S_W)(1 - R_W) m_{CO_2\ water}] + \left(A\ h\ \varphi\ S_W R_w \rho_{CO_2}\right)$	Derived by a numerical simulation method
Saline aquifer	CSLF	Structural/ stratigraphic	$G_e = Ah\varphi\rho_{CO_2}(1 - S_{wirr}) C_c$	Not defined
		Solubility	$G_e = Ah\varphi\left(\rho_{w_s} X_s^{CO_2} - \rho_{w_0} X_0^{CO_2}\right) C$	
		Residual	$G_t = \Delta V_{trap} \rho_{CO_2} \varphi S_{CO_2 trap}$	
	USDOE	Structural/ stratigraphic	$G_e = Ah\varphi\rho_{CO_2} E$	$E = \left(E_{An/At} \times E_{Hn/Hg} \times E_{\varphi e/\varphi t}\right) E_A E_V E_G E_D$
	USGS	Buoyant and residual	$G_{tech} = \rho_{CO_2} V_b E_b + \sum_{i=1}^{3} [\rho_g (AH\varphi - V_b) R_i R_w E_r]$	$E_r = \frac{\left(S_{CO_2 irr}/(1 - S_{wirr})\right)^2}{0.9\lambda + 0.49}$
	Zhou et al.[8]	Compressibility	$G_e(t_i) = Ah\varphi\rho_{CO_2} E$	$E = \left(\beta_p + \beta_w\right) \Delta P_{max}$

Modified by Goodman et al. [10]

2 The Storage Capacity Estimation in Oil and Gas Reservoirs

Oil and gas reservoirs are considered ideal geologic storage sites because they have held hydrocarbons over thousands to millions of years. Furthermore, their architecture and properties are well known as a result of exploration and production of these hydrocarbons. CO_2 storage capacity estimation is generally based on reservoir characteristic (pressure, temperature, effective volume) and resources (e.g., the Original Gas or Oil in Place-OGIP and OOIP- respectively, and the recovery factor), as well as in situ CO_2 properties.

2.1 The CSLF Methodology

The CSLF methodology [2, 7] proposed two approaches. The first (Eqs. 1 and 2) is based on OGIP and OOIP, respectively, at surface conditions and assumes that the volume previously occupied by hydrocarbons can be available for CO_2 storage once they are extracted:

$$G_t = \rho_{CO_2} R_f (1 - F_{\mathrm{IG}})\, OGIP \left[\frac{\mathrm{P_s Z_r T_r}}{\mathrm{P_r Z_s T_s}}\right] \tag{1}$$

where, F_{IG} is the fraction of injected gas.

$$G_t = \rho_{CO_2} \left[\frac{R_f OOIP}{B_f} - V_{wi} + V_{wp}\right] \tag{2}$$

The second is based on the volume of reservoir (Eq. 3):

$$G_t = \rho_{CO_2} \left[R_f A h \varphi (1 - S_w) - V_{wi} + \mathrm{V}_{wp}\right] \tag{3}$$

where, V_{wi} and V_{wp} (applicable in the case of oil reservoirs) can be calculated from production records.

In the case of reservoirs underlain by aquifers, the hydrocarbons extraction produces a pressure decline leading the formation waters to invade the pore space. Injected CO_2 can partially displace the water, since some water can be retained in pore space by capillary trapping [30], thus resulting in a net reduction of CO_2 storage capacity. This reduction process can be expressed by a capacity coefficient [31] as follows:

$$G_e = CG_t = C_m C_b C_h C_w C_a G_t \tag{4}$$

where C is the capacity coefficient and the subscripts *m, b, h, w, a* stand for CO_2 mobility with respect to oil and water, buoyancy of CO_2 on oil and water, reservoir heterogeneity, water saturation and aquifer strength, respectively.

2.2 The USDOE Method

USDOE method [3] for oil or gas reservoirs is proposed at the field scale. CO_2 storage capacity is computed by both volumetric basis and amount of deliverable oil and gas. The volumetric estimate is based on the standard industry method to calculate OOIP and OGIP by the formation volume factor (B_f) [10, 32] as follows:

$$G_e = AH\varphi_e(1 - S_w)B_f\rho_{CO_{2\,std}}E \tag{5}$$

The storage efficiency factor (E) reflects a fraction of the total pore volume from which oil and/or gas has been produced and that can be filled by CO_2. E can be derived from local CO_2-Enhanced Oil Recovery experience or reservoir simulations as standard volume of CO_2 per volume of OOIP [10].

A comparison between CSLF and USDOE algorithms (Eqs. 3, 4 and 5, respectively) shows that the two methodologies are basically equivalent if injected (V_{wi}) and produced (V_{wp}) water are not considered. Thus:

$$E = R_f \times C \tag{6}$$

2.3 The IEA-GHG Method

The IEA Greenhouse Gas R&D Programme (IEA – GHG) joined with Pöyry Energy Consulting, Element Energy and BGS developed a capacity estimation method, specific for gas reservoirs, assuming that a depleted gas field could be refilled with CO_2 up to its initial pre-production pressure [18]. Their algorithm is based on the Ultimately Recoverable Reserves of gas at standard conditions ($URR_{gas_{std}}$) as follows:

$$G_e = URR_{gas_{std}}B_f\rho_{CO_2}E \tag{7}$$

Here B_f corresponds to the reciprocal of the GEF (Gas Expansion Factor) from reservoir to standard conditions and depends on reservoir temperature, pressure and gas composition. For world CO_2 capacity estimations, IEA-GHG assumed a storage efficiency of 75 %.

3 The Storage Capacity Estimation in Coal Seams

CO_2 storage within unmineable coal seams can be combined with the Enhanced Coal Bed Methane (ECBM) recovery to increase methane production, since coal naturally contains varying amounts of methane adsorbed onto pore surfaces. Storage capacity evaluations in these reservoirs assume that the injected CO_2 will replace the methane in coal since it has a higher affinity for CO_2 than for methane.

3.1 The CSLF Method

The CSLF methodology [2, 7] is based on both the Initial-Gas-In-Place (IGIP) absorbed in the coal and the reservoir deliverability ($R_f C^{'}$). Effective storage capacity can be calculated as:

$$G_e = \rho_{CO_2 std} IGIP R_f C', \tag{8}$$

where C' is the completion factor which represents an estimate of the coal portion zone that contribute to gas production or storage. In this formalism:

$$IGIP = AH\rho_{coal} G_{cs}(1 - f_a - f_m) \tag{9}$$

where, G_{cs} is the coal gas content (dry, ash free) assuming a coal fully saturated with CO_2, f_a and f_m are the ash and moisture weight fraction of coal, respectively. G_{cs} is generally assumed to follow a pressure-dependent Langmuir isotherm:

$$G_{CS} = V_L \frac{P}{P + P_L} \tag{10}$$

where V_L and P_L are the Langmuir volume and pressure.

3.2 The USDOE Method

The USDOE [3–6] proposed a volumetric method to estimate the capacity:

$$G_e = A h C \rho_{CO_2 std} E \tag{11}$$

where C is the concentration of CO_2 standard volume per unit of coal volume (Eq. 10) assuming 100 % CO_2 saturated coal conditions [6]. E was estimated by Log Odds method with Monte Carlo sampling, as function of volume available to CO_2 storage and displacement [10]:

$$E = \left(E_{An/At} \times E_{Hn/Hg} \right) E_A E_V E_G E_D \tag{12}$$

where, the net-to-total area $E_{An/At}$ is the fraction of the basin containing coal, $E_{Hn/Hg}$ is the net-to-gross thickness that has adsorptive capability. E_A and E_V represent the fraction of areal and vertical section that can be contacted by CO_2 from a single vertical well. E_G express the effect of density differences between CO_2 and the formation water in the cleats. E_D reflects the degree of saturation achievable for in

situ coal compared with the theoretical maximum predicted by the CO_2 Langmuir isotherm. Goodman et al. [10] provided E values based on coal bed methane production and computer modeling observations [3–5], ranging from 21 %, 37 % and 48 % over the 10th, 50th and 90th percentile, respectively. If $E_{An/At}$, $E_{H_{Hg}}$ are known, only displacement factors contribute to E value, which ranges from 38 %, 64 % and 77 %, over the 10th, 50th and 90th percentile, respectively [10].

3.3 The Zhao et al. (2015) Methodology

Zhao et al. [16] proposed an alternative approach to evaluate CO_2 storage capacity in coal beds where formation waters are present. The storage capacity is given by sum of CO_2 adsorption in coal beds, CO_2 solubility in water and CO_2 displacement to formation waters, as follows:

$$G_t = \left(\frac{0.1 \times Ah\rho_{coal}G_{cs}R_f\, ER\rho_{CO_{2std}}}{10^6}\right) + [Ah\varphi\,(1 - S_W)(1 - R_W)m_{CO_2\,water}] + \left(A\,h\,\varphi\,S_W R_w \rho_{CO_2}\right) \tag{13}$$

where G_{cs} is the coal beds gas content, ER is the replacement coefficient which reflects the CH_4 replaced by CO_2 in coal beds. R_f, R_w can be achieved by the reservoir numerical simulation method.

4 The Storage Capacity Estimation in Saline Aquifers

Saline aquifers are recognized to have the greatest capacity compared to the other reservoir types, due to their worldwide availability [1]. Despite this, their CO_2 capacity estimates involve a high degree of uncertainties, mainly due to the fact that the knowledge of saline formations is quite limited [13, 27, 33]. Moreover, in deep saline aquifers, the various trapping mechanisms interact with each other, even though they are active at different times during the storage process [2, 13]. For structural and stratigraphic traps, maximum storage capacity is obtained at the injection end, whereas in open systems the time of CO_2 immobilization occurs after the cessation of injection by solubility and residual trapping. This temporal factor introduces a further degree of complexity in the capacity estimation, since it depends on the time period over which such estimate is done [27]. Basically, saline aquifers storage capacity can be estimated by the volumetric-based or pressure-limited approaches.

4.1 The CSLF Method

The CSLF methodology [2, 7] considers several trapping mechanisms, namely, structural and stratigraphic trapping, residual and solubility trapping providing individual equations for each one.

The CSLF method for structural and stratigraphic traps assumes a complete displacements of native formation water down to spill point:

$$G_e = A\,h\,\varphi\,\rho_{CO_2}(1 - S_{wirr})C_c \tag{14}$$

where C_c is a capacity coefficient accounting for trap heterogeneity, CO_2 buoyancy and sweep efficiency. The term $(1 - S_{wirr})C_c$ corresponds to storage efficiency factor (E). Its values are defined as a function of lithological characteristics of reservoir for clastic (1.86, 2.70, 6.0 %), dolomite (2.58, 3.26, 5.54 %) and limestone (1.41, 2.04, 3.271 %), based on their 10th, 50th and 90th percentiles [19].

The CSLF method by solubility trapping is based on the fraction of CO_2 meeting native formation waters [2]. This trapping mechanism is a time-dependent process and should be determined through numerical modeling at the local and site-specific scales. On the other hand, at the basin- and regional-scale, the following relation can be applied [34]:

$$G_e = A\,h\,\varphi\left(\rho_{w_s} X_s^{CO_2} - \rho_{w_0} X_0^{CO_2}\right)C \tag{15}$$

where C is a coefficient accounting for all factors that affect the spread and dissolution of CO_2 in the aquifer volume [2, 7]. The fraction of dissolved CO_2 increases with pressure and decreases with temperature and water salinity as ruled by several equations of state [35].

The CSLF residual trapping is based on the irreducible gas saturation in the pore space after the stoppage of injection [36]. This mechanism is time-dependent:

$$G_t = \Delta V_{trap}\,\rho_{CO_2}\,\varphi\,S_{CO_{2trap}} \tag{16}$$

$S_{CO_{2trap}}$ and ΔV_{trap} can be determined at a specific time only through numerical simulations in local- and site-scale assessments [36, 37].

4.2 The USDOE Method

The USDOE methodology [3–6, 10] is mainly volumetric and compressibility based and estimates CO_2 capacity at basin level. Solubility and mineral trapping are not taken into account because they depend on in situ conditions and their contribution is likely insignificant during the injection phase of a CO_2 storage operation [38]. Effective CO_2 storage capacity at open conditions is [4–6]:

$$G_e = A\,h\,\varphi\,\rho_{CO_2}E \tag{17}$$

E was determined by the Log Odds method with Monte Carlo sampling, which includes terms to define the pore volume available to CO_2 storage ($E_{An/At}$, $E_{H\eta/Hg}$, $E_{\varphi e/\varphi t}$) and both macroscopic (E_A, E_V, E_G) and microscopic (E_D) displacement efficiency terms to define the pore volume immediately surrounding a single CO_2 injector well [4, 5, 10, 17] as follows:

$$E = \left(E_{An/At} \times E_{Hn/Hg} \times E_{\varphi e/\varphi t}\right) E_A E_V E_G E_D \tag{18}$$

where $E_{An/At}$ is the net-to-total area, $E_{H\eta/Hg}$ is the net-to-gross thickness, $E_{\varphi e/\varphi t}$ is the effective to total porosity. If these parameters are known, $E_{An/At}$, $E_{H\eta/Hg}$, $E_{\varphi e/\varphi t}$ values can be set to 1. E_A and E_v represent the fraction of areal and vertical section of the aquifer contacted by CO_2 in a single vertical well. E_G express the effect of density and viscosity contrast between CO_2 and saline formation waters. E_D represents the fraction of water-saturated pore volume replaced by CO_2 [10, 27]. Goodman et al. [10] have calculated E values for clastic (0.5, 2.0, 5.4 %), dolomite (0.64, 2.2, 5.5 %) and limestone (0.4, 1.5, 4.1) lithologies based on their 10th, 50th and 90th percentiles, respectively [4, 5].

4.3 The USGS Method

In 2007 the United States Geologic Survey (USGS) carried out a national assessment in conjunction with the Environmental Protection Agency (EPA) and DOE, developing a new method to assess CO_2 resources in USA [9, 14]. The USGS approach defines Storage Assessment Units (SAUs), i.e., mappable subsurface bodies of rock characterized by common geologic and hydrologic characteristics such as depth and confinement at scale from regional to sub-basinal [9, 14, 21]. This methodology focuses on the technically accessible resource, i.e., using present-day geological and engineering knowledge to optimize storage efficiency. Technically accessible storage resource (G_{tech}) can be obtained by the sum of the buoyant trapping at the top and lateral seal of a stratigraphic and structural trap and residual trapping in the open part of the aquifer:

$$G_{tech} = \rho_{CO_2} V_b E_b + \sum_{i=1}^{3} \left[\rho_{CO_2}(AH\varphi - V_b) R_i R_s E_r\right] \tag{19}$$

where V_b is the buoyant trapping pore volume and E_b is the buoyant trapping storage efficiency. E_b values are based on hydrocarbon production, undiscovered resources and volume calculations of geologic traps [15], and range among 20 %,

30 % and 40 % based on their 10th, 50th and 90th percentiles, respectively [14]. Each of the three terms in the summation is a residual trapping storage resource, apportioned into three injectivity classes (R_i) by rock permeability (k) characteristics ($k > 1$ D, 1 mD $< k <$ 1 D; $k <$ 1 mD, respectively) [14], the sum of which must be to one. R_s is the area fraction of the SAU available for storage, depending on U.S. Environmental Protection Agency (EPA) water-quality guidelines or highly fractured seals. E_r is the residual trapping storage efficiency. E_r values are calculated by the McMinn et al. [39] model, which assumes an homogeneous isotropic aquifer with no horizon interface between reservoir and caprock. This model uses an equation that employs the capillary trapping number divided by an approximation involving the mobility factor (λ):

$$E_r = \frac{\left(S_{CO_2 irr}/(1 - S_{wirr})\right)^2}{0.9\lambda + 0.49} \tag{20}$$

$$\lambda = k_{rCO_2}\mu_w/\mu_{CO_2} \tag{21}$$

Residual trapping efficiencies range from 1.35 to 8.1 % for standard SAU (914–3962 m depth) and from 4 to 22 % for deep SAU (>3962 m depth) by rock class [15, 21, 22].

4.4 The Pressure-Limited Systems

The pressure-limited systems [8, 23] estimate capacity as the maximum amount of gas that can be injected before reaching a maximum allowed pressure. The maximum pressure is generally defined by regulatory mechanisms in order to avoid geo-mechanical damages [8, 24, 40] that could create or enhance leakage pathways from the aquifer, as well as induced seismicity by fault (re-)activation [1, 41, 42]. Depending on the national regulatory, maximum allowed pressure generally corresponds to the 50 % of the initial hydrostatic pressure or the 60 % of initial lithostatic pressure at the top of the storage formation.

Zhou et al. [8] proposed a quick assessment method to provide capacity estimates at early stages of site selection in closed and semi-closed systems, when data are sparse. In this method, accommodation space for the injected CO_2 is provided by expanded pore volume of medium and water in the storage formation and the seals, and the increased brine density in response to pressure buildup in the storage formation as follows:

$$G_e(t_i) = A\,h\,\varphi\,\rho_{CO_2}E \tag{22}$$

$$E = \left(\beta_p + \beta_w\right)\Delta P_{max} \tag{23}$$

Pore compressibility for deep formations generally has large variability, from 4.5×10^{-11} to 4.5×10^{-9} Pa^{-1} [8], whereas water compressibility is in the range

of 3–6 $\times 10^{-10}$ Pa^{-1} for typical CO_2 storage reservoirs [43]. Depending on β_p, E would vary in the range of 0.08–0.75 % per 1 MPa increase in average aquifer pressure, but more typical values would be in the order of 0.1 % per MPa [27]. In semi-closed systems, caprock would allow pressure dissipation throughout vertical leakage and brine displacement [8], depending on their permeability (on the order of 10^{-18} m^2) [25].

4.5 Comparison of Saline Aquifers Methodologies

Several analyses have been conducted to compare the above cited methodologies in order to identify gaps and to estimate the storage efficiency range [33]. From a statistical point of view, CSLF [2, 7], USDOE [3–5] and USGS [9, 21] approaches can be considered equivalent [33], with E ranging from 1.5 to 3.6 % in open systems [26]. Similarly, closed and open system approaches cannot be statistically distinguished, although in some cases, conflicting results due to the differences in the assumptions and lacking of data are obtained. Generally, the uncertainty in the geological properties has a much greater impact on capacity estimates than the chosen methodology [33]. A comparison between open and closed approaches with flow models [24], showed that the firsts can over-estimate the storage capacity because they do not account for pressure build up in the reservoir, whereas the seconds are approximately close to the flow-model derived capacity.

5 World Examples

As shown in the previous paragraphs, several methods have been proposed to estimate CO_2 storage capacity in oil and gas reservoirs, coal beds and saline aquifers. Most of today's world storage estimates are based on the CSLF method, whereas in United States the most commonly used methods are USDOE and USGS. Some worldwide examples are shown below.

U.S. & Canada Recently in US and Canada a CO_2 storage capacity estimation has been performed by DOE-NETL jointly with RCSPs (Regional Carbon Sequestration Partnerships) and NATCARB (Natural Carbon Sequestration Database and Geographic Information System). A volumetric approach (see Sect. 2, 3, 4) has been proposed for oil and gas reservoirs, unmineable coal and saline aquifers. The CO_2 storage capacity in oil and gas reservoirs in North America were estimated on 33 provinces [6]. No range of capacity values was proposed and not all potential mature oil and gas reservoirs have been examined. DOE's RCSPs have documented the location of approximately 226 Gt of CO_2 storage resource [6] mainly distributed in Texas, Oklahoma, U.S. Federal Offshore, Alberta, Louisiana, New Mexico, Saskatchewan, West Virginia, Pennsylvania and North Dakota. CO_2 storage

resources in Texas and Oklahoma are able to retain the CO_2 at current emission rates for 260 years and 550 years, respectively [6]. The CO_2 storage capacity in unmineable coal was evaluated in 32 provinces of North America considering reservoirs at shallower depths than oil and gas reservoirs and saline formations, since CO_2 need not be in supercritical condition to be adsorbed by coal. DOE's RCSPs documented the location of approximately 56–114 Gt of potential CO_2 storage resources in unmineable coal [6]. The best areas are located in Texas, Alaska, Louisiana, Mississippi, Wyoming, Alabama, Arkansas, Illinois, Florida and Washington. At current CO_2 emission rate, Texas and Alaska are able to store CO_2 for 35–80 years and 610–1420 years, respectively [6]. Saline formations are fairly widespread throughout North America, occurring in both onshore and offshore sedimentary basins [6]. DOE's RCSPs estimated a CO_2 storage resource ranging from approximately 2102 to more than 20,043 Gt of CO_2 [6]. The areas with largest CO_2 storage capacity were identified in U.S. Federal Offshore, Texas, Louisiana, Alabama, Mississippi, Montana, Wyoming, Florida, Washington and California. At current emission rate of Texas and Louisiana, storage capacity is for 880–11,200 years and 1000–16,000 years, respectively [6].

China A recent work which was carried out proposed a new estimate of CO_2 storage capacity in coal beds in China [16]. The evaluation has been done considering not only CO_2 adsorption in coal beds but also CO_2 dissolution and displacement to formation water. This new approach arises out of the consideration that most coal beds in the world host water and the physical and solubility trapping should be not ignored in the CO_2 storage capacity estimate. The capacity was calculated for the Qinshui Basin, at the southeastern end of Shanxi province. The results show a CO_2 storage resource of 1720, 15 and 46 Gt for adsorption, dissolution and displacement mechanisms, respectively.

Japan Since 2005, Research Institute of Innovative Technology for the Earth (RITE) in cooperation with Engineering Advancement Association of Japan (ENAA) conducted a re-evaluation of CO_2 storage capacity in Japan [44]. A first assessment was carried out by Tanaka et al [45] in saline aquifers (91.5 Gt of CO_2). This new estimation was conducted by the CSLF method, including two storage categories (A–B) which depend on the trap mechanism and the amount of acquired data. The A-category refers to aquifers in the structural traps, including depleted oil and gas reservoirs. The B-category is relative to aquifers in stratigraphic and residual trap, both in offshore sedimentary basins, where the sea floor is less than 200 m deep, and in onshore gas fields [44]. The results show a CO_2 storage capacity of 30 Gt and 116 Gt, for category A and B, respectively, sum total 146 Gt, about 54.5 Gt more than previous storage estimations [45].

Mozambique A recent study published by Solomon et al. [46] proposed a CO_2 storage capacity evaluation in saline formations, in the Mozambique Basin. The estimation was performed following the USDOE volumetric approach [3–6]. The estimated CO_2 capacity ranges from 2.4 to 228 Gt of CO_2 as a function of the net-to-gross ratio and the storage efficiency factor (1 to 2 %) [46].

Northern Europe In 2011 Höeller and Viebahn [47] computed the CO_2 storage capacity in deep saline aquifers and depleted oil and gas fields for Germany and its neighboring countries (Netherlands, France, Denmark, Norway, UK and Poland) where German CO_2 emissions could possibly be stored. The effective capacity of deep saline aquifer was estimated by the volumetric method for closed systems [8], whereas for depleted oil and gas fields cumulative production and reserve data were used. In this case the volume of ultimately recoverable gas at the surface is multiplied by CO_2 density, gas expansion factor/formation volume factor and sweep efficiency to determine the theoretical capacity estimation. Based on the recent studies [19] only 75 % replacement of original oil and gas is expected. The results for the Northern Europe show a conservative CO_2 storage capacity of 49 Gt, the offshore in the North Sea and UK are the most promising areas.

Greece A preliminary evaluation of the theoretical CO_2 storage capacity in Greece was performed by Koukouzas et al. [48]. The estimate was carried out on depleted and unexploited oil fields and saline aquifers. A complete evaluation was possible only for Prinos-Kavala sedimentary basin, in the North Aegean Sea, following the CSFL method. The storage capacity of the Prinos oil field was estimated at 19 Mt CO_2, based on Ultimately Recoverable Reserves and assuming the CO_2 injection ends when the initial reservoir pressure is reached. For unexploited oil field an evaluation of the 32 Mt of CO_2 was performed considering the probable oil-in-place volume. The storage capacity of the saline formations in the offshore Prinos Basin was estimated as 1350 Mt of CO_2. The total capacity of the Prinos-Kavala basin is 1.4 Gt of CO_2 (Fig. 1).

6 Italian Case Study

The CO_2 storage assessment in geo-dynamically active areas is rather challenging. For a reliable estimation, a careful characterization of a reservoir is a pre-requisite. Among the already defined CO_2 storage suitable areas in Italy [28, 29] a potential reservoir in Po Plain (Northern Italy) was selected as a case study for CO_2 capacity estimation.

6.1 Geological and Seismotectonic Background

The area of interest for the study is located in the Western part of the Po Plain, among the cities of Cremona, Mantova and Reggio Emilia (Fig. 2). The Po Plain represents the foreland of two mountain belts: the NNE-verging Northern Apennines and the S-verging Central-Southern Alps. The Po Plain area recently underwent a continuous subsidence which allowed the sedimentation of huge thicknesses (from few hundred meters on top of the shallowest buried anticlines

Fig. 1 Map of the CO_2 storage capacity of reported examples (See Sect. 5). For each considered example, the maximum capacity (Gt) is indicated; only for USA & Canada the min and max capacity is listed

to several thousand meters in the depocenters between the main thrust fronts; Fig. 2) of Plio-Quaternary foredeep terrigenous units [49, 50]. Since, these areas have been extensively investigated for hydrocarbons exploration purposes, with several oil and gas fields still in production [51, 52], a great amount of underground data are available (e.g., seismic profiles, well logs and structural maps, made available by the Italian Ministry of Economic Development, UNMIG) [53]. These data allowed a refined interpretation of underground structures, which are mostly represented by blind ramp anticlines and anticlinal stacks belonging to the Northern Apennines arcs, currently buried below the Plio–Quaternary sequence (Fig. 2). Several detailed stratigraphical analyses, based on geophysical well logs, were also conducted in order to deeply characterize the whole sedimentary cover down to the pre-foredeep basement units. Even if these data show a complex geological variability, the general stratigraphy can be summarized in several group of units which have been coherently observed throughout the whole Po Plain basin [51, 54]; from the top: (*i*) Quaternary sequence made up by alluvial deposits, clays, silts, and sands (e.g., alluvial sediments, Sabbie di Asti, Ravenna Fm.); *(ii)* Pliocene group mainly characterized by clay, silt, and sand (e.g., Argille del Santerno, Portocorsini Fm., and Garibaldi Fm.); (*iii*) Messinian group consisting of sand, clay, and sandstone with gypsum (e.g., Gessoso-Solfifera and Colombacci Fms.); (*iv*) Flyschoid group consisting of syn- and post-orogenic terrigeneous sequences (e.g., Marne di Gallare, Marnoso-Arenacea and Cervarola unit); and (*v*) Meso-Cenozoic calcareous and marly sequence (e.g., Scaglia and Maiolica Fms.) present everywhere below the foredeep basin units.

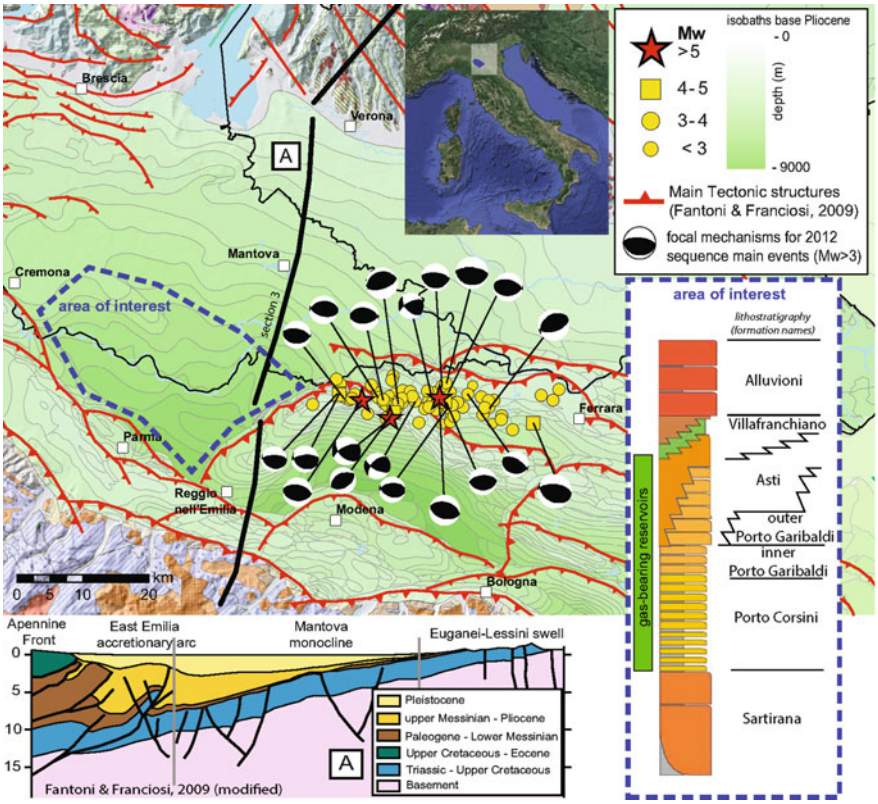

Fig. 2 Structural setting of the study area with isobaths contours of Pliocene units below the whole Po Plain [50] and main tectonic lineaments [49]. Geological cross section modified from Fantoni and Franciosi [49] and the main events of the 2012 seismic sequence with moment tensors solutions (Modified after Ref. [55]). The general stratigraphy in the area of interest is summarized highlighting the presence of gas-bearing reservoir units (Modified after Ref. [51])

The whole Po Plain area has been historically interested by diffuse seismicity [56, 57]. In addition to this the 2012 Emilia seismic sequence brings important information concerning the geometry of Northern Apennine fold-and-thrust outer belt (Fig. 3a). The 20th and 29th May 2012 main shocks and aftershocks seismic sequence concentrated within the Mesozoic–Tertiary carbonates [58] below the terrigenous sedimentary cover, compatibly with the reactivation of pre-existing normal faults inherited from the previous Mesozoic extensional tectonics [59]. The few epicenters located in the area of interest generally have a depth between 25 and 30 km, possibly addressable to deep transverse structures perpendicular to the chain elongation (sensu [60]), sensibly far from the depths of the sedimentary units target of this evaluation.

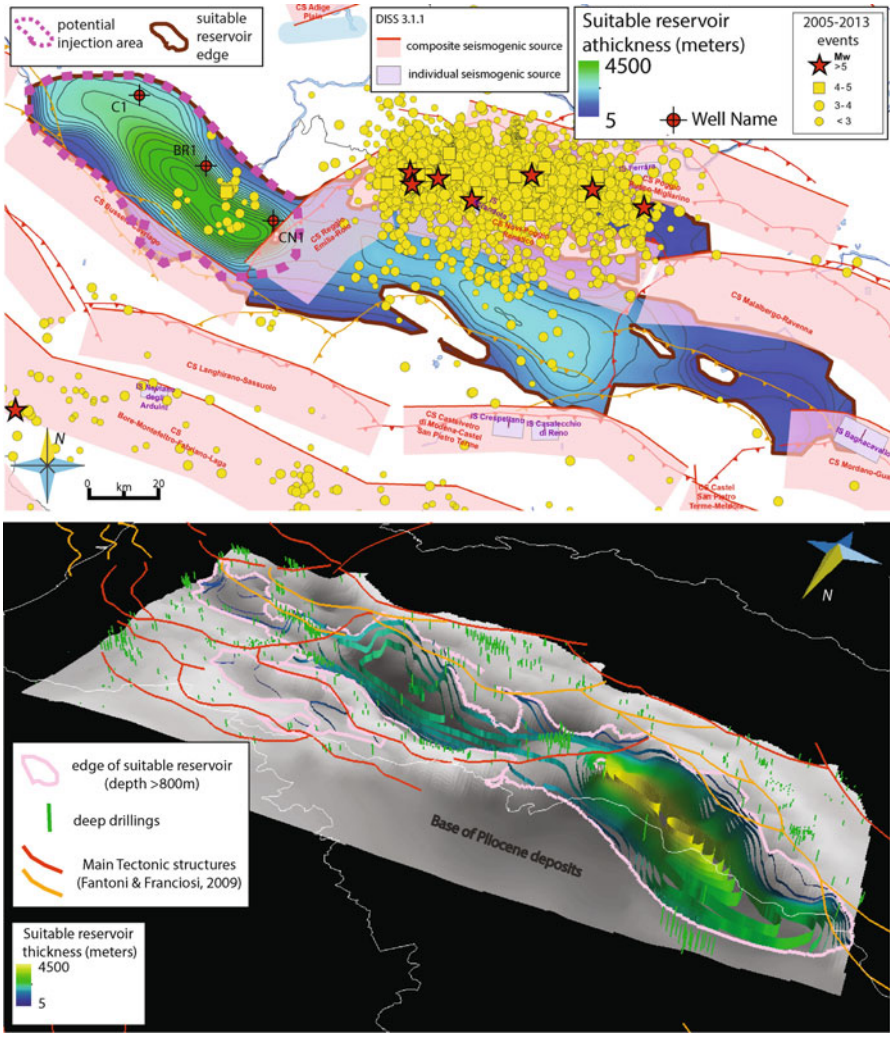

Fig. 3 *Upper panel*: 2D reconstruction of the potential reservoir compared with the distribution of seismic events extracted from INGV catalogues for the period 2005–2013 [57]. *Brown line* defines the extension of the reservoir below the depth of 800 m. The location of Cantoni 1 (*C1*), Bosco Rosso 1 (*BR1*) and Castelnuovo 1 (*CN1*) available wells, used to extract reservoir parameters is reported. *Lower panel*: 3D model of the base of Pliocene deposits surface (*grey scale*). *Blue* to *yellow* isopachs stripes define the thickening of the reservoir in northeastern sector of the study area, where storage capacity calculations have been conducted (view from North-West to South-East)

6.2 Reservoir Characterization

The published interpretations of Po Plain structural setting as well as the available underground datasets [50, 53, 61–64] were reviewed in order to check the reconstructions of Pliocene base surface and the sedimentary sequence above it. The Pliocene base surface defines the reservoir bottom in these areas, which is constituted by the Porto Corsini, the Porto Garibaldi and minorly the Asti formations [51] (Fig. 2). The caprock is constituted by a huge thickness of clays which is an excellent seal, as it has a proven capability to retain the hydrocarbons in the Po Plain fields. A 3D geological model of the reservoir was developed based on the available isopachs maps of the Porto Corsini and Porto Garibaldi units [53]. The bi-dimensional and tridimensional geometry (geocellular model) of the reservoir was defined (Fig. 3), also comparing the distribution of reservoir layers with the seismic events in the area.

The highest thickness of reservoir units is located just toward the NE with respect to the Cremona-Parma-Reggio nell'Emilia thrust front (Fig. 2) [65]. Here the reservoir is generally developed between approximately 2 and 8 km of depth, while the top surface varies from 1 to 3.5 km. The potential reservoir is widespread over an area of approximately 8.56×10^8 m^2 and its average gross thickness is about 1300 m (Fig. 2). Well log information of Cantoni 1, Bosco Rosso 1 and Castelnuovo 1 wells [53], drilled in the area of interest, report an average net-to-gross ratio (n/g) of 60 % for Porto Corsini and Porto Garibaldi formations. The average porosity of the reservoir units from well log analysis is around 25 %. This value is in line with the already published 30 % for similar reservoir units [29]. Authors would point out that this porosity values have not been estimated throughout a strict sensitivity analysis, since such kind of data is generally scarce for those areas, and only a few are published in literature. Moreover no information about permeability values is available, except for those related to clay layers, which are mineralized with natural gas, where it has been calculated between 1 and 6.5 mD. Salinity of formation waters (NaCl), extrapolated by well log analyses of Bosco Rosso 1 is 50 g/L. Empirical evaluations from oil and gas companies unpublished charts for the reservoirs of Po Plain areas allow to set the irreducible water saturation to 10 %. The average lithostatic pressure applied to the reservoir can be estimated using the 21 MPa/km gradient extracted by well log analyses [54], which should be about 50 MPa at reservoir top. According to the temperature log from Bosco Rosso 1 well, the temperature of the reservoir is around 46 °C at a depth of 2850 m. These conditions are adequate to maintain CO_2 in its supercritical state. Together with the hydrostatic pressure (28.5 MPa at a depth of 2850 m) these values influence the density of the CO_2 at reservoir conditions, which could be then calculated in 876.6 kg/m^3 [66].

6.3 CO_2 Capacity Estimation

CO_2 capacity estimation for the selected reservoir is based on static volumetric approaches. Since the well data of this area don't report any presence of oil and gas accumulations, it would be more appropriate to use only the equations for storage calculations for saline aquifers (see Sect. 4). Although the published comparisons on such volumetric methodologies show that they are statistically equivalent [33], some differences can be found between open and closed systems. Therefore in this study we applied the commonly used equations for open systems proposed by CSLF (Eq. 14) and USDOE (Eq. 17) avoiding the USGS one, since it tends to overestimate the storage evaluations [24]. Furthermore as a conservative end member for closed systems we also applied the approach proposed by Zhou et al. [8] (Eq. 22). Since in all the used methodologies, contribution of solubility and residual during injection time is considered rather small, therefore it has been neglected for this case study. For each considered approaches both theoretical and geocellular reservoir volumes were used. The theoretical reservoir volume ($A \times h$) is 1.156×10^{12} m^3, while the more realistic geocellular volume (V_{geoc}) extracted from 3D geological model is 1.28×10^{12} m^3. The latter, together with the net-to-gross ratio (n/g) were used to compute a more realistic storage capacity. Authors therefore introduced a slight change in the common USDOE formalism, as follow:

$$G_{e-geoc} = V_{geoc} \varphi \rho_{CO_2} \frac{n}{g} E \tag{24}$$

Storage efficiency factors for CSLF ($(1 - S_{wirr})C_c$) and USDOE were directly used from the statistical classes (over the 10th, 50th and 90th percentile) proposed for clastic reservoirs by IEA-GHG [19] and [4], respectively; whereas the efficiency factor adopted in Zhou et al. [8] approach were calculated using the reservoir bulk compressibility multiplied to the maximum allowed pressure (Eq. 23). An average bulk compressibility of 7×10^{-4} MPa^{-1} was estimated by Baù et al. [67] for gas reservoirs hosted in Quaternary and Upper Pliocene deposits of the Northern Adriatic sedimentary basin, at depth between 900 and 7000 m. This value agrees with literature data for pore and water compressibility typical CO_2 storage reservoirs [8]. Italy lacks a specific regulation on the maximum allowed overpressure during fluid geological storage operations. Thus the ΔP_{max} value has been set to 7 % of the initial lithostatic pressure (i.e., 3.5 MPa). This value is based on the overpressure already granted by the UNMIG at Settala natural gas field (to the NW of Po Plain) during seasonal injection operations (http://7unmig.sviluppoeconomico.gov.it/deposito/titoli/decreti/2813_20101025.pdf). Results shows that for the Italian selected case study the effective storage capacity ranges from 0.60 to 16.88 Gt, based on the assigned E values. A summary of the capacity calculations is reported in Table 2.

Table 2 CO_2 storage capacities and efficiency factor values calculated for the selected structure

	E %			G_e (Gt)			$G_{e\text{-}geoc}$ (Gt)		
Approach	10th	50th	90th	10th	50th	90th	10th	50th	90th
CSLF	1.86	2.70	6.0	4.54	6.58	14.63	5.23	7.60	16.88
USDOE	0.5	2.0	5.4	1.22	4.88	13.17	1.41	5.63	15.19
Zhou et al. [8]	0.245			0.60			0.69		

Ge is calculated following the Eqs. 14, 17, 22, while $G_{e\text{-}geoc}$ is calculated on the basis of the geocellular model volume (Eq. 24)

7 Discussion and Conclusion

CO_2 storage capacity estimation is still a challenge since many approaches are available. In this work a detailed review of most commonly used algorithms was carried out for oil and gas reservoirs, coal beds and saline aquifers. Several examples of capacity estimation in some part of the world show a wide range of estimates. From a statistical point of view the volumetric methods can be considered equivalent. Although major differences still exist in the basic assumptions made for closed and open systems, they cannot be statistically distinguished.

A practical example of a storage capacity estimate was performed for an Italian reservoir. The commonly established capacity methodology of CSLF and USDOE for open systems and the Zhou et al. [8] approach for closed systems were applied. The analysis indicates that the main factor influencing the effective storage capacity is the storage efficiency coefficient, since it could account for different storage features (reservoir characteristics, boundary conditions and regulatory constraints).

Results show that for the Italian selected case study the effective storage capacity ranges from 0.60 to 13.17 Gt, based on the assigned *E* values. A more reliable estimation was calculated adopting a geocellular volume extracted from 3D model of the reservoir instead of the theoretical volume. The geocellular capacity (0.69–16.88 Gt) is in the same order of magnitude of the effective one. The slight difference is explained by a larger geocellular volume that surely approximate in a more realistic way the actual volume occupied by the reservoir. It is remarked that the performed analyses represent only preliminary evaluations. Major uncertainties in the capacity estimations results are due to the lack of geological data, the assumptions and simplifications made to define the reservoir conceptual model, as well as the general inability to investigate the variability ranges of used parameters. Although uncertainties are observed, this study demonstrates that the selected structure has favorable characteristics for CO_2 geological storage.

The 2012 Italian CO_2 emissions were 386.667 equivalent million tons (Mt) [68]. The 10 % of it can be addressed to the Emilia Romagna region, which actually covers the most part of the Po Plain. At current emission rates (39.163 CO_2 equivalent Mt of 2012) [69] the selected structure could cover the whole Emilia Romagna CO_2 emissions for several decades.

Finally the obtained results encourage further detailed investigations in order to define the practical and matched storage capacities of the structure, as well as the deep characterization regarding the containment and leakage risk assessment.

Acknowledgments The authors thank the Midland Valley company for providing an educational license of the Move software, which was used for the seismic interpretations and reservoir geometries reconstructions.

Nomenclature and Greek Letters

Nomenclature

A	Geographical/Trap area of the storage site
B_f	Formation volume factor: converts oil/gas volume from standard to reservoir conditions (15 °C and 1 bar)
D	Depth to top of the aquifer
E	CO_2 storage efficiency factor
E_f	Sweep efficiency
G	Acceleration gravity
G_e	Effective storage capacity by CO_2 mass
G_{e-geoc}	Effective storage capacity by CO_2 mass computed by geocelluar volume
G_t	Theoretical storage capacity by CO_2 mass
G_{tech}	Technically accessible storage resource by CO_2 mass
H	Average gross thickness of the reservoir
H	Net thickness of the reservoir
K	Rock permeability
k_{CO_2r}	CO_2 relative permeability
L_T	Length of domain for migration model
m_{CO_2}	CO_2 solubility coefficient. Subscripts oil and water stand for CO_2 solubility in oil and water, respectively
P	Pressure. Subscripts r and s stand for reservoir and surface conditions; respectively
P_{frac}	Fracture pressure
ΔP_{max}	Maximum allowed pressure
R_f	Recovery factor
R_w	Recovery of reservoir water
S_{CO_2}	CO_2 saturation within the Volume where CO_2 plume is present
$S_{CO_{2irr}}$	Irreducible CO_2 saturation within the Volume where CO_2 plume is present
$S_{CO_{2trap}}$	Trapped CO_2 saturation after flow reversal
S_w	Water saturation
S_{wirr}	Irreducible water saturation
T	Time
T	Temperature. Subscripts r and s stand for reservoir and surface conditions; respectively

V_{geoc} Reservoir volume computed by £G geological models
V_w Water volume. Subscripts i and p stand for injected and produced; respectively
ΔV_{trap} Rock volume previously saturated with CO_2 that is invaded by water
W Width of the well array
X^{CO2} CO_2 mass fraction in formation water. Subscripts 0 and s stand for initial and CO_2 content at saturation, respectively
Z Gas compressibility. Subscripts r and s stand for reservoir and surface conditions; respectively

Greek Letters

B Bulk compressibility. Subscripts p and w stand for porous medium and water, respectively
M Dynamic viscosity. Subscripts CO_2 and w stand for initial CO_2 and water, respectively
ρ_{CO_2} Density of CO_2 at reservoir pressure and temperature conditions. Subscripts std indicate standard conditions (15 °C and 1 bar)
ρ_{coal} Bulk coal density
ρ_w Density of water at reservoir pressure and temperature conditions. Subscripts 0 and s stand for initial and CO_2 content at saturation, respectively
Φ Average porosity of reservoir, subscript e stand for effective porosity

References

1. Metz B, Davidson O, de Coninck H, Loos M, Meyer L (2005) Carbon dioxide capture and storage. In: Intergovernmental Panel on Climate Change: underground geological storage. Cambridge University Press, Cambridge, England
2. Bachu S, Bonijoly D, Bradshaw J et al (2007) CO_2 storage capacity estimation: methodology and gaps. Int J Greenhouse Gas Control 1(4):430–443
3. USDOE (U.S. Department of Energy) (2007) Carbon sequestration atlas of United States and Canada, 1st edn. USDOE (U.S. Department of Energy), Morgantown
4. USDOE (U.S. Department of Energy) (2010) Carbon sequestration atlas of the United States and Canada, 3rd edn. USDOE (U.S. Department of Energy), Morgantown
5. USDOE (U.S. Department of Energy) (2010b) Site screening, selection and characterization for storage of CO_2 in deep geologic formations. United State Department of Energy: National Energy Technology Laboratory. http://www.netl.doe.gov/technologies/carbon seq/refshelf/BPM-SiteScreening.pdf
6. USDOE (U.S. Department of Energy) (2012) Carbon sequestration atlas of the United States and Canada, 4th edn. USDOE (U.S. Department of Energy), Morgantown
7. CSLF (2008) Comparison between methodologies recommended for estimation of CO_2 storage capacity in geological media. In: Bachu S (ed) Carbon Sequestration Leadership Forum (CSLF) http://www.cslforum.org/publications/documents/PhaseIIIReportStorageCapacityEstimationTaskForce0408.pdf

8. Zhou Q, Birkholzer JT, Tsang C-F et al (2008) A method for quick assessment of CO_2 storage capacity in closed and semi-closed saline formations. Int J Greenhouse Gas Control 2 (4):626–639
9. Brennan ST, Burruss RC, Merrill MD et al (2010) A probabilistic assessment methodology for the evaluation of geologic carbon dioxide storage. In: USGS Open-File Report 2010–1127, p 31
10. Goodman A, Hakala A, Bromhal G et al (2011) U.S. DOE methodology for development of geologic storage potential for carbon dioxide at national and regional scale. Int J Greenhouse Gas Control 5(4):952–965
11. Szulczewski ML, McMinn CW, Herzog HJ et al (2012) Lifetime of carbon capture and storage as a climate-change mitigation technology. PNAS 109(14):5185–5189
12. Szulczewski ML, McMinn CW, Juanes R (2014) Theoretical analysis of how pressure buildup and CO_2 migration both constrain storage capacity in deep saline aquifers. Int J Greenhouse Gas Control 23:113–118
13. Bradshaw J, Bachu S, Bonijoly D et al (2007) CO_2 storage capacity estimation: issues and development of standards. Int J Greenhouse Gas Control 1(1):62–68
14. Blondes MS, Brennan ST, Merrill MD et al (2013) National assessment of geologic carbon dioxide storage resources– methodology implementation. In: USGS Open-File Report 2013–1055, p 26
15. Brennan ST (2014) The U. S. geological survey carbon dioxide storage efficiency value methodology: results and observations. Energy Procedia 63:5123–5129
16. Zhao X, Liao X, He L (2015) The evaluation methods for CO_2 storage in coal beds, in China. J Energy Inst. doi:10.1016/j.joei.2015.03.001
17. Gorecki CD, Sorensen JA, Bremer JM et al (2009) Development of storage coefficients for determining the effective CO_2 storage resource in deep saline formations. SPE paper 126444
18. IEA-GHG (International Energy Agency Greenhouse Gas Programme) (2009a) CO_2 storage in depleted gas fields. In: IEA Greeenhouse Gas R&D Programme (IEA-GHG), Report Number 2009/01
19. IEA-GHG (International Energy Agency Greenhouse Gas Programme) (2009b) Development of storage coefficients for CO_2 storage in deep saline formations. In: IEA Greenhouse Gas R&D Programme (IEA-GHG), Report Number 2009/13
20. Wang Y, Xu Y, Zhang K (2012) Investigation of CO_2 storage capacity in open saline aquifers with numerical models. Procedia Eng 31:886–892
21. USGS (United States Geological Survey) (2013a) National assessment of geologic carbon dioxide storage resources – results. USGS Circular 1386, 41
22. USGS (United States Geological Survey) (2013b) National assessment of geologic carbon dioxide storage resources – data. USGS Data Series 774, 13, plus appendices and data files
23. Economides MJ, Ehlig-Economides CA (2009) Sequestering carbon dioxide in a closed underground volume. Society of Petroleum Engineers, SPE 124430, pp 8
24. Thibeau S, Bachu S, Birkholzer JT et al (2014) Using pressure and volumetric approaches to estimate CO_2 storage capacity in deep saline aquifers. Energy Procedia 63:5294–5304
25. Cavanagh A, Wildgust N (2011) Pressurization and brine displacement issues for deep saline formation CO_2 storage. Energy Procedia 4:4814–4821
26. van der Meer LGH, Egberts PJP (2008) A general method for calculating subsurface storage capacity. OTC Paper 19309
27. Bachu S (2015) Review of CO_2 storage efficiency in deep saline aquifers. Int J Greenhouse Gas Control. doi:10.1016/j.ijggc.2015.01.007
28. Buttinelli M, Procesi M, Cantucci B et al (2011) The geo-database of caprock quality and deep saline aquifers distribution for geological storage of CO_2 in Italy. Energy 36:2968–2983
29. Donda F, Volpi V, Persoglia S et al (2011) CO_2 storage potential of deep saline aquifers: the case of Italy. Int J Greenhouse Gas Control 5:327–335
30. Stevens SH, Kuuskra VA, Gale J (2001) Sequestration of CO_2 in depleted oil & gas fields: global capacity, costs and barriers. In: Williams DJ, Durie RA, McMullan P, Paulson CAJ,

Smith AY (eds) Proceedings of the fifth international conference on greenhouse gas control technologies. CSIRO Publishing, Collingwood, pp 278–283
31. Doughty C, Pruess K (2004) Modeling supercritical carbon dioxide injection in heterogeneous porous media. Vadose Zone J 3(3):837–847
32. Lake LW (1989) Enhance oil recovery. Prentice Hall, Englewood Cliffs
33. Goodman A, Bromhal G, Strazisar B et al (2013) Comparison of methods for geologic storage of carbon dioxide in saline formations. Int J Greenhouse Gas Control 18:329–342
34. Bachu S, Adams JJ (2003) Sequestration of CO_2 in geological media in response to climate change: capacity of deep saline aquifers to sequester CO_2 in solution. Energy Convers Manag 44(20):3151–3175
35. Duan Z, Sun R (2003) An improved model calculating CO_2 solubility in pure water and aqueous NaCl solutions from 273 to 533 K and from 0 to 2000 bar. Chem Geol 193:257–271
36. Juanes R, Spiteri EJ, Jr O et al (2006) Impact of relative permeability hysteresis on geological CO_2 storage. Water Resour Res 42, W12418. doi:10.1029/2005WR004806
37. Kumar A, Noh MH, Sepehrnoori K et al (2005) Simulating CO_2 storage in deep saline aquifers. In: Benson SM (ed) Carbon dioxide capture for storage in deep geologic formations-results from the CO_2 capture project, vol 2, Geologic storage of carbon dioxide with monitoring and verification. Elsevier, London, pp 898–977
38. Espie T, Woods A (2014) Testing some common concepts in CO_2 storage. Energy Procedia 63:5450–5460
39. McMinn CW, Szulcczewski ML, Juanes R (2010) CO_2 migration in saline aquifers. Part 1: capillary trapping under slope and groundwater flow. J Fluid Mech 662:329–351
40. Rutqvist J, Birkholzer JT, Cappa F et al (2007) Estimating maximum sustainable injection pressure during geological sequestration of CO_2 using coupled fluid flow and geomechanical fault-slip analysis. Energy Convers Manag 48:1798–1807
41. Cappa F, Rutqvist J (2011a) Impact of CO_2 geological sequestration on the nucleation of earthquakes. Geophys Res Lett 38. doi:10.1029/2011GL048487
42. Cappa F, Rutqvist J (2011b) Modeling of coupled deformation and permeability evolution during fault reactivation induced by deep underground injection of CO_2. Int J Greenhouse Gas Control 5. doi:10.1016/j.ijggc.2010.08.005
43. Thibeau S, Mucha V (2011) Have we overestimated saline aquifer CO_2 storage capacities? Oil Gas Sci Technol Rev IFP Energies nouvelles 66(1):81–92
44. Takahashi T, Ohsumi T, Nakayama K (2009) Estimation of CO_2 aquifer storage potential in Japan. Energy Procedia 1:2631–2638
45. Tanaka S, Koide H, Sasagawa A (1995) Possibility of underground CO_2 storage in Japan. Energy Convers Manage 36:527–530
46. Solomon S, Bureau-Cauchois G, Ahmed N et al (2014) CO_2 storage capacity assessment of deep saline aquifers in the Mozambique Basin. Energy Procedia 63:5266–5283
47. Höeller S, Viebahn P (2011) Assessment of CO_2 storage capacity in geological formations of Germany and Northern Europe. Wuppertal Institute for Climate, Environment and Energy, Berlin
48. Koukousaz N, Ziogou F, Gemeni V (2009) Preliminary assessment of CO_2 geological storage opportunities in Greece. Int J Greenhouse Gas Control 3:502–513
49. Fantoni R, Franciosi R (2010) Tectono-sedimentary setting of the Po Plain and Adriatic foreland. Rendiconti Lincei 21(1):197–209
50. Consiglio Nazionale delle Ricerche (1992) Structural model of Italy and gravitymap, scale 1:500000. In: Progetto Finalizzato Geodinamica. Quad Ric Sci 114, Rome
51. Bertello F, Fantoni R, Franciosi R et al (2010) From thrust and fold belt to foreland: hydrocarbon occurrences in Italy. In: Vining BA, Pickering SC (eds) Petroleum geology: from mature basin to new frontiers. Proceedings of the 7th petroleum geology conference, Geol Soc, pp 113–126
52. Casero P (2004) Structural setting of petroleum exploration plays in Italy. Italian Geological Society special volume of the Italian Geological Society for the IGC 32 Florence-2004

53. ViDEPI Project (Visibility of petroleum exploration data in Italy). http://unmig.sviluppoeconomico.gov.it/videpi/videpi.asp
54. Montone P, Mariucci MT (2015) P-wave velocity, density, and vertical stress magnitude along the crustal Po Plain (Northern Italy) from Sonic Log Drilling Data. Pure Appl Geophys 172:1547–1561
55. Malagnini L, Herrmann RB, Munafò I et al (2012) The 2012 Ferrara seismic sequence: regional crustal structure, earthquake sources, and seismic hazard. Geophys Res Lett. doi:10.1029/2012GL053214
56. Chiarabba C, Jovane L, DiStefano R (2005) A new view of Italian seismicity using 20 years of instrumental recordings. Tectonophysics 395(3):251–268, ISO 690
57. ISIDe Working Group (INGV, 2010), Italian Seismological Instrumental and parametric database. http://iside.rm.ingv.it
58. Govoni A, Marchetti A, De Gori P et al (2014) The 2012 Emilia seismic sequence (Northern Italy): imaging the thrust fault system by accurate aftershocks location. Tectonophysics. doi:10.1016/j.tecto.2014.02.013
59. Chiarabba C, De Gori P, Improta L et al (2014) Frontal compression along the Apennines thrust system: the Emilia 2012 example from seismicity to crustal structure. J Geodyn 82:98–109
60. Vannoli P, Burrato P, Valensise G (2014) The seismotectonics of the Po Plain (northern Italy): tectonic diversity in a blind faulting domain. Pure Appl Geophys 172(5):1105–1142
61. Boccaletti M, Bonini M, Corti G et al (2004) Carta simotettonica della regione Emilia Romagna, 1:250.000 e note illustrative. SELCA Editore, Firenze
62. RER, ENI-Agip (1998) Riserve idriche sotterranee della Regione Emilia-Romagna, Publication Regione Emilia Romagna
63. Maesano FE, D'Ambrogi C, Burrato P et al (2015) Slip-rates of blind thrusts in slow deforming areas: examples from the Po Plain (Italy). Tectonophysics 643:8–25
64. Molinari I, Argnani A, Morelli A et al (2015) Development and testing of a 3D seismic velocity model of the Po Plain Sedimentary Basin, Italy. Bull Seismol Soc Am. doi:10.1785/0120140204
65. Buttinelli M, Procesi M, Cantucci B et al (2013) An overview on the outermost buried fronts of northern Apennines: hints, insights, limits and constraints for fluids geological storage. In: Proceedings of Geoitalia 2013 congress – IX edizione del Forum Italiano di Scienze della Terra "Le Geoscienze per la Società" – Pisa, 15–18 Settembre 2013
66. Duan Z, Møller N, Weare JH (1992) An equation of state for the CH_4-CO_2-H_2O system – II. Mixtures from 50 to 1000 °C and 0 to 1000 bar. Geochim Cosmochim Acta 56:2619–2631
67. Baù D, Ferronato M, Gambolati G et al (2002) Basin-scale compressibility of the northern Adriatic by the radioactive marker technique. Geotechnique 52:605–616
68. De Lauretis R, Romano D, Vitullo M et al (2014) National greenhouse gas inventory system in Italy- year 2014. ISPRA- Institute for Environmental Protection and Research Environment Department, Rome
69. INEMAR – Arpa Emilia-Romagna (2013) INEMAR, Inventario Emissioni in Atmosfera: emissioni in Regione Emilia-Romagna nell´anno 2010 – Arpa Emilia-Romagna

Part III
CO_2 Storage in Deep Saline Aquifers

Trapping Mechanism of CO_2 Storage in Deep Saline Aquifers: Brief Review

Richa Shukla Potdar and V. Vishal

Abstract Global CO_2 storage capacity of saline aquifers is much greater than other alternative reservoirs, but suitability of a potential site must be investigated carefully. Saline aquifers that have sandstone as reservoir rock at a depth greater than 800 m below the ground surface are ideal reservoirs for injection and storage of CO_2, provided a good cap-rock exists to act as the seal. The geochemical maturity and geomechanical characteristics of the reservoirs are of prime importance. Highly mineralized brine present in a typical saline aquifer has been found to enhance the process of mineral trapping of CO_2 through rock-brine-CO_2 interaction. The challenge though is that CO_2 thus stored, should not escape or leak from the reservoir under any circumstance. In this chapter, a comprehensive study of various CO_2 trapping mechanisms in a saline aquifer is presented. A brief review of previous works is also presented to highlight the immense storage potential of the suitable aquifers. Injected CO_2 in such a reservoir may be stored as structural/stratigraphic trapping, diffusion/solubility trapping, residual trapping, and mineral trapping/ mineralization.

1 Introduction

Geo-sequestration of carbon dioxide is argued to be the strongest option available to reduce the greenhouse effect and maintain safe levels of CO_2 in the atmosphere for a sustainable future [1–7]. Saline aquifers are the most abundant fluid reservoirs with immense capacity to store CO_2 and contain it safely for geologically significant periods of time. Sincere initiative from the commercial and scientific entities is hence required to enable the development of new and large-scale projects that could sequester greater volumes of anthropogenic CO_2 safely, efficiently and economically. Five scenarios of possible traps for geological sequestration of

R. Shukla Potdar (✉)
GHD Consultants, 180 Lonsdale Street, Melbourne, VIC, Australia 3000
e-mail: Richa.Potdar@ghd.com

V. Vishal
Department of Earth Sciences, Indian Institute of Technology Bombay, Mumbai, India
e-mail: drvikramvishal@gmail.com

V. Vishal, T.N. Singh (eds.), *Geologic Carbon Sequestration*,
DOI 10.1007/978-3-319-27019-7_3

CO_2 exist in suitable geological formations i.e. the abandoned hydrocarbon reservoirs, brown oil field, saline reservoir, non-economic coal seams and shale formations, and basalt formations have been discussed by Dimri [8].

Saline formations provide excellent options for carbon sequestration as they are found in abundance all over the world and often in close vicinity to CO_2 point sources. The concept is to inject captured and compressed CO_2 into deep reservoir rocks which are capped by very low permeability seals such as layers of mudstones or shales. The presence of fluid traps or sealing faults can boost the efficiency of the reservoirs by trapping the CO_2 structurally or stratigraphically, but even in their absence it is suggested by several studies that the CO_2 could be simply stored in the pore spaces of reservoir rocks (usually limestone or sandstone) [1, 9–11]. A large amount of the CO_2 can be stored in the free state, some of the CO_2 may remain dissolved in the formation water and some is expected to react with the rock minerals in the reservoir. Finally the CO_2 is anticipated to stay locked and subsequently ultimately mitigate to form other stable forms of carbon over geologically large time scales. Many studies have been conducted in the field [10, 12–14].

Reservoir rocks require high permeability and strength to allow safe dissipation of induced stresses and fluid pressures from CO_2 injection. Sandstones fit this criterion perfectly as they generally possess high porosity and permeability, and natural sandstone formations are abundantly available in nature at desirable depths containing highly saline brine which is geochemically favourable for CO_2 sequestration [12, 13, 15–17].

Several sequestration projects are already functioning today, which have injected millions of tonnes of CO_2 into deep saline aquifers at different locations around the globe. The Sleipner Project in the Utsira formation in the North Sea was started in October 1996 and has already injected more than 8 million tonnes of CO_2 successfully [18]. Another such project in South Ontario, investigates two reservoirs with an approximate storage capacity of about 700 million tonnes of CO_2, which will otherwise be emitted from a nearby coal-fired power plant in the next 10–17 years. The main reservoir is the saline aquifer of Mt. Simon sandstone in the Michigan and Appalachian basins. The available caprock, which is about 95 m in total depth, is a combination of two formations, i.e. Shadow Lake formation and Eau Claire formation. Certainly, much remains to be studied about the phenomena involved in the process of final mitigation of the CO_2 injected into saline aquifers and the effects that this CO_2 may have on the integrity and efficiency of reservoir and cap-rocks.

2 Storage Capacity

The total storage capacity estimate of individual reservoirs is questionable even when using well-established reservoir simulators with well-known parameters. The storage efficiency of a CO_2 reservoir system depends on the fraction of the reservoir

available to be filled with CO_2 and it varies considerably for different reservoirs [19, 22]. The major global estimates of storage capacity are based on assumptions about the storage concept and the volumes of storage space accessible for these storage concepts. This means that the major storage capacity estimates in research studies by Bachu et al. [12] and Kide et al. [20] may be highly erroneous. Several reservoir models that have been developed in the past which suggest that if a realistic injection rate is assumed, only a small proportion of the pore space in a structure can be occupied by injected CO_2 before the gravitational effect prevails and viscous fingering begins and the CO_2 starts to escape from the trap [19]. The upper estimates consider that a substantial fraction of the pore volume of saline aquifers could be used for CO_2 storage, whereas the lower estimates consider that only a small fraction of the pore space which makes up the conventional fluid traps present in saline aquifers could be used for CO_2 storage [21]. As illustrated in Table 1, global saline aquifers have the capacity to contain from 20 to 500 % of the total CO_2 estimated to be emitted in the next 50 years.

Koide et al. [17] used an aerial method to estimate the global underground CO_2 storage capacity assuming 1 % of the onshore sedimentary basins of the world to be useful for CO_2 storage and considering the offshore basins would increase the storage capacity significantly. The estimate of global storage capacity of saline aquifers is more than about 367 Gt CO_2, when only the fluid traps in the aquifers are considered ignoring the possible available proportions of the pore space of the aquifer. Bachu et al. [12] used both the fluid traps as well as the pore spaces of aquifers and indicated that the total underground storage capacity of the Alberta Basin, Canada, is 20 Gt CO_2 [12]. This made up about 16 % of the underground CO_2 storage capacity estimated by [17].

The difference between the total capacity for CO_2 at saturation and the total inorganic carbon currently in solution in that aquifer is known as the ultimate CO_2 sequestration capacity in solution (UCSCS) of an aquifer. It depends on the pressure, temperature and salinity of the formation water. Bachu and Adams [10] state that the UCSCS of an aquifer is calculated by considering the effect of dissolved CO_2 on the formation water density, the aquifer thickness and porosity to account for the volume of water in the aquifer pore space and for the mass of CO_2

Table 1 Storage capacity for several geological storage options

Reservoir type	Lower estimate of storage capacity (Gt CO_2)	Upper estimate of storage capacity (Gt CO_2)	Upper estimate as a proportion of total emissions in next 50 years (%)
Depleted oil and gas fields	675	900	45
Deep saline reservoirs	1000	400–10,000	20–500
Unmineable coal seams	3–15	200	>1

dissolved in the water currently and at saturation. They conducted experimental and geochemical modelling of the Viking aquifer in the Alberta basin in western Canada and calculated its capacity to be 100 Gt. The Southeast Regional Carbon Sequestration Partnership (SECARB), deals with multiple regional-scale geologic storage opportunities, including deep saline formations, depleted oil and gas fields, organic-rich shale formations. Petrusak et al. [22] present an updated assessment of the CO_2 storage capacity for the SECARB region and state that these regions offer sufficient capacity to sequester the region's major point source CO_2 emissions for decades.

Gunter et al. [13] studied the relationship between CO_2 storage capacity and the quality of pore fluid available in the saline aquifers in terms of mineralogical trapping. They presented modelling results that indicated that brackish or relatively dilute formation waters (i.e. total dissolved solids between 1000 and 10,000 mg/l) in saline aquifers can take up more CO_2 than brine formation waters (i.e. total dissolved solids greater than 100,000 mg/l). They state that although the geochemical trapping of CO_2 in the rocks plays an important role in CO_2 trapping, it would not cause any dramatic increase in the storage capacity to significant levels. They concluded that brackish or dilute formation waters are favoured for CO_2 capture, since the maximum solubility of CO_2 is limited in brines due to the salting-out effect at higher ionic strengths. Furthermore, siliciclastic aquifers (rich in magnesium and calcium with feldspars and clay) that contain brackish formations are the most suitable CO_2 sequestration reservoirs as they can trap the maximum amount of CO_2 [13]. Labus and Bujok [23] conducted hydrochemical modeling and experimental tests of rock-water-gas interactions to assess the suitability of saline aquifers within the Upper Silesian Coal Basin (USCB), as potential greenhouse gas repositories from the territory of the USCB. Evaluation of mineral-trapping mechanisms and assessment of storage capacity of the aquifers is based on two stages of modeling enabled prediction of the immediate changes in the aquifer and insulating rocks impacted by the beginning of CO_2 injection, and the assessment of long-term effects of sequestration [23]. In the analyzed sandstone aquifers the minerals able to trap CO_2 are dawsonite and dolomite, while siderite or calcite is able to degrade. The phases capable of mineral CO_2 trapping in the cap rocks are: dawsonite, dolomite, and siderite. Mineral-trapping capacity, for the sandstone aquifers is relatively low: 1.2–1.9 kg CO_2 /m^3, with the exception of the Upper Silesian Sandstone Series – over 6.6 kg CO_2 /m^3. The solubility trapping capacity does not exceed 4.07 kg CO_2 /m^3.

3 CO_2 Trapping Mechanisms

Several mechanisms lead to the final disposition of CO_2 in a reservoir. The mechanisms include structural or stratigraphic trapping, residual trapping, solubility trapping and mineral trapping. These mechanisms come into effect at different time periods in the total lifespan of the CO_2 mitigation process. For

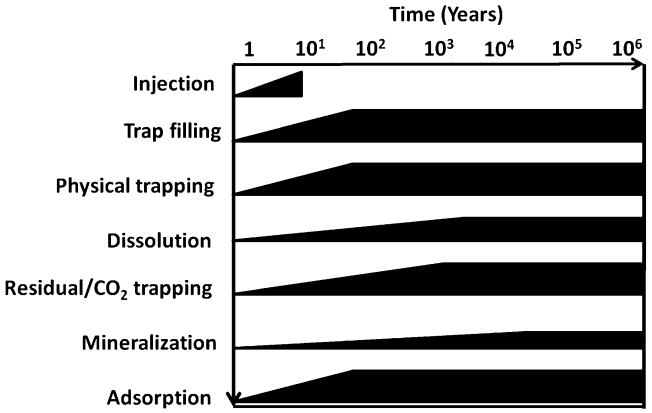

Fig. 1 Life cycle of CO_2 mitigation evolving over time in a saline aquifer through different trapping mechanisms

example, structural trapping is responsible for the initial containment and safe storage of the CO_2. Residual and solubility trapping play an important role in the distribution and migration of the CO_2 plume and assist in making the geochemical trapping faster as the CO_2 comes in contact with more and more rock minerals as it spreads outwards in the reservoir layer. When geochemical trapping or mineralization begins, the CO_2 will no longer be able to escape the reservoir in any form and the CO_2 geological storage project can be deemed secure as the risks of leakage are minimised. Figure 1 illustrates the contribution and duration of these sequestration mechanisms towards the ultimate fixation of the injected CO_2 over thousands of years. These trapping mechanisms are explained in detail in the following sections.

3.1 Structural/Stratigraphic Trapping

When the injected CO_2 migrates upwards towards the caprock under buoyancy, most CO_2 eventually accumulates in the topographical highs or spaces. This purely physical entrapment of CO_2 in the reservoir due to its intactness and containment is known as structural or stratigraphic trapping [24]. Structural trapping forms the largest possible means of CO_2 trapping and without a structural trap the injected CO_2 might eventually migrate from the injection site to other subterranean sites where storage is not desirable or even to where it can escape to the atmosphere. However, the latest studies suggest that the need of structural traps can be reduced if the injection of CO_2 is done at a good distance from the aquifer or reservoir boundaries.

3.2 *Diffusion/Solubility Trapping*

Solubility trapping involves the dissolution of CO_2 into a fluid phase, including both aqueous brines and oil. Hildenbrand et al. [25] conducted experiments on argillaceous rocks to monitor the migration of CO_2 and the diffusion process. It was established that the migration of gas through lithologies with low permeabilities (10^{-21} m^2) can occur by pressure-driven volume flow and by molecular diffusion. In initially water-saturated rocks, the former process involves capillary pressure phenomena (gas breakthrough) and two-phase flow. The gas flux that results from this gas breakthrough is monitored as a function of time and pressure gradient by means of pressure changes in a closed downstream reservoir of known volume. After breakthrough, the effective permeability to the gas phase (k_{eff}) decreases with decreasing differential (capillary) pressure due to re-imbibition of water into the interconnected gas-conducting pore system (Fig. 2).

Nominal effective permeability coefficients in the range of 10–24 m appear to represent a lower limit for pressure-driven volume flow (Darcy flow) under experimental conditions. Below these values, it is no longer possible to differentiate between the Darcy flow and molecular diffusion of the gas. Diffusion is not considered an important process for CO_2 leakage through caprocks, even on geological time scales.

van der Meer et al. [26] also discuss the effects of solubility on the sequestration of CO_2. Saripalli et al. [27] built a model of a sequestration reservoir using

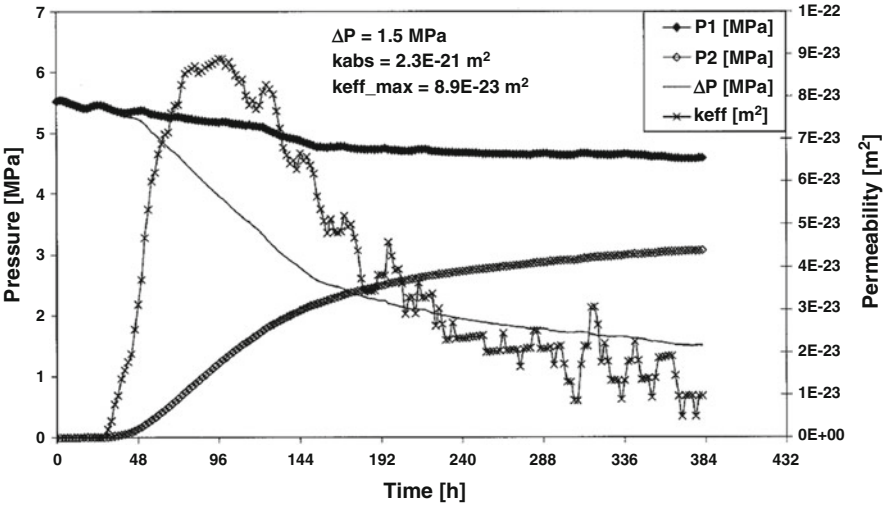

Fig. 2 Experimental capillary breakthrough curves (upstream pressure, P1, and downstream pressure, P2) for CO_2 and effective permeability vs. experimental time [25]

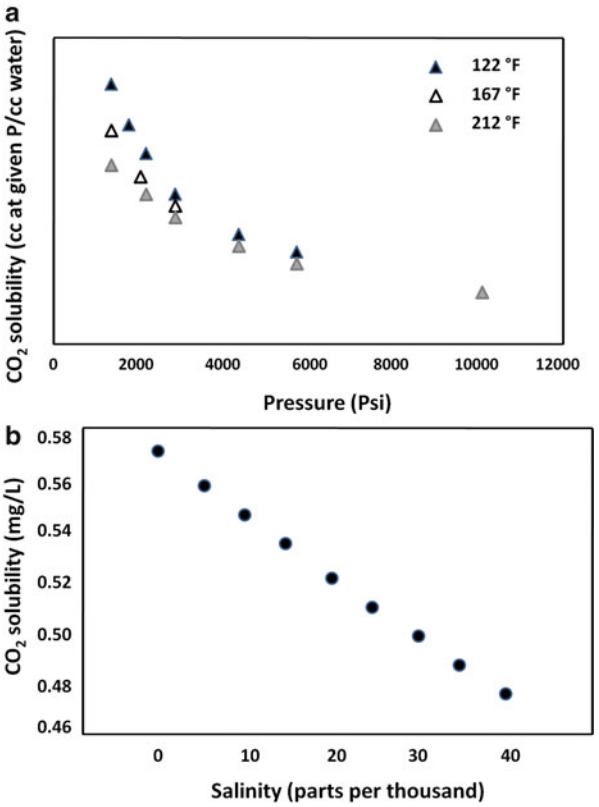

Fig. 3 Effect of increasing (**a**) injection pressure and (**b**) pore water salinity on CO_2 solubility [27]

TOUGHREACT and found that solubility is decreased with increasing injection pressure and increasing salinity of the pore fluid (<10 % reduction in solubility as salinity increases from 0 to 25 parts per thousand) (Fig. 3a, b).

3.3 Residual Trapping

Residual trapping is the term given to the trapping of CO_2 in the capillary pores of the reservoir rock after a particular saturation level under the influence of the capillary forces. After injection, the gas bubble slowly moves upwards and while trying to escape, the bubble loses its CO_2 concentration due to the other carbon mitigation mechanisms like dissolution and rock-mineral interaction, which further enhance the process of residual trapping. This trail of the CO_2 plume that is left behind in the rock pores as the major bubble of CO_2 moves upwards towards the

caprock seal is highly influenced by the relative permeability hysteresis of the rock matrix and the fluid phases. This physical trapping of the CO_2 bubbles is the safest and quickest CO_2 mitigating mechanism.

3.4 Mineral Trapping/Mineralization

The CO_2 trapping capacity varies considerably with reservoir rock type and depends significantly on mineral composition of the rock as well as of the pore fluid. Mineral trapping is a long-term storage mechanism and it involves the integration of CO_2 into a solid phase, for example, the precipitation of carbonate minerals. This process traps carbon in the form of solid carbonate salts. This process occurs slowly in nature and is responsible for the deposition and accumulation of limestone (calcium carbonate) over geologic time. Numerous uncertainties and scientific gaps still exist in quantifying CO_2 -brine-mineral interactions at reservoir conditions, because supercritical CO_2 is buoyant, displaces huge volumes of formation water and becomes reactive to minerals, and well cements and pipes when dissolved in the formation water. Carbonic acid in groundwater slowly reacts with complex silicates to dissolve calcium, magnesium, alkalis and silica and leave a residue of clay minerals. The dissolved calcium and magnesium react with bicarbonate to precipitate calcium and magnesium carbonates, a process that organisms use to make shells. When the organisms die, their shells are deposited as sediment and eventually turn into limestone. Limestones have accumulated over billions of years of geologic time and contain much of the Earth's carbon. Xu et al. [28] and Bachu et al. [12] have also studied the process and importance of mineral trapping.

The chemical reactions that are most probable to occur between the reservoir rock, the brine and CO_2 are explained by Ortoleva et al. [29]. The time frame for CO_2 sequestration is a function of reaction kinetics. They explain that the process begins with the dissolution of CO_2 in the brine/pore water to produce weak carbonic acid and bicarbonate ions which increase the acidity of the pore solution (Eqs. 1a, 1b). The next stage is the dissolution of many primary minerals to the reservoir rock which results in progressive dissolution of the cations with the bicarbonate ions (Eq. 2). These dissolved bicarbonates then interact with the divalent cations precipitating carbonate minerals (Eqs. 3a, 3b, 3c). Along with mineral precipitation, alkaline aluminosilicate minerals also dissolve under the effect of CO_2, leading to increase in soluble carbonates and bicarbonates in the solution, which means enhancement of the solubility trapping process.

$$CO_2 + H_2O \rightarrow H_2CO_3 \tag{1a}$$

$$H_2CO_3 \rightarrow H^+ + HCO_3^- \tag{1b}$$

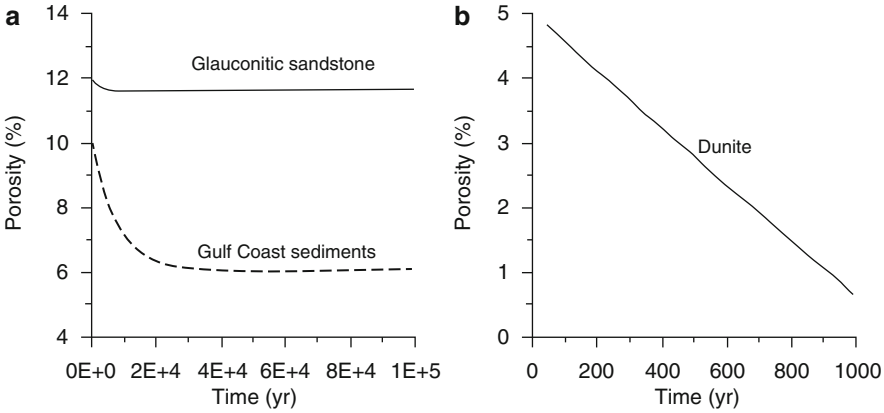

Fig. 4 Porosity evolution of three different types of rocks with CO_2 mineralisation at 260 bar over time [28]

$$Ca^{2+} + HCO_3^- \rightarrow CaHCO_3^+ \tag{2}$$

$$HCO_3^- + Ca^{2+} \rightarrow CaCO_3 + H^+ \tag{3a}$$

$$HCO_3^- + Mg^{2+} \rightarrow MgCO_3 + H^+ \tag{3b}$$

$$HCO_3^- + Fe^{2+} \rightarrow FeCO_3 + H^+ \tag{3c}$$

Carbonic acid formed in the above processes can also attack the silicate minerals as shown in the reaction below:

$$2CO_2 + H_2O + CaSiO_3 \rightarrow Ca^{++} + 2HCO_3 + SiO_2 \tag{3d}$$

Xu at al. [28] showed that the reservoir rock undergoes physical alteration after CO_2 injection which results in decrease in porosity. They suggest that this may be because the CO_2 mass is added to the solid matrix due to mineral trapping (Fig. 4). Kaszuba et al. [30] also conducted experimental studies on geochemical reactions relating to supercritical CO_2 injection into saline aquifers at high pressure and temperature conditions. Their results present details of reaction kinetics in a brine-aquitard reservoir system as they report abundant magnesite precipitation and significant reactions of the silicate minerals. Cole et al. [31] conducted detailed chemical and isotopic analyses of water, associated gases, and added tracers obtained from Frio I and II field tests, near Houston, Texas. The study tracked the successful injection and flow of CO_2 in the reservoir sandstone alongside detecting that some CO_2 leaked into the overlying layers. It also showed mobilization of metals (Fe, Mn, Pb, etc) and toxic organic compounds following CO_2 injection and major changes in chemical and isotopic compositions of formation water, including a dramatic drop in calculated brine pH, from 6.3 to 3.0.

4 Conclusion

The geomechanics of reservoirs and saline aquifers is a vast area of research and it has been studied thoroughly in the past few decades. CCS concept is attracting great interest, and is being verified by scientists around the world. The basic knowledge of rock mechanics and reservoir engineering is readily applied to CCS projects but there are still some unforeseen scenarios that can emerge in the long term storage of CO_2 underground. As discussed earlier, the safety and feasibility of any sequestration project largely depend on the efficiency and integrity of the caprock and the sustainability of the seals and pre-existing faults. Triaxial and uniaxial compressive testing of rock cores from reservoirs and caprocks provides a substantial understanding of the mechanisms of CO_2 flow and behaviour through the rocks. The application of multi-phase hydro-thermo-geo-mechanical data in numerical modelling of CO_2 injection, dispersion and long term storage will assist in measuring, monitoring and estimating rockmass integrity and help minimise the risk of possible CO_2 leakage.

A review of past literature shows that vast amount of research that has been done in the fields supporting carbon geo-sequestration and geomechanics. However, it also suggests that there is still a need to further explore some of the more complex phenomena that occur in real-life CCS projects. These processes include the CO_2-brine-rock mineral interactions between different types of rocks and clays and the different salinity brines that occur in natural saline aquifer systems. The possible leakage paths of the stored CO_2 must also be thoroughly studied in order to establish the success of CCS as the ultimate CO_2 mitigation option.

The possible hazards from natural phenomena like earthquakes and other tectonic activities must also be investigated in detail when planning a CCS project. Supercritical carbon dioxide is a highly reactive and corrosive fluid and it is likely to interact with the geochemical and geophysical environment in the caprock formation after sequestration. A number of studies have been conducted and several carbon sequestration pilot projects are still taking place, but the mechanisms of carbon dioxide trapping and mitigation taking place in situ are not yet fully understood.

References

1. Houghton JT, Ding Y, Griggs DJ, Noguer M, van der Linden PJ, Dai X, Maskell K, Johnson CA (2001) IPCC 2001: the scientific basis. Contribution of working group I in the third assessment report of Intergovernmental Panel on Climate Change, Cambridge University Press, Accessed online (on 12/01/2016) at: http://www.grida.no/publications/other/ipcc_tar/?src=/climate/ipcc_tar/
2. Shukla R, Ranjith PG, Haque A, Choi X (2010) A review of studies on CO_2 sequestration and caprock integrity. Fuel 98(10):2651–2664
3. Shukla R, Ranjith PG, Choi SK, Haque A (2010) Study of caprock integrity in geosequestration of carbon dioxide. Int J Geomechanics 11(4):294–301

4. Shukla R, Ranjith PG, Choi SK, Haque A (2012) A novel testing apparatus for hydromechanical investigation of rocks: geo-sequestration of carbon dioxide. Rock Mech Rock Eng 45 (6):1073–1085
5. Vishal V, Ranjith PG, Singh TN (2015) An experimental investigation on behaviour of coal under fluid saturation, using acoustic emission. J Nat Gas Sci Eng 22:428–436
6. Vishal V, Singh TN (2015) A laboratory investigation of permeability of coal to supercritical CO_2. Geotech Geol Eng 33(4):1009–1016
7. Vishal V, Singh TN, Ranjith PG (2015) Influence of sorption time in CO_2-ECBM process in Indian coals using coupled numerical simulation. Fuel 139:51–58
8. Dimri V P (2008) (National Geophysical Research Institute, India) Reducing global warming by CO_2 injection in suitable geological formations. Source: International Geological Congress, Abstracts, Congres Geologique International, Resumes, 33, 33rd
9. Bachu S (2000) Sequestration of CO_2 in geological media: criteria and approach for site selection in response to climate change. Energy Convers Manag 41:953–970
10. Bachu S, Adams JJ (2003) Sequestration of CO_2 in geological media in response to climate change: capacity of deep saline aquifers to sequester CO_2 in solution. Energy Convers Manag 44:3151–3175
11. Shukla R, Ranjith PG, Choi SK, Haque A, Yellishetty M, Hong L (2013) Mechanical behaviour of reservoir rock under brine saturation. Rock Mech Rock Eng 46(1):83–93
12. Bachu S, Gunter WD, Perkins EH (1994) Aquifer disposal of CO_2: hydrodynamic and mineral trapping. Energy Convers Manag 35(4):269–279
13. Gunter WD, Perking HP, McCann TJ (1992) Aquifer disposal of CO_2-rich gases: reaction design for added capacity. Energy Conserv Manag 34(9–1):941–948
14. Kumar A, Noh M, Pope GA, Sepehrnoori K, Bryant S, Lake LW (2004) Reservoir simulation of CO_2 storage in deep saline aquifers. Soc Pet Eng J 10(3):336–348
15. Rosenbauer RJ, Koksalan T, Palandri JL (2005) Experimental investigation of CO_2-brine–rock interactions at elevated temperature and pressure: implications for CO_2 sequestration in deep-saline aquifers. Fuel Process Technol 86:1581–1597
16. Rutqvist J, Tsang CF (2002) A study of caprock hydromechanical changes associated with CO_2-injection into a brine formation. Environ Geol 42:296–305
17. Koide H, Tazaki Y, Noguchi Y, Nakayama S, Iijima M, Ito K, Shindo Y (1992) Subterranean containment and long-term storage of carbon dioxide in unused aquifers and in depleted natural gas reservoirs. Energy Convers Manag 33(5–80):619–626
18. Torp TA, Gale J (2004) Demonstrating storage of CO_2 in geological reservoirs: the Sleipner and SACS projects. Energy 29:1361–1369
19. van der Meer LGH (1995) The CO_2 storage efficiency of aquifers. Energy Conserv Manag 36 (6–9):513–518
20. Koide HG, Tazaki Y, Noguchi Y, Iijirna M, Ito K, Shindo Y (1993) Carbon dioxide injection into useless aquifers and recovery of natural gas dissolved in fossil water. Energy Convers Manag 34(9–11):921–924
21. Holloway S (1997) An overview of the underground disposal of carbon dioxide. Energy Convers Manag 38(1):S193–S198
22. Petrusak R, Riestenberg D, Goad P, Schepers K, Pashin J, Esposito R, Trautz R (2009) World class CO_2 sequestration potential in saline formations, oil and gas fields, coal, and shale: the US southeast regional carbon sequestration partnership has it all. Source: SPE International Conference on CO_2 Capture, Storage, and Utilization, pp 136–153
23. Labus K, Bujok P (2011) CO_2 mineral sequestration mechanisms and capacity of saline aquifers of the Upper Silesian Coal Basin (Central Europe) – modeling and experimental verification. Energy 36(8):4974–4982
24. Johnson JW, Nitao JJ, Steefel CI, Knauss KG (2001) Reactive transport modelling of geologic CO_2 sequestration in saline aquifers: the influence of intra-aquifer shales and the relative effectiveness of structural, solubility, and mineral trapping during prograde and retrograde sequestration. In: Proceedings of the 1st national conference on Carbon sequestration, Washington, DC, pp 60

25. Hildenbrand SS, Krooss BM, Littke R (2004) Gas breakthrough experiments on pelitic rocks: comparative study with N_2, CO_2 and CH_4. Geofluids 4:61–80
26. van der Meer LGH, Cor H, Bogdan O (2009) The fluid flow consequences of CO_2 migration from 1000 to 600 metres upon passing the critical conditions of CO_2. Energy Procedia 1:3213–3220
27. Saripalli P, McGrail P (2002) Semi-analytical approaches to modeling deep well injection of CO_2 for geological sequestration. Energy Convers Manag 43(2):185–198
28. Xu T, Apps JA, Pruess K (2004) Numerical simulation of CO_2 disposal by mineral trapping in deep aquifers. Appl Geochem 19(6):917–936
29. Ortoleva PJ, Dove P, Richter F (1998) Geochemical perspectives on CO_2 sequestration. In: US Department of Energy Workshop on Terrestrial sequestration of CO_2-an assessment of research needs. Gaithersburg
30. Kaszuba JP, Janecky DR, Marjorie GS (2003) Carbon dioxide reaction processes in a model brine aquifer at 200 °C and 200 bars: implications for geologic sequestration of carbon. Appl Geochem 18(7):1065–1080
31. Cole D R, Kharaka Y, Bullen TD, Hovorka SD (2010) Environmental impacts of CO_2 sequestration in sedimentary basins. Source: Abstracts: Annual Meeting – American Association of Petroleum Geologists

Monitoring of CO_2 Plume Migration in Deep Saline Formations with Kinetic Interface Sensitive Tracers *(A Numerical Modelling Study for the Laboratory)*

Alexandru Bogdan Tatomir, Apoorv Jyoti, and Martin Sauter

Abstract Monitoring CO_2 plume migration in deep saline aquifers is essential for improving the design and operation of the storage. Therefore, the development of new efficient monitoring techniques is an on-going area of research. Tracer techniques have been extensively used to study the movement of gas and liquids in porous media systems. Their main advantage is that they can provide direct information about the hydraulic, transport and reactive processes and parameters of the reservoir. Kinetic interface sensitive (KIS) tracers represent a novel class of reactive tracers for quantifying the interfacial area between CO_2 and brine and its development with time. The theoretical development of KIS tracers is described, including the conceptual and mathematical models. Through numerical modelling, a sensitivity analysis with regard to the key flow and transport parameters of CO_2 storage reservoir is performed.

1 Introduction

This chapter describes the theoretical development of a novel tracer-based monitoring technique for quantifying the supercritical CO_2 plume migration in deep saline formations. It is a well known fact that the technological development of improved CO_2 monitoring techniques is essential for the widespread commercial deployment of the CCS, and for countering the criticism that the technology is not yet proven.

First, the essential parameters for CO_2 storage in deep saline formations are introduced, together with the current state of the art in the monitoring techniques. Next, the conceptual and mathematical models of the kinetic interface sensitive tracers are described. Through numerical modelling, a sensitivity analysis with regard to the key flow and transport parameters of a CO_2 storage reservoir is performed.

A.B. Tatomir (✉) • A. Jyoti • M. Sauter
Department of Applied Geology, Geoscience Center of the University of Göttingen, Goldschmidtstr. 3, 37077 Göttingen, Germany
e-mail: alexandru.tatomir@geo.uni-goettingen.de

V. Vishal, T.N. Singh (eds.), *Geologic Carbon Sequestration*,
DOI 10.1007/978-3-319-27019-7_4

1.1 Key Parameters of CO_2 Storage in Deep Saline Formations

Geological CO_2 storage (GCS) in deep saline formations is technically feasible and it is considered by many, to be the most viable option to reduce the greenhouse gas emissions [5, 11, 12, 20, 35, 37]. Among the underground geological formations for CO_2 storage (e.g. oil/gas fields, coal seams, salt caverns, etc.), deep saline formations have the largest volumetric potential with an estimated storage capacity of at least 1000 Gt CO_2, with some studies suggesting even one order of magnitude higher than this [20]. Sedimentary rocks are usually the building blocks of the deep saline aquifers, which commonly occur at depths greater than fresh-water aquifers. Due to the high salt content and due to laying at great depths, the brine (saline water) cannot be used commercially or technologically for surface applications. However, in most cases, the regulators allow water to be drawn from, and fluids to be injected into deep saline formations.

During the last 15 years, carbon dioxide has come to be regarded as a waste product, and therefore, similarly to how waste products are dealt with, CO_2 storage appears to be a more viable alternative than sequestration. The basic criteria for choosing long-term CO_2 storage site are:

- *Size*: Spatial extent of the reservoir must be large enough to store large amounts of carbon dioxide
- *Porosity* and *Permeability*: Large porosity ensures the volume for storage while a large permeability correlates with a good injectivity. As carbon dioxide is injected into the reservoir it begins to displace the brine present in its pores. If the permeability is too low or there are certain barriers in the system to the fluid flow, this would lead to an increase in the pressure at the injection point and thus limit the amount of carbon dioxide that could be stored inside that reservoir or endanger the integrity of the cap rock.
- *Depth*: Most commonly depths below 800 m ensure that CO_2 exists in supercritical form (critical point without impurities being 7.38 MPa and 31.1 °C) which occupies approximately two orders of magnitude less pore volume than in gaseous form. This in turn makes the storage economical.
- *Overlying cap rock* must be impermeable to the passage of CO_2. The cap rock's low porosity, low permeability and high entry pressure stops the buoyant supercritical CO_2 from leaking. The integrity of the cap rock is highly dependent on the ability of the reservoir to dissipate the additional pressure (over pressure) created by injection. An increase in the injection rate leads to pressure increase which should be kept below the cap rock fracture pressure.

Besides the above mentioned criteria, the geological (e.g., fault zone presence), petrophysical and chemical heterogeneities (e.g., distributed relative mineral surface area) influence the migration of CO_2 plume and determine the efficiency of the trapping mechanisms (Fig. 1; [20]). One known challenge for the reservoir engineers is the existence of heterogeneities at different scales (i.e. pore scale up to field, and regional scale) which can lead to unexpected reactive transport behaviour.

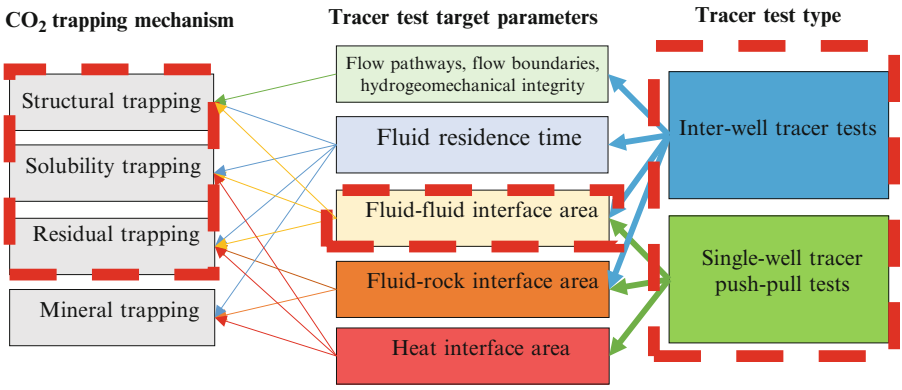

Fig. 1 Schematic overview of tracer test types, their determined parameters and parameter relevance to the CO_2 trapping mechanisms. For this study (*dashed red line*) we address to fluid-fluid interface sensitive tracers, conducted both in single- and inter-well configurations which are relevant for structural, solubility and residual trapping (After Tatomir et al. [50])

1.2 CO_2 Plume Monitoring

Monitoring in the context of GCS has a variety of purposes (e.g. risk management, safety, performance assessment, closure and post-closure control; [20, 40]). One of the most important purposes is the CO_2 plume monitoring. The main objectives of plume monitoring are to improve the understanding of the plume movement in the subsurface, to prevent leakage, and to measure the pressure build-up, which relates to reservoir and seal integrity. In general, the monitoring costs are small compared to the storage costs. Nevertheless, they depend strongly on the regulatory requirements [19, 20].

The monitoring techniques for supercritical carbon dioxide ($scCO_2$) injected in deep saline formations can be classified in two broad categories: direct and indirect. The direct monitoring techniques include sampling methods, chemical sensors, monitoring wells which are rather limited in availability [32]. A much broader applicability is offered by the indirect techniques, e.g., seismic, electromagnetic. The main functioning concept behind most of the geophysical monitoring techniques relies on the contrast in fluid properties. Since the compressibility and the density of the supercritical CO_2 is different from the saline water present in the aquifer, the pore space in the aquifer will be filled with less compressible and less dense fluid after the substitution of the residual saline water by injected CO_2.

Table 1 lists the most commonly used geophysical methods for the monitoring of the injected CO_2 [23]. An overview of different geophysical techniques can be found in Sayers and Wilson [43]. Also, a recent review of small-scale GCS projects worldwide was done by Cook et al. [12]. One of the main focuses of investigation in these small-scale GCS projects is the development of efficient CO_2 injection strategies and reliable, real-time monitoring techniques. Among the most recent, state-of-the-art plume monitoring methods is the satellite interferometry, which measures the land surface deformation [25, 36].

The main focus of this research is on the tracer tests that are applicable both in the pre- CO_2 injection stage for reservoir characterization and also in the post- CO_2

Table 1 The Common geophysical methods for plume monitoring

Measurement method	Physical parameter	Literature
Seismic	Seismic velocities, density	Arts [3]
Geo electrical	Electrical resistivity	Kiessling et al. [26]
Electromagnetic	Electrical resistivity	[10, 47]
Gravity	Density	Alnes et al. [1]
Borehole	Pressure, temperature, salinity	–

injection stage as a direct monitoring technique for the CO_2 plume development, the determination of residual CO_2 saturation and the displacement of brine.

1.3 Tracer Techniques for CO_2 Plume Monitoring

Chemical tracers have been extensively used to study the movement of gas and liquids in porous media systems. Their main advantage is that they can provide direct information about the hydraulic, transport and reactive processes and parameters of the reservoir. Within the context of CCS projects, tracer methods can provide an understanding over the subsurface movement of the CO_2 plume [9, 15, 53, 54], characterize geochemical processes [4, 30], assess the residual trapping capacity [29, 33, 39, 58], determine the containment and leakage rates for monitoring and verification programs [46, 56, 57], or provide information about individual trapping mechanisms.

The tracer tests (Fig. 1) can be conducted in a single-well push-pull configurations, (e.g. [39, 52]), in multi-well configurations and sometimes in combinations of the two (e.g., [8]).

Until now, chemical tracers which can effectively determine the brine-sc CO_2 interfacial area and its time-dependent development are not available in practice. Current studies are mostly limited to equilibrium tracers (Table 2). Volume sensitive partitioning tracers [32, 33] are used to quantify the amount or the saturation of the immiscible phases.

Anionic surfactants, such as linear alkylbenzenesulfonates [27, 42], adsorb exclusively on the interface between the water and the non-aqueous phase. Hence, these tracers are interface-sensitive. But similar to conventional partitioning tracers, a thermodynamic equilibrium between water and liquid/liquid-interface is assumed. Therefore, the application is only useful in static time-independent systems. Furthermore, these tracers are dissolved in the water phase and cannot be injected together with the $scCO_2$ phase. A wide range of commercially available cyclic perfluoro carbons tracers like perfluoromethylcyclohexane (PMCP) etc. are particularly suitable for labelling tracers in multi-injection wells [32].

Examples of tracers which can be used for the determination of the CO_2 plume in deep saline formations are listed in Table 2. One category is represented by the volume sensitive tracers which rely on the retardation process resulting from partitioning between two phase volumes, or from adsorption on the fluid-fluid interface. A more challenging category are the reactive tracers [44, 45, 50].

Table 2 Chemical tracers with potential for monitoring CO_2 plume development in deep saline formations [44, 45, 50]

	Underlying process	Compound examples	Literature
Volume-sensitive tracers / Retardation	Partitioning between two phase volumes	Alcohols (1-hexanol, 1-heptanol)	Annable et al. [2]
			Dwarakanath and Pope [14]
		Gases (SF6 and Kr)	Vulava et al. [55]
		Fluorinated hydrocarbons	McCallum et al. [31]; Wells et al. [31]
	Partitioning between two phase volumes	Naturally occurring isotopes 222Rn	Hunkeler et al. [18]; Semprini et al. [59]; Davis et al. [13]
Interfacial tracers / Retardation	Adsorption on liquid/ liquid interface	Anionic surfactants (Alkylbenzenesulfonates)	Saripalli et al. [41, 42]
	Adsorption on liquid/gas interface	High molecular weight alcohols	Kim et al. [27] and Rao et al. [38]
Reactive tracers	Kinetic interface sensitive tracers (KIS)/ Hydrolysis at fluid-fluid interface	Non-polar, hydrophobic esters	Schaffer et al. [44]
	Thermo-sensitive tracers	Polar, anionic esters	Nottebohm et al. [34]
	Biogeochemical reactive tracers	Inorganic electron acceptors or donors (O2, NO3-, SO42-, H2)	Istok et al. [21]
		Low weight alcohols, benzoate, sugars	Rao et al. [38]
		Caffeine	Hillebrand et al. [17]

2 Theoretical Background and Conceptual Model of KIS Tracers for CO_2 Storage in Deep Saline Formations

Kinetic interface sensitive (KIS) tracers represent a novel class of reactive tracers (Table 2) for quantifying the interfacial area between the two fluid phases ($scCO_2$ and brine). KIS tracers have the potential to describe the CO_2 plume movement in the saline formations and its interface development with time. These tracers undergo a known hydrolysis reaction across the fluid-fluid interface. For the development of the KIS tracers with desired properties (i.e. reaction kinetics, pH, temperature), molecular target design method was used [44].

The interfacial area between $scCO_2$ and brine controls the amount of dissolution and also implicitly the solubility trapping mechanism. The larger the interface, the larger is the dissolved mass. Thus, to increase the storage effectiveness the interface

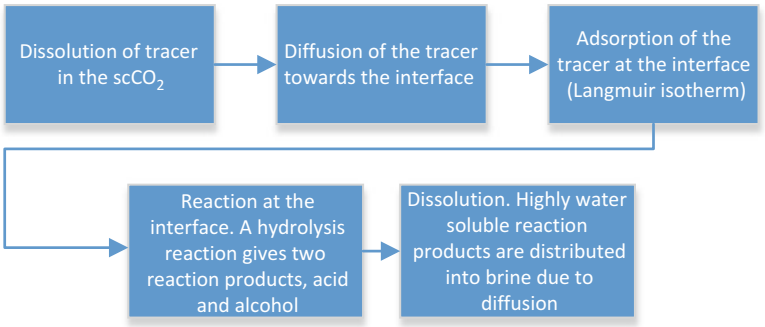

Fig. 2 Flow chart of the underlying reaction process for Kinetic interface tracers

between the two fluids should be maximized. In this sense, being able to characterize the development of the plume and its interface in the reservoir, the novel KIS tracers help to build optimized injection strategies for maximum interface creation.

The basis of the kinetic interface tracer lies in the hydrolysis reaction Eq. (1), which happens on the interface of the fluids. As the two phases increase their interfacial area, the hydrolysis reaction of the kinetic interface tracer increases and this leads to the formation of the by-products from the reaction. Here the KIS tracer dissolved in the $scCO_2$ (A_{scCO_2}) reacts irreversibly at the interface to form the reaction products B_{H_2O}(acid) and C_{H_2O} (alcohol), which are highly soluble in water. According to [44] the reaction can be written as:

$$A_{scCO_2} + H_2O \xrightarrow{k^R_{n\to w}} B_{H_2O} + C_{H_2O} \tag{1}$$

where the hydrolysis reaction rate $k^R_{n\to w}$ of the tracer depends on the chemical and physical conditions (pressure, temperature, pH, impurities, etc.).

Apart from this, additional physico-chemical processes have to be taken into account. Figure 2 shows the flowchart of all the steps involved in the KIS tracer flow, transport and reaction in brine saturated porous media. First, the tracer dissolved in the $scCO_2$ is transported through advection and diffusion towards the interface. It is assumed that A_{scCO_2} is fully dissolved in the supercritical CO_2. Next the tracer is adsorbed at the interface which is assumed to be always saturated with tracer molecules, due to the high diffusion rates and the initial excess of tracer. This reaction process usually follows an isotherm adsorption such as Langmuir isotherm [22] and the absolute amount of adsorbed tracer depends on the interfacial area linearly [44].

$$\theta_{c_p} = \frac{K_{eq} \cdot c_{KIS}}{1 + K_{eq} \cdot c_{KIS}} \tag{2}$$

Here θ_{c_p} is the fractional coverage of the fluid-fluid interfacial surface where sorption is occurring, c_{KIS} is the predefined concentration of the KIS tracer that we are injecting in the system, and K_{eq} is the Langmuir constant. The amount of

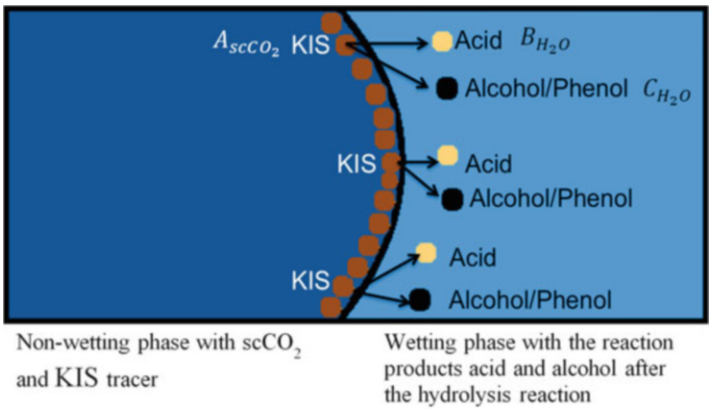

Fig. 3 Kinetic interface sensitive tracers (*KIS*) conceptual model. KIS tracer (A_{scCO_2}) dissolved in the $scCO_2$ saturates the interfacial area and hydrolyses to form acid (B_{H_2O}) and alcohol (C_{H_2O}) dissolved in the wetting phase

interfacial area formed between the two phases during this process is calculated using a biquadratic Eq. (15). After the adsorption is completed at the interface, the tracer reacts in the presence of water following a first order kinetic reaction.

At the end of the process a mass transfer between non-wetting and wetting phase occurs. The highly water soluble reaction products B_{H_2O} and C_{H_2O} are distributed into the brine but away from the interface.

A graphical representation of KIS tracer conceptual model is given in Fig. 3. It is shown how the KIS tracer molecules are transported towards the interface remaining in the non-wetting phase, then are adsorbed on the fluid-fluid interface until its saturation, and finally they hydrolyse to form the water-soluble by-products.

3 Mathematical Model of KIS Tracers for CO_2 Storage in Deep Saline Formations

The conceptual model of the KIS tracer flow, transport and reaction in deep saline formations is translated into a mathematical model. This is done in two steps. The first step is the formulation of the mathematical model of $scCO_2$ and brine movement in porous media and the second step is the formulation of the transport of KIS tracer and acid in the $scCO_2$ phase, respectively in the brine phase. The two phase flow equations using Darcy's extended law [1] is:

$$\frac{\partial(\phi S_\alpha \rho_\alpha)}{\partial t} - \nabla \cdot \left\{ \rho_\alpha \frac{k_{r\alpha}}{\mu_\alpha} \boldsymbol{K}(\nabla p_\alpha - \rho_\alpha g) \right\} = q_\alpha \rho_\alpha \tag{3}$$

where ϕ is the porosity, K is the intrinsic permeability, S_α is the saturation, ρ_α is the density, k_{ra} is the relative permeability, and p_a is the pressure of the fluid-phase

$\alpha = (w, n)$. Next, the classic two-phase flow coupling relationships are defined. The first one states that the sum of the saturation of both phases is equal to unity. In the second relation, the capillary pressure can be defined as the difference between the pressure of the non-wetting and the wetting phase.

$$S_w + S_n = 1 \tag{4}$$

$$p_c = p_n - p_w \tag{5}$$

Here p_c is the capillary pressure, p_n is the pressure of the non-wetting phase and p_w is the pressure of the wetting phase.

3.1 Supercritical CO_2 and Brine Flow in Porous Media

In the preceding paragraph, Eq. (3) together with the capillary pressure relationship (4) and (5) represents a coupled dynamic system of equations describing the two-phase immiscible flow in porous media. The resulting systems of equation are highly parabolic in nature [16]. The pressure–saturation formulation is used because of its advantage over the other two-phase flow formulations, so that it can be applied to a situation where in the gradient of the capillary pressure is really small.

It is assumed that the pressure, temperature and chemical conditions in the investigated domain do not change strongly, so that the density variations are minimal. Additionally, the source and sink term is left out.

After including Eq. (5) it results:

$$\phi\rho_n \frac{\partial(S_n)}{\partial t} - \nabla \cdot \left(\lambda_n \rho_n K \nabla p_w + \lambda_n \rho_n K(\nabla p_c - \rho_n g)\right) = 0 \tag{6}$$

For one-spatial direction it can be written that $\nabla p_c = \left(\frac{\partial p_c}{\partial x}\right)\left(\frac{\partial S_n}{\partial S_n}\right)$. A variable switch is performed for the numerical implementation in the multiphase flow simula tor: $\nabla p_c = \left(\frac{\partial p_c}{\partial S_n}\right)\nabla S_n$. Applied in (6) results:

$$\phi\rho_n \frac{\partial(S_n)}{\partial t} - \nabla \cdot \left(\lambda_n \rho_n K \nabla p_w + \lambda_n \rho_n K\left(\left(\left(\frac{\partial p_c}{\partial S_n}\right)\nabla S_n - \rho_n g\right)\right)\right) = 0 \tag{7}$$

The derivative of capillary pressure with respect to saturation of non-wetting phase ($\frac{\partial p_c}{\partial S_n}$) can be derived as:

$$\left(\frac{\partial p_c}{\partial S_n}\right) = (1/\lambda) p_d (1 - S_n)^{\left(-\frac{1}{\lambda}-1\right)} \tag{8}$$

Therefore after inserting Eq. (8) in (7) the final balance equations expressed with only the primary variables can be written:

For the wetting phase:

$$-\frac{\partial(S_n\phi\rho_w)}{\partial t}-\nabla\cdot\left(\frac{\rho_w \mathrm{K}k_{rw}}{\mu_w}(\nabla p_w-\rho_w \mathrm{g})\right)=\rho_w q_w \tag{9}$$

For the non-wetting phase:

$$\frac{\partial(S_n\phi\rho_n)}{\partial t}-\nabla\cdot\left(\frac{\rho_n \mathrm{K}k_{rn}}{\mu_n}\nabla p_w+\frac{\rho_n \mathrm{K}k_{rn}}{\mu_n}\left(\left(\frac{\partial p_c}{\partial S_n}\right)\nabla S_n-\rho_n g\right)\right)=\rho_n q_n \tag{10}$$

The constitutive relationship between the capillary pressure and saturation is formulated using the Brooks-Corey [6] model:

$$p_c(S_w)=p_d S_e^{-\frac{1}{\lambda}}, \text{where } S_e=\frac{S_w-S_{wr}}{1-S_{wr}-S_{nr}} \tag{11}$$

Here $S_e$is the effective saturation, p_d is the entry pressure, S_{wr} is the residual wetting phase saturation, S_{nr} is the residual non-wetting phase saturation and λ is the parameter in Brooks-Corey formulation.

The combination of the Burdine model with the Brooks-Corey one expresses the relative permeabilities:

$$k_{rw}=S_e^{\frac{2+3\lambda}{\lambda}} \text{ and } k_{rn}=(1-S_e)^2\left(1-S_e^{\frac{2+\lambda}{\lambda}}\right) \tag{12}$$

Here k_{rw} is the relative permeability of the wetting phase and $k_{rn}$is the relative permeability of the non-wetting phase.

4 Tracer Transport and Interface Hydrolysis Reaction

A first numerical model of the interface sensitive tracers was introduced by Tatomir et al. [48] for immiscible two-phase flow. An extended two-phase multi-component model accounting for the dissolution of CO_2 is presented in Tatomir et al. [51].

This model assumes that the two phases are immiscible. The KIS tracer molecules react at the interface and produce two by-products namely acid and alcohol/phenol. Two separate transport models are defined complementary to the two-phase immiscible model. The first transport model tracks the concentration of the KIS tracer whose molecules remain at all times in the non-wetting phase and react at the interface. And the second transport model is for tracking the acid whose

molecules remain in the wetting phase. The solute transport equation for tracer concentration C (KIS, acid) is:

$$\phi \frac{\partial (C)}{\partial t} - \nabla \cdot (\mathrm{C}v_\alpha - \phi D_\alpha \nabla C) - q^R_{n \to w} = 0 \tag{13}$$

For the KIS tracer, the transport velocity is that of the non-wetting phase, v_n, while for acid is that of the wetting phase, v_n.

The hydrolysis reaction is represented averaged over the entire elementary volume by an effective specific interfacial area term and an effective rate coefficient. It is assumed that the reaction follows a zero order kinetic law [44, 48]:

$$q^R_{n \to w} = k^R_{n \to w} a_{wn} \tag{14}$$

The specific interfacial area between the two phases (a_{wn}) can be expressed averaged on a representative elementary volume (REV) with the following relationship [48, 49, 51]:

$$a_{wn} = a_0 (S_w)^{a1} (1 - S_w)^{a2} \left(p_c{}^{max} - p_c\right)^{a3} \tag{15}$$

Here: $a_0 = 1, a_1 = 2, a_2 = 2, a_3 = 1.2$

The adsorption of the tracer on the fluid-fluid interface Eq. (2) can be included in the mathematical model by multiplying the reaction rate with the function θ_{cp}, which accounts for the Langmuir isotherm.

5 Laboratory Column Flooding Experiment

The current development status of KIS tracer requires testing in the laboratory column experiments before field deployment. The main aim of the experiment is to understand the main flow and transport processes of the KIS tracer in the CO_2-brine systems. A sensitivity analysis is performed to investigate the influence of the key flow and transport parameters on the breakthrough curves (BTC) behaviour. Also, it assesses the relevant parameter ranges and the response in the arrival times of the plume.

Four parameters are investigated through numerical modelling: porosity, permeability, size of the investigation domain, and the injection rate of CO_2. As discussed in "Introduction" they are the key parameters for the geological storage of CO_2. The practical range for the kinetic rates of the KIS tracers is determined by Tatomir et al. [51]. The coupled system of partial differential equations Eqs. (9, 10, 11, 12, 13, and 14) is implemented and solved in a finite element simulation

software (COMSOL Multiphysics 2014). The technical details of implementation are described and discussed in Tatomir et al. [49] and Jyoti [24].

5.1 Model Setup

The setup is a laboratory column with the length of 1.5 m and a diameter of 0.03 m. A sketch of the model setup with the assigned boundary conditions is given in Fig. 4. The non-wetting phase is injected with KIS tracer dissolved through an injection pump from the left boundary of the domain. For the right side of the domain we set up a Dirichlet boundary condition with the saturation of the non-wetting phase set at "0.0" and the wetting pressure equal to 1.0 e7 Pa. The top and the bottom boundaries of the domain are set to Neumann no–flow boundary conditions and the initial conditions in the system are defined to be the same as the Dirichlet condition at the outlet (right hand side).

The injection rate is set at $0.0008(kg/m^2 \cdot s)$. This injection rate is optimum for the experiment because the steady state is reached after 1 day. Table 3 gives the flow and transport parameters of the column experiment which are in the typical range of sandstone reservoirs (e.g., [53]). The Brooks-Corey model is used to define the properties of the porous media and relative permeability (Table 3). The effect of gravity is neglected which leads to a quasi 1D problem.

An unstructured triangular conforming mesh is used for the computation. The minimum finite element size is 0.000113 m. A time step of 0.01 day is used and the model is run for a time period of 1 day.

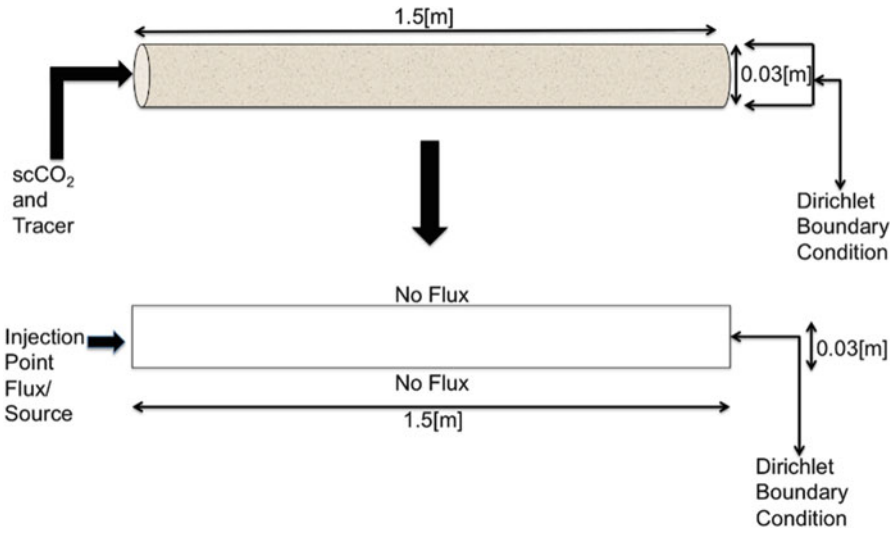

Fig. 4 Model setup with boundary conditions

Table 3 Parameters to simulate the laboratory core flooding case

Parameter	Laboratory-scale values
ϕ	0.2
K	$10^{-11}\,(m^2)$
ρ_w	$1000\,(kg/m^3)$
ρ_n	$700\,(kg/m^3)$
λ	2
p_d	2000 (Pa)
p_w	10^7 (Pa)
S_n	0.0
Q_{in}	$10^{-4}\,(kg/m^2 \cdot s)$
μ_n	$10^{-4}\,(Pa \cdot s)$
μ_w	$10^{-3}\,(Pa \cdot s)$
$k^R_{n\to w}$	$10^{-6}\,(kg/m^2 \cdot s)$

5.2 Simulation Results and Discussion

A sensitivity analysis has been performed in order to determine the tracer behaviour with regard to changes in flow and transport parameters (porosity, permeability). Furthermore, the effects of the sand column and length and the injection rates on the breakthrough curves (BTC) is investigated. The results of the sensitivity analysis are described below and the robustness of the model is tested.

In Fig. 5 the profile of the non-wetting phase saturation is observed as it gets injected into a fully wetting phase saturated porous media from the left boundary of the domain. The fate of the non-wetting phase is observed as it displaces the wetting phase which saturates the domain at T = 0 day. Then slowly the non-wetting phase displaces the wetting phase in the domain until the end of the simulation at T = 1 day when the whole domain is saturated with non-wetting phase. The blue colour as given on the legend below the figure represents that the saturation of non-wetting phase is zero ($S_n = 0$) and the red color represents that the saturation of the non-wetting phase is close to 45 % ($S_n \cong 0.45$).

5.2.1 Sensitivity Analysis with Regard to Effective Porosity

The first parameter that is being investigated is the effective (connected) porosity of the system. The simulations are run on various porosity values ranging from a very low porous system of 0.1 to a very high porous system of 0.5. According to [28], the range of porosity values selected to run this sensitivity analysis cover almost all the major reservoir types.

In Fig. 6a the BTCs for the saturation of the non-wetting phase for different values of porosity are plotted. The graph shows that when the system has the lowest porosity, the saturation front moves the fastest and reaches the maximum value in the shortest time. Next, in Fig. 6b the BTCs for the formulation of interfacial area with changing porosity values are plotted. The interfacial area reaches its maximum

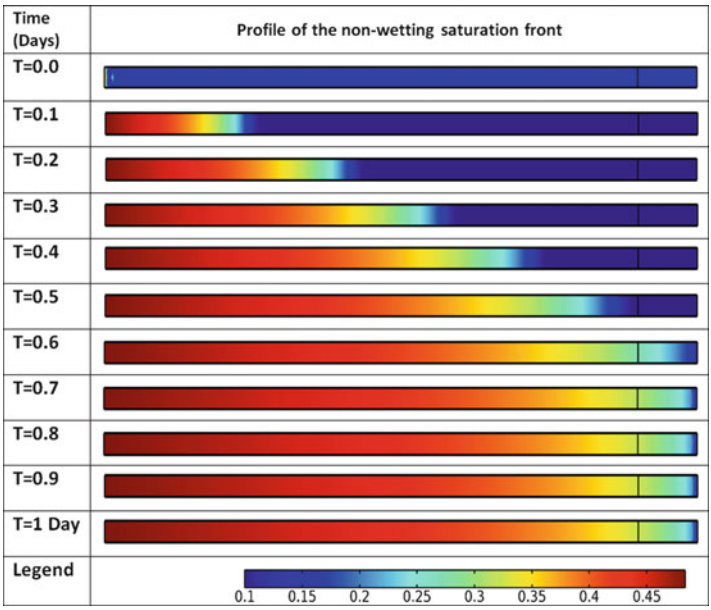

Fig. 5 Results for lab scale KIS model, representing the fate of $S_n$in the domain

value when the non-wetting saturation front reaches 50 % of its value. Once the saturation front reaches 50 %, the amount of interfacial area starts to decrease. Similar to non-wetting saturation behaviour, the maximum interfacial area is reached in the least amount of time for lowest porosity. Figure 6c shows the BTCs of KIS tracer concentration. The highest concentration is reached in the shortest amount of time with the system of lowest porosity. With an increase in porosity, the saturation front takes more time to migrate through the domain. As expected, the front is slowest for the highest porosity. Next, in Fig. 6d, the BTC of the concentration of acid with respect to time are plotted. As described in the theoretical background section, the acid is the by-product of the reaction at the interface.

High porosities lead to increased travel times and a delay in reaching the maximum non-wetting saturation and interfacial area. The maximum interfacial area which determines the reaction rate and implicitly the amount of acid formed (14) is reached faster for the systems with low porosity. This means more acid is produced if the reaction is kept at the maximum rate for a longer period of time. Therefore, it can be seen (Fig. 6d) that as the porosity is increased the concentration of the acid decreases. These results, however, do not include the interface adsorption.

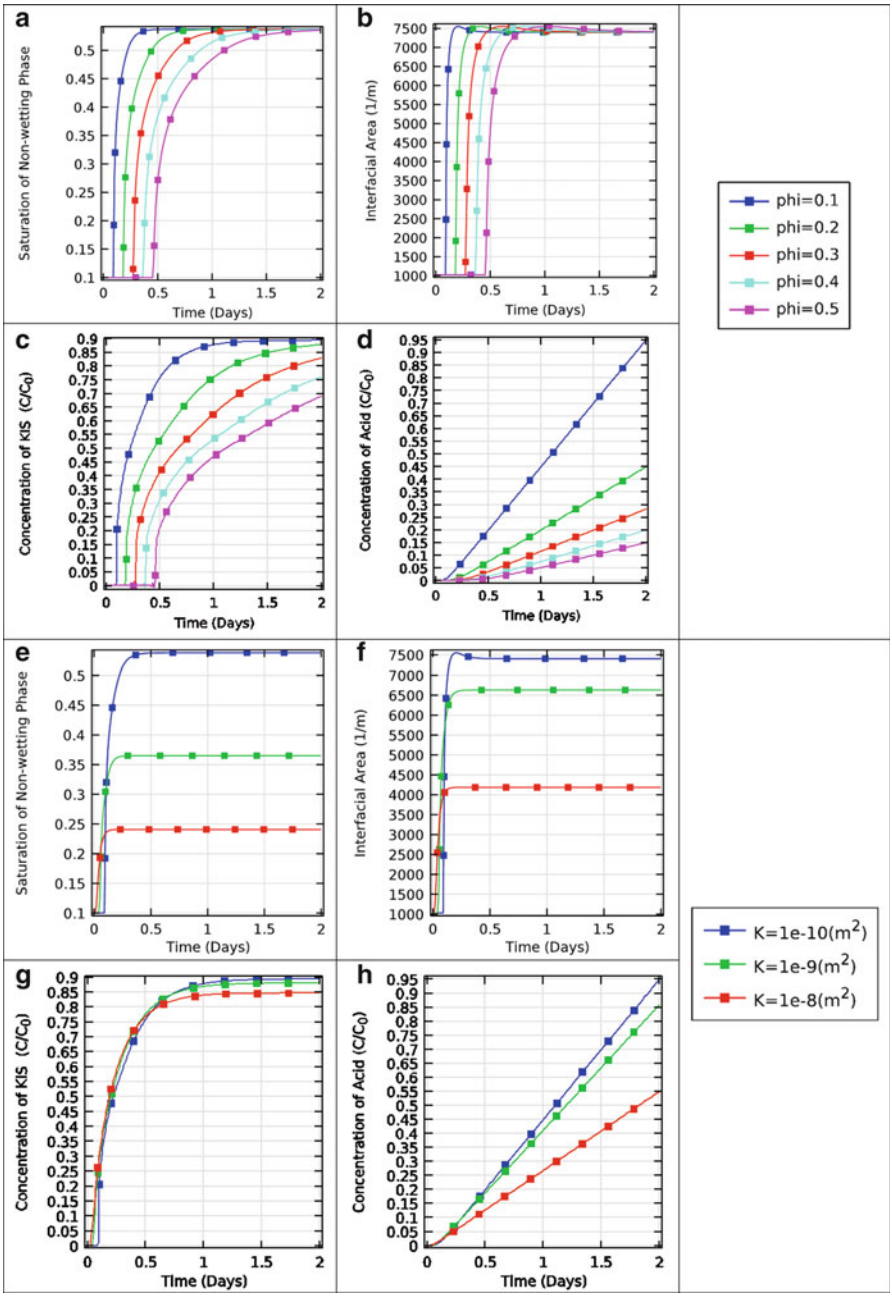

Fig. 6 Sensitivity analysis of KIS tracers for change in porosity (**a**–**d**) and for change in intrinsic permeability (**e**–**h**); (**a**) Saturation of non-wetting phase; (**b**) Specific interfacial area; (**c**) Concentration of KIS tracer; (**d**) Concentration of acid; (**e**) Saturation of non-wetting phase; (**f**) Specific interfacial area; (**g**) Concentration of KIS tracer; (**h**) Concentration of acid

5.2.2 Sensitivity Analysis with Regard to Intrinsic Permeability

The intrinsic permeability of the system is changed in the second sensitivity analysis. The intrinsic permeability is a property of a porous medium characterizing its ability to let a fluid pass through it. Here the porous medium is the system in which the wetting phase is already present and we are injecting the non-wetting phase in the media. So the permeability has a large effect on the system, which can also be seen in the conservation equations that are being used in the model. The model is run at three different values of intrinsic permeability that are 1.0e-10 (m^2), 1.0e-9 (m^2) and 1.0e-8 (m^2). Figure 6e shows the impact of change in the intrinsic permeability of the system on the saturation of the non-wetting phase with respect to time. All the graphs are plotted for a location in the center of the domain.

The non-wetting saturation reaches its maximum value when the permeability is at its minimum and when the permeability increases, the maximum saturation value reached by the model decreases. In Fig. 6f the BTC for the formation of the specific interfacial area with respect to time on different values of permeability are plotted. It can be seen in the graph that as the permeability of the system increases, the amount of interfacial area produced decreases. The maximum amount of interfacial area is reached when the intrinsic permeability is at its minimum. It is known from the interfacial area equation that the interfacial area is highly dependent on the saturation front but it should also be noted that when the saturation point reached 50 %, the amount of interfacial area starts to decrease till it reaches a stable value towards the end of the simulation (after 2 days).

The graphs display two more important properties of the system. In Fig. 6g the BTCs for the concentration of the KIS tracer are plotted for systems having different permeability. At the end of the 2nd day of simulation, it can be concluded that a higher concentration of KIS tracer is reached in the system when the permeability is decreased and a lower concentration of the tracer is reached when the permeability is increased. Next Fig. 6h shows the concentration of the acid in the system. It can be concluded from the graphs that an increase in the permeability of the system leads to a decrease in the maximum value of interfacial area and implicitly a decrease in the concentration of the acid produced. Analogously, a decrease in the permeability, leads to an increase in the concentration of the acid produced.

5.2.3 Sensitivity Analysis with Regard to the Domain Lengths

The simulations are run for different domain (column) lengths to design the optimal column so as to conduct laboratory experiments. The standard length to run the laboratory–scale model is 1.5 m. In this sensitivity analysis 5 different lengths are being investigated, i.e. 1.5, 2, 2.5, 3, 3.5 and 4 m.

In Fig. 7a, the BTC for the saturation of the non-wetting phase with respect to time on different column lengths of the domain are plotted. With the increasing

domain length, the saturation front takes more time to reach the centre of the domain and the maximum saturation also increases. For all simulations the injection rate of 0.0008 $(kg/m^2 \cdot s)$ is applied. In Fig. 7b, the BTC for the specific interfacial area formulation with respect to time on different column lengths are plotted. With an increase in the length of the domain, the time taken for reaching the peak of interfacial area increases. Though they reach the same maximum value (~7500 1/m) for all the investigated domain lengths, the smallest sized domain with the length of 1.5[m] takes the least amount of time and the lengthiest domain of 4 [m] takes the maximum time to reach the maximum value of the interfacial area. This effect is mainly influenced by the boundaries when the quasi-steady state regime is reached. In Fig. 7c the BTC of the concentration of the kinetic interface tracer with respect to time for changing domain lengths are plotted. The concentration of the tracer slightly decreases with an increase in the domain length. The longer the domain length the smaller is the concentration of the KIS tracer. The Fig. 7d, shows that with an increase in the domain length, the concentration of the acid decreases. These values correlate with the values of the interfacial area (Fig. 7b) and reach a quasi-steady state regime.

5.2.4 Sensitivity Analysis with Regard to CO_2 Injection Rates

The next parametric study investigates the injection rate of the non-wetting phase (Q_{in}) which is one of the most important user controlled parameters. Five different injection values starting from 3.0e-4 $(kg/m^2 \cdot s)$ to a maximum value of 3.0e-3 $(kg/m^2 \cdot s)$ are simulated. The injection rate determines the speed of the saturation front and so it also influences the amount of time that the KIS tracer gets to react with the wetting phase inside the porous medium. The injection rate has to be administered carefully as a low injection rate will result in a slow system in which the saturation front will take a longer time to reach to the other end of the domain. On the other hand, a high injection rate is not beneficial since the saturation front will pass through the domain at a very high speed and the desired reactions and results cannot be observed within the spatial domain. In Fig. 7e the BTCs of the non-wetting phase saturation are plotted for different injection rates. As expected, with increasing injection rates more mass enters the system. Thus, the non-wetting saturation front moves faster and reaches higher values. In Fig. 7f the BTCs for the formulation of the interfacial area at different injection rates are plotted. The highest S_n value is reached for the highest considered injection rate of 3.0e-3 $(kg/m^2 \cdot s)$. Analogously, least amount of interfacial area is formed when the injection rate is the lowest, respectively 3.0e-4 $(kg/m^2 \cdot s)$. In Fig. 7g, h, the BTCs of the KIS tracer, and acid concentration are plotted for the different range of injection rates. The concentration of the acid increases with an increase in the injection rate. The contrast between the BTCs is greater for KIS tracer than for acid. This effect can be explained from the lower value in the interfacial area (resulting at low injection rates).

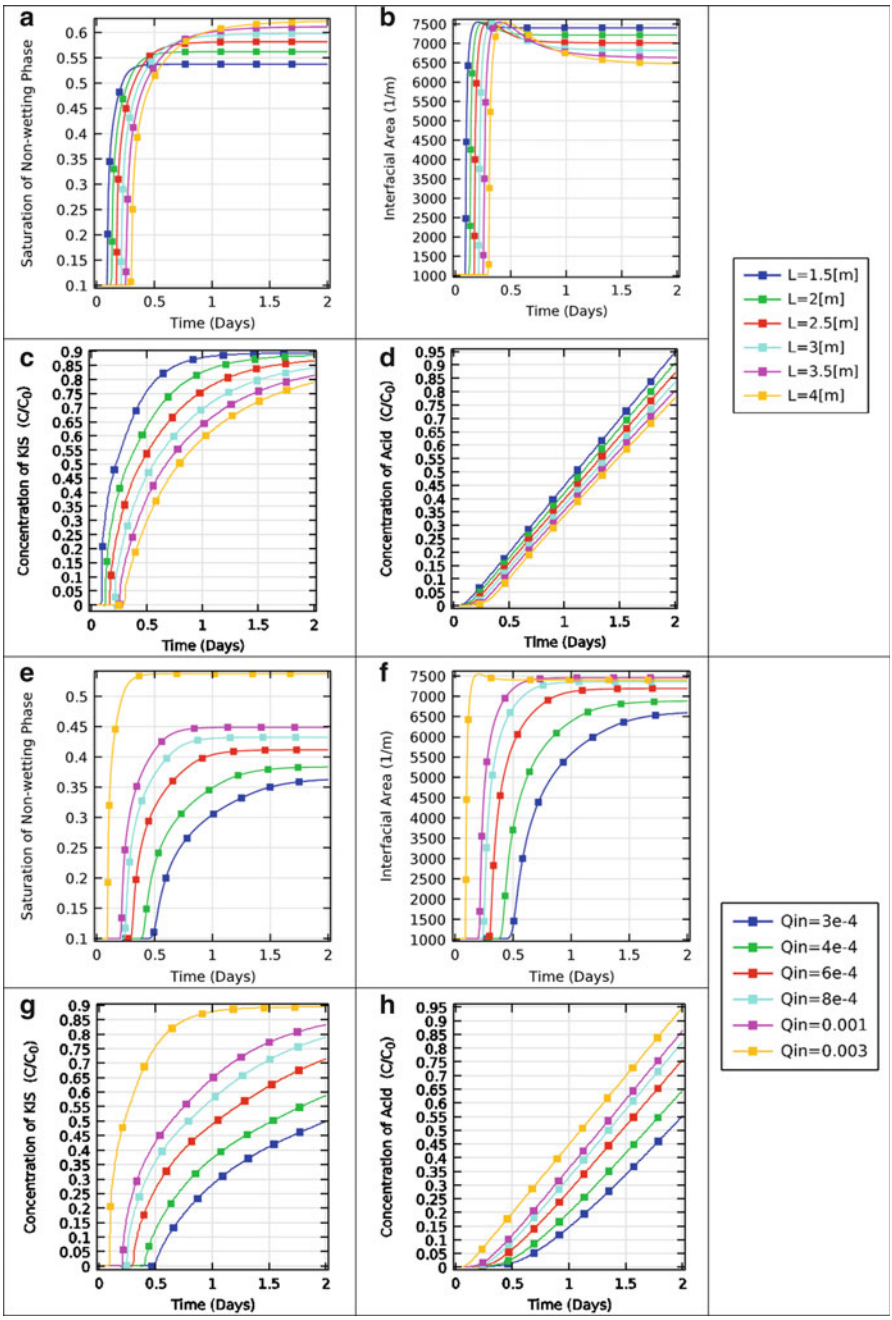

Fig. 7 Sensitivity analysis of KIS tracers for change in column length (**a**–**d**) and for change in injection rate (**e**–**h**); (**a**) Saturation of non-wetting phase; (**b**) Specific interfacial area; (**c**) Concentration of KIS tracer; (**d**) Concentration of acid; (**e**) Saturation of non-wetting phase for changing injection rates, (**f**) Specific interfacial area; (**g**) Concentration of KIS tracer; (**h**) Concentration of acid

6 Summary and Conclusions

Geological carbon storage projects can be successful only if they rely on efficient, robust monitoring systems. Tracer methods represent powerful monitoring tools which can determine the processes in the saline formation before, during and after the CO_2 injection, e.g., leakage pathways, boundaries of the reservoir, chemical activity, extent of the CO_2 plume and its location, size of the brine- CO_2 interfacial area and its evolution with time, amount of residual CO_2, etc. Monitoring techniques can also help to improve the public perception on the GCS technology, to prove that it is safe, and to show that leakages can be accurately detected and prevented with a stringent monitoring routine.

An overview of the fundamental chemical tracers together with the key parameters relevant for the GCS projects was presented. The main focus was to emphasize the importance of the interfacial area between brine and supercritical CO_2. Afterwards, conceptual and mathematical models of the KIS tracer were introduced. The mathematical model and the robustness of the implementation are tested in a laboratory column CO_2 flooding experiment. Several sensitivity analyses with regard to the key flow and transport parameters improve the understanding of the model behaviour over the whole parameter range.

Sensitivity analysis with regard to porosity shows that this parameter induces strong variations in the alcohol and KIS tracers BTCs. Porosity has the strongest influence among the four investigated parameters. This is important as porosity is vital to any GCS enterprise in that it determines the storage capacity. The sensitivity of the KIS tracers BTC with regard to intrinsic permeability is small. On the other hand, the size of the specific interfacial areas increases with the decrease in permeability which leads to higher alcohol concentrations for lower permeabilities. Column length between 1.5 and 4 m show small variation in the acid BTCs, and greater variation for the KIS tracer BTCs. For practical reasons, shorter columns are easier to handle. The simulation results indicate that for an accurate reconstruction of the $scCO_2$ –brine interfacial area and its evolution with time besides the acid tracer detection, measuring the KIS tracer in the non-wetting phase and the CO_2 saturation are required, which and can reduce the uncertainty.

Designing tracer tests, for the field and even for laboratory experiments prove to require interdisciplinary expertise of chemists, engineers, modellers, geologist etc. And even though the theoretical background of the tracer methods is well developed,. the new challenges arise for the GCS in saline aquifers due to complex phase behaviour of CO_2. Reactive tracers, and in particular the KIS tracers represent the leading edge innovation in the field of GCS. For the field application of the KIS tracers, a number of the physico-chemical factors still need to be considered (pH, temperature, salinity, fluid composition, etc.). The present study can be regarded as a prerequisite to continue the KIS tracer development by improving the understanding of the effect of reservoir and operational parameters on the tracer BTC.

The future work includes the validation of the model with the laboratory experiments. If the lab validation is successful then the final objective would be to develop appropriate tracer tests like push-pull, dipole or a combination of both which then can be used and implemented in a pilot test site.

Acknowledgments This research has received funding from the European Community's 7th Framework Programme through the MUSTANG (grant agreement no. 227286) and TRUST (grant agreement no. 309067) projects.

References

1. Alnes H, Eiken O, Nooner S, Sasagawa G, Stenvold T, Zumberge M (2011) Results from Sleipner gravity monitoring: updated density and temperature. Energy Procedia 4:5504–5511
2. Annable MD, Rao PSC, Hatfield K, Graham WD, Wood AL, Enfield CG (1998) Partitioning tracers for measuring residual NAPL: field-scale test results. J Environ Eng 124:498–503
3. Arts R, Eiken O, Chadwick A, Zweigel P, van der Meer L, Zinszner B (2004) Monitoring of CO2 injected at Sleipner using time-lapse seismic data. Energy 29:1383–1392
4. Assayag N, Matter J, Ader M, Goldberg D, Agrinier P (2009) Water–rock inter-actions during a CO_2 injection field-test: implications on host rock dissolution and alteration effects. Chem Geol 265:227–235
5. Bachu S (2003) Screening and ranking of sedimentary basins for sequestration of CO2 in geological media in response to climate change. Environ Geol 44:277–289. doi:10.1007/s00254-003-0762-9
6. Brooks RH, Corey AT (1964) Hydraulic properties of porous media. Hydrology papers, vol 3. Colorado State University, Fort Collins
7. Bear J (1972) Dynamics of fluids in porous media. Elsevier Scientific Publishing, New York
8. Behrens H, Ghergut J, Bensabat J, Niemi A, Sauter M (2014) Merging single- and inter-well tracer tests into one forced-gradient dipole test, at the Heletz site within the MUSTANG project. Energy Procedia 59:249–255
9. Boreham C, Underschultz J, Stalker L, Kirste D, Freifeld B, Jenkins C, Ennis-King J (2011) Monitoring of CO2 storage in a depleted natural gas reservoir: gas geochemistry from the CO2CRC Otway project, Australia. Int J Greenhouse Gas Control 5:1039–1054
10. Carcione JM, Gei D, Picotti S, Michelini A (2012) Cross-hole electromagnetic and seismic modeling for CO2 detection and monitoring in a saline aquifer. J Pet Sci Eng 100:162–172. doi:10.1016/j.petrol.2012.03.018
11. Celia MA, Nordbotten JM (2009) Practical modeling approaches for geological storage of carbon dioxide. Ground Water 47:627–638. doi:10.1111/j.1745-6584.2009.00590.x
12. Cook P, Causebrook R, Gale J, Michel K, Watson M (2014) What have we learned from small-scale injection projects. Energy Procedia 63(0):6129–6140. http://dx.doi.org/10.1016/j.egypro.2014.11.645
13. Davis BM, Istok JD, Semprini L (2002) Push–pull partitioning tracer tests using radon-222 to quantify non-aqueous phase liquid contamination. J Contam Hydrol 58:129–146
14. Dwarakanath V, Pope GA (1998) New approach for estimating alcohol partition coefficients between non-aqueous phase liquids and water. Environ Sci Technol 32:1662–1666
15. Freifeld BM, Trautz RC, Kharaka YK, Phelps TJ, Myer LR, Hovorka SD, Collins DJ (2005) The U-tube: a novel system for acquiring borehole fluid samples from a deep geologic CO2 sequestration experiment. J Geophys Res Solid Earth (1978–2012): 110(B10)

16. Helmig R (1997) Multiphase flow and transport processes in the subsurface: a contribution to the modelling of hydro systems, 1st edn. Springer, Berlin/New York
17. Hillebrand O, Nödler K, Licha T, Sauter M, Geyer T (2012) Identification of the attenuation potential of a karst aquifer by an artificial dual tracer experiment with caffeine. Water Res 46:5381–5388
18. Hunkeler D, Hoehn E, Höhener P, Zeyer J (1997) 222 Rn as a partitioning tracer to detect diesel fuel contamination in aquifers: laboratory study and field observations. Environ Sci Technol 31:3180–3187
19. IEA (2008) CO2 capture and storage – a key carbon abatement option. IEA Publications, Paris
20. IPCC (2005) IPCC special report on carbon dioxide capture and storage. In: Metz B, Davidson O, de Coninck HC, Loos M, Meyer LA (eds) Prepared by working group III of the Intergovernmental Panel on Climate Change. Cambridge University Press, Cambridge
21. Istok JD, Humphrey MD, Schroth MR, Hyman MR, O'Reilly KT (1997) Single-well, push–pull test for in situ determination of microbial activities. Ground Water 35:619–631
22. Langmuir I (1915) Chemical reactions at low pressures. J Am Chem Soc 37:1139–1167. doi:10.1021/ja02170a017
23. JafarGandomi A, Curtis A (2011) Detectability of petrophysical properties of subsurface CO2 – saturated aquifer reservoirs using surface geophysical methods. Lead Edge 30:1112–1121
24. Jyoti A (2015) Numerical simulations of fluid-fluid interface sensitive tracers in two-phase porous media systems. Master thesis, University of Goettingen, Göttingen
25. Ketelaar VBH (2009) Satellite radar interferometry, remote sensing and digital image processing. Springer, Dordrecht
26. Kiessling D, Schmidt-Hattenberger C, Schuett H, Schilling F, Krueger K, Schoebel B, Danckwardt E, Kummerow J, CO2 SINK Group (2010) Geoelectrical methods for monitoring geological CO2 storage: first results from cross-hole and surface-downhole measurements from the CO2 SINK test site at Ketzin (Germany). Int J Greenhouse Gas Control 4:816–826
27. Kim H, Suresh P, Rao PSC, Annable MD (1999) Consistency of the interfacial tracer technique: experimental evaluation. J Contam Hydrol 40:79–94
28. Kopp A, Class H, Helmig R (2009) Investigations on CO2 storage capacity in saline aquifers: Part 1. Dimensional analysis of flow processes and reservoir characteristics. Int J Greenhouse Gas Control 3:263–276. doi:10.1016/j.ijggc.2008.10.002
29. LaForce T, Ennis-King J, Boreham C, Paterson L (2014) Residual CO2 saturation estimate using noble gas tracers in a single-well field test: the CO2CRC Otway project. Int J Greenhouse Gas Control 26:9–21. doi:10.1016/j.ijggc.2014.04.009
30. Matter JM, Takahashi T, Goldberg D (2007) Experimental evaluation of in situ CO2–water–rock reactions during CO2 injection in basaltic rocks: implications for geological CO2 sequestration. Geochem Geophys Geosyst 8, Q02001
31. McCallum SD, Riestenberg DE, Cole DR, Freifeld BM, Trautz RC, Hovorka SD, Phelps TJ (2005) Monitoring geologically sequestered CO2 during the Frio Brine pilot test using perfluorocarbon tracers. In: Proceedings of the 4th annual conference on carbon capture and sequestration DOE/NETL, Alexandria
32. Myers M, Stalker L, Pejcic B, Ross A (2013) Tracers – past, present and future applications in CO2 geosequestration. Appl Geochem 30:125–135
33. Myers M, Stalker L, Ross A, Dyt C, Ho K-B (2012) Method for the determination of residual carbon dioxide saturation using reactive ester tracers. Appl Geochem 27:2148–2156
34. Nottebohm M, Licha T, Sauter M (2012) Tracer design for tracking thermal fronts in geothermal reservoirs. Geothermics 43:37–44
35. Oldenburg CM, Bryant SL, Nicot J-P (2009) Certification framework based on effective trapping for geologic carbon sequestration. Int J Greenhouse Gas Control 3:444–457. doi:10.1016/j.ijggc.2009.02.009
36. Onuma T, Ohkawa S (2009) Detection of surface deformation related with CO2 injection by DInSAR at In Salah, Algeria. Energy Procedia, Greenhouse Gas Control Technologies 9. In: Proceedings of the 9th international conference on Greenhouse gas control technologies

(GHGT-9), Washington DC, USA, 16–20 November 2008, 2177–2184. doi:10.1016/j.egypro.2009.01.283
37. Pires JCM, Martins FG, Alvim-Ferraz MCM, Simões M (2011) Recent developments on carbon capture and storage: an overview. Chem Eng Res Des 89:1446–1460. doi:10.1016/j.cherd.2011.01.028, Special Issue on Carbon Capture & Storage
38. Rao PSC, Annable MD, Kim H (2000) NAPL source zone characterization and remediation technology performance assessment: recent developments and applications of tracer techniques. J Contam Hydrol 45:63–78
39. Rasmusson K, Rasmusson M, Fagerlund F, Bensabat J, Tsang Y, Niemi A (2014) Analysis of alternative push–pull-test-designs for determining in situ residual trapping of carbon dioxide. Int J Greenhouse Gas Control 27:155–168. doi:10.1016/j.ijggc.2014.05.008
40. Rütters H, CGS Europe partners (2013) State of play on CO2 geological storage in 28 European countries. CGS Europe report No. D2.10
41. Saripalli KP, Kim H, Rao PSC, Annable MD (1997) Measurement of specific fluid-fluid interfacial areas of immiscible fluids in porous media. Environ Sci Technol 31:932–936
42. Saripalli KP, Rao PSC, Annable MD (1998) Determination of specific NAPL–water interfacial areas of residual NAPLs in porous media using the interfacial tracers technique. J Contam Hydrol 30:375–391
43. Sayers C, Wilson T (2010) An introduction to this special section on CO2 sequestration. Lead Edge 29:148–149
44. Schaffer M, Maier F, Licha T, Sauter M (2013) A new generation of tracers for the characterization of interfacial areas during supercritical carbon dioxide injections into deep saline aquifers: kinetic interface-sensitive tracers (KIS tracer). Int J Greenhouse Gas Control 14:200–208. doi:10.1016/j.ijggc.2013.01.020
45. Schaffer M (2013b) On the possibility of using organic molecules in the characterization of subsurface processes. PhD thesis, University of Goettingen, Goettingen, Germany
46. Strazisar BR, Wells AW, Diehl JR, Hammack RW, Veloski GA (2009) Near-surface monitoring for the ZERT shallow CO2 injection project. Int J Greenhouse Gas Control 3:736–744
47. Streich R, Becken M, Matzander U, Ritter O (2011) Strategies for land-based controlled-source electromagnetic surveying in high-noise regions. Lead Edge 30:1174–1181
48. Tatomir A, Maier F, Schaffer M, Licha T, Sauter M (2013) Modelling of kinetic interface sensitive tracers for two-phase systems. In: Hou MZ, Xie H, Were P (eds) Clean energy systems in the subsurface: production, storage and conversion, Springer series in geomechanics and geoengineering. Springer, Berlin/Heidelberg, pp 65–74
49. Tatomir A, Jyoti A, Maier F, Sauter M (2014) Modelling of kinetic interface sensitive tracers for two phase immiscible flow in porous media with COMSOL Multiphysics®. In: COMSOL conference, Cambridge, UK
50. Tatomir AB, Ghergut I, Sauter M (2016) Tracer methods for characterization and monitoring of the CO2 storage in geological formations. In: Niemi A, Bear J, Bensabat J (eds) Geological storage of CO2 in deep saline formations. Springer (to appear in 2016)
51. Tatomir AB, Schaffer M, Kissinger A, Hommel J, Nuske P, Licha T, Helmig R, Sauter M (2015) Novel approach for modeling kinetic interface-sensitive (KIS) tracers with respect to time-dependent interfacial area change for the optimization of supercritical carbon dioxide injection into deep saline aquifers. Int J Greenhouse Gas Control 33:145–153. doi:10.1016/j.ijggc.2014.11.020
52. Tomich JF, Dalton RL, Deans HA, Shallenberger LK (1973) Single-well tracer method to measure residual oil saturation. J Pet Technol 25
53. Underschultz J, Boreham C, Dance T, Stalker L, Freifeld B, Kirste D, Ennis-King J (2011) CO2 storage in a depleted gas field: an overview of the CO2CRC Otway project and initial results. Int J Greenhouse Gas Control 5:922–932
54. Vandeweijer V, van der Meer B, Hofstee C, Mulders F, D'Hoore D, Graven H (2011) Monitoring the CO2 injection site: K12-B. Energy Procedia 4:5471–5478

55. Vulava VM, Perry EB, Romanek CS, Seaman JC (2002) Dissolved gases as partitioning tracers for determination of hydrogeological parameters. Environ Sci Technol 36:254–262
56. Wells AW, Diehl JR, Bromhal G, Strazisar BR, Wilson TH, White CM (2007) The use of tracers to assess leakage from the sequestration of CO2 in a depleted oil reservoir, New Mexico, USA. Appl Geochem 22(5):996–1016
57. Wells A, Strazisar B, Diehl JR, Veloski G (2010) Atmospheric tracer monitoring and surface plume development at the ZERT pilot test in Bozeman, Montana, USA. Environ Earth Sci 60:299–305
58. Zhang Y, Freifeld B, Finsterle S, Leahy M, Ennis-King J, Paterson L, Dance T (2011) Single-well experimental design for studying residual trapping of supercritical carbon dioxide. Int J Greenhouse Gas Control 5:88–98
59. Semprini L, Hopkins OS, Tasker BR (2000) Laboratory, field and modeling studies of Radon - 222 as a natural tracer for monitoring NAPL contamination. Transp Porous Media 38:223–240 doi:10.1023/A:1006671519143

Monitoring of Soil Gases in the Characterization Stage of CO_2 Storage in Saline Aquifers and Possible Effects of CO_2 Leakages in the Groundwater System

Javier Elio, Marcelo F. Ortega, Luis F. Mazadiego, Barbara Nisi, Orlando Vaselli, and Maria Jesus Garcia-Martinez

Abstract The main objective of this chapter is to describe which analytical methodologies and procedures can be applied at the surface to monitor and verify the feasibility of geologically stored carbon dioxide.

The reported techniques are mainly focused on the measurements of diffuse soil gas. The soil-gas measurements include the determination of CO_2 flux and the application to natural trace gases (e.g. radon) that may help to detect any CO_2 leakage. In particular, the accumulation chamber method was used to measure the diffuse emission of CO_2 at the soil-atmosphere interface. This technique was considered to be of utmost importance to adapt the optimum methodology for measuring the CO_2 soil flux and estimate the total CO_2 output. During the pre-injection phase CO_2 fluxes are expected to be relatively low compared to the intra- and post-injection phases. If leakages are occurring, small variation in CO_2 flux might be detected when the CO_2 "noise" is overcoming that produced by the biological activity of the soil.

Once the CO_2 flux measurements are completed and anomalies zones are detected, the total CO_2 output is estimated to quantify the amount of CO_2 released to the atmosphere. For the estimation of the CO_2 output six statistical methods can satisfactorily be applied, namely, arithmetic mean, minimum variances unbiased estimator, bootstrap resample, partitioning of data into different normal populations with a graphical and a maximum likelihood procedures, and sequential Gaussian simulation.

Leakages of CO_2 toward the surface are also expected to modify the chemical composition of the groundwater system with which they may interact. Thus, a specific

J. Elio • M.F. Ortega (✉) • L.F. Mazadiego • M.J. Garcia-Martinez
Department of Energy and Fuels, Universidad Politécnica de Madrid, Madrid, Spain
e-mail: mf.ortega@upm.es

B. Nisi
CNR-IGG Institute of Geosciences and Earth Resources, Pisa, Italy

O. Vaselli
Department of Earth Science, Florence, Italy

CNR-IGG Institute of Geosciences and Earth Resources, Florence, Italy

V. Vishal, T.N. Singh (eds.), *Geologic Carbon Sequestration*,
DOI 10.1007/978-3-319-27019-7_5

section of this paper will be dedicated to the expected variations by considering the equilibrium of the carbon species, which also includes the effects on the isotopic composition of dissolved CO_2 and Total Dissolved Inorganic Carbon (TDIC), these parameters likely being the most sensitive and affected by any leakage.

1 Monitoring During Geological Storage of CO_2

Projects aimed to capture and store CO_2 underground necessarily require monitoring techniques to ensure that the containment of CO_2 is effective. These techniques are aimed to detect CO_2 leakages and, if recognized, to identify and quantify them. Monitoring programs are to be planned before, during and after the CO_2 injection stage.

Preliminarily, the CO_2 injection has to be preceded by three fundamental steps, as follows:

1. Ensuring that operations, i.e. construction of CO_2 capture plants, transportation systems, gas injection and storage, are carried out safely;
2. Keeping a detailed and comprehensive register of the site;
3. Contributing to the trust and acceptance by the society and local communities to develop such projects.

Furthermore, specific and detailed information on the geological, geostructural and hydrogeological features of the selected area and geochemical characterization of the discharging waters (springs and wells) and soil gases needs to be acquired.

Although studies and developments of new monitoring strategies and/or techniques are continuously improved, the basic objectives of a monitoring approach when CO_2 is to be stored at depth are, as follows [1]:

1. Characterization of the site and reconnaissance of preferential and potential pathways along which leakages may occur;
2. Definition of leakage risks that can be obtained by combining site characterization and modeling of CO_2 behavior;
3. Verification of any CO_2 leakage and CO_2 behavior as it is injected. Then, updating of models;
4. Recording the CO_2 injected and the emissions from storage.

Geophysical, geochemical, seismic and ground deformation monitoring contribute to these objectives. The critical point is the knowledge of the "baseline", which is the distribution/concentration of the studied variables (e.g. concentrations and CO_2 fluxes) under undisturbed conditions. As outlined by Stenhouse [2], knowing the initial conditions in a selected storage site allows an extrapolation to future scenarios, which can be modeled in the case of a CO_2 escape. Therefore, monitoring is intimately connected to migration and leakage.

At the "European CO_2 Capture and Storage Conference" [3], three different terms were defined:

- Migration: horizontal or vertical movement of CO_2 (or other acid gases) within the geological formation selected for injection; the fluid remains "trapped";
- Leakage: movement of CO_2 (or other gases) outside the geological formation where CO_2 was injected. Movement through the formation boundary seals or through bore-holes;
- Seepage: movement of fluids from the geosphere to the biosphere.

In the case of leakage CO_2 may appear at the surface as diffuse and/or punctual discharges or dissolved in groundwater via springs or domestic/industrial wells. Moreover, CO_2 migration and leakage have the following general characteristics:

1. Range migration (and leakage) is not constant over time.
2. Migration flows (and leakage) are spatially inhomogeneous.

According to the IPCC [4], major routes of CO_2 leaks (Table 1) may occur even at several kilometers from the site of injection. Thus, it is essential to characterize the leakage by developing an appropriate monitoring plan.

As reported by Hannis [5]: "*the ultimate purpose of monitoring is to confirm safe and permanent storage of CO_2 in the reservoir*". As a consequence, monitoring plays a fundamental role in any geological storage of CO_2 projects. Prolonged confinement of CO_2 does not generate negative impacts on the environment and is an effective technique to reduce greenhouse gas emissions.

This implies that, in addition to the previously mentioned objectives, any kind of monitoring is expected to [6]:

- Identify storage processes and verify its integrity.
- Evaluate the interaction of CO_2 with rock and formation fluid.
- Evaluate the environmental consequences of a possible leak of CO_2.
- Evaluate the remediation processes when a leak occurs.
- Define legal disputes arising from any impact generated during storage.

For each site a specific monitoring has to be built and it may also vary according to the stage of the project. In developing the monitoring plan one must take into account these specific needs to select the best available techniques to be applied.

There is a wide range of monitoring techniques. Those able to perform the best results for the achievement of objectives of monitoring are to be applied. Thus, it is rather difficult to present a list, which contains the techniques that should be used at each stage. Therefore, the most appropriate and available techniques should be selected on the basis of the site features in accordance with the advancement of the CO_2 project. In this respect it is important to know which are the objectives of the monitoring and hence, select those techniques that better technically and economically match these objectives.

Table 1 Main types of CO_2 leakage

Types of emission	Routes/Sources of potential emissions	Comments	Phases in which may occur
Leakage pathways through wells and bore-holes	Operative or abandoned wells	It is important to identify all the abandoned wells on the site (or close to it)	Characterization
			Injection
			Post-injection
		These wells can become major routes of leakage	
	Blowouts (uncontrolled emissions from injection wells)	This can cause high leakage flows in short periods of time	Injection
		It is considered that this is unlikely to cause accidents if the safety standards are met during drilling	
	Future extraction of CO_2 reservoirs	It can be a problem in the reservoirs of coal deposits	Post-injection
Leakage pathways and natural migrations	Through faults and fractures (natural or induced)	Possible source of high flows leakage	Characterization
			Injection
		The correct characterization of the site can reduce the risk of leakage	Post-injection
	By dissolving CO_2 in a fluid and subsequent transport by natural circulation of fluid	Proper site characterization (evaluation of hydrogeology) may reduce the risk of leaks	Characterization
			Injection
			Post-injection
	If the cap rock is absent in site	The characterization and appropriate site selection can reduce the risk of leakage	Characterization
	Through a cap rock degraded by CO_2-water-rock interaction processes	Studies of the cap rock and geochemical factors during site characterization can help to reduce risk of gas leaks	Characterization
			Injection
			Post-injection
	Through the pore system in low permeability rocks when the capillary entry pressure is exceeded or if the CO_2 is in solution	Proper site characterization can reduce the risk of leaks	Characterization
			Injection
		An exhaustive control of the injection pressure is needed	
	By a spill if the reservoir overflows	Proper site characterization can reduce the risk of leaks	Injection
			Post-injection
Another type of leakage	There may be leakage of methane as a result of the displacement of CH_4 by CO_2	It can happen in depleted reservoirs of oil and gas or processes enhanced coal bed methane recovery and enhanced oil recovery rate	Characterization
			Injection
			Post-injection

From http://www.ipcc-nggip.iges.or.jp/public/2006gl/spanish/pdf/2_Volume2/V2_5_Ch5_CCS.pdf

2 Monitoring During Pre-Injection Operations

Before any CO_2 storage project, monitoring campaigns are required in order to carry out geological, geophysical and geochemical characterization of the site where carbon dioxide is to be injected, and identify the associated risks and potential pathways for the release of CO_2. Initial site conditions are established at this stage, i.e. the definition of a baseline.

Monitoring should continue for a suitable time to explain the variation model, for example, seasonal type (in the case of estimation CO_2 flux baseline; [7]). The works at this stage are aimed towards the following objectives:

- Characterization of site:
  It is provided by collecting information on seismicity (estimated probability of earthquake occurrence), hydrology (recharge parameters and infiltration), meteorology and climatology, hydrology (conductivity, temperature, water flow speed and direction), hydrogeochemistry [8] (water chemistry, pH, Eh, salinity, chemical composition of the dissolved ions) and structural geology (fractures and faults).
- Establishment of baseline:
  The estimation of initial conditions is expected to allow to understand the future evolution of the storage system and serves as a basis for further numerical modeling. It should be commenced before any operation.
- Identification of migration routes and escape of CO_2:
  This aspect is aimed to detect all possible weaknesses in the system, such as fracture and faulting zones from which CO_2 can migrate and reach the surface.
  Measurements of soil gases and CO_2 and other gases (e.g. He, Rn, CH_4, etc.) can help to estimate the fracture density and locate the preferred paths where uprising gases may reach the surface.
- Development of numerical models
  The collected data can be used to build three-dimensional static geological models and simulate dynamic modeling of CO_2 injection at various intervals of time with the corresponding sensitivity analysis. Numerical simulations for non-isothermal multiphase reactive geochemical transport of fluids in porous and fractured media can be performed when the chemical-physical and geological data of the reservoir and those of the cap-rock the surrounding areas, if hydraulically connected, are known by using specific simulation codes.
- Risk Analysis
  Risk analysis allows to quantify the probability that a particular adverse event may be occurring and evaluate its impact on human health and/or ecosystems. Therefore, a proper site management can be coped to ensure safety.
  The monitoring data are useful for a correct assessment of exposure to the effects of a possible CO_2 release, based on: environmental characteristics, distribution and activities of the population and behavior and possible destination in the case of a unlikely event of leakage. The effects of exposure are based on the sensitivity of species susceptible to potential leakage episodes of both CO_2 and substances which may be displaced by injecting CO_2.

3 Soil Gas

An appropriate detection system and a quantification of the amount of the CO_2 leakage are necessary to assess the risks related to a possible release of CO_2 at the surface. Practically, the characteristics of the migration, the water-rock interaction processes, the different sources of carbon dioxide, the various gas compounds entrained with the CO_2 flow, the substances dissolved and mobilized by CO_2-rich waters and the effects on human health and ecosystems of high CO_2 concentration and related compounds have to be known.

It is to be pointed out that one of the main problems in detecting and quantifying possible leakages is to evaluate the difference between the amount of the naturally occurring CO_2 and that released at the surface once CO_2 is injected. CO_2 is indeed present in soil gases and the atmosphere. Moreover, in the pedological cover its concentration can vary over time due to different natural processes (e.g. soil respiration). Therefore, understanding the sources and behavior of CO_2 is vital in selecting the different monitoring techniques.

Commonly, the gas composition recovered at the surface in the soil pores can be regarded as a gas mixture originated by deep, i.e. mantle and/or hydrothermal, (hypogean gases), shallow (supergene gases) and soil (e.g. decomposition of organic matter, soil respiration) sources and atmospheric gases. A schematic representation of the different gas sources and the main processes that can affect the primary gas reservoirs is reported in Fig. 1.

As shown in Fig. 1, the interpretation of the soil gases can be complicated because each gas can be affected by: (i) dilution processes with the atmosphere, (ii) reactions with the soil matrix and other gases or water, (iii) oxidation processes and (iv) biological reactions. At which extent each process and/or source can affect the soil gas composition is rather difficult to be evaluated and in addition, each site may show significant differences in terms of seasonal or, even, diurnal variations.

In most CO_2 geological storage projects, interstitial soil gas and diffuse flux of CO_2 are commonly analyzed. Carbon dioxide (CO_2) is an odorless, colorless and slightly acid gas. The concentration of CO_2 in the atmosphere has recently achieved 400 ppm by volume (NOAA-ESRL data, February 2015) whereas in the soil it is usually in the range of 0.2–4 % by vol [9, 10]. It is slightly denser than air and tends to accumulate in low areas. Consequently, in open areas if the climatic conditions are favorable (e.g. absence of wind and solar irradiation, cloud cover) CO_2 can accumulate in lowlands (e.g. [11–13]), and seriously affect vegetation, animals and people.

4 Monitoring with the Accumulation Chamber Method

This method has widely been applied in volcanic and geothermal areas [14–16], as well as to define soil respiration in agricultural practices [15]. Other researchers have employed this technique in CO_2 storage projects [17–21].

The theory is relatively simple: the CO_2 flux to the atmosphere is measured as the increase of the CO_2 concentration into the accumulation chamber with time.

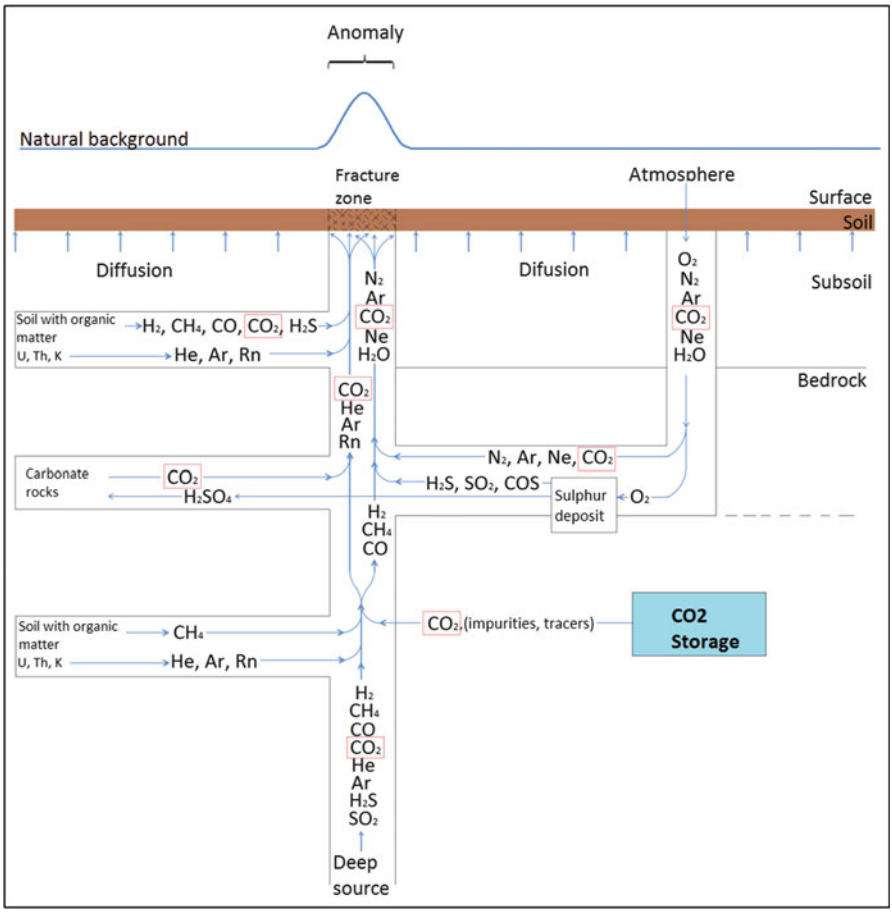

Fig. 1 Simplified representation of the source of gases, which can be retrieved at the soil surface (Modified after Rose et al. [9])

The slope in the concentration curve versus time (dC/dt as ppmv/s) diagram is calculated in order to determine the CO_2 flux ([22]). A low-flux pump ($20\ ml \cdot s^{-1}$) transfers the soil gas through a silicone tube to an Infra-Red (IR) spectrophotometer (Licor® Li-820, infra-red sensor detector, measuring range of 0–20,000 ppm, accuracy of 4 % of reading). Between the chamber and the CO_2 sensor a magnesium perchlorate filter and a 0.45 μm PTFE particle filter are interposed to remove humidity and soil particle, respectively [14, 23, 24] and avoid interference with the measurement.

To express the flux in g m^2 d^{-1}, the following conversion is applied:

$$\Phi\left(g \cdot m^{-2} \cdot day^{-1}\right) = \frac{dC}{dt}\left(\frac{ppmV}{s}\right) \cdot \frac{V(m^3)}{A(m^2)} \cdot \frac{\left({}^{1}/_{10^3 m^3}\right)}{1ppmV} \cdot \frac{86400s}{1day} \cdot \frac{P(bar) \cdot PM(g/mol)}{R\left({}^{bar \cdot l}/_{K \cdot mol}\right) \cdot T(K)}$$

Where:

dC/dt = Slope of the concentration curve versus time.
V = Net volume of the chamber (including the total volume through which the soil gas passes, i.e. sensor, pump and connection tubes).
P = Atmospheric pressure. One standard atmosphere = 1.01325 bar.
PM = Molecular weight of the gas (for CO_2 = 44.01 g/mol).
R = Gas constant for an ideal gas (0.08314510 bar L K^{-1} mol^{-1}).
T = Air temperature (K).

A summary of applicability and limitations of the accumulation chamber method when applied to CO_2 storage site is reported in Table 2.

Table 2 Summary of limitations of accumulation chamber method

Objectives	Detection limit	Applicability	Limitations	State of technology
Detects any flow from soil by, for example, infrared gas detectors	Detect CO_2 flux from 0.04 $g \cdot m^2 \cdot d^{-1}$	In-land and on surface (rivers, lakes) waters	The sample area is limited	Implemented by the scientific community
	There is background noise in the signal by biological activity. Detecting deep sources is usually carried out in winter (low activity) than in summer	Application in water layers being evaluated	Only provides an instantaneous measurement of system	
	It requires the completion of a pre-injection baseline for a long time (1 year or more) to understand local flow variations	Appropriate detectors can be used to measure the flow of other gases, e.g. CH_4, Rn, etc	Seasonal and temporal variation in measurement due to the difference in biological activity or environmental conditions	
	The flow measurements are performed on a small area ($\approx cm^2$). Punctual leakages may not detected	Equipments measuring diffuse soil CO_2 flow of at pre-set time intervals can be installed in fixed positions (useful to control the evolution of a leak)	Measurements are not effective if the soil is too wet or frozen	
			If there is a large and thick shallow aquifer. The leaks may not be detected due to the dilution of CO_2	
			Late detection of a leak	

5 Measurement Protocol

According to Lewicki [24], the methodology can influence the calculated value of CO_2 within the measurement area as well as the magnitude of the uncertainty associated with the estimator used. Likewise, in sites with strong winds the contact between the bottom of the chamber and soil surface must be sealed. If not, a dilution effect or an increased flux due to the Bernoulli effect can be provoked. Accumulation chamber users usually apply a concentric protective screen around the chamber. Alternatively, the chamber is positioned a few centimeters into the ground. Physical properties of the ground can change then a potential alteration in CO_2 flux can occur [25].

The studied area lies close to the village of Hontomín (Burgos, Spain). This area is located in the northeastern part of the Duero Basin, where Mesozoic, Cenozoic and Quaternary sedimentary rocks dominate (Sheet 167/19-9 Montorio, Geological Map of Spain, scale 1:50.000, IGME, 1991). The CO_2 injection is into a saline water-bearing stratum located at a depth of 1500 m.

Elio et al. [26] have suggested a measurement protocol aimed to minimize the error with the accumulation chamber method. Summarizing, four linear mixed models were used taking into account the following variables: (a) three different measurement approaches, (1) cleaning and immediate measurement, (2) non-cleaning and (3) cleaning and preparation of the sampling area, (b) different lithological features of the substratum and (c) the spatial situation where the flux is measured. The model selection was made according to the criteria of maximum likelihood, followed by different graphic and geostatistical studies [23]. Finally, the procedure validation campaigns were conducted.

In Fig. 2, the different steps to obtain an accurate measurement are reported.

- Using a trowel, the sampling area covered by the chamber is prepared by removing vegetation and the very first layer of the topsoil (1–2 cm).
- Waiting (about 1 h) to prevent flux perturbation due to the soil removal.
- Measuring until the concentration of CO_2 recorded by the instrument is approximately equal to that of the atmosphere. Then, the instrument is set to that value.
- Placing the chamber on the ground. The interested area is sealed with soil to prevent the entrance of air and avoid exchanges with the open atmosphere.

Fig. 2 Protocol of CO_2 measurement (**a**). Cleaning, (**b**). Waiting and (**c**). Measuring

- After the placement of the chamber, the increase in the concentration of CO_2 is measured inside the chamber within the allotted time span (ppm/s)
- The temperature and atmospheric pressure values are used to calculate the soil CO_2 flux in g m^{-2} day^{-1}.

6 Estimation of Total Output of Diffuse Soil CO_2 Flux

There is a wide range of methodologies that allow to estimate the total CO_2 flux output [14, 23, 27]. It is important to understand each of them in order to apply the most appropriate method for the studied area.

This is a critical task to detect and quantify leakages during operational and post-operational stages.

At least six statistical methods to evaluate the total CO_2 output can be applied, as follows: arithmetic mean, minimum variances unbiased estimator, bootstrap resample, partitioning of data into different populations with a graphical and a maximum likelihood procedures, and sequential Gaussian simulation

For the comparative study each method was applied to two scenarios. In natural analogues of CO_2 storage and in the Hontomín CO_2 Storage Technology Development Plant (Burgos, Spain), a total of eight field campaigns were carried out. The CCS site area is characterized by low CO_2 flux associated with biological activity (mean values from 5 to 13 $g \cdot m^2 \cdot d^{-1}$ [28]). In addition to the CO_2 flux, in each measurement point meteorological parameters such as pressure, temperature, relative humidity and wind speed were recorded.

The distribution of the CO_2 flux is usually characterized by different lognormal populations, which are related to different geochemical processes or CO_2 sources. The partitioning in different populations helps to differentiate background values of biological activity from deep geological sources. For example, in geothermal areas it is common to distinguish two populations, a background CO_2 flux and a hydrothermal high CO_2 fluxes connected to the degassing process from deep sources [23, 29].

Partitioning of CO_2 values into different lognormal population to estimate the parameters can be carried out by two methods. One based in the graphical Sinclair's method [29], representing the probabilistic graph, and a second one that applies a maximum-likelihood method [30, 31].

In Fig. 3 an example of isoflux CO_2 values in $g \cdot m^2 \cdot day^{-1}$ of Sequences Gaussian Simulation (sGs) applying a trans-Gaussian kriging to calculate baseline in Hontomin CO_2 Storage Technology Development Plant (Burgos, Spain) is shown. The sampling area is 625 ha with a regular grid of 100 by 100 m.

The estimation of the total CO_2 output is of paramount importance to quantify the magnitude of the leakage. The estimation procedure after measuring the CO_2 flux with the accumulation chamber is to apply a variogram analysis. If the relation between the data can be explained with the variogram, the best technique to calculate the total CO_2 output and its confidence interval is sGs. In the case that

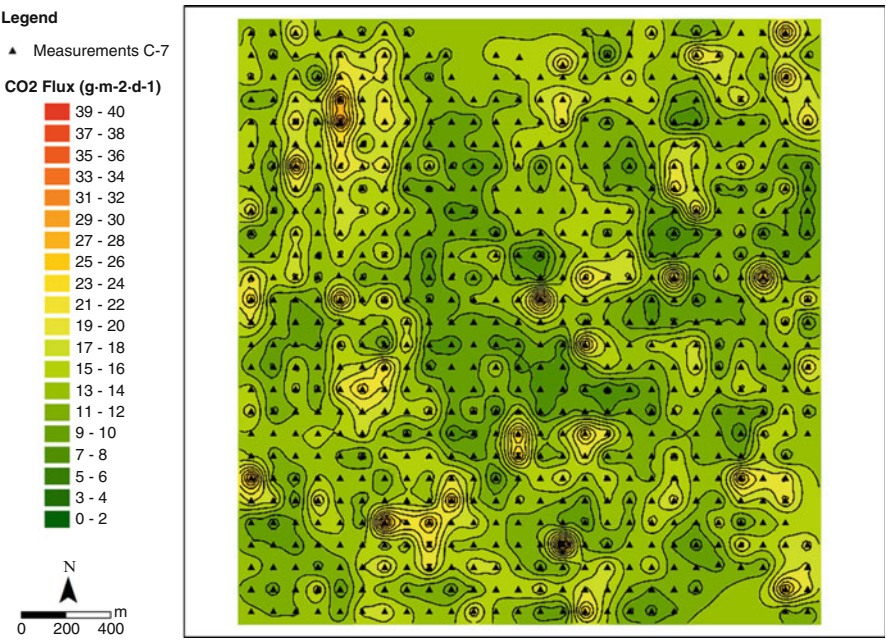

Fig. 3 Isovalues of CO_2 flux

the CO_2 flux data are independent (no variogram), their distribution is to be analyzed. For normal and log-normal distribution the most appropriate methods are the arithmetic mean and minimum variance unbiased estimator (MVUE), respectively. If the data are not normal (log-normal) or are a mixture of population the best method is the bootstrap re-sampling.

7 CO_2 Leakage and Expected Effects on the Groundwater Chemistry: Possible Modifications of Carbonate Equilibria

Similarly to what described for the definition of a geochemical baseline of the diffuse CO_2 soil flux, geochemical and isotopic data of ground waters collected at different depths during the pre-injection phase are considered a key pre-requisite to assess possible subsequent CO_2 leakages. This implies that pH values, alkalinity, major, minor and trace dissolved species are to be determined along with stable isotopic ratios of H_2O and stable and radiogenic isotopes of other dissolved solutes, e.g. sulfur and oxygen in sulfate, boron, strontium and so forth ([30] and references therein). Pre-injection monitoring by water geochemistry may also reveal the presence of seasonal variation and anthropogenic contributions, which cannot be neglected when evaluating the effects expected by a CO_2 leakage [7].

It is expected that if the injected CO_2 is leaking, the original carbonate equilibrium, i.e. TDIC (Total Dissolved Inorganic Carbon), pCO_2 and the related dissolved species such as H_2CO_3, HCO_3^- and CO_3^{2-}, can be modified.

The mass action law (Eq. 1) regulates the P_{CO2} interval in waters, as follows:

$$H_2CO_3^* = CO_{2(g)} + H_2O;\ K_H = \frac{f_{CO_2}}{a_{H_2CO_3^*}} = \frac{f_{CO_2}}{\left(m_{H_2CO_3^*} \cdot \gamma_{H_2CO_3^*}\right)} = 10^{+1.47} \quad 25\ ^\circ C \tag{1}$$

Where $H_2CO_3^*$ is referred to carbonic acid, which includes the true carbonic acid ($H_2CO_3^\circ$) and the dissolved molecular carbon dioxide ($CO_{2(aq)}$). K_H is the Henry constant of gaseous CO_2 to the content of H_2CO_3, the latter being the main acidic substance driving mineral dissolution reactions in most natural environments. Water-rock interaction processes progressively reduce the amount of carbonic acid, essentially mimicking an acid–base titration or a neutralization reaction, which leads to the conversion of both carbonic acid to the conjugate base, bicarbonate ion (Eq. 2), and the latter to carbonate ion (Eq. 3) at higher pH values:

$$H_2CO_3^* = HCO_3^- + H^+;\ K_1 = \frac{\left(a_{H^+} \cdot m_{HCO_3^-} \cdot \gamma_{HCO_3^-}\right)}{\left(m_{H_2CO_3^*} \cdot \gamma_{H_2CO_3^*}\right)} = 10^{-6.35} \quad 25\ ^\circ C \tag{2}$$

$$HCO_3^- = CO_3^{2-} + H^+;\ K_2 = \frac{\left(a_{H^+} \cdot m_{CO_3^{2-}} \cdot \gamma_{CO_3^{2-}}\right)}{\left(m_{HCO_3^-} \cdot \gamma_{HCO_3^-}\right)} = 10^{-10.33} \quad 25\ ^\circ C \tag{3}$$

Carbonic acid, total bicarbonate (and related complexes) and total carbonate ion (and related complexes) represent the Total Dissolved Inorganic Carbon (TDIC), which can be described by Eq. 4:

$$m_{TDIC} = m_{H_2CO_3^*} + m_{HCO_3^-} + m_{CO_3^{2-}} + \sum m_{HCO_3^- - complexes} + \sum m_{CO_3^{2-} - complexes} \tag{4}$$

As carbonic acid converts to the conjugate bases during weathering, TDIC remains constant only for closed systems with respect to $CO_{2(g)}$. This means that no loss/acquisition of gaseous CO_2 is occurring from an external reservoir and no carbonate minerals are precipitating. On the other hand, this process favours the increase of the water carbonate alkalinity, which can be expressed by the sum of total bicarbonate and total carbonate concentrations in equivalent units, as follows:

$$Alk_c = m_{HCO_3^-} + 2 \cdot m_{CO_3^{2-}} + \sum m_{HCO_3^- - complexes} + 2 \cdot \sum m_{CO_3^{2-} - complexes} \tag{5}$$

In open system, i.e. under natural conditions of constant supply of gaseous CO_2, e.g. biological activity and organic matter decomposition in soils, the acid-base neutralization process produces an increase in carbonate alkalinity and TDIC, the latter being generated by carbonate and silicate minerals such as those characterizing the sedimentary geological formations at Hontomín. Both the TDIC concentrations and $\delta^{13}C\text{-}_{TDIC}$ values will result to be affected by these processes. The carbon isotopic ratios may be changing when either isotope fractionation processes affect the transformation of carbon or mixing of carbon from different sources occurs. TDIC concentrations and $\delta^{13}C\text{-}_{TDIC}$ values are routinely used in studies of carbon geochemistry of natural waters.

Monitoring stable carbon isotopes and the subsequent determination of isotope mass balance allow to evaluate the fate of CO_2 and TDIC distribution in deep aquifers. This approach can be applied to several studies related to CCS [32–34]. The investigation of the isotopic carbons in dissolved CO_2 and TDIC related to surface, spring and well waters can be used in order to verify whether CO_2 leakages, induced by the injection of CO_2, are able to affect the quality of the waters in the local hydrological circuits [7] Thus, water and soil gas geochemistry are necessarily to be coupled as they play a key role in detecting CO_2 leakages from the reservoir since if occurring they may reach the shallow groundwater systems as well as the topsoil. As a consequence, measurements of TDIC concentrations, $\delta^{13}C\text{-}_{TDIC}$ and diffuse CO_2 soil flux are important CO_2 leaking tracers and should be considered when a geochemical monitoring will be designed.

For the water system, the establishment of a geochemical baseline through monitoring programs should include the acquisition of large spectrum of chemical and isotopic parameters (in particular those referring to the carbonate equilibria), before commencing the pre-injection of CO_2 for assuring that during operational and post-operational phases no modifications have occurred. The baseline geochemical parameters may be changing as an event of CO_2 leakage is occurring. Consequently, if the CO_2 plume released from the storing reservoir is interacting with the shallow groundwater system, the geochemical processes governing the water and dissolved gas composition will significantly be modified with respect to those recorded during the pre-injection phase.

8 Conclusions

Diffuse CO_2 soil flux measurements and water geochemical parameters, such as carbonate equilibria and the carbon isotopes of dissolved CO_2 and TDIC can be considered good tracers for CCS areas where large injection of CO_2 are involved. Monitoring activities of CO_2 soil fluxes may have some limitations due to the sensitivity of the accumulation chamber method as low leakages may be masked by seasonal and/or soil respiration variations if a proper pre-injection "geochemical baseline" is not performed. The carbonate equilibria can also be affected by similar variations but a recognizable increase in the (bi)carbonate species may be expected.

Carbon isotopic variations cannot be recorded in the case that the injected CO_2 is not isotopically distinct with respect to that recovered in the groundwater system.

Despite the limitations, which are however affecting any kind of monitoring surveys, geochemical investigations on soil gases and waters can be regarded as powerful tools for assessing CO_2 movements and potential leakages.

References

1. Dixon T, Romanak KD (2015) Improving monitoring protocols for CO_2 geological storage with technical advances in CO2 attribution monitoring. Int J Greenhouse Gas Control 41:29–40. doi:10.1016/j.ijggc.2015.05.029
2. Stenhouse MJ, Zhou W, Arthur R (2006) Assessment of the long-term fate of CO injected into the Weyburn field: system-level modeling of CO migration and potential impacts. In: Lombardi S et al (eds) Advances in the geological storage of carbon dioxide. Springer, Dordrecht, pp 231–242
3. Fouillac C (2005) Monitoring of geological storage of CO_2: protocols and research needs. European CO_2 capture and storage conference, Bruselas, 13–15 April 2005
4. IPPC (2005) IPCC special report on carbon dioxide capture and storage. In: Metz B, Davidson O, de Coninck HC, Loos M, Meyer LA (eds) Prepared by working group III of the Intergovernmental Panel on Climate Change. Cambridge University Press, Cambridge/New York, p 442
5. Hannis SD (2013) Monitoring of geological storage of CO2. In: Gluyas J, Mathias S (eds) Geological storage of carbon dioxide (CO2). Woodhead Publishing Limited, Cambridge
6. NETL (2009) Best practices for: monitoring, verification, and accounting of CO_2 stored in deep geologic formations. National Energy Technology Laboratory DOE/NETL-311/081508
7. Etheridge D, Leuning R, de Vries D (eds) (2005) Atmospheric monitoring and verification technologies for CO_2 storage at geosequestration sites in Australia, CO2CRC publication number RPT05-0134. Cooperative Research Centre for Greenhouse Gas Technologies, Canberra, p 83
8. Nisi B, Vaselli O, Tassi F, Elío J, Delgado A, Mazadiego LF, Ortega MF (2013) Hydrogeochemistry of running and spring waters in the Hontomín-Huermeces area (Burgos Spain). Int J Greenhouse Gas Control 14:151–168
9. Rose AW, Hawkes HE, Webb JS (1979) Geochemistry in mineral exploration, vol 2. Academic, London, 657 p
10. IPCC (2007) Climate change 2007: synthesis report. In: Core Writing Team, Pachauri RK, Reisinger A (eds) Contribution of working groups I, II and III to the fourth assessment report of the Intergovernmental Panel on Climate Change. IPCC, Geneva, 104 pp
11. Baxter PJ (1990) Medical effects of volcanic eruptions: 1. Main causes of death and injury. Bull Volcanol 52:532–544
12. Baxter PJ, Baubron JC, Coutinho R (1999) Health hazard and disaster potential of ground gas emissions at Furnas volcano, São Miguel, Azores. J Volcanol Geotherm Res 92:95–106
13. Melian Rodríguez GV (2008) Emisión difusa de dióxido de carbono y otros volátiles en el volcán Póas, Costa Rica, América Central. Tesis doctoral, Química analítica, nutrición y bromatología, Facultad de química, Universidad de la Laguna, Tenerife: División de Medio Ambiente, Instituto Tecnológico y de Energías Renovables (ITER)
14. Chiodini G, Cioni R, Guidi M, Raco B, Marini L (1998) Soil CO2 flux measurements in volcanic and geothermal areas. Appl Geochem 13(5):543–552
15. Farrar D, Neil JM, Howle JF (1999) Magmatic carbon dioxide emissions at Mammoth Mountain, California, Water-resources investigations. U.S. Geological Survey, Sacramento

16. Hui Yim M, Jin Joo S, Nakane K (2002) Comparison of field methods for measuring soil respiration: a static alkali absorption method and two dynamic closed chamber methods. For Ecol Manag 170:189–197
17. Klusman RW (2003) A geochemical perspective and assessment of leakage potencial for a mature carbon dioxide enhanced oil recovery project and as a prototype for carbon dioxide sequestration, Rangely field, Colorado. Editado por The American association of petroleum geologist. AAPG Bull 87(9):1485–1507
18. Klusman RW (2005) Baseline studies of surface gas exchange and soil-gas composition in preparation for CO2 sequestration research:Teapot Dome, Wyoming. Editado por The American Association of Petroleum Geologists. AAPG Bull 89(8):981–1003
19. Klusman RW (2003) Rate measurements and detection of gas microseepage to the atmosphere from an enhanced oil recovery/sequestration project, Rangely, Colorado, USA. Appl Geochem 18:1825–1838
20. Lewicki JL, Hilley GE, Oldenburg CM (2005) An improved strategy to detect CO2 leakage for verification of geologic carbon sequestration. Geophys Res Lett 32:L19403. doi:10.1029/2005GL024281
21. Klusman RW (2003) Evaluation of leakage potential from a carbon dioxide EOR/sequestration project. Energy Convers Manag 44:1921–1940
22. West Systems (2009) Portable diffuse flux meter. Handbook, release 8.0. Pontedera, November de 2009
23. Lewicki JL, Bergfeld D, Cardellini C, Chiodini G, Granieri D, Varley N, Werner C (2005) Comparative soil CO2 flux measurements and geostatistical estimation methods on Masaya volcano, Nicaragua. Bull Volcanol 68:76–90
24. Lewicki JL, Connor C, St-Amand K, Stix J, Spinner W (2003) Self-potential, soil CO2 flux, and temperature on Masaya volcano, Nicaragua. Geophys Res Lett (American Geophysical Union) 30(15):1817
25. Gerlach TM, Doukas MP, McGee KA, Kessler R (2001) Soil efflux and total emission rates of magmatic CO2 at the Horseshoe Lake tree kill, Mammoth Mountain, California, 1995–1999. Chem Geol 177:101–116
26. Elío J, Ortega MF, Chacón E, Mazadiego LF, Grandia F (2012) Sampling strategies using the "accumulation chamber" for monitoring geological storage of CO2. Int J Greenhouse Gas Control 9:303–311
27. De Bortoli D, Panosso AR, Pelegrino CE, Pereira GT, La Scala N (2011) Soil CO2 emission estimated by different interpolation techniques. Plant Soil 345:187–194
28. Elío J, Nisi B, Ortega MF, Mazadiego LF, Vaselli O, Grandia F (2013) CO2 soil flux baseline at the technological development plant for CO2 injection at Hontomín (Burgos, Spain). Int J Greenhouse Gas Control 18:224–236
29. Cardellini C, Chiodini G, Frondini F (2003) Application of stochastic simulation to CO2 flux from soil: mapping and quantification of gas release. J Geophys Res 108:2425
30. Benaglia T, Chaveau D, Hunter DR, Young DY (2009) mixtools: an R package for analyzing finite mixture models. J Stat Softw 32:1–29
31. Young DS, Hunter DR (2010) Mixtures of regression with predictor-dependent mixing proportions. Comput Stat Data Anal 54–10:2253–2266
32. Mayer B, Humez P, Becker V, Dalkhaa C, Rock L, Myrttinen A, Barth JAC (2015) Assessing the usefulness of the isotopic composition of CO2 for leakage monitoring at CO2 storage sites: a review. Int J Greenhouse Gas control 37:46–60
33. Becker V, Myrttinen A, Blum P, van Geldern R, Barth JAC (2011) Predicting $\delta^{13}C_{DIC}$ dynamics in CCS: a scheme based on a review of inorganic carbon chemistry under elevated pressures and temperatures. Int J Greenhouse Gas Control 5:1250–1258
34. Myrttinen A, Becker V, Barth JAC (2012) A review of methods used for equilibrium isotope fractionation investigations between dissolved inorganic carbon and CO_2. Earth Sci Rev 115:192–199

CO_2 Storage Capacity Estimates for a Norwegian and a Swedish Aquifer Using Different Approaches – From Theoretical Volumes, Basin Modelling to Reservoir Models

Ane E. Lothe, Per E.S. Bergmo, Benjamin U. Emmel, and Gry Møl Mortensen

Abstract Open dipping aquifers might offer a unique possibility to store huge quantities of carbon dioxide. Many different modelling approaches have been used to quantify possible storage capacities often giving very diverse results. In this study, we applied three different methods to calculate and model theoretical volumes, structural trapping volumes using a basin modelling tool and capacities obtained from dynamic reservoir simulations. We tested end-member scenarios for different critical parameters. The results for two stratigraphic confined open/semi-closed dipping saline aquifers, the Garn Formation (Norwegian Sea, Norway) and the Faludden sandstone (Baltic Sea, Sweden) show broad variations. For the Garn Formation CO_2 storage capacities vary from 2.0 to 8.4 Gt. Taking into accounts all results, we estimated a representative storage capacity ranging between 2.0 and 3.5 Gt. In the case of the Faludden sandstone the different modelled scenarios give a spread from 10 to 836 Mt and a representative capacity of 250–435 Mt was defined. We will show and discuss how the different estimates are calculated, how they are related to each other and finally exclude unreliable results. Furthermore we compare our results with published data from the same areas. This will demonstrate the complexity and difficulty of a direct comparison of geological CO_2 storage estimates and pinpoint to the need for a general strategy to compare modelling results for geological CO_2 storage estimates.

A.E. Lothe (✉) • P.E.S. Bergmo • B.U. Emmel
SINTEF Petroleum Research, Sluppen, P.O. Box 4763, 7465 Trondheim, Norway
e-mail: ane.lothe@sintef.no

G.M. Mortensen
Sveriges geologiska undersökning (SGU), Kiliansgatan 10, 223 50 Lund, Sweden

V. Vishal, T.N. Singh (eds.), *Geologic Carbon Sequestration*,
DOI 10.1007/978-3-319-27019-7_6

1 Introduction

In the coming years underground storage of carbon dioxide in sedimentary basins is required to reduce global warming. The International Energy Agency released in their *Energy Technology Perspectives 2012* [1] actions required for their goal to limit the average global temperature increase by 2 °C until 2050. In a business-as-usual scenario, the temperature would increase up to 6 °C until 2050. To avoid such a scenario a drastic reduction of CO_2 emission is required. Thereby, carbon capture and storage (CCS) should contribute to one-sixth of CO_2 emission reduction until 2050, and 14 % of the cumulative emission reduction between 2015 and 2050. For OECD Europe, this implies that 1.4 Gt CO_2 needs to be captured and stored until 2030 and 10.2 Gt until 2050. In order to fulfil these requirements for OECD Europe mapping, characterisation and modelling of saline aquifers for CO_2 storage have to be performed. Since the early nineties, the evaluation of potential locations for CO_2 storage in sedimentary basins have been carried out for Western Europe [2, 3] the Norwegian continental shelf [4, 5] and Swedish aquifers [6, 7]. The evaluation of geological CO_2 storage capacities can be described in a step-wise manner. Beginning with the first estimates during a screening phase towards a final estimate during the injection phase when a reservoir is evaluated in detail and possible test injections have been made (Fig. 1). However, carbon storage in sedimentary basins deals with many uncertainties which can only be monitored by well data, indirect by seismic interpretation and be evaluated by mathematical modelling and numerical simulations describing the subsurface CO_2 flow and dissolution behaviour. These models are often based on a wide variety of assumptions and approaches leading to variable estimates at different stages of the storage capacity evaluation which might confuse the reader.

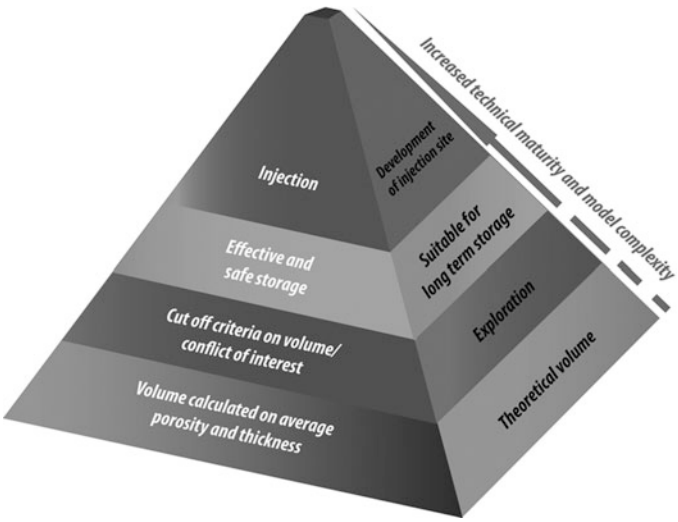

Fig. 1 The maturation pyramid picturing the step-wise approximation to evaluation of CO_2 storage suitability and capacity [5]

In this contribution we will introduce calculations and modelling results describing the climbing from the base of the CO_2 storage maturation pyramid to a higher level (Fig. 1). We will show and describe the different estimates for the Garn Formation (Fm.) (Trøndelag Platform, Norway) and the Faludden sandstone (Baltic Sea, Sweden). Both study areas are very large (Trøndelag Platform ca. 15,000 km^2, Faludden member ca. 33,000 km^2) and might be capable of storing huge quantities of CO_2. We will focus on some key aspects that can have a large impact on possible storage capacity e.g., the effect of sealing faults on trap capacities, the dissolution of CO_2 into the formation water and the residual trapping during migration.

2 Definition of Trapping Mechanisms

Saline aquifers suitable for CO_2 storage should (i) have sufficient porosity and permeability to allow injection of large volumes of CO_2 (ii) be located below a certain depth (temperature dependent) so that the injected CO_2 stays in liquid or supercritical phase and (iii) be overlain by a sealing formation to prevent migration to shallower stratigraphic units, the surface or the sea floor. The CO_2 storage capacity evaluation of a formation can be classified [8] by technical and economic feasibility and maturity (Fig. 1).

The main CO_2 trapping mechanisms in deep geological formations can be divided into structural and stratigraphic trapping (Fig. 2), residual trapping, solubility trapping and mineral trapping [8]. (1) Structural and stratigraphic trapping occurs when CO_2 is immobilised by capillary forces below sealing layers of rocks (Fig. 2). Residual trapping immobilises the CO_2 also by capillary forces in the pore space as residual gas saturation. (2) Solubility trapping occurs when CO_2 dissolves in the formation water which again enables further mineral trapping. The duration and influence on the total storage budget for these trapping mechanisms might vary depending on geological setting and operational parameters.

3 Methodologies

For storage capacity estimates several approaches can be applied depending on the size of the study area, dominating type of trapping mechanisms and the amount of available data. Here we focus on the theoretical volume calculations, modelling of structural trapping capacities and finally injection of CO_2 and simulation of migration in a full dynamic reservoir model.

3.1 Theoretical Volumes

A common approach to calculate the theoretical volume is to use an efficiency factor which represents the assumed fraction of pore volume that will be occupied

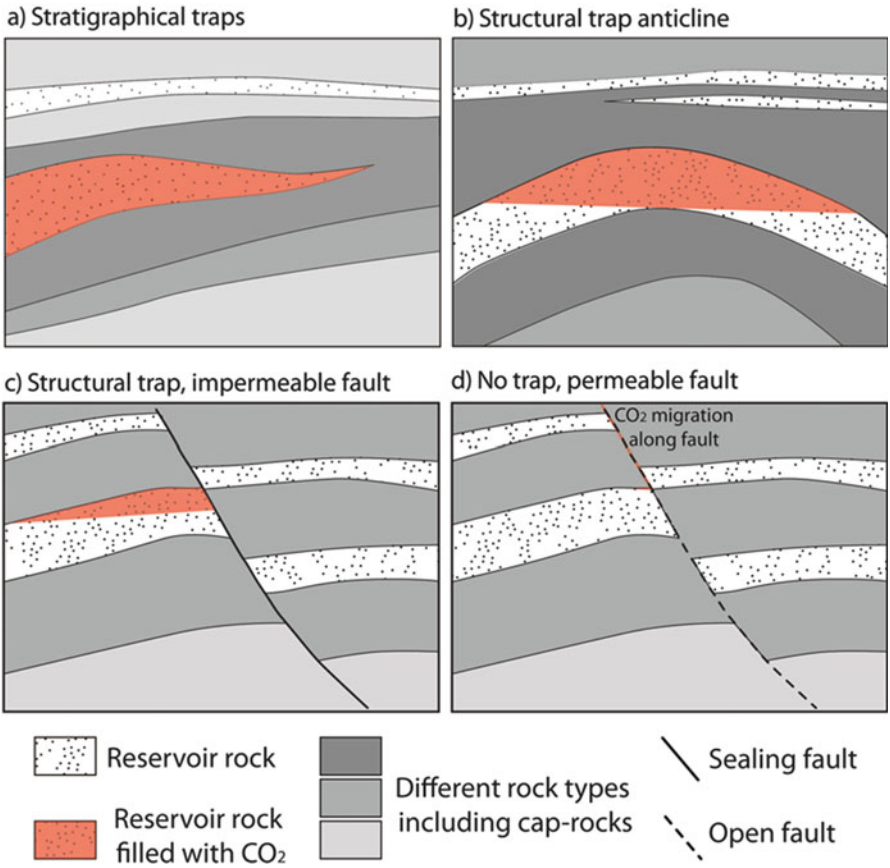

Fig. 2 Different structural and stratigraphic trap types for CO_2 storage (**a**) Stratigraphical maps. (**b**) Structural trap anticline. (**c**) Structural trap impermeable fault. (**d**) No trap permeable fault (Modified from [5])

by CO_2 [8]. The U.S. Department of Energy [9] has proposed the following equation for calculating the mass of CO_2 that can be stored:

$$M_{co_2} = Ah\phi\rho_{co_2}\mathrm{E}$$

Where M_{CO2} is the mass of CO_2, A is the area of interest, h is net height of storage formation, ϕ is the porosity, ρ_{CO2} is the density of CO_2 at storage conditions and E is the storage efficiency factor. The parameters h, ϕ, ρ_{CO2} can vary within a storage aquifer and are not known in detail; therefore average values have to be used. Additionally, E will vary for different storage sites depending on characteristics of the storage aquifer, characteristics of the confining aquifers, storage operations and regulator constrains [see detailed overview in 10]. The value of

the storage efficiency factors reported in the literature varies in a wide range from <1 to >10 %, by a factor of 20 and even higher and no single set can be universally used [10].

3.2 Structural Trapping Volumes – SEMI

In order to estimate the structural trapping volumes we used the basin modelling tool SEMI [11]. The software has been developed to model hydrocarbon migration and exploration risk over geological time scales. It uses a ray-tracing technique to migrate fluids and gases within a reservoir unit below sealing cap-rocks. The technique uses the dip of the top reservoir unit to determine pathway directions. Phase pressure, volume and temperature are computed for each trap during the simulations. To quantify CO_2 structural trapping volumes [12] the SEMI methodology was enhanced by including (i) trapping of CO_2 along migration pathway and (ii) dissolution of CO_2 at gas-water-contact within trap entities [13]. The simulator workflow starts with tracking every migration path within the storage unit and correspondingly identifies all drainage areas. The injected CO_2 will then migrate towards its nearest trap structure along the identified paths. If the CO_2 volume is larger than the trap capacity, the remaining volume of CO_2 will be spilled along a path till a neighbouring trap structure. These processes will take place, till no more CO2 volume is left to migrate.

3.3 Reservoir Simulation – Eclipse

The ECLIPSE 100 reservoir simulator from Schlumberger is used to perform dynamic modelling of CO_2 injection into deep saline aquifers. The simulator is fully implicit; three phases three dimensional which simulate all trapping mechanism involved in CO_2 storage except mineral trapping. For a detail description of the capabilities and applied methods we refer to the ECLIPSE user manual [14].

4 Geological Setting of the Storage Units

Two study areas have been chosen to present the work-flow for the different capacity estimates (Figs. 3 and 4). The Trøndelag Platform is located offshore mid Norway (Fig. 3a). The part of the Platform which was included in the modelling study covers an area of ca. 15,000 km^2. The water depth is between ca. 80 and 515 m and the storage unit is at a depth of ca. 1.2–1.75 km.

The Faludden storage unit is located within the Baltic Sea offshore south-eastern Sweden (Fig. 4a). The whole study area covers an area of ca. 33,000 km^2 but only ca. 11,000 km^2 are below a depth of 800 m [17]. The storage unit is at an average depth of ca. 0.83 km.

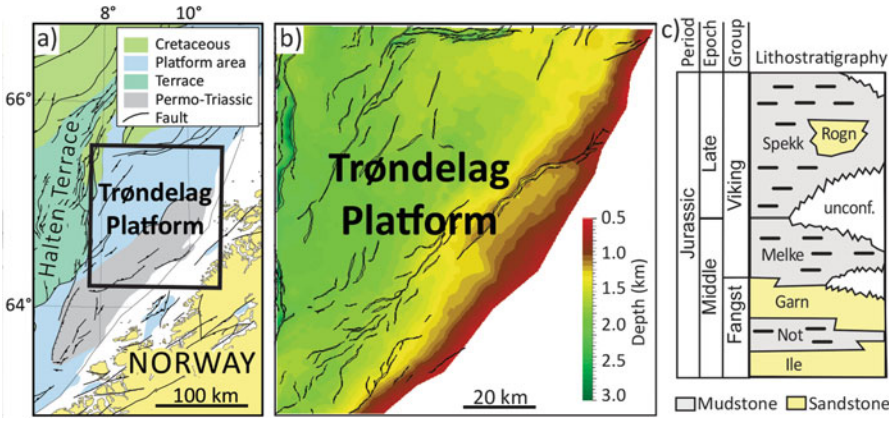

Fig. 3 Location of the Trøndelag Platform, offshore Mid-Norway (**a**). (**b**) Depth map of the top Garn Formation with faults as *black lines*. (**c**) Simplified lithostratigraphic column of the Norwegian Sea [15]

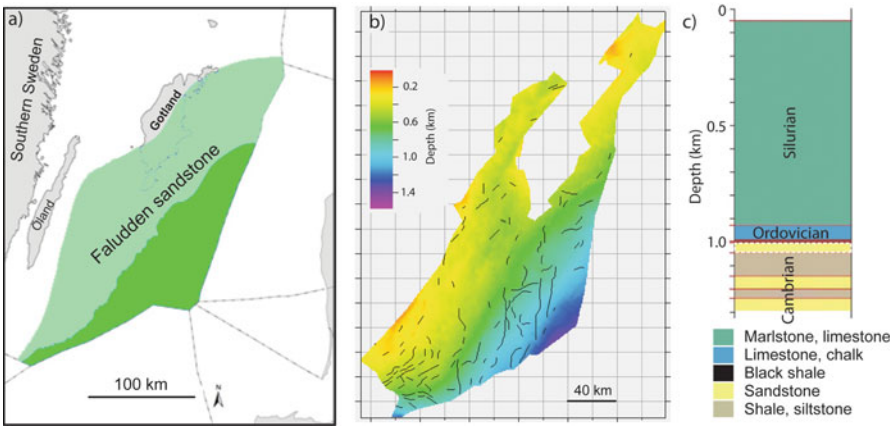

Fig. 4 (**a**) The Faludden sandstone is situated offshore south-east Sweden. (**b**) Depth map of the top Faludden sandstone (km) with faults marked as *black lines* (**c**) lithostratigraphy from well B-9 (Based on [16])

4.1 Garn Fm. – Trøndelag Platform

The Middle Jurassic sandstones of the Garn Fm. have been deposited in a near shore, wave dominated shallow marine environment. The sandstones are medium to coarse grained, moderately to well-sorted interlayered by mica-rich zones [15]. At the Halten Terrace area (Fig. 3a) at a depth <2.2 km, the Garn Fm. has porosities varying between 25 and 34 %, and permeability's (Klingenberg method) ranging from 1129 mD to 13,451 mD [18]. However, an average permeability of 400 mD is

reported by [5]. The thickness of the Garn Fm. in type well 6407/1-3 is 104 m, but may increase up to ca. 150 m on the Trøndelag Platform [5]. Average net to gross ratio from exploration wells is estimated to be 0.85. Above the Garn Fm., mudstones and shales of the Viking Group with Melke and Spekk formations provide a good seal for the reservoir unit (Fig. 3c). Thick sequences of Cretaceous and Tertiary fine-grained sedimentary deposits and Quaternary glacial deposits overlie the Viking Group. As a response to Neogene erosion events the Mesozoic and Early Cenozoic succession crop out at the seafloor directly beneath Quaternary deposits close to the Norwegian coast (Fig. 3a). Thus, the migration through the formation has to be evaluated carefully.

4.2 Faludden Sandstone – Baltic Sea

The Faludden sandstone was deposited in Middle Cambrian times in the Baltic syneclise which is the largest tectonic element within the south-western margin of the East-European Craton [19].

The sandstone was deposited in a relatively stable tectonic environment with slow and uniform sedimentation resulting with a high homogeneity over a large area. The sandstone was deposited near shore and has a basin wards progradation from east to west. Minor variations represented by interbeds of shale and siltstone reflect distance to the palaeo- shore line, fluvial and deltaic influences and water depths [20]. The Faludden sandstone has a large lens shaped distribution, weakly dipping ($<1°$) towards the east-south-east. In the Baltic Sea the Faludden sandstone is pinching out in a north-east to south-west line between the islands of Gotland and Öland (Fig. 4b). Beneath the island of Gotland it is at depth of ca. 400 m and in the deepest part offshore Sweden at a maximum depth of ca. 1000 m. Thickness varies from 1 to 49 m increasing towards the Swedish south-eastern border. Average thickness is 10 m onshore and 45 m offshore [16].

The Faludden sandstone consists of a clean, fine- to medium- grained, well sorted, calcite cemented quartz sandstone with local interbeds of shale and siltstone. In general, the upper 3–5 m of the sandstone is very hard and clayey with low porosity [16]. The estimated net to gross ratio is as high as 90 % [17] and silica oxide content is between 85 and 98 % [20]. Maximum bottom hole temperature is in the range from 30 to 35 °C indicating a geothermal gradient of ca. 30–50 °C/km. Logs together with well cores show porosities from 8 to 20 % with an average of 14 %, and permeabilities between 0.67 and 1255 mD, averaging 147 mD. The Faludden sandstone sequence is followed by ca. 80 m Ordovician limestone, with bentonitic limestone in the bottom (ca. 50 m), which is overlain by ca. 500 m of Silurian marlstone (Fig. 4c).

5 Model Set Up

For all approaches we used the same surface and fault maps to calculate the storage volume. However, we varied some specific parameters and modelling assumptions. The input parameters are given in Tables 1 and 2.

5.1 Garn Fm. – Trøndelag Platform

To calculate the theoretical volume for the Gran Fm. we used a net height of the storage formation of 127 m, an average porosity of 34 %, and a CO_2 density at storage conditions of 0.65 g /cm3 and a storage efficiency factor varying between 0.5 and 2 % (Table. 1). To estimate the structural trapping volumes, we used the interpreted top Garn Fm. map, the present seabed map and an interpreted fault map

Table 1 Input parameters for modelling of CO_2 storage volumes of the Garn Formation

Parameters	TV	STV (SEMI)	RM (ECLIPSE 100)
Average net permeability (D)		1	0.05–10, a log linear relation between porosity and permeability
CO_2 density at storage conditions [g/cm^3]	0.65		pVT properties for CO_2 from Span & Wagner, 1996
Polygon fault map		Interpreted fault map at top Garn Formation	Interpreted fault map at top Garn Formation
Porosity [%]	34	Compaction curve from Sclater and Christie (1980) calibrated vs. data from Ehrenberg (1990)	15–41 % (depth dependent); Ehrenberg (1990) with cut-off at 41 %
Pressure [MPa]		Hydrostatic conditions	Hydrostatic conditions
Storage efficiency [%]	0.5–2.0		
Surface temperature [°C]		4	4
Thermal gradient [°C/km]		40	40
Thickness maps[a] [m]	127	127	127
Top reservoir map		Interpreted top Garn Formation seismic map (surface)	Interpreted top Garn Formation seismic map (surface)
Total injected CO_2 [Mt]		Infinite	3500–7000
Water depth [m]		Present day seabed	Present day seabed

For theoretical volumes (*TV*) we used average formation properties, the structural trapping volumes (*STV*) were modelled with SEMI and for the reservoir model (*RM*) we used ECLIPSE 100
[a]Well date from six wells: 64076-3, 64076-5, 64076-4, 64076-1, 64079-7, and 6408/4-1

Table 2 The parameters used for modelling of CO_2 storage volumes of the Faludden sandstone

Parameters	TV	STV (SEMI)	RM (ECLIPSE 100)
Average net permeability [mD]		147	147
CO_2 density at storage conditions [g/cm^3]	0.662		P VT properties for CO_2 from Span & Wagner, 1996
Polygon fault map		Interpreted fault map at top Faludden sandstone	Interpreted fault map at top Faludden sandstone
Porosity [%]	14	14	14
Pressure [M Pa]		Hydrostatic conditions	Hydrostatic conditions
Reservoir thickness [m]	41	Thickness map	Thickness map
Surface temperature [°C]		4	4
Storage efficiency [%]	0.5–2.0		
Thermal gradient [°C/km]		40	40
Top reservoir map		Interpreted top Faludden sandstone map (surface)	Interpreted top Faludden sandstone seismic map (surface)
Total dissolved salts		–	0.6
Total injected CO_2 [Mt]		Infinite	250–500
Water depth [m]		Present day seabed	Present day seabed

Abbreviation, see Table 1. Surfaces and fault maps were constructed from interpreted seismic and well data [16, 17], bathymetric maps [21], and the thickness map for the Faludden sandstone [20] and further reworked

at top Garn Fm. (Fig. 3b). The horizontal grid dimension was 200 m × 200 m. Furthermore, we introduced a "pseudo" CO_2 layer below the storage unit in order to guarantee maximum filling of the structures [12]. Two end-member models were performed assuming open and sealing faults.

Log data and the interpreted top Garn Fm. map (Fig. 3) have been used to build a 3D reservoir model with grid dimension 500 m × 500 m. Vertical layer thickness below the top is in average 16 m. Faults were implemented as geometrical characteristics but with no transmissibility modifications. Net-to-gross values were set between 0.7 and 1 with random variation in the storage layer (Fig. 5a). Two scenarios were tested: A high permeability scenario assuming permeabilities from 0.5 to 10 D (Fig. 5b). A total amount of 3.5 Gt CO_2 was injected into 34 wells (Fig. 5c). In the second scenario we injected 7 Gt of CO_2 into the same well locations but assuming lower permeabilities (50–1000 mD).

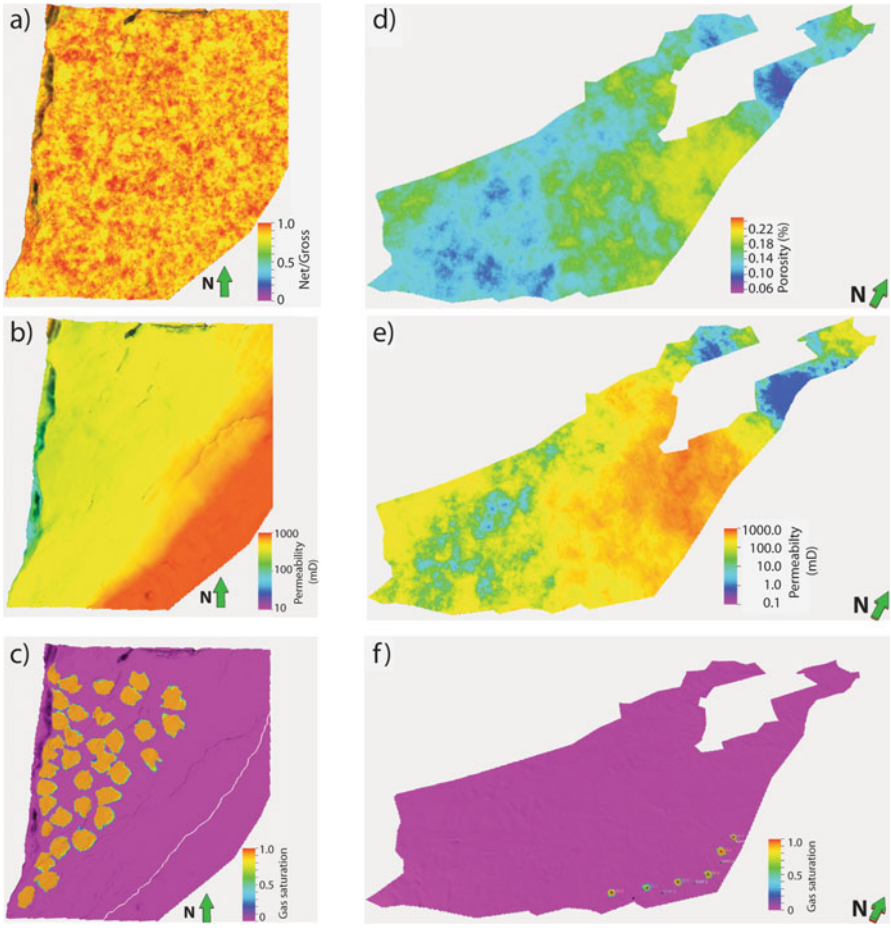

Fig. 5 Examples of input parameters into the reservoir model for the Garn Fm. (**a**, **b**, **c**) and the Faludden sandstone (**d**, **e**, **f**). Maps for Garn Fm. represent (**a**) net/gross, (**b**) permeability and (**c**) CO_2 plumes after the injection of 7 Gt. Maps for Faludden sandstone shows: (**d**) porosity, (**e**) permeability, (**c**) CO_2 distribution at top of the Faludden sandstone 10 years after the injection started. Additionally the locations of injection and production wells are shown

5.2 Faludden Sandstone- Baltic Sea

To calculate the theoretical volume for the Faludden sandstone we used a net height of storage formation of 41 m, an average porosity of 14 %, a CO_2 density at storage conditions of 0.662 g/cm^3 and a storage efficiency factor varying between 0.5 and 2 % (Table 2).

For the modelling of structural trapping volumes, we used a map of interpreted seismic horizons at top Faludden sandstone, a thickness map, the present day

seabed, and an interpreted fault map at top of the Faludden sandstone (Fig. 4b). The horizontal grid dimension was set to 500 m × 500 m. In the same way as described for the Garn Formation, we introduced a "pseudo" CO_2 layer below the reservoir unit in order to guarantee maximum filling of the structures [12]. Two end-member models were performed assuming open and sealing faults. The net-to-gross value was set to 0.9.

The reservoir model for the Faludden aquifer unit has been constructed using available well and seismic map data. Capillary pressure between CO_2 and water was set to zero [22]. A simulation grid with approximately 1.3 million grid blocks has been constructed based on the top Faludden depth surface, the Faludden isopach map and the interpreted fault lines. The lateral grid block resolution is 500 × 500 m and the grid has four layers with the upper two layers refined to 1 m thickness. Based on the interpretation from available well logs, the reservoir model was populated using a stochastic Gaussian distribution function to add heterogeneity into the model. Only one realisation with the given reservoir properties has been generated (Fig. 5d, e).

To represent the part of the formation not included in the model, pore volumes of the boundary grid blocks to the East and South-East has been increased by a factor of 500 (pore volume multiplier). This is more than a doubling of the total pore volume of the formation. This will help dissipate the induced pressure from injecting CO_2 into the formation. However, to enable a relatively high injection rate and better utilisation of the storage resource, water production wells are required to keep the injection pressure below an assumed safe pressure limit (75 % of lithostatic pressure). A series of test runs were performed to optimise the location, number and rates for injection wells. In addition, five production wells producing at constant bottom hole pressure (hydrostatic pressure) were positioned down-flank from the injectors. Figure 5f displays CO_2 saturation at the top, after 10 years injection indicating the positions of the injection and production wells.

Two final scenarios were simulated. For both the scenarios the injection rates are the same with 1 Mt/year for the four central wells and 0.5 Mt/year for the northernmost and southernmost wells (Fig. 5f) but we modelled different injection periods: (i) scenario one: 250 Mt CO_2 over 50 years; (ii) scenario two: 500 Mt CO_2 over 100 years.

After the end of injection the simulation was run for a total of 6000 years to model the migration of CO_2 towards the shallower regions, the dissolution of CO_2 in the formation water and the residual trapping of the migrating CO_2.

6 Results

In this article we report total storage capacity results for the theoretical volume, the structural trapping volumes and capacities obtained from simulations on formation reservoir models. For the structural trapping volumes we present the

results of two end-member models assuming sealing or closed faults. We point out that all results are based on different assumptions and model complexities which have to be taken into account during the interpretation of these results. An important assumption counting for all modelling approaches is that the reservoir unit is overlain by sealing cap-rocks preventing vertical CO_2 migration out of the reservoir unit.

6.1 *Storage Capacities for the Garn Fm. – Trøndelag Platform*

The theoretical CO_2 storage capacity for the Garn Fm. ranges between 2.1 and 8.4 Gt (efficiency factors between 0.5 and 2 %). For the structural trapping volumes modelling, results indicate a capacity of ca. 2.0 Gt for the no faults scenario and a significantly higher value of 5.2 Gt if sealing faults were taken into account (Fig. 6).

Also in the reservoir simulation approach we tested two scenarios (high and low permeability). In the high permeability scenario (0.5–10 D) 3.5 Gt CO_2 were injected. After 3000 year 23.5 % were dissolved and 0.1 % migrated to a depth shallower than 800 m (Fig. 7a, 8a). In the low permeability scenario (50–1000 mD) we injected 7 Gt CO_2. After 3000 year 22.1 % was dissolved and 1.4 % reached depths shallower than 800 m (Figs. 7b and 8b). Storage efficiency factors obtained from reservoir simulations indicate values between 0.8 and 1.7 %.

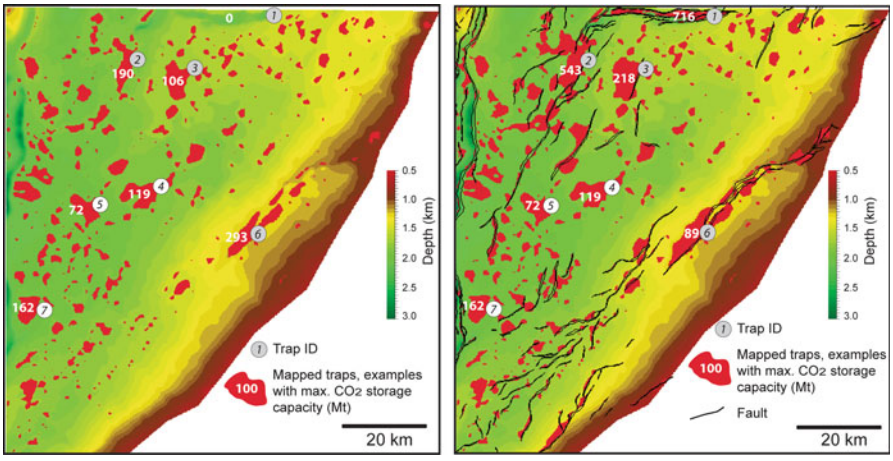

Fig. 6 Modelled structural trapping of CO_2 shown on the Garn Fm. depth map, with the area "flooded" with CO_2 and all traps were filled. (**a**) First scenario without faults: a total trap storage capacity of ca. 2.0 Gt was modelled. (**b**) The scenario with sealing faults gave a total trap storage capacity of ca. 5.2 Gt [12]

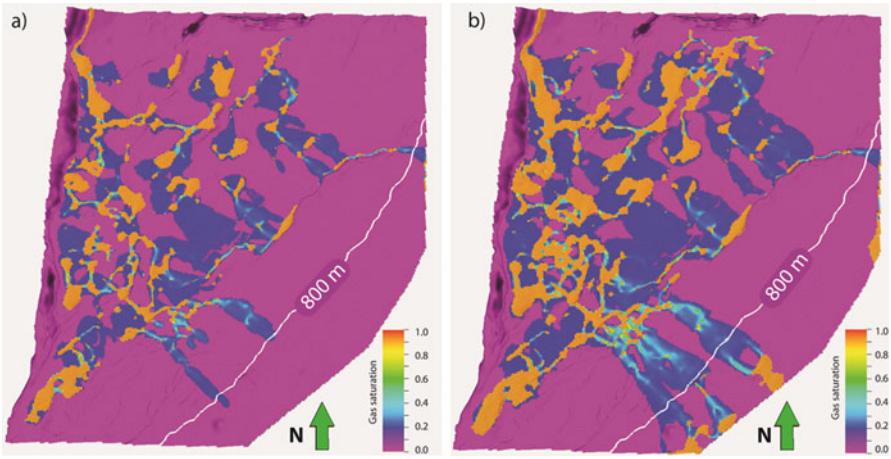

Fig. 7 Results of the reservoir models for the Garn Fm. 3000 years after CO_2 injection. (**a**) The high permeability scenario where 3.5 Gt of CO_2 were injected. (**b**) The low permeability scenario with 7 Gt CO_2 injected

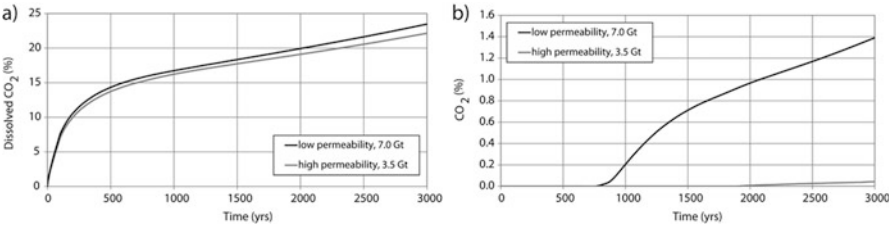

Fig. 8 Results of the two reservoir modelling scenarios for the Garn Fm. (**a**) Showing the percentage of dissolved CO_2 after the injection. (**b**) Depicts the percentage of injected CO_2 which migrated into an area shallower than 800 m

6.2 Storage Capacities for the Faludden sandstone – Baltic Sea

For the Faludden sandstone we report for the theoretical and structural trapping capacities values for the whole reservoir unit and the part situated deeper than 800 m. The theoretical CO_2 storage capacity varies between 0.63 and 2.46 Gt. For the part below 800 m the estimated volumes range from 209 to 836 Mt (for storage efficiency factors of 0.5 and 2 %).

The structural trapping volume for the open fault scenario is 561 Mt. Thereby the traps below 800 m can only store 10 Mt. If sealing faults are assumed, the total values increase to 602 Mt for the whole sandstone and 70 Mt for the area deeper than 800 m (Fig. 9).

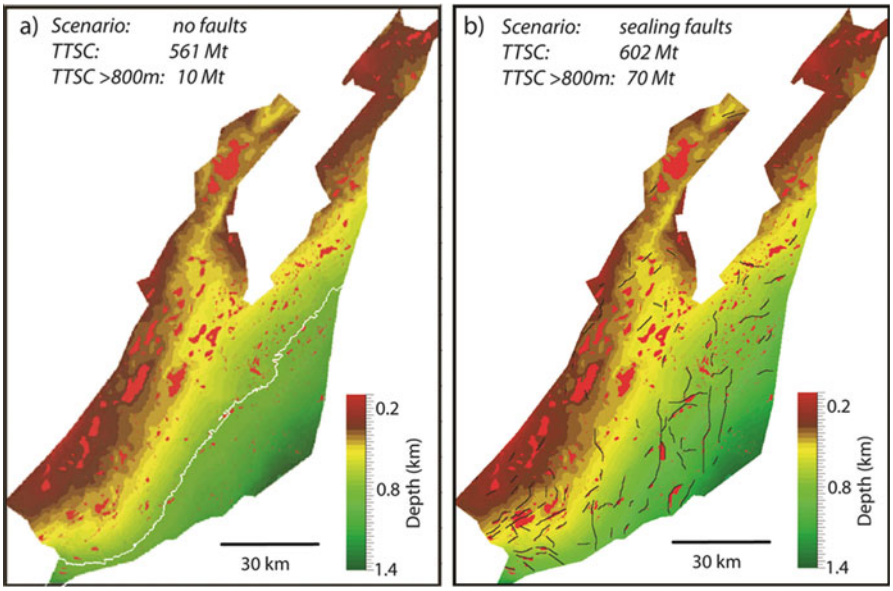

Fig. 9 Estimates of the total trap storage capacity (TTSC) for the Faludden sandstone with (**a**) open faults and (**b**) sealing faults. The maps are top surfaces of the Faludden units overlain by traps (*red areas*), *black lines* are faults (**b**) and the *white line* is (**a**) the 800 m depth isoline

For both reservoir modelling scenarios parts of the injected CO_2 migrate to structural traps that are shallower than 600 m (Fig. 10). In scenario one (250 Mt CO_2) 4.1 % of the injected CO_2 ends up in traps shallower than 600 m and 9.1 % is located in the depth region between 600 and 800 m. For scenario two (500 Mt CO_2) 13 % ends up in traps shallower than 600 m and 10.8 % is located between 600 and 800 m (Fig. 11). Note that a large part of the injected CO_2, is capillary trapped as residual gas (Fig. 10; blue colour saturation). Figure 11a shows the amount of dissolved CO_2 in the two cases. After 6000 year the total amount of dissolved CO_2 is 39 % for scenario one and 42.5 % for scenario two. Storage efficiency factors obtained from reservoir simulations indicate values between 0.45 and 0.9 %.

7 Discussions

In terms of CO_2 storage, the Garn Fm. and the Faludden sandstone represent stratigraphic confined open/semi-closed dipping saline aquifers with large lateral distributions. Such aquifers might be capable to trap and to solve huge volumes of CO_2. However, in public perception CO_2 injection in saline aquifers might be associated with potential risks such as brine/CO_2 leakage into shallow drinking water aquifers [23], induced seismicity [24] and pollution of seawater [25]. Thus,

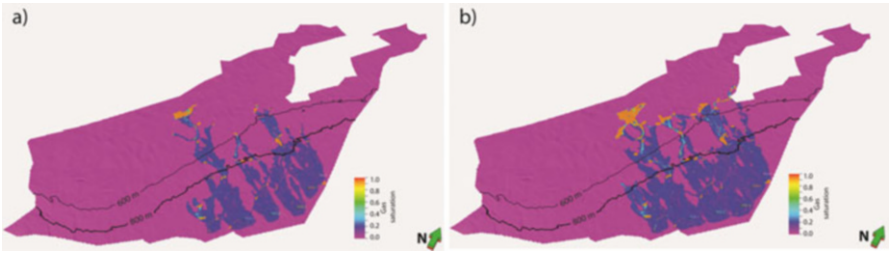

Fig. 10 CO_2 saturation after 6000 years in the case with (**a**) 250 Mt CO_2 injected and (**b**) 500 Mt CO_2 injected

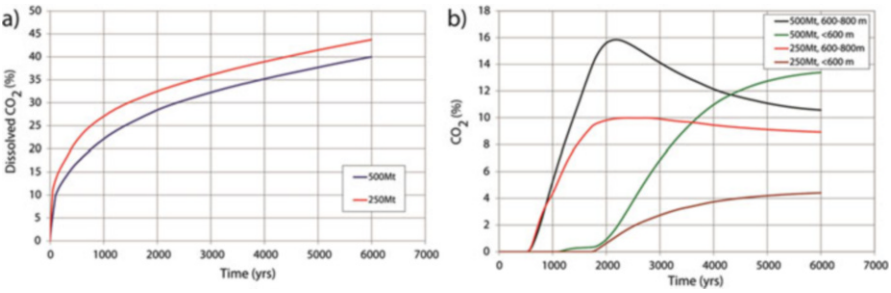

Fig. 11 Results of the reservoir modelling scenarios for the Faludden sandstone. (**a**) Shows percentage of dissolved CO_2 vs. time (years) after the injection. (**b**) Percentage of injected CO_2 which migrated into areas 600–800 m and <600 m

the CO_2 storage potential of these aquifers has to be evaluated in detail taking into account different trapping mechanisms and different modelling assumptions.

Here we present three approaches from two different areas varying the most uncertain parameters. The estimated storage volumes show a very broad variation. For the Garn Fm. volumes vary between 2.1 and 8.4 Gt and for the Faludden sandstone capacity estimates span from 10 to 836 Mt (Fig. 12). These numbers illustrate the complexity of the problem and challenge the trust in the significance of this data. As mentioned above, the interpretation of these modelling results is intricate and thus we will first discuss our own results in Sect. 7.1 before we compare the data with published estimates in Sect. 7.2.

7.1 Comparison of Different Storage Capacities

7.1.1 Garn Fm

The theoretical capacity estimates assuming an efficiency factor of 2 % revealed the highest values of ca. 8.4 Gt. Compared to the other modelling results and the estimates of the reservoir simulations (0.8–1.7 %) this seems to be rather unrealistic

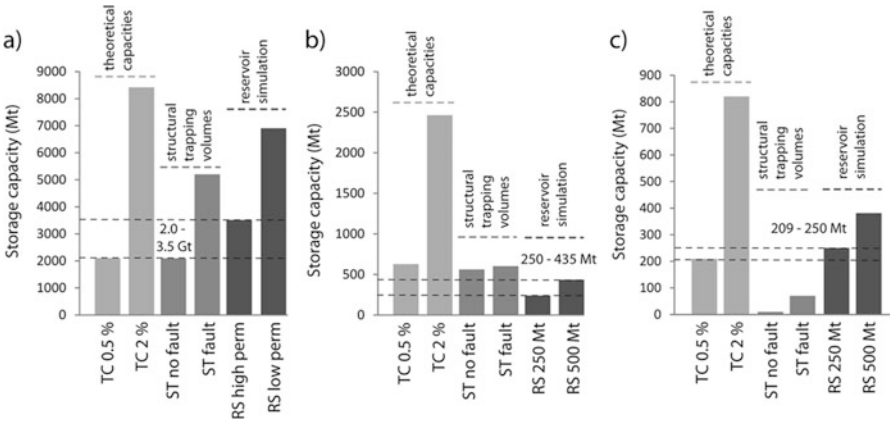

Fig. 12 Comparison of the results of the modelling approaches. (**a**) Capacity estimates for the Garn Formation (**a**), the whole Faludden sandstone (**b**), and parts of the Faludden aquifer >800 m (**c**). The dashed line indicates the lowest modelled storage capacities and volumes are given. Abbreviations: TC 0.5 % and 2 %: theoretical capacity applying an efficiency factor of 0.5 % and 2 %; *ST no fault*: structural trapping assuming open faults; *ST fault*: structural trapping assuming sealing faults; *RS high perm*: reservoir simulation with high permeability scenario; *RS low perm*: reservoir simulation with low permeability scenario; RS 250 Mt and RS 500 Mt: reservoir simulation injecting CO_2 over a period of 50 year and 100 year

and a lower efficiency has to be assumed. In the Garn Fm. the structural trapping has a huge influence on the final storage capacity. Hereby, especially the fault sealing properties influences migration pathways and storage capacities. Modelling results suggest a 2.6 times higher structural trapping capacity if the mapped faults are sealing (Fig. 7a, b). Varying closed and open faults, some traps show major variations e.g. trap 1 is not filled with open faults whereas up to 716 Mt of CO_2 can be trapped if all faults are sealing (Fig. 7a, b). In general, the faults situated in the northern part of the study area, have more influence on the trap capacity (Fig. 7 e.g. traps 1, 2, 3) compared to the traps located in the center of the study area with similar results for both scenario (Fig. 7. e.g. traps 4, 5, 7). A key question to discuss, is whether faults with small throw, will have any influence on lateral CO_2 fluid flow. Oil field studies indicate that also small faults, fractures and deformation bands associated with larger faults represent potential barriers for fluid flow [26]. The fault permeability is dependent on clay smear, maximum burial depth and mineralogy [27]. For our study areas these relationships are unknown, therefore we analysed two end member models assuming open or closed faults. Generally, we believe that the results illustrate the importance to consider different fault sealing behaviors during the determination of structural trapping volumes.

Also the reservoir simulations indicate the importance of structural trapping on the final total capacity estimates. For both simulated scenarios highest gas saturations are associated with structural traps (compare Figs. 7 and 8) even though transmissibility was varied (comparable to the open fault scenario). However, for both scenarios also, a significant amount of CO_2 (22.1 and 23.5 % of the injected

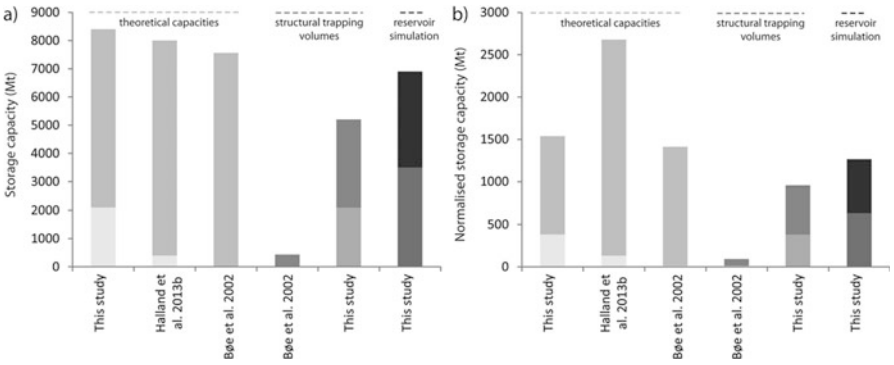

Fig. 13 (**a**) Comparison of own results with published estimates for storage capacities for the Garn Fm. Note that different modelling assumption are made on: the size of the investigated area, structures, included, and rock physical parameters. (**b**) Comparison of normalised storage capacities (per 100 km^3 total pore volume). Total pore volumes are calculated by multiplying the area size, thickness, porosity and the net to gross value. For the Garn Fm. we used a total pore volume of 550 km^3, [5] reported 300 km^3 and [28] used 540 km^3. Dark grey represent the maximum values and bright grey the minimum values

CO_2) was dissolved 3000 year after the injection (Fig. 9a). Taking into account the results from all three approaches we would suggest a representative CO_2 storage volume between 2.0 and 3.5 Gt (Fig. 13a). This would guarantee that a huge quantity of the injected CO_2 could be trapped into structures, and hence major uncertainties regarding the residual, solubility and mineral trapping would not be the determining factors.

7.1.2 Faludden Sandstone

The total capacity estimates from the Faludden sandstone show a large variation spanning from only 10 Mt to 2.5 Gt (Fig. 12b, c). The highest values relate to the theoretical capacity estimates assuming an efficiency factor of 2 %. Compared to the other modelling results including the estimates of the reservoir simulations (0.8–1.7 %) this seems to be rather unrealistic and a lower efficiency has to be assumed.

The structural trapping volumes for open and sealing faults indicate that the fault sealing behaviour in the sandstone should be investigated in detail. For the whole working area the structural trapping capacity is 1.07 times higher assuming sealing faults (Fig. 9 a, b) and in the parts deeper than 800 m the structural trapping capacity increases significantly (7 times higher) if faults are sealing (Fig. 9a, b). Compared to the Garn Fm., the Faludden sandstone structural trapping volumes are very low. The major reason for this is the ca. 3.2 times higher total pore volume of the Garn Fm. and more structural traps. However, the low amount of structural traps within the Faludden sandstone might be associated with the low resolution of the interpreted seismic surface. The seismic interpretation is based on 2D lines from

the 1970s with a coarse resolution and potentially minor traps are not imaged and maintained in the modelling results.

The reservoir simulations clearly indicate that a high quantity of the injected CO_2 is residually trapped or dissolved after 6000 year (39–42.5 %). However, Fig. 11 indicates that for both the scenarios, part of the injected CO_2 migrates to structural traps that are shallower than 600 m. At these depths the CO_2 is no longer in dense phase (temperature dependent) but since it is retained in structural traps no further migration is expected. In the case of the Faludden sandstone we suggest as a representative total storage volumes for the whole working area the results from the reservoir simulations (250–435 Mt, Fig. 12b). In the deeper part (>800 m) the structural trapping is ineffective, thus we use the theoretical volume (with an efficiency factor of 0.5 %) and the results of the reservoir simulation (RS 250 Mt) to constrain the representative total storage volume of 209–250 Mt (Fig. 12c).

7.2 Comparison with Published Data

Several studies have been published aiming to quantify the CO_2 storage capacity of the Garn Fm. [5, 28] and the Faludden sandstone [6, 7, 20]. Thereby different methodologies have been applied to different main target areas giving a large spread in estimated CO_2 storage capacities (Figs. 13 and 14). Thus, a direct comparison of these estimates is not possible. Results of similar approaches can be compared under the consideration of the different total pore volumes of the areas. This will be demonstrated on the example of the Garn Formation.

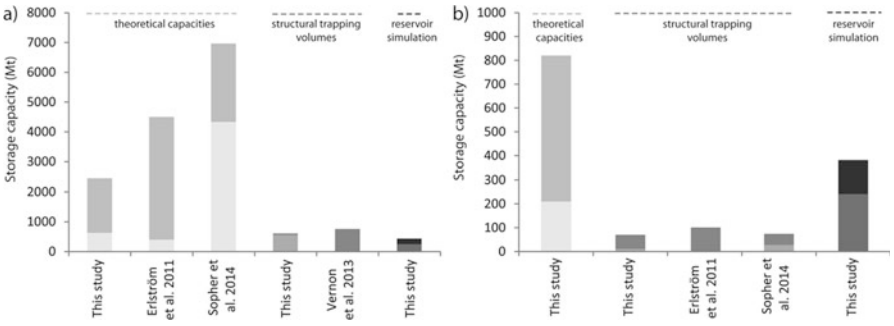

Fig. 14 Comparison of own results with published estimates for storage capacities from the Faludden sandstone. (**a**) Capacities for the whole reservoir unit. (**b**) Capacities for the part below 800 m (reservoir model below 600 m). Note that different modelling assumptions are made on: the size of the investigated area, structures, included, and rock physical parameters. *Dark grey* represent the maximum values and *bright grey* the minimum values

7.2.1 Garn Fm

The theoretical storage capacities reported here give similar results to previous publications (Fig. 13a) even so [5] revealed their estimates from a larger area, including also the underlying Ile Fm. (thickness from 30 to 60 m; [5]). However, in order to compare the results we normalised the storage capacities and reported them as capacities related to a total pore volume of 100 km^3 (Fig. 14b). In this way theoretical capacities used in this study and reported by [28] gave similar results. The maximum theoretical capacities given by [5] might be an overestimate. They used storage efficiency factors up to 4 % which is too high compared to our results based on reservoir simulations (0.8–1.7 %). The structural trapping volumes reported here a significantly higher than values published by [28]. Even our minimum estimate of 2.1 Gt exceeds the estimates from [28] by more than 1.6 Gt's. The main reason for the large difference is that [28] used an arbitrary storage efficiency factor of 0.12 % for the whole working area to calculate structural trapping volumes. We are confident that our approach, measures these volumes more accurate. This has been demonstrated in numerous industry related studies to estimate gas and oil volumes in traps [5].

7.2.2 Faludden Sandstone

The theoretical storage capacities reported here give different results compared to previous publications (Fig. 14a). Unfortunately not all parameters necessary to normalise these results are available for us. However, the theoretical capacities reported by [6] are between 4.3 and 6.9 Gt and are clearly higher than all our estimates (Fig. 14). The main reason for this is that they used efficiency factors ranging between 3.8 and 14.4 % which definitely is contradictory to the results of our reservoir simulations (0.8–1.7 %).

All studies revealed that the structural trapping volumes are relatively low in the whole area (maximum estimate ca. 760 Mt) and even insignificant in the areas deeper than 800 m (maximum estimate 100 Mt, Fig. 14b). It should be mentioned that the published structural trapping volumes included the Dalders structure south-west of our working area.

8 Conclusions

We demonstrated the potential of open dipping aquifers to store high volumes of CO_2. For the Garn Fm. representative storage capacities range between 2.0 and 3.5 Gt and for the Faludden sandstone representative estimates vary between 250 and 435 Mt. This study also identified the difficulties related to unknown parameters in the two working areas. Furthermore, we showed the importance for

the CO_2 storage community to find a solution to compare different modelling results obtained from the same areas. We suggest using normalised storage capacities (demonstrated for the Garn Fm.) or storage efficiency factors together with the target storage pore volume to communicate results more transparent to public readers.

Acknowledgments The work has been supported by the NORDICCS Centre, as part of the Nordic Innovation and Top-level Research Initiative CO_2 Capture and Storage Program (Project number: 11029). Statoil is thanked for providing the data from the Trøndelag Platform.

References

1. IEA (2012) Energy technology perspectives 2012 pathways to clean energy system, Paris, France, OECD/IEA, 690 p
2. Holloway S, Heederik JP, van der Meer LGH (1996) The underground disposal of carbon dioxide – summary report. BGS report for JOULE II project CT92-0031, 21 p
3. Christensen NP, Holloway S (2004) The GESTCO project – summery report, 2nd edn. EU 5th framework programme for eesearch & development ENK6-CT-1999-00010, 32 p
4. Lindeberg E, Vuillaume JF, Ghaderi A (2009) Determination of the CO_2 storage capacity of the Utsira formation. Energy Procedia 1(1):2777–2784
5. Halland EK, Mujezinovic J, Riis F (2014) CO_2 storage Atlas Norwegian continental shelf, Stavanger, Norway, NPD publications, 163 p
6. Sopher D, Juhlin C, Erlström M (2014) A probabilistic assessment of the effective CO_2 storage capacity within the Swedish sector of the Baltic Basin. Int J Greenh Gas Control 30:148–170
7. Vernon R, O'Neil N, Pasquali R, Nieminen M (2013) Screening of prospective sites for geological storage of CO_2 in the Southern Baltic Sea, Espoo 2013, VTT Technology, 101 p
8. Bachu S, Bonijoy D, Bradshaw J (2007) CO_2 storage capacity estimation: methodology and gaps. Int J Greenh Gas Control 1:430–443
9. US Department of Energy (2007) Carbon sequestration Atlas of United States and Canada, p 1
10. Bachu S (2015) Review of CO_2 storage efficiency in deep saline aquifers. Int J Greenh Gas Control 40:188–202
11. Sylta Ø (2004) Hydrocarbon migration modelling and exploration risk. NTNU, Trondheim
12. Lothe AE, Emmel B, Grøver A et al (2014) CO_2 storage modelling and capacity estimation for the Trøndelag platform offshore Norway – using a Basin modelling approach. Energy Procedia 63:3648–3657
13. Grøver A, Rinna J, Lothe AE et al (2013) How and when could basin modelling approaches be useful for CO_2 storage assessment? The 7th Trondheim CCS conference, 4–5 June 2013
14. ECLIPSE 100 (2014) Eclipse reference manual. Schlumberger Information Solutions, 2014.1, Houston
15. Dalland AG, Worsley D, Ofstad K (1988) A lithostratigraphic scheme for the Mesozoic and Cenozoic succession offshore mid-and northern Norway. Norw Petr Directorate, p 65
16. Oljeprospektering (OPAB) AB (1976) Baltic sea, exploration activities 1971─1976, geology and petroleum prospects. Oljeprospektering AB, Exploration Department, 70 p
17. Mortensen GM (2014) CO_2 storage atlas for Sweden – a contribution to the Nordic Competence Centre for CCS, NORDICCS. 31st Nordic geological winter meeting, Lund
18. Ehrenberg SN (1990) Relationship between diagenesis and reservoir quality in sandstones of the Garn Formation Haltenbanken, mid-Norwegian continental shelf. AAPG 74:1538–1558

19. Brangulis AP, Kanev SV, Margulis LS et al (1993) Geology and hydrocarbon prospects of the Paleozoic in the Baltic region. In: Parker JR (ed) Petr of Northwest Europe. Proceedings of the 4th conference, The Geol Society, London, pp 651–656
20. Erlström M, Frederiksson D, Juhojuntti N et al (2011) Lagring av koldioxid i berggrunden – krav, förutsättningar och möjligheter. SGU, Rapporter och meddelanden 131
21. The Baltic Sea Hydrographic Commission (2013) Baltic Sea Bathymetry Database v 0.9.3
22. Bergmo PE, Polak S, Aagaard P et al (2013) Evaluation of CO_2 storage potential in Skagerrak. Energy Procedia 37:4863–4871
23. Zheng L, Apps JA, Zhang Y (2009) On mobilization of lead and arsenic in groundwater in reponse to CO_2 leakage from deep geological storage. Chem Geol 268:281–297
24. Zoback MD, Gorelick SM (2012) Earthquake trigging and large-scale geologic storage of carbon dioxide. In: Proceeding in the National Academy of Sciences. www.pnas.org/cgi/doi/10.1073/pnas.1202473109
25. Kikkawa T, Sato T, Kita J et al (2006) Acute toxicity of temporally varying seawater CO_2 conditions on juveniles of Japanese sillago (Sillago japonica). Mar Pollut Bull 52:621–625
26. Knipe RJ (1992) Faulting processes and fault seal. In: Larsen RM et al (eds) Structural and tectonic modelling and its application to petroleum geology, NPF special publication 1. Elsevier, Stavanger, pp 325–342
27. Sperrevik S, Gillespie PA, Fisher QJ et al (2002) Empirical estimation of fault rock properties. In: Koestler AG, Hunsdale R (eds) Hydrocarbon seal quantification, NPF special publication 11. Elsevier, Burlington, pp 109–125
28. Bøe R, Magnus C, Osmundsen PT et al (2002) CO_2 point sources and subsurface storage capacities for CO_2 in aquifers in Norway. NGU report 2002.010

Determination of CO_2-Brine-Rock Interactions for Carbon Dioxide Sequestration Using SEM-EDS Methods

Magdalena Wdowin and Wojciech Franus

Abstract The article constitutes a review of so far obtained results of the mineralogical changes occurs in reservoir and cap rocks due to the effect of carbon dioxide injection and storage in the presence of saline. The impact of CO_2 was observed based on the determination of mineralogical changes by SEM-EDS method. In order to evaluate such interactions (changes) a numerous laboratory investigations were carried our using special designed devices for this purposes where samples of rocks were flooded in artificial brines and closed in autoclaves. Next the CO_2 stream was driven. The investigations were performed at different conditions of pressure, temperature and period of time. To determine the changes in the individual minerals, via the scanning electron microscopy method, the results of mineralogical observations of the same sort of minerals in rock samples before and after the experiment were described. In all investigated cases the minerals precipitation and dissolution processes were observed as the result CO_2-brine-rock interactions. The changes were detected on the following minerals: feldspars, micas, dolomite, calcite, anhydrite, kaolinite, pyrite.

1 Introduction

Carbon dioxide is the main greenhouse gas emitted through human activities such as industrialization and socioeconomic development where the fossil fuel use is the primary source of CO_2 [34, 40, 41]. Considering only fossil fuel according to International Energy Agency (IEA) in 2010, 44 % of carbon dioxide emissions established from fuel combustion were produced from coal, 36 % from oil and 20 % from gas. Therefore, there is an urgent need for neutralization of the gas. Actually there are three considered primary methods for reducing anthropogenic CO_2 in the atmosphere:

M. Wdowin (✉)
Division of Geotechnology, The Mineral and Energy Economy Research Institute, Polish Academy of Sciences, Wybickiego 7, 31-261 Kraków, Poland
e-mail: wdowin@meeri.pl

W. Franus
Civil Engineering and Architecture Faculty, Lublin University of Technology, Nadbystrzycka 40, 20-618 Lublin, Poland

V. Vishal, T.N. Singh (eds.), *Geologic Carbon Sequestration*,
DOI 10.1007/978-3-319-27019-7_7

- employing energy efficiency and conservation practices;
- using carbon-free or reduced-carbon energy resources;
- carbon capture and storage (CCS) either from fossil fuels or from the atmosphere.

The last option is promising because in many countries using a carbon-free energy source is too expensive. The CCS method is a technique that enables the capture of carbon dioxide from combustion of fuel or other industrial processes, next the transport of CO_2 via pipelines, ships or cars, and its storage underground, in depleted gas and oil fields or deep saline formations. CCS technology can, therefore, have a unique and important significance in the global transition to a sustainable low-carbon economy, in both power generations as well industry [15].

Considering the last stage of CO_2 sequestration i.e. geological storage according to Cook [7] six options are distinguished for CO_2 storage:

- in depleted oil and gas reservoirs,
- use of CO_2 to enhance oil recovery (EOR),
- in deep unmineable coal seams,
- use of CO_2 in enhanced coal bed methane recovery (ECBMR),
- in deep unused saline water-saturated reservoir rocks – deep saline aquifer,
- Other suggested options (basalts, oil shales, cavities etc.).

Taking into account geological storage of CO_2 in deep saline aquifer, this option is considered to be one of the key strategies within portfolio of actions to reduce CO_2 emission to the atmosphere. In the systems of deep saline aquifer it can be assumed initial physico-chemical equilibrium between fluid and rock. But the CO_2 injection into these saline aquifer formations disturbs this initial equilibrium and will cause chemical interaction between injected of CO_2. The chemical reactions are related to dissolution and precipitation of some mineral phases [9].

Studying of CO_2-brine-rock interactions is very important for planning safe underground CO_2 storage operations, because any unawareness in these areas can cause the gas leakage from the underground reservoir [37]. Therefore a laboratory experiment of CO_2-brine-rock interaction is considered to be one of the ways to explore and understand the processes and mechanisms of CO_2 geological storage [21]. However such investigations very often are complemented by modeling of CO_2 sequestration to predict the extents and rates of subsurface CO_2–brine–rock interactions [1, 43].

There are many methods for observation of CO_2-water-rock interactions changes. Considering those changes on the mineral grains, the easiest and the fast method is using scanning electron microscopy (SEM).

The main aim of this study was to present so far investigation of mineral changes on mineral surface as a result of CO_2-brine-rock interactions using SEM analysis.

2 CO_2-Brine-Rock Interactions Experiment

In order to determine changes in mineral grains (precipitation or dissolution) the experiments at laboratory scale are performed. So far a number of investigations by other authors were carried out. Generally most of the experiments had the same scheme (as presented in the Fig. 1), where samples of rocks (reservoir and cap rocks) or only reactive minerals, were placed in autoclaves and flooded in artificial brine (often only NaCl solution) and sealed. Next the system was connected with a CO_2-supplying medium. Additionally in these systems there are established different conditions of temperature, pressure and duration time. Many authors try to establish reservoir conditions in autoclaves depending on tested formations. For example tested temperatures were from 40 °C [9] to even 70 °C [22], and the pressure from 5.5 [9] to 20 MPa [22]. Sometimes the reservoir conditions are as high as 30 bar and 125 °C [14]. The duration time simulated *in situ* condition is approximately above 1 year [9, 22].

But it is important that in the area of low pressure (5–6 MPa) increase in temperature causes small changes in the density of CO_2 (Fig. 2). In the case of supercritical pressures the density increases and for expected *in situ* pressure (10–12 MPa) amounts to approx. 350 kg/dm^3. It is not a significant difference in relation to the conditions of the carried out experiment, and affects only a slight acceleration of the kinetic reactions in a CO_2-brine-rock system. Therefore Wdowin et al. [43] carried out experiments under the room conditions of T = 25 °C and P = 6 MPa. Rock samples were placed for a period of 18 months in a special for this purpose designed apparatus system.

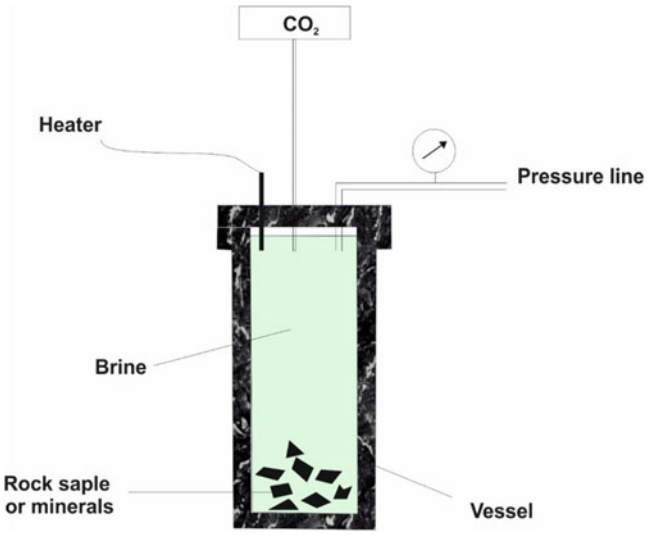

Fig. 1 Simplified scheme of apparatus to tests of CO_2-brine-rock interactions

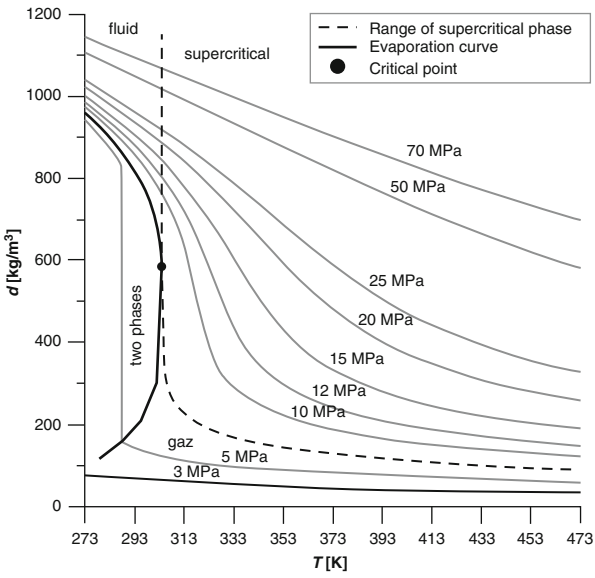

Fig. 2 Dependence of density as a function of temperature and pressure (based on Span and Wagner [35])

Many authors in order to speed up CO_2-brine-rock interactions, significantly increased temperature and pressure instead of using the *in situ* condition. For example Kaszuba et al. [20] carried out experiments in high temperature (200 °C) and pressure at 20 MPa. The duration time of experiment was 139 days. Bateman et al. [2] used 130 °C and the pressure of 30 MPa (duration time – 3–5 months). Liu et al. [25] conducted tests at 200 °C and 300 bars with a period of time up to 60 days.

The considered fluids to such experiments also are very different. Some authors tried to create artificial brine based on chemical composition of brine occurring within tested geological formation [9, 37, 43]. In order to avoid mistakes and difficulties in the interpretation of results others [29] used only NaCl solution at different concentration of sodium chlorides (because sodium ions are predominant components of brine). Rimmeléet et al. [32] used distilled water to observe only the influence of CO_2 on rock. Hug et al. [15] used two sort of brine i.e. NaCl solution and $CaCl_2$ solution. Hu et al. [12] applied solutions of 1 M NaCl, 0.4 M $MgCl_2$ and 0.4 M $CaCl_2$ in order to establish which cations played a key role in reaction with minerals.

To evaluate the impact of CO_2-brine-rock interactions many parameters were considered due to importance of them in CO_2 injection and storage operations i.e.:

(1) Observation of changes in petrophysical parameters of tested rocks.
(2) Observation of changes in minerals of rock (qualitative and quantitative evaluations).
(3) Observation of chemical composition changes in taken to the experiment brine.
(4) Observation of changes on surface of minerals occurring in investigated rocks.

(5) Geochemical modeling.

The petrophysical investigation of rocks taken to the experiment play a key role in the evaluation of suitability of geological structures considered to CO_2 storage. The most important parameters are porosity and permeability of tested rocks because porosity is related to injection capacity, and permeability is related to injection rate. The changes in this parameter can be dangerous for safe underground CO_2 storage. They are also related to the changes in mineralogical composition during CO_2-brine-rock interactions (e.g. dissolution of some minerals could result in increase of the rock porosity) [10, 37]. In the case of caprocks such formations should have good sealing properties (to avoid leakage of CO_2 from reservoir) by low permeability and low porosity. According to Plewa and Plewa [31] permeability below 0.1 mD have impermeable rocks, and porosity below 10 % have rocks with reduced porosity. Opposite situation is for reservoir rocks where important is to retain a quit large values of these parameters i.e. permeability above 10 mD – for permeable rocks, porosity above 15 or 20 % – for rocks with increased porosity and rocks with high porosity [31, 37].

Changes in mineral composition depend on pH of CO_2-brine-rock system, presence of reactive minerals (feldspar, carbonates, kaolinite, biotite, pyrite, and anhydrite), and concentration of brine. But to evaluate such alterations in detail, such experiments have to be carried out carefully. Because tested rocks sandstones, clay stones, mudstones, anhydrite, dolomite, limestone very often are inhomogeneous, therefore quantitative mineral composition have to be carried out within the same area of samples, which very often is difficult.

More reliable seems to be the chemical analysis of brines. It is expected that after experiments a TDS (Total Dissolved Solids) will increase as a result of dissolution, for example of plagioclase, K-feldspar and anhydrite [9]. This phenomenon may cause subsequent precipitation of carbonate phases [8, 18, 30, 31]. Also increase in concentration of some ions such as calcium, magnesium, sodium and potassium ions is a result of mineral dissolution [43].

Numerous experiments have different conditions (temperature, time of reaction, pressure, composition of brine). Therefore kinetic reaction during CO_2-brine-rock interactions can be modeled by different softwares e.g. PHREEQC [36, 39]. Besides geochemical modeling of deep underground fluids behavior at presence of CO_2, is a basic procedure that is used to investigate the variations in brine composition caused by injection of CO_2 and brine–rock interactions, as well as to track the fate of the injected CO_2 plume. To such modeling, the mineralogical geochemical results (among others mineral composition of rocks, chemical composition of brine, *in situ* condition of reservoir formation i.e. pressure and temperature etc.) are applied in order to establish numerical model of deep geochemical processes (by saturation indexes, thermodynamic database, activities and speciation calculations of liquid phase). Obtained in modeling parameters give the information about theoretical reservoir equilibrium conditions between several phases and to

reconstruct physico-chemical variations of different phases at non-equilibrium conditions on the basis of kinetically controlled reactions (e.g. [5, 24, 28]). Such calculations are helpful to assess the geochemical behavior of CO_2 in saline aquifer formations, including its dissolution in brine, as well as interactions with minerals, etc. [38], which enables to determine the suitability of tested geological structures for CO_2 storage [23, 24].

3 SEM Observation of Mineral Changes

The very simple method to evaluate the impact of CO_2 onto rock formation during carbon dioxide storage is Scanning Electron Microscopy (SEM). To evaluate changes caused by CO_2 injection to the rock system with brine, a morphology observation of the mineral grains are needed. Using this method, mainly reactive minerals are observed such as: feldspar, biotite, muscovite, calcite and dolomite, kaolinite, pyrite, anhydrite. Some minerals after CO_2 injection to the system of brine-rock can corrode or some minerals can precipitate in the pore spaces of rocks.

3.1 Feldspar

In the case of feldspars, placed in incongruent dissolution, where a part of the dissolved components go into solution, while a part of them is bonded with the other components to form new mineral phases [46]. Dissolution of these minerals is caused by the acidic environment associated by dissolving of CO_2 in the brine [19, 26, 43]. Depending on the environment of reaction as a result of feldspar corrosion, it is observed precipitation of muscovite, kaolinite or gibbsite. Sample of reactions were presented below [27]:

$$2KAlSi_3O_8(\text{K-feldspar}) + 2H^+ + 9\,H_2O \leftrightarrow Al_2Si_2O_5(OH)_4(\text{kaolinite}) + 2K^+ + 4H_4SiO_4 - \text{reaction of kaolinitzation}$$

$$3KAlSi_3O_8(\text{K-feldspar}) + 2H^+ + 12H_2O \leftrightarrow KAl_3Si_3O_{10}(OH)_2(\text{muscovite}) + 2K^+ + 6H_4SiO_4 - \text{reaction of sericitization}$$

$$KAl_3Si_3O_{10}(OH)_2(\text{K-feldspar}) + 2H^+ + 12H_2O \leftrightarrow 3Al(OH)_3(\text{gibbsite}) + K^+ + 3H_4SiO_4$$

If after the dissolution of feldspars the brine in unsaturated appropriate ions to form muscovite or kaolinite on the surface of feldspar grains, only corrosion is observed [9, 43, 44] as is presented in the Fig. 3.

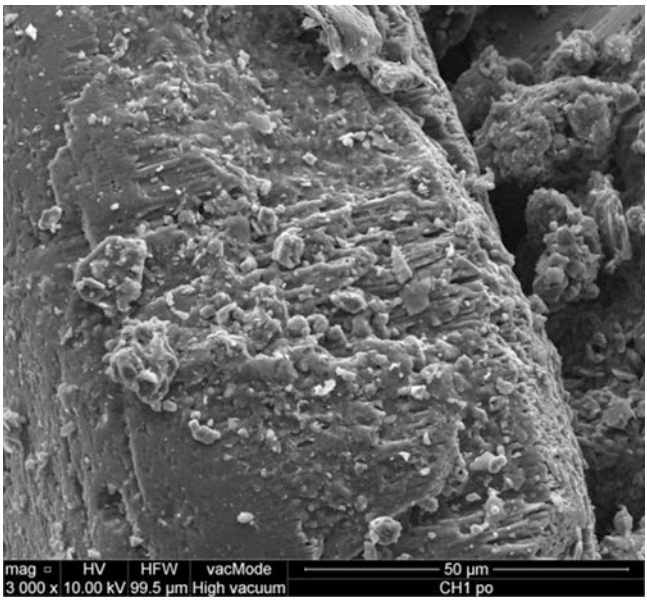

Fig. 3 Corrosion of K-feldspar (From Wdowin et al. [43])

3.2 Micas

Micas (muscovite, biotite, phlogopite etc.) due to their structure including many cations on ion-exchange position will react with CO_2 and brine. Observed alterations (corrosion; Fig. 4) of micas could easily lead to the clay minerals formation, such as kaolinite (kaolinitization, reaction below), illite (illitization) and chlorite (chloritization), which may have a significant influence on petrophysical properties of the reservoir [9].

$$2KAl_3Si_3O_{10}(OH)_2(\text{muscovite}) + 2H^+ + 3H_2O \leftrightarrow 3Al_2Si_2O_5(OH)_4(\text{kaolinite}) + 2\,K^+$$

Investigations carried out by Hu et al. [12] on biotite grains have shown that depending on predominant cations in brine the different changes will be observed. So we can conclude that the cations present in the brine can control the ion exchange reactions with biotite interlayer K, and the resulting surface morphological growths and biotite framework ion release (Mg, Al, Fe, and Si). Besides the authors observed that the relative plenty of morphologies caused by swelling (such as cracks, bulges and bumps) and that the early stage release rate of biotite framework ions followed the same order: $CaCl_2 > MgCl_2 > NaCl \gg$ water, which approved with the order of the hydrated cation size [16, 17] and the expansion is caused by the different ion exchange reactions [3]. Therefore the authors concluded that the larger hydrated cations can cause more stress on the structure of biotite over

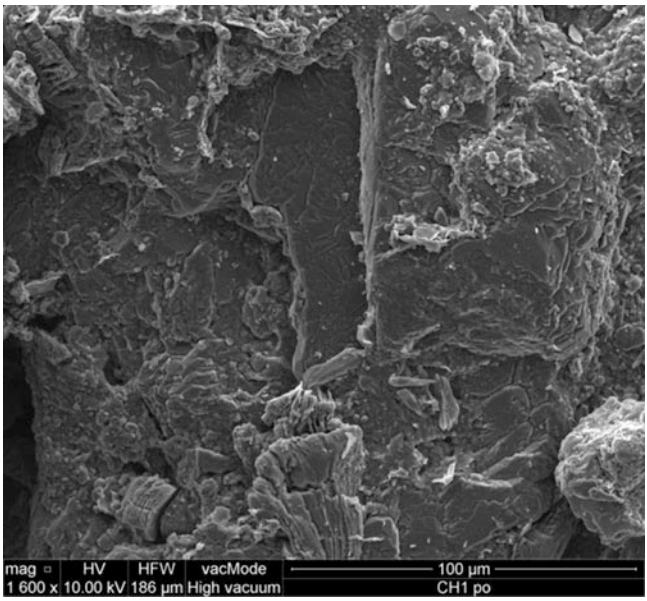

Fig. 4 SEM microphotograph of corroded muscovite (Form Wdowin et al. [43])

ion exchange reaction, which can promote the release of the biotite framework ions, as well as bump, bulge, and crack formation.

3.3 Carbonate Minerals

When the CO_2 injection is related to contact with carbonates and brine, we observed dissolution of carbonate mineral. In case of calcite, product of reaction is $CaCl_2$ [29]. But with time the dissolved brine minerals tend to precipitate as calcite and dolomite – most reactive minerals [4, 33]. In this process, CO_2 is permanently and long term trapped in the form of minerals (mostly carbonates) precipitated in open spaces as secondary phases, such as calcite $CaCO_3$, magnesite $MgCO_3$, siderite $FeCO_3$, dolomite $CaMg(CO_3)_2$ and dawsonite $NaAlCO_3(OH)_2$. This process has a major impact on the physical properties of reservoir rocks [42].

Example of the reactions occurring during CO_2 sequestration into deep saline aquifer was proposed by Xu et al. [45]:

(a) dissolution of CO_2 and the formation of carbonic acid:

$$CO_{2(g)} + H_2O \Leftrightarrow H_2CO_3$$

(b) immediate dissociation of carbonic acid to form the bicarbonate ion (dominant form of carbonate ion in the pH range encountered in brines):

$$H_2CO_3 \Leftrightarrow H^+ + HCO_3^-$$

This reaction may be accompanied by simultaneous dissolution of carbonate minerals and CO_2:

$$CO_2 + CaCO_3 + H_2O \Leftrightarrow Ca^{2+} + 2HCO_3^-$$

(c) reaction with metal ions present in solution and precipitation of carbonate minerals:

$$Ca^{2+} + HCO_3^- \Leftrightarrow CaCO_3 \downarrow + H^+$$
$$Mg^{2+} + HCO_3^- \Leftrightarrow MgCO_3 \downarrow + H^+$$
$$Fe^{2+} + HCO_3^- \Leftrightarrow FeCO_3 \downarrow + H^+$$

SEM-EDS analysis allows the corrosion evaluation of tested carbonates and precipitation of such minerals in the pore spaces of tested rocks.

3.4 Kaolinite

Precipitation of kaolinite during CO_2 injection is a well-known phenomenon. Kaolinite can be formed from a various of reactions (dependent on the mineral composition of the rock subjected to this type of experiments) [10, 11, 13]. Example is presented below [27]:

(a) the dissolution of Calcium feldspar leading to the formation of kaolinite:

$$2H^+ + CaAl_2Si_2O_8 + H_2O \leftrightarrow Ca^{2+} + Al_2Si_2O_5(OH)_4$$
$$CaAl_2Si_2O_8 + H_2CO_3 + H_2O \leftrightarrow CaCO_3 + Al_2Si_2O_5(OH)_4$$

(b) dissolution of microcline yielding kaolinite:

$$2KAlSi_3O_8 + 9H_2O + 2H^+ \leftrightarrow Al_2Si_2O_5(OH)_4 + 2K^+ + 4H_4SiO_4$$

(c) formation of kaolinite from albite:

$$NaAlSi_3O_8 + CO_2 + 5.5H_2O \leftrightarrow Na^+ + HCO_3^- + 2\,H_4SiO_4 + 0.5Al_2Si_2O_5(OH)_4$$

The SEM-EDS observations enable to observe a precipitation of kaolinite in the form of vermiform intergrowths (Fig. 5). Sometimes this mineral is observed in the form of imperfectly crystalized kaolinite. Such phenomenon may indicate its origin as a result of the CO_2-brine-rock experiment in the presence of brine that was not

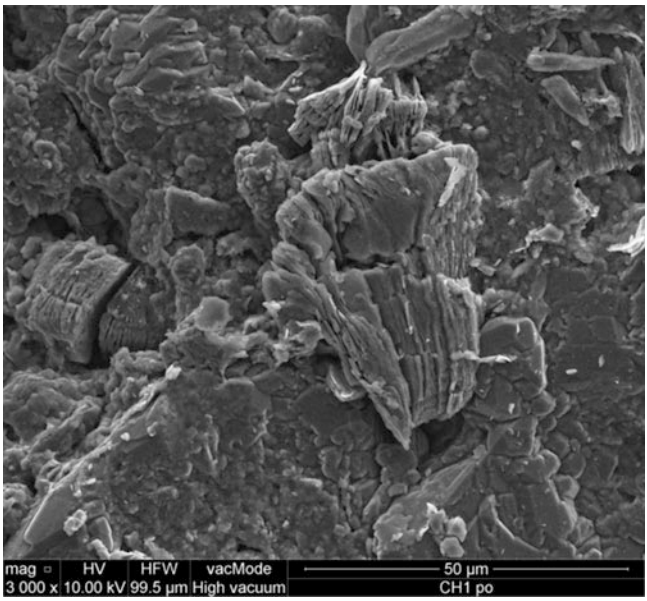

Fig. 5 SEM microphotograph of well-formed vermiform intergrowths of kaolinite

sufficient saturated of ions forming the kaolinite. Furthermore, kaolinitization process can be observed on the surfaces of muscovite or feldspars [43].

3.5 Anhydrite

Brine with high sulfate ions causes the precipitation of anhydrite ($CaSO_4$) according to model presented by Mandalaparty [27]. In cases where CO_2 is injected to anhydrite formation we also can observe a corrosion of this mineral [25]. Anhydrite dissolves only slightly along the CO_2 front, but precipitates in higher proportions near the well bore.

3.6 Pyrite

Pyrite has a tendency of corrosion during CO_2-brine-rock interaction. Changes are seen with cracks on mineral grains and corrosion on the edges of euhedral grains [6, 43]. Example of corrosion of well-formed pyrite grains in presented in the Fig. 6.

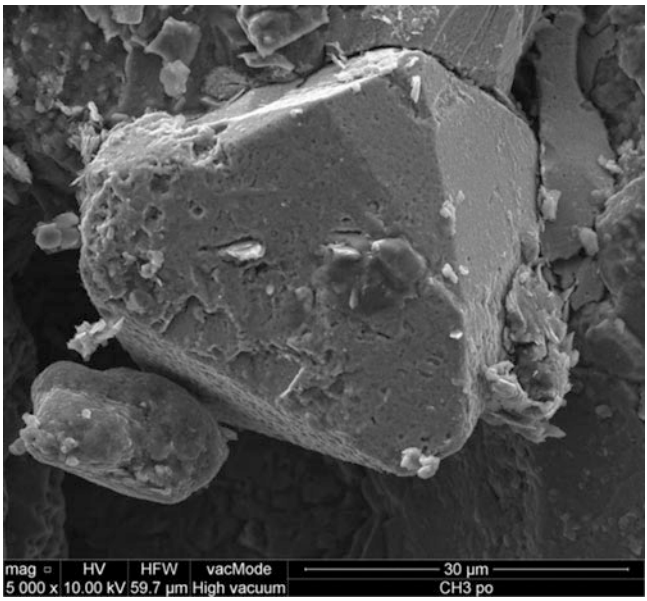

Fig. 6 SEM microphotograph of corroded pyrite (From Wdowin et al. [43])

3.7 Halite

Also in many cases, as a result of evaporation of brine on the surface of the mineral grains or generally in rocks, precipitation of halite is observed both in the form of well-formed cubic crystals or as a coatings (as it is observed in the Fig. 7).

4 Conclusion

SEM investigation of changes is the easiest method to evaluate the impact of CO_2-brine-rock interactions on the rock formations. The changes are revealed mainly by corrosion of mineral grains (in case of dissolution of minerals) or precipitation of some minerals in the pore spaces of the rocks (in case of precipitation on mineral grains from brine solution). In order to evaluate if observed changes (corrosion or precipitation) are caused by the experiment, it is important to investigate the same rock samples or minerals before and after experiment. It is significant to take into consideration that the time of mineral forming or dissolution of minerals is very long. We can speed up such kinetic reaction by the significant increase of temperature and pressure. But it is safer to carry out long term experiment.

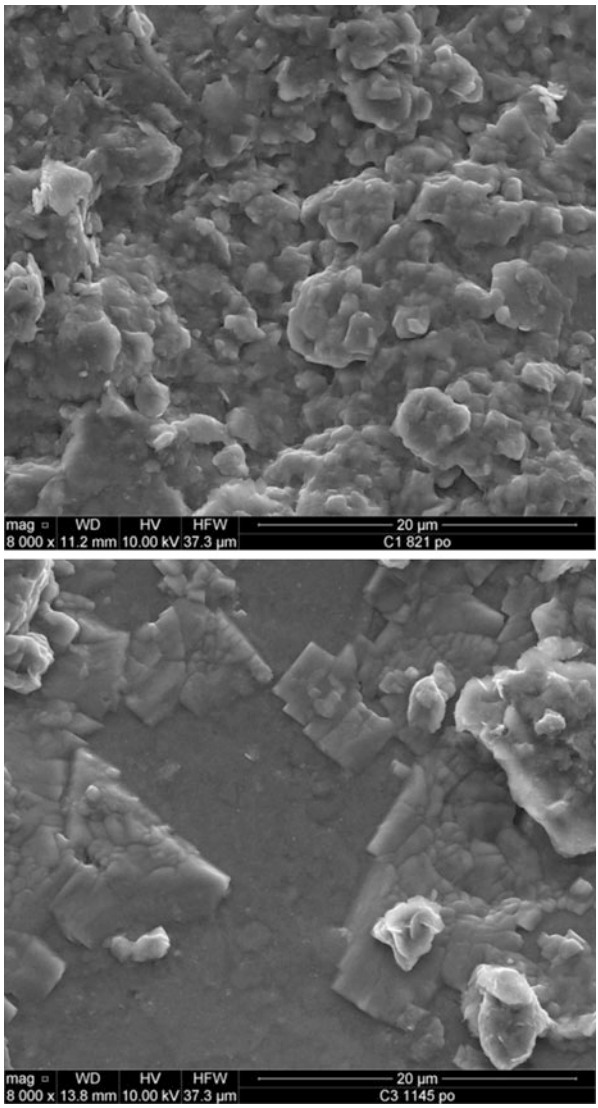

Fig. 7 SEM microphotograph of coatings of halite on the surface of rock (*above*) and cubic crystals and coatings of halite (*below*) (From Wdowin et al. [43])

Acknowledgements This work was financed from the statutory work of The Mineral and Energy Economy Research Institute of the Polish Academy of Sciences

References

1. Balashov VN, Guthrie GD, Hakala JA, Lopano Ch L, Rimstidt JD, Brantley SL (2013) Predictive modeling of CO_2 sequestration in deep saline sandstone reservoirs: impacts of geochemical kinetics. Appl Geochem 30:41–56
2. Bateman K, Rochelle C, Lacinska A, Wagner D (2011) CO_2-porewater-rock reactions – large-scale column experiment (Big Rig II). Energy Procedia 4:4937–4944
3. Bortun AI, Bortun LN, Khainakov SA, Clearfield A (1998) Ion exchange properties of the sodium phlogopite and biotite. Solvent Extr Ion Exch 16(4):1067–1090
4. Calabrese M, Blunt MJ (2005) Simulation of physical-chemical processes during carbon dioxide sequestration in geological structures. Paper SPE 95820 presented at SPE Annual technical conference and exhibition, Dallas, Texas, USA
5. Cantucci B, Montegrossi G, Vaselli O, Tassi F, Quattrocchi F, Perkins EH (2009) Geochemical modeling of CO_2 storage in deep reservoirs: the Weyburn Project (Canada) case study. Chem Geol 265(1-2):181–197. doi:10.1016/j.chemgeo.2008.12.029
6. Chopping C, Kaszuba JP (2012) Supercritical carbon dioxide–brine–rock reactions in the Madison Limestone of Southwest Wyoming: an experimental investigation of a sulfur-rich natural carbon dioxide reservoir. Chem Geol 322–323:223–236
7. Cook PJ (1999) Sustainability and nonrenewable resources. Environ Geosci 6(4):185–190
8. Czernichowski-Lauriol I, Rochelle C, Gaus I, Azaroua lM, Pearce J, Durst P (2006) Geochemical interactions between CO_2, pore-water and reservoir rock. Adv Geolog StorageCarbonDioxide 65:157–174
9. Fischer S, Liebscher A, Wandrey M, The CO2SINK Group (2010) CO_2–brine–rock interaction — first results of long-term exposure experiments at in situ P–T conditions of the Ketzin CO_2 reservoir. Chem Erde Geochem 70(S3):155–164
10. Gaus I (2010) Role and impact of CO_2-rock interactions during CO_2 storage in sedimentary rocks. Int J Greenh Gas Con l4:73–89
11. Hitchon B, Gunter WD, Gentzis T, Bailey RT (1999) Sedimentary basins and greenhouse gases: a serendipitous association. Energy Conserv Manage 40:825–843
12. Hu Y, Ray JR, Jun YS (2013) Na+, Ca^2+, and Mg^2+ in brines affect supercritical CO_2-brine-biotite interactions: ion exchange, biotite dissolution, and illite precipitation. Environ Sci Technol 47(1):191–197
13. Hu Y, Ray JR, Jun Y (2011) Biotite-brine interactions under acidic hydrothermal conditions: fibrous illite, goethite, and kaolinite formation and biotite surface cracking. Environ Sci Technol 45:6175–6180
14. Huq F, Haderlein SB, Cirpka OA, Nowak M, Blum P, Grathwohl P (2015) Flow-through experiments on water–rock interactions in a sandstone caused by CO_2 injection at pressures and temperatures mimicking reservoir conditions. Appl Geochem 58:136–146
15. IEA – International Energy Agency (2012) CO_2 emissions from fuel combustion highlights, 2012th edn. OECD/IEA, Paris
16. Ikeda T (2007) Hydration of alkali ions from first principles molecular dynamics revisited. J Chem Phys 126:034501
17. Ikeda T (2007) Hydration properties of magnesium and calcium ions from constrained first principles molecular dynamics. J Chem Phys 127:074503
18. Kampman N, Bickle M, Becker J, Assayag N, Chapman H (2009) Feldspar dissolution kinetics and Gibbs free energy dependence in a CO_2-enriched groundwater system, Green River. Utah Earth Planet Sci Lett 284:473–488

19. Kaszuba JP, Janecky DR (2013) Geochemical impacts of sequestering carbon dioxide in Brine Formations. In: Sundquist E, McPherson B (eds) Carbon sequestration and its role in the global carbon cycle, Geophysical monograph 183. American Geophysical Union, Washington, DC
20. Kaszuba JP, Janecky DR, Snow MG (2003) Carbon dioxide reaction processes in a model brine aquifer at 200 °C and 200 bars: implications for geologic sequestration of carbon. Appl Geochem 18(7):1065–1080
21. Ketzer JM, Iglesias R, Einloft S, Dullius J, Ligabue R, de Lima V (2009) Water–rock– CO_2 interactions in saline aquifers aimed for carbon dioxide storage: experimental and numerical modeling studies of the Rio Bonito Formation (Permian), southern Brazil. Appl Geochem 24:760–767
22. Kjøller C, Weibel R, Bateman K, Laier R, Nielsen LH, Frykman P, Springer N (2011) Geochemical impacts of CO_2 storage in saline aquifers with various mineralogy-results from laboratory experiments and reactive geochemical modeling. Energy Procedia 4:4724–4731
23. Labus K, Tarkowski R, Wdowin M (2010) Assessment of CO_2 sequestration capacity based on hydrogeochemical model of water-rock-gas interactions in the potential storage site within the Bełchatów area (Poland). Gosp Sur Min- Min Res Manage 26(2):69–84
24. Labus K, Tarkowski R, Wdowin M (2015) Modeling gas–rock–water interactions in carbon dioxide storage capacity assessment: a case study of Jurassic sandstones in Poland. Int J Environ Sci Technol 12(8):2493–2502. doi:10.1007/s13762-014-0652-6
25. Liu F, Lu P, Griffith C, Hedges SW, Soong Y, Hellevang H, Zhu C (2012) CO_2–brine–caprock interaction: reactivity experiments on Eau Claire shale and a review of relevant literature. Inter J Greenh Gas Con 7:153–167
26. Luo X, Yang W, Li R, Liping G (2001) Effects of pH on the solubility of the feldspar and the development of secondary porosity. Bull Miner Petrol Geochem 02:103–107
27. Mandalaparty P (2012) Reaction chemistry in carbon dioxide sequestration. University of Utah, Utah, 164 pp
28. Marini L (2007) Geological sequestration of carbon dioxide: thermodynamics, kinetics and reaction path modeling. Elsevier XV, Amsterdam, 453 pp
29. Mohamed I, He J, Nasr-El-Din HA (2013) Effect of brine composition on CO_2/limestone rock interactions during CO_2 sequestration. J Pet Sci Res 2(1):14–26
30. Parry WT, Forster CB, Evans JP, Bowen BB, Chan MA (2007) Geochemistry of CO_2 sequestration in the Jurassic Navajo Sandstone, Colorado Plateau, Utah. Environ Geosci 14 (2):91–109
31. Plewa M, Plewa S (1992) Petrofizyka. Wydawnictwa Geologiczne, Warszawa
32. Rimmelé G, Barlet-Gouédard V, Renard F (2010) Evolution of the petrophysical and mineralogical properties of two reservoir rocks under thermodynamic conditions relevant for CO_2 geological storage at 3 km depth. Oil Gas Sci Technol Rev IFP 65(4):565–580. doi:10.2516/ogst/2009071
33. Rochelle CA, Czernichowski-Lauriol I, Milodowski AE (2004) The impact of chemical reactions on CO_2 storage in geological formations: a brief review, Spec publ. 233. Geological Society, London, pp 87–106
34. Shukla R, Ranjith P, Haque A, Choi X (2010) A review of studies on CO_2 sequestration and caprock integrity. Fuel 89(10):2651–2664
35. Span R, Wagner W (1996) A new equation of state for carbon dioxide covering the fluid region from the triple-point temperature to 1100 K at pressures up to 800 MPa. J Phys Chem Ref Data 25:1509–1596
36. Tarkowski R, Manecki M (red.) (2009) Badania oddziaływania CO_2 na mezozoiczne skały zbiornikowe w celu określenia ich przydatności do geologicznej sekwestracji dwutlenku węgla. Wyd. IGSMiE PAN, Kraków, 114 pp
37. Tarkowski R, Wdowin M (2011) Petrophysical and mineralogical research on the influence of CO_2 injection on Mesozoic Reservoir and Caprocks from the Polish Lowlands. Oil Gas Sci Technol Rev IFP Energies nouvelles 66(1):137–150

38. Trémosa J, Castillo C, Vong CQ, Kervévan C, Lassin A, Audigane P (2014) Long-term assessment of geochemical reactivity of CO_2 storage in highly saline aquifers: application to Ketzin, in Salah and Snøhvit storage sites. Int J Greenh Gas Con 20:2–26
39. Van Pham TH, Aagaard P, Hellevang H (2012) On the potential for CO_2 mineral storage in continental flood basalts – PHREEQC batch- and 1D diffusion–reaction simulations. Geochem Trans 13(5):2–12. doi:10.1186/1467-4866-13-5
40. Vishal V, Singh TN, Ranjith PG (2015) Influence of sorption time in CO_2-ECBM process in Indian coals using coupled numerical simulation. Fuel 139:51–58
41. Wang T, Wang H, Zhang F, Xu T (2013) Simulation of CO_2–water–rock interactions on geologic CO_2 sequestration under geological conditions of China. Mar Pollut Bull 76 (1–2):307–314
42. Wdowin M (2015) The CO_2-Brine-rock interactions as a result of carbon dioxide sequestration, In: Pant KK, Sinha S, Bajpai S, Govil JN [red.] (eds) Advances in petroleum engineering II: petrochemical. Studium Press LLC, USA, pp 155–178
43. Wdowin M, Tarkowski R, Franus W (2014) Determination of changes in the reservoir and cap rocks of the Chabowo Anticline caused by CO_2–brine–rock interactions. Int J Coal Geol 130:79–88
44. Wigand M, Carey JW, Schütt H, Spangenberg E, Erzinger J (2008) Geochemical effects of CO_2 sequestration in sandstones under simulated in situ conditions of deep saline aquifers. Appl Geochem 23:2735–2745
45. Xu T, Sonnenthal E, Spycher NF, Pruess K (2004) TOUGHREACT user's guide: a simulation program for non-isothermal multiphase reactive geochemical transport in variable saturated geologic media. Lawrence Berkeley National Laboratory LBNL-55460, Berkeley
46. Zhu H, Qu X, Liu L, Yu Z, Zhang L, Tang H (2011) Study on interaction between the feldspar and CO_2 fluid. J Jilin Univ (Earth Sci Ed) 41(03):697–706

Part IV
CO_2 Storage in Coal

Geological Considerations for CO_2 Storage in Coal

Jack C. Pashin

Abstract Coal has potential as a high-capacity sink for anthropogenic emissions of CO_2 and can be considered an attractive geologic storage target from a variety of standpoints. Many geologic factors need to be considered when evaluating coal as a reservoir rock, and the same applies to developing a CO_2 storage strategy for coal. This chapter provides a review of the principal geologic considerations for the storage of CO_2 in coal and for enhanced coalbed methane recovery. The literature on this topic is vast and growing rapidly, and so the objective is not to furnish an exhaustive review, but to provide a synopsis of the critical geologic factors that should be considered when developing geologic storage and enhanced recovery strategies for coal. The discussion begins with a review of the stratigraphy and sedimentation of some of the most prolific CBM reservoirs and continues with a discussion of structural geology and tectonics. The focus then shifts toward hydrodynamics and geothermics, and the discussion concludes with a synthesis of coal quality parameters and their impact on the storage potential and permeability of coal-bearing strata.

1 Introduction

Coal has potential as a high-capacity sink for anthropogenic emissions of CO_2 and can be considered an attractive geologic storage target from a variety of standpoints [1–5]. First, coal has stored large volumes CO_2 naturally through large spans of geologic time and across a broad range of geological conditions [6, 7]. Second, coal stores gases primarily in an adsorbed state, which facilitates high concentration at shallow depth low temperature, and low pressure. In contrast to buoyant trapping of free gas, moreover, adsorption onto the microporous framework of coal can help limit leakage risks that may be posed by imperfect reservoir seals. Third, coal is a proven natural gas reservoir that accounts for a significant proportion of the

J.C. Pashin (✉)
Boone Pickens School of Geology, Oklahoma State University, 105 Noble Research Center, Stillwater, OK 74078, USA
e-mail: jack.pashin@okstate.edu

V. Vishal, T.N. Singh (eds.), *Geologic Carbon Sequestration*,
DOI 10.1007/978-3-319-27019-7_8

world's unconventional production [8, 9]. Last but not least, injection of CO_2 into coal has been proven to enhance recovery of coalbed methane (CBM), thereby offsetting part of the cost of geologic storage while adding to the natural gas supply [10]. Indeed, the global capacity for CO_2 storage in coal is estimated to be on the order of 500 Gt, and the CO_2-enhanced gas recovery potential is perhaps on the order of 50 Tcm, which arguably exceeds the potential for primary CBM production [4].

Although coal is classified as a continuous-type unconventional gas reservoir, continuity does not imply a lack of heterogeneity that affects reservoir performance and storage potential. Many geologic factors need to be considered when evaluating coal as a reservoir rock, and the same applies to developing a CO_2 storage strategy for coal [1, 11–13] (Fig. 1). Coal originally accumulated as peat in wetlands, and so many of its characteristics were determined in the original depositional environment. Hence, delineating the stratigraphic and sedimentologic framework in an essential step in reservoir evaluation. Following sedimentation, folding, faulting, and fracturing affect the geometry and transmissivity of coal-bearing strata, thus structure and tectonics are critical considerations. Indeed, cleat systems are closely spaced fracture systems in coal that control permeability and support commercial flow rates in coal seams. In addition to gas, coal contains large volumes of water, and basin hydrodynamics determine water chemistry and reservoir pressure. During burial, coal bearing strata undergo a complex burial and thermal history that determines many basic coal properties, and geothermics are a major consideration for assessing reservoir capacity and dynamics. Coal quality includes many compositional parameters, including type, rank, and grade, which control adsorption capacity. And ultimately, the ability of coal to store and transmit fluids determines whether gas production, CO_2 storage, and enhanced gas recovery are technically and economically feasible.

This chapter provides a review of the principal geologic considerations for the storage of CO_2 in coal and for enhanced coalbed methane recovery (ECBM). The literature on this topic is vast and growing rapidly, and so the objective is not to furnish an exhaustive review, but to provide a synopsis of the critical geologic factors that should be considered when developing geologic storage and enhanced recovery strategies for coal. The discussion begins with a review of the stratigraphy and sedimentation of some of the most prolific CBM reservoirs and continues with a discussion of structural geology and tectonics. The focus then shifts toward hydrodynamics and geothermics, and the discussion concludes with a synthesis of coal quality parameters and their impact on the storage potential and permeability of coal-bearing strata.

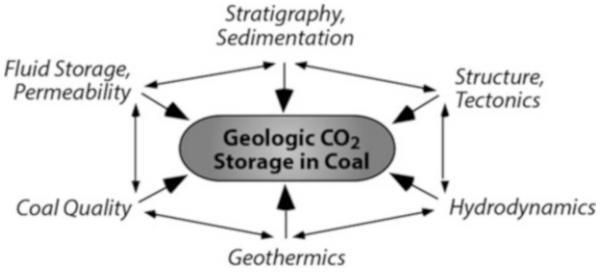

Fig. 1 Conceptual framework showing fundamental geologic considerations for storage of CO_2 in coal

2 Stratigraphy and Sedimentation

The natural history of economic coal seams and CBM reservoirs is linked to the evolution of plants, as well as interwoven tectonic, climatic, and biotic events. The earliest vascular plants are psilophytes, which form thin coal seams in the Silurian system of eastern Europe [14]. Woody gymnosperm floras composing bright-banded coal became increasingly abundant as plants radiated during the Devonian but are not of commercial consequence. Coal seams of commercial thickness for mining (>1 m) and gas production (>0.3 m) became widespread during the Carboniferous in Europe, North America, and China. Floras were dominated by lycophytes, sphenophytes, and other common Paleozoic plants and formed principally in the tropics. By contrast, major coal seams of Permian age that are important development targets are widespread in the Gondwanan basins of South America, Africa, India, and Australia and originated as *Glossopteris* peat in high-latitude, subglacial swamps [15]. A major gap in the coal-bearing stratigraphic record occurred following the terminal Permian extinction, and peat-forming flora apparently did not recover until the mid Triassic [16]. Mesozoic and Cenozoic coal-bearing floras show marked radiation and diversification of plant communities, with floras including conifers, cycads, and ultimately angiosperms replacing the lycopod-dominated assemblages that were so characteristic of the late Paleozoic. Significant CBM development is occurring in Jurassic seams in the Surat basin in eastern Australia [17], and development has been highly successful in the Cretaceous-Tertiary strata of western North America [18]. Analysis of the natural history of coal demonstrates that a great diversity of swamp types formed from equatorial to polar latitudes and hosted an ever-changing suite of floral communities. Because of this, coal composition has changed through geologic time, as have the characteristics of coal as a reservoir rock and geologic carbon sink. Thus, development protocols applied to coal of a given age or in a given area may not be transferrable to other regions. For example, Wilkins and George stated that woody plant material became waxier and thus more oil-prone in the Cretaceous and Tertiary, which may affect basic reservoir properties, including gas storage potential [19].

The stratigraphic and depositional architecture of coal-bearing strata varies considerably among sedimentary basins and has a strong influence how reservoirs

are developed and managed. For example, coal of Late Carboniferous age is productive in many North American and Chinese basins and is prospective in European basins. Late Carboniferous coal-bearing strata in North America and Europe were deposited in or near the humid equatorial belt as the Pangaea supercontinent was assembled. Widespread orogenic activity at this time facilitated subsidence and the accumulation of thick clastic wedges. Meanwhile, waxing and waning glaciers in the southern hemisphere drove high-frequency and changes of sea level. This resulted in cyclothemic intercalation of marine and nonmarine sediment and the formation of numerous thin coal seams (0.1–4 m) that scattered throughout the stratigraphic section as exemplified by the highly productive CBM reservoirs in the Black Warrior Basin in the southeastern USA [13] (Fig. 2).

The majority of CBM produced in North America comes from Cretaceous strata in the Rocky Mountain foreland. The San Juan is the most prolific of these basins, and significant production also comes from the Raton, Uinta, and Alberta basins [18, 20]. The stratigraphic style of Cretaceous CBM reservoirs contrasts sharply with that in the Carboniferous, as exemplified by the Fruitland Formation in the San Juan Basin (Fig. 3). The Late Cretaceous was a time of exceptionally warm global climate when glaciation was too limited to drive the type of sea-level change that was so characteristic of the Carboniferous. Episodic vertical stacking of shoreline sandstone units facilitated formation of extensive backshore wetland complexes [21]. Hence, Cretaceous coalbed methane reservoirs tend to be concentrated in isolated coal zones thinner than 150 m containing seams typically ranging in thickness from 3 to 10 m. In basins where multiple coal zones are present, reservoir development in a given area typically focuses on a single coal zone.

Prolific CBM reservoirs have been developed in Tertiary (Paleocene-Eocene) strata in the Powder River Basin [18, 22], and potential for development exists in other Tertiary successions, such as the Wilcox Group of the Gulf of Mexico Basin [23]. Tertiary strata in other parts of the globe, such as southeast Asia, are just beginning to be explored [8]. The Powder River Basin is a giant Rocky Mountain basin that was initially occupied by a large lake (Lebo Shale Member, Fort Union Formation) (Fig. 4). Infilling of the lake set the stage for widespread peat accumulation, as represented by coal seams in the Tongue River Member of the Fort Union Formation. One school of thought holds that the Tongue River coal seams are part of a deltaic succession [18, 24], whereas another favors peat accumulation amidst fluvial tributary networks [25]. Whereas the Cretaceous coal seams in the San Juan Basin are an order of magnitude thicker than the Carboniferous seams in the Black Warrior Basin, the seams in the Powder River Basin are commonly 10–100 m thick, and thus an order of magnitude thicker than those in the San Juan. Coal seams in the Fort Union Formation have extremely complex geometry, thus reflecting physical and biotic interactions between siliciclastic depositional systems and wetland plant communities. This heterogeneity underscores the importance of stratigraphic and sedimentologic analysis whether exploring for CBM or developing a CO_2 storage strategy.

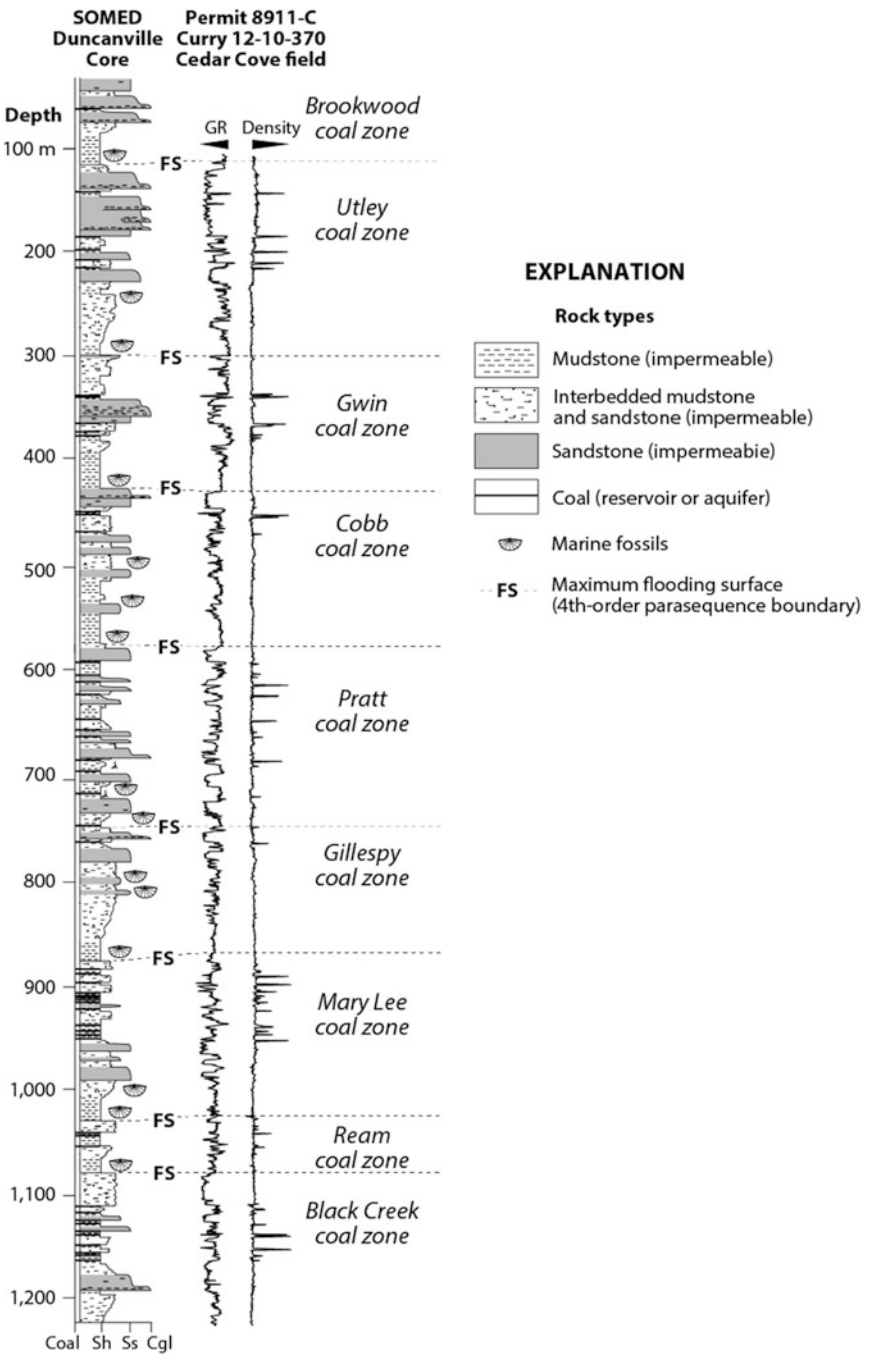

Fig. 2 Core log and geophysical well log of Upper Carboniferous coal-bearing strata in the Black Warrior Basin, southeastern United States

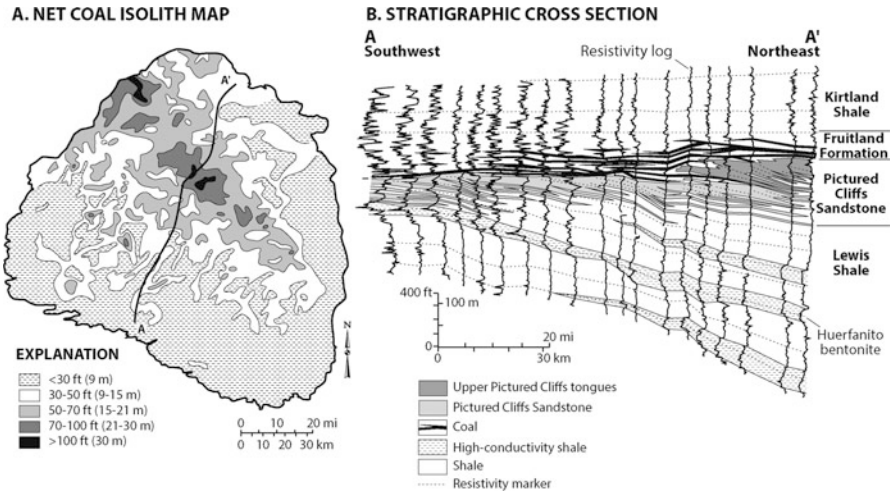

Fig. 3 Net coal isolith map and stratigraphic cross section showing the distribution of coal and stratal geometry in Upper Cretaceous coalbed methane reservoirs of Fruitland Formation and associated strata, San Juan Basin, southwestern United States (**a**) Net coal isolith map. (**b**) Stratigraphic cross section (After Ayers and Kaiser [24])

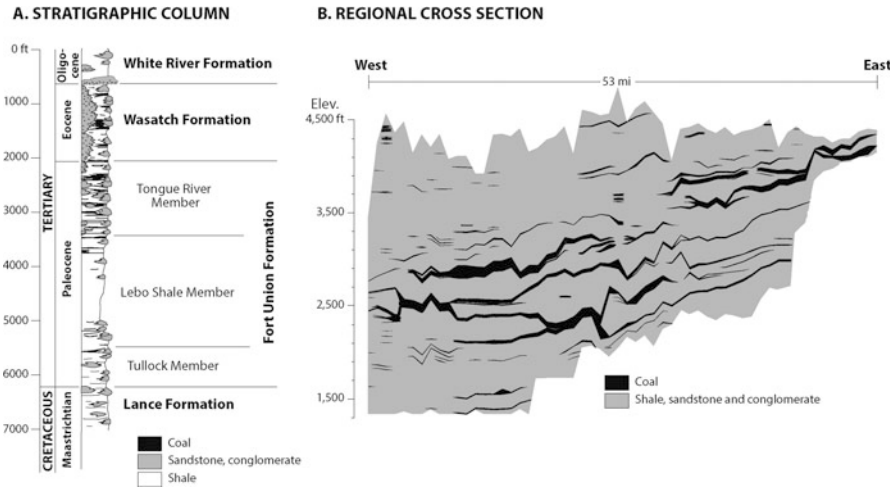

Fig. 4 Stratigraphic column and cross section showing distribution of coal and complex coal-body geometry in the Paleocene strata of the Fort Union Formation, Powder River Basin, northwestern United States (**a**) Stratigraphic column. (**b**) Regional cross section (After Flores [22])

3 Structure and Tectonics

The structural and tectonic framework of any coal-bearing succession evolves throughout the history of a sedimentary basin. Indeed, folding and faulting may be contemporaneous with sedimentation and can occur at any time during any

number of subsequent burial and unroofing episodes. Natural fractures are important conduits for the movement of fluid in the subsurface and are abundant in many coal-bearing successions. Not only do faults and fractures form an important part of the subsurface plumbing system, they also can be prime determinants of whether coal seams are hydraulically confined or may leak during injection [13, 26].

Sedimentary basins are typically classified in terms of crustal type (continental, transitional, oceanic), tectonic motion (extensional, compressional, transcurrent), and tectonic setting (plate margin, plate interior) [27]. Reservoir-class coal seams occur in virtually any type of basin capable of supporting peat-forming plant communities, which includes a great range of continental and transitional crustal settings and precludes oceanic settings. Common continental settings include cratonic basins (e.g., Illinois and Surat basins), foreland basins (Black Warrior and Alberta basins), and intermontaine basins (Powder River and Stellarton basins). Transitional basins include rift basins (Damodar Valley coal basins of India) and passive margin basins (Gulf of Mexico Basin).

Although sedimentary basins are typically classified as extensional (e.g., rift basins like those of the Damodar Valley), compressional (foreland basins like the Black Warrior) or transcurrent (intermontaine pull-apart basins like the Stellarton), any given basin can contain a diverse assemblage of extensional, compressional, and transcurrent structures. In the Black Warrior foreland basin, for example, compressional folds and thrust faults are present along the basin margin, transcurrent faults are developed along the lateral margins of the thrust structures, and normal faults formed by regional bending of the crust occur in the interior of the basin [28]. Folding and faulting can affect the viability of coal as a reservoir rock and geologic CO_2 sink in a variety of ways. For example, large folds commonly bring reservoir coal seams to the surface, which has a strong effect on basin hydrology [29, 30]. Structural style in the interiors of sedimentary basins varies greatly. In some regions, like the eastern flank of the Alberta Basin, strata dip gently and may lack significant folds and faults at a regional scale [31]. In folded regions, productivity sweet spots can occur along structural hinges [28] (Fig. 5). Normal faults, by comparison, may partition CBM reservoirs into structural blocks with different production characteristics.

Without natural fractures, coal would have no practical utility as a reservoir rock or as a geologic CO_2 sink. Fracture networks in coal-bearing strata include cleats in coal, joints in the intervening siliciclastic and carbonate rocks, and shear fractures that are typically associated with faults. Cleat and joint systems are orthogonal networks of opening-mode fractures; that is, the fractures form under tensional stress and exhibit no offset parallel to the fracture plane. Joint and cleat systems form localized to regional networks that are sensitive recorders of stress at the time of formation. At a grand scale, these types of fractures can maintain similar orientation across basins and continents [32]. Cleat systems are restricted to the host coal bed and are thus strata-bound. They commonly display a distinct hierarchy in which primary or master cleats cut complete beds or benches, secondary cleats cut a series of bands, and tertiary cleats cut single vitrain bands [26]. Cleat spacing can be on the order of a meter to a millimeter and typically decreases as rank increases,

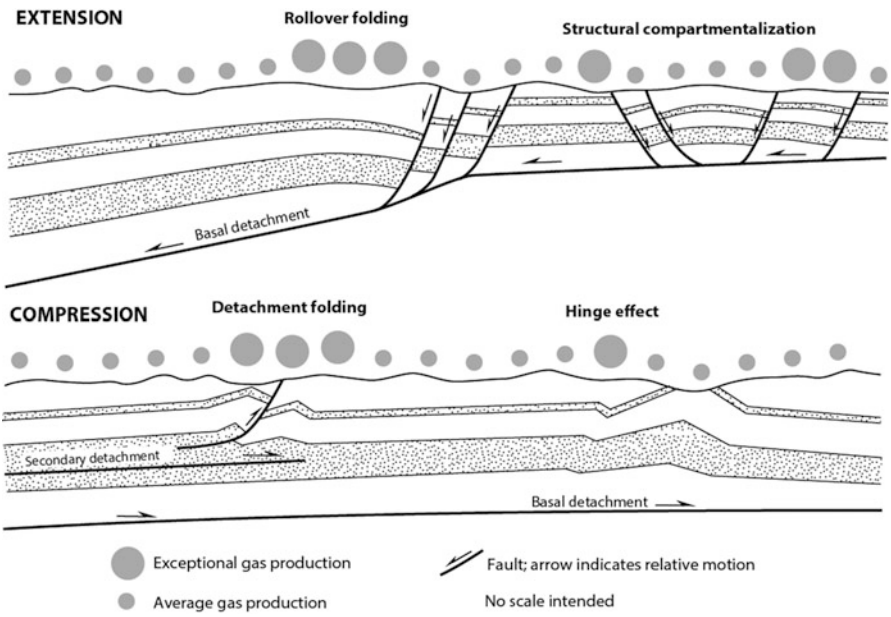

Fig. 5 Structural controls of coalbed methane production in extensional and compressional tectonic settings of the Black Warrior Basin (After Pashin and Groshong [28])

suggesting a relationship to stresses generated by devolatization of coal during thermal maturation [33]. Joints may resemble cleats in terms of geometry but have greater spacing by at least an order of magnitude. Tectonic stress and elevated pore pressure are considered to be the main mechanisms of joint formation [34]. Different rock types have different mechanical properties, and so interlayering of brittle and ductile rock types is a source of heterogeneity that facilitates the development of strata-bound joint networks, as well as trans-stratal fracture systems.

Faults can be viewed as fundamental reservoir discontinuities. Dislocated strata along major fault panes indicates formation under shear stress, and types of faults are identified by geometry (planar, listric, decollement, etc.) and relative displacement (normal, reverse, and strike-slip). Fault zones commonly contain intensely deformed gouge along the fault plane, and swarms of dipping shear fractures that extend into the adjacent country rock [35]. Faults can act as reservoir seals or as conduits for cross-formational flow [36, 37]. Indeed, assessing seals and cross-formational flow conduits is an important consideration for CO_2 storage in coal. Adsorption theory dictates that pressure is a more important factor for storage than the presence of a confining layer. From the standpoint of CBM production, the principal import of hydraulic confinement is isolation of reservoir coal seams from external sources of water that may dilute produced gas. In many situations, faulting as a reservoir discontinuity that limits reservoir drainage may be more of a concern than faulting as a source of cross-formational flow. For CO_2 storage and ECBM, however, hydraulic confinement is required to keep injectate in the target coal

seams and to ensure effective reservoir sweep [38]. Faults and other cross-formational flow conduits thus pose significant leakage risks, and avoiding them is a vital consideration in the design of storage and enhanced recovery programs [13].

4 Hydrodynamics

Water chemistry and reservoir pressure are two critical variables for evaluating coal as a reservoir rock or as a CO_2 sink. Basin hydrodynamics have long played a central role in coalbed methane exploration and development [29, 30] and are strongly related to stratigraphic and structural architecture (Fig. 6). Water produced from coal ranges from potable (TDS <300 mg/L) to hypersaline (TDS >36,000 mg/L) [39]. Large volumes of water are co-produced with CBM, and so understanding water chemistry is essential for developing a viable water management strategy [9]. Even in instances where CO_2 may be injected into coal without co-production of water from ECBM or pressure maintenance wells, water chemistry remains an essential part of the decision process. In most nations, formation water with TDS >10,000 mg/L is protected as an underground source of drinking water (USDW) and is thus not available for underground injection. In the USA and other nations with similar regulatory structure, however, an aquifer exception is available for underground injection wells used for enhanced oil and gas recovery, including ECBM.

Water in coal seams is typically fresh to brackish water of Na-HCO_3 type and brackish to hypersaline water of Na-Cl type [39]. In many productive basins, Na-HCO_3 water occurs in fresh-water intrusions that are fed by meteoric recharge along basin margins (Fig. 6). In the Black Warrior and San Juan basins, fresh-water intrusions originate in structurally upturned margins of the basin where reservoir coal seams are exposed [11, 30]. In the Uinta Basin, by contrast, fresh water charges coal seams by percolation down faults [40].

The interface between near-surface Mg- and Ca-bearing SO_4 and HCO_3 waters is a significant region of microbial methanogenesis. Microbial methanogens also inhabit in the interiors of many coal basins [41]. Indeed, coal seams contain a combination of thermogenic and late-stage biogenic gases, and the proportions of these gas types is determined by the thermal and burial history of the basin, as well as the geochemistry, hydrodynamics, and nutrient flux in the coal-borne water. Indeed, the recharge system is thought to play a vital role in the introduction and sustenance of microbial communities in coal. These communities are thought to be most active above a temperature of 80 °C, which is considered the effective biogenic floor of a sedimentary basin [42]. Pressure has two major components in sedimentary basins: lithostatic pressure and hydrostatic pressure. Lithostatic pressure is caused by the mass of the overburden and has a vertical gradient of ~23 kPa/m. Hydrostatic pressure is caused by reservoir fluid (i.e., pore pressure) and opposes lithostatic pressure. A normal fresh-water hydrostatic pressure gradient in which

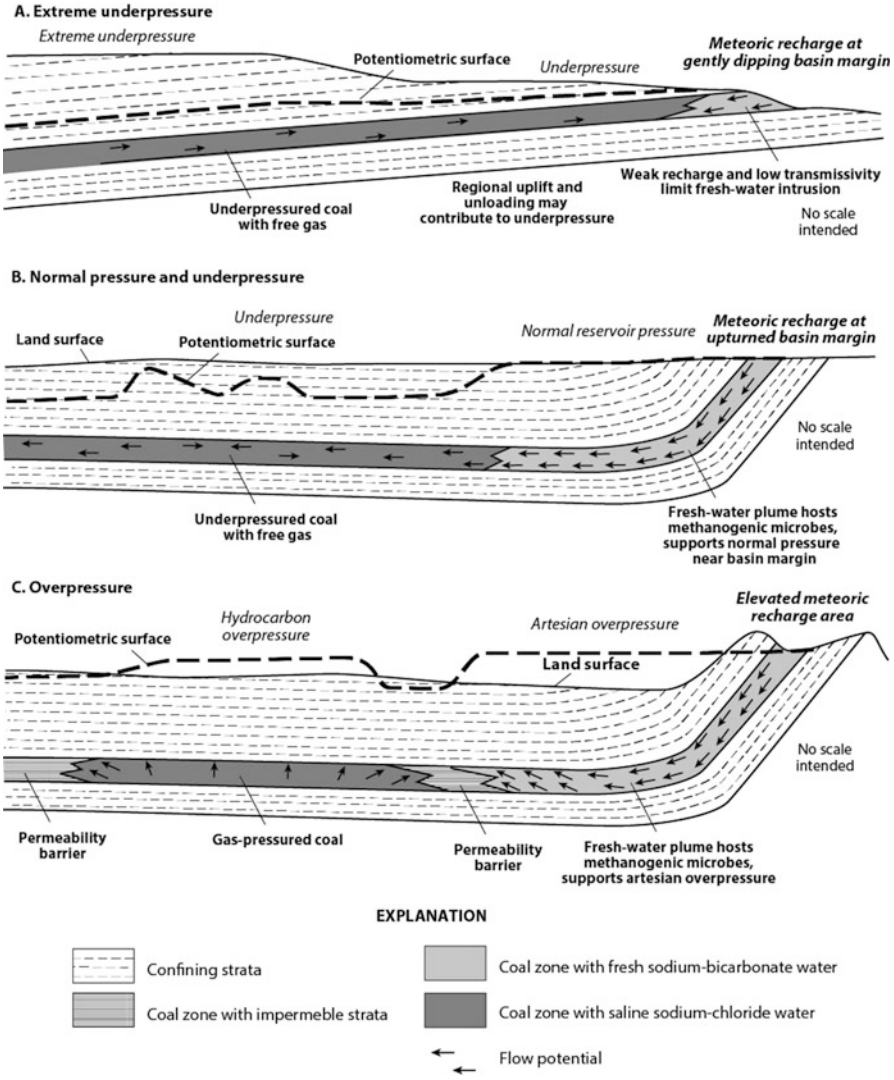

Fig. 6 Hydrodynamic models showing basic mechanisms of recharge, gas charge, and pressuring in coal basins. (**a**) Extreme underpressure. (**b**) Normal pressure and underpressure. (**c**) Overpressure

water in an open well will rise to the level of the land surface is ~9.7 kPa/m. Abnormal hydrostatic pressure is common in the subsurface and includes underpressure (gradient <9.7 kPa/m) and overpressure (gradient >9.7 kPa/m). Topographically driven flow and dilation of fractures in response to the removal of overburden have a strong influence on the pressure regime in the shallow reaches

of sedimentary basins, whereas active hydrocarbon generation may influence pore pressure at depth.

Coal basins can have widely variable reservoir pressure, and numerous examples of underpressure, normal pressure, and overpressure are documented (Fig. 6). Perhaps the most prominent case of underpressure is in the Alberta Basin, where Cretaceous coal of the Horseshoe Canyon Formation has hydrostatic pressure gradients as low as 0.9 kPa/m [31]. Diverse factors contribute to underpressure, including ineffective recharge related to low dip at the basin margin, as well as elevation of the basin interior relative to the basin margin (Fig. 6a). Melting of ~3 km of glacial ice after the Pleistocene is thought to have contributed to extreme underpressure in Alberta [43], which facilitates gas production from coal without co-produced water.

Black Warrior CBM reservoirs are characterized by normal reservoir pressure and underpressure [30, 44]. Normal pressure is supported by fresh-water intrusions that originate at a structurally upturned recharge area with land elevation similar to that in the interior of the basin (Fig. 6b). The plumes support normal pressure to modest underpressure up to 25 km from the basin margin. Northwest of the plumes, underpressure predominates, with hydrostatic gradients locally lower than 4.5 kPa/m.

Overpressure in coal basins includes artesian overpressure and hydrocarbon overpressure. Artesian overpressure is driven by a recharge area that is elevated above the basin interior (Fig. 6c). Artesian overpressure is thought to be effective in the San Juan Basin, where a highly elevated recharge area occurs along the basin margin and supports hydrostatic gradients as high as 14 kPa/m [29]. Hydrocarbon overpressure is typically developed in geologically young strata that are enveloped by a low-permeability barrier that prevents hydrocarbons from migrating. A widely cited example of hydrocarbon overpressure is in the Cameo coal zone of the Piceance Basin in the Rocky Mountains, where large volumes of thermogenic hydrocarbons have charged not only coal, but basin-centered gas accumulations in tight sandstone [12, 45].

Native reservoir pressure is of primary concern for geologic CO_2 storage in areas where reservoir pressure has not been perturbed by anthropogenic activity, such as CBM production and underground coal mining. In virgin areas, highly pressured reservoirs may provide limited headroom for CO_2 storage between hydrostatic pressure and fracture pressure. Indeed, exceeding fracture pressure would facilitate loss of hydraulic confinement and migration of CO_2 out of the injection zone. Anthropogenic sources of underpressure related to mining and hydrocarbon production are a key issue when assessing CO_2 storage and ECBM potential. In the Black Warrior Basin, for example, longwall mining has resulted in major pressure sinks in an otherwise normally pressured region [44]. In Europe, investigators have analyzed the feasibility of storing CO_2 in abandoned underground coal mines [46, 47]. Long-term production of CBM results in significant pressure depletion throughout the development area. Indeed, wellhead gauge pressures of mature wells in some regions may be <60 kPa [48]. These values indicate that CO_2 injection for

storage and ECBM may commence under effective vacuum conditions, which can facilitate high initial injectivity in mature reservoirs.

5 Geothermics

Temperature is another dynamic variable that must be considered when evaluating coal as a gas reservoir or a geologic carbon sink. Indeed, the burial history of a sedimentary basin has long been understood to result in major temperature transients that affect the generation, expulsion, and retention of hydrocarbons [49]. Biogenic gas generation appears to be widespread at temperature <80 °C, whereas thermogenic gas generation is thought to begin at ~100 °C [42, 50]. Coal appears capable of generating 4–10 times more gas than can be retained at temperatures of thermogenesis [51], and this excess gas will either migrate updip, be expelled, and fracture the coal and adjacent strata depending on amount generated and the degree of hydraulic confinement.

Temperature has an inverse relationship to the adsorption capacity of coal [52]. Because of this, coal is a relatively weak sorbent during active thermogenesis and a much stronger sorbent at the lower temperatures facilitating biogenesis. Hence, CBM reservoirs are commonly undersaturated with thermogenic gas, and late-stage biogenic gas is a critical component of economic gas charge in many basins [6, 12]. Relationships among temperature, pressure, burial history, and gas saturation are complex, and so geologically young basins may be saturated with thermogenic gas for some time, whereas older basins that have undergone major uplift and unroofing may be greatly undersaturated in the absence of migrated gas or late-stage biogenic charge [53].

Modern reservoir temperature in CBM reservoirs is variable, with geothermal gradients ranging from <11 to >60 °C/km [44, 54]. Heat flow in the sedimentary column is influenced by the thermal conductivity of the sedimentary column, as well as advective effects associated with the flow of ground water [55]. Most studies of coal-bearing strata emphasize thermal conduction, and Burra et al have documented advective cooling in shallow coal seams in the Sydney Basin [54]. Adiabatic effects related to the expansion and contraction of free gas is another factor requiring significant attention in coal [56]. For example, Pashin et al., found that reservoir temperature had fallen ~8 °C after 12 years of CBM production prior to converting a well into a CO_2 injector [48]. This result underscores the importance of measuring reservoir temperature in mature reservoirs rather than relying on temperature logs and bottom-hole temperatures that were measured prior to gas production. In a recent CO_2 injection test in the Appalachian Basin, temperature logging was employed in concert with spinner surveys to identify which coal seams were accommodating flow [57]. In that study, temperature changes across coal seams proved to be more effective than the spinner surveys for determining which seams were taking the injected CO_2.

6 Coal Quality

Coal can be defined simply as a rock containing more than 50 % organic matter by weight. However, coal is an incredibly diverse of rock with many properties that can be used for characterization and to determine its utility as a natural resource. Most techniques used to classify and characterize coal were derived when it was used chiefly for generating steam to drive engines and generators and for metallurgical applications. All of these techniques remain relevant for characterizing coal as a petroleum source rock, reservoir rock, and geologic carbon sink. Coal quality is typically characterized in terms of type, grade, and rank parameters. Type parameters are used to characterize the composition of coal, whereas grade parameters are used to characterize purity. Rank, by comparison, is determined using parameters that relate to calorific value and thermal maturity.

Important type parameters include lithotype and maceral composition. Reservoir coal seams are predominantly bright-banded and are composed principally of bright lithotypes that can be classified as vitrain and clarain and dull lithotypes classified as durain and fusain. Macerals constitute the microscopic organic constituents of coal and comprise three major groups: vitrinite, inertinite, and liptinite. Vitrinite macerals appear gray in reflected light and are the vitrified remains of woody plant tissue. Intertinite macerals appear white in reflected light and are oxidized plant and fungal remains. Oxidation processes recorded by inertinite include atmospheric exposure and canopy fires. Liptinite macerals can be strongly fluorescent under blue light and are dark gray in reflected white light. These macerals are derived from waxy organic matter, such as leaves, cuticles, palynomorphs, resin, and algae. The proportions of macerals can vary substantially within and among seams, regions, and geologic time periods [14]. For example, coal seams in North America and Europe are typically bright-banded and commonly contain >75 % vitrinite and <5 % liptinite. Australian coal seams, in contrast, can be highly variable in composition, with many containing >60 % intertinite and others containing mostly algal liptinite (i.e., alginite). Indeed, maceral composition varies sufficiently that the decades of experience with North American CBM reservoirs does not necessarily transfer to other regions, where fundamental coal properties can be vastly different.

The maceral groups in coal are analogous to kerogen in other rock types and thus differ in the capacity to generate, store, and transmit natural gas and CO_2. Kerogen is the dispersed organic matter in sedimentary rocks that is insoluble in aqueous alkaline solvents and common organic solvents. The organic matter in coal and other rock types is classified as types I-IV on the basis of C, H, and O content. Type I organic matter is predominantly alginite, which is H-rich and highly oil-prone. Type II organic matter has a lower H:C ratio than Type I and includes most of the other liptinite macerals (e.g., sporinite, cutinite, and resinite). Type II organic matter yields less oil than Type I organic matter. Vitrinite group macerals constitute type III organic matter, which is coalified humic material, including wood. Type III organic matter has a low H:C ratio and a broad range of O:C ratios that decrease as

coal rank increases. Vitrinite group macerals are typically gas-prone and also store large volumes of natural gas and CO_2 [58]. Inertinite macerals constitute type IV organic matter, which has very low H:C and O:C ratios. Type IV organic matter has no generative potential but can store significant volumes of gas [59].

Grade parameters relevant to CBM and CO_2 storage are ash content, sulfur content, and mineral matter content [60, 61]. Ash is the residue that remains after coal is combusted and can be used to characterize the inorganic fraction of coal. Mineral matter content can be estimated from ash content using the Parr formula, which accounts for the materials lost from minerals during combustion, specifically moisture and sulfur. Common minerals in coal are quartz, feldspar, clay minerals, carbonate, and pyrite. Detrital mineral matter, such as quartz and clay, was deposited during events like floods and volcanic ash falls. Pyrite contains most sulfur in coal and most commonly is a product of early diagenesis driven by microbial SO_4 reduction in peat [62]. Mineral matter also can fill cleats and consists of epigenetic carbonate, silicate, oxide, sulfide, and clay minerals. Organic matter is diluted by mineral matter, which thus has an inverse volumetric relationship to adsorption capacity. Hence, the volume of inorganic constituents in coal is more important than weight percent, and a basic method to quantify the effect of ash and mineral matter on gas storage in coal is available in [12].

The principal variables used to measure the rank of CBM reservoirs, and hence thermal maturity, are volatile matter (dry, ash-free basis), fixed carbon (dry, ash-free basis), moisture (ash-free), and vitrinite reflectance (R_o, % basis). Rank affects many basic reservoir properties, including gas capacity and geomechanics. Rank parameters are used to classify coal as lignite, subbituminous, bituminous, semi-anthracite, anthracite, and meta-anthracite. Coal type is useful for understanding the generative potential and gas storage characteristics of coal, whereas rank parameters provide information on what hydrocarbons were probably generated and the amounts of specific gases that may be stored.

Peat is considered to have been transformed to lignite when cellulose is absent, moisture falls below 75 %, and fixed carbon (dry, ash-free basis) is >~60 %. As coal progresses through lignite and subbituminous rank, lignin and the remaining cellulosic substances are transformed to humic compounds. In lignite and subbituminous coal, H_2O, CO_2, and biogenic CH_4 are the dominant volatile compounds generated, and most of the gas is expelled by compaction [63]. Liptinite can begin to exude oil at lignite rank, although only liptinitic (i.e., boghead and cannel) coal seams are thought to be effective source rocks for oil [19]. At bituminous rank, devolatization becomes the main factor driving volumetric changes in coal, with moisture decreasing from 15 % at the subbituminous-high volatile C bituminous transition to only ~1 % at medium volatile bituminous rank. Major thermogenic gas generation begins as coal reaches high volatile A bituminous rank (R_o ~0.80) [50], which is near peak oil generation. As rank continues increasing, significant amounts of N_2 may be generated, and rather than expelling oil, one thought is that it is stored in vitrinite and cracked into gas prior to explusion [19]. As coal reaches anthracite rank (R_o >3.00), the capacity to generate thermogenic hydrocarbons is thought to be exhausted.

Geomechanical parameters that exhibit at least some degree of rank-dependence include mechanical strength and cleat development. A widely used proxy for the mechanical strength of coal is the Hardgrove Grindability Index (HGI). Hydrofracturing and cavity completions in coal appear to be most effective at medium-low volatile bituminous rank [64], which is where HGI is greatest [65]. Rank dependence of cleating is thought to be influenced by mechanical strength, and most specifically by pore pressure exceeding fracture during devolatization [33]. However, the cleat-rank relationship can be indistinct in some basins and obvious in others. In the Black Warrior Basin, for example, primary cleat spacing decreases from ~10 to 2 cm at the edge of the thermogenic gas window and is commonly on the order of 1 mm at medium volatile bituminous and higher rank [83]. A prime example of different expressions of cleating at elevated rank comes from the Appalachians, where anthracite classically exhibits conchoidal fracture and is effectively impermeable, and China where some anthracite is finely cleated and produces CBM [66]. This is yet another difference that underscores how fundamental observations of coal properties in one region may not be transferrable to another.

7 Fluid Storage and Permeability

Gas in coal is stored in adsorbed and free states, with the adsorbed gas stored mainly in organic matrix and the free gas stored in macropores, including cleats and other voids, which are most common in fusain bands. Macroporosity in coal is <5 % of bulk rock volume and is typically <1 % at reservoir depth [67]. Free gas is thought to contribute significantly to storage and production locally, and examples include the crestal regions of anticlines in the Powder River and Appalachian basins [9, 18] and the exceptionally underpressured Horseshoe Canyon reservoirs of the Alberta Basin [31]. But these are exceptional cases—the vast majority of the gas in coal is adsorbed, and adsorption is thus the focus of the discussion here.

The Langmuir isotherm depicts how adsorption capacity changes with pressure at constant temperature and is an important tool for evaluating CBM reservoirs and CO_2 sinks (Fig. 7). A detailed review of storage as it relates to CBM and CO_2 storage has been published by [68]. Absolute isotherms are expressed as curves in which the slope is high at the origin and decreases progressively as it approaches infinite pressure. Two basic parameters are used to describe the shape of the isotherm: Langmuir volume and Langmuir pressure. Langmuir volume is total adsorption capacity at infinite pressure. Langmuir pressure, by comparison, is the pressure at which adsorption capacity equals 50 % of Langmuir volume. Whereas Langmuir pressure describes the ultimate adsorption capacity of a coal sample, Langmuir pressure is used to describe the shape of the isotherm curve. If Langmuir pressure is low, the slope of the curve is high near the origin, and the curve flattens at elevated pressure. If Langmuir pressure is high, the slope of the curve is lower near the origin, and the curve maintains slope at high pressure.

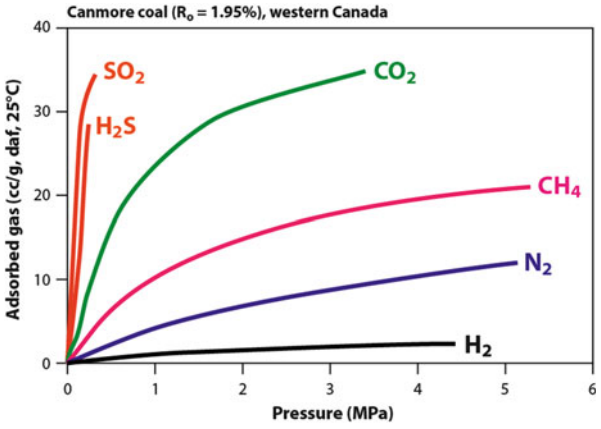

Fig. 7 Adsorption isotherms for various gases in a high-rank coal sample from western Canada (After Chikatamarla et al. [69]). Note high adsorption capacity of CO_2 relative to other common coal seam gases (CH_4 and N_2). High capacity for other acid gases (SO_2, H_2S) at less than 0.2 MPa indicates potential for other by-products of power generation in coal

If gas content and pressure data are plotted with the isotherm, saturated coal samples plot on the isotherm curve, and undersaturated coal samples plot below the curve. As a practical matter, there is no such thing as oversaturated coal – excess gas would go to free storage. If a data point plots above the isotherm, there is either analytical error or a significant amount of a different gas in the sample. The shape of the isotherm has important implications for CO_2 storage in coal. Steep slope near the origin indicates that the vast majority of the adsorption capacity can be accessed lower pressure than 3 MPa. Hence, there is no advantage in trying to pressure up a large reservoir volume. Rather, the only reason to inject as a supercritical phase or at elevated pressure is to propel CO_2 deep into the formation.

Indeed, a given coal sample has different capacity for different gases. Chickatamarla et al plotted isotherms for a series of gases in a high-rank coal sample from western Canada [69] (Fig. 7). Langmuir volume for each gas increases with molecular size such that capacity for H_2 is minimal, capacity for CH_4 at high pressure is about twice as high as N_2, and capacity for CO_2 is about twice as high as CH_4. Chickatamarla et al also plotted isotherms for SO_2 and H_2S, which show potential for storage of other acid waste gases generated by the energy industry [69]. The adsorption capacity of coal, as well as the precise proportions of different gases that can be adsorbed, is influenced by a number of factors, including type, mineral matter, and rank. Holding other variables constant, adsorption capacity can correlate positively with vitrinite and intertinite content [58, 59] and, as already mentioned, negatively with mineral matter content [12].

Rank parameters, including moisture, volatile matter, and vitrinite reflectance have long been known to correlate with adsorption capacity [70, 71]. As a rule, adsorption capacity increases with rank, but CO_2 is an exceptional gas because of high solubility in water (Fig. 8). McVay et al documented exceptional CO_2 storage capacity in low-rank coal of the Gulf of Mexico Basin [23]. Moisture in lignite and subbituminous coal ranges from 75 to 15 %, and so one idea is that much of this storage can be attributed to hydrolysis rather than true adsorption. At bituminous and higher rank, CO_2 adsorption capacity does commonly appear to increase with

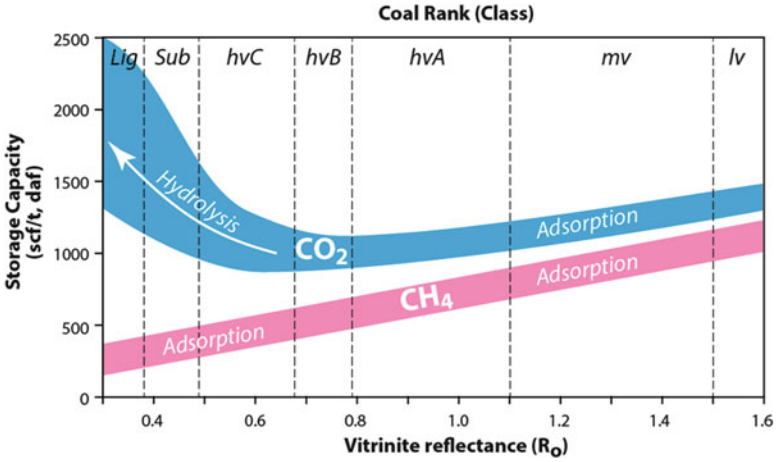

Fig. 8 Generalized relationship between adsorption capacity and coal rank. At low rank, high moisture content facilitates major storage of CO_2 by hydrolysis. At bituminous and higher rank, CO_2 capacity increases modestly with increasing thermal maturity. Hydrolysis effects on CH_4 storage are minimal, and so adsorption capacity tends to increase uniformly with rank

rank, but several workers have noted that this increase is not as pronounced as for CH_4 [68].

Flow within coal matrix is thought to occur primarily by Fickian diffusion, which is a response to concentration gradients, whereas flow within cleat networks can be characterized using Darcy's Law, in which fluid flows in response to pressure gradients. Natural and induced fractures provide the essential permeability enabling commercial CBM production and ECBM operations, and characterization of the permeability field requires knowledge of fracture architecture, lithostatic stress, and hydrostatic stress, and the volumetric changes that occur in coal matrix as gas is adsorbed and desorbed.

Coal is an exceptionally stress-sensitive rock when compared with siliciclastic and carbonate rocks, and high compressibility leads to an exponential decrease of permeability with increasing lithostatic stress [67, 72]. Coal can have Darcy-class permeability near the surface, as is the case in the Powder River Basin [18], and some basins like the Black Warrior have very high permeability-depth gradients in which permeability lower than 1 mD is common only 700 m below the land surface [67]. In this area, stacked coal seams commonly have permeability spanning three orders of magnitude (Fig. 9). In the San Juan basin, by contrast, favorable tectonic stress tends to prop cleats open, with permeability in some areas exceeding 100 mD below depths of 1000 m [26]. And in most regions, geological heterogeneity results in variations of permeability exceeding an order of magnitude at any given depth [35].

Remarkably, permeability in CBM reservoirs is a transient reservoir property. As gas desorbs during production, coal matrix shrinks and cleat apertures widen, thereby improving permeability [73]. In some cases, matrix shrinkage may result in

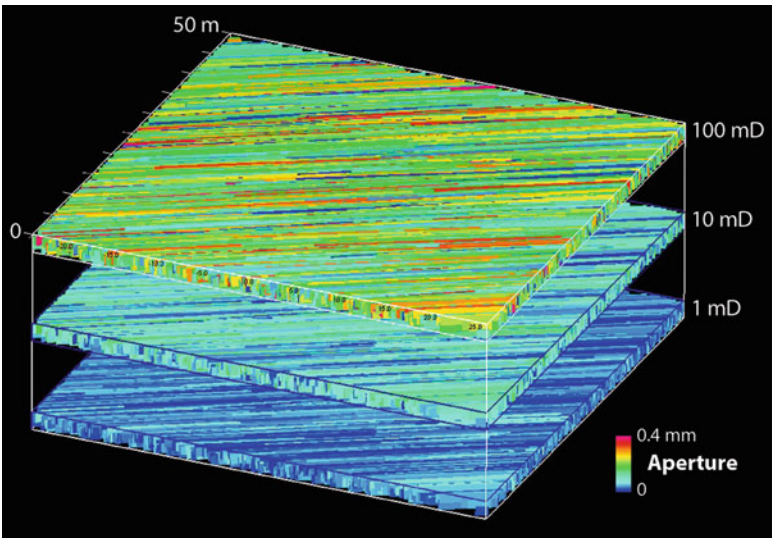

Fig. 9 Discrete fracture network model showing decrease of face cleat aperture with increasing overburden stress as a function of depth. Where coal seams are distributed through a thick stratigraphic section, permeability may vary by more than three orders of magnitude. Swelling of coal matrix and narrowing of cleat aperture in response to CO_2 adsorption may further reduce permeability and injectivity

order-of-magnitude increases of permeability over the life of a well. The opposite happens when CO_2 is injected into coal, and the end result can be the reduction of permeability relative to the virgin reservoir condition by more than an order of magnitude [68]. The swelling phenomenon has been observed in coal from virtually all major mining and gas production regions [74] and is a fundamental variable that must be taken into account when organizing CO_2 injection programs. However, geomechanical models indicate that transient permeability effects are extremely variable when tested in the field, and co-injection of N_2 may be a viable method to limit swelling issues where they pose difficulty. Indeed, permeability in coal seams is the result of a delicate balance among numerous variables, including pore pressure, overburden stress, tectonic stress, Young's modulus, and Poisson's ratio, all of which must be taken into account [75, 76].

Permeability anisotropy is yet another factor affecting CBM production and CO_2 injection operations. Multi-well interference tests in the Black Warrior Basin demonstrated that permeability anisotropy on the order of 15:1 is expressed in shallow, well-cleated coal seams, but that deeper coal seams with low permeability did not exhibit similar anisotropy [77]. Recent CO_2 injection tests employing multi-zone and multi-well monitoring designs detected similar anisotropy in the Illinois and Black Warrior basins [48, 78]. In the Black Warrior test, for example, injection-falloff results indicate significant pressure response in monitor wells located relative to the injection well in the hydrofracture and face cleat directions; no response was observed in a third monitoring well that was located along the butt cleat

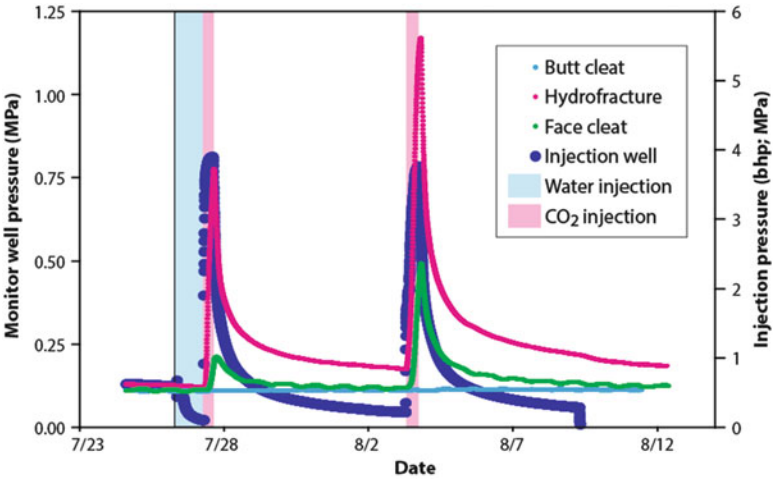

Fig. 10 Slug test results showing anisotropic reservoir response to CO_2 injection in the Pratt coal zone, Blue Creek Field, Black Warrior Basin

direction (Fig. 10), confirming that anisotropy is an important factor affecting reservoir drainage and sweep that should be taken into account when planning production and injection operations.

Injection pilot programs for CO_2 storage and ECBM have now been conducted successfully in numerous basins around the globe from well-test to commercial scale and in coal ranging from lignite to anthracite [79–82]. Each of these programs provides a knowledge base that that helps light the path toward widespread deployment of CO_2 storage and ECBM operations in coal. Much work remains to be done to ensure that CO_2 storage technology can be implemented safely and effectively in coal, and understanding the geologic controls affecting storage potential will remain a prime topic for research for many years to come.

References

1. Gentzis T (2000) Subsurface sequestration of carbon dioxide—an overview from an Alberta (Canada) perspective. Int J Coal Geol 43:287–305
2. White CW, Strazisar BR, Granite EJ, Hoffman JS, Pennline HW (2003) 2003 critical review: separation and capture of CO_2 from large stationary sources and sequestration in geological formations—coalbeds and deep saline aquifers. J Air Waste Manage Assoc 53:645–715
3. Pashin JC (2008) Coal as a petroleum source rock and reservoir rock. In: Ruiz IS, Crelling JC (eds) Applied coal petrology—the role of petrology in coal utilization. Elsevier, Amsterdam, pp 227–262
4. Godec ML, Jonsson H, Basava-Reddi L (2013) Potential global implications of gas production from shales and coal from geological CO_2 storage. Energy Procedia 37:6656–6666
5. Vishal V, Singh TN, Ranjith PG (2015) Influence of sorption time in CO_2-ECBM process in Indian coals: numerical simulation. Fuel 139:51–58

6. Scott AR, Kaiser WR, Ayers WB Jr (1994) Thermogenic and secondary biogenic gases, San Juan Basin, Colorado and New Mexico—implications for coalbed gas producibility. AAPG Bull 78:1186–1209
7. Faiz MM, Saghafi A, Barclay SA, Stalker L, Sherwood NR, Whitford DJ (2007) Evaluating geological sequestration of CO_2 in bituminous coals: the southern Sydney Basin, Australia as a natural analogue. Int J Greenhouse Gas Control 1:223–235
8. Moore TA (2012) Coalbed methane: a review. Int J Coal Geol 101:36–81
9. Pashin JC (2014) Geology of North American coalbed methane reservoirs. In: Thakur P, Schatzel SA, Aminian K (eds) Coalbed methane: from prospect to pipeline. Elsevier, Amsterdam, pp 31–61
10. Byrer CW, Guthrie HD (1999) Appalachian coals: potential reservoirs for sequestering carbon dioxide emissions from power plants while enhancing CBM production. In: International Coalbed Methane Symposium proceedings, University of Alabama, Tuscaloosa, pp 319–327
11. Ayers WB Jr, Kaiser WA (1994) Coalbed methane in the Upper Cretaceous Fruitland Formation, San Juan Basin, Colorado and New Mexico. Texas Bureau of Economic Geology Report of Investigations 218, pp 216
12. Scott AR (2002) Hydrogeologic factors affecting gas content distribution in coal beds. Int J Coal Geol 50:363–387
13. Pashin JC, McIntyre MR, Carroll RE, Groshong RH Jr, Bustin RM (2009) Carbon sequestration and enhanced recovery potential of mature coalbed methane reservoirs in the Black Warrior basin. AAPG Stud Geol 59:125–147
14. Diessel CFK (1992) Coal-bearing depositional systems. Springer, Berlin, 721 pp
15. Fielding CR, Frank TD, Birgenheier LP, Rygel MC, Jones AT, Roberts J (2008) Stratigraphic imprint of the Late Paleozoic ice age in eastern Australia: a record of alternating glacial and nonglacial climate regime. J Geol Soc Lond 165:129–140
16. Retallack GJ, Veevers JJ, Morante R (1996) Coal gap between Permian-Triassic extinction and Middle Triassic recovery of peat-forming plants. Geol Soc Am Bull 108:95–207
17. Hamilton SK, Esterle JS, Golding SD (2012) Geological interpretation of gas content trends, Walloon Subgroup, eastern Surat Basin, Queensland, Australia. Int J Coal Geol 101:21–35
18. Ayers WB Jr (2002) Coalbed gas systems, resources, and production and a review of contrasting cases from the San Juan and Powder River Basins. AAPG Bull 86:1853–1890
19. Wilkins RWT, George SC (2002) Coal as a source rock for oil: a review. Int J Coal Geol 50:317–361
20. Eberth DA, Braman DR (2012) A revised stratigraphy and depositional history for the Horseshoe Canyon Formation (Upper Cretaceous), southern Alberta plains. Can J Earth Sci 49:1053–1086
21. Ambrose WA, Ayers WB Jr (2007) Geologic controls on transgressive-regressive cycles in the upper Pictured Cliffs Sandstone and coal geometry in the lower Fruitland Formation, northern San Juan Basin New Mexico and Colorado. AAPG Bull 91:1099–1122
22. Flores RM (2004) Coalbed methane in the Powder River Basin, Wyoming and Montana: an assessment of the Tertiary-Upper Cretaceous coalbed methane total petroleum system. U.S. Geological Survey Digital Data Series DDS 69-C, Reston, Virginia, 56 pp
23. McVay DA, Gonzalo Hernandez A, Bello RO, Ayers WB Jr, Rushing JA, Ruhl SK, Hoffmann MF, Ramazanova RI (2009) Evaluation of the technical and economic feasibility of CO_2 sequestration and enhanced coalbed methane recovery in Texas low-rank coals. AAPG Stud Geol 59:665–688
24. Ayers WB Jr, Kaiser WR (1984) Lacustrine interdeltaic coal in the Fort Union Formation (Paleocene), Powder River Basin, Wyoming and Montana, U.S.A. International Association of Sedimentologists Special Publication 7:61–84
25. Flores RM, Bader LR (1999) Fort Union coal in the Powder River Basin, Wyoming and Montana—a synthesis. US Geological Survey Professional Paper 1625–A, pp PS1–PS71
26. Laubach SE, Marrett R, Olson JE, Scott AR (1998) Characteristics and origins of coal cleat: a review. Int J Coal Geol 35:175–207

27. Kingston DR, Dishroon CP, Williams PA (1983) Global basin classification system. AAPG Bull 67:2175–2193
28. Pashin JC, Groshong RH Jr (1998) Structural control of coalbed methane production in Alabama. Int J Coal Geol 38:89–113
29. Kaiser WR, Hamilton DS, Scott AR, Tyler R (1994) Geological and hydrological controls on the producibility of coalbed methane. J Geol Soc Lond 151:417–420
30. Pashin JC (2007) Hydrodynamics of coalbed methane reservoirs in the Black Warrior Basin: key to understanding reservoir performance and environmental issues. Appl Geochem 22:2257–2272
31. Gentzis T (2010) Coalbed natural gas activity in western Canada: the emergence of major unconventional gas industry in an established conventional province. In: Reddy KJ (ed) Coalbed natural gas, energy and environment. Nova, New York, pp 377–399
32. Engelder T, Whitaker A (2006) Early jointing in coal and black shale: evidence for an Appalachian-wide stress field as a prelude to the Alleghanian orogeny. Geology 34:581–584
33. Ting FTC (1977) Origin and spacing of cleats in coal beds. J Press Vessel Technol 99:624–626
34. Pollard DD, Aydin A (1988) Progress in understanding jointing over the last century. Geol Soc Am Bull 100:1181–1204
35. Pashin JC (1998) Stratigraphy and structure of coalbed methane reservoirs in the United States: an overview. Int J Coal Geol 35:207–238
36. Allan US (1989) Model for hydrocarbon migration and entrapment within faulted structures. AAPG Bull 78:355–377
37. Knipe RJ (1997) Juxtaposition and seal diagrams to help analyze fault seals in hydrocarbon reservoirs. AAPG Bull 81:187–195
38. Grimm RP, Eriksson KA, Ripepi N, Eble C, Greb SF (2012) Seal evaluation and confinement screening criteria for beneficial carbon dioxide storage with enhanced coal bed methane recovery in the Pocahontas Basin, Virginia. Int J Coal Geol 90:110–125
39. Van Voast WA (2003) Geochemical signature of formation waters associated with coalbed methane. AAPG Bull 87:667–676
40. Stark TJ, Cook CW (2009) Factors controlling coalbed methane production from Helper, Drunkards Wash, and Buzzard Bench fields, Carbon and Emery Counties, Utah. AAPG Search and Discovery Article 90090
41. Flores RM (ed) (2008) Microbes, methanogenesis, and microbial gas in coal. Int J Coal Geol 76:1–185
42. Shurr GW, Ridgley JL (2002) Unconventional shallow biogenic gas systems. AAPG Bull 86:1939–1969
43. Bachu S, Michael K (2003) Possible controls of hydrogeological and stress regimes on the producibility of coalbed methane in Upper Cretaceous-Tertiary strata of the Alberta Basin, Canada. AAPG Bull 87:1729–1754
44. Pashin JC, McIntyre MR (2003) Temperature-pressure conditions in coalbed methane reservoirs of the Black Warrior Basin, Alabama, U.S.A: implications for carbon sequestration and enhanced coalbed methane recovery. Int J Coal Geol 54:167–183
45. Law BE (2002) Basin-centered gas systems. AAPG Bull 86:1891–1919
46. Piessence K, Dusar M (2004) Feasibility of CO_2 sequestration in abandoned coal mines in Belgium. Geol Belg 7:165–180
47. Busch A, Krooss BM, Kempka T, Waschbüsch M, Fernández-Steeger T, Schlüter R (2009) Carbon dioxide storage in abandoned coal mines. AAPG Stud Geol 59:643–653
48. Pashin JC, Clark PE, McIntyre-Redden MR, Carroll RE, Esposito RA, Oudinot AY, Koperna GJ Jr (2015) SECARB CO_2 injection test in mature coalbed methane reservoirs of the Black Warrior Basin, Blue Creek Field, Alabama. Int J Coal Geol 144:71–87
49. Waples DW (1980) Time and temperature in petroleum formation. AAPG Bull 64:916–926
50. Jüntgen H, Klein J (1975) Entstehung von Erdgas aus kohligen Sedimenten. Erdöl und Kohle, Erdgas Petrochemistrie, Ergängsband 1, pp 52–69

51. Zhang E, Hill RJ, Katz BJ, Tang Y (2008) Modeling of gas generation from the Cameo coal zone in the Piceance Basin, Colorado. AAPG Bull 92:1077–1106
52. Yang RT, Saunders JT (1985) Adsorption of gases on coals and heat-treated coals at elevated temperature and pressure. Fuel 64:616–620
53. Bustin AMM, Bustin RM (2008) Coal reservoir saturation: impact of temperature and pressure. AAPG Bull 92:77–86
54. Burra A, Esterle JS, Golding SD (2015) Use of temperature logs in coal seam gas distribution mapping. Int J Coal Geol 144:68–77
55. Jessop AM (1989) Hydrological distortion of heat flow in sedimentary basins. Tectonophysics 164:211–218
56. Kopp A, Ebigbo A, Bielinski A, Class H, Helmig R (2009) Numerical simulation of temperature changes caused by CO_2 injection in geological reservoirs. AAPG Stud Geol 59:439–456
57. Ripepi NS (2009) Carbon dioxide storage in coal seams with enhanced coalbed methane recovery: geologic evaluation, capacity assessment and field validation of the central Appalachian basin. Blacksburg, Virginia Tech, Ph.D. dissertation, 237 pp
58. Mastalerz M, Gluskoter H, Rupp J (2004) Carbon dioxide and methane sorption in high volatile bituminous coals from Indiana, USA. Int J Coal Geol 60:43–55
59. Crosdale PJ, Beamish BB, Valix M (1998) Coalbed methane sorption related to coal composition. Int J Coal Geol 35:147–158
60. Spears DA (1987) Mineral matter in coals, with special reference to the Pennine Coalfields, Special Publication 32. Geological Society, London, pp 171–185
61. Faraj SM, Fielding CR, MacKinnon IDR (1996) Cleat mineralization of upper Permian Baralaba/Rangal coal measures, Bowen Basin, Australia, Special Publication 109. Geological Society, London, pp 151–164
62. Casagrande DJ (1987) Sulphur in peat and coal, Special Publication 32. Geological Society, London, pp 87–105
63. Levine JR (1993) Coalification: the evolution of coal as a source rock and reservoir rock for oil and gas. AAPG Stud Geol 38:39–77
64. Young GBC, Kelso BS, Paul GW (1994) Understanding cavity well performance. Soc Petrol Eng Pap 28579:16 pp
65. Esterle JS (2008) Mining and beneficiation. In: Ruiz IS, Crelling JC (eds) Applied coal petrology—the role of petrology in coal utilization. Elsevier, Amsterdam, pp 61–83
66. Su X, Lin X, Zhao M, Song Y, Liu S (2005) The upper Paleozoic coalbed methane system in the Qinshui Basin, China. AAPG Bull 89:81–100
67. McKee CR, Bumb AC, Koenig RA (1988) Stress-dependent permeability and porosity of coal and other geologic formations. Soc Petrol Eng Form Eval, 3(1):81–91
68. Busch A, Gensterblum Y (2011) CBM and CO_2-ECBM related sorption processes in coal: a review. Int J Coal Geol 87:49–71
69. Chikatamarla LM, Bustin RM, Cui X (2009) CO_2 sequestration into coalbeds: insights from laboratory experiments and numerical modeling. AAPG Stud Geol 59:457–474
70. Joubert JL, Grein CT, Bienstock D (1973) Sorption of methane in moist coals. Fuel 52:181–185
71. Kim AG (1977) Estimating methane content of bituminous coals from adsorption data: U.S. Bureau of Mines report of investigations 2845, 22 pp
72. Vishal V, Ranjith PG, Pradhan SP, Singh TN (2013) Permeability of sub-critical carbon dioxide in naturally fractured Indian bituminous coal at a range of down-hole stress conditions. Eng Geol 167:148–156
73. Harpalani S, Chen G (1995) Influence of gas production induced volumetric strain on permeability of coal. Geotech Geol Eng 15:303–325
74. Vishal V, Ranjith PG, Singh TN (2013) CO_2 permeability of Indian bituminous coals: implications for carbon sequestration. Int J Coal Geol 105:36–47
75. Palmer I, Mansoori J (1998) How permeability depends on stress and pore pressure in coalbeds: a new model. Soc Petrol Eng Reserv Eval Eng, paper SPE 52607:539–544

76. Pekot LJ, Reeves SR (2003) Modeling the effects of matrix shrinkage and differential swelling on coalbed methane recovery and carbon sequestration. In: International Coalbed Methane Symposium proceedings, paper 0328, Tuscaloosa, 16 pp
77. Koenig RA (1989) Hydrologic characterization of coal seams for optimal dewatering and methane drainage. Q Rev Methane Coal Seams Technol 7:30–31
78. Morse DG, Mastalerz M, Drobniak A, Rupp JA, Harpalani S (2010) Variations in coal characteristics and their possible implications for CO_2 sequestration: tanquary injection site, southeastern Illinois, USA. Int J Coal Geol 84:25–38
79. Reeves SR (2001) Geological sequestration of CO_2 in deep, unmineable coalbeds: an integrated research and commercial-scale field demonstration test. Soc Petrol Eng Paper 71749, 11 pp
80. van Bergen F, Pagnier H, Krzystolik P (2006) Field experiment of enhanced coalbed methane-CO_2 in the upper Silesian Basin of Poland. Environ Geosci 13:201–224
81. Wong S, Law D, Deng X, Robinson J, Kadatz B, Gunter WD, Jianping Y, Sanli F, Zhiqiang F (2007) Enhanced coalbed methane and CO2 storage in anthracitic coals—micro-pilot test at south Qinshui, Shanxi, China. Int J Greenhouse Gas Control 1:215–222
82. NETL (2012) The United States carbon utilization and storage atlas, 4th edn. U.S. Dept. of Energy National Energy Technology Laboratory, Pittsburgh, 129 pp
83. Pashin JC, Carroll RE, Hatch JR, Goldhaber MB (1999) Mechanical and thermal control of cleating and shearing in coal: examples from the Alabama coalbed methane fields, USA. In: Mastalerz M, Glikson M, Golding S (eds) Coalbed methane: scientific, environmental and economic evaluation. Kluwer, Dordrecht, pp 305–327

A Review Summary on Multiple Aspects of Coal Seam Sequestration

V. Vishal, Ashwin Sudhakaran, Ashwani Kumar Tiwari, Sarada Prasad Pradhan, and T.N. Singh

Abstract Presence of natural gas in adsorbed form in coal seams is the primary reason for scientists to attempt CO_2 sequestration in the same. The economic analysis states that the additional methane in case of coupled enhanced coalbed methane recovery (ECBMR) with sequestration partly offsets the cost of the operation. Injected CO_2 reduces the partial pressure of methane and enhances its desorption from the matrix. Furthermore, CO_2 is preferentially adsorbed onto the porous surface of the coal thereby displacing methane from adsorption sites. Apart from estimation of coal gas reserves, several technical parameters related to the adsorption capacity of coals and suitable trapping/sealing mechanism must be ensured before utilizing coal as a CO_2 sink.

Parameters such as geomechanical characteristics, swelling/shrinkage, CO_2 permeability in coal, role of effective stresses at higher confining pressure corresponding to deeper target coal seams etc. should be studied in detail before embarking on such problems in the field scale. Various studies ranging from experimental to analytical and numerical modeling have been conducted in the past. This chapter reviews the literature in CO_2 geosequestration in coal with/without ECBMR covering the physical aspects like fluid flow in coal, fluid storage in the adsorbed form, matrix deformation of the porous media, effect of shrinkage/swelling, flow permeability, existence of fluid in its different phases etc. in context to coals worldwide.

V. Vishal (✉) • T.N. Singh
Department of Earth Sciences, Indian Institute of Technology Bombay, Mumbai, India
e-mail: drvikramvishal@gmail.com; tnsingh@iitb.ac.in

A. Sudhakaran
Department of Environmental Engineering and Earth Sciences, Clemson University, Anderson, South Carolina, USA

A.K. Tiwari
Department of Environment, Land and Infrastructure Engineering, Politecnico di Torino, Turin, Italy

S.P. Pradhan
Department of Earth Sciences, Indian Institute of Technology Roorkee, Uttarakhand, India

V. Vishal, T.N. Singh (eds.), *Geologic Carbon Sequestration*,
DOI 10.1007/978-3-319-27019-7_9

1 Introduction

Coal is composed of solid matrix blocks bound by a well-defined network of a pore system. Coal is a heterogeneous porous organic rock composed of micropores/primary porosity and macropores/secondary porosity and is otherwise known as a dual porosity porous media. Micropores form the major share of the porous structure and are responsible for storage and concentration gradient based movement of fluid molecules. On the other hand, macropores are the cleats/fractures formed in response to local stresses, and serve as the medium for pressure driven fluid flow. These porous networks represent the domain of fluid existence in the porous media and control the interactions and movement of the fluid in the solid matrix, which in turn depends upon the coal characteristics and fluid properties. The gas flow effectively involves three mechanisms: desorption from the pores, diffusion through micropores to the cleat network, and flow to the outlet by Darcy's laminar flow and Knudsen diffusion.

The fractures/cleats system of coal is complex. There are mutually perpendicular face cleats and butt cleats that comprise the extensively developed fracture network (Fig. 1 from [1]). Compositionally, coal comprises organic and inorganic matter along with volatiles. The organic matter is constituted of "macerals" that are the organic equivalents of minerals in rocks and are broadly classified as vitrinite, exinite and inertinite. The inorganic matter of coal includes the different minerals that are non-combustible. These form the ash that is left after burning of coal. Volatiles in coal mainly include moisture, and other gases. Moisture in coal includes internal, inherent as well as external water. Coal is therefore, a

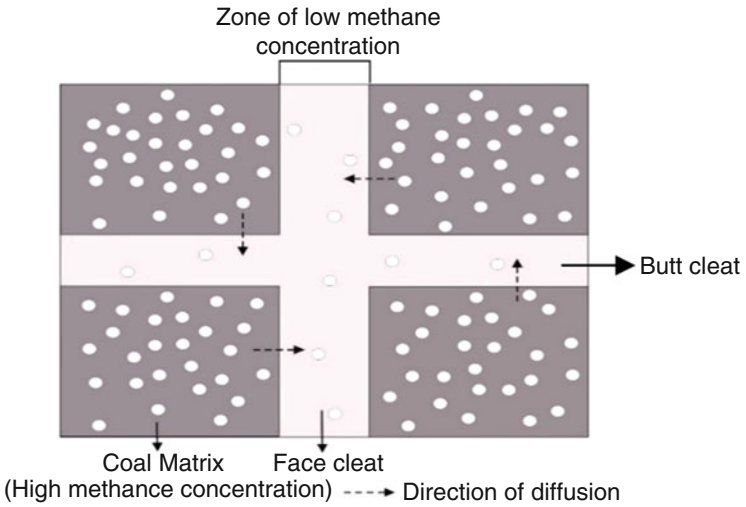

Fig. 1 Cleats orientation and gas desorption in coal [1]

non-volatile, non-crystalline, insoluble, and highly complex mixture of organic molecules of diverse sizes and structures [2].

2 Existence of Gases in Coal

The gases present in coal are formed during the process of coalification and may either be biogenic or thermogenic in origin. Biogenic methane is generated when peat forms as a result of decomposition of organic matter at temperatures below 50 °C. The later stages of coalification witness a high temperature due to an increase in burial depth and influence of magmatic activities because of which, coals of a higher rank are formed. Gases that form in this period of coal formation are referred to as thermogenic methane. Although the gases in coal seams comprise methane dominantly, they also include carbon dioxide, carbon monoxide, and nitrogen from organic decay; in some cases, hydrogen sulphide is generated in trace amounts from the humic source substance. Some higher hydrocarbons are also present in a very small proportion. Methane is dominantly retained in coal seams as adsorbed molecules on the organic micropore surfaces. These pores are mostly inaccessible to formation water and have a diameter <2 nm, qualifying as micropores according to International Union on Pure and Applied Chemistry (IUPAC) classification [3]. It is well understood that more than 95 % of gases in coal beds are stored by the mechanism of physical adsorption or sorption. Minute quantities may be present as free gas in pores and fractures or as dissolved in solutions within the coal beds [4, 5].

2.1 Adsorption/Desorption of Gases in Coal

The recovery of methane from the coals is initiated on creating certain favorable conditions that are different from those applicable in conventional gas reservoirs. Removal of water from the CBM reservoirs generates a pressure gradient due to the depressurization of the coal seam, causing gases to desorb from the pores, diffuse through the matrix and finally catch the pressure gradient in cleat network [6]. This is known as primary recovery of coal bed methane. Other possibilities of extraction of methane include the injection of gases more sorptive than methane, by which the coal automatically releases the methane due to its affinity for the injected gas. The third alternative is injection of gases to reduce the partial pressure of methane that causes methane release from coals. The latter two options of methane recovery are referred to as enhanced coal bed methane recovery. At this point it is worthwhile to understand the gas storage mechanism and the adsorption phenomenon with respect to coal. Various physical models are used to study the adsorption/desorption

mechanisms. They are called adsorption isotherms and help to determine the gas storage capacity of coal with respect to gas pressures (or concentrations) at a given temperature. The models are based on various assumptions surrounding the very basic attributes of adsorption.

2.1.1 Models to Predict Gas Adsorption Capacity

Langmuir Model

The most common model used for studying the adsorption mechanism in porous media like coal is the Langmuir equation and it is based on the dynamic equilibrium created between the adsorbent and adsorbate molecules with respect to the pressure and temperature of adsorbate [7]. Langmuir isotherm is produced when the extent of adsorbing molecules coverage is believed to be limited to one molecular layer (Type I). It assumes that each site accommodates one adsorbate molecule and hence, maximum adsorption occurs when a monolayer of adsorbate occupies all the adsorptive sites.

The equation for the Langmuir isotherm for a single gas phase is given as:

$$V = V_L \frac{p}{p + p_L} \tag{1}$$

where, V is the volume of gas adsorbed per unit mass and p, the pressure of the system. V_L and p_L are the Langmuir volume constant and pressure constant respectively. These constants vary from material to material and are obtained from the best fit of the adsorption/desorption information. The isotherm, when modified for coal systems accounting for the ash and moisture content in gas volume estimation, may be written as:

$$V = V_L[1 - (w_a + w_m)]\frac{p}{p + p_L} \tag{2}$$

where, V is gas volume in coal, V_L is dry, ash-free gas Langmuir volume; w_a is weight fraction of ash content, w_m is weight fraction of equilibrium moisture content, p is pressure and p_L is Langmuir pressure. The utility of adsorption isotherms in CBM exploration lies in the estimation of desorption pressure, rate of release of gas due to pressure decline and the volume of gas remnant in the coals after primary recovery. Figure 2 shows a typical Langmuir adsorption graph where the matrix gas content is plotted against the system pressure.

To account for intermolecular interactions, the equation is modified in the case of gas mixtures. Arri et al. [8] formulated the extended Langmuir equation for gas mixtures based on their experiments on methane-nitrogen and methane-carbon dioxide mixtures:

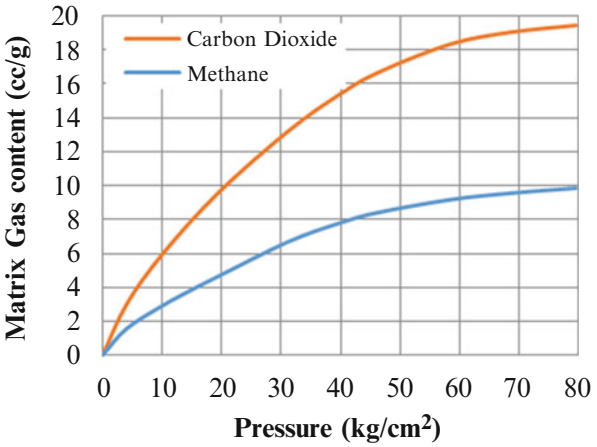

Fig. 2 Langmuir adsorption curves for Raniganj basin coal (After Mendhe et al. [10])

$$v_i = (v_L)_i p \frac{\frac{r_i}{(p_L)_i}}{1 + p\sum_i \frac{r_i}{(p_L)_i}} \tag{3}$$

There are other versions of extended Langmuir isotherm equations [9].

Langmuir's isotherm model is most commonly used for ideal solutions. It is, however, less competent to handle non-idealities in adsorbed phase.

BET Model

The Brunauer, Emmett and Teller (BET) model extends the Langmuir model to multilayers and hence, is applicable to different isotherm types [11]. This accounts well for the enthalpy of sorption and may be used for adsorption of gases at high pressures as well. The heat of adsorption is assumed to be equal to the molar heat of condensation in all the layers. The adsorbed molecules do not interact and the surface of adsorbent is assumed to be energetically uniform. The BET isotherm equation may be defined as:

$$\frac{1}{V\left[(p_o/p) - 1\right)\right]} = \frac{1}{V_m C} + \frac{(C-1)}{V_m C}\frac{p}{p_o} \tag{4}$$

where, V is the gas volume in coal, V_m is the monolayer volume, C is a constant and p_o is the saturation vapor pressure under experimental temperature conditions. The term p/p_o is known as the relative pressure of the reduced pressure. The rate at which the multilayers form is directly related to the constant C, which is usually

greater than unity. BET theory enables experimental determination of the number of molecules required to form a monolayer. At the same time, it establishes that in a multilayer adsorption, the equilibrium of the matrix with gas phase is dynamic and that the actual locations of surface sites covered by one, two or more layers may vary; the number of molecules in every layer, however, will be constant [12]. Although this equation rarely fills to the experimental isotherms for coal matrix, it is still considered to be a useful tool in qualitative study using various isotherm shapes. The model is usually valid between relative pressure values (p/p_o) of 0.05–0.35, when most of the monolayers are completed [13, 14].

Dubinin-Polanyi's Model

Polanyi's Potential theory assumes the existence of a potential field surrounding the adsorbents and immediately above the solid matrix that contains equipotential lines following the contour of surface potential [15, 16]. The space between each set of equipotential surfaces corresponds to a definite adsorbed volume. The adsorption potential may be described as the isothermal work done per mole of adsorbate in transferring molecules from the gaseous state to adsorbed state. Therefore, the adsorption potential, A, depends solely on the volume of gaseous phase, V, held by the equipotential surface surrounding the adsorbent matrix and is directly proportional to it. The plot of V versus A is known as the characteristic curve as this is characteristic of a gas-solid system. Thus, the potential theory of Polanyi holds that for an adsorbate in adsorbed form, the adsorption potential is given by:

$$A = RT\ln(Po/P) \tag{5}$$

where R is the universal gas constant, P is the adsorption pressure and P_o is the saturation vapour pressure of the adsorbate at adsorption temperature, T.

Dubinin [17] used this concept of potential theory to discuss the adsorption phenomenon and formulated the theory of volume filling of micropores (TVFM) that is based on the concept of pore filling. Adsorption in micropores, according to TVFM, happens when the fluid occupies the pore volume by volume filling and not by forming discrete monolayers on homogeneous adsorbent surface. These molecules fit into the micropores and are pressed further inside on compression until the pressure exceeds the vapor pressure, when the adsorbed phase turns into liquid. The theory was worked upon and a simple mathematical relationship was proposed as:

$$V = Vo\exp - (A/E)^2 \tag{6}$$

where E is the characteristic energy parameter of the adsorption system. It depends on the adsorbate and adsorbent properties and their association [17].

The D–P equations were primarily developed for adsorption of vapors below critical point, although, they have been modified for vapors above critical point as well. The characteristic curve can be derived from a single isotherm at any

particular temperature; from the characteristic curve, the isotherm at any other temperature may be obtained. This is a unique advantage of D–P equations adding another dimension of estimation of stored gas volume for coal reservoirs that have high variations in temperature, with the use of limited data.

2.1.2 Validation of Various Adsorption Models Through Different Research Works

For a variety of coals, several researchers reported a close approximation of the Langmuir isotherm with their experimental results. Scientists have found that the experimental results on various American, Canadian and Indian coals correspond to Langmuir's isotherm [10, 18–20].

While considering CO_2 driven ECBM recovery, it is important to understand the adsorption of gas mixtures to coal which have been studied for a number of scenarios. The following research works show the application of the Ideal Adsorbed Solution (IAS) Theory and an extended Langmuir equation to successfully validate the data and use them for estimating the adsorption isotherms of gas mixtures. Stevenson et al. [21] measured the adsorption isotherms for binary and ternary mixtures of CH_4, CO_2 and N_2 on coal at 30 °C and pressures up to 5.2 MPa. They obtained varying proportions of adsorbed gases on the coal surfaces and the total amount of gas mixture adsorbed was strongly dependent on the composition and pressure, validating the utility of the IAS theory for successful estimation of gas adsorption behavior of coal. Arri et al. [8] investigated the adsorption of binary mixtures of methane-nitrogen and methane-carbon dioxide at a temperature of 46.11 °C and pressures up to 10.34 MPa for wet coals. They concluded that instead of independent gas adsorption on to the micropores, the two gases competed for the same sorption sites and Langmuir curves were still valid.

Experimental findings of Busch et al. [22] and Ozdemir et al. [23] further corroborate this theory of competition for adsorption sites. Pariti and Harpalani [24] established the adsorption isotherms for ternary adsorption / desorption data from saturated coals at 319.15 K and their data also fit the extended Langmuir isotherm. Detailed experiments were carried out by De Gance et al. [25] on pure and multi component isotherms of CH_4, N_2 and CO_2 using two dimensional equations of state, IAS theory and extended Langmuir equation and obtained matching adsorption isotherms. For wet coals, they found that the Equation of State models matched the results. For the same gas mixtures and pure forms, Hall et al. [26] studied for adsorption of gas mixtures and established that it is the IAS and 2D Equation of State models that provide a better fit to the data than the Langmuir isotherms, which were only useful for pure gaseous phases; thus, they highlighted the findings of Stevenson et al. [21] who advocated the best fit using the IAS theory. Clarkson and Bustin [27] made a comparative analysis of various model predictions for adsorption/desorption in binary/ternary gas mixtures and found that the IAS model most suitably predicted the experimental results. Some early researchers used the dual sorption mechanism to predict the adsorption of gases on coal partly

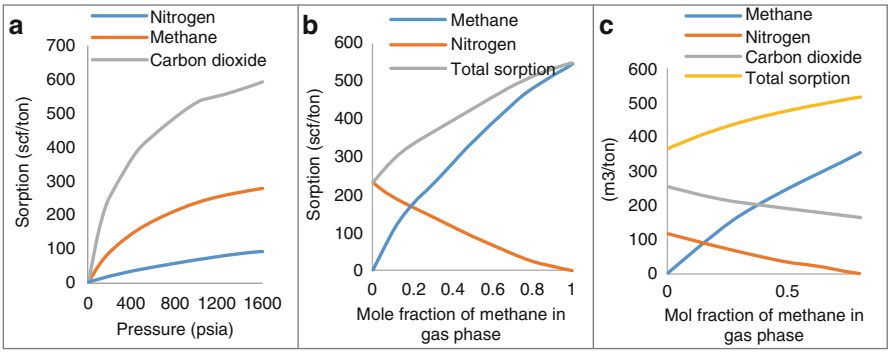

Fig. 3 (**a**) Single component sorption isotherms (dry coal basis) for wet Fruitland coal B at 115 °F, (**b**) $N_2 + CH_4$ mixture sorption isotherms (dry coal basis) for wet Mary Lee coal at 80 °F and 830 psi, (**c**) $N_2 + CH_4 + CO_2$ mixture sorption isotherms (dry coal basis) for wet Fruitland coal C at 115 °F and 526 psi, $y_{CO2} = 0.142$ [31]. It has now been significantly established that there is a preference of adsorption of different gases onto the micro pores of coal—the order from high to low being carbon dioxide, methane, hydrogen, nitrogen—the actual quantities in the proportion varying for different coals [8, 31, 33–36]

based on the solution theory and partly on adsorption [28, 29]. Huddleston et al. [30] studied the adsorption of methane under a temperature of 51.8 °C (125 °F) and pressures up to 15.17 MPa and validated that the Langmuir model could fit the isotherm results at low pressure and a third-order polynomial could fit the whole isotherm. Chaback et al. [31] studied the adsorption/desorption of pure gases and gas mixtures for ECBM recovery process on Fruitland and Mary Lee coals at 46 °C and pressure up to 11 MPa and concluded that the extended Langmuir isotherm was adequate to define the gas adsorption for mixtures as well as for pure forms (Fig. 3). Vishal et al. [1, 32] used the information on Indian coal from previous works and applied the Langmuir models for prediction of CO_2 enhanced coalbed methane extraction and achieved good results on matrix methane saturation, water extraction and volumes of gases released from the chosen coal block.

Although extended Langmuir equations and IAS models fit most of the coal adsorption/desorption data for varying pressures, some data have got a reasonably good fit using the Brunauer, Emmett and Teller (BET) model, Polayni's potential theory and DR and DA models.

3 Coal Matrix Deformation

The gases stored in the coal are adsorbed onto the micropores and desorption is associated with a reduction in the pressure in the coal seam. The natural fractures are widened by this effect enhancing permeability. This occurs in case of sorptive

gases when coal swells or expands due to adsorption and shrinks or contracts during desorption. This widening of cleat apertures due to coal shrinkage during desorption results in an increase in macroporosity in coal and vice versa. The phenomenon of adsorption induces swelling in the coal matrix, which is due to the viscoelastic relaxation of the highly crossed macromolecular structure that is strained [37–40]. Upon adsorption of molecules, new bonds that induce swelling are formed between the adsorbate and adsorbent [40, 41]. Increase in gas pressure leads to an increase in swelling and a decrease in the time required to reach the maximum swelling. This confirms that there is a kinetic process involved in the swelling [42]. The other idea maintains that swelling may be an attribute of forces exerted by the adsorbate on to the molecular structure of the adsorbent at high pressures; here, the injected gas behaves like a high density liquid, by which the energy of the system changes. This leads to volumetric changes [43–45].

Several experimental investigations have been conducted to investigate the swelling/shrinkage behavior of coal and to quantify the linear or volumetric strains due to adsorption/desorption of sorptive gases in strained and unstrained conditions. Sorption induced strain have been calculated for pure gases as well as gas mixtures for different types of coals, worldwide. The quantification is important to understand the behavior of coal in the course of methane extraction as well as for gas injection for ECBM recovery. Although most workers have assumed the linear deformation curve for coal to be elastic, it is really not so evident from other key research works [46, 47].

It is important to comprehend the stress-strain relation for coal in order to enable an accurate estimation of matrix deformation at low and high stresses. Researchers have conducted experiments and have presented theoretical models for quantifying the sorption induced strain on coal, using pure gases as well as gas mixtures at varying pressure and temperature conditions. Most of the research have been carried out for coal under unstrained conditions, while a more realistic approach would have been to analyze the rock deformation behavior in strained conditions. The rocks underground are subject to a certain amount of overburden pressure and undergo some compression causing closure of cleats during removal of gas during desorption. However, the two are not independently active and so, may not be the actual case [48] though the effects of overburden stress cannot be totally neglected.

3.1 Reviewing Development of Understanding on Coal Matrix Deformation

Briggs and Sinha [49] determined the sorption-related changes in coal at 2.07 MPa in CH_4 and CO_2 and found that the axial strain for methane ranged from 0.06 % to 0.30 %. Though the values for CO_2 induced swelling were higher, ranging from 0.34 % to 0.58 %, they showed that the induced strain is recoverable at ambient

pressure. Reucroft and Patel [50] conducted dialatometric studies on elongate coal samples due to adsorption of N_2, He, Xe and CO_2. Volume increase of up to 1.3 % were obtained on exposure to CO_2, while negligible effects were obtained on exposure to N_2, He, and Xe. Reucroft and Sethuraman [42] obtained significant swelling from 0.75 % under 0.5 MPa to 4.18 % under 1.5 MPa for Kentucky coals of varying ranks. The magnitude of swelling decreased with increasing ranks and increasing moisture content of coals. Walker et al. [51] studied the deformational behavior of coals of varying ranks when subjected to CO_2 at different pressures and found that the maximum coal swelling increased from nearly 1 % at 0.68 MPa to around 4 % at 4.8 MPa. They observed an interesting phenomenon: expansion of coals at high pressures was not fully reversible when the pressure was reduced, due to permanent structural deformation as a result of CO_2 dissolution. The percentage of swelling increased with increasing pressure and decreased with high ranks. Although similar observations were made by earlier workers too when Moffat and Weale [52] reported that coal matrix swelling using methane recorded a maximum strain of 1.75 % with increase in pressure while the strain associated with desorption of methane was 1.49 % resulting in residual volumetric strain of 0.27 % for Cannock Wood Coal.

Harpalani and Schraufnagel [53] used methane gas for their study and obtained a linear increase in volume by 0.48 % due to adsorption, with maximum CH_4 pressure as 6.2 MPa. The decrease in the matrix volume was nonlinear as the pressure was completely reduced, resulting in a residual expansion. Ceglarska-Stefanska and Czaplinski [54] used CO_2 on coking coal as well as an anthracite and obtained differential swelling in directions parallel (maximum linear strain = 0.65 %) to and perpendicular (maximum linear strain = 0.92 %) to the bedding at pressures around 4.8 MPa. Ceglarska-Stefanska [55] compared the rates of adsorption/desorption with the rates of swelling/shrinkage using CH_4 at pressures reaching up to 4 MPa, keeping the temperature constant at 25 ° C and found that gas adsorption/desorption occurred faster than the matrix swelling/shrinkage. Differential swelling was found in directions parallel (maximum linear strain = 0.134 %) to and perpendicular (maximum linear strain = 0.175 %) to the bedding at a gas pressure of 3.04 MPa and the shrinkage was not the same as swelling leading to some residual expansion. The observation on differential rates of sorption and swelling was also made when the sorption of carbon dioxide was faster than the development of swelling strain, but at higher pressures (>4 MPa) the two occur simultaneously [56]. No change in sample dimensions were observed upto 60 % of gas adsorption in both the studies at low pressure levels for which it was hypothesized that “the delay in coal dilation at the initial low pressure levels causes the gas to enter the coal macro-pores, causing a minimum of volume change; increased swelling of coal takes place when the gas, at higher pressures, is forced into the micro-pores” [56].

Harpalani and Chen [57] attempted to eliminate the effects of overburden in matrix compression in experiments to study shrinkage of coal due to desorption of CH_4. They obtained a strain of 0.21 % due to desorption when pressure was reduced from 10.3 MPa to 0 MPa and found a linear relation between matrix shrinkage and adsorbed volume. Levine [58] used CH_4 and CO_2 for determination of matrix

shrinkage/swelling in coal and found that swelling was greater in the plane perpendicular to the bedding in both the cases. The data also showed that sorption strain is not linear with pressure, but exhibits a curvilinear form that is steeper at a low pressure, becoming flatter at a higher pressure, resembling the sorption isotherm in shape. Ceglarska-Stefanska and Holda [59] also conducted studies to understand the sorption of various gases by the coal matrix and obtained a maximum swelling for CH_4 as 0.36 %. The other gases like H_2, N_2 and Ar induced swelling of 0.05 %, 0.15 % and 0.18 % respectively. There was almost negligible interaction between He and coal substrate. George and Barakat [48] used gas-saturated coals and found that the swelling due to adsorption was 2.16 % with CO_2, 0.38 % with CH_4 and 0.17 % with N_2 while there was a negligible compression of coal using He. The volume shrinkage in coals were less during desorption resulting in a permanent strain. Ceglarska-Stefanska et al. [60, 61] used a mixture of CH_4 and CO_2 and found that the matrix swelling perpendicular to bedding increased with pressure and reached upto 0.249 % at 3.70 MPa gas-mixture pressure while the same set of samples when exposed to pure methane pressure of 2.83 MPa manifested a strain of 0.16 %.

Chikatamarla et al. [62] examined the matrix deformation behavior of West Canadian sedimentary basin samples with different ranks—from sub-bituminous to medium volatile coals—using various gases. They showed that the volumetric strains are proportionate to the volume of the adsorbed gas. Maximum volumetric strains obtained were 9.33 % for H_2S, nearly 14 times greater than CO_2 (0.66 %), 20 times more than CH_4 (0.30 %), while nitrogen induced strain was almost negligible (0.03 %). Mazumder et al. [63] conducted experiments to replicate the underground in-situ conditions at total gas (CH_4 and CO_2) pressures ranging from about 4 MPa to nearly 23 MPa and obtained linear strains on the coal equal to 0.6 %. Siemons and Busch [64] obtained the swelling of coal at high gas pressures up to 20 MPa using an indirect approach and found that it ranged from 3 to 13 % depending on the type of coal. Day et al. [65] experimented on three Australian high volatile bituminous coals with gas pressures up to 15 MPa and obtained a maximum volumetric swelling ranging from 1.7 to 1.9 % with indications of a relationship between the percentage of swelling and the volume of CO_2 adsorbed. Zarebska and Ceglarska-Stefanska [66] experimentally studied the linear strains of coal for varying mixtures of CO_2 and CH_4, with maximum values ranging from 0.45 % to 0.8 % and 0.4 % for pure CO_2 and CH_4 sorption, respectively, for gas mixtures. Pone et al. [67] reported a three dimensional strain distribution due to interaction of CO_2 when injected in bituminous coal in which the positive strain due to swelling was 0.93 %, 0.94 % and 0.30 % along X, Y, and Z axes, respectively. However, the average volumetric strain was reported to be negative, indicating an overall volumetric reduction as an influence of stresses. Majewska et al. [68] conducted binary gas sorption experiments and found that swelling strain at 4.0 MPa was equal to 1.2 %. The maximum volumetric strain varied from 0.9 to 1.4 % for pure CO_2 and 0.25 to 0.35 % for pure CH_4. The volumetric strain consistently decreased due to increasing CH_4/CO_2 binary ratio. Pini et al. [69] investigated the role of adsorption and swelling on the dynamics of gas injection in

coal; they obtained the swelling isotherms as a function of different gas pressures, using CO_2 and N_2 with maximum strain corresponding to maximum gas pressure. Detailed studies were carried out by van Bergen et al. [70] on the development of strain in unconfined coals for different gases and they established that the maximum equilibrated strain due to CO_2 was 2.24 % at 8.2 MPa while CH_4 and Ar showed maximum strain of approximately 0.65 % and 0.50 %, respectively. Swelling and sorption experiments by Battistutta et al. [71] revealed a fully reversible swelling in case of CO_2 with a maximum swelling nearly equal to 1.44 %. They obtained the swelling ratios between the maximum value in excess sorption as 1:1.5:2.6 for N_2:CH_4:CO_2 at 318 K.

Day et al. [73] experimented on the moist coals with pressures up to 16 MPa and found that the maximum volumetric swelling occurred from 2 to 5 % under dry conditions depending on the rank of coals. Day et al. [74] conducted swelling measurements in Australian coals for CO_2 and CH_4 and mixtures of both in fixed compositions. Helium was seen to completely displace an already swelled coal with CO_2 at 15 MPa. In another experiment, it was observed that the CO_2 completely displaced an already saturated coal with CH_4; swelling of coal was higher than before, supporting the fact that CO_2 has higher affinity for adsorption. Syed et al. [75] conducted swelling strain measurements and the results suggested that the sample pore size distribution has higher role in determining the swelling induced by CO_2 adsorption compared to adsorption of other gas molecules. Majewska et al. [76] simultaneously measured the induced strain, stress and acoustic emissions in coal upon sorption of CO_2 and observed that the swelling reduced by about 60 % upon application of axial stress. Vishal et al. [72] conducted triaxial experiments on Indian coal and measured coal swelling using a radial strain gauge put over coal core sample in triaxial conditions; they reported a deformation ranging 0.041–0.062 % due to the initial CO_2 flow (Fig. 4). Anggara et al. [77] experimented on low rank coals with supercritical CO_2. They observed that moisture was the deciding factor for swelling extent whereas the swelling behavior with

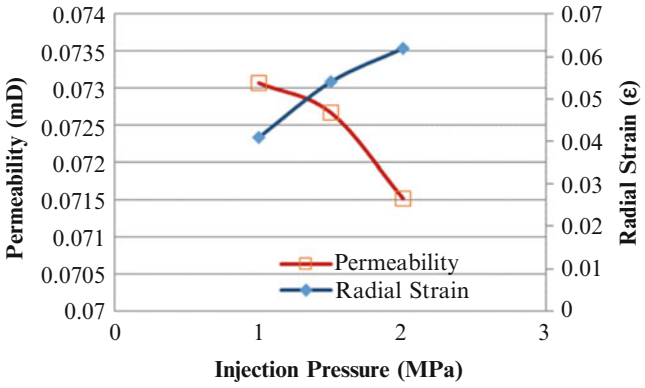

Fig. 4 Coal matrix swelling corresponds to the reduction in permeability with injection pressure during initial gas flow [72]

respect to bedding orientation was dependent upon megascopic texture. Works continue to establish this phenomenon and characterize coal from different basins from across the globe and this appears to be a significant challenge not only for the operations of CO_2 injection in coal but also the overall safety and stability of the system.

4 Permeability of Gas in Coal

Permeability in coal is a critical parameter that is affected by several inter-related phenomena such as shrinkage/swelling of coal matrix, gas slippage, geomechanical effects, cleat anisotropy and effective stresses. The coal matrix undergoes volumetric deformation, typically, swelling and shrinkage with gas adsorption and desorption, respectively; this alters the cleat apertures and therefore, significantly influences the in situ reservoir permeability. Further, permeability in coal is dependent on the effective stress. Several permeability models have been developed for coal seam gas production in the past few years [78–84]. Permeability in coal is commonly estimated using the Darcy's Law for interpretation of experimental results, provided the volumetric flow rate varies linearly with pressure gradient across the ends of the sample [85]. For higher flow rates, the pressure gradient may exceed that which is predicted by Darcy's law; such behavior is known as non-Darcy flow. In recent times, studies have been done in permeability evolution upon variation of different parameters [1, 32]. As discussed earlier, coal contains dual porosity. Similarly, on the basis of disposition and arrangement of cleats, coal exhibits flow anisotropy. Permeability of coal is at its maximum in the direction of the face cleats. From several studies [86–88], the importance of permeability anisotropy calculation for the coal seam/basin for correct estimation of gas flow behavior during coal bed methane production and/or carbon dioxide sequestration is established.

Coal exhibits differential sorption affinity to different gases and hence, depending on the sorptive and non-sorptive gas type, the permeability of coal varies. Early research works established that coal permeability is significantly lower for methane as compared to nitrogen primarily because of the high sorption affinity of methane in coal [89, 90]. Patching [89] however, concluded that the molecular diameter of gas type inversely affected the permeability attributes of coal. Skawinski [91] showed that CO_2 resulted in still higher reduction in coal permeability as compared to CH_4 and N_2 due to the high adsorption affinity of the coal mass towards CO_2. Cui [82] found that the molecule size of the flowing medium along with the pore structure of coal influenced the selective adsorption and gas diffusion in coal. Results showed that the gas desorption and diffusion rate was inversely related to its kinetic diameter, while it varied directly with sorption affinity. This established that the pore structure and molecular geometries of the phases play a more dominant role over mere sorption affinity. Robertson [92] also demonstrated a decreasing order of coal permeability with N_2,

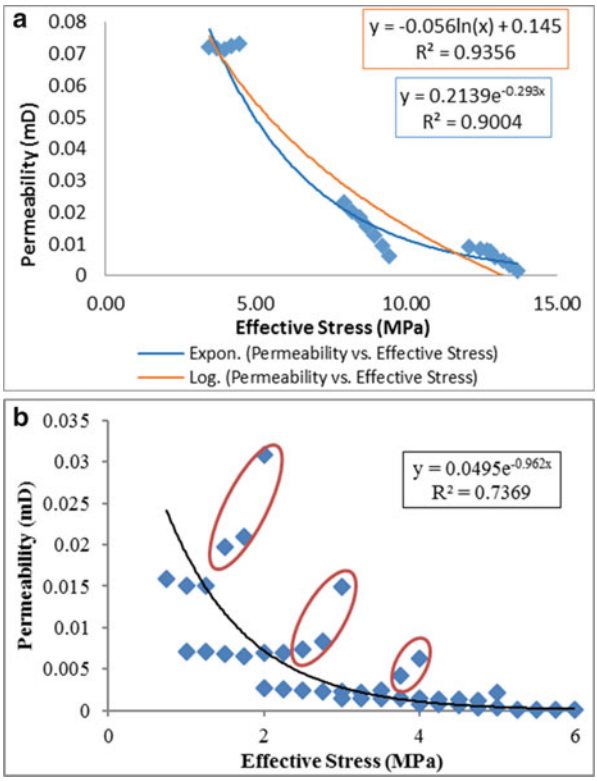

Fig. 5 Variation of permeability of coal in intact (**a**) and fractured (**b**) coal specimens [1]

CH_4 and CO_2, respectively. The major application of this phenomenon would be in enhanced recovery of CBM using CO_2 sequestration.

Al-hawaree [93] tested the change of permeability of coal samples from Alberta, Canada using CO_2 and CH_4 and found that at a constant effective stress in coal, permeability to CO_2 reduced upto 84 %, while that in CH_4 reduced upto 50 % in a comparable range of increasing pore pressure. Li et al. [94] used Powder River Basin coal and utilized pure N_2, CH_4, CO_2 and mixtures of N_2 and CO_2 under a constant effective stress. They established that coal permeability decreased with an increase in the gas sorption pressure, while an increase in the CO_2 component in the flowing mixtures reduced permeability to a greater extent. For pure gases, CO_2 caused the highest permeability reduction followed by CH_4 and finally N_2. Vishal et al. [1] estimated the changes in permeability of intact and fractured coal respectively with effective stresses (Fig. 5a, b).

Several field based studies have also demonstrated reduction in coal permeability with different phases of gas. Reeves [95] detailed the observations from first field scale pilot of enhanced CBM recovery using CO_2 in San Juan Basin, USA. Reduction in injection rate of CO_2 took place with time, from 5mscf/day to 3mscf/day due to loss in injectivity, which shows influence of CO_2 on permeability of coal. Mavor et al. [96] reported a reduction of nearly four times in CO_2 permeability in

coal in ECBM pilot tests in Alberta, Canada. Shi et al. [97] showed that injection of pure N_2 over some days could reverse the permeability reduction due to CO_2 injection in coal beds of Yubari pilot project, Japan. Botnen et al. [98] showed that a reduction by nearly ten times in CO_2 permeability took place in Williston Basin (North Dakota) for lignite.

Mazumder et al. [99] observed multifold increase in CO_2 permeability with respect to reservoir pressure owing to matrix shrinkage. Qu et al. [100] developed models to see the evolution of permeability with CO_2 injection at different temperatures. They observed a maximum permeability reduction of 95 % at 278.15 K. Sander et al. [101] performed core-flood experiments of CO_2-ECBM on two different samples of Australian coal and found the results to be similar to that observed in past studies. No permeability changes were observed in reverse core flood with CH_4 displacing CO_2, thus agreeing with the fact that CO_2 has greater affinity to coal.

5 Adsorptive Weakening of Coal

Previous studies conducted on coal from different basins around the globe have established the adsorptive weakening of coal. Ettinger and Lamba [102] mechanically crushed the coal samples and used the amount of 0.5-mm sieve dust residue as an indicator of coal strength. The samples were first evacuated and then subjected to air and CO_2 saturation at a pressure of 4.0 MPa. The results indicated that the "disturbed" coal samples showed strength reduction by a factor of 0.75 in CO_2 environment as compared to air. Similarly, Tankard [103], measured the changes in surface area of crushed coal due to gas adsorption to understand the influence of sorptive and non sorptive gases on coal. Czaplinski and Holda [104] experimented on the crushing strength of coal in normal air at 0.1 MPa and in CO_2 environment at 2.0 MPa and found that the amount of coal extracted by crushing was much higher when saturated with CO_2 than in air. Holda [105] used the same setup and introduced methane along with CO_2 and air in the scope of investigation. The results revealed that major reduction in coal strength was observed in samples saturated with CO_2 than the ones with CH_4. In contrast to the findings of earlier researchers, Ates and Barron [106] conducted Brazilian tests on Canadian and Australian coals and indicated that no significant reduction in coal strength occurred due to CO_2 saturation upto gas pressure less than 20 atm. Later, Aziz and Ming-Li [107] investigated the effects of gas sorption induced changes in coal strength in terms of coal drillability characteristics. They used pure CO_2 and CH_4 along with their mixtures at variable pressures. The results indicated that CO_2 caused maximum reduction in coal strength as a higher drilling rate and coarser drilling particles were observed in this case. They also showed that an increase in gas pressure increased the drilling rate. This implies that gas type as well as gas pressure influence the strength characteristics of coal.

Table 1 Comparative chart on saturation effects on the uniaxial compressive strength (UCS) and Young's modulus (E) of bituminous coal, Jharia [112]

Condition	UCS (MPa)	ΔUCS (%)	E (GPa)	ΔE (%)
Untreated	15.29 ± 0.32	–	5.34 ± 0.19	–
CO_2	12.62 ± 0.44	17.6	3.94 ± 0.25	26.2
Water	11.39 ± 0.59	25.5	3.32 ± 0.27	37.8
Water + CO_2	$10.95 + 0.41$	28.4	2.79 ± 0.24	47.8

The explanation to this was found in Viete and Ranjith [108] who explained that with an increase in confinement on coal, there was reduction in lowering of adsorptive surface energy and hence, not much weakening was observed. For reduction in the strength of coal under triaxial conditions, the confinement on the coal must be less than the tensile stress of the coal. Karacan [109] explained that coal matrix swelling due to gas adsorption led to an increase in the distance between the atoms in the coal, leading to reduction in its strength. The increase in vitrinite content and increasing CO_2 pressure lead to higher strain and therefore higher reduction in the strength of the coal [109]. These studies are limited to only certain coal and the role of gas injection in coal strength under varied conditions of confinement, coal types and gas phases are still ambiguous and need further investigation. Different ranks of coal, coal with different maceral content are expected to undergo differential reduction in strength due to gas injection. Another study by Pan et al. [110] on Australian black coal indicated no direct evidence of the sorptive weakening character of coal and they suggested that the effect might vary from one coal type to the other.

Hol and Spiers [111] from the laboratory experiments, emphasized on the effects of plasticization that is believed to weaken the internal bonds in coal. They observed that most of the microfractures developed parallel to the bedding plane. A detailed investigation was conducted by Vishal et al. [112] on behavior of coal under saturation with both CO_2 and moisture. They found that the CO_2 treatment of moisture saturated coal reduced the strength of coal by almost 28 % and the Young's modulus by nearly 48 % (Table 1). The acoustic emission results also showed major difference in the pattern of failure of these samples in uniaxial loading. These findings highlight the sorption induced weakening in coal and that it should be addressed before any CO_2 storage operation in coal seams.

6 Conclusions

This chapter reviews the physical attributes associated with the coal-fluid interactions during CO_2 sequestration with/without simultaneous CBM recovery. It is evident that adsorption of CO_2 in coal causes coal matrix swelling which in turn leads to reduction in the strength of coal. Different adsorption models are applied to understand the adsorption phenomenon in coal. Permeability is one of the most

important parameters in methane extraction or CO_2 injection. It depends on several factors such as confining pressure, effective stresses, pore pressure, coal deformation, gas type etc.

CO_2 storage in coal seams has been tested in the past for feasibility at all levels ranging from laborious laboratory scale experiments to pilot scale demonstrations and there is still scope for more research at these levels of testing. But the present scenario demands urgent deployment of such techniques to be able to allow mankind to continue using fossil fuels for a time, until sustainable energy can take charge, without disrupting the climate change predictions. The major advantage of sequestration in coal is that due to the widespread scenario of coal worldwide, technology transfer is the easiest in contrast to geological storage in aquifers and basalt. Geosequestration may be the fastest mode to effectively tune the anthropogenic CO_2 cycle thus making it a forerunner in climate change mitigation initiatives and a buffer directed towards any delay in sustainable energy commercialization.

Acknowledgements This study was conducted as a part of the DST INSPIRE Faculty Award Grant (IFA-13-EAS-07). VV is thankful to the Department of Science and Technology, Government of India, New Delhi for the research grant.

References

1. Vishal V, Ranjith PG, Singh TN (2013) CO_2 permeability of Indian bituminous coals: implications for carbon sequestration. Int J Coal Geol 105:36–47
2. Haenel MW (1992) Recent progress in coal structure research. Fuel 71:1211–1223
3. IUPAC (1972) International union of pure and applied chemistry, manuals of symbols and terminology for physico chemical quantities and units. Butterworth, London
4. Shi JQ, Durucan S (2005) A model for changes in coalbed permeability during primary and enhanced methane recovery. SPEREE 8 SPE 87230-PA 291–299
5. Vishal V (2007) Coal bed methane: an introduction. Indian J Earth Sci 33(1–4):76–79
6. Law DHS, Van der Meer LGH, Gunter WD (2003) Comparison simulators for greenhouse gas sequestration in coalbeds, part III, More complex problems. In: Proceedings of the national energy technology laboratory publication, Conference proceedings of the 2nd annual conference carbon sequestration, Alexandria, Virginia, 5–8 May
7. Langmuir I (1916) The constitution and fundamental properties of solids and liquids. J Am Chem Soc 38:2221–2295
8. Arri LE, Yee D, Morgan WD, Jeansonne MW (1992) Modelling coalbed methane production with binary gas sorption. SPE Rocky Mountain Region Meeting, Casper, Wyoming, SPE-24363
9. Siperstein F, Myers AL (2001) Mixed-gas adsorption. AIChE J 47:1141–1159
10. Mendhe VA, Singh H, Prashant, Sinha A (2011) Sorption capacities for enhanced coalbed methane recovery through CO_2 sequestration in unmineable coal seams of India. In: International conference unconventional source fossil fuels carbon management, GERMI, Gujrat, India
11. Brunauer S, Emmett PH, Teller E (1938) Adsorption of gases in multimolecular layers. J Am Chem Soc 60:309–319
12. Lowell S, Shields JE, Thomas MA, Thommes M (2004) Characterization of porous solids and powders: surface area, pore size and density. Kluwer Academic Publishers, Dordrecht

13. Gregg SJ, Sing KSW (1982) Adsorption surface area and porosity, 2nd edn. Acad Press, New York, p 303
14. Lowell S, Shields JE (1984) Powder surface area and porosity, 2nd edn. John Wiley, New York
15. Polanyi M (1914) ber die Adsorption vom Standpunkt des dritten Wirmesatzes. Verh Dtsch Phys Ge 16:1012–1016
16. Polanyi M (1932) Theories of the adsorption of gases: A general survey and some additional remarks. Trans Faraday Soc 28:316–333
17. Dubinin MM (1967) Adsorption in micropores. J. Colloid Interface Sci. 23(4):487–499
18. Yang RT, Saunders JT (1985) Adsorption of gases on coals and heat treated coals at elevated temperature and pressure: adsorption from hydrogen and methane as single gases. Fuel 64:616–620
19. Patching TH, Mikhail MW (1986) Studies of gas sorption and emission on Canadian coals. CIM Bull 79(887):104–109
20. Mavor MJ, Owen LB, Pratt TJ (1990) Measurement and evaluation of coal isotherm data. In: 65th annual technical conference exhibition and society of petroleum engineers, Richardson, Texas, USA, SPE 20728
21. Stevenson MD, Pinczewski WV, Somers ML, Bagio SE (1991) Adsorption/desorption of multicomponent gas mixtures at in-seam condition. SPE Asia-Pacific conference society of petroleum engineers, Richardson, Texas, USA, SPE 23026
22. Busch A, Krooss BM, Gensterblum Y (2003) Methane and CO_2 sorption and desorption measurements on dry Argonne Premium coals: pure components and mixtures. Int J Coal Geol 55:205–224
23. Ozdemir E, Schroeder K, Morsi BI (2004) CO_2 adsorption capacity of Argonne premium coals. Fuel 83:1085–1094
24. Pariti UM, Harpalani S (1993) Study of coal sorption isotherms using a multicomponent gas mixture. In: International coalbed methane symposium, Tuscaloosa, Alabama, USA, 9356
25. DeGance AE, Morgan WD, Yee D (1993) High pressure adsorption of methane, nitrogen and carbon dioxide on coal substrates. Fluid Phase Equilib 82:215–224
26. Hall FE, Zhou C, Gasem KAM, Robinson Jr RL (1994) Adsorption of pure methane, nitrogen, and carbon dioxide and their binary mixtures on Wet Fruitland Coal. In: East regional conference exhibition, society petroleum engineers, Richardson, Texas, USA, SPE 29194
27. Clarkson CR, Bustin RM (1999) The effect of pore structure and gas pressure upon the transport properties of coal: a laboratory and modeling study. 1. Isotherms and pore volume distributions. Fuel 78(11):1333–1344
28. Barrer RM (1984) Diffusivities in glassy polymers for the dual mode sorption model. J Membr Sci 18:25–32
29. Koros WJ (1980) Model for sorption of mixed gases in glassy polymers. J Polym Sci Polym Phys 18:981–989
30. Huddleston JC, Marshall JS, Pilcher RC (1995) Analysis of sorption and thermodynamic data and a discussion of an empirical model for sorbed gases in coal. In: International unconventional gas symposium, University Alabama, Tuscaloosa, Alabama, USA, 9523
31. Chaback J, Morgan W, Yee D (1996) Sorption of nitrogen, methane, carbon dioxide and their mixtures on bituminous coals at in-situ conditions. Fluid Phase Equilib 117:289–296
32. Vishal V, Singh TN, Ranjith PG (2015) Influence of sorption time in CO_2-ECBM process in Indian coals using coupled numerical simulation. Fuel 139:51–58
33. Gunter WD, Gentzis T, Rottenfuser BA, Richardson RJH (1997) Deep coalbed methane in Alberta, Canada: a fossil resource with the potential of zero greenhouse gas emissions. Energy Convers Manage 38:217–222
34. Gentzis T (2000) Subsurface sequestration of carbon dioxide – an overview from an Alberta (Canada) perspective. Int J Coal Geol 43:287–305
35. Mastalerz M, Gluskoter H, Rupp J (2004) Carbon dioxide and methane sorption in high volatile bituminous coals from Indiana, USA. Int J Coal Geol 6(1):43–55

36. Mazumder S, Karnik AA, Wolf KHAA (2006) Swelling of coal in response to CO_2 sequestration for ECBM and its effect on fracture permeability. SPE J 11(3):390–398
37. Larsen JW, Kovac J (1978) Polymer structure of bituminous coals. ACS Symp Ser 71:36–49
38. Brenner (1985) The macromolecular nature of bituminous coal. Fuel 64:167–173
39. Larsen JW, Flowers RA II, Hall P, Carlson G (1997) Structural rearrangement of strained coals. Energy Fuel 11:998–1002
40. Larsen JW (2004) The effects of dissolved CO_2 on coal structure and properties. Int J Coal Geol 57:63–70
41. Karacan CO (2003) Heterogeneous sorption and swelling in a confined and stressed coal during CO_2 injection. Energy Fuel 17:1595–1608
42. Reucroft PJ, Sethuraman AR (1987) Effect of pressure on carbon dioxide induced coal swelling. Energy Fuel 1:72–75
43. Astakhov AV, Shirochin DL (1991) Capillary-like condensation of sorbed gases in coals. Fuel 70:51–56
44. Jakubov TS, Mainwaring DE (2002) Adsorption-induced dimensional changes of solids. Phys Chem Chem Phys 4(22):5678–5682
45. Pan Z, Connell LD (2007) A theoretical model for gas adsorption-induced coal swelling. Int J Coal Geol 69(4):243–252
46. Hobbs DW (1964) The strength and the stress-strain characteristics of coal in triaxial compression. J Geol 72(2):214–231
47. Czaplinski A, Gustkiewicz J (1990) Sorption stresses and deformations in coal. Strata Multiph Med (in Polish, Eng ver prov by second auth) 2:455–468
48. George JD, Barkat MA (2001) The change in effective stress associated with shrinkage from gas desorption in coal. Int J Coal Geol 45:105–113
49. Briggs H, Sinha RP (1933) Expansion and contraction of coal caused respectively by the sorption and discharge of gas. Proc Roy Soc Edinb 53:48–53
50. Reucroft PJ, Patel H (1986) Gas-induced swelling in coal. Fuel 65:816–820
51. Walker PL, Verma SK Jr, Rivera-Utrilla J, Khan MR (1988) A direct measurement of expansion in coals and macerals induced by carbon dioxide and methanol. Fuel 67:719–726
52. Moffat DH, Weale KE (1955) Sorption by coal of methane at high pressure. Fuel 34:449–462
53. Harpalani S, Schraufnagel RA (1990) Shrinkage of coal matrix with release of gas and its impact on permeability of coal. Fuel 69:551–556
54. Ceglarska SG, Czaplinski A (1993) Correlation between sorption and dilatometric processes in hard coals. Fuel 72(3):413–417
55. Ceglarska-Stefanska G (1994) Effect of gas pressure in methane induced swelling on the porous structure of coals. Stud Surf sci Catal 87:671–677
56. Czaplinski A (1971) Simultaneous testing of kinetics of expansion and sorption in coal of carbon dioxide. Archiv Gornick 16:227–231
57. Harpalani S, Chen G (1995) Estimation of changes in fracture porosity of coal with gas emission. Fuel 74(10):1491–1498
58. Levine JR (1996) Model study of the influence of matrix shrinkage on absolute permeability of coal bed reservoirs. Coalbed methane and coal geology. Geology of Society, London, pp 197–212
59. Ceglarska-Stefanska G, Holda S (1994) Effect of sorption of vapours of gases and fluids on properties of hard coal. In: Czaplinski, A (ed.) Chapter 13, Acad min metal, Krakow, Poland, 183–202
60. Ceglarska-Stefańska G, Zarębska K, Aleksandrowicz K (2002) Displacement sorption of CO_2 and CH_4 on low rank hard coal within a low gas pressure range. Arch Min Sci 47:157–173
61. Ceglarska-Stefanska G, Zarebska K (2002) The competitive sorption of CO_2 and CH_4 with regard to the release of methane from coal. Fuel Process Technol 77–78:423–429

62. Chikatamarla L, Cui X, Bustin RM (2004) Implications of volumetric swelling/shrinkage of coal in sequestration of acid gases. In: International coalbed methane symposium, University of Alabama, Tuscaloosa, Alabama, USA, 0435
63. Mazumder S, van Hemert P, Busch A, Wolf KHA, Tejera-Cuesta P (2006) Flue gas and pure CO_2 sorption properties of coal: a comparative study. Int J Coal Geol 67:267–279
64. Siemons N, Busch A (2007) Measurement and interpretation of supercritical CO_2 sorption on various coals. Int J Coal Geol 69(4):229–242
65. Day S, Fry R, Sakurovs R (2008) Swelling of Australian coals in supercritical CO_2. Int J Coal Geol 74:41–52
66. Zarebska K, Ceglarska-Stefanska G (2009) The change in effective stress associated with swelling during carbon dioxide sequestration on natural gas recovery. Int J Coal Geol 74(3–4):167–174
67. Pone JDN, Halleck PM, Mathews JP (2010) 3D characterization of coal strains induced by compression, carbon dioxide sorption and desorption at in situ stress conditions. Int J Coal Geol 82:262–268
68. Majewska Z, Ceglarska-Stefanska G, Majewski S, Zietek J (2009) Binary gas sorption/desorption experiments on a bituminous coal: simultaneous measurements on sorption kinetics, volumetric strain and acoustic emission. Int J Coal Geol 77(1–2):90–102
69. Pini R, Ottiger L, Storti G, Mazzotti M (2009) Role of adsorption and swelling on the dynamics of gas injection in coal. J Geophys Res Solid Earth 114(B4):B04203
70. van Bergen F, Spiers C, Floor G, Bots P (2009) Strain development in unconfined coals exposed to CO2, CH4 and Ar: effect of moisture. Int J Coal Geol 77(1–2):43–53
71. Battistutta E, Van Hemert P, Lutynski M, Bruining H, Wolf KH (2010) Swelling and sorption experiments on methane, nitrogen and carbon dioxide on dry Selar Cornish coal. Int J Coal Geol 84:39–48
72. Vishal V, Singh L, Pradhan SP, Singh TN, Ranjith PG (2013) Numerical modeling of Gondwana coal seams in India as coalbed methane reservoirs substituted for carbon dioxide sequestration. Energy 49:384–394
73. Day S, Fry R, Sakurovs R (2011) Swelling of moist coal in carbon dioxide and methane. Int J Coal Geol 86:197–203
74. Day S, Fry R, Sakurovs R (2012) Swelling of coal in carbon dioxide, methane and their mixtures. Int J Coal Geol 93:40–48
75. Syed A, Durucan S, Shi J, Korre A (2013) Flue gas injection for CO_2 storage and enhanced coalbed methane recovery: mixed gas sorption and swelling characteristics of coals. Energy Procedia 37:6738–6745
76. Majewska Z, Majewski S, Zietekm J (2013) Swelling and acoustic emission behaviour of unconfined and confined coal during sorption of CO_2. Int J Coal Geol 116:17–25
77. Anggara F, Sasaki K, Rodrigues S, Sugai Y (2014) The effect of megascopic texture on swelling of a low rank coal in supercritical carbon dioxide. Int J Coal Geol 125:45–56
78. Gray I (1987) Reservoir engineering in coal seams: part 1—the physical process of gas storage and movement in coal seams. SPE Reserv Eng 2:28–34
79. Palmer I, Mansoori J (1998) How permeability depends on stress and pore pressure in coalbeds: a new model. SPEREE 1(6):539–544, SPE-52607-PA
80. Pekot LJ, Reeves SR (2003) Modeling the effects of matrix shrinkage and differential swelling on coalbed methane recovery and carbon sequestration. In: International coalbed methane symposium, University of Alabama, Tuscaloosa, 0328
81. Shi JQ, Durucan S (2004) Drawdown induced changes in permeability of coalbeds: a new interpretation of the reservoir response to primary recovery. Transp Porous Media 56:1–16
82. Cui X, Bustin RM (2005) Volumetric strain associated with methane desorption and its impact on coalbed gas production from deep coal seams. AAPG Bull 89(9):1181–1202
83. Cui X, Bustin RM, Chikatamarla L (2007) Adsorption-induced coal swelling and stress: implications for methane production and acid gas sequestration into coal seams. J Geophys Res 112:B10202

84. Wang GX, Massarotto P, Rudolph V (2009) An improved permeability model of coal for coalbed methane recovery and CO_2 geosequestration. Int J Coal Geol 77:127–136
85. Darcy H (1856) Les Fontaines publiques de la ville de Dijon. V. Dalmont, Paris
86. Pomeroy CD, Robinson DJ (1967) The effect of applied stresses on the permeability of a middle rank coal to water. Int J Rock Mech Min Sci 4:329–343
87. Koenig RA, Stubbs PB (1986) Interference testing of a coalbed methane reservoir, SPE unconventional gas technology symposium society of petroleum engineers, Richardson, Texas, USA, SPE 15225
88. Gash BW, Volz RF, Potter G, Corgan JM (1993) The effects of cleat orientation and confining pressure on cleat porosity, permeability and relative permeability in coal. In: International coalbed methane symposium, University of Alabama, Tuscaloosa, Alabama, USA. SPE–9321
89. Patching TH (1965) Variations in permeability of coal. In: Proceedings of the Rock mechanics symposium, University of Toronto, pp 185–194
90. Somerton WH, Soylemezoglu IM, Dudley RC (1975) Effect of stress on permeability of coal. Int J Rock Mech Min Sci Geomech Abstr 12:129–145
91. Skawinski R (1999) Considerations referring to coal swelling accompanying the sorption of gases and water. Arch Min Sci 44:425–434
92. Robertson EP (2005) Measurement and modeling of sorption-induced strain and permeability changes in coal. Idaho National Laboratory, INL/EXT-06-11832
93. Al-hawaree M (1999) Geomechanics of CO_2 sequestration in coalbed methane reservoir. Thesis Master Degree, Department of Civil Environment Engineer, University of Alberta, Edmonton, Alberta, Canada
94. Li X, Nie B, Ren T (2008) Analysis and research on influencing factors of coal reservoir permeability. In: Coal operators conference, Wollongong, Australia, University of Wollongong, 197–201
95. Reeves SR (2001) Geological sequestration of CO_2 in deep, unmineable coalbeds: an integrated research and commercial-scale field demonstration project. SPE annual technical conference exhibition, Society of petroleum engineers, Richardson, Texas, USA, SPE 71749
96. Mavor MJ, Gunter WD, Robinson JR (2004) Alberta multiwell micro-pilot testing for CBM properties, enhanced recovery. Society of petroleum engineers, Richardson, Texas, USA, SPE-90256
97. Shi JQ, Durucan S, Fujioka M (2008) A reservoir simulation study of CO_2 injection and N_2 flooding at the Ishikari coalfield CO_2 storage pilot project, Japan. Int J Greenhouse Gas Control 2:47–57
98. Botnen LS, Fisher DW, Dobroskok AA, Bratton TR, Greaves KH, McLendon TR et al (2009) Field test of CO_2 injection and storage in lignite coal seam in North Dakota. Energy Procedia 1(1):2013–2019
99. Mazumder S, Scott M, Jiang J (2012) Permeability increase in Bowen Basin coal as a result of matrix shrinkage during primary depletion. Int J Coal Geol 96:109–119
100. Qu H, Liu J, Chen Z, Wang J, Pan Z, Connell L, Elsworth D (2012) Complex evolution of coal permeability during CO_2 injection under variable temperatures. Int J Greenhouse Gas Cont 9:281–293
101. Sander R, Connell LD, Pan Z, Camilleri M, Heryanto D, Lupton N (2014) Core flooding experiments of CO_2 enhanced coalbed methane recovery. Int J Coal Geol 131:113–125
102. Ettinger IL, Lamba EG (1957) Gas medium in coal-breaking processes. Fuel 36(3):298–306
103. Tankard JHG (1958) The effect of sorbed carbon dioxide upon the strength of coals. MS thesis, Department of Mining Engineering, University of Sydney
104. Czapliński A, Holda S (1982) Changes in mechanical properties of coal due to sorption of carbon dioxide vapour. Fuel 61(12):1281–1282
105. Holda S (1986) Investigation of adsorption, dilatometry and strength of low rank coal. Archiw GornicTom 3:599–608

106. Ates Y, Barron K (1988) The effect of gas sorption on the strength of coal. Min Sci Technol 6(3):291–300
107. Aziz NI, Ming-Li W (1999) The effect of sorbed gas on the strength of coal: an experimental study. Geotech Geol Eng 17(3):387–402
108. Viete DR, Ranjith PG (2007) The mechanical behaviour of coal with respect to CO_2 sequestration in deep coal seams. Fuel 86:2667–2671
109. Karacan CO (2007) Swelling-induced volumetric strains internal to a stressed coal associated with CO_2 sorption. Int J Coal Geol 72:209–220
110. Pan Z, Connell LD, Camilleri M (2010) Laboratory characterisation of coal reservoir permeability for primary and enhanced coalbed methane recovery. Int J Coal Geol 82:252–261
111. Hol S, Spiers CJ (2012) Competition between adsorption-induced swelling and elastic compression of coal at CO_2 pressures up to 100 MPa. J Mech Phys Solids 60(11):1862–1882
112. Vishal V, Ranjith PG, Singh TN (2015) An experimental investigation on behaviour of coal under fluid saturation, using acoustic emission. J Nat Gas Sci Eng 22:428–436

Part V
CO_2 Storage in Oil Reservoirs

Storage of CO_2 in depleted/producing oil reservoirs

Amin Ettehadtavakkol

Abstract This chapter presents a framework for an environmental based assessment of CO_2 storage operations in depleted/producing oil reservoirs. We specially focus on the CO_2 enhanced oil recovery (EOR) and storage as the primal advantage of the storage in producing and depleted oilfields. We begin with a qualitative assessment of the physical aspects of EOR-storage process. Then we present a basic quantitative method for the EOR-storage performance evaluation. Finally, we discuss the field scale development of EOR operation for industrial CO_2 storage and address the environmental assessment of the EOR-storage operation. The contents of this chapter aim to benefit reservoir engineers and geologists who seek to upscale and communicate the technical knowledge on field-scale CO_2-EOR operations into tangible environmental and technical performance measures that are better observed by managers and policy makers.

1 Introduction

CO_2 storage in depleted and producing oil reservoirs follows two objectives: utilization of CO_2 for enhanced oil recovery and permanent underground CO_2 storage. CO_2-EOR is a well-established technology that produces oil from the already-developed oilfields. The CO_2-EOR process inevitably stores substantial volumes of CO_2 in the subsurface formations, but the storage is not the prime benefit of the process. The storage aspect becomes an objective when anthropogenic CO_2 is used instead of the natural CO_2.

The synergy between the CO_2-EOR and the anthropogenic CO_2 storage provides an attractive alternative for the short-term mitigation of the greenhouse gas emissions. From an environmental view point, a portion of the CO_2 emissions from the oil production and consumption operations is offset via geological storage. From an economic viewpoint, a portion of the costs of CO_2 capture, transport and injection

A. Ettehadtavakkol (✉)
Bob L. Herd Department of Petroleum Engineering, Texas Tech University, Lubbock, TX, Box 43111, 79409-3111, USA
e-mail: amin.ettehadtavakkol@ttu.edu

V. Vishal, T.N. Singh (eds.), *Geologic Carbon Sequestration*,
DOI 10.1007/978-3-319-27019-7_10

processes are compensated by the incremental oil production. In the long-term, the EOR-storage projects have the following benefits.

1. Increase in the domestic oil production and energy security enhancement,
2. Promotion of the oilfield operators participation in the CO_2 storage projects because of tax credits [1],
3. Expansion of the carbon capture, utilization and storage (CCUS) infrastructure, especially the pipeline network.

The EOR-storage projects need to overcome some major challenges, before they become stablished as an industrial practice. A considerable impact on carbon emission reduction requires sustainable large-scale CO_2 storage for decades. This requires that the pipeline network and infrastructure, subsurface uncertainties, regulatory framework, long-term liability, and public acceptance issues are all resolved.

The individual processes of CO_2-EOR and CO_2 storage have been addressed from different perspectives and we will cover the major aspects in this chapter. Our main focus, however, will be on the fundamental physical model of the EOR-storage process.

1.1 Physical Aspects of CO_2-EOR and CO_2 Storage Processes

The objective of any EOR process is to maximize the recovery efficiency (E) which is a product of the displacement efficiency (E_d) and the volumetric sweep efficiency, i.e. $E = E_d \times E_v$. This section is dedicated to the parameters that affect the recovery efficiency and the design parameters that improve the recovery. The CO_2 storage process has the same physical foundation as EOR, though the subjects of dissolution, capillary trapping, plume migration and leakage are more emphasized. Therefore, one can easily extend the basic model of CO_2-EOR process to EOR-storage to predict and interpret the results.

The CO_2-EOR process is characterized as a multi-phase and multi-component displacement process. In the CO_2-EOR process the super critical CO_2 is injected to an oilfield at some state of maturity, typically after the secondary recovery phase. Figure 1a shows the sequence and the typical oil recovery range of the primary, secondary water flooding and the tertiary EOR phases. CO_2 is normally injected in alternating cycles with water, a process that is referred to as water-alternating-gas (WAG) injection. The major physical aspects of the WAG injection process follow.

1. Miscibility is a key phase behavior concept that determines the displacement efficiency and storage capacity at pore scale [2]. The two phases of oil and CO_2 are miscible if they mix in all properties and form one "oleic" phase. The reservoir pressure, temperature and the oil composition determine the CO_2 miscibility with oil. Numerous studies investigated the effect of reservoir fluid

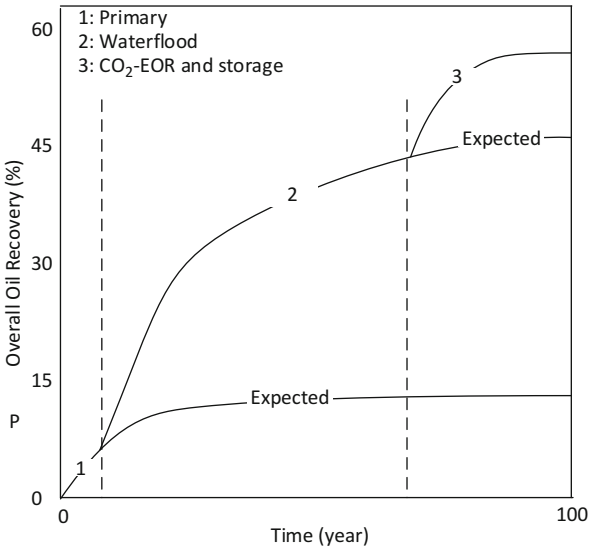

Fig. 1 Incremental oil recovery from the primary, secondary (waterflood), and tertiary (CO_2-EOR and storage) phases. A typical recovery range and duration is shown for each stage. The expected projection of recovery is shown after the transition to the new phase

and conditions on the CO_2 miscibility. In general, high pressure (greater than 1500 psi), low temperature (less than 140 °F), high concentration of intermediate components (C4-C6), and low oil density (API greater than 30°) are the favorable conditions for the miscibility development.

2. When CO_2 develops miscibility with oil, the oleic phase mobility improves through the swelling, density reduction, viscosity reduction, and increase of oleic phase saturation. These help the viscous forces, which tend to push the oil out towards the producers, to overcome the capillary forces, which tend to keep the oil trapped in the rock pores. As a result of miscibility, the mobile, swelled oleic phase is "dragged and pushed" from the injectors towards the producers.
3. The oleic phase ahead of the injected CO_2 plume forms an oil bank. In fact, the observation of a big oil peak at the producer after the injection of CO_2 is the sign of a successful WAG injection.
4. The oil production will follow an exponential-type decline after the oil peak due to the formation of low resistance CO_2 flow paths from the injectors to the producers. CO_2 has a high mobility and is less dense than water and oil; therefore, it tends to "channel" through the high permeability layers and "finger" through the sweep area between the producer and injector. These effects reduce the volumetric sweep efficiency if CO_2 is continuously injected. To resolve the associated challenges of pure CO_2 injection, the CO_2 and water are injected in alternating cycles (WAG). The objective of the WAG injection is to maximize the volumetric sweep efficiency through the adjustment of CO_2 and water half-cycle durations. The WAG process mitigates the unfavorable side effects of the high mobility of CO_2 [3] and ultimately improves the vertical and areal sweep efficiencies.

5. The reservoir heterogeneity and anisotropy have an unfavorable effect on the volumetric sweep efficiency. These effects are mitigated through the design of injection patterns, selective well injection, and zonal isolation and completion operations.
6. The EOR-storage projects will require a cyclic WAG process because the produced water is required to be re-injected to maintain the reservoir pressure, reduce the unfavorable effects of viscous fingering and channeling, reduce the CO_2 trapping, and minimize the environmental footprint of the operation.
7. The choice of the WAG ratio is a critical design parameter of the EOR-storage projects [4]. Figure 2 illustrates the typical oil production response to a WAG injection process. Figure 2a shows an idealized cyclic WAG injection for a tuned reservoir model representing 6 injectors and 8 producers in the Sacroc Unit, Permian Basin. Figure 2b shows the corresponding oil production response. The ideal oil production response to the simultaneous WAG injection is an oil peak followed by a long-tailed exponential-type decline. A low WAG ratio increases the CO_2 storage capacity but decreases the pace of the fieldwide implementation of the EOR project. In practice, water and CO_2 are not injected as regularly as shown in Figure 2a and the oil production response is not as smooth and predictable as shown in Figure 2b.

In the storage process, the CO_2 displaces the mobile resident fluids of the pores and pushes them out to other zones and layers or towards the producers [5]. This process involves both convection and diffusion mechanisms and results in the partial trapping of the injected CO_2 in the reservoir pores or as a dissolved component in the aqueous and oleic phases.

The CO_2 trapping mechanisms are divided into four types: structural, capillary, dissolution, and mineral trapping [6]. The environmental risk of the trapping depends on the contribution of each mechanism. Normally, the structural trapping is the least secure and mineral trapping is the most secure mechanism and the capillary and dissolution mechanisms fall in between. The risk of CO_2 leakage is high through the injection after the completion of injection phase because the contribution of the structural and capillary trapping mechanisms are high. The risk of CO_2 leakage reduces over time as the contribution of the more secure dissolution and mineral trapping mechanisms become larger. This transition of trapping mechanisms normally takes decades to centuries [7].

In the WAG injection, the injected water displaces a large portion of the CO_2 that is trapped through the structural mechanism and takes up the pore space that would otherwise be occupied by the CO_2 plume. This is evidently detrimental to the long-term storage objective. However, the injection of water is crucial environmentally for the produced water management and economically for the volumetric sweep efficiency improvement. This, highlights the importance of the adjustment of the WAG ratio in the EOR-storage design. The water injection has minimal effect on the dissolved- or capillary-trapped CO_2 because of the hysteresis effects on the capillary and relative permeability curves [8]. The mineral trapping is far too slow to substantially affect the injection phase.

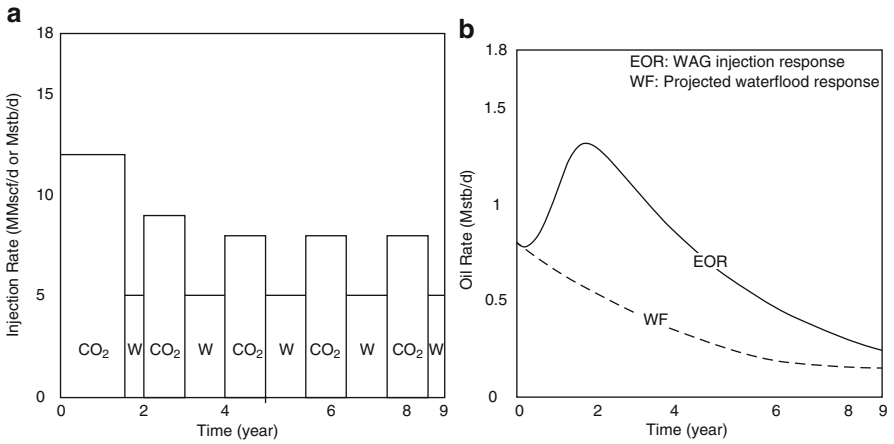

Fig. 2 (**a**) Schematic WAG injection process, the WAG ratio increases with time in an industrial EOR application (**b**) oil production response to the simultaneous WAG injection for a block of 8 producers in the Sacroc Unit, Permian Basin

1.2 CO_2-EOR and Storage Mechanism

This section discusses the physical governing equations of the CO_2-EOR and storage process. The fractional flow theory and the method of characteristics form the foundations of the analysis [9, 10]. We use a graphical solution approach presented by Walsh and Lake [10] that greatly simplifies the analytical results. However, the reader needs a background on the theoretical subject to fully benefit from the discussion.

The method of characteristics assumes the following idealizations for the EOR-storage model:

1. One-dimensional flow at a constant rate in a homogeneous and isothermal permeable medium. At most three components, i = 1(water), 2(oil), and 3 (CO_2), and two phases, j = w (aqueous) and o (oleic), are present. The aqueous phase contains water and dissolved CO_2 but no oil. The oleic phase contains oil and CO_2 components but no water. The CO_2 solubility in the oleic phase is orders of magnitude greater than that of the aqueous phase.
2. The fluids are in local thermodynamic equilibrium do not react with the rock and mix ideally. CO_2 is miscible with oil and the miscibility is achieved at a rate substantially faster than the fluid flow rate. Ideal mixing means that no volume changes occur through mixing and we can transform mass concentrations into volume fractions.
3. The rock and fluid properties are independent from pressure, implying that the rock and fluids are incompressible and volumetric flowrates are conservative of the mass balance. This assumption will introduce an error to the fractional flow solution compared to the practical cases in which the injection and production

pressures are fairly stable and the rate varies with time; however, the general insight obtained is still valuable.

4. Dissipation phenomena, including phase capillary pressure and dispersion and diffusion between components in a single phase are negligible.
5. CO_2 and water are simultaneously injected. In practice, CO_2 and water are injected in alternating cycles as shown in Fig. 2. Under this assumption, we slightly overestimate the oil recovery; but again, the general insight obtained is valuable.

With the above assumptions, the material balance for component i is given as,

$$\frac{\partial C_1}{\partial t_D} + \frac{\partial F_1}{\partial x_D} = 0 \tag{1a}$$

$$\frac{\partial C_2}{\partial t_D} + \frac{\partial F_2}{\partial x_D} = 0 \tag{1b}$$

for the water (i = 1) and oil (i = 2) components and C and F are the corresponding concentration and fractional flow, respectively. The independent variables in Eq. (1) are dimensionless time defined as the cumulative pore volume injection $t_D = q \times t/v_p$, and dimensionless position, defined as $x_D = x/L$, q is the flowrate, v_p is the total pore volume and L is the length of the permeable medium.

Since two phases are present, the overall composition and flow of any component is given as,

$$C_i = S_w C_{iw} + (1 - S_w) C_{io} \tag{2a}$$

$$F_i = f_w C_{iw} + (1 - f_w) C_{io} \tag{2b}$$

Where C_{iw} and C_{io} denote the volume fractions of component i in the aqueous and oleic phases, respectively, S_w is the aqueous phase saturation and f_w is the fractional flow of the aqueous phase. Water does not dissolve into the oleic phase and oil does not dissolve in the aqueous phase either. Therefore,

$$C_1 = S_w C_{1w} \tag{3a}$$

$$F_1 = f_w C_{1w} \tag{3b}$$

$$C_2 = (1\text{-}S_w) C_{2o} \tag{3c}$$

$$F_2 = (1\text{-}f_w) C_{2o}. \tag{3d}$$

CO_2 slightly dissolves in the aqueous phase and mainly in the oleic phase, therefore,

$$C_3 = S_w C_{3w} + (1\text{-}S_w) C_{3o} \tag{3e}$$

$$F_3 = f_w C_{3w} + (1\text{-}f_w) C_{3o}. \tag{3f}$$

The fractional flow f_w is generally a non-linear function in the aqueous phase

saturation S_w and the phase properties. The aqueous phase fractional flow for a dipping reservoir with constant dip angle α is given as,

$$f_w = \frac{\lambda_{rw}}{\lambda_{rw} + \lambda_{ro}} \left\{ 1 - \frac{k\lambda_{ro}(\rho_w - \rho_o)g}{u} \sin\alpha \right\} \tag{4}$$

where u is the total Darcy velocity of the two phases $u = u_w + u_o$, k is absolute permeability, and λ_{rw} and λ_{ro} are the relative mobilities of the aqueous and oleic phases, respectively. The relative mobility is defined as the ratio of relative permeability to the viscosity for each phase, for the aqueous phase, for example $\lambda_{rw} = k_{rw}/\mu_w$. The oleic phase viscosity is a function of the oil concentration C_{2o}; however, we assume a constant viscosity for oleic phase. We also assume that the dip angle is zero. Under these assumptions, the fractional flow is a function of S_w only.

The overall fluxes F_1 and F_2 are functions of C_1 and C_2 only. Given a value of C_1 and C_2, a flash calculation can be performed to find the equilibrium phase compositions c_{1w} and c_{2o}, and then the phase saturations can be calculated. From the saturations, the relative permeabilities (k_{rw} and k_{ro}) and mobilities are calculated. These will provide all the data required for Eq. (4) to calculate the fractional flows. Therefore, the objective is to find C_1 and C_2 at all times and positions.

The corresponding eigenvalue problem to the system of partial differential equations in Eq. (1) has two solutions, a tieline eigenvalue λ_t and a non-tieline eigenvalue λ_{nt}.

$$\lambda_t = \frac{\partial F_1}{\partial C_1} \tag{5a}$$

$$\lambda_{nt} = \frac{F_1 - 1}{C_1 - 1} \tag{5b}$$

These eigenvalues are associated with two eigenvectors, a tieline eigenvector e_t and a non-tieline eigenvector e_{nt},

$$\vec{e}_t = \begin{pmatrix} 1 \\ 0 \end{pmatrix} \tag{5c}$$

$$\vec{e}_{nt} = \begin{pmatrix} 1 \\ \dfrac{\lambda_{nt} - \lambda_t}{f_1} \end{pmatrix} \tag{5d}$$

The eigenvalues and eigenvectors determine the compositional velocity and the compositional paths, respectively. The compositional solution path can theoretically take any arbitrary path. However, the variation of compositional velocity and path is strictly governed by the phase behavior, material balance and the initial and injection conditions.

The ternary phase diagram of the water, oil and CO_2 system, shown in Fig. 3, provides important information for the calculation of eigenvalues and eigenvectors, as follows:

1. The two phase region is expanded almost all over the phase diagram. The only single-phase regions are the line connecting the CO_2 and oil ($c_{1w} = 0$) and the single pure water corner ($c_{1w} = 1$).
2. The compositional solution may travel on the two-phase tielines. These tielines appear as the water-oil and CO_2-water edges of the ternary diagram. Each tieline is associated with a tieline eigenvalue and eigenvector. The velocity and direction of compositional change along the tielines are determined by Eqs. (5a) and (5c).
3. The injection condition J falls on the CO_2-water tieline and the initial condition I falls on the water-oil tieline. These two tielines are important because the compositional solution will pass through them. In fact, the water-oil and CO_2-water tielines are the only two tielines that particularly matter to the EOR-storage problem.
4. The compositional path has to switch at some point from the injection tieline and travel through a non-tieline path to reach the initial tieline. The velocity and direction of the compositional change along this non-tieline path is determined by Eqs. (5b) and (5d).
5. The tielines all intersect at one point, either at the pure water corner if $c_{1w} = 1$ or $c_{1w} \sim 1$ if the small CO_2 solubility exists in aqueous phase. When the tielines all meet at one point, the non-tieline compositional velocity λ_{nt} has a constant value [11].

We assume that the CO_2 solubility in the aqueous phase is so small that it negligibly affects the fractional flow of water. This reasonable assumption simplifies the composition path along the tielines. The fractional flow of any component along the tieline paths is now a function of water saturation only,

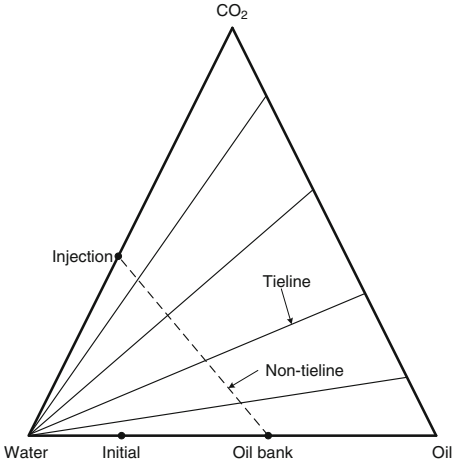

Fig. 3 Phase diagram of water-oil-CO_2 system. The tieline and non-tieline paths with the initial, injection and the oil bank compositions are shown. The two-phase tielines pass through the pure water point

$$\lambda_t = \frac{\partial F_1}{\partial C_1} = \frac{d(C_{1w} f_w)}{d(C_{1w} S_w)} \simeq \frac{df_w}{dS_w} \tag{6}$$

The graphical interpretation of the tieline path is the well-known Buckley-Leverett solution. Therefore, we need to consider two f_w-S_w tieline equations, one for water-oil $\lambda_{t,wo}$ and one for CO_2-water$\lambda_{t,CO2w}$. Equation (4) is used to find the corresponding relations. The saturation path along these tielines will either follow the f_w-S_w curve or form a shock depending on the initial and final saturations [2].

The solution to the EOR-storage problem is a set of saturation paths that connects the initial reservoir condition (I) and the injection condition (J). These two saturations fall on different tielines, namely CO_2-water and water-oil. Therefore, the saturation path may require a switch path from the CO_2-water to the water-oil tieline. This switch path occurs along the non-tieline path. With the assumption of negligible impact of CO_2 solubility in aqueous phase and the presence of residual oil saturation, the non-tieline velocity for the water component given in Eq. (5b) simplifies to a straight line with slope of λ_{nt},

$$\lambda_{nt} = \frac{f_{w,s} - b}{S_{w,s} - a} \tag{7a}$$

$$a = \frac{1 - S_{oc}(1 - C_{3o})}{1 - C_{3w}} \tag{7b}$$

$$b = \frac{1}{1 - C_{3w}} \tag{7c}$$

where C_{3w} is the CO_2 volume fraction in the aqueous phase, S_{oc} is the residual oil saturation with respect to miscible CO_2 flood, C_{3o} is the volume fraction of the CO_2 in the oleic phase. The graphical interpretation of the non-tieline velocity on the f_w-S_w plot is a straight line passing through points (a,b) and ($S_{w,s}$,$f_{w,s}$) on the CO_2-water fractional flow curve.

Given that the non-tieline velocity is constant we get the same component velocity for the oil.

$$\lambda_{nt} = \frac{f_{w,OB} - 1}{S_{w,OB} - c} \tag{7d}$$

$$c = 1 - S_{oc}(1 - C_{3o}) \tag{7e}$$

The non-tieline velocity is independent of the component type and therefore the water and oil component velocities are equal. The same result can also be inferred from that of the coherence condition. The graphical interpretation of the non-tieline velocity on the f_w-S_w plot is a straight line passing through points (c,1) and ($S_{w,OB}$, $f_{w,OB}$) on the water-oil fractional flow curve. Note that $1 \leq c \leq a$, because the CO_2 solubility in the oleic phase is greater than the aqueous phase. Therefore, the point (c,1) always falls to the left of the point (a,b) on the fractional flow plot.

Based on the phase behavior discussions, we know that the saturation path will travel first along the water-solvent tieline from the injection condition J ($S_{w,J}$,$f_{w,J}$) to a switch point ($S_{w,s}$,$f_{w,s}$); then the saturation follows a straight non-tieline line towards the water-oil tieline and lands on ($S_{w,OB}$,$f_{w,OB}$); from there it follows a tieline path towards the initial condition ($S_{w,I}$,$f_{w,I}$). However, the values of the switch points are not determined through phase behavior. The material balance determines these values. The material balance implies that the switch points must satisfy two conditions:

1. The velocity of the upstream saturations should not be greater than the downstream saturations. This implies that $\lambda_{t,CO2w} \leq \lambda_{nt} \leq \lambda_{t,wo.}$ The graphical interpretation of this condition is that the slope of the saturation paths should be non-decreasing from the upstream injection condition to the downstream initial condition.
2. The saturations should have a unique velocity. The graphical interpretation of this condition is to prevent the tieline and non-tieline paths from intersecting at multiple points.

The initial and injection conditions considerably affect the results. The initial condition depends on the reservoir's state of maturity. The initial condition greatly affects the EOR-stroage performance. The EOR-storage implementation after a primary production phase implies that the initial oil saturation is relatively high, for example $S_{oI} = 1\text{-}S_{wir}$ where S_{wir} is the irreducible water saturation. The EOR-storage implementation after a secondary waterflood phase implies that the initial oil saturation is near the residual saturation to water, for example, $S_{oi} = S_{orw}$where S_{orw} is the residual oil saturation to water. Since there is no CO_2 present in the reservoir at the beginning of injection, the corresponding concentrations of the three components are equal to the initial saturations (Eq. 3).

The injection condition, specifically the WAG ratio, is an important parameter. The water fractional flow is related to the WAG ratio W_R as,

$$f_{wJ} = \frac{W_R}{1 + W_R} \tag{8}$$

With the WAG ratio known, f_{wJ} and S_{wJ} are consecutively calculated from Eqs. (4) and (8). A WAG ratio of zero implies a pure CO_2 injection and increasing the WAG ratio reduces the CO_2 fraction of the total injection.

Based on the initial reservoir condition and the choice of the WAG ratio we may consider three operational conditions for the EOR-storage.

1. *Secondary WAG injection*: A depleted oil reservoir after the primary recovery phase that is flooded with CO_2 and water injection, implying that,

$$S_{oI} = 1 - S_{wir}, \qquad t_D = 0, \quad 0 < x_D \leq 1, \tag{9a}$$

$$f_{wJ} = W_R/(1 + W_R), \qquad x_D = 0. \tag{9b}$$

2. *Tertiary CO_2 injection*: A depleted oil reservoir near the end of waterflood phase that is flooded with CO_2 only. This condition indicates that,

$$S_{oI} = S_{orw}, \qquad t_D = 0, \quad 0 < x_D \leq 1, \tag{9c}$$

$$f_{wJ} = 0, \qquad x_D = 0. \tag{9d}$$

3. *Tertiary WAG injection*: A depleted oil reservoir near the end of waterflood phase that is flooded with CO_2 and water. This case has the same initial condition as Eq. (9c) and injection condition as Eq. (9b).

The last consideration is on the calculation of EOR-storage performance measures. These are mainly based on the cumulative oil and CO_2 production, and cumulative CO_2 injection. These are calculated as,

$$P_{oD}(t_D) = \int_0^{t_D} F_2|_{x_D=1} dt_D' \tag{10a}$$

$$P_{CO_2D}(t_D) = \int_0^{t_D} F_3|_{x_D=1} dt_D' \tag{10b}$$

$$I_{CO_2D}(t_D) = \frac{t_D}{1 + W_R} \tag{10c}$$

Where P_{oD} and P_{CO2D} are the dimensionless pore volume of oil and CO_2 production, respectively, and I_{CO2D} is the dimensionless pore volume of CO_2 injection.

All the requirements for the quantitative graphical solution are ready to present the solution to the EOR-storage problem.

1. Collect the following inputs (1) relative permeability data for water-oil and water-CO_2 systems (2) water, oil and CO_2 viscosity (3) CO_2 solubility in the aqueous (C_{3w}) and oleic phases (C_{3o}), and (4) residual oil saturation with respect to CO_2 (S_{oc}). If the water-CO_2 relative permeability data are not available, use the water-oil data instead
2. Calculate λ_{ro}, λ_{rw} and calculate the fractional flow of aqueous phase f_w using Eq. (4). Plot the two fractional flow curves as a function of aqueous phase saturation. These are the tieline paths.
3. Calculate the solubility parameters a, b and c according to Eq. (7). Calculate the injection condition according to Eq. (8). Mark the points I, J, (a,b) and (c,1) on the fractional flow plot.
4. Find the non-tieline path by choosing from the set of parallel lines from (a,b) to the CO_2-water fractional flow curve and from (c,1) to the water-oil curve. The solution non-tieline path will be the one that honors the two material balance

conditions. This step requires some algorithmic trial and error. Mark the switch points ($S_{w,s}$,$f_{w,s}$) and ($S_{w,OB}$,$f_{w,OB}$) on the CO_2-water and water-oil fractional flow curves, respectively.
5. Use the Buckley-Leverett method to construct the tieline solution path from the injection condition J to the first switch point ($S_{w,s}$,$f_{w,s}$) on the CO_2-water curve. Follow a similar process for ($S_{w,OB}$,$f_{w,OB}$) and initial condition on the water-oil curve.
6. Generate the corresponding saturation profile at different pore volume injections t_D (e.g. $t_D = 0.2$) and the effluent history at $x_D = 1$.
7. Calculate the cumulative oil and CO_2 production and cumulative CO_2 injection according to Eq. (10).

1.3 Example CO_2-EOR and Storage Problems

We present two examples in this section. The first one addresses secondary WAG injection and the second addresses tertiary WAG injection with significant trapping of the oleic phase, including CO_2 and oil.

Secondary WAG Injection Figure 4a presents the secondary WAG injection with the typical S-shape CO_2-water and water-oil fractional flow curves. The initial reservoir condition is at the irreducible water saturation of 0.25 ($S_{wI} = S_{wir} = 0.25$) and the injection condition has a 0.4 WAG ratio ($f_{ws} = 0.29$). We also assume that $C_{3w} = 0.02$ and $C_{3o} = 0.2$ and $S_{oc} = 0.15$. All parameters for the calculation of a, b, c, S_{ws} and f_{ws} are ready. The point (c,1) approximately falls on the CO_2 velocity line for the cases of secondary WAG and tertiary CO_2 injection.

The non-tieline line passes through (a,b) and connects the CO_2-water curve at the residual water saturation to CO_2 which is 0.25. In this case the residual water saturation to CO_2 is equal to the irreducible water saturation on the water-oil tieline. From the injection condition to the switch point ($S_{w,s}$,$f_{w,s}$) a shock forms (Buckley-Leverett solution); then the saturation switches to the non-tieline path whose velocity is V_{CO2} followed by a switch to the water-oil tieline path at ($S_{w,OB}$,$f_{w,OB}$). This point also falls on the initial condition I. Therefore, three points are overlapping: the switch points ($S_{w,s}$,$f_{w,s}$) and ($S_{w,OB}$,$f_{w,OB}$) along the non-tieline path and the initial condition I. The injected water has a lower velocity V_w.

The resulting saturation profile reflects a piston-like displacement of initial oil by a CO_2 bank and the injected water lags behind. This condition is favorable to the storage objective because a CO_2 bank is formed behind the displaced oil and takes a larger portion of the storage capacity while the incremental oil production remains the same.

The presented solution in Fig. 4a is the only consistent solution that honors both material balance and phase behavior conditions. The displacement profile consists of an immiscible shock from J to ($S_{w,s}$,$f_{w,s}$) which is the same point as I. The injected CO_2 then switches to the faster non-tieline path with velocity V_{CO2}. The

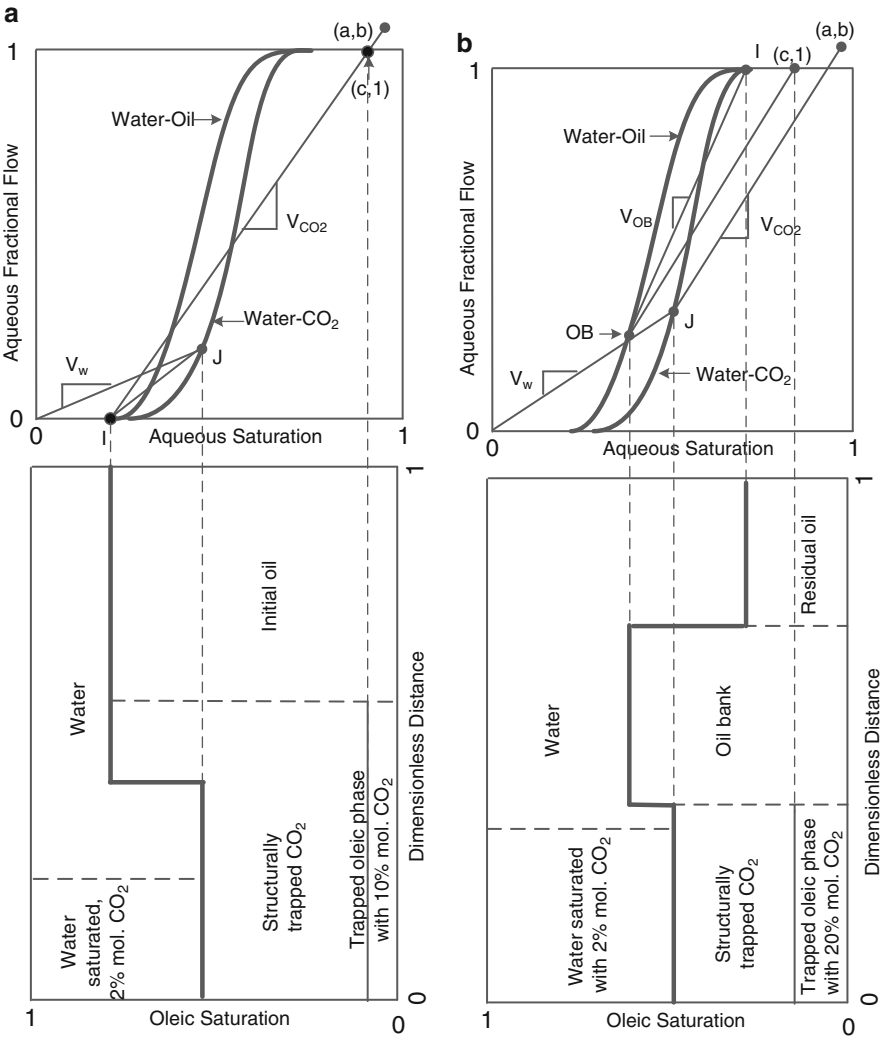

Fig. 4 Fractional flow solution to the WAG injection (**a**) secondary WAG injection at a low WAG ratio of 0.34 (**b**) tertiary WAG Injection with high residual oleic phase saturation and moderate WAG ratio of 0.75. Graphic presentation adopted from Walsh and Lake [10]

injected water has a slow velocity V_w because the injected water volume is relatively small. This is a typical condition after the primary recovery phase. The additional CO_2 in the absence of water displaces the oil in a piston-like manner along the water-oil tieline with the same velocity $V_{OB} = V_{CO2}$. Therefore, the phase behavior requirements and material balance condition are both satisfied $(\lambda_{t,\ CO2w} \leq \lambda_{nt} = \lambda_{t,wo})$.

Even though the secondary WAG problem has many idealizations, it presents the following valuable conclusions for practical EOR-storage applications.

1. The reservoir's storage capacity is limited. Increasing the WAG ratio may increase the water production and reduce the CO_2 storage capacity. It may also delay the incremental oil production if the injection condition J is above the intersection of the non-tieline path and the CO_2-water curve.
2. The choice of a high WAG ratio is in favor of the EOR objective because it produces substantial volumes of oil with a relatively small CO_2 slug. At the same time, a high WAG ratio is detrimental to the storage objective because the majority of storage capacity is occupied by water rather than CO_2.

Tertiary WAG Injection Figure 4b presents the tertiary WAG injection with the same CO_2-water and water-oil fractional flow curves. The initial reservoir condition is at the residual oil saturation of 0.35 and the injection condition has a 0.8 WAG ratio. The residual oil saturation to CO_2 is 0.25. The rest of parameters are the same as the previous problem. Because of the tertiary nature of this process a large portion of the injected CO_2 and residual oil is trapped by the surrounded aqueous phase. The large water saturation prevents CO_2 from contacting the residual oil and traps a larger portion of the injected CO_2. This results in an increased residual oil saturation to CO_2 and reflects a shift of the point (c,1) further to the left on the fractional flow diagram.

The non-tieline path passes through $(S_{w,s},f_{w,s})$ which in this case falls on the injection condition J, and switches to the water-oil tieline at $(S_{w,OB},f_{w,OB})$. The slopes of the two lines are equal since all non-tielines have a constant velocity. The saturation path then follows a shock on the water-oil tieline to the initial condition I (Buckley-Leverett). The injected water has a slightly lower velocity than the injected CO_2 and therefore it lags behind. However, no CO_2 bank is formed in this case. The tertiary WAG problem provides several important observations.

1. An oil bank forms with a moderate oil saturation. The high value of residual oleic saturation prevents the accumulation of CO_2 behind the oil bank. The CO_2 is instead trapped as a residual phase (solubility and capillary trapping).
2. A bigger portion of the CO_2 is trapped through the dissolution or capillary trapping mechanisms. This may lower the risk of a CO_2 leakage.
3. Decreasing the WAG ratio will increase the oil saturation in the oil bank as it will shift the oil bank's water saturation (OB) down the water-oil curve. Therefore, decreasing the WAG ratio accelerates the incremental oil production and increases the CO_2 storage.

Other initial and injection conditions may be solved and analyzed to get a better insight on the physical aspects of EOR-storage. These problems all follow the same rules as presented in this section. Due to the space limitation of this chapter, we leave them as exercise.

2 Field Scale Development of EOR-Storage Operation

The best source of the performance evaluation and prediction is the actual field practices. There are few CO_2-EOR projects worldwide with an active storage objective. These are In-Salah (Nigeria) [12] and Weyburn (Canada) [13]. There are EOR projects such as Cransfield (Mississippi, U.S.) with the secondary objective of understanding the field-scale storage via EOR [14]. On the other hand, there are currently 136 active EOR projects worldwide, most of which are implemented in North America, such as Permian Basin (West Texas and East New Mexico), Rangely field, Weber formation (Colorado, U.S.) and Weyburn field (Saskatchewan, Canada) [15]. The projected performances for the future EOR-storage prospects is expected to be affected by the EOR experience in these regions. Therefore, we dedicate this section to the important implications of the EOR's operational aspects for the future EOR-storage projects.

2.1 Operational Aspects of CO_2-EOR and Storage

The industry experience with anthropogenic CO_2 storage in the saline aquifers and oil and gas fields faces a long maturity path. On the other hand, the industry experience with CO_2-EOR is rich and well-developed. CO_2-EOR was first implemented at field-scale in the 1970s in the Permian Basin, located in West Texas and southeastern New Mexico, and expanded mainly in North America over the past 40 years [15].

A CO_2-EOR and storage project may be implemented as an extension of an existing CO_2-EOR project or directly implemented after a secondary recovery phase (see Fig. 1). Implementation of EOR-storage before a secondary recovery phase is possible from a technical viewpoint; however the economics of an early implementation may not be favorable.

Most of the CO_2 supply for the EOR projects is provided from natural sources. Anthropogenic CO_2 can be potentially utilized as well if it meets the pipeline quality requirements. Any impurity, especially if it exceeds 5 % molar concentration, significantly deteriorates the CO_2 miscibility. The presence of oxygen and hydrogen sulfide are detrimental to the pipelines and facilities. Table 1 presents the CO_2 specifications for the Canyon Reef and Weyburn pipelines.

EOR-storage operations at industrial scale often require more producers and injectors than the size of a typical oilfield. Depending on the reservoir properties and the choice of the EOR-storage design, mainly the WAG ratio, the number of producers and injectors may change through time. In such cases, several fields are considered and an optimum sequence of development is specified as shown in Fig. 3a. Figure 3b shows a qualitative example.

Table 1 CO_2 quality specifications of Canyon Reef and Weyburn pipelines [6]

Property	Canyon Reef	Weyburn
Pipeline transport	12,000 tonne/day (4.4 MM tonne/year)	5000 tonne/day (1.8 MM tonne/year)
Carbon dioxide	≥95 mole percent	≥96 mole percent
Temperature	≤48.9 °C	n/a
Water content	No free water	No free water
	≤20 ppm by weight in vapor phase	≤20 ppm by weight in vapor phase
Hydrogen Sulfide	≤1500 ppm by weight	≤0.9 mole percent
Nitrogen	≤4 mole percent	≤300 ppm
Total Sulfur	≤1450 ppm by weight	n/a
Hydrocarbons	≤5 mole percent of hydrocarbons	≤0.7 mole percent methane
	dew point of hydrocarbon product ≤−28.9 °C	≤2.3 mole percent C2+
Oxygen	≤10 ppm by weight	≤50 ppm by weight
Glycol	$\leq 4 \times 10^{-5} l/m^3$	n/a
	no glycol in a liquid state at any time	
Carbon monoxide	n/a	≤0.1 mole percent

1. The fresh CO_2 feed is initially sufficient to cover a certain portion of the field, namely the White Region.
2. After the CO_2 breakthrough, the produced CO_2 is recycled and used along with the fresh CO_2 to flood the white Region 1, and the light-grey Region
3. The CO_2 production will increase with time and that will allow for flooding the dark-grey Region 3. This process may continue until the entire target field is flooded or the storage project is complete.

The choice of the sequence of field development is often determined by the available logistics and the willingness of the operators to participate in the EOR-storage plan. However, if all the reservoir regions are available to begin the EOR-storage operation, one should begin with the area of best historical oil production performance to maximize the economic benefits and the CO_2 utilization. For the mature fields with an established history of waterflooding, the EOR-storage implementation should follow an optimum sequence by ranking the regions or zones in a descending potential performance order [16].

After the CO_2 breakthrough the produced CO_2 is separated from the other fluids, dried, compressed and re-injected. The recycling of the produced CO_2 is critical to the economics of EOR as the oilfield operator would otherwise have to purchase the fresh CO_2. Therefore, the operator needs to inject two CO_2 inflow streams after the CO_2 breakthrough, fresh CO_2 coming from the capture source and produced CO_2. This requires that the operator maintains a sufficient injection capacity at all times by gradually expanding the scope of EOR-storage implementation through several

phases. The concept of sequential expansion is a unique feature of EOR-storage projects. If the objective is EOR only, then the fresh CO_2 would continuously decrease after the breakthrough down to a stabilized level. This is a common practice that prevents the need for field wide expansion.

The CO_2 plume behavior should be monitored after the completion of the injection phase. This requires proper sealing of the injectors and producers, installation of monitoring equipment, drilling of additional monitoring wells and standard monitoring tests. The monitoring aspects of CO_2 sequestration are addressed in other literature [17, 18]. The monitoring of the plume is again an exclusive feature of EOR-storage. The monitoring for CO_2 leakage detection is a common practice for EOR, but the monitoring of the plume after the injection is not critical because the scale of operation is relatively small and the CO_2 injection normally declines with time.

2.2 Potential Targets for EOR-Storage Projects

There are four potential targets for the EOR-storage projects implementation

(1) Mature oilfields that experienced long periods of primary and secondary recovery, especially waterflooding
(2) Depleted oilfields that experienced the primary recovery phase and some secondary recovery method such as the artificial lift
(3) Depleted gas fields, and
(4) Capillary transition zones (CTZ) and residual oil zones (ROZ) below the main pay zone (MPZ).

The target zone for the first three categories is the main pay zone (MPZ) which is above the water-oil contact or the water-gas contact. The initial water saturation in MPZ is at the residual water saturation. The MPZ is conventionally perforated for the primary and secondary recovery phases to avoid the excessive water production. Figure 4 schematically shows the MPZ, CTZ and ROZ under the static capillary-gravity equilibrium.

The CTZ is developed as the result of vertical equilibrium of the capillary forces and gravity forces under the static conditions between the water-oil and oil-gas zones. Residual oil zone (ROZ) is an attractive target for the EOR-storage operation. The ROZ should not be confused with the capillary transition zone (CTZ). The residual oil zone may develop by the natural waterflood of the oil trap through a geologic time scale. The nature's waterflood process may be triggered after second-stage tectonic activities such as basin tilt, breached seals, and uplift and lateral sweep an active aquifer exists [19].

There are three types of screening criteria for the identification of EOR-storage candidates: logistic, geological/reservoir, and crude oil criteria [20–23]. A brief description of the parameters under each category is listed in Table 2. For each

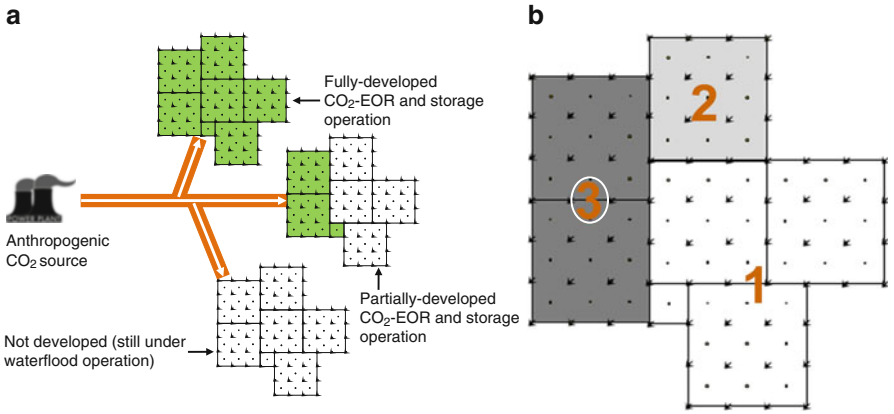

Fig. 5 Field-scale operation of EOR-storage (**a**) captured CO_2 from an industrial source is sufficient for EOR operation in multiple fields (**b**) Optimum sequence of EOR-storage implementation. Region 1 has a better historical waterflood performance and therefore is first selected for EOR-storage, followed by regions 2 and 3 16 [16]

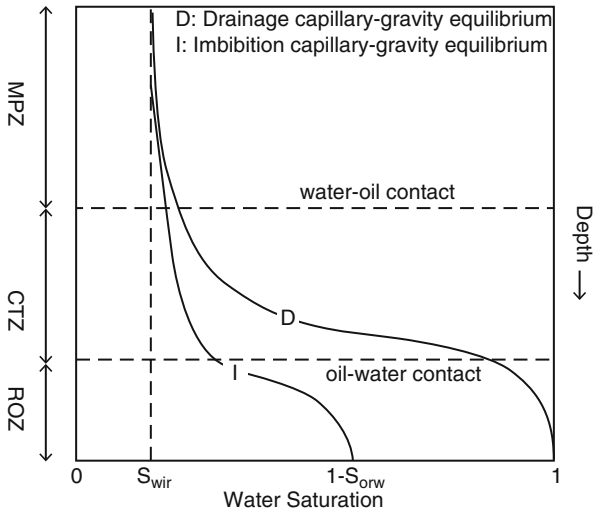

Fig. 6 Water saturation distribution for water-oil system under the capillary-gravity equilibrium. The columns of main pay zone (*MPZ*), capillary transition zone (*CTZ*) and residual oil zone (*ROZ*) develop after the natural imbibition of water (natural waterflood). The ROZ thickness may vary according to the geological structure and the strength of the aquifer

parameter, a threshold value is presented, along with a recommended (R) value. There are few potential targets, if any, around the world that meet all these criteria. The logistic screening criteria are often prioritized to the geological/reservoir or the crude oil criteria because the logistics determine the capital investments on the CO_2 capture and transport [24].

Table 2 Screening criteria for miscible CO_2-EOR and storage projects. Symbol "R" represents the recommended value or range

Property	Favorable Range	Notes
Logistic criteria		
Distance from the CO_2 source (mile)	≤ 200, $R \leq 62$	Transportation cost, energy consumption and carbon footprint rapidly increase beyond 62 miles
Distance from municipal area (mile)	$50 \leq R \leq 200$	Acquiring the permits and addressing the public safety Public opinion is against the underground CO_2 storage if the storage site is close to the municipal areas.
Access to nearby saline aquifer (mile)	$0 \leq R \leq 50$	Saline aquifers serve as a potential storage backup. This improves storage compliance and the economics of EOR-storage.
Geological/Reservoir criteria		
Formation type	Sandstone or carbonate	The mineral type is not important as long as the reservoir is permeable and fairly homogeneous though these conditions are more observed in sandstones.
Caprock	Shale or siltstone	Multiple thick layers of shale or siltstone with strong integrity are ideal. A net thickness of 4 ft or better in every 10 ft of caprock may reduce the vertical leakage risk down to 1 %.
Formation depth (ft)	>2500, $4000 \leq R \leq 10{,}000$	Deep formations are favorable for miscibility development and environmental safety. However, the cost of deep formation development and operation exponentially increases beyond 4000 ft depth.
Temperature (°F)	$110 \leq R \leq 200$	Low temperature and high pressure causes the supercritical CO_2 to behave similar to a liquid. Ideally low temperature and high reservoir pressure is required.
Heterogeneity, Dykstra-Parsons coefficient	$V_{DP} \leq 0.65$, $R \leq 0.5$	Small vertical and horizontal Dykstra-Parsons coefficients are preferred as homogenous reservoirs respond better to CO_2 injection.
	$H_{DP} \leq 0.6$, $R \leq 0.4$	
Average permeability (md)	$k_h \geq 5$, $R \geq 15$	Strongly affects the CO_2 injectivity, vertical sweep efficiency, and the pace of recovery and storage. Shale barriers in the pay zone are detrimental to the vertical sweep and storage capacity but beneficial to structural and capillary trapping enhancement.
	$k_v \geq 0.1k_h$	
Net thickness (ft)	≥ 30, $R \geq 100$	
CTZ and ROZ thicknesses (ft)	Not critical, $R \geq 30$	Presence of CTZ and/or ROZ is not critical. CTZ and ROZ are favorable targets for EOR-storage due to the safety considerations.

(continued)

Table 2 (continued)

Property	Favorable Range	Notes
Crude oil criteria		
Oil gravity (°API)	≥22, R ≥ 36	Minimum of 22°API is successfully tested only at lab scale. 36° or more recommended and verified at field scale
Oil saturation (%)	≥40, R ≥ 50	At least a 40 % oil saturation to ensure a 20 % recoverable oil. About 50 % of the recoverable oil will remain in the reservoir after EOR. 50 % oil saturation yields about 15 % incremental recovery at favorable conditions.
Nitrogen (% mol.)	≤4, R ≤ 1	Presence of Nitrogen is detrimental to miscibility. Hydrogen sulfide on the other hand is favorable to the miscibility though detrimental to the facilities.
Light hydrocarbons C1-C2 (% mol.)	≤25, R ≤ 15	≤15 % mol. methane and ≤10 % mole percent ethane is favorable. Light components deteriorate the miscibility.
Intermediate hydrocarbons C4-C6 (% mol.)	≥15, R ≥ 20	Intermediate components are the primary driver of miscibility development

2.3 Measures of EOR-Storage Performance

Three design parameters control the reservoir response to the EOR-storage process: gas injection rate, injection duration, and the WAG ratio; and three parameters describe the reservoir response:

1. Average oil production performance, defined as total oil production rate divided by the number of active producers.
2. Net CO_2 utilization, defined as the amount of CO_2 stored per incremental barrel of produced oil.
3. CO_2 recycle ratio, defined as the ratio of the CO_2 production rate to the fresh CO_2 injection rate.

Figure 7 shows an example on the effect of the WAG ratio on two EOR-storage performance criteria, oil production and net CO_2 utilization. Decreasing the WAG ratio slightly improves the production but significantly increases the utilization. This means that more CO_2 is stored to produce oil. This is good for the storage objective but detrimental to the EOR objective in the long-term because it delays the EOR expansion to other wells, phases and fields.

The EOR-storage performance parameters determine the pace of field development, the number of producers and injectors required at any time, the CO_2 separation plant size, and the compression power and energy consumption requirements. These parameters are necessary for the facility design and the associated economic assessments [4].

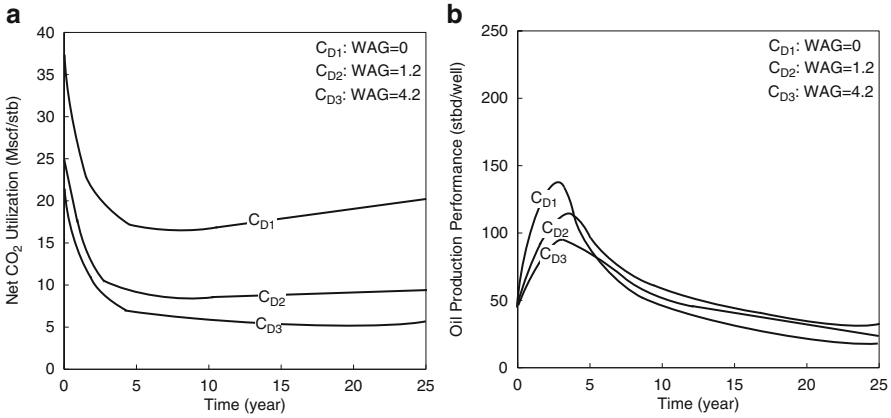

Fig. 7 Reservoir response to the WAG ratio as a design parameter (**a**) the net CO_2 utilization increases with decreasing the WAG ratio (**b**) the oil production performance increases with decreasing the WAG ratio [4]

2.4 EOR-Storage Performance Evaluation and Prediction

Figure 8 shows a workflow for the performance evaluation of the EOR-storage process. Every evaluation model takes a certain set of input parameters and delivers a set of outputs. Depending on the subsurface modelling tool the inputs and outputs may vary. The common inputs of such models are (1) total project duration and fresh CO_2 slug size (2) annual fresh CO_2 injection rate (3) the WAG ratio (4) water and CO_2 injection rates or injection pressure (5) total producers and injectors in one flood pattern. The major outputs are (1) oil production (2) water production (3) gross and net CO_2 utilization (4) CO_2 recycle ratio, and (5) EOR-storage performance curve.

There are two common methods for the development of the EOR-storage subsurface model (1) reservoir simulation (2) statistical and experimental models. These are briefly presented in the following.

2.4.1 Reservoir Simulation

The physical process of EOR-storage is a fairly complicated problem that requires appropriate tools for modeling multiphase fluid flow of compositional phases in a heterogeneous permeable medium. No closed-form set of analytical equations may predict the oil production response to the alternating injection of water and gas without making significant simplifying assumptions.

Reservoir simulation is a suitable tool for modelling and performance prediction of CO_2 sequestration processes including EOR-storage. The capability of modelling compositional fluid flow in complicated geological structures over long time

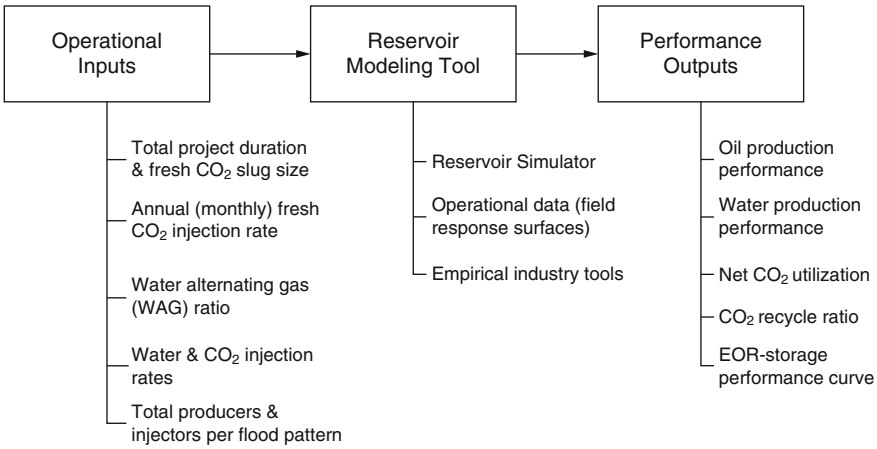

Fig. 8 Conceptual model of the CO_2-EOR and storage predictive tool

periods is an important advantage. Simulators are able to deliver both qualitative and quantitative estimations on the EOR-storage performance parameters and predict the reservoir behavior under various operating conditions [16].

One may gather the following inputs by integrating the available data with the general literature on CO_2-EOR studies.

1. Geological structure and reservoir properties (reservoir extent, flow barriers and pay thickness, natural fractures frequency and orientation, heterogeneity)
2. Rock-fluid properties (relative permeability curves, capillary pressure curves and hysteresis)
3. Fluid properties (fluid compositions, phase behavior, minimum miscibility pressure, mixture properties etc.)
4. Rock properties (porosity and permeability and compaction)
5. Operating conditions (bottomhole pressure and flow rate constraints, monitoring threshold, maintenance schedule, operational interruptions, surface facility constraints, and perforation intervals)

The reservoir response to the WAG injection should be similar to the real CO_2 projects. This means that the three measures of EOR-storage performance: oil production, net CO_2 utilization and CO_2 recycle ratio should follow the same range and trend, as the field EOR practices. The operational conditions of the simulation should be similar to those of field practices. Many of the operating constrains are difficult to predict over long time periods especially for the mature oilfields. Thus, certain simplifications will be inevitable.

The simplifying assumptions should be tested to realize their impacts. The following list of assumptions is commonly observed in simulation studies (1) the reservoir has been under a waterflood operation long enough to reach an economic

limit before the EOR-storage phase begins (2) the well-pattern design and the well-spacing do not change before or during the operations; this means no infill drilling or producer-injector switches occur, (3) the producers and injectors are assumed to operate all the time and there are no redundant wells.

The interpretation of the simulation output should be aligned with the EOR-storage objectives. This process should aim to maximize the incremental oil production and CO_2 storage simultaneously; these objectives are not in the same direction. Therefore, one should look for the optimum operating conditions that satisfy both objectives.

2.4.2 Statistical and Experimental Models

Statistical and experimental predictive tools rely on the actual performance of the current EOR experience over the past 40 years. They analyze the data and propose a set of experimental equations that statistically describe the output performance parameters of EOR projects as a function of the input design parameters [25].

The statistical tools may rely on the results of the tuned reservoir simulation models that are generalized to non-dimensional performance curves for a range of operating conditions. Kinder Morgan (KM) spread sheets is an example of the CO_2-EOR screening tool. The advantage of the KM spreadsheets is the ease of applicability for quick performance and economic assessment of an EOR prospect.

2.4.3 Environmental Impact of EOR-Storage

The environmental assessment of the EOR-storage operation has been broadly covered in the literature [26–29]. The environmental considerations expand across several major disciplines including engineering and operational aspects, geological aspects, government regulations, and legal and liability considerations.

There are several technical considerations that may be addressed as the exclusive environmental aspects of EOR-storage. These include,

1. *Disposal of produced water*: CO_2 dissolves in water in small fractions. Produced waters contain a small fraction of dissolved CO_2. A portion of the produced water may be re-injected through the WAG process along with CO_2. The produced water may also be injected in saline aquifers, or purified and utilized for agricultural or industrial purposes.
2. *CO_2 leakage through the abandoned wells*: The presence of abandoned wells is a common concern in the mature oilfields. They penetrate through the cap rock which is supposed to be a sealing barrier. If the well is not properly sealed, CO_2 may pass through the caprock by penetrating through and around the bore hole [30, 31]. Therefore, the drilling history of all successful and unsuccessful wells over the entire life of the field is acquired. All the wells should be tested to ensure the proper sealing. This process may take time but can be gradually

completed through the CO_2 injection phase which takes several decades. The risk of CO_2 leakage after the injection completion remains high because of the local pressure gradients and the high CO_2 mobility. Therefore, the monitoring of the abandoned wells and the previously-active wells may continue through several decades after the injection.

3. *Storage compliance*: CO_2 storage compliance refers to the consistent storage of a captured anthropogenic CO_2 slug in an underground geological structure. Storage compliance requires the operator to maintain sufficient CO_2 injection and storage capacities throughout the EOR-storage project life. The uncertainty in two operational parameters may raise a compliance consideration: annual captured CO_2 from the power plant and CO_2 injection loss in the oilfield. The operator should maintain sufficient CO_2 injection and storage capacities and maximize the economic benefits from the EOR-storage operation. The appropriate adjustment of the WAG ratio increases both the compliance and the economic benefits. A CO_2 storage backup in a saline aquifer allows the oilfield operator to implement more profitable EOR-storage designs and ensure a full compliance level [32].

References

1. Ettehadtavakkol A, Lake LW, Bryant SL (2014). Impact of storage tax credit on economic viability of CO storage with EOR. In: SPE Hydrocarbon Economics, Houston, TX, May 19. Society of Petroleum Engineers. doi:10.2118/169838-MS
2. Green DW, Willhite GP (1998) Enhanced oil recovery. Henry L. Doherty Memorial Fund of AIME. Society of Petroleum Engineers: Richardson, TX
3. Pariani G et al (1992) An approach to optimize economics in a west Texas CO_2 flood. J Pet Technol 44(9):984–988
4. Ettehadtavakkol A, Lake LW, Bryant SL (2014) CO_2-EOR and storage design optimization. Int J Greenh Gas Control 25:79–92
5. Kumar A et al (2004). Reservoir simulation of CO2 storage in deep saline aquifers. Society of Petroleum Engineers, January 1. SPE/DOE symposium on improved oil recovery, 17–21 April, Tulsa, Oklahoma. doi:10.2118/89343-MS
6. Metz B (2007) Climate change 2007-Mitigation of climate change: working group III contribution to the fourth assessment report of the IPCC, 4th edn. Cambridge University Press, Cambridge
7. Noh MH et al (2007) Implications of coupling fractional flow and geochemistry for CO_2 injection in aquifers. SPE Reserv Eval Eng 10(04):406–414
8. Burton M, Kumar N, Bryant SL (2009) CO_2 injectivity into brine aquifers: why relative permeability matters as much as absolute permeability. Energy Procedia 1(1):3091–3098
9. Orr FM (2007) Theory of gas injection processes. Tie-Line Publications, Copenhagen
10. Walsh MP, Lake LW (1989) Applying fractional flow theory to solvent flooding and chase fluids. J Pet Sci Eng 2(4):281–303
11. Cere A, Zanotti F (1985) Sharpening behaviour and dispersion in chemical flooding. In: Proceedings of the third European meeting on Improved oil recovery, Rome
12. Riddiford F et al (2003) A cleaner development: the in salah gas project Algeria. Greenh Gas Control Technol 1:595–600
13. Malik QM, Islam MR (2000). CO_2 injection in the Weyburn Field of Canada: optimization of enhanced oil recovery and greenhouse gas storage with horizontal wells, January 1. Society of

Petroleum Engineers. SPE/DOE improved oil recovery symposium, 3–5 April, Tulsa, Oklahoma. doi:10.2118/59327-MS
14. Hovorka SD et al (2011) Monitoring a large volume CO_2 injection: year two results from SECARB project at Denbury's Cranfield, Mississippi USA. Energy Procedia 4:3478–3485
15. Kuuskraa V, Wallace M (2014) CO_2-EOR set for growth as new CO_2 supplies emerge. Oil Gas J 112(5):92–92
16. Ettehadtavakkol A (2013) CO_2 EOR-storage design optimization under uncertainty. University of Texas, Austin, USA
17. White D et al (2004) Greenhouse gas sequestration in abandoned oil reservoirs: the international energy agency Weyburn pilot project. GSA today 14(7):4–11
18. White D (2009) Monitoring CO_2 storage during EOR at the Weyburn-Midale Field. Lead Edge 28(7):838–842
19. Melzer LS, Kuuskraa VA, Koperna GJ (2006). The origin and resource potential of residual oil zones. Society of Petroleum Engineers, January 1. doi:10.2118/102964-MS
20. Damen K et al (2005) Identification of early opportunities for CO_2 sequestration—worldwide screening for CO_2-EOR and CO_2-ECBM projects. Energy 30(10):1931–1952
21. Van Bergen F et al (2004) Worldwide selection of early opportunities for CO_2-enhanced oil recovery and CO_2-enhanced coal bed methane production. Energy 29(9):1611–1621
22. Núñez-López V et al (2008) Quick-look assessments to identify optimal CO_2 EOR storage sites. Environ Geol 54(8):1695–1706
23. Kovscek A (2002) Screening criteria for CO_2 storage in oil reservoirs. Pet Sci Technol 20 (7–8):841–866
24. Wei N et al (2015) Regional resource distribution of onshore carbon geological utilization in China. J CO2 Util 11:20–30
25. Azzolina NA et al (2015) CO_2 storage associated with CO_2 enhanced oil recovery: a statistical analysis of historical operations. Int J Greenh Gas Control 37:384–397
26. Herzog H, Golomb D (2004) Carbon capture and storage from fossil fuel use. Encycl Energy 1:1–11
27. Koornneef J et al (2012) The environmental impact and risk assessment of CO_2 capture, transport and storage–an evaluation of the knowledge base. Prog Energy Combust Sci 38 (1):62–86
28. Koornneef J, Faaij A, Turkenburg W (2008) The screening and scoping of environmental impact assessment and strategic environmental assessment of carbon capture and storage in the Netherlands. Environ Impact Assess Rev 28(6):392–414
29. Bachu S (2008) CO_2 storage in geological media: role, means, status and barriers to deployment. Prog Energy Combust Sci 34(2):254–273
30. Nordbotten JM et al (2005) Semianalytical solution for CO_2 leakage through an abandoned well. Environ Sci Technol 39(2):602–611
31. Ebigbo A, Class H, Helmig R (2007) CO_2 leakage through an abandoned well: problem-oriented benchmarks. Comput Geosci 11(2):103–115
32. Ettehadtavakkol A (2014) Storage compliance in coupled CO_2-EOR and storage. Greenh Gas Sci Technol 4(1):66–80

Part VI
CO_2 Storage in Other Sites

Mineral Carbonation in Ultramafic and Basaltic Rocks

Pablo García del Real and V. Vishal

Abstract Carbon capture and storage in the form of mineral carbonation in ultramafic and basaltic rocks offers a geologically stable repository of anthropogenic CO_2. This chapter provides fundamental, theoretical and applied concepts relevant to mineral carbonation in peridotite, serpentinite and basaltic rocks. We explore the general global distribution of these lithologies and bring to the discussion the potential role of sedimentary serpentine, so far an overlooked type of rock that may offer both reactive silicate minerals and requisite permeability for CO_2 injection. The chapter recalls chemical reactions, field observations, and historical perspectives that have informed experimental and modeling developments in the area of mineral carbonation. Encouraging scientific results have inspired the injection of CO_2 in basaltic rocks in Iceland and Washington, USA, and proposed drilling in Oman. Besides the high economic cost of mineral carbonation, other limitations include the availability of water, distance between CO_2 sources and target rocks, and various coupled geochemical and physical aspects that remain to be further addressed.

1 Introduction

Carbon dioxide (CO_2) storage in ultramafic and basaltic rocks via mineral carbonation represents a long-term mechanism for removing CO_2 from the fluid envelopes of Earth, including CO_2 from anthropogenic sources. Mineral carbonation of ultramafic and basaltic rocks complements the current array of mechanisms and

P. García del Real (✉)
Department of Geological Sciences, Stanford University, 450 Serra Mall, Bldg. 320, Stanford, CA 94305, USA
e-mail: gdelreal@stanford.edu

V. Vishal
Department of Earth Sciences, Indian Institute of Technology Bombay, Mumbai, India
e-mail: drvikramvishal@gmail.com

V. Vishal, T.N. Singh (eds.), *Geologic Carbon Sequestration*,
DOI 10.1007/978-3-319-27019-7_11

technologies in carbon capture and storage (CCS) aimed at mitigating global anthropogenic CO_2 emissions to the atmosphere. Regarded as a prime option to counteract output of CO_2 and to mitigate global warming (*e.g.* [1, 2]), CCS contributes to other proposed routes for achieving cleaner energy, such as (*a*) improving energy transfer and utilization efficiency; (*b*) opting for low-carbon mechanisms; (*c*) enhancing biological CO_2 fixation; and (*d*) reducing the emissions of non-CO_2 greenhouse gases. CO_2 storage in geologic reservoirs such as ultramafic and basaltic rocks is an effective method to create an extended window for the development and deployment of renewable sources of energy [3, 4]. To meet the 2°C per century reduction climate goal, implementing CCS in various underground reservoirs is necessary, and remains a technically viable solution to arrest CO_2 build-up in the atmosphere [5, 6].

Global geologic reservoirs suitable for CO_2 storage include: (*a*) depleted and active hydrocarbon reservoirs; (*b*) saline aquifers; (*c*) coals seams; (*d*) salt caverns; (*e*) oil/gas shale; (*f*) geothermal fields; and (*g*) mafic and ultramafic rocks (Fig. 1). These potential CO_2 storage reservoirs are selected on the basis of fundamental technical parameters such as requisite capacity, injection considerations, robust caprock sealing mechanisms, basin suitability, and environmental compatibility [5–9]. Other storage techniques such as biomass sequestration, ocean injection, and conversion of CO_2 to useful products, are not expected to sequester carbon at a large-scale. It has been proposed, however, that geological storage techniques, including mineral carbonation, are among the most efficient methods for CO_2 disposal [10]. Mineral carbonates, in fact, constitute the largest carbon storage

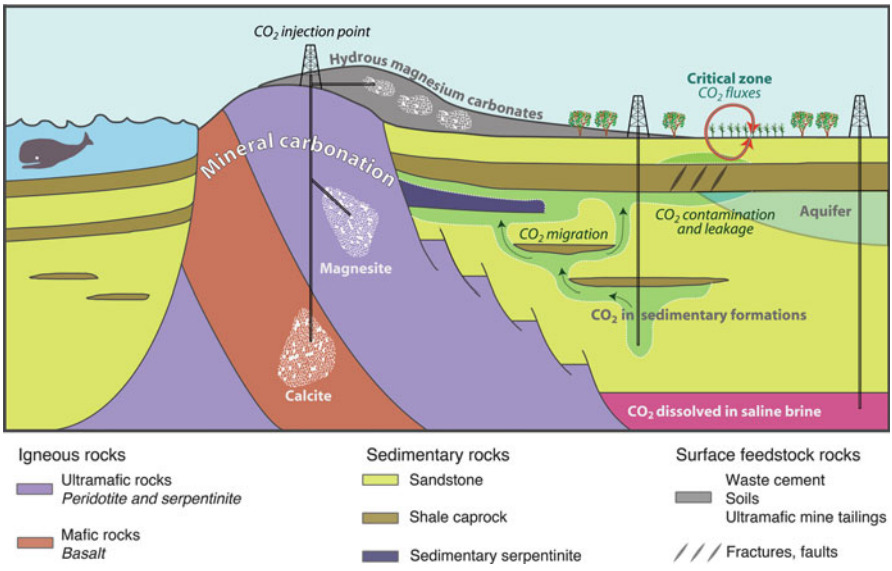

Fig. 1 Cross section showing mineral carbonation in ultramafic and basaltic rocks, as well as other approaches and risks to carbon storage

capacity (1 million Gt carbon) and the longest storage time (>100,000 years) on Earth in comparison to other sequestration methods [10].

For our discussion, ultramafic rocks refer to peridotite, serpentinized peridotite, and serpentinite. Peridotite broadly describes a group of dense, intrusive igneous rocks whose mineral assemblage is dominated by olivine and pyroxene (Sect. 3). When peridotite rocks are in contact with water, they become partially (serpentinized peridotite) and wholly hydrated (serpentinite). Basaltic rocks are variably porous, extrusive igneous rocks composed mainly of plagioclase and pyroxene (Sect. 4). Upon cooling and crystallization, ultramafic and basaltic rocks exhibit a wide range of crystallinity, mineral and chemical profiles, and physical configuration (total porosity, permeability). Common in all continents and within reachable depths, ultramafic and basaltic rocks provide the highest availability of requisite cations (mostly Mg and Ca, but also Fe, Mn) for mineral carbonation.

A fundamental difference between mineral carbonation and other CO_2 sequestration mechanisms is the permanent immobilization of CO_2 that results upon transformation to solid carbonates—*e.g.,* magnesite [$MgCO_3$], calcite [$CaCO_3$] (Fig. 1). Other mechanisms rely on sequestering CO_2 by structural traps or caprocks (hydrodynamic trapping in sedimentary formations) or by dissolving CO_2 in basinal waters/saline brines (Fig. 1). In both cases, the CO_2 remains in fluid phase, which renders it mobile and susceptible to migration and leakage. Figure 1 highlights the importance of water availability for deployment of CCS. As noted by Gislason and Oelkers [11], CO_2 injection into basalts in Iceland (see Sect. 4.1) requires a fluid that is 5 % dissolved CO_2 and 95 % water. Access to water (*e.g.* groundwater, seawater) is thus an important component during CO_2 injection, when water acts as the solvent and transports CO_2. In the case of mineral carbonation in ultramafic rocks, examples of naturally occurring carbonation point towards the indispensable role of CO_2-charged waters to regulate reactions and subsequent magnesite mineralization. Prospective drilling in ultramafic rocks in Oman, for instance, aims to investigate the mobility and role of water (*e.g.* fresh groundwater, seawater) and CO_2-rich solutions in the alteration and carbonation of ultramafic masses (see Sect. 3.1).

In addition to subsurface ultramafic and basaltic rocks, mineral carbonation can also occur in industrial wastes, which provide feedstock (*e.g.* rocks, cement waste) for carbonation at the Earth's surface (Fig. 1). For example, mine tailings of ultramafic rocks can be readily reutilized for mineral carbonation purposes (*e.g.* [12]). Similarly, sedimentary serpentinite—a sedimentary rock composed primarily of serpentinite detritus (clasts or fragments)—can provide a highly reactive, porous and more permeable feedstock in comparison to crystalline rocks such as peridotite and serpentinite. Mineral carbonation is also intrinsically related to surface and groundwater processes—the 'critical zone' (Fig. 1), where human activity also affects CO_2 fluxes, particularly in relation to weathering. It is at the intersection represented by the 'critical zone' where humans are vulnerable to how we opt to manage carbon; for example, the effect of carbon imbalances and CO_2 leakages on agriculture, water supplies, biodiversity and human health.

Mineral carbonation in peridotite and basalt can be achieved by two fundamental methods: *in-situ* and *ex-situ* mineral carbonation. *In-situ* mineral carbonation depends on point sources of CO_2 (*e.g.* coal-powered electric plants or other high-output industries) from where CO_2 is physically manipulated and transported to the injection site near the target peridotite and/or basalt formations. *Ex-situ* mineral carbonation relies on mining and crushing the rocks to be hauled to industrial configurations where mineral carbonation is induced by the influx of CO_2 in large batch reactors. At the end of the process, remaining liquid materials must be separated and disposed of in environmentally sensible conditions; likewise, depending on reaction extent and resultant carbonate purity, the solid carbonated materials could probably be returned to the mine or used in a different industrial process. Based on technical and economic factors [13], *ex-situ* mineral carbonation is regarded to be unfeasible in the timeframe and scale required for offsetting CO_2 emissions. Preferred technically and economically over *ex-situ* approaches [14], *in-situ* methodologies could be broadly applicable when suitable geologic conditions (*e.g.* tectonic framework, stress, pressure and temperature regimes, permeability and porosity) as well as access to CO_2 point sources are available.

Mineral carbonation relies on the transformation of CO_2 from fluid to solid phase, whereby the CO_2 incorporates elements (chiefly Mg, Ca) from ultramafic and basaltic rocks to produce solid carbonate minerals (Fig. 1). The end product of mineral carbonation is a thermodynamically stable and inert compound—a carbonate, which effectively and irreversibly traps CO_2 over geologic timescales [15]. However, in some cases carbonate minerals are unstable and dissolve when acid solutions react with them. In nature, ultramafic and basaltic rocks trap CO_2 by the transformation of fluid $CO_{2(aq)}$ to solid carbonate minerals through a broad variety of long and short-term geologic processes. Seifritz [16] first suggested the possibility of using silicates rocks (such as ultramafic and basaltic rocks) to chemically bind CO_2 for storage purposes—an idea further refined by a few other initial researchers [17, 18] before research in the domain exponentially increased. Our challenge is to understand natural processes of mineral carbonation, and to safely replicate and enhance them using current technical and engineering capabilities of fluid injection into the subsurface.

This chapter further explores the fundamental processes underpinning mineral sequestration of CO_2, including the (*a*) global distribution of peridotite and basalt provinces; (*b*) geologic, chemical and physical constraints on carbonate formation in peridotite and basalt; and (*c*) case studies of ongoing and future CO_2 injection into peridotite and basalt.

2 Distribution of Ultramafic and Basaltic Provinces

Representative worldwide distribution of ultramafic rocks (including serpentinized peridotite and serpentinite), sedimentary serpentinite, and basaltic rocks is shown in Fig. 2. Ultramafic rocks cover approximately 1 % of Earth's surface and shallow

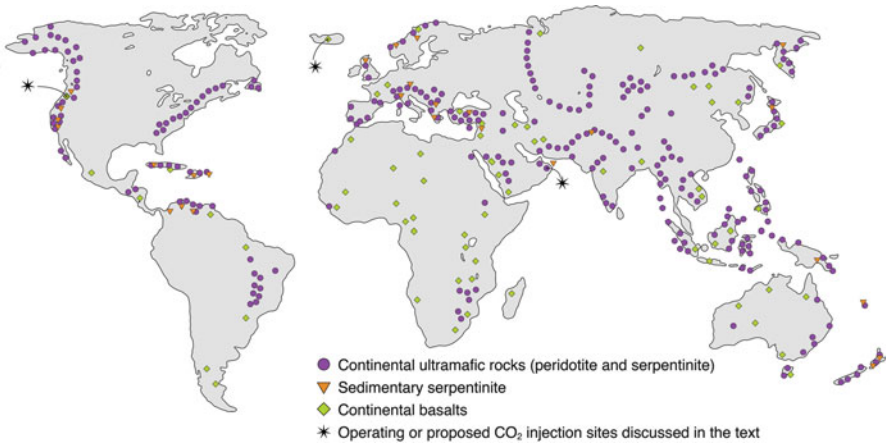

Fig. 2 World map distribution of (*a*) continental crystalline ultramafic rocks (peridotite and serpentinite), (*b*) sedimentary serpentinite, and (*c*) basaltic rocks. Also shown is where injection of CO_2 has occurred in the past, continues to this day, or is projected in the near future. Data points display general location of lithologies and are not representative of the size or extent of the rock exposures. Ultramafic rocks location data from Oze et al. [19], sedimentary serpentinite from Lockwood [22], and basalts from Oelkers et al. [14]

crust [19] and are widespread in most continents. Ultramafic rocks, mostly members of ophiolite sequences (portion of ocean crust), tend to be exposed in the continents following linear trends. These ultramafic belts are a result of orogenic processes, usually at convergent margins, that emplace segments of ophiolites onto the continental lithosphere. The largest ultramafic rock exposures are located in Oman, New Caledonia, Papua New Guinea, the east coast of the Adriatic Sea [20], as well as in highly industrialized and populated areas in North America, China, India, and Japan (Fig. 2).

Basaltic rocks are one of the most abundant rocks on Earth, covering less than 10 % of the continental surface [12] and occur in the form of massive basalt flows in large igneous provinces, continental flood basalts (CFBs), volcanic passive margins, and oceanic plateaus [21]. Basaltic rocks are also members of ophiolites and overlie ultramafic rocks in ophiolitic sequences. Once interspersed in the continental crust, basalt provinces host ore deposits, aquifers and even petroleum. Massive volumes of basalt are present in northwestern USA (Columbia River Basalt), Mexico (Sierra Madre Occidental and Trans-Mexican Volcanic Belt), South America (Paraná Traps), Namibia and Angola (Etendeka Province), East African Rift, India (Deccan Traps), Russia (Siberian Traps and Kamchatka), Iceland, Indonesia, Australia, Arabian Peninsula and the Middle East (Fig. 2).

3 Mineral Carbonation in Ultramafic Rocks

Ultramafic rocks are chiefly comprised of relatively coarse primary magnesium silicate minerals olivine [$(Mg,Fe)_2SiO_4$] and pyroxene [$(Mg,Fe)SiO_3$], and minor chromite (or Cr-spinel), ±plagioclase, and ±amphibole. When ultramafic rocks react with circulating waters, some charged with CO_2, primary minerals become hydrated and transform to serpentine minerals ([$Mg_3Si_2O_5(OH)_4$], antigorite, lizardite, chrysotile). Most peridotite rocks exposed on the continents record variable degrees and multiple generations of serpentinization. As such, peridotite rocks almost invariably contain serpentine minerals and can be completely replaced to become serpentinite (Fig. 3). Mineralogical heterogeneity and resultant structural changes to the peridotite protolith due to serpentinization need to be taken into account in modelling and implementation of mineral carbonation of ultramafic rocks.

Magnesium carbonate, magnesite ($MgCO_3$), is the main resultant product of mineral carbonation in ultramafic rocks. Ultramafic rocks, rich in magnesium silicate minerals, supply alkaline earth cations (*e.g.* Mg^{2+}) that react with CO_2 to form magnesite. The structural and thermal stability of magnesite, coupled with its multiple industrial applications (*e.g.* cement, refractory material, fertilizers, welding), render it a safe and economically viable sink for CO_2. However, a fundamental problem is the formation of magnesite at low, surface temperatures (<25°C) is kinetically inhibited —and it is difficult to produce in the laboratory. In lieu of magnesite, laboratory and field observations suggest that metastable hydrous and hydroxy- magnesium carbonates are kinetically favoured (*e.g.* [12]). Observations of widespread magnesite (Fig. 3) and hydrous magnesium carbonate mineralization in ultramafic rocks in a wide variety of geologic environments have furnished fundamental data on the transformation of CO_2 to solid carbonate in ultramafic rocks. For a streamlined discussion, we focus on the mineralization pathways for magnesite.

The reaction of olivine, one of the main magnesium silicate minerals in ultramafic rocks, with carbon dioxide produces magnesite [$MgCO_3$] and silica ([SiO_2], aqueous, amorphous silica, opal or quartz, depending on conditions of pressure, temperature and composition), represented by

$$Mg_2SiO_4 + 2CO_2 \rightarrow 2MgCO_3 + SiO_2 \quad (1)$$

Similarly, depending on pressure, temperature and composition, in the presence of water, which is a more likely process in nature and in controlled experiments, the carbonation of olivine proceeds to form serpentine [$Mg_3Si_2O_5(OH)_4$] and magnesite

$$2Mg_2SiO_4 + CO_2 + 2H_2O \rightarrow Mg_3Si_2O_5(OH)_4 + MgCO_3 \quad (2)$$

and when serpentine reacts with CO_2-rich fluids to form magnesite

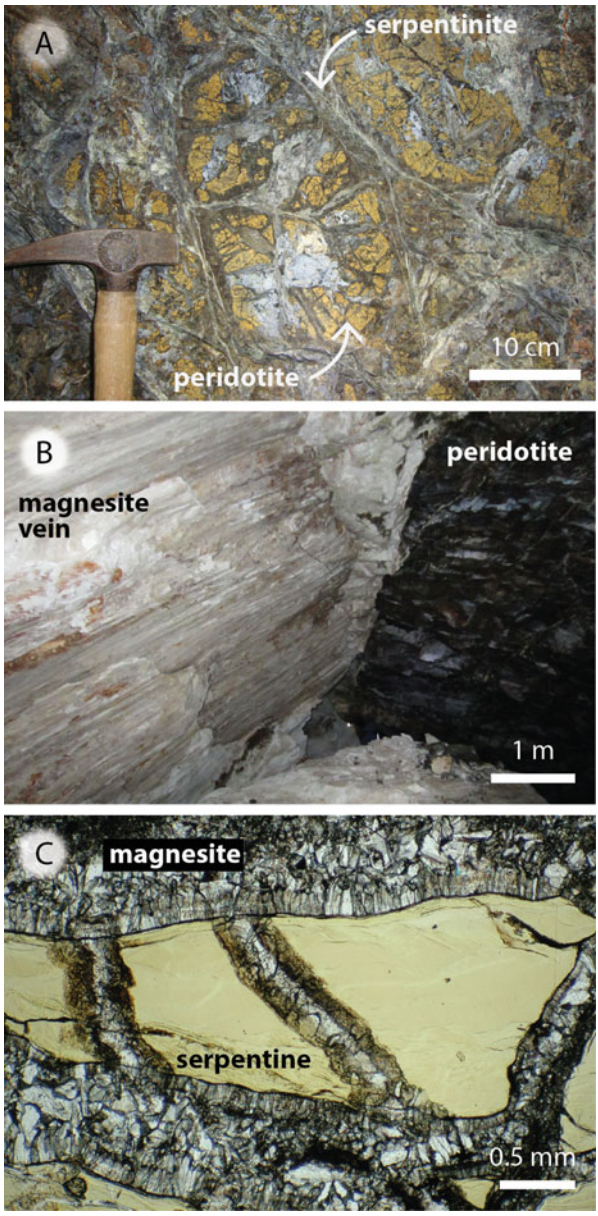

Fig. 3 Examples of mineral carbonation in ultramafic rocks. (**a**) A variably serpentinized peridotite and related mineral and structural heterogeneity typical of ultramafic lithologies. Serpentine veins (*light green color*) and older serpentinite (*dark rims*) pervade the peridotite mass, the original configuration of which can still be recognized. *Yellow* staining of the peridotite is due to oxidation of olivine during exposure to atmosphere and water. (**b**) A massive (>20 m *wide*) magnesite vein (to the *left, white*) in sharp contact with peridotite (to the *right, dark*) (Red Mountain magnesite mine, California, USA). (**c**) A micrograph under plane light of serpentine minerals (*green*) in contact with carbonate veins (*white*) (Field of view 5 mm). Examples and photographs from the serpentinized peridotite of the Del Puerto ophiolite, California (USA) taken by the author

$$Mg_3Si_2O_5(OH)_4 + 3CO_2 + 2H_2O \rightarrow 3MgCO_3 + 2H_4SiO_4 \quad (3)$$

The dissolution of CO_2 in water produces is represented by

$$CO_2 + H_2O \rightarrow H_2CO_3 \quad (4)$$

$$H_2CO_3 \rightarrow H^+ + HCO_3^- \quad (5)$$

$$HCO_3^- \rightarrow H^+ + CO_3^{2-} \tag{6}$$

such that Reactions (1), (2) and (3) can cast in terms of acidic conditions related to CO_2 dissolution as stated in Reactions (4) and (5)

$$Mg_2SiO_4 + 4H^+ \rightarrow 2Mg^{2+} + SiO_2 + 2H_2O \tag{7}$$

$$HCO_3^- + Mg^{2+} \rightarrow MgCO_3 + H^+ \tag{8}$$

$$CO_3^{2-} + Mg^{2+} \rightarrow MgCO_3 \tag{9}$$

where Reaction (6) and (9) suggest that the formation of magnesite is favored in basic environments. For a discussion and recent developments on magnesite thermodynamic parameters and databases, and thermodynamic constraints on mineral carbonation refer to [23, 24]. Marini [25] offers a comprehensive treatment of thermodynamic and kinetic concepts, as well as modeling of dissolution and precipitation processes for mineral carbonation in ultramafic rocks and other silicate rocks.

Linking studies of geologic natural analogues, experiments and modeling to large-scale implementation of mineral carbonation is fundamental to reach a suitable scientific and technical understanding of the complex factors that control CO_2 injection and reactivity in ultramafic substrates. Power et al. [12] provide a comprehensive examination of scientific and economic perspectives on mineral carbonation (also referred to as carbon mineralization) in ultramafic rocks. Natural analogues of mineral carbonation that have provided fundamental knowledge on the rates and processes governing formation of carbonates in ultramafic rocks include: (*a*) magnesite veins (see Fig. 3; *e.g.* [26, 27]); (*b*) travertines [26]; (*c*) silica-carbonate alteration or listwanite [28, 29]; (*d*) hydrothermal magnesite [30]; and (*e*) hydrous magnesium carbonates in mine tailings [31–33], playa lakes [34, 35], and mine adits [36]. Experimental studies provide insight into replicating mineral carbonation in ultramafic rocks, for example: (*a*) Percolation experiments using dunite (>90 % olivine) under in-situ carbonation conditions (160°C) point to engineering optimum injection (flow rate) conditions, based on observations where reduction of the permeability occurs at low flow rates and carbonation potential is decreases at higher injection rates [37]; (*b*) Experiments of dissolution of ultramafic rocks and precipitation of magnesium carbonates at variable fluid compositions (*e.g.* CO_2 content, organic compounds, electrolytes), pressure, and temperature determine rates (kinetics), fluid-rock chemistry after reaction, resultant precipitates besides carbonate minerals (*e.g.* SiO_2, NaCl, iron oxides), and extent and mode of carbonation [38–42]. To couple field observations with experimental constraints, various modeling approaches have further expanded our understanding of mineral carbonation in ultramafic rocks, namely: (*a*) Numerical modeling to constrain thermodynamic properties of carbonation reactions, including heterogeneous phase equilibria and chemical speciation at various temperatures (100–400°C) [24]; (*b*) reactive transport modeling that demonstrates under which conditions the rate of carbonation and mineralization efficiency could be theoretically enhanced following natural

constraints [43], (*c*) how water-rock interaction can be modeled to understand the role of meteoric water in mineral carbonation and injection of CO_2 in particular geologic settings [44]; (*d*) general carbonation mechanisms in hypothetical dunite [45]; and modeling of carbonation in near surface conditions [46, 47].

3.1 Scientific Drilling in the Samail Ophiolite

The Samail ophiolite located in the Sultanate of Oman and the United Arab Emirates (Fig. 2) is the largest exposed section of oceanic crust in the world and preserves most, if not all, of the representative rocks of the ophiolite sequence. Scientific drilling of the ophiolite, including the peridotite, has been proposed to the International Continental Drilling Program (Oman Drilling project; www.ldeo.columbia.edu/gpg/projects/icdp-workshop-oman-drilling-project). The proposed drilling, coring and sampling are inspired by the vast number of scientific inquiries that drilling into ophiolitic subsurface affords: from mantle geochemistry and rheology to plate tectonics to fluid (including CO_2) and biological interactions [48]. On land, peridotite sections of the Samail Ophiolite exhibit high-temperature (~200°C) and low-temperature (<50°C) mineral carbonation [29, 49], both of which have shed light on processes of natural CO_2 uptake by ultramafic rocks. The carbonate-bearing areas of the Oman peridotite have also served as model for reaction-driven cracking, whereby volume change during carbonate precipitation enhance the permeability by opening new reactive surfaces for continued carbonation in ultramafic rocks [50]. One of the principal objectives of the proposed drilling is the injection (with or without tracers) and pumping of fluids to measure permeability, geomechanical properties, and microseismicity in the peridotite.

4 Mineral Carbonation in Basalts

Basalt is a common rock found in all continents (Fig. 2) and can attain a wide range of geochemical and morphological configurations based on the origin and emplacement of the lavas from which it solidifies. In general, however, pyroxene [$(Mg,Fe)SiO_3$], plagioclase [$CaAl_2Si_2O_8$-$NaAlSi_3O_8$], other feldspars [$KAlSi_3O_8$], ±olivine minerals and ± basaltic glass constitute a typical basalt assemblage (Fig. 4). Chemical composition, fluid content, mode of eruption and other parameters affect the morphology and structure of basalt exposures. Typically, basaltic rocks contain vesicles and extensive vesicle zones, brecciated flow-tops, interconnected pores, contractional joints and fractures (Fig. 4), which result in much larger porosity and enhanced permeability in comparison to crystalline peridotite and serpentinite. Permeability and porosity in basalts control the transport and delivery of reactive CO_2 fluids as well as CO_2 storage capacity of basaltic rocks.

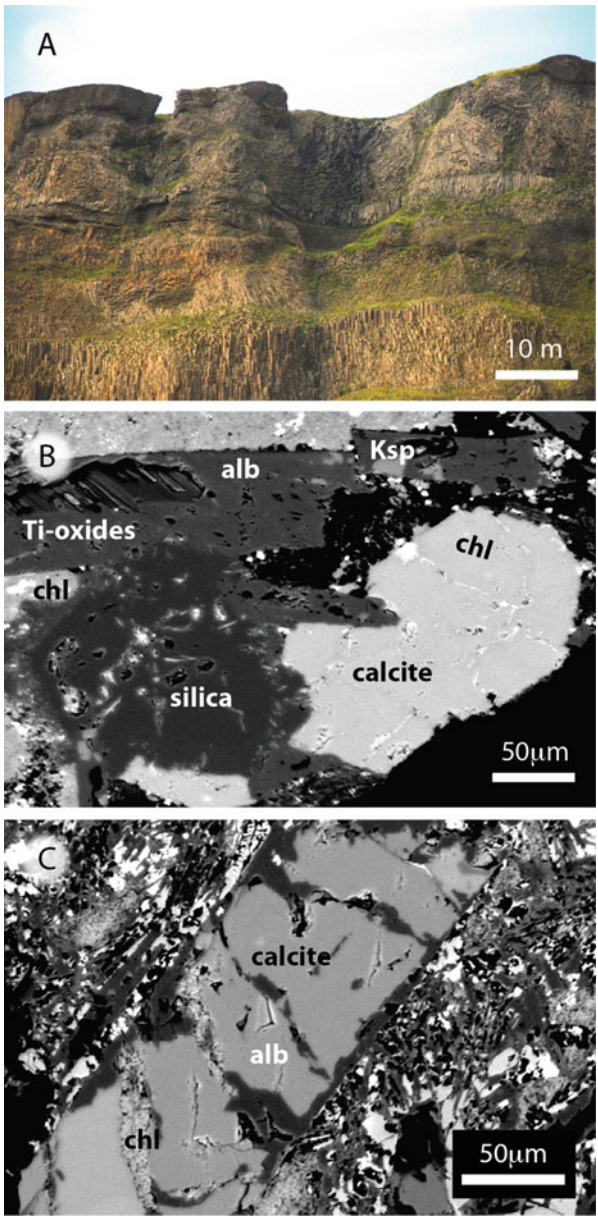

Fig. 4 Examples of basalt exposures and carbonate alteration in basalt (Iceland). (**a**) Example of columnar basalt sill, layered basalts and fanning columns that highlights the extent, as well as the structural and morphological complexity of basalt fields. Important structural features of basalt fields also include flow textures, brecciation, platy fracturing, vesicular zones, sheets and cylinders, columns, and spiracles (*e.g.* [21]) (**b**) Scanning electron microscopy (*SEM*) backscatter image of a section of altered basalt showing pseudomorphic replacement of pyroxene for calcite, cogenetic silica (SiO_2), chlorite, and primary albite and potassium feldspar. (**c**) SEM image showing the alteration in basalt and resultant calcite, chlorite, and primary albite laths with a matrix that contains feldspar minerals, glass and abundant porosity. (**b**) and (**c**) are drill cuttings from the Seydisholar area of the South Iceland Seismic Zone. Photo credit: Dana Thomas (Stanford University)

Natural basalt carbonation captures ~1.8×10^8 tons of CO_2 annually in basalt provinces worldwide [51], which has led to the study of analogues of CO_2 reactions in basalt. In addition to the mineral carbonation that results from weathering of basalt exposed to the atmosphere, other geologic processes also activate mineral carbonation such as low-temperature geothermal fields and hot

hydrothermal systems (Fig. 4). Basalt carbonation is simplified following the general reaction:

$$\left(Ca^{2+}, Mg^{2+}, Fe^{2+}\right) + CO_2 + H_2O \rightarrow (Ca, Mg, Fe)CO_3 + 2H^+ \qquad (10)$$

where the cations (Ca^{2+}, Mg^{2+}, Fe^{2+}) are furnished by the mineral assemblage that constitutes basalt. Unlike peridotite, basaltic minerals contain varying amounts of calcium, magnesium, and iron, which results in the formation of solid solutions of calcite [$CaCO_3$], dolomite [$CaMg(CO_3)_2$], and more rarely magnesite [$MgCO_3$] and siderite [$FeCO_3$]. Concomitant formation of other secondary minerals can also occur in CO_2-altered basalts, including clays, zeolites, metal hydroxides, chlorite, metal oxides, and silica (amorphous or quartz). Some of these secondary minerals may impede the completion of carbonation reactions by competing for the cations expected to bind to CO_2 species and form carbonates.

Mineral carbonation of basalts requires the combination of field-based research, experimental work, and modeling approaches, which in turn have guided the development of pilot injection projects of CO_2 into crystalline basalt. Natural analogues of mineral carbonation in basalt include, for example: (*a*) assessment of CO_2 injection in deep-sea basalts and oceanic ridges [52, 53]; (*b*) the relation between fluid evolution, metal mobility and toxicity during CO_2 alteration in basalt [54, 55]; and (*c*) stratigraphy, petrology, and chemical characterization of specific field sites in Iceland [56, 57]. Experiments that have yielded insight into carbonate mineralization reactions in basalt include: (*a*) variations in mineralization rates and precipitation dynamics in mineralogically similar basalt from USA, India and Africa [58]; (*b*) deep reservoirs (>5 km) and supercritical conditions [59]; (*c*) experimental constraints on basaltic glass dissolution in H_2O-CO_2 mixtures [60]; and (*d*) water-saturated hydrothermal laboratory experiments using Indian basalts from the Deccan plateau [61].

Models and simulations of mineral carbonation in basalt incorporate the variety of scenarios expected in injection of CO_2: (*a*) coupled injection of CO_2 and H_2S impurities in brecciated basalt, which generates calcite and pyrite [62]; (*b*) the dissolution of diopside (a pyroxene) and basaltic glass and influence on mineral carbonation [63]; (*c*) multidimensional, field scale reactive and mass transport modeling of injection of 1.2×10^3 and 4.0×10^5 tons of CO_2 [64]; (*d*) simulation of low temperature alteration and carbonation of basalt [65–68]; and (*e*) critique of thermodynamic criteria for accurate modeling of mineral carbonation in basalt [69].

4.1 Field Scale CO_2 Injection Projects in Basalt

4.1.1 CarbFix Project, Iceland

The CarbFix project (www.carbfix.com) in Iceland is a CO_2 injection project located 30 km south-east of the capital, Reykjavik. CarbFix aims to sequester CO_2 produced at the Hellisheidi geothermal power plant into underground basaltic rocks [70] at depths between 400 and 800 m, and variable temperatures (15–35°C) and pH (8.4–9.8)

[56]. The target formation consists of olivine tholeiite basalt, which contains on average 6 moles of cations (mainly Ca^{2+}) per 1 kg of rock and is overlain by hyaloclastities (glass-bearing rocks formed during glaciations) that serve as cap rock [56]. Injection of CO_2 started in January 2012, and in May 2012, approximately 170 tons of CO_2 were injected at the CarbFix site. As an analogue, it has been estimated that geothermal wells in Icelandic basalts have naturally already fixed about 30–40 Gt CO_2 [53]. Studies of reservoir modeling coupled with reaction chemistry predicted 100 % mineral fixation in 10 years [64]. Post-injection monitoring deemed the storage reservoir effective in terms of mineral reactivity [71].

4.1.2 Big Sky Carbon Sequestration Partnership (BSCP), Washington, U.S.A

Supercritical CO_2 ($scCO_2$) injection near Wallula, Washington, USA represents a pilot project of mineral carbonation in the Columbia River Basalt Group [72]. The first injection of ~1000 MT $scCO_2$ started in July 2013 and lasted for 25 days [72]. Results from post-injection well logging, soil gas analysis and fluid samples confirm the absence of vertical migration of CO_2 and leakage [72]. Fluid samples exhibit elevated concentration of Ca, Mg, Fe and Mn, as expected from basaltic mineralogies, as well as changes in the values of carbon ($\delta^{13}C$) and oxygen ($\delta^{18}O$) isotope compositions, which may represent reaction of basalt with $scCO_2$. The extent of mineral carbonation induced by injection of $scCO_2$ is unknown, core sampling and modeling will provide a better understanding of the mechanisms controlling injection of $scCO_2$ and subsequent mineral carbonation in basalt.

5 Seismic Risk

CO_2 injection in the subsurface changes the general structure of the formations, distribution of governing stresses, pore fluid pressures and resultant fracturing [73, 74]. Substantial development in the past few years have produced a more comprehensive understanding of induced seismicity during injection in sedimentary reservoirs [75]. In case of injection of CO_2 in peridotite and basaltic rocks, [76] suggest that mineral carbonation reduces the contact area among grains, which results in a reduction of effective pore fluid pressure, distributes deviatoric stress, and improves frictional contact. By coupling the effects of carbonation, stress state, and injection/pumping rates, mineral carbonation could in fact reduce seismic risk [76]. In the case of mineral precipitation and consumption of CO_2 fluid, expected total volume alters the internal pore pressure and stresses at the injection area [77], possibly extending to projected mineralized horizons. Seismicity during CO_2 injection into peridotite and basalt requires further research involving modeling and experimental work to incorporate lithological inhomogeneity, rheological changes, and changes of reaction rates dependent on pressure, temperature, and composition of both the mineralizing fluid and the reacting host rock.

6 Conclusions

Ultramafic and basaltic rocks contain the array of reactive Mg-Ca-Fe silicate minerals required for mineral carbonation. Natural examples of mineral carbonation provide us with first-order observations and data on the mobilization of CO_2-rich fluids in ultramafic and basaltic rocks. Ultramafic rocks are more reactive in comparison to basalt, but the latter have higher reactive surface area owing to higher permeability and porosity. Besides such fundamental difference, ultramafic and basaltic rocks are not mutually exclusive lithologies: they often occur in close genetic association in ophiolite sequences. As such, lithological heterogeneity and spatial relationships afforded by ophiolitic structures need to be coupled to progress mineral carbonation in ultramafic and basaltic rocks.

For example, schematic reconstruction of ophiolites suggest the progression, from bottom to top, of ultramafic rocks (peridotite, serpentinites, and dikes of variable composition), gabbro sections, basalt sequences of highly variable chemistry and morphologies (basalt breccia, pillow basalt, columnar basalt, and multiple dike and sill intrusions), and capping sedimentary rocks such as chert and shale (*e.g.* [78]). This portrayal of stacked ophiolitic sequences thus represents an idealized model where CO_2 may react with deeper peridotite segments, then with mafic sections, and should any remaining fluid migrate, the chert layers may act as a trap. Sedimentary serpentinite formations, also associated with ophiolitic peridotite, need to be revisited and assessed for their potential for engineered mineral carbonation. Deposits of sedimentary serpentinite can reach thickness of 3 km and may extend laterally for 10s of kilometers [22], offering a conceivable repository for CO_2 in highly reactive and permeable sedimentary sequences.

Refinement in the implementation of CCS in ultramafic and basaltic rocks include progress on various fronts, namely: (*a*) determination of enhanced dissolution rates of heterogeneous rocks, attendant to the effects of temperature, crystal and solution chemistry, and surface passivation; (*b*) H_2O-CO_2-brine-organics fluid properties and ability to induce substantial carbonate mineralization in nature and in controlled environments; (*c*) enhancement of nucleation and precipitation of magnesium carbonates in experiments and in the field at ambient or near-ambient conditions; (*d*) the evolution of porosity and permeability in competing dissolution-precipitation processes; and (*e*) comprehensive seismic risk during CO_2 injection and subsequent mineralization.

Acknowledgments We thank Dana Thomas (Stanford University) for furnishing basalt photographs and SEM images, and Anna Harrison (Stanford University) for insightful revisions.

References

1. IPCC (2005) IPCC special report on carbon dioxide capture and storage. Prepared by working group III of the Intergovernmental Panel on Climate Change IPCC. doi:10.1021/es200619j
2. Scott V, Gilfillan S, Markusson N et al (2013) Last chance for carbon capture and storage. Nat Clim Chang 3:105–111. doi:10.1038/nclimate1695
3. Gerlagh R, van der Zwaan B (2003) Gross world product and consumption in a global warming model with endogenous technological change. Resour Energy Econ 25:35–57. doi:10.1016/S0928-7655(02)00020-9
4. van der Zwaan B, Gerlagh R (2009) Effectiveness of CCS with time-dependent CO_2 leakage. Energy Procedia 1:4977–4984. doi:10.1016/j.egypro.2009.05.002
5. Bachu S (2003) Screening and ranking of sedimentary basins for sequestration of CO_2 in geological media in response to climate change. Environ Geol 44:277–289. doi:10.1007/s00254-003-0762-9
6. Bachu S (2008) CO_2 storage in geological media: role, means, status and barriers to deployment. Prog Energy Combust Sci 34:254–273. doi:10.1016/j.pecs.2007.10.001
7. Bradshaw J, Allinson G, Bradshaw B et al (2004) Australia's CO_2 geological storage potential and matching of emission sources to potential sinks. Energy 29:1623–1631. doi:10.1016/j.energy.2004.03.064
8. Vishal V, Ranjith PG, Singh TN (2013) CO_2 permeability of Indian bituminous coals: implications for carbon sequestration. Int J Coal Geol 105:36–47. doi:10.1016/j.coal.2012.11.003
9. Vishal V, Singh L, Pradhan SP et al (2013) Numerical modeling of Gondwana coal seams in India as coalbed methane reservoirs substituted for carbon dioxide sequestration. Energy 49:384–394. doi:10.1016/j.energy.2012.09.045
10. Lackner KS (2003) Climate change: a guide to CO_2 sequestration. Science 300:1677–1678. doi:10.1126/science.1079033
11. Gislason SR, Oelkers EH (2014) Carbon storage in basalt. Science 344(6182):373–374. doi:10.1126/science.1250828
12. Power IM, Harrison AL, Dipple GM et al (2013) Carbon mineralization: from natural analogues to engineered systems. Rev Mineral Geochem 77:305–360. doi:10.2138/rmg.2013.77.9
13. Gerdemann SJ, O'Connor WK, Dahlin DC et al (2007) Ex situ aqueous mineral carbonation. Environ Sci Technol 41:2587–2593
14. Oelkers EH, Gislason SR, Matter J (2008) Mineral carbonation of CO_2. Elements 4:333–337. doi:10.2113/gselements.4.5.333
15. Sanna A, Uibu M, Caramanna G et al (2014) A review of mineral carbonation technologies to sequester CO_2. Chem Soc Rev 43:8049–8080. doi:10.1039/c4cs00035h
16. Seifritz W (1990) CO_2 disposal by means of silicates. Nature 345:486–486. doi:10.1038/345486b0
17. Dunsmore HE (1992) A geological perspective on global warming and the possibility of carbon dioxide removal as calcium carbonate mineral. Energy Convers Manag 33:565–572. doi:10.1016/0196-8904(92)90057-4
18. Lackner KS, Wendt CH, Butt DP et al (1995) Carbon dioxide disposal in carbonate minerals. Energy 20:1153–1170. doi:10.1016/0360-5442(95)00071-N
19. Oze C, Bird DK, Fendorf S (2007) Genesis of hexavalent chromium from natural sources in soil and groundwater. Proc Natl Acad Sci U S A 104:6544–6549. doi:10.1073/pnas.0701085104
20. Matter JM, Kelemen PB (2009) Permanent storage of carbon dioxide in geological reservoirs by mineral carbonation. Nat Geosci 2:837–841. doi:10.1038/ngeo683
21. McGrail BP, Schaef HT, Ho AM et al (2006) Potential for carbon dioxide sequestration in flood basalts. J Geophys Res 111:B12201. doi:10.1029/2005JB004169
22. Lockwood JP (1971) Sedimentary and gravity-slide emplacement of serpentinite. Geol Soc Am Bull 82:919. doi:10.1130/0016-7606(1971)82[919:SAGEOS]2.0.CO;2
23. Bénézeth P, Saldi GD, Dandurand J-L, Schott J (2011) Experimental determination of the solubility product of magnesite at 50–200 °C. Chem Geol 286:21–31. doi:10.1016/j.chemgeo.2011.04.016

24. Klein F, Garrido CJ (2011) Thermodynamic constraints on mineral carbonation of serpentinized peridotite. Lithos 126:147–160. doi:10.1016/j.lithos.2011.07.020
25. Marini L (2007) Geological sequestration of carbon dioxide: thermodynamics, kinetics, and reaction path modeling, 1st edn. Elsevier Ltd, Amsterdam
26. Kelemen PB, Matter J (2008) In situ carbonation of peridotite for CO_2 storage. Direct 105:17295–17300. doi:10.1073/pnas.0805794105
27. Oskierski HC, Dlugogorski BZ, Jacobsen G (2013) Sequestration of atmospheric CO_2 in a weathering-derived, serpentinite-hosted magnesite deposit: ^{14}C tracing of carbon sources and age constraints for a refined genetic model. Geochim Cosmochim Acta 122:226–246. doi:10.1016/j.gca.2013.08.029
28. Kelemen PB, Matter J, Streit EE et al (2011) Rates and mechanisms of mineral carbonation in peridotite: natural processes and recipes for enhanced, in situ CO_2 capture and storage. Annu Rev Earth Planet Sci 39:545–576. doi:10.1146/annurev-earth-092010-152509
29. Streit E, Kelemen P, Eiler J (2012) Coexisting serpentine and quartz from carbonate-bearing serpentinized peridotite in the Samail Ophiolite, Oman. Contrib Miner Petrol 164:821–837. doi:10.1007/s00410-012-0775-z
30. Boschi C, Dini A, Dallai L et al (2009) Enhanced CO_2-mineral sequestration by cyclic hydraulic fracturing and Si-rich fluid infiltration into serpentinites at Malentrata (Tuscany, Italy). Chem Geol 265:209–226. doi:10.1016/j.chemgeo.2009.03.016
31. Harrison AL, Power IM, Dipple GM (2013) Accelerated carbonation of brucite in mine tailings for carbon sequestration. Environ Sci Technol 47:126–134. doi:10.1021/es3012854
32. Wilson SA, Dipple GM, Power IM et al (2009) Carbon dioxide fixation within mine wastes of ultramafic-hosted ore deposits: examples from the clinton creek and cassiar chrysotile deposits, Canada. Econ Geol 104:95–112. doi:10.2113/gsecongeo.104.1.95
33. Wilson SA, Barker SLL, Dipple GM, Atudorei V (2010) Isotopic disequilibrium during uptake of atmospheric CO_2 into mine process waters: implications for CO_2 sequestration. Environ Sci Technol 44:9522–9529. doi:10.1021/es1021125
34. Power IM, Wilson SA, Thom JM et al (2009) The hydromagnesite playas of Atlin, British Columbia, Canada: a biogeochemical model for CO_2 sequestration. Chem Geol 260:302–316. doi:10.1016/j.chemgeo.2009.01.012
35. Power IM, Wilson SA, Harrison AL et al (2014) A depositional model for hydromagnesite-magnesite playas near Atlin, British Columbia. Canada Sedimentol 61(6):1701–1733. doi:10.1111/sed.12124
36. Beinlich A, Austrheim H (2012) Carbonation of mine shafts in serpentinized peridotite – in situ sequestration of modern CO_2 at low temperature, 14:4693
37. Andreani M, Luquot L, Gouze P et al (2009) Experimental study of carbon sequestration reactions controlled by the percolation of CO_2-rich brine through peridotites. Environ Sci Technol 43(4):1226–1231. doi:10.1021/es8018429
38. Saldi GD, Jordan G, Schott J, Oelkers EH (2009) Magnesite growth rates as a function of temperature and saturation state. Geochim Cosmochim Acta 73:5646–5657. doi:10.1016/j.gca.2009.06.035
39. Daval D, Sissmann O, Menguy N et al (2011) Influence of amorphous silica layer formation on the dissolution rate of olivine at 90 °C and elevated pCO_2. Chem Geol 284:193–209. doi:10.1016/j.chemgeo.2011.02.021
40. Saldi GD, Schott J, Pokrovsky OS et al (2012) An experimental study of magnesite precipitation rates at neutral to alkaline conditions and 100–200 °C as a function of pH, aqueous solution composition and chemical affinity. Geochim Cosmochim Acta 83:93–109. doi:10.1016/j.gca.2011.12.005
41. Johnson NC, Thomas B, Maher K et al (2014) Olivine dissolution and carbonation under conditions relevant for in situ carbon storage. Chem Geol 373:93–105. doi:10.1016/j.chemgeo.2014.02.026
42. Olsson J, Bovet N, Makovicky E et al (2012) Olivine reactivity with CO_2 and H_2O on a microscale: implications for carbon sequestration. Geochim Cosmochim Acta 77:86–97. doi:10.1016/j.gca.2011.11.001

43. Paukert AN, Matter JM, Kelemen PB et al (2012) Reaction path modeling of enhanced in situ CO_2 mineralization for carbon sequestration in the peridotite of the Samail Ophiolite, Sultanate of Oman. Chem Geol 330–331:86–100. doi:10.1016/j.chemgeo.2012.08.013
44. Cipolli F (2004) Geochemistry of high-pH waters from serpentinites of the Gruppo di Voltri (Genova, Italy) and reaction path modeling of CO_2 sequestration in serpentinite aquifers. Appl Geochem 19:787–802. doi:10.1016/j.apgeochem.2003.10.007
45. Xu T, Apps J, Pruess K (2000) Analysis of mineral trapping for CO_2 disposal in deep aquifers. Lawrence Berkeley National Laboratory, Berkeley. Retrieved from: http://escholarship.org/uc/item/59c8k6gb
46. Harrison AL, Dipple GM, Power IM, Mayer KU (2015) Influence of surface passivation and water content on mineral carbonation rates: implications for CO_2 sequestration in mine tailings. Geochim Cosmochim Acta 148:477–495. doi:10.1016/j.gca.2014.10.020
47. Wilson SA, Harrison AL, Dipple GM et al (2014) Offsetting of CO_2 emissions by air capture in mine tailings at the Mount Keith Nickel Mine, Western Australia: rates, controls and prospects for carbon neutral mining. Int J Greenh Gas Control 25:121–140. doi:10.1016/j.ijggc.2014.04.002
48. Kelemen P, Rajhi AA, Godard M et al (2013) Scientific drilling and related research in the Samail Ophiolite. Sultanate Oman Sci Drill 15:64–71. doi:10.2204/iodp.sd.15.10.2013
49. Falk ES, Kelemen PB (2015) Geochemistry and petrology of listvenite in the Samail ophiolite, Sultanate of Oman: complete carbonation of peridotite during ophiolite emplacement. Geochim Cosmochim Acta 160:70–90. doi:10.1016/j.gca.2015.03.014
50. Rudge JF, Kelemen PB, Spiegelman M (2010) A simple model of reaction-induced cracking applied to serpentinization and carbonation of peridotite. Earth Planet Sci Lett 291:215–227. doi:10.1016/j.epsl.2010.01.016
51. Dessert C, Dupré B, Gaillardet J et al (2003) Basalt weathering laws and the impact of basalt weathering on the global carbon cycle. Chem Geol 202:257–273. doi:10.1016/j.chemgeo.2002.10.001
52. Goldberg DS, Takahashi T, Slagle AL (2008) Carbon dioxide sequestration in deep-sea basalt. Proc Natl Acad Sci U S A 105:9920–9925. doi:10.1073/pnas.0804397105
53. Snæbjörnsdóttir SÓ, Wiese F, Fridriksson T et al (2014) CO_2 storage potential of basaltic rocks in Iceland and the oceanic ridges. Energy Procedia 63:4585–4600. doi:10.1016/j.egypro.2014.11.491
54. Flaathen TK, Gislason SR, Oelkers EH, Sveinbjörnsdóttir ÁE (2009) Chemical evolution of the Mt. Hekla, Iceland, groundwaters: a natural analogue for CO_2 sequestration in basaltic rocks. Appl Geochem 24:463–474. doi:10.1016/j.apgeochem.2008.12.031
55. Galeczka I, Wolff-Boenisch D, Gislason S (2013) Experimental studies of basalt-H_2O-CO_2 interaction with a high pressure column flow reactor: the mobility of metals. Energy Procedia 37:5823–5833. doi:10.1016/j.egypro.2013.06.505
56. Alfredsson HA, Oelkers EH, Hardarsson BS et al (2013) The geology and water chemistry of the Hellisheidi, SW-Iceland carbon storage site. Int J Greenhouse Gas Control 12:399–418. doi:10.1016/j.ijggc.2012.11.019
57. Alfredsson HA, Hardarson BS, Franzson H, Gislason SR (2008) CO_2 sequestration in basaltic rock at the Hellisheidi site in SW Iceland: stratigraphy and chemical composition of the rocks at the injection site. Mineral Mag 72:1–5. doi:10.1180/minmag.2008.072.1.1
58. Schaef HT, McGrail BP, Owen AT (2010) Carbonate mineralization of volcanic province basalts. Int J Greenh Gas Control 4:249–261. doi:10.1016/j.ijggc.2009.10.009
59. Schaef HT, McGrail BP, Owen AT (2011) Basalt reactivity variability with reservoir depth in supercritical CO_2 and aqueous phases. Energy Procedia 4:4977–4984. doi:10.1016/j.egypro.2011.02.468
60. Galeczka I, Wolff-Boenisch D, Oelkers EH, Gislason SR (2014) An experimental study of basaltic glass–H_2O–CO_2 interaction at 22 and 50 °C: implications for subsurface storage of CO_2. Geochim Cosmochim Acta 126:123–145. doi:10.1016/j.gca.2013.10.044
61. Rani N, Pathak V, Shrivastava JP (2013) CO_2 mineral trapping: an experimental study on the carbonation of basalts from the Eastern Deccan Volcanic Province, India. Procedia Earth Planet Sci 7:806–809. doi:10.1016/j.proeps.2013.03.069

62. Bacon DH, Ramanathan R, Schaef HT, McGrail BP (2014) Simulating geologic co-sequestration of carbon dioxide and hydrogen sulfide in a basalt formation. Int J Greenhouse Gas Control 21:165–176. doi:10.1016/j.ijggc.2013.12.012
63. Stockmann G, Wolff-Boenisch D, Gíslason SR, Oelkers EH (2008) Dissolution of diopside and basaltic glass: the effect of carbonate coating. Mineral Mag 72:135–139. doi:10.1180/minmag.2008.072.1.135
64. Aradóttir ESP, Sonnenthal EL, Björnsson G, Jónsson H (2012) Multidimensional reactive transport modeling of CO_2 mineral sequestration in basalts at the Hellisheidi geothermal field, Iceland. Int J Greenh Gas Control 9:24–40. doi:10.1016/j.ijggc.2012.02.006
65. Gysi AP, Stefánsson A (2012) Experiments and geochemical modeling of CO_2 sequestration during hydrothermal basalt alteration. Chem Geol 306–307:10–28. doi:10.1016/j.chemgeo.2012.02.016
66. Gysi AP, Stefánsson A (2011) CO_2–water–basalt interaction. Numerical simulation of low temperature CO_2 sequestration into basalts. Geochim Cosmochim Acta 75:4728–4751. doi:10.1016/j.gca.2011.05.037
67. Gysi AP, Stefánsson A (2008) Numerical modelling of CO_2-water-basalt interaction. Mineral Mag 72:55–59. doi:10.1180/minmag.2008.072.1.55
68. Gysi AP, Stefánsson A (2012) CO_2-water–basalt interaction. Low temperature experiments and implications for CO_2 sequestration into basalts. Geochim Cosmochim Acta 81:129–152. doi:10.1016/j.gca.2011.12.012
69. Aradóttir ESP, Sonnenthal EL, Jónsson H (2012) Development and evaluation of a thermodynamic dataset for phases of interest in CO_2 mineral sequestration in basaltic rocks. Chem Geol 304–305:26–38. doi:10.1016/j.chemgeo.2012.01.031
70. Gislason SR, Wolff-Boenisch D, Stefansson A et al (2010) Mineral sequestration of carbon dioxide in basalt: a pre-injection overview of the CarbFix project. Int J Greenh Gas Control 4:537–545. doi:10.1016/j.ijggc.2009.11.013
71. Matter JM, Stute M, Hall J et al (2014) Monitoring permanent CO_2 storage by in situ mineral carbonation using a reactive tracer technique. Energy Procedia 63:4180–4185. doi:10.1016/j.egypro.2014.11.450
72. McGrail BP, Spane FA, Amonette JE et al (2014) Injection and monitoring at the wallula basalt pilot project. Energy Procedia 63:2939–2948. doi:10.1016/j.egypro.2014.11.316
73. Rutqvist J, Tsang C-F (2002) A study of caprock hydromechanical changes associated with CO_2-injection into a brine formation. Environ Geol 42:296–305. doi:10.1007/s00254-001-0499-2
74. Rutqvist J, Birkholzer JT, Tsang C-F (2008) Coupled reservoir–geomechanical analysis of the potential for tensile and shear failure associated with CO_2 injection in multilayered reservoir–caprock systems. Int J Rock Mech Min Sci 45:132–143. doi:10.1016/j.ijrmms.2007.04.006
75. Zoback MD, Gorelick SM (2012) Earthquake triggering and large-scale geologic storage of carbon dioxide. Proc Natl Acad Sci 109:10164–10168. doi:10.1073/pnas.1202473109
76. Yarushina VM, Bercovici D (2013) Mineral carbon sequestration and induced seismicity. Geophys Res Lett 40:814–818. doi:10.1002/grl.50196
77. Kelemen PB, Hirth G (2012) Reaction-driven cracking during retrograde metamorphism: olivine hydration and carbonation. Earth Planet Sci Lett 345–348:81–89. doi:10.1016/j.epsl.2012.06.018
78. Page BM (1972) Oceanic crust and mantle fragment in subduction complex near San Luis Obispo, California. Bull Geol Soc Am 83:957–972. doi:10.1130/0016-7606(1972)83[957:OCAMFI]2.0.CO;2

Ocean Applications for Carbon Dioxide Sequestration

N. Thulasi Prasad, K.N.V.V. Murthy, Sridhar Muddada, Sucheta Sadhu, G. Dharani, S. Ramesh, S.V.S. Phani Kumar, M.B. Venkata Rao, A. Syamsundar, and M.A. Atmanand

Abstract Increase in the concentration of carbon dioxide (CO_2) in the atmosphere is being attributed to the adverse effects such as warming of the planet; increase in the sea level; variation in the atmospheric and ocean circulation patterns; snow cover variation; and, sea ice extent. One of the common approaches followed in the mitigation efforts is the study on the reduction of the emissions of CO_2 from the major point sources such as coal fired power plants, steel plants, cement industries. Direct injection of the carbon dioxide into the deep oceans, mineral carbonation applications, in situ replacement of the gas hydrate into the carbon dioxide hydrates, micro algal sequestration and iron fertilization are some of the ocean sequestration options studied in the literature. Present chapter studies the feasibility of different ocean sequestration methods in comparison with the technological requirements for the realization of these methods.

The relative merits of the methods, the technological challenges, ecological and environmental issues needing detailed studies for the application are discussed in this chapter. The experiments conducted on the mineral carbonation of industrial wastes such as steel slag using direct and indirect methods are discussed, considering the Linz-Donawitz converter slag. The carbonation efficiency for different conditions is compared and the structure of the resulting materials is analyzed. The prospective applications for coastal protective measures and artificial reef growth and the state of the art in similar applications using the concrete structure are discussed. The chapter discusses in detail the energy requirements in mineral carbonation methodology using the steel slag.

N.T. Prasad • K.N.V.V. Murthy • S. Muddada • S. Sadhu • G. Dharani • S. Ramesh
S.V.S. Phani Kumar (✉) • M.A. Atmanand
Earth Systems Science Organisation - National Institute of Ocean Technology (ESSO-NIOT), Velacherry-Tambaram Main Road, Narayanapuram, Pallikaranai, Chennai 600 100 Tamil Nadu, India
e-mail: phani@niot.res.in

M.B.V. Rao • A. Syamsundar
Visakhapatnam Steel Plant (VSP), Visakhapatnam, India

V. Vishal, T.N. Singh (eds.), *Geologic Carbon Sequestration*,
DOI 10.1007/978-3-319-27019-7_12

1 Introduction

The role of the increasing amount of anthropogenic emissions of greenhouse gases including the carbon dioxide in the atmosphere is being studied to ascertain the adverse effects on the global climate. Considering, the current level of the mean monthly concentrations of carbon dioxide (CO_2) in the atmosphere reportedly reaching 400 ppm [1], it is highly imperative to take note of the Intergovernmental Panel on Climate Change observation to take necessary steps to study the effects and to identify the possible means of mitigation of the global warming [2]. The immediate attention is thus being drawn to the point sources of carbon dioxide emissions such as power plants, iron and cement industries, etc. Ocean, along with the terrestrial vegetation, plays an important role as a natural sink to about 50 % of the anthropogenic CO_2 emissions. Detailed experiments on the increasing atmospheric concentration indicated correlation with the drop in the ocean pH [3, 4]. It is essential to understand in detail the impacts of the pH changes in the ocean on the global climate and also on the marine life, apart from the concentrated efforts to mitigate the global warming effects by CO_2 sequestration.

The options for CO_2 sequestration involving its capture and long term storage by geological and biological means are studied to mitigate the global warming [5]. The options studied on ocean CO_2 sequestration include the storage of carbon dioxide by either directly injecting carbon dioxide to stable depths [6]; or at intermediate depths [7]. The state of the art of the ocean technology for development of applications up to 6000 m water depth, as demonstrated at Earth Systems Science Orgnization – National Institute of Ocean Technology (ESSO-NIOT) [8] and other pioneering institutes worldwide, would not only provide a glimpse of the technological challenges for the direct injection methods, but also suggest innovative eco-friendly marine application options with sustainable coastal protection.

Use of the carbonated materials as artificial reefs for coastal protection structures is studied in one such technique, combining industrial mineral carbonation with coastal protection structures as shown in the Fig. 1. Test blocks prepared from carbonated materials are subjected to trials in seawater environment. Carbonated material is also found to be an ideal substrate for settlement and growth of coral and diverse marine organisms. Further studies are aimed at the use of the carbonated steel slag, and there by the carbon dioxide emission and waste product from the industry, towards sustainable development and harnessing of the marine ecosystem.

2 Role of Ocean as a Natural Sink

The ocean, in association with the terrestrial biosphere has been a natural sink for anthropogenic carbon dioxide [4]. The ocean is estimated to absorb 1 million tons of CO_2 per hour with about 530×10^9 metric tons of fossil fuel CO_2 accumulated in ocean waters [6]. Various naturally occurring currents in the ocean circulate the

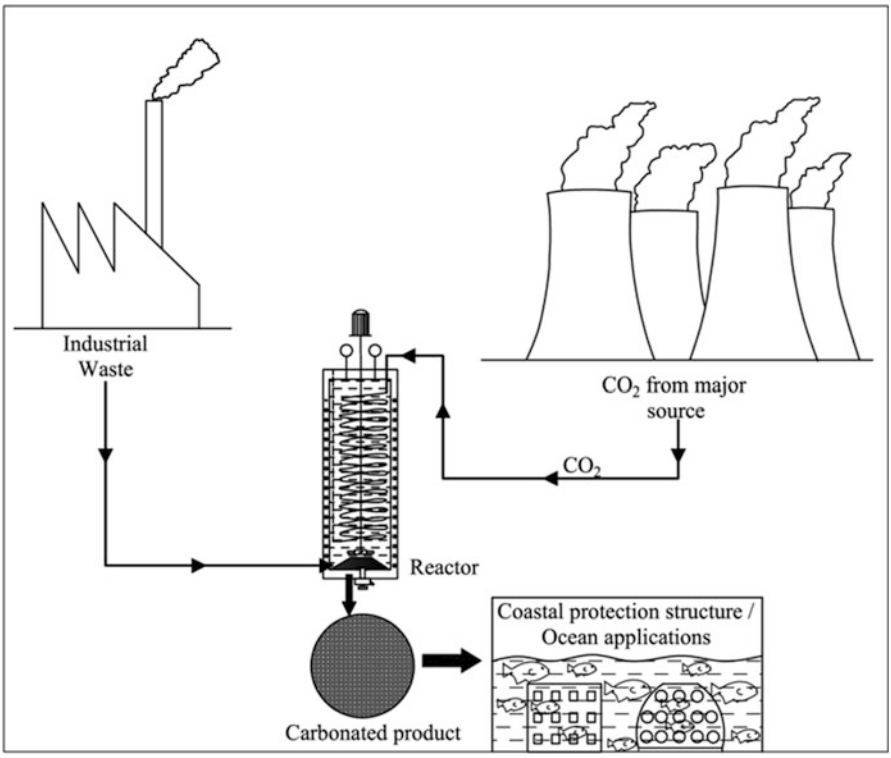

Fig. 1 Schematic of the of carbonation process for ocean applications

dissolved CO_2 to the deeper depths, resulting in the lowering of the pH and thus affecting the saturation state of the calcium carbonate particles and biological system. While some studies concentrated on the ocean–atmosphere to understand the dynamics of the absorption and its after effects, others concentrated on the impacts of acidification on the marine life such as coral reefs [3] and other calcareous organisms [6].

3 Ocean CO_2 Sequestration Techniques

The basic approach of CO_2 storage in ocean consisted of compressing the CO_2 stream captured from the industry and transporting it to the deep ocean for release at a stable depth. Direct injection of liquefied CO_2 into the deep ocean waters was first proposed by Marchetti [9], to increase the degree of isolation of CO_2 from atmosphere [10].

The stratified ocean, with its vertical profiles, is characterized by an upper mixed layer of about 100 m deep, a thermocline region extending to about a depth of

1000 m, and a deep region. The upper mixed layer features near-constant density and temperature profiles over the depth and the gaseous concentration levels are in equilibrium with the atmosphere. The thermocline is stably stratified by large temperature and density gradients that inhibit vertical mixing. The deep ocean has near-constant temperatures in the range of 2–5 °C. The increase in the pressure of about 1 bar per 10 m depth would ensure that CO_2 would be a gas approximately above 500 m depth and a liquid below that depth.

Field experiments are conducted to test the ideas for the disposal of fossil fuel carbon dioxide in the ocean as a solid hydrate at depths ranging from 349 to 3627 m [6]. The experiments indicated that the Liquid CO_2 on the seafloor within the water depths of 2700–4500 m would quickly react with water, form a hydrate and swell many times than its original volume. The liquid CO_2 would be positively buoyant down to about 3000 m, but negatively buoyant below that depth. At about 3700 m, the liquid becomes negatively buoyant compared to seawater saturated with CO_2. Although quite long residence times are possible, first in the hydrate phase and later because of the long ocean circulation time scales and the necessity of the equality of chemical potential in all the three phases (aqueous solution, CO_2 and clathrate) as a condition for the hydrate stability has long been known [11], the background ocean CO_2 levels are far from saturation.

The technological feasibility of the transportation and disposal of carbon dioxide at these depths and the environmental impact of any destabilizing effects due to the natural disasters need to be ascertained to go forward with the method. Considering the formation of CO_2 hydrate beyond the water depths of about 500 m depending on the relative compositions, several methods of injecting CO_2 in the ocean are proposed such as: Direct injection; Dry ice; CO_2 hydrate; and Gas Lift Advanced Device (GLAD) system.

3.1 Direct Injection

The, CO_2 recovered from the industry is liquefied and then transported to a floating platform supporting a vertical pipe to inject liquid-CO_2 directly into the ocean. At depths of 3000 m, 90 % of the CO_2 is expected to be stored for at least 500 years. The energy required for CO_2 liquefaction by the use of a compression unit is estimated to be 120 kWh per ton CO_2. Energy requirements for compression and injection from the floating platform are estimated to be about 40–50 kWh per ton CO_2 [12].

The options of pumping along an inclined pipeline traversing the seabed and a 500 m long pipe towed by a vessel are two other variations studied for the direct injection. The distance to the potential site with a minimum water depth of 3000 m, the requirements for the platform, loading and unloading of the vessel and the vessel time for the operation and the mechanisms to ensure operational safety are some of the challenges to be understood in detail so as to take the technology forward.

3.2 Dry Ice

The Solid CO_2 or dry ice blocks, with a specific gravity of 1.5 to readily sink into the ocean on disposal from a moving ship, is another option that is studied. The energy requirement for making and maintaining dry ice, the point of insertion and detailing the dry ice interaction with its surroundings while sinking are some of the issues that need immediate attention [13].

3.3 CO_2 Hydrate

The liquefied CO_2 is transported by pipe to a hydrate reactor and injected as hydrates into the ocean at depths of 1000–1500 m. The CO_2-hydrates will sink to reach complete dissolution at a depth of 2500 m. Some parts of the ocean are reported to hold enormous natural resources of methane hydrates. Global reserves of methane in hydrate reservoirs are estimated to be up to 120×10^{15} m^3 with about $1900x10^9$ m^3 reported to be trapped under Indian waters [14]. One of the concepts for methane extraction involves pumping CO_2 into the reserves to replace the methane in the reservoir [15, 16], being used by the Conoco-Philips demonstration project at Ignik Sikumi field site in Arctic Circle. While sequestering the CO_2 in the process of extraction of the methane, the process also aims at restoring the stability of the reservoir [17].

3.4 Gas Lift Advances Device (GLAD) System

The recovered CO_2 is passed to an inverse j-tube gas-lift pump system [18] immersed in the ocean at about 200 m below the surface. The buoyancy of the gas is utilized to ensure complete dissolution in ocean water as the gas rises. The hydraulic head created as the dissolving gas rises and the momentum of the carbonate solution at the highest position is ensured to sink the carbonate solution through the longer arm of the system to depths beyond 3000 m where the solution is negatively buoyant. The system is capable of sequestering low purity CO_2 emissions sources and bypasses the liquefaction stage for CO_2. However, the system still needs to address the technological challenges, issues of operational safety of carrying the gas to the system, maintenance of the system and the environmental performance of the system [19].

3.5 Artificial Upwelling

Upwelling is the natural process that occurs in the ocean where cold deep sea nutrient rich water is brought back to ocean surface. Upwelling in the ocean is caused by the combination of wind, Coriolis effects, and Ekman transport. Five types of upwelling, namely, coastal, wind driven, eddy driven, topographically associated and diffusive, are reported in the world oceans. The rate of upwelling is reported to be about 1 % of the down welling but accounts for 5 % of global marine productivity [20]. Generally the offshore open oceans are oligotrophic in nature because of the sinking of the organic matter to deep water and the replenishment of nutrient from deep sea waters are less due to the difference in the density between the warm surface water and the cold deep ocean water [21]. Artificial upwelling is another form of ocean fertilization where in the cold nutrient rich deep ocean water are brought back to surface of the ocean by engineering techniques. The artificial upwelling of cold deep sea water provides a continuous supply of plant nutrient to the surface water and promotes phytoplankton bloom, there by fixing an equivalent proposition of CO_2.

Pumping of deep ocean water from 1200 m for Ocean thermal energy conversion (OTEC) was attempted by ESSO-NIOT during 2000 and continuous pumping of water from 300 m for the low temperature thermal desalination (LTTD) at three Islands of Lakshadweep group of Islands since 2005 has been achieved by ESSO-NIOT. In OTEC it was proposed to pump deep sea cold water continuously from 1200 m depth at 2.1 m^3/s. The deep sea cold water from 1000 m deep has characteristics of 8 °C temperature, 3.4, 6.2 and 27.3 μmole of phosphate, nitrate and silicate respectively which is several fold higher that the surface water. Experiments conducted onboard on the effect of mixing of deep sea cold water and surface warm water at a ratio of 1:1 increased the phytoplankton production up to 20 fold higher when compared to the surface water. Similarly at Lakshadweep group of Islands 12 °C cold deep sea water is pumped from 300 m at a rate of 0.15 m^3/s. Artificial upwelling of deep sea cold water with rich nutrients also bring significant amount of carbon dioxide back to the surface water and subsequently to the atmosphere. However the amount of carbon fixed by phytoplankton due to the nutrient enrichment offsets the surfaced CO_2. Some of the phytoplankton species produce Dimethylsulphoniopropionate (DMSP) in natural upwelling regions, which degrades to Dimethylsulfide (DMS) that is oxidized by hydroxyl radicals to form sulfate particles which contribute to an increase in cloud cover.

3.6 Other Options for Ocean Sequestration

Iron fertilization deals with the introduction of iron particles into the ocean to increase the biological productivity of the phytoplankton species that in turn fixes the carbon dioxide. The lack of understanding of the long term environmental

effects of the process is one of the main factors that discouraged sustained studies on the topic [22].

Studies on the micro algal production for biodiesel and neutraceuticals concentrate on the growth enhancement mechanisms of the algae. The algae can sustain growth in high CO_2 concentrations while fixing a part of the CO_2. The sensitivity of the algal strains for high temperatures and the limitations in the scale and continuous utilization of CO_2 streams are some of the challenges being addressed in the studies [23].

3.7 Mineral Carbonation and Coastal Protection

The coastal regions are constantly shaping under the influence of natural forces such as wind, waves and currents. The landward displacement of the shoreline caused by the combined energy of these forces is termed as coastal erosion. Coastal erosion, or coastal instability, affects the human activities near the shore, properties and businesses. The great concentration of national resources in the coastal zones requires the understanding of the coastal change. Structures are installed in the shallow depths to absorb the incident wave energy to reduce the erosion. Some forms of these structures eventually harness the marine growth and grow in size to form reefs. Mineral carbonation process, using the industrial wastes such as steel slag produces the carbonates of calcium and magnesium that could in turn be used in the construction of these structures.

4 Steel Slag and Carbonation Methods

Mineral Carbonation is a process to store CO_2 in a geologically stable, solid final form. The basic concept behind mineral CO_2 sequestration is that the calcium or magnesium containing minerals react with CO_2 and form solid calcium or magnesium carbonates, shown in Eq. (1).

$$(\mathrm{Ca,Mg})\mathrm{SiO_3(s)} + \mathrm{CO_2(g)} \rightarrow (\mathrm{Ca,Mg})\mathrm{CO_3(s)} + \mathrm{SiO_2(s)} \tag{1}$$

The mineral carbonation that mimics naturally occurring rock weathering processes of calcium and magnesium minerals being converted into their respective carbonates [24, 25] is described with Eqs. (2), (3), and (4).

$$\mathrm{CO_2(g)} + \mathrm{H_2O(l)} \rightarrow 2\mathrm{H^+(aq)} + \mathrm{CO_3^{2-}(aq)} \tag{2}$$

$$\mathrm{CaSiO_3(s)} + 2\mathrm{H^+(aq)} \rightarrow \mathrm{Ca^{2+}(aq)} + \mathrm{SiO_2(s)} + \mathrm{H_2O} \tag{3}$$

$$Ca^{2+}(aq) + CO_3^{2-}(aq) \rightarrow CaCO_3 \downarrow (s) \tag{4}$$

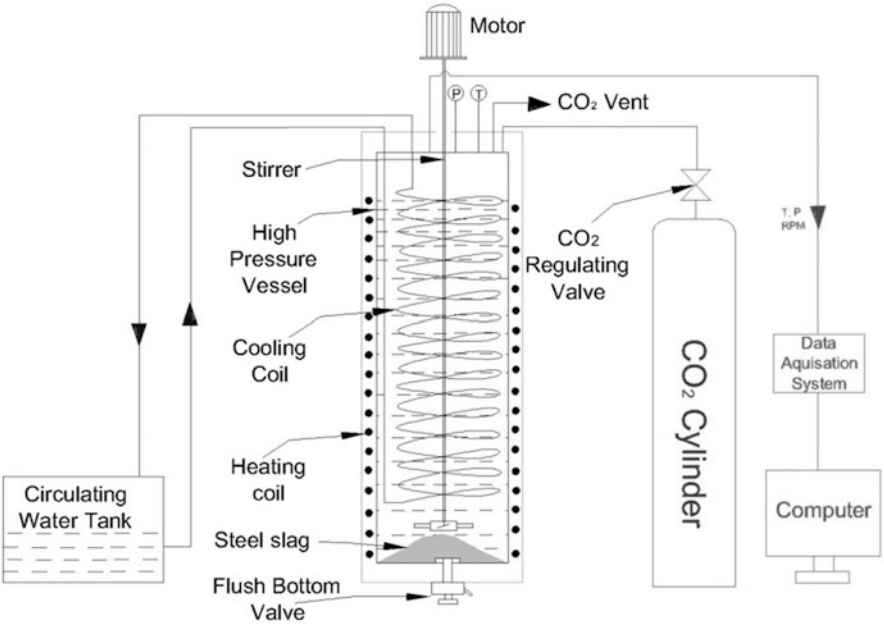

Fig. 2 Schematic diagram of carbonation reactor set up

Naturally occurring weathering process is extremely slow and takes place over thousands of years. Attempts were made to study the process efficiency by changing different process parameters such as particle size, temperature, pressure, stirring rate and catalysts.

The experiments were performed [26] with various particle sizes ranging from <75 μm to 1000 μm in a reactor of 1000 ml volume equipped with heater and stirrer. In the carbonation method, steel slag weighing 50 g was placed in 500 ml distilled water, with a liquid-to-solid (L/S) ratio of 10 kg/kg. The stirring rate was varied between 200 and 800 rpm, the reactor pressure was between 5 and 30 bar and temperature range was between 40 and 100 °C with the entire process time of reaction as 5 h in the presence of carbon dioxide supplied through a regulator controlled cylinder as shown in Fig. 2. The carbonation efficiency of the process was estimated using the pressure drop method [24, 26].

4.1 Particle Size

Reduction in the size of the particles from 1000 μm to <75 μm increased the carbonation efficiency as observed in the Fig. 3a. Decrease in the particle size of the slag increased the exposed surface area of the particles undergoing the reaction, in turn increasing the efficiency of the reaction. Higher carbonation efficiency is

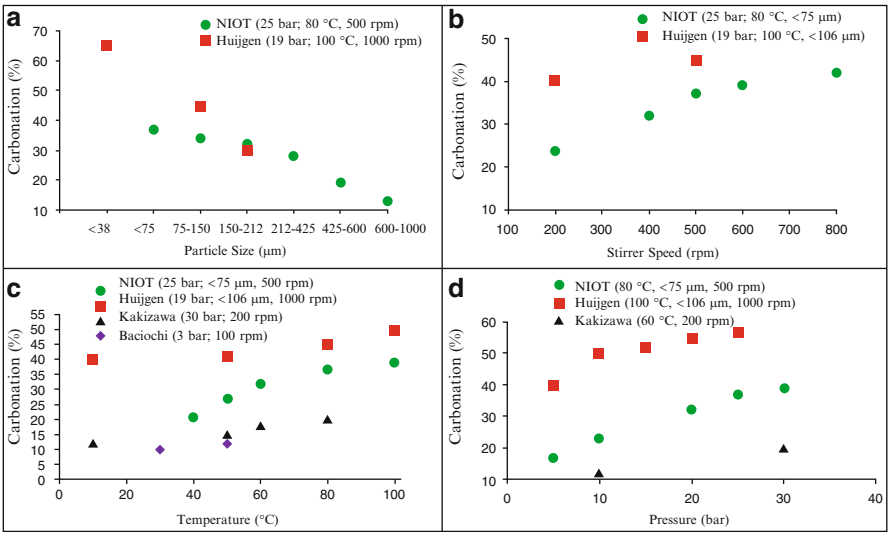

Fig. 3 (**a**) Variation of carbonation efficiency with particle size; (**b**) Variation of carbonation efficiency with stirrer speed; (**c**) Variation of carbonation efficiency with increase in temperature; and, (**d**) Variation in carbonation efficiency with increase in pressure

observed in Huijgen [24] in Fig. 3a compared to that of Prasad et al. [27] due to the reaction temperature being higher by 20 °C and stirrer rotation being higher by 500 rpm in Prasad et. al [27]. For the particle sizes between 75 and 150 μm the carbonation efficiency reported by Prasad et al. [27] was 38 % and that by Huijgen [24] was 47 %.

4.2 Stirring Rate

The rotation rate of the stirrer was varied between 200 and 800 rpm as shown in Fig. 3b. The rotation of the stirrer enhances the reaction of the steel slag in the water simultaneously releasing the oxides of the calcium and magnesium. At 500 rpm the 34 % carbonation observed by Prasad et al. [27] was relatively less compared to 43 % observed by Huijgen et al. [24] due to the higher operating temperature of the later.

4.3 Temperature

The temperature of the reaction was varied between 200 and 800 °C by keeping other parameters constant. Increase in temperature is expected to enhance the leaching of calcium or magnesium oxides from the steel slag and in turn the

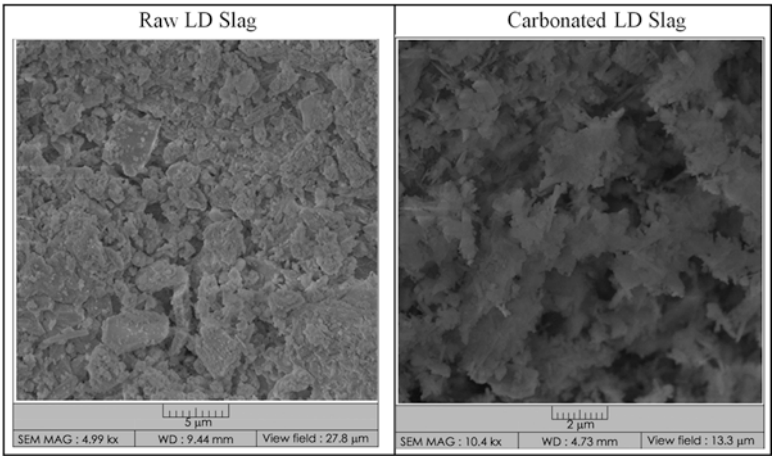

Fig. 4 Scanning Electron Microscope image of Linz-Donawitz converter slag (Size: 212–425 µm, Pressure: 20 bar, Temperature: 60 °C, Stirrer speed: 500 rpm)

carbonate conversion. However higher temperature is associated with the consumption of more energy. It is essential to find the optimum temperature for the energy efficiency process. From Fig. 3c, it was observed that the carbonation efficiency at 50 °C as reported by Prasad et al. [27] was higher than that of Kakizawa [28] and Baciochi [29], but lower than that of Huijgen [24] due to the difference in the stirrer speed.

4.4 Pressure

From Fig. 3d it was observed that the carbonation efficiency reported by Prasad et al. [26] was higher than that of Kakizawa [27] but lower than that of Huijgen [24]. An increase in the pressure was found to increase the carbonation efficiencies. At a pressure of 10 bar the carbonation efficiency was 12 %, 23 % and 48 % respectively for [24], [26] and [27] due to the difference in the stirrer speed.

The structural morphology of the sample before and after carbonation reaction was studied using a Scanning Electron Microscope (make: TESCAN Vega 3). The reacted and un-reacted slag samples were dried and coated with palladium gold with an ion sputtering device (make: Quorum) and the predominant structures were identified using a microscope. Even-though silica was the dominating component in steel slag, the reacted slag showed the formation of carbonates in the form of scaleno-hedral shape as shown in Fig. 4 [30].

4.5 Indirect Carbonation Process

Indirect carbonation was also studied using acetic acid and ammonium chloride [31, 32]. The indirect method involves a two step procedure namely the extraction of calcium ions from the calcium silicate [24] as shown in Eqs. (5) and (6) [28, 33] and after filtering the silica out of the solution, pumping carbon dioxide into the solution at 25 bar pressure for carbonation as indicated in Eq. (7) and (8).

$$CaSiO_3 + 2CH_3COOH \rightarrow Ca^{2+} + 2CH_3COO^- + SiO_2 + H_2O \quad (5)$$

$$2CaSiO_3 + 4NH_4Cl \rightarrow 2CaCl_2 + 4NH_3 + 2H_2O + 2SiO_2 \quad (6)$$

$$Ca^{2+} + 2CH_3COO^- + CO_2 + H_2O \rightarrow CaCO_3(\downarrow) + 2CH_3COOH \quad (7)$$

$$2CaCl_2 + 4NH_3 + 2H_2O + 2CO_2 \rightarrow 2CaCO_3 + 4NH_4Cl \quad (8)$$

X-Ray Fluorescence Spectroscopy (XRF) analysis was conducted for raw Linz-Donawitz converter slag, and the residues from indirect carbonation on Linz-Donawitz converter slag with ammonium chloride and acetic acid. The results as shown in Table 1 revealed the presence of 45.2 %, 5.88 %, 21.1 % of calcium oxide, magnesium oxide and silica respectively. The concentration of calcium oxide decreased and the concentration of silica increased in the residues from indirect carbonation on Linz-Donawitz converter slag with ammonium chloride and acetic acid [28, 31, 33].

Titration analysis [34] of the residues of indirect carbonation on Linz-Donawitz converter slag revealed a carbonation efficiency of 85 % with acetic acid and that of 97 % with ammonium chloride. Even-though the carbonation is high in the case of indirect process, the energy requirement for the indirect process is more when compared with direct process [35].

The X-ray diffraction analysis for the raw Linz-Donawitz converter slag and its residues from indirect carbonation with ammonium chloride was analyzed and is shown in Fig. 5. It was observed that the peaks coincided with calcite form.

Table 1 Composition of Linz-Donawitz Converter Steel Slag and the residues resulting from indirect carbonation with Ammonium Chloride (NH_4Cl) and Acetic Acid (CH_3COOH)

	Weight (%)						
	MgO	Al_2O_3	FeO	CaO	SiO_2	MnO	P_2O_5
Raw LD Slag	5.88	1.9	20.3	45.2	21.1	2.94	1.28
Residue of Indirect car-bonation with NH_4Cl	7.32	3.5	21.3	36.1	27.5	0.97	1.66
Residue of Indirect car-bonation with CH_3COOH	5.72	7	32.7	6.7	41.3	0.97	3.4

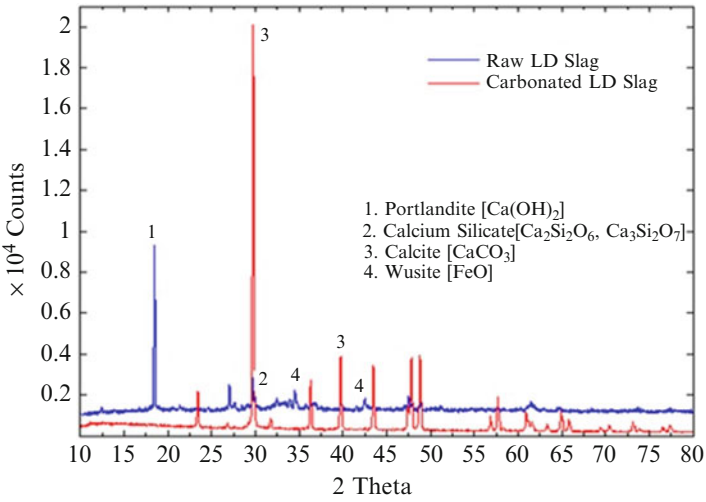

Fig. 5 XRD Analysis of raw slag and carbonated ammonium chloride extraction process

5 Feasibility Study to Use Converted Carbonates as Coastal Protection Structures

Carbonated wastes were proposed to be used in the preparation of the coastal structures. Studies [36] showed that the blocks made out of carbonated industrial wastes could also be used for the artificial growth of corals in the sea. Coastal regions experience depletion of beach sand that is identified to contribute to the erosion and loss of reef crests and increased wave energy at the shore. Use of artificial reefs for the coastal protective measures was demonstrated by ESSO-NIOT. 750 concrete artificial reef modules of 3 different shapes with typical dimensions of 1 m × 1 m that were designed and deployed along Odisha coast during 2011 have supported the growth of a variety of invertebrates. It was estimated that the artificial reef structures supported approximately 150 MT of biomass, there by contributing to carbon recycling.

The carbonated slag was used in the preparation of test blocks [27] and was immersed in seawater to study its pH changes as shown in Fig. 6 indicating the leaching process in marine environment. On comparison with the blocks made of raw slag and concrete, no significant impact was observed due to the use of carbonated slag in the blocks [35]. Artificial reefs show high stability in sea water due to the presence of calcium carbonate and can act as substrate for sea weeds and corals [37].

Coal combustion waste [38] was used in making blocks that were deployed as a fishing reef and extensive studies were conducted. While the plant settlement was not observed due to low light penetration in the area of deployment, during the first year the animal life was found to settle on the block surface. About 50 % of the surface was observed to be covered on the top and the sides while the bottom appeared to be more covered (Fig. 7).

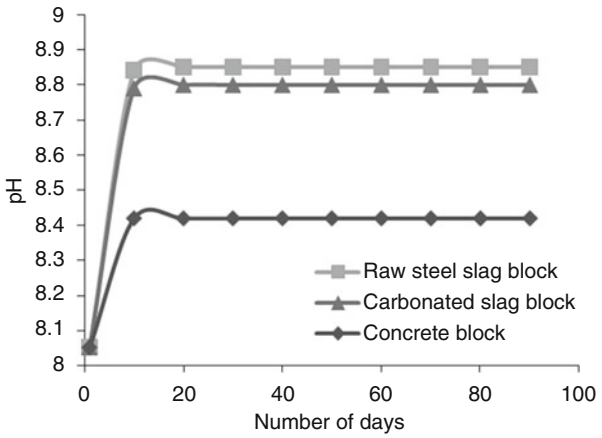

Fig. 6 pH change after soaking blocks of concrete, steel slag and carbonated slag in sea water

Fig. 7 Marine growth on artificial reef and congregation of groupers

6 Conclusions

The ocean is the largest sink for the storing of CO_2 as compared to all other sequestration options. Various options for the ocean CO_2 sequestration are discussed and the technological challenges, ecological and environmental issues need further extensive studies for the safe and permanent storage of CO_2 in the ocean. Studies indicate that the carbonation from industrial wastes can be optimized for energy efficiency and in turn can be utilized as artificial reef blocks to store carbon dioxide for long-term. Storage in marine environment as artificial reefs will be eco-friendly to the marine biotic life cycle.

Acknowledgements Authors from ESSO-NIOT would like to thank Ministry of Earth Sciences, Govt. of India for financial support and encouragement. Authors would also like to thank Visakhapatnam Steel Plant for inputs and providing steel slag during the course of the studies.

References

1. Tans P, Keeling R (2015) Concentrations of CO_2 in earth's atmosphere derived from in situ air measurements at Mauna Loa Observatory, Hawaii, USA. National Oceanic and Atmospheric Administration, Earth Research Laboratory data sets, hosted at http://www.esrl.noaa.gov/gmd/ccgg/trends//co2_mm_mlo.txt
2. Field CB et al. (eds) (2014) Intergovernmental Panel on Climate Change (IPCC): climate change 2014: impacts, adaptation, and vulnerability. Part A: global and sectoral aspects. Contribution of working group II to the fifth assessment report of the Intergovernmental Panel on Climate Change. Cambridge University Press, Cambridge/New York
3. Sabine CL et al (2004) Current status and past trends of the global carbon cycle. In: Field CB, Raupach MR (eds) The global carbon cycle: integrating humans, climate, and the natural world, Scope 62. Island Press, Washington, DC, pp 17–44
4. Feely RA, Doney SC, Cooley SR (2007) Present conditions and future challenges in a high CO_2 world. Oceanography 22(4):36–47
5. Yang H, Xu Z, Fan M, Gupta R, Slimane RB, Bland AE, Wright I (2008) Progress in carbon dioxide separation and capture: a review. J Environ Sci 20(1):14–27
6. Brewer PG, Friederich G, Peltzer ET, Orr FM Jr (1999) Direct experiments on the ocean disposal of fossil fuel CO_2. Science 284:943–945
7. Sarv H (1999) Large-scale CO_2 transportation and deep ocean sequestration. Phase I final report. McDermott Technology Inc
8. Atmanand MA (2013) Development in underwater technologies – Indian scenario. In: Proceedings of the international symposium on underwater technologies, The University of Tokyo, Tokyo, Japan, 5–8 March 2013
9. Marchetti C (1977) On geoengineering and the CO_2 problem. Clim Chang 1:59–68
10. Brewer PG (2009) A changing ocean seen with clarity. Proc Natl Acad Sci U S A 106:12213–12214
11. Bakker RJ, Dubessy J, Cathelineau M (1996) Improvements in clathrate modeling I: the H2O-CO2 system with various salts. Geochim Cosmochim Acta 60(10):1657–1681
12. Khoo HH, Tan RBH (2006) Life cycle investigation of CO_2 recovery and sequestration. Environ Sci Technol 40(12):4016–4024
13. Murray CN, Visintini L, Bidoglio G, Henry G (1996) Permanent storage of carbon dioxide in the marine environment: the solid CO_2 penetrator. Energy Convers Manag 37(6–8):1067–1072
14. Sain K, Ojha M, Satyavani N, Ramadass GA (2012) Gas hydrates on Krishna-Godavari and Mahanadi basins: new data. J Geol Soc India 79:553–556
15. Ohgaki K, Takano K, Sangawa H, Matsubara T, Nakano S (1996) Methane exploitation by carbon dioxide from gas hydrates-phase equilibria for CO_2-CH_4 mixed hydrate system. J Chem Eng Japan 29(3):478–483
16. Hirohama S, Shimoyama Y, Wakabayashi A, Tatsuta S, Nishida N (1996) Conversion of CH4-hydrate to CO_2-hydrate in liquid CO_2. J Chem Eng Japan 29(6):1014–1020
17. Duyen LQ, Herri JM, Yamina O, Nam TH, Du LQ (2012) CO_2-CH_4 exchange in the context of CO_2 injection and gas production from methane hydrates bearing sediments. Petrovietnam 10:38–45
18. Saito T, Kajishima K (2000) CO_2 sequestration at sea by gas-lift system of shallow injection and deep releasing. Environ Sci Technol 34:4040–4045
19. Saito T, Kajishima K, Tsuchiya K (2011) Deep ocean CO_2 sequestration via GLAD (gas-lift advanced dissolution) system. J Environ Eng 6(2):412–415
20. Carr ME (2002) Estimation of potential productivity in eastern boundary currents using remote sensing. Deep Sea Res II Top Stud Oceanogr 49:59–80
21. Stowe K (1996) Exploring ocean science, 2nd edn. Wiley, New York
22. Blain S et al (2007) Effect of natural iron fertilization on carbon sequestration in the Southern Ocean. Nature 446:1070–1074

23. Salih FM (2011) Microalgae tolerance to high concentrations of CO_2: a review. J Environ Prot 2:618–654
24. Huijgen WJJ, Witkamp GJ, Comans RNJ (2005) Mineral CO2 sequestration by steel slag carbonation. Environ Sci Technol 39(24):9676–9682
25. Huijgen WJJ, Witkamp GJ, Comans RNJ (2006) Mechanisms of aqueous wollastonite carbonation as a possible CO_2 sequestration process. Chem Eng Sci 61(13):4242–4251
26. Prasad NT, Sadhu S, Murthy KNVV, Srinivasula Reddy P, Ramesh S, Phani Kumar SVS, Dharani G, Atmanand MA, Venkata Rao MB, Dey TK, Syamsundar A (204) CO2 fixation by artificial reef development in marine environment using carbonated slag material from steel plant. In: Proceedings of OCEANS'14 MTS/IEEE Taipei, 7–10 April 2014
27. Prasad NT, Sadhu S, Murthy KNVV, Dharani G, Phanikumar SVS, Ramesh S, Atmanand MA, Venkatarao MB, Dey TK, Balachandrarao P, Syamsundar A (2015) Carbon dioxide fixation: waste material utilization for under water applications. International symposium on underwater technology, Chennai, India, 23–25 February 2015
28. Kakizawa M, Yamasaki A, Yanagisawa Y (2001) A new CO_2 disposal process via artificial weathering of calcium silicate accelerated by acetic acid. Energy 26(4):341–354
29. Baciocchi R, Costa G, Polettini A, Pomi R (2009) Influence of particle size on the carbonation of stainless steel slag for CO_2 storage. Energy Procedia 1:4859–4866
30. Specialty Minerals – Minerals Technologies (2015) Available from http://www.mineralstech.com/Pages/SMI/Precipitated-Calcium-Carbonate-(PCC).aspx Accessed 2 Mar 2015
31. Teir S, Eloneva S, Fogelholm CJ, Zevenhoven R (2006) Stability of calcium carbonate and magnesium carbonate in rainwater and nitric acid solutions. Energy Convers Manag 47:3059–3068
32. Zevenhoven R, Elovena S, Teir S (2006) Chemical fixation of CO_2 in carbonates: routes to valuable products and long-term storage. Catal Today 115:73–79
33. Kodama S, Nishimoto T, Yamamoto N, Yogo K, Yamada K (2008) Development of a new pH-swing CO_2 mineralization process with a recyclable reaction solution. Energy 33 (5):776–784
34. Muller G (1967) Methods in sedimentary petrology. Hafner Publishing Company, New York, p 255
35. Mun M, Cho H (2013) Mineral carbonation for carbon sequestration with industrial waste. Energy Procedia 37:6999–7005
36. Mohammad TA, Hamed A, Habi NF, Ezz-El Arab MA, El-Mose Ihy KHM (2012) Coral rehabilitation using steel slag as a substrate. Int J Environ Prot 2(5):1–5
37. Lim M, Han GC, Ahn JW, You KS (2010) Environmental remediation and conversion of carbon dioxide (CO_2) into useful green products by accelerated carbonation technology. Int J Environ Res Pub Health 7(1):203–228
38. Woodhead PMJ, Parker JH, Duedall IW (1982) The coal-waste artificial reef program (C-WARP): a new resource potential for fishing reef construction. Mar Fish Rev 44 (6–7):16–23

Part VII
Risk Assessment of CO_2 Storage

Risk Assessment of the Geological Storage of CO_2: A Review

Qi Li and Guizhen Liu

Abstract The geological storage of carbon dioxide (CO_2) is a key approach that responds to climate change by reducing the emission of anthropogenic greenhouse gases. However, the CO_2 that is injected into deep geological formations can possibly leak into the paths of wells, cap rock, geological faults, and fractures. Such leakage could allow the CO_2 to move into shallow geological formations or into the atmosphere, thereby polluting shallow underground water, soil, rivers, lakes, and air, all of which could damage the ecological system and cause hazards to human health. Risk assessment studies have identified the main risk scenarios and identified the potential threats and vulnerabilities in order to guarantee the safe and secure storage of captured CO_2. Many qualitative and quantitative methods have been developed and used in existing CCS/CCUS (Carbon dioxide Capture and Storage/Carbon dioxide Capture, Utilization and Storage) projects or assumed sites, such as CO_2-FEP (Feature, Event, and Process), Certification Framework, RISQUE (Risk Identification and Strategy using QUantitative Evaluation), and others. Risk assessment is the overall process of identifying, analyzing, and evaluating potential risks. In this chapter, the health, safety, and environmental risks associated with the geological storage of CO_2 are addressed in detail. Various assessment methods for different stages of the risk management are discussed, including the application of risk assessment practices in various field cases. The risk management measures, which include monitoring, remediation, and emergency plans, also are reviewed for use by engineers, technicians, and policy makers.

Acronyms/Abbreviations

AGI	Acid Gas Injection
AHP	Analytical Hierarchy Process
AIST	National Institute of Advanced Industrial Science and Technology
ALARP	As Low As Reasonably Practicable
AOR	Area of Review

Q. Li (✉) • G. Liu
State Key Laboratory of Geomechanics and Geotechnical Engineering, Institute of Rock and Soil Mechanics (IRSM), Chinese Academy of Sciences, Xiaohongshan 2, Wuchang Wuhan 430071, China
e-mail: qli@whrsm.ac.cn

V. Vishal, T.N. Singh (eds.), *Geologic Carbon Sequestration*,
DOI 10.1007/978-3-319-27019-7_13

BRGM	Bureau de Recherches Géologiques et Minières (French Geological Survey)
CASSIF	CArbon Storage Scenario Identification Framework
CCS	Carbon dioxide Capture and Storage
CCUS	Carbon dioxide Capture, Utilization and Storage
CF	Certification Framework
CGS	CO_2 Geological Storage
CO_2	Carbon dioxide
CO_2-PENS	CO_2 Predicting Engineered Natural Systems
CSA	Canadian Standards Association
DFMEA	Design Failure Mode and Effects Analysis
DNV	Det Norske Veritas
ECA	Emission Credits and Atmosphere
EFMEA	Equipment Failure Mode and Effects Analysis
EOR	Enhance Oil Recovery
EPA	Environmental Protection Agency
ESL	Evidence Support Logic
EU	European Union
FDIS	Final Draft International Standard
FEP	Feature, Event, and Process
FMEA	Failure Mode and Effects Analysis
FTA	Fault Tree Analysis
GERAS-CO_2GS	Geo-Environmental Risk Assessment System - CO_2 Geological Storage
GHGs	Greenhouse Gases
HMR	Hydrocarbon and Mineral Resource
HSE	Health, Safety, and Environment
IBDP	Illinois Basin – Decatur Project
ICARAS	Integrated CArbon Risk ASsessment
IEA	International Energy Agency
IEA GHG	IEA Greenhouse Gas R&D Programme
IFPEN	Institut Francais du Petrole Energies Nouvelles
INERIS	French National Institute for Industrial Environment and Risks
IPCC	Intergovernmental Panel on Climate Change
ISO	International Standardization Organization
KPIs	Key Performance Indicators
LIV	Leakage Impact Valuation
MEP	Ministry of Environmental Protection
MMV	Measurement, Monitoring, and Verification
MOSAR	Organized and Systemic Method of Risk Analysis
MUSTANG	A MUltiple Space and Time scale Approach for the quaNtification of deep saline formations for CO_2 storaGe
NCR	Natural CO_2 reservoirs
NSE	Near-Surface Environment
P&R	Performance and Risk

PFMEA	Process Failure Mode and Effects Analysis
QRA	Quantitative Risk Assessment
QRTT	Quantitative Risk Through Time
RD&D	Research, Development and Demonstration
RISCS	Risk Interference Subsurface CO_2 Storage
RISQUE	Risk Identification and Strategy using QUantitative Evaluation
SFMEA	System Failure Mode and Effects Analysis
SINTEF	Stiftelsen for INdustriell og TEknisk Forskning (Foundation for Scientific and Industrial Research at the Norwegian Institute of Technology)
SQL	Structured Query Language
SRF	Screening and Ranking Framework
SWIFT	Structured What-If Technique
TNO	Nederlandse Organisatie voor Toegepast Natuurwetenschappelijk Onderzoek (Netherlands Organization for Applied Scientific Research)
UDIW	Underground Disposal of Industrial Waste
UDNW	Underground Disposal of Nuclear Waste
US	United States
USDW	Underground Source of Drinking Water
USGS	United States Geological Survey
USNG	Underground Storage of Natural Gas
VEF	Vulnerability Evaluation Framework
WRI	World Resources Institute

1 What Is Risk?

Various equations have been written that define risk, including "risk = uncertainty + damage," "risk = $\frac{\text{hazard}}{\text{safeguards}}$" [1], and " risk = frequency × consequences" [2]. It also was defined as the "effect of uncertainty on objectives" in ISO 31000:2009 [3]. An "effect" is a deviation from the positive and/or negative outcomes expected in the definition, while "objectives" address different aspects, such as health, safety, financial and environmental considerations, and they are applied at different levels, such as strategic, organization-wide, project, product, and process levels. "Uncertainty" is the state of deficiency of information related to the understanding or knowledge of an event (even if the uncertainty is only partial) and its consequence or likelihood. Normally, risk is characterized by reference to potential events and consequences, or a combination of the two, and it is expressed in terms of a combination of the consequences of an event, including changes in the circumstances and the associated likelihood of occurrence [4].

As mentioned above, the risks associated with the geological storage of CO_2 in deep subsurface formations can be understood as a combination of natural and

technology hazards. Thus, the potential causes of possible leaks do not only depend on the operation of technology as is usually the case in industrial plants, and, consequently, the causes are not perfectly known or understood [5].

2 Risks Associated with the Geological Storage of CO_2

A conceptual risk profile for CCS (Carbon dioxide Capture and Storage) projects was depicted by Benson [6] (Fig. 1). The concept is that most of the possible issues associated with storage projects occur during the operational stage, and the risk of the release of CO_2 is expected to decrease when injection stops and the secondary trapping mechanisms take effect. Even so, the concept also shows that the risk will remain greater than zero for a long time.

The potential risks of CO_2 storage in a geological reservoir can be divided into five categories, i.e., CO_2 leakage, CH_4 leakage, seismicity, ground movement, and displacement of brine [7]. Clearly, the hot spot of risk research is CO_2 leakage, because there is a need to guarantee, to the extent possible, that the injected CO_2 stays safely underground. Figure 2 shows the possible leakage pathways of CO_2 from wells, cap rock or seals, and geological faults and fractures.

There are two broad categories of risks potentially associated with the leakage of CO_2 from geological storage reservoirs, i.e., global risks and local risks. The global risks may are related primarily to uncertainties concerning the effectiveness of CO_2 containment. Local risks can be categorized as the health, safety, and environmental risks, and they are associated with three processes, i.e., (1) the elevation of CO_2 concentrations due to the flux of CO_2 through the shallow subsurface to the atmosphere, (2) the chemical effects of dissolved CO_2 in the subsurface, and (3) the effects that arise from the displacement of fluids by the injected CO_2 [10] (Fig. 3).

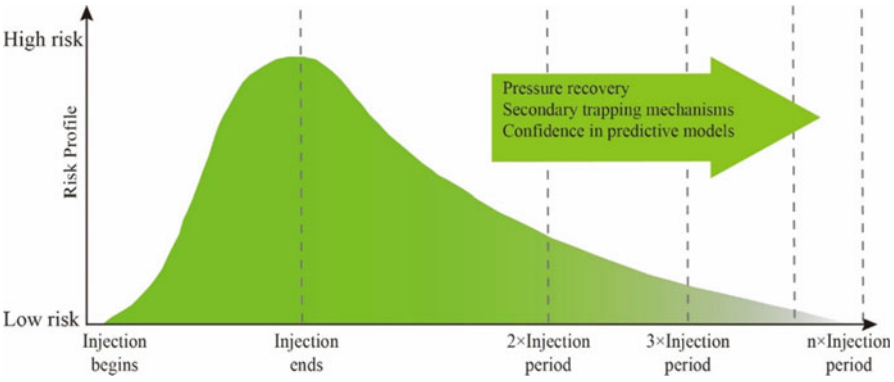

Fig. 1 Conceptual risk profile of CO_2 geological storage (Adapted from Ref. [6])

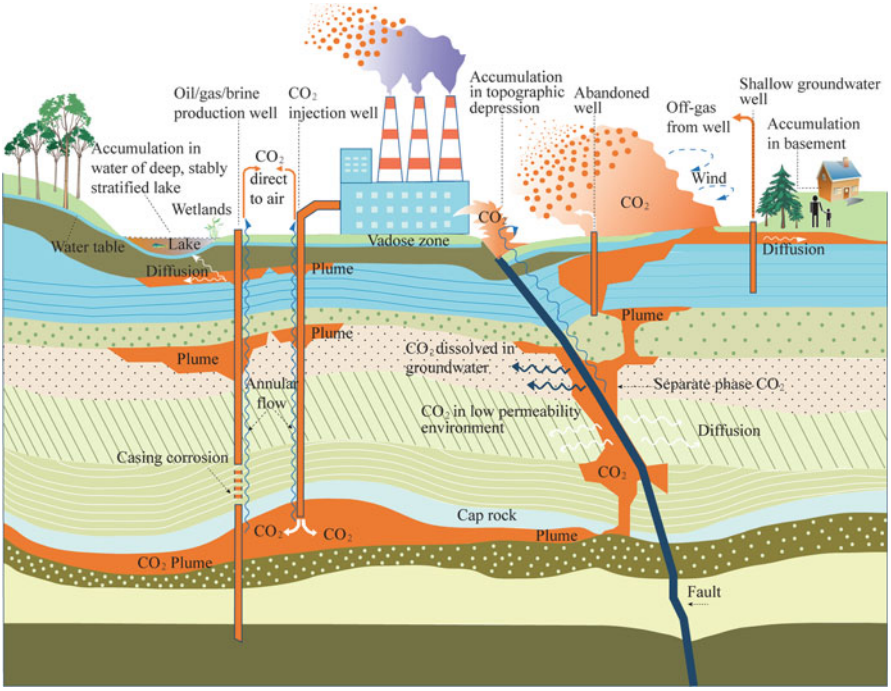

Fig. 2 Possible leakage pathways of sequestered CO_2 (Adapted from Ref. [8, 9])

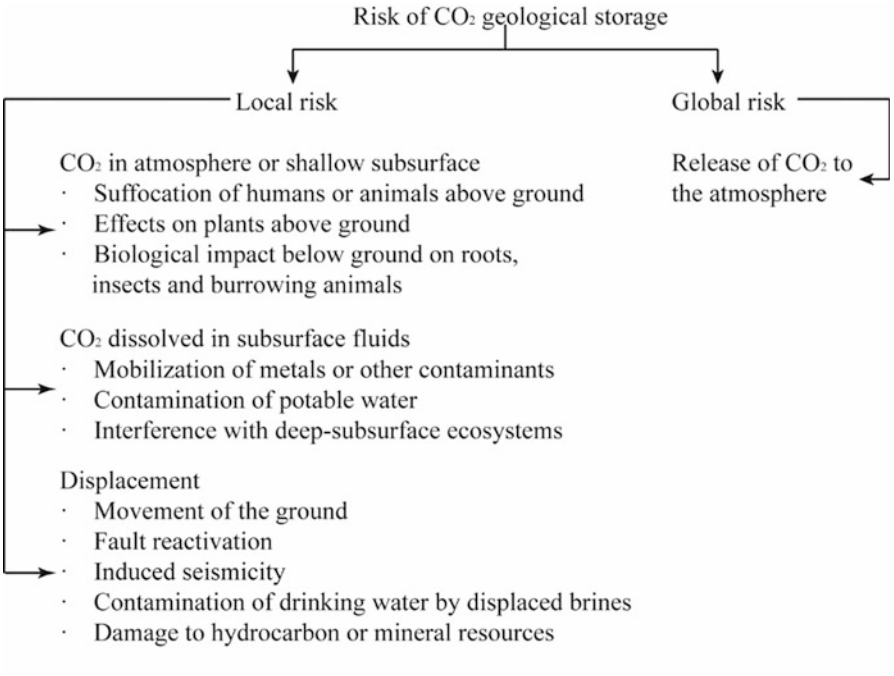

Fig. 3 Taxonomy of risks associated with the geological storage of CO_2 (Adapted from Ref. [10])

3 Regulations for Risk Assessment of the Geological Storage of CO_2

3.1 EU Directive

EU (European Union) directive 2009/31/EC (European Communities) defines the criteria for the characterization and assessment of potential storage complexes and the surrounding areas. Sensitivity characterization and risk assessment must be included in the characterization of the dynamic behavior of a storage complex, and the risk assessment must include hazard characterization, exposure assessment, effects assessment, risk characterization, and other assessments, as deemed appropriate depending on site-specific characteristics [11].

3.2 CSA Z741

The CSA (Canadian Standards Association) Z741 Standard for the Geological Storage of Carbon Dioxide provides guidance on all steps of the risk management process except the actual implementation of risk treatment, i.e., only risk treatment planning, follow-up, and review are addressed. The risk management process described in the Standard is consistent with the risk management process described in ISO 31000 [12].

3.3 WRI Guidelines

In the WRI (World Resources Institute) Guidelines for the capture, transport, and storage of CO_2, the proposed guidelines for assessing the risk associated with the storage of CO_2 are as follows storage risk assessment [13]:

(a) For all storage projects, a risk assessment should be required, along with the development and implementation of a risk management and risk communication plan, for all storage projects. At a minimum, risk assessments should examine the potential for leakage of injected or displaced fluids via wells, faults, fractures, and seismic events and examine the fluids' potential impacts on the integrity of the confining zone and their potential endangerment of human health and the environment.
(b) Risk assessments should address the potential for leakage during the operational phase and during the long-term after the operational phase has ended.
(c) Risk assessments should help identify priority locations and approaches for enhanced MMV (Measurement, Monitoring and Verification) activities.
(d) Risk assessments should provide the basis for mitigation/remediation plans for response to unexpected events; such plans should be developed and submitted to the regulator in support of the proposed MMV plan.

(e) Risk assessments should guide operational decisions, including setting an appropriate injection pressure that will not compromise the integrity of the confining zone.
(f) Periodic updates to the risk assessment should be conducted throughout the project's lifecycle based on updated MMV data and revised models and simulations, as well as knowledge gained from ongoing research and the operation of other storage sites.
(g) Risk assessments should encompass the potential for leakage of injected or displaced fluids via wells, faults, fractures, and seismic events, with a focus on the potential impacts on the integrity of the confining zone and endangerment of human health and the environment.
(h) Risk assessments should include site-specific information, such as the terrain, potential receptors, proximity of USDWs (Underground Sources of Drinking Water), faults, and the potential for unidentified borehole locations within the project's footprint.
(i) Risk assessments should include non-spatial elements or non-geologic factors (such as population, land use, or critical habitat) that should be considered in evaluating a specific site.

3.4 Technical Guidelines of MEP (China) for the Environmental Risk Assessment of CCUS

Exposure draft of technical guidelines for a CCUS environmental risk assessment were developed by the Ministry of Environmental Protection (MEP) of China. In the guidelines, the risk assessment process was based on the ISO 31000, including [14]:

(i) Systematically identify potential sources and critical receptors of environmental risk;
(ii) Determine environmental risk assessment methods, defining impacts and possibilities;
(iii) Assess the impacts and likelihood of environmental risks and estimate the environmental risk level of each source and receptor of risk; and
(iv) Identify the environmental risk management measures that will be taken to reduce the environmental risk to an acceptable level.

The MEP guidelines define surrounding area of a project may be threatened by the injection activity as the assessment space of utilization and storage of CO_2, and the time scale for the risk assessment is divided into the pre-injection, injection, closure, and post-closure periods. A risk matrix is recommended in this guideline, and the risk level is divided into three categories, i.e., low, moderate, and high. The potential levels of impacts on the receptors are divided into five categories, i.e., light, serious, major, severe, and extreme. The possibility of adverse effects divided into five categories, i.e., very likely, likely, medium likelihood, unlikely and very unlikely (Table 1).

Table 1 Regulations of CO_2 Geological Storage (CGS) risk assessment

Organization	Framework	Details
EU	Hazard characterization	The Hazard characterization shall cover the full range of potential operating conditions, and the following shall be included:
	Exposure assessment	(a) potential leakage pathways;
		(b) potential magnitude of leakage events for identified leakage pathways (flux rates);
	Effects assessment	(c) critical parameters that affect potential leakage (for example, maximum pressure in the reservoir, maximum injection rate, temperature, sensitivity to various assumptions in the static geological Earth model(s));
	Risk characterization	(d) secondary effects of storage of CO_2, including displaced formation fluids and new substances created by the storing of CO_2;
		(e) any other factors that could pose a hazard to human health or the environment (for example, physical structures associated with the project).
CSA	Consistent with ISO 31000	The risk identification process shall include the following activities:
	Risk identification	(a) Threats to each of the following project criteria: capacity, injectivity, containment, geomechanical stability, adequate knowledge of the baseline, technical and economic feasibility, operational safety and environmental protection;
	Risk analysis	(b) Risk scenarios for each threat;
	Risk evaluation	(c) Biosphere and economic resources in the geosphere;
		(d) Interdependencies among different risk scenarios.
WRI	Hazard identification	The potential for leakage of injected or displaced fluids via wells, faults, fractures, and seismic events, and the fluids' potential impacts on the integrity of the confining zone and endangerment to human health and the environment.
	Evaluation of impacts on the receptors	
	Risk management	
	Mitigation or remediation planning	
MEP	Based on ISO 31000	Risk source: CO_2 and/or other risk material, supporting equipment on the surface for capture and transport, existing or added wells or other possible ways for leakage to occur.
	Risk identification	
	Risk analysis	
	Risk evaluation	Assessment indicator: characteristics of the geological structure, CO_2 injection parameters, numbers and depths of existing and added wells in the storage area, CO_2 migration, engineering construction, resource extraction activities, mechanical instability.
		Risk Acceptors: environmental media, population, animals and plants, microorganisms.

4 Risk Assessment

4.1 Risk Assessment Framework for the Geological Storage of CO_2

Currently, risk assessments often proceed based on the ISO Standards or a self-developed workflow.

4.1.1 Risk Management Based on ISO Standards

According to ISO 2009:31000, risk assessment is an integral part of risk management, and it is the overall process of risk identification, risk analysis, and risk evaluation [4]. In this definition, risk identification is the process of identifying, recognizing, and describing risks, involving the identification of risk sources, events, their causes, and their potential consequences. Risk analysis, including risk estimation, is a process designed to comprehend the nature of risk and to determine the level of risk, which provide the basis for risk evaluation and decisions about risk treatment. Risk evaluation is process of comparing the results of risk analysis with criteria to determine whether the risk and its magnitude are acceptable or tolerable [4] (Fig. 4).

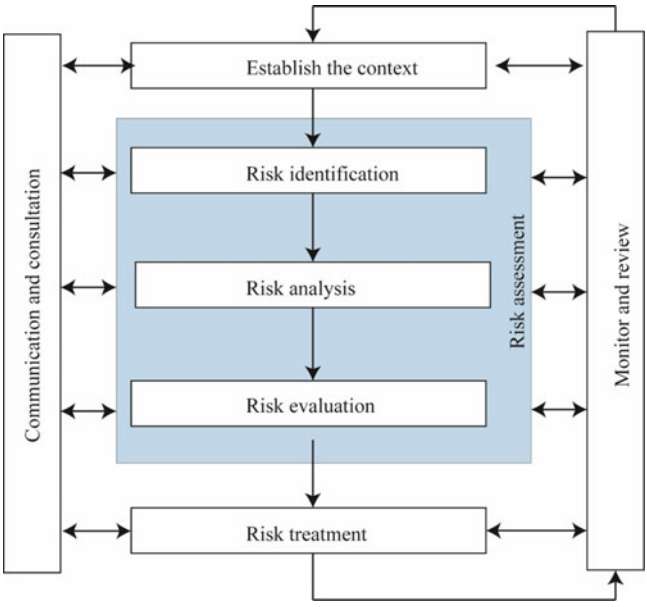

Fig. 4 Risk management process from ISO 31000:2009 [3]

Risk Assessment of the MUSTANG Project

This risk management process adapted and applied by OXAND[1] for the MUSTANG (MUltiple Space and Time scale Approach for the quaNtification of deep saline formations for CO_2 storaGe) project with (1) risk management policy added at the beginning of the process and (2) risk profile and action added between the risk evaluation and risk treatment process. The risk assessment of the MUSTANG project contains all eight of the processes in Fig. 5. In the assessment, the consequence grid describes the different severity levels that were identified and adapted for each project objective. And the systematic approach FMEA (Failure Mode and Effects Analysis) was proposed for risk identification, and, then, the "bow-tie" diagram was created to define the risks, their causes, and their consequences in the project. In the MUSTANG project, numerical model development and modeling were done, and the modeling results were used to assess the severity levels of the identified risks in the risk estimation process [15].

Integrated Risk Assessment for CCS

Risk assessment of ISO 31000 also was applied to the integrated risk assessment for the CCS system, including the capture, transport, and storage sections [16]. An overview of the aspects should be addressed when establishing the context for a risk assessment, i.e., stakeholders, CCS system, time scales, risk aspects, and metrics. Then, three qualitative tools, i.e., (1) brainstorming, (2) risk register, and (3) bow tie diagram, and one quantitative tool, i.e., Bayesian Belief Networks [91], were suggested for the risk assessment.

4.1.2 Risk Management Workflow

The IEA Greenhouse Gas R&D Programme (IEA GHG) [17] developed a risk management workflow diagram for the deployment of a commercial-scale storage program [18, 19]. Figure 6 shows that risk assessment begins with risk source assessment and proceeds through exposure assessment, effects assessment, and risk characterization.

4.1.3 Integrated Carbon Risk Assessment (ICARAS)

ICARAS is a comprehensive and transparent risk assessment methodology developed by IFPEN (IFP Energies nouvelles), SINTEF (the Foundation for Scientific

[1] An international engineering and consulting firm based in France. It specializes in the risk-based management of industrial infrastructure.

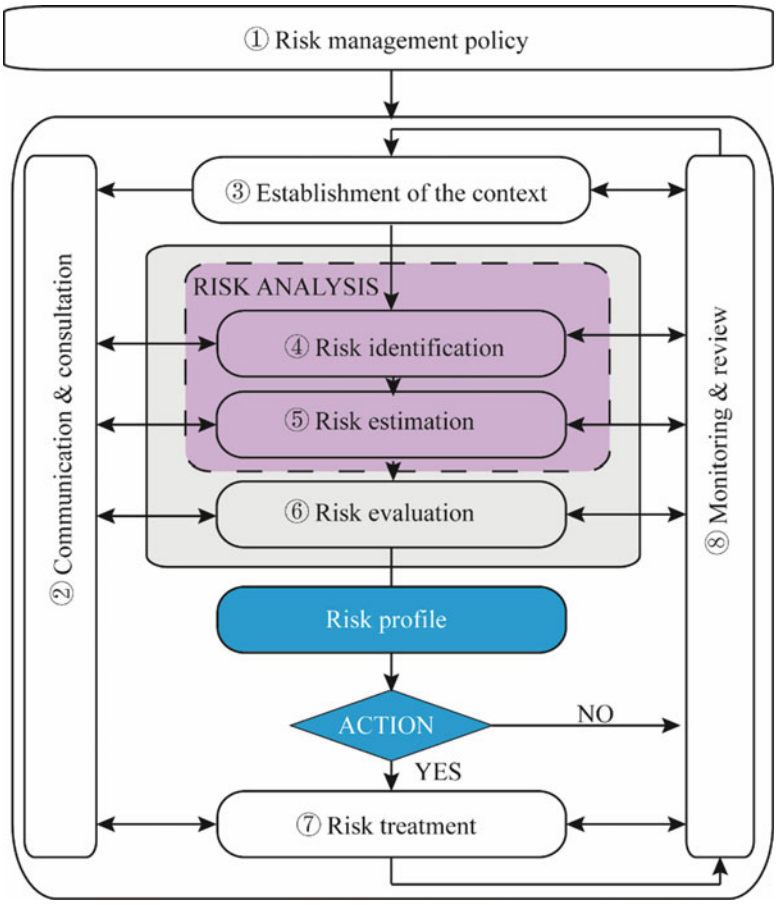

Fig. 5 The risk management process according to ISO/FDIS 31000 [15]

and Industrial Research at the Norwegian Institute of Technology), and TNO (the Netherlands Organization for Applied Scientific Research) [20]. It provides an Integrated CArbon Risk ASsessment (ICARAS) workflow for CO_2 geological storage (Fig. 7). Figure 8 shows the four modules that are included in the workflow, and the approaches used in the four modules are provided below.

Scenario Definition: Carbon Storage Scenario Identification Framework (CASSIF) based on FEP.

Scenario Analysis: Modeling of the reservoir is based on two complementary approaches, i.e., the use of COSE (a simplified tool) to simulating CO_2 storage

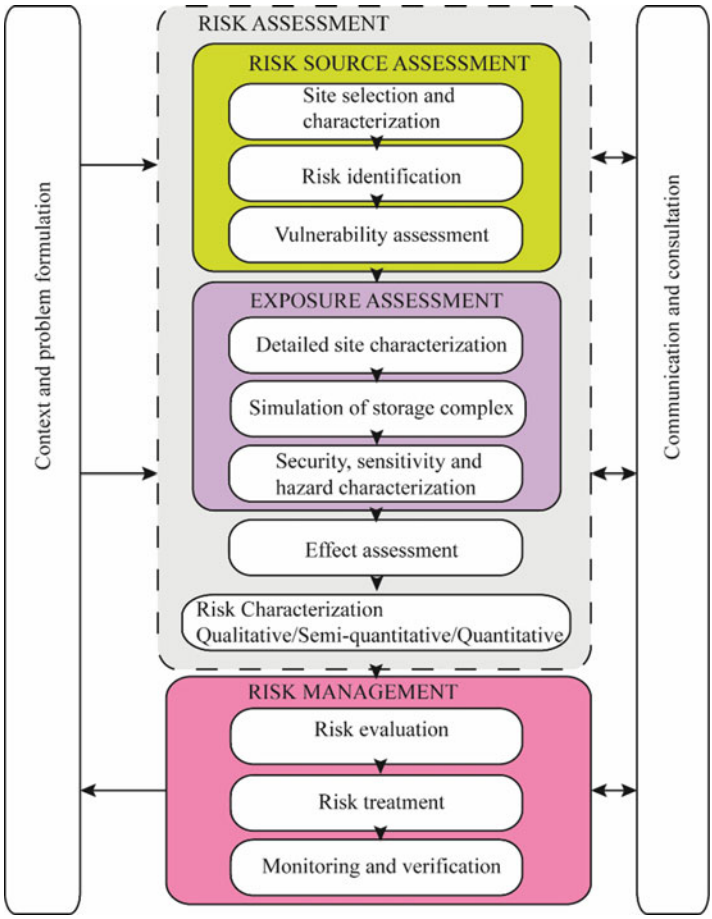

Fig. 6 Diagram of risk management workflow for a commercial-scale storage deployment program (Adapted from Ref. [17])

and possible leakage on different synthetic scenarios and simplification of detailed reservoir simulation models. PFRAC (a simple analytical tool) based on the Mohr-Coulomb criterion was developed in the ICARAS project for geomechanical modeling that, given an initial stress state, provided the fracturing limit pressure. SEMI (SINTEF's in-house basin modelling software) was extended to include specific CO_2 behaviors in the migration model. And a combination is being developed that consists of a statistical risk ranking tool for wells and a specified assessment of the actual performance of the wellbore materials. This combination will allow the determination of the risks related to the wells in the storage complex within ICARAS.

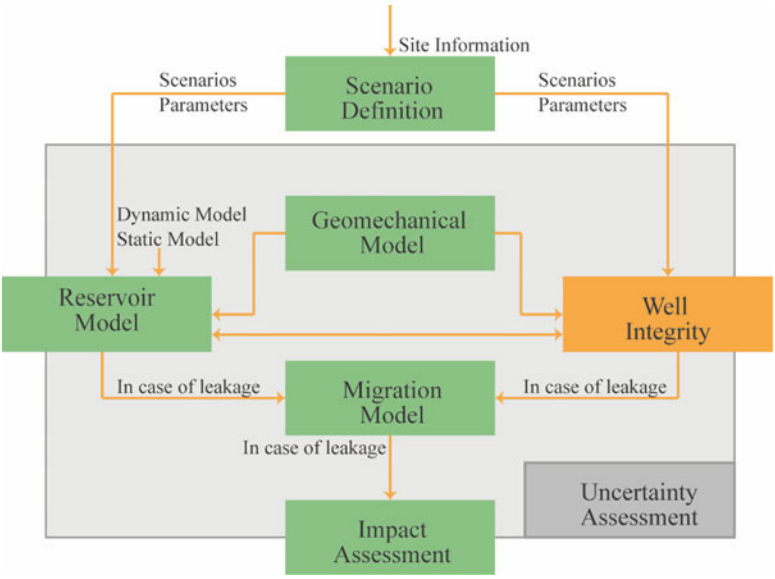

Fig. 7 Integrated Carbon Risk Assessment (ICARAS) workflow [20]

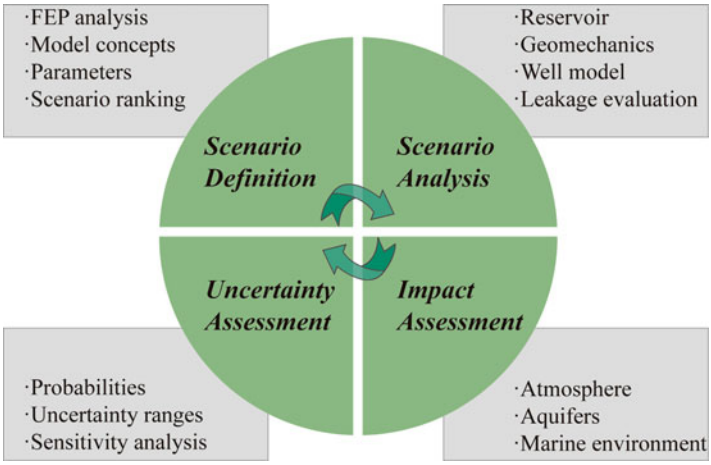

Fig. 8 Integrated Carbon Risk Assessment (ICARAS) modules [20]

Uncertainty Assessment: The commercial software, Cougar™, was used in modeling.

Impact Assessment: Two commercial software packages both from TNO were used, i.e., EFFECTS and RISKCURVES.

4.1.4 Risk Management Workflow – Schlumberger Carbon Services

The risk management workflow was initiated by Schlumberger Carbon Services to evaluate and manage project risk in the Illinois Basin – Decatur Project (IBDP) [21, 22]. The features of IBDP's initial risk–assessment process are (1) project status at the time of the risk assessment workshop, (2) time constraints, (3) composition of the expert panel, (4) information available, (5) entities evaluated, (6) at-risk entities, (7) evaluation criteria, (8) L (Likelihood of the negative impact) and S (Severity of the negative impact) scales, (9) elicitation format, and (10) collected data. The "risk entities" that were evaluated first were the features, events, and processes (FEPs) based on the list published by Quintessa Limited (www.quintessa.org). Risk was defined as the product of the likelihood of negative impact multiplied by its severity, i.e., $L \times S$. Five values of the project were evaluated in the assessment, i.e., Health and Safety, Finance, Environment, Research, and Industrial Viability (Fig. 9). Consensus results were displayed on risk matrices for each of six working groups, i.e., Air-Atmosphere, Surface-Near Surface, CO_2 Delivery, Subsurface, Community, and Ownership-Environment groups, during the process of risk assessment.

4.1.5 Containment Risk Management – Shell

Two techniques were used to assess the suitability and containment risks of the Goldeneye candidate CO_2 storage site. One was the methodology based on Evidence Support Logic, as implemented in TESLA software, and it was used to assess the suitability of the site, while the specific containment risk was assessed using the Bow-tie risk assessment methodology, which is an integral part of the process that was used to demonstrate that the risks were As Low As Reasonably Practicable (ALARP) [23].

4.2 Risk Identification

For the most part, risk identification is qualitative. Risk sources, events, their causes, and their potential consequences are identified according to expert judgment based on practical experience or according to a reference framework, e.g., FEP (Fig. 10).

4.2.1 Identification of Risk by Expert Judgment Based on Practical Experience

The practical experience discussed here includes three categories, i.e., analogues, existing CCS projects, and regulatory experience.

Industrial and natural analogues, such as enhanced oil recovery with CO_2 (EOR) [24], acid gas injection (AGI) [25], underground disposal of industrial waste (UDIW), underground disposal of nuclear waste (UDNW), underground storage

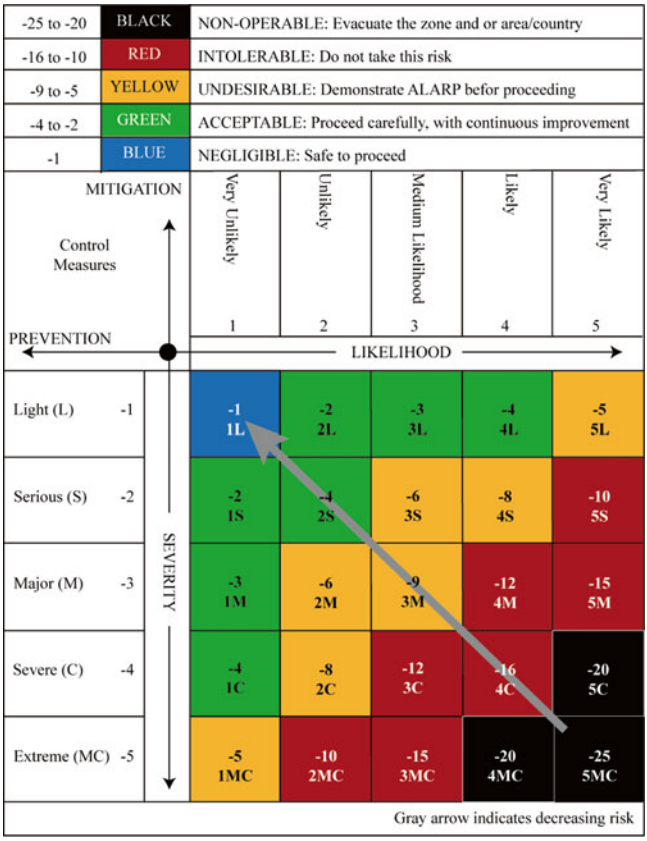

Fig. 9 Risk matrix used by Schlumberger [21, 92]

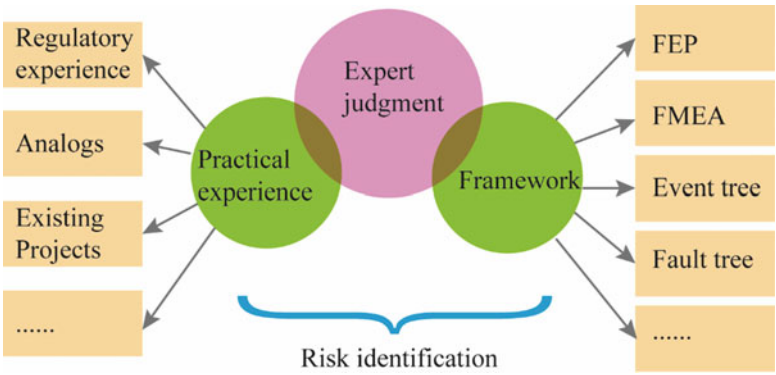

Fig. 10 Identification process of risk

of natural gas (USNG), and natural CO_2 reservoirs (NCRs) were compared to underground storage of CO_2 to understand the risk of the CGS [7, 26–29].

In 2015, there are approximately 55 large-scale CCS projects in different phases of development all over the world, and 13 of them are in operation. These existing projects provide valuable information for understanding and assessing the risks associated with CGS, such as those in In Salah, Algeria [30, 31]; Sleipner, Norway [32]; and Snøhvit, Norway [33].

With the research, development, and demonstration (RD&D) of CCS, WRI, EU, US EPA, Canada, and others have promulgated regulations for CGS risk assessment that provide references for risk identification, as shown in sect. 3.

4.2.2 Framework for the Identification of Risk

Existing frameworks, such as FEP, FMEA, and Event tree, have been used to identify the risks associated with CGS.

FEPs

Features, Events, and Processes (FEPs) were developed in the nuclear waste area, and they have been proposed for application to CGS. *Processes* influence the evolution of the system, while *events* can be viewed as *processes* that take place on comparatively short timescales [34]. Thus, the scenarios of CGS risk can be identified according to analyses of the features, events, and processes of the system.

A generic database of FEPs for CGS has been developed with the chosen FEPs being included based on their relevance to the long-term safety and performance of the storage system after the injection of carbon dioxide has been completed, and the injection boreholes have been sealed [35]. The database provides a centralized source of information on the relevant technical and scientific considerations that relate to the long-term geological storage of carbon dioxide, and it can be used as part of the systematic assessments of safety and performance.

Databases of FEPs provide a tool to support the assessment of long-term safety and performance of CGS. There are eight categories of FEPs, i.e., assessment basis, external factors, CO_2 storage, CO_2 properties, geosphere, boreholes, near-surface environment, and impacts. There are two main approaches to the analysis of FEPs, and they have been described as ‘top-down’ and ‘bottom-up’ approaches.

RITE-DB

The RITE-DB was improved by adding new FEPs concerning Japan to Quintessa’s database of FEPs and some tools to manipulate FEPs. Two types of hypothetical site conditions were defined and used for the scenario analysis, i.e., one in which

Table 2 Characteristics of the three FEPs database

Database	Developer	Description	Components	Application	References
CO_2 FEP database	Quintessa	On-line tools to support the assessment of long-term safety and performance of CGS	Descriptions of FEPs	Weyburn/ Williston Basin/In Salah	[35]
			Explanations of their relevance		
			Bibliographies		
			Links to external web sites		
CASSIF	TNO	Define CO_2 release scenarios based on the three major scenarios: well, fault and seal	FEPQuest	NA	[37]
			FEPMan: Seal/Well/ Fault		
			FEPChain		
			FEPMon		
RITE-DB	RITE	Based on Quintessa's database, and providing a Japanese context	NA	Hypothetical site: structural CO_2 trap hydrodynamic trap	[36]

there is a structural CO_2 trap (termed the 'structural site') and one in which there is a hydrodynamic trap (termed the 'non-structural site') [36].

Storage

CASSIF - Carbon Storage Scenario Scenario Identification Framework: Second-generation analysis tool for CO_2 FEPs was developed by TNO and named CASSIF. It is a framework of an SQL database combined with a web interface and workshop visualization software [37] (Table 2).

Fault Trees

The French National Institute for Industrial Environment and Risks (INERIS) designed fault trees as a practical method to identify the relevant risk scenarios and took an application to the different life stages of deep aquifer storage, combining long-term and short-term issues. The possible high content of impurities, and therefore the different exposure routes for people and the soil/water environment, were taken into account [38].

FMEA (Failure Mode and Effects Analysis)

FMEA was one of the first systematic techniques used for failure analysis. It was developed by reliability engineers in the 1950s to study problems that might arise from the malfunctions of military systems. A few different types of FMEA analyses exist, such as Design FMEA (DFMEA), Process FMEA (PFMEA), Equipment FMEA (EFMEA), and System FMEA (SFMEA) [15, 39].

4.3 Risk Analysis and Evaluation

The risk analysis and evaluation methodologies for CGS are classified into three types, i.e., qualitative and quantitative methodologies and combinations of the two. Qualitative risk assessment does not provide concrete or numerical results, such as VEF. Quantitative methods are used in the well-known systems in which the level of uncertainty is relatively low, such as CF and P&R [40].

4.3.1 Qualitative Risk Assessment

VEF (Vulnerability Evaluation Framework)

The VEF is a qualitative method that EPA has used to assess the risks associated with geological storage systems. The system is characterized in terms of the CO_2 stream that is injected, the confining system, the injection zone, and a series of geological attributes that could influence the vulnerability of the system to unanticipated migration [41], leakage, and undesirable changes in pressure. A binary classification of low and elevated vulnerability was defined qualitatively for the VEF [42] (Fig. 11).

The Structured What-If Technique (SWIFT)

SWIFT involves the use of expert panels. It is a form of Delphi risk analysis used by DNV (Det Nopske Veritas) for the qualitative identification of hazards. DNV undertook a risk analysis assessment of a system combining SWIFT and QRA for the capture, transport, and storage of CO_2 [43]. It consists of a series of questions, e.g. "what ifs. . .?" or "How could. . .?" to identify situations, issues, or threats that had the potential to cause harm. SWIFT produced good, focused results that stimulated in-depth discussion and brought diverse parties to a common understanding [44].

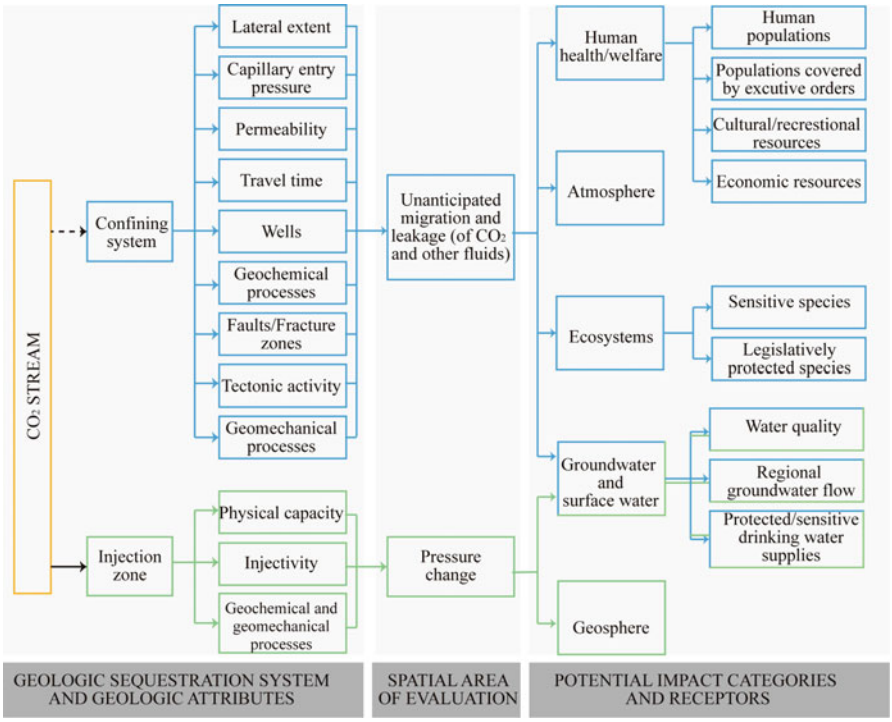

Fig. 11 Depiction of the conceptual approach to the Vulnerability Evaluation Framework (VEF) (Adapted from Ref. [42])

The Evidence Support Logic (ESL)

ESL involves systematically breaking down the question or hypothesis under consideration into a logical hypothesis model, the elements of which identify the basic judgments and opinions that relate to the quality of the evidence associated with a particular interpretation or proposition. It also establishes the level of confidence that one can place in the relevant judgments [45]. During the CO_2ReMoVe project, a software tool named TESLA was developed based on ESL [46]. It also was combined with another method for assessing performance [47, 48]. The suitability of a storage site was assessed using TESLA by Shell [23].

Bow-Tie Diagram

A bow-tie diagram is built by a step-by-step process to produce a qualitative risk assessment of the hazard being considered in this method. It provides a readily understandable representation of the relationships between the causes of unwanted events, the escalation of such events to a range of possible outcomes, the controls

required to prevent the event from occurring, and the mitigation measures that exist to limit the consequences. The diagram method was used by Shell to manage containment risk in a depleted gas field [23], by BRGM, France to build GERICO database for managing the risk of geological storage [49], and by OXAND to identify the risks associated with the MUSTANG project [15].

Screening and Ranking Framework (SRF)

SRF was developed to evaluate potential sites for the geological storage of CO_2 on the basis of health, safety, and environmental (HSE) risks that might occur as the result of CO_2 leakage [50]. SRF is a three-grade ranking system. The highest level grade is based on the assumption that the risk of CO_2 leakage depends on three basic characteristics of a potential geological storage site for CO_2, i.e., the potential the target formation has for long-term containment of CO_2, the potential for secondary containment if the primary site were to leak, and the potential the site has to attenuate and/or disperse leaking CO_2 if the primary formation leaks and the secondary containment fails. The three basic characteristics above form the main grade indicators, i.e., potential for primary containment, potential for secondary containment, and attenuation potential. A SRF spreadsheet was designed to provide a qualitative and independent assessment. Some examples were used, including the Rio Vista gas field, the Ventura oil field, and the Mammoth Mountain oil field, all of which are in the state of California in the U.S. [50].

The SRF also was used in the Shenhua CCS pilot project in China with a few modifications [51]. Large quantities of data are required by the SRF, and primary and secondary containments are difficult to define for some special sites, such as the Ordos basin in China, because it has with multi-layers of thin formations [52, 53].

4.3.2 Quantitative Risk Assessment

Risk Interference Subsurface CO_2 Storage (RISCS)

RISCS is the model of a methodology for assessing the impact of the risk of basin-scale leakage and the resulting impacts on stakeholders [54]. This model combines several aspects of risk, including (1) probabilistic magnitudes of CO_2 and brine leakage and their spatial extents based on simulations of geophysical fluid flow, (2) three-dimensional geospatial data, and (3) estimates of potential costs triggered by leakage. For (1), Bielicki et al. [54] used the Estimating Leakage Semi-Analytically (ELSA) model; for (2), they compiled data that were acquired from the United States Geological Survey (USGS) and the Michigan Department of Environmental Quality; for (3), they used the Leakage Impact Valuation (LIV) method to estimate the financial consequences of leakage [54]. This methodology was applied to two injection locations in the Michigan sedimentary basin (USA).

Analytical Hierarchy Process (AHP)

AHP and Fault Tree Analysis (FTA) methods have been proposed for use in quantifying the risks associated with CCS projects [55]. AHP is a mathematical method that is used in many fields [56, 57]. The process consists of five steps, i.e., (1) defining the objective; (2) structuring the elements into criteria, sub-criteria, and alternatives; (3) making a pair-wise comparison of the elements in each group and then calculating the weighting and the consistency ratio; (4) evaluating the alternatives using the weightings; and (5) obtaining the ranking.

Certification Framework (CF)

The CF was developed for use in certifying the safety and effectiveness of geological carbon storage sites [58]. Simplicity was achieved in the CF by using several different assumptions and aspects related to the sites, i.e., (1) wells and faults as the potential leakage pathways, (2) compartments to represent environmental resources that may be impacted by leakage, (3) CO_2 fluxes and concentrations in the compartments as proxies for impact to vulnerable entities, (4) broad ranges of storage formation properties to generate a catalog of simulated plume movements, and (5) probabilities of intersection of the CO_2 plume with the conduits and compartments. In the CF, impacts can occur to the various compartments, such as Hydrocarbon and Mineral Resources (HMRs), Health and Safety, Underground Source of Drinking Water (USDW), Near-Surface Environment (NSE), and Emission Credits and Atmosphere (ECA) [58]. The CF was used in a dynamic context for the assessment of the risk of leakage in the In Salah CO_2 storage facility in Algeria [30].

Performance and Risk (P&R)

P&R is a risk-based methodology that was developed by OXAND and Schlumberger and is used to evaluate the performance and risks associated with the integrity of wells. In the P&R methodology, a risk is estimated (1) as a failure event represented by specific well integrity conditions to which a probability of occurrence is proposed and (2) the magnitude of the impact of a leakage is assessed with respect to all of the stakeholders involved in the project. The main steps of P&R are (1) data collection and functional analysis; (2) the development and use of static and dynamic models; (3) defining scenarios and modeling with SIMEO™--Stor; (4) the quantification of risks; and (5) the implementation of actions to treat and/or mitigate risks [59, 60].

CO_2-PENS (Predicting Engineered Natural Systems)

CO_2-PENS is a system-level model that can be used to predict the overall performance of sequestration systems. It was developed at Los Alamos National Laboratory (U.S.) using the commercially-available GoldSim system [18, 61, 62]. CO_2-PENS describes the entire CO_2 sequestration pathway, starting from the capture of the CO_2 at a power plant, and following it through pipelines to the injection site and into the reservoir. The capabilities of this method include CO_2 capture and transport calculations, reservoir injectivity and capacity calculations, wellbore, fault and cap rock leakage estimates, shallow groundwater impacts, leakage to the atmosphere, screening mode, site selection mode, and economic impacts [63]. It has been used for CO_2 sequestration studies, performance assessment, CO_2 sequestration at the Rock Spring Uplift in Wyoming (U.S.), and others [62].

GERAS-CO_2GS

GERAS-CO_2GS (Geo-Environmental Risk Assessment System - CO_2 Geological Storage) is risk assessment tool that is being developed to analyze risks related to the migration of injected CO_2 and to assist safety and risk management by National Institute of Advanced Industrial Science and Technology (AIST), Japan. GERAS-CO_2GS contains four major routines with specific functions, i.e., (1) calculating CO_2 retention and leakage; (2) defining and editing of risk data; (3) Processing the dispersion of CO_2 on the surface; and (4) evaluating risk [64].

4.3.3 Combined Analysis

RISQUE (Risk Identification and Strategy Using Quantitative Evaluation)

RISQUE is the research module of the GEODISC program. The method is consistent with the Australian Risk Management Standard. It is a systematic, quantitative process based on the judgment of a panel of experts. The approach relies on quantitative techniques to characterize risks in terms of both the likelihood of the occurrence of identified risk events and their consequences, with examples of the former being the escape of CO_2 and inadequate injectivity into the storage site and examples of the latter being environmental damage and the loss of life. Three Key Performance Indicators (KPIs) were developed to address the risk assessment aims, i.e., the performance of the reservoir, greenhouse benefits, and community impacts. The RISQUE research module consists of five stages, i.e., (1) establishing the context, (2) identifying the risk, (3) analyzing the risk, (4) developing a strategy for managing the risk, and (5) implementing the risk management strategy. Monte Carlo simulation was used for the risk analysis [65].

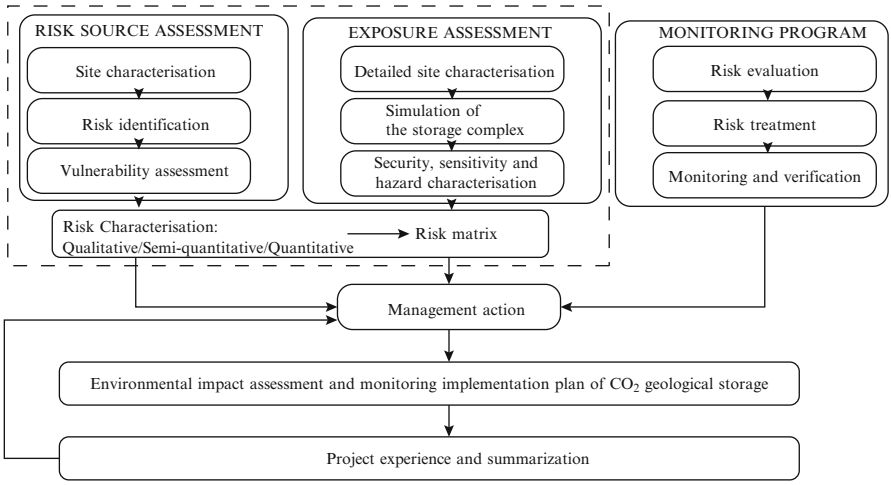

Fig. 12 Workflow of the CO2RISKEYE (Adapted from Ref. [67, 68])

MOSAR (Organized and Systemic Method of Risk Analysis)

MOSAR is a method that can be used to analyze the technical risks and to identify the means by which the risks can be prevented or neutralized. It consists of two steps, i.e., step A, which allows the analysis of major risks, and step B, in which a detailed analysis of the implementation of the project is prepared, including the specific implementation of safety tools relating to the possible technical dysfunction of machines and devices [66].

CO2RISKEYE

CO2RISKEYE is an assessment prototype for environmental risk assessment of CO_2 geological storage that is being developed by Li, IRSM-CAS, China (Fig. 12) [67, 68]. It combines different assessment methods for different purposes, including a modified version of Oldenburg's SRF [50], Bachu's site-screening method [69], a fuzzy AHP method [56], and others. It can be tailored for different stages of CO_2 geological storage, also can integrate monitoring data and functional analysis. The core simulator of CO2RISKEYE is AEEA coupler [70], an in-house program developed at IRSM-CAS under the financial support of national research foundation and industrial funding by linking two commercial software packages, Simulia ABAQUS and Schlumberger ECLIPSE, both of which are widely used and highly recognized in their respective fields.

4.4 Summary of the Risk Assessment Methods

A summary of the risk assessment methods, including the organization or researcher who developed them, the assessment methods used, and the associated tools and properties is provided below (Table 3).

4.5 Cases of Application of the Risk Assessment Methods

The risk assessment methods have been used in different projects and at different sites, such as Weyburn, In Salah, Gorgon, Latrobe Valley, and Otway. More than one method usually was used to a project, as was the case at Weyburn and In Salah (see Table 4).

4.5.1 Weyburn, Canada

The long-term behavior of the CO_2 and its leakage risks at Weyburn were assessed within a methodological framework based on the FEPs [71]. Quintessa's on-line Generic CO_2 FEP Database was developed initially through international collaboration under the Weyburn project via a series of expert workshops [72]. Several simulations were performed for the long-term assessment, such as the modeling of CO_2 migration through the geosphere, CO_2 leakage through abandoned wells, and potential environmental impacts from CO_2 leakage to the biosphere [73]. Based on the data from the Williston basin, a typical simulation of a hypothetical sequestration system in the Weyburn oilfield in Saskatchewan, Canada was conducted by CQUESTRA, a risk and performance assessment semi-analytical code for CGS [74].

4.5.2 In Salah, Algeria

Several methods were used at the In Salah project [75], i.e., (1) systematic FEP and scenario analysis to provide a framework for assessing long-term performance [31]; (2) the RISQUE QRA process developed for CO2CRC [65]; (3) the Certification Framework in a dynamic context [30]; (4) the Quantitative Risk Through Time Analysis (QRTT), an approach developed by British Petroleum (BP), and (5) CO_2TESLA based on ESL for integrating and communicating performance-relevant information [4].

Some methodologies and some results of risk assessments of CO_2 storage projects have been summarized according to descriptions of failure scenarios, the receiving environmental compartment, and results and indicators [33].

Table 3 Summary of risk assessment methods

Organization/ Researcher	Assessment method	Toolbox		Category[a]
		Name	Release[b]	
Quintessa	FEP (Feature, Event, and Process)	Quintessa FEP database	O	P
Quintessa	PA (Performance Assessment)	TESLA, QPAC-CO_2, Quintessa FEP database	O	S
Quintessa	ESL (Evidence Support Logic)	NA	NA	S
TNO	TNO risk assessment method	SIMED II	I	Q
TNO	CASSIF (Carbon Storage Scenario Identification Framework)	FEP database based on SQL, VUE for FEP interactive visualization	I	P
TNO	ICARAS (Integrated Carbon Risk Assessment)	CASSIF, COSE, PFRAC, SEMI, Cougar™, EFFECTS, RISKCURVES	I/O	S
RITE	FEP	RITE-DB	I	P
URS	RISQUE (Risk Identification and Strategy using Quantitative Evaluation)	MS Excel	I	S
AIST	Quantitative assessment based on prior probability	GERAS-CO_2GS	I	Q
LANL	CO_2-PENS	Developed based on Goldsim, FEHM	I	Q
LANL	IAM (Integrated Assessment Modelling)	NA	NA	Q
DNV	CO_2 QUALSTORE Directive	NA	NA	S
DNV	SWIFT (Structured What-If Technique)	NA	NA	P
Schlumberger Carbon Services	Carbon Workflow (Based on FEP)	NA	NA	S
OXAND	P&R (Performance & Risk Methodology)	SIMEO™-STOR	I	Q
U.S. EPA	VEF (Vulnerability Evaluation Framework)	NA	NA	P
BRGM	Bow-tie diagrams	GERICO database	I	P
Shell	ESL (Evidence Support Logic), Bow-tie diagrams, ALARP (As Low As Reasonably Practicable)	TESLA	O	P
INERIS	FT (Fault Trees)	BowTie	O	P
C.M. Oldenburg	CF (Certification Framework)	TOUGH2, CMG-GEM	O	Q

(continued)

Table 3 (continued)

Organization/ Researcher	Assessment method	Toolbox		Category[a]
		Name	Release[b]	
C.M. Oldenburg	SRF (Screening and Ranking Framework)	MS Excel		P
Ecofys	DPSIR (Drivers, Pressures, State, Impact, and Responses) framework	NA	NA	P
J.M. Bielicki	RISCS (Risk Interference Subsurface CO_2 Storage)	NA	NA	Q
B. Oraee-Mirzamani	FTA & AHP (Fault Tree Analysis & Analytical Hierarchy Process)	NA	NA	P
A. Cherkaoui	MOSAR (Method Organized for a Systematic Analysis of Risk)	NA	NA	S
Q. Li	Prototype for environmental risk assessment of CO_2 geological storage	CO2RISKEYE	I	S

[a]P: Qualitative method; Q: Quantitative method; S: Combined method.
[b]O: Open code or program; I: In-house code or program; NA: Not available.

Table 4 Application of risk assessment methods at some typical projects or sites

Project/Site	Method
Weyburn	FEPs (Quintessa's online generic CO_2 FEP Database), RISQUE, Probabilistic scenario (CQUESTRA), Reservoir model (ECLIPSE E-300),
In Salah	FEPs (Quintessa's online generic CO_2 FEP Database), RISQUE, CF, QRTT, CO_2TESLA based on ESL
Otway	RISQUE
Schweinrich	FEP, Simulation discrete scenarios with stochastically varied parameters in reservoir model (SIMED-II)
Gorgon	RISQUE
Shenhua CCS	SRF, Modified SRF, AHP, Bachu's site selection method

5 Risk Management Measures

5.1 Monitoring

Monitoring is an important part of the overall risk management for CGS. When the injection starts, the risks associated with CGS increase until the injection stops, after which the risk decreases. Sequestered CO_2 must be monitored to verify that there is no leakage and to provide confidence in the predictions of its long-term behavior in the future. First, baseline monitoring must be conducted to provide background values. The baseline monitoring must include the atmosphere, soil

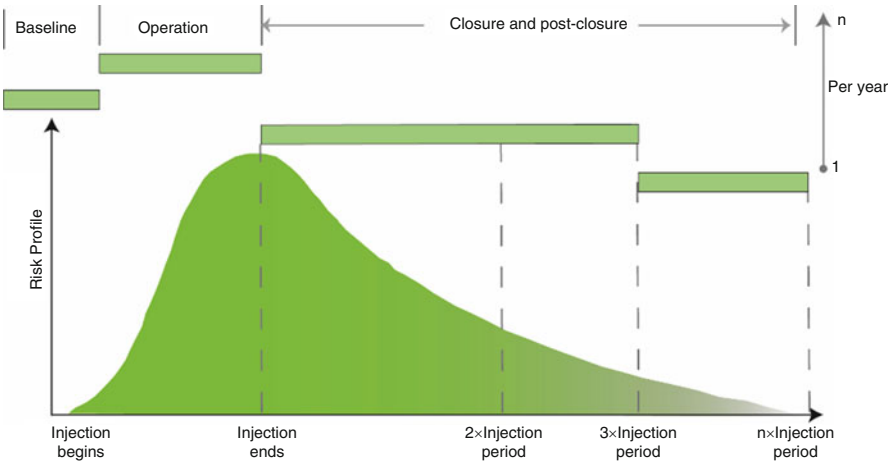

Fig. 13 Monitoring frequency in the life cycle of CO_2 geological storage [79]

gases, water (surface water, shallow groundwater, and reservoir water), the migration of fluids, the vegetation ecosystem, and others [76–78]. The frequency of routine monitoring must increase when the injection starts due to the increased risk. After the injection is stopped, other trapping mechanisms begin to work, and the risk will decrease, so the frequency of monitoring can be reduced (Fig. 13).

Various monitoring technologies are chosen depending on the corresponding risk, and they have been used in different projects (Table 5).

5.2 Emergency Response

In accordance with the requirements of the risk analysis, an emergency response plan should be developed to stop the unexpected movement of carbon dioxide. If such movement or any other emergency events occur, the response plan describes the actions that those in charge must be prepared to take.

The IEA Greenhouse Gas R&D Programme (IEA GHG) [82] conducted research concerning the planning of emergency procedures that should be developed and ready for use at CCS projects. IEA GHG indicated that emergency planning is affected by uncertainties in the consequence modeling for CO_2 and recommended that a "live" model should be available to the emergency coordinator so that the dispersion pattern can be predicted on the day the event occurs. A best-practice emergency response plan for CO_2 should be developed, and the following contents are recommended:

1. Information about where members of the public should go in an emergency;
2. The potential impairment of people's responses in an atmosphere with a high concentration CO_2 because of its asphyxiant and physiological properties;

Table 5 Monitoring technologies and corresponding risk for some CGS projects [76, 80, 81]

Monitoring technology	Risk	Application
3D Seismic	Plume migration;	In Salah/Gorgon/Sleipner/ Snøhvit/Weyburn
	Underground characteristics	
VSP Seismic	Plume migration;	In Salah/CO_2SINK/Gorgon/ RECOPOL/Weyburn
	Underground characteristics	
Gravity survey	Plume migration;	In Salah/Sleipner
	Underground characteristics	
Microseismic	Cap rock integrity	In Salah/Weyburn
InSAR monitoring	Plume migration	In Salah/Weyburn
	Cap rock integrity	
	Pressure development	
Tiltmeters/GPS	Plume migration	In Salah
	Cap rock integrity	
	Pressure development	
Shallow aquifer wells	Cap rock integrity	In Salah/CO_2SINK
	Potable aquifer contamination	
Wellhead/Annulus samples	Wellbore integrity	In Salah
	Plume migration	
Tracers	Plume migration	In Salah/CO_2SINK/ RECOPOL/Weyburn
Surface Flux/Soil Gas	Surface seepage	In Salah/Gorgon/CO_2SINK/ RECOPOL/Weyburn
Microbiology	Surface seepage	In Salah
CO_2 injection rate and pressure (wellhead and bottom-hole)	Wellbore integrity	In Salah/Gorgon/CO_2SINK/ RECOPOL/Weyburn
Pressure of monitoring wells and pressure manage wells (wellhead and bottom-hole)	Wellbore integrity	In Salah/Gorgon/CO_2SINK/ RECOPOL/Weyburn
Wireline	Wellbore integrity	In Salah/Gorgon/RECOPOL/ Weyburn
Logging	Subsurface characterization	

3. The possibility of providing indicators/monitors for CO_2;
4. Drastic reductions in visibility in the case of larger releases, and such releases also will cause significant local cooling that could impact all equipment and components of the system. Consideration should be given to the survivability of the equipment and components and whether their failure could lead to escalation of the dangers involved. Equipment required for use in an emergency response must be designed and/or protected so that they will operate under such conditions.

Finally, IEA GHG proposes that any incidents that require an emergency response should be monitored and recorded in order to learn from experience [82].

The MEP guideline requires that the emergency measures should include, but not be limited to, the following. The main measures are: (1) establish a restricted construction area to prevent risk; (2) have functional alert monitors in place; (3) develop an emergency plan, including approaches for reducing the risk level and the corresponding response procedures required; (4) set up an emergency organization; and (5) have an emergency monitoring plan in place [14].

An emergency and remedial response plan has been developed for the CCS#1 Illinois Basin-Decatur Project (IBDP). This plan describes actions that the owner/operator shall take to address movement of the injection fluid or formation fluids in a manner that may endanger an underground source of drinking water (USDW) during Class VI activities, including post-injection site care, for the IBDP CCS#1 well [83]. There are seven parts in the plan:

1. Local resources and infrastructure;
2. Potential risk scenarios: well integrity failure, potential brine or CO_2 leakage to USDW, natural disaster, induced seismic event;
3. Emergency identification and response actions;
4. Response personnel and equipment;
5. Emergency communications plan;
6. Plan review;
7. Staff training and exercise procedures

An emergency and remedial response plan also has been developed for FutureGen 2.0 Morgon County CO_2 storage site Well#1. This plan describes actions the permittee will take at the storage site in the unlikely event of an emergency that could endanger any underground source of drinking water within the project Area of Review (AOR) during construction, operation, or post-injection site care. Such events may include the unplanned release of CO_2 or the detection of unexpected movement of CO_2 or associated fluids in or from the injection zone [84].

Sacuta et al. [85] developed an emergency response plan for the Illinois Basin–Decatur Project (IBDP) as an example of international collaboration in the CCS community's outreach and project development efforts. This plan is a process for planning vital communications during a crisis. In their opinion, any communication plan for a crisis situation at a CCS project should recognize the value of removing barriers to providing information to other projects before any crisis has occurred and, especially, in the event of such a crisis.

5.3 Remediation

Geological storage sites will be selected based on risk assessment findings to avoid leakage and to ensure systematic operation. However, in rare cases, leakage may

occur and remediation measures will be needed, either to stop the leakage or to prevent adverse impacts to people and/or the ecosystem.

Benson and Hepple [86] discussed the possibility of early detection of leakage from CGS projects and the availability of remediation options for many of the types of leakage that may occur. Seven potential leakage routes and remediation techniques for CO_2 injected into saline formations were illustrated in Intergovenmental Panel on Climate Change (IPCC) [87], and remediation options for different scenarios for CGS were presented, as listed below:

1. Leakage up faults, fractures, and spill points;
2. Leakage through active or abandoned wells;
3. Accumulation of CO_2 in the vadose zone and soil gas;
4. Leakage into the vadose zone and accumulation in soil gas;
5. Large releases of CO_2 into the atmosphere;
6. Accumulation of CO_2 in indoor environments with chronic low-level leakage;
7. Accumulation in surface water.

A technical study of the remediation of leakage from CO_2 storage reservoirs was conducted by IEA GHG [88], and full details were presented in the report on the following topics: (1) the five-part strategy for seepage prevention and remediation; (2) classification of a CO_2 seepage event; (3) remediation procedures of CO_2 seepage well; (4) remediation of the subsurface impacts of CO_2 migration; (5) cost of CO_2 seepage prevention and remediation.

The effectiveness of some of the remediation measures was studied via simulations. Two types of vadose zone remediation of CO_2 leakage from CGS were compared [8]. First, they considered passive remediation with and without barometric pumping; then, they considered active methods involving extraction wells in both vertical and horizontal configurations. They defined the half-life of the CO_2 plume as a convenient measure of the CO_2 removal rate. The results of the simulations showed that, for passive remediation approaches, thicker vadose zones generally require longer times, while the half-life of the CO_2 plume without barometric pumping was longer than that for somewhat thicker vadose zones. As for active strategies, the results showed that a combination of horizontal and vertical wells was the most effective strategy among those that were investigated.

The use of wells in the remediation of possible leakage from geologic CO_2 storage reservoirs into groundwater aquifers also has been discussed [89, 90]. Three types of remediation measures, i.e., the extraction of the CO_2, injection water, and the injection of water followed by extraction were compared based on the results of the TOUGH2 simulation. Based on the simulations that were analyzed, multiple conclusions were made concerning the effectiveness of various remediation scenarios. With one vertical extraction well, the optimal scenario for the larger leakage cases was a multi-step extraction process that initially removed mobile CO_2 from the high-concentration areas. A horizontal extraction well in the middle of the aquifer was much more efficient than vertical wells for removing CO_2. Water injection effectively and quickly reduced the mobile phase CO_2, with tradeoffs between the injection rates and increases in pressure. The most effective scenario

over a longer time period included injection for a short time followed by extraction from four vertical wells. For the most rapid reduction of the CO_2, four injector wells with high flow rates and one extraction well were the most effective approach in cases of large quantities of CO_2 leakage [89, 90].

6 Concluding Remarks

This article provided a brief review of the geological storage of CO_2 and an introduction to the risk assessment associated with such storage, including risk scenarios, risk assessment methods and applications, and risk management measures. Various methods have been applied to assess the risks associated with the geological storage of CO_2, but, none of them can be used for all such projects or phases. Thus, care must be exercised in selecting suitable methods for different CCS projects that have different features, purposes, and designs.

In the ISO/TC 265 (carbon dioxide capture, transportation, and geological storage), Working Group 5 discussed the lifecycle risk management for an integrated CCS project. It is our hope that an ISO standard will be developed for the risk assessment of the geological storage of CO_2 that provides well-documented, comprehensive information concerning appropriate approaches to risk assessment.

Acknowledgments The authors acknowledge with grateful appreciation the funding support provided by the China Australia Geological Storage of CO_2 (CAGS), the China CDM Fund (Environmental Impact Assessment of CCS), NZEC IIA (Risk Management and Public Acceptance of CCS Pilot Project), the National Key Technology R&D Program (Grant No. 2012BAC24B05), the National Department Public Benefit Research Foundation of MLR, China (Grant No. 201211063-4-1), and the Hundred Talent Program of Chinese Academy of Sciences.

References

1. Kalan S, Garrick BJ (1981) On the quantitative definition of risk. Risk Anal 1:11–27
2. Deel D, Mahajan K, Mahoney CR, McIlvried HG, Srivastava RD (2006) Risk assessment and management for long-term storage of CO_2 in geologic formations – United States Department of Energy R&D. In: Callaos N, Zinn D, Savoie MJ, Hu X, Hill R, Haga H (eds) 10th world multi-conference on systemics, cybernetics and informatics/12th international conference on information systems analysis and synthesis, Orlando, FL, USA 16–19 July 2006. International Institute of Informatics & Systemics, pp 326–331
3. Purdy G (2010) ISO 31000:2009-setting a new standard for risk management. Risk Anal 30:881–886. doi:10.1111/j.1539-6924.2010.01442.x
4. International Standardization Organization (2009) 31000:2009, risk management – principles and guidelines. ISO, Geneva
5. Morgado CdRV, Esteves VPP (2011) Technological challenges in risk management of carbon capture and geological storage (CCGS) projects. Paper presented at the proceedings of the

2011 international conference on industrial engineer and operations management, Kuala Lumpur, Malaysia, 22–25 January 2011. pp 158–163
6. Benson SA (2007) Geological storage of CO_2: analogues and risk management. Paper presented at the Carbon Sequestration Leadership Forum, Pittsburgh, PA, USA, 7 May 2007
7. Damen K, Faaij A, Turkenburg W (2003) Health, safety and environmental risks of underground CO_2 storage – overview of mechanisms and current knowledge. Utrecht University, Utrecht, The Netherlands, p 30
8. Zhang Y, Oldenburg CM, Benson SM (2004) Vadose zone remediation of carbon dioxide leakage from geologic carbon dioxide sequestration sites. Vadose Zone J 3:858–866. doi:10.2113/3.3.858
9. Liu L-C, Li Q, Zhang J-T, Cao D (2016) Toward a framework of environmental risk management for CO_2 geological storage in China: gaps and suggestions for future regulations. Mitig Adapt Strateg Glob Chang 21:191–207. doi:10.1007/s11027-11014-19589-11029
10. Wilson EJ, Johnson TL, Keith DW (2003) Regulating the ultimate sink: managing the risks of geologic CO_2 storage. Environ Sci Technol 37:3476–3483. doi:10.1021/es021038+
11. European Union (EU) (2009) Directive 2009/31/EC of the european parliament and of the council of 23 April 2009 on the geological storage of carbon dioxide and amending council Directive 85/337/EEC, European Parliament and Council Directives 2000/60/EC, 2001/80/EC, 2004/35/EC, 2006/12/EC, 2008/1/EC and Regulation (EC) No 1013/2006 (Text with EEA relevance). Off J Eur Union:114–135
12. Canadian Standards Association (2011) CSA Z741: geological storage of carbon dioxide (draft issued for public review 27 october 2011). CSA, Mississauga, Canada
13. World Resources Institute (2008) Guidelines for carbon dioxide capture, transport, and storage. WRI, Washington, DC
14. Ministry of Environmental Protection of China (2015) CCUS environmental risk assessment technical guidelines (exposure draft). MEP. http://www.mep.gov.cn/gkml/hbb/bgth/201501/W020150108344992053747.pdf
15. Dias S, Guen YL, Poupard O, Shtivelman V (2011) Risk assessment of MUSTANG project experimental site – methodological development. Energy Procedia 4:4109–4116. doi:10.1016/j.egypro.2011.02.354
16. Gerstenberger MC, Christophersen A, Buxton R, Allinson G, Hou W, Leamon G, Nicol A (2013) Integrated risk assessment for CCS. Energy Procedia 37:2775–2782. doi:10.1016/j.egypro.2013.06.162
17. IEA Greenhouse Gas R&D Programme (IEA GHG) (2009) A review of the international state of the art in risk assessment guidelines and proposed terminology for use in CO_2 geological storage. IEA GHG, Cheltenham, UK
18. National Energy Technology Laboratory (2011) Best practices for: risk analysis and simulation for geologic storage of CO_2, 1st edn. National Energy Technology Laboratory, Morgantown, WV, USA
19. Pawar RJ et al (2015) Recent advances in risk assessment and risk management of geologic CO_2 storage. Int J Greenhouse Gas Control 40:292–311. doi:10.1016/j.ijggc.2015.06.014
20. Wollenweber J et al (2013) Integrated carbon risk assessment (ICARAS). Energy Procedia 37:4825–4832. doi:10.1016/j.egypro.2013.06.392
21. Hnottavange-Telleen K, Chabora E, Finley RJ, Greenberg SE, Marsteller S (2011) Risk management in a large-scale CO_2 geosequestration pilot project, Illinois, USA. Energy Procedia 4:4044–4051. doi:10.1016/j.egypro.2011.02.346
22. Hnottavange-Telleen K, Krapac I, Vivalda C (2009) Illinois Basin-Decatur Project: initial risk-assessment results and framework for evaluating site performance. Energy Procedia 1:2431–2438. doi:10.1016/j.egypro.2009.02.004
23. Tucker O, Holley M, Metcalfe R, Hurst S (2013) Containment risk management for CO_2 storage in a depleted gas field, UK North Sea. Energy Procedia 37:4804–4817. doi:10.1016/j.egypro.2013.06.390

24. Lv GZ, Li Q, Wang S, Li X (2015) Key techniques of reservoir engineering and injection-production process for CO_2 flooding in China's SINOPEC Shengli Oilfield. J CO_2 Util 11:31–40. doi:10.1016/j.jcou.2014.12.007
25. Li Q, Liu X, Du L, Bai B, Fang Z, Jing M, Li X (2013) Economics of acid gas reinjection with comparison to sulfur recovery in China. Energy Procedia 37:2505–2510. doi:10.1016/j.egypro.2013.06.132
26. Heinrich JJ, Herzog HJ, Reiner DM (2003) Environmental assessment of geologic storage of CO_2. Paper presented at the second national conference on carbon sequestration, Washington, DC, 5–8 May 2003
27. Stenhouse M (2009) Natural and industrial analogues for geological storage of carbon dioxide. IEA Greenhouse Gas R&D Programme, Cheltenham, UK
28. Benson SM, Hepple R, Apps J, Tsang C-F, Lippmann M (2002) Lessons learned from natural and industrial analogues for storage of carbon dioxide in deep geological formations. Lawrence Berkeley National Laboratory, Berkeley, CA, USA
29. Li Q, Song R, Liu XH, Liu GZ, Sun Y-K (2016) Monitoring of carbon dioxide geological utilization and storage in China: a review. In: Wu Y, Carroll JJ, Zhu W (eds) Acid gas extraction for disposal and related topics. Wiley, New York, USA, pp 331–358
30. Oldenburg CM, Jordan PD, Nicot J-P, Mazzoldi A, Gupta AK, Bryant SL (2011) Leakage risk assessment of the In Salah CO_2 storage project: applying the certification framework in a dynamic context. Energy Procedia 4:4154–4161. doi:10.1016/j.egypro.2011.02.360
31. Paulley A, Metcalfe R, Limer L (2011) Systematic FEP and scenario analysis to provide a framework for assessing long-term performance of the Krechba CO_2 storage system at In Salah. Energy Procedia 4:4185–4192. doi:10.1016/j.egypro.2011.02.365
32. Verdon JP, Kendall JM, Stork AL, Chadwick RA, White DJ, Bissell RC (2013) Comparison of geomechanical deformation induced by megatonne-scale CO_2 storage at Sleipner, Weyburn, and In Salah. Proc Natl Acad Sci U S A 110:E2762–E2771. doi:10.1073/pnas.1302156110
33. Koornneef J, Ramirez A, Turkenburg W, Faaij A (2012) The environmental impact and risk assessment of CO_2 capture, transport and storage – an evaluation of the knowledge base. Prog Energ Combust Sci 38:62–86. doi:10.1016/j.pecs.2011.05.002
34. Savage D, Maul PR, Benbow S, Walke RC (2004) A generic FEP database for the assessment of long-term performance and safety of the geological storage of CO_2. Quintessa, Oxfordshire, UK
35. Quintessa (2010) Generic CO_2 FEP database. Quintessa Limited. http://www.quintessa.org/co2fepdb/
36. Yamaguchi K, Takizawa K, Komaki H, Hayashi E, Murai S, Ueta S, Tsuchiya M (2011) Scenario analysis of hypothetical site conditions for geological CO_2 sequestration in Japan. Energy Procedia 4:4052–4058. doi:10.1016/j.egypro.2011.02.347
37. Yavuz F, van Tilburg T, David P, Spruijt M, Wildenborg T (2009) Second generation CO_2 FEP analysis: CASSIF – carbon storage scenario identification framework. Energy Procedia 1:2479–2485. doi:10.1016/j.egypro.2009.02.010
38. Farret R, Gombert P, Lahaie F, Cherkaoui A, Lafortune S, Roux P (2011) Design of fault trees as a practical method for risk analysis of CCS: application to the different life stages of deep aquifer storage, combining long-term and short-term issues. Energy Procedia 4:4193–4198. doi:10.1016/j.egypro.2011.02.366
39. Flaus J-M (2013) Risk analysis: socio-technical and industrial systems. Wiley-ISTE, London, UK
40. Condor J, Unatrakarn D, Wilson M, Asghari K (2011) A comparative analysis of risk assessment methodologies for the geologic storage of carbon dioxide. Energy Procedia 4:4036–4043. doi:10.1016/j.egypro.2011.02.345
41. Birkholzer JT, Oldenburg CM, Zhou Q (2015) CO_2 migration and pressure evolution in deep saline aquifers. Int J Greenhouse Gas Control 40:203–220. doi:10.1016/j.ijggc.2015.03.022
42. Environmental Protection Agency (EPA) (2008) Vulnerability evaluation framework for geologic sequestration of carbon dioxide. U.S. Environmental Protection Agency. http://www.epa.gov/climatechange/ccs/federal.html

43. IEA Greenhouse Gas R&D Programme (2004) BP risk assessment. In: Risk assessment workshop, DTI conference centre, London, UK, 11–12 February 2004. IEA, p 458
44. Vendrig M (2004) The use of SWIFT and QRA in determining risk of leakage from CO_2 capture, transport and storage systems. IEA Greenhouse GAS R&D Programme and BP Risk Assessment Workshop, London, UK
45. Quintessa Limited Evidence support logic: a guide for TESLA users. http://www.quintessa.org/evidence-support-logic-guide.pdf. 2015
46. Metcalfe R, Paulley A, Suckling PM, Watson CE (2013) A tool for integrating and communicating performance-relevant information in CO_2 storage projects: description and application to In Salah. Energy Procedia 37:4741–4748. doi:10.1016/j.egypro.2013.06.383
47. Egan M, Bowden R (2004) Application of evidence support logic to the role of palaeohydrogeology in long-term performance assessment. Report QRS-1219A-1v1, prepared for UK Nirex Ltd by Quintessa Ltd
48. Egan M, Paulley A, Lehman L, Lowe J, Rochette E, Baker S, Enterprises U (2009) Assessing confidence in performance assessments using an evidence support logic methodology: an application of TESLA–9484. Paper presented at the waste management symposium (WM2009 Conference), Phoenix, AZ, USA, 1–5 March 2009
49. Guénan TL, Manceau J-C, Bouc O, Rohmer J, Ledoux A (2011) GERICO: a database for CO_2 geological storage risk management. Energy Procedia 4:4124–4131. doi:10.1016/j.egypro.2011.02.356
50. Oldenburg CM (2008) Screening and ranking framework for geologic CO_2 storage site selection on the basis of health, safety, and environmental risk. Environ Geol 54:1687–1694. doi:10.1007/s00254-007-0947-8
51. Li Q, Liu GZ, Liu XH, Li XC (2013) Application of a health, safety, and environmental screening and ranking framework to the Shenhua CCS project. Int J Greenhouse Gas Control 17:504–514. doi:10.1016/j.ijggc.2013.06.005
52. Li Q, Fei W, Liu XH, Wei XC, Jing M, Li XC (2014) Challenging combination of CO_2 geological storage and coal mining in Ordos basin, China. Greenhouse Gases: Sci Technol 4:452–467. doi:10.1002/ghg.1408
53. Wei XC, Li Q, Li X-Y, Sun Y-K, Liu XH (2015) Uncertainty analysis of impact indicators for the integrity of combined caprock during CO_2 geosequestration. Eng Geol 196:37–46. doi:10.1016/j.enggeo.2015.06.023
54. Bielicki JM, Pollak MF, Wilson EJ, Fitts JP, Peters CA (2013) A methodology for monetizing basin-scale leakage risk and stakeholder impacts. Energy Procedia 37:4665–4672. doi:10.1016/j.egypro.2013.06.375
55. Oraee-Mirzamani B, Cockerill T, Makuch Z (2013) Risk assessment and management associated with CCS. Energy Procedia 37:4757–4764. doi:10.1016/j.egypro.2013.06.385
56. Liu GZ, Li Q (2014) A basin-scale site selection assessment method for CO_2 geological storage under the background of climate change. Clim Chang Res Lett 3:13–19. doi:10.12677/ccrl.2014.31003 (in Chinese)
57. Li Q, Kuang D, Liu GZ, Liu XH (2014) Acid gas injection: a suitability evaluation for the sequestration site in Amu Darya Basin, Turkmenistan. Geol Rev 60:1133–1146 (in Chinese)
58. Oldenburg CM, Bryant SL, Nicot J-P (2009) Certification framework based on effective trapping for geologic carbon sequestration. Int J Greenhouse Gas Control 3:444–457. doi:10.1016/j.ijggc.2009.02.009
59. Guen YL, Huot M, Loizzo M, Poupard O (2011) Well integrity risk assessment of Ketzin injection well (ktzi-201) over a prolonged sequestration period. Energy Procedia 4:4076–4083. doi:10.1016/j.egypro.2011.02.350
60. Meyer V, Houdu E, Poupard O, Le Gouevec J (2009) Quantitative risk evaluation related to long term CO_2 gas leakage along wells. Energy Procedia 1:3595–3602. doi:10.1016/j.egypro.2009.02.154
61. Viswanathan HS et al (2008) Development of a hybrid process and system model for the assessment of wellbore leakage at a geologic CO_2 sequestration site. Environ Sci Technol 42:7280–7286. doi:10.1021/es800417x

62. Stauffer PH et al (2011) Application of the CO_2-PENS risk analysis tool to the Rock Springs Uplift, Wyoming. Energy Procedia 4:4084–4091. doi:10.1016/j.egypro.2011.02.351
63. Los Alamos National Laboratory CO_2-PENS. http://co2-pens.lanl.gov/. Accessed 5 Jan 2015
64. Tanaka A, Sakamoto Y, Higashino H, Suzumura M, Komai T (2013) Development of a risk assessment tool for CO_2 geological storage: 'GERAS-CO_2GS'. Energy Procedia 37:2828–2839. doi:10.1016/j.egypro.2013.06.168
65. Bowden AR, Rigg A (2004) Assessing reservoir performance risk in CO_2 storage projects. Paper presented at the GHGT-7, Regina, Canada
66. Cherkaoui A, Lopez P (2009) CO_2 storage risk assessment: feasibility study of the systemic method MOSAR. Saf Secur Eng III 108:173–184. doi:10.2495/Safe090171
67. Li Q, Li XC (2012) Recommended risk method related to CO_2 geological storage in China. Paper presented at the CSLF/GCCSI /IEA workshop on risk and liability of CO_2 geologic storage, Paris, France, 7 Oct 2012
68. Li Q, Liu L-C (2013) Environmental impact and risk assessment for CO_2 geological utilization and storage. Paper presented at the CAGS2 Training School 1, Chengdu, China, 14–17 Oct 2013
69. Bachu S (2003) Screening and ranking of sedimentary basins for sequestration of CO_2 in geological media in response to climate change. Environ Geol 44:277–289. doi:10.1007/s00254-003-0762-9
70. Fei W, Li Q, Wei XC, Song R, Jing M, Li XC (2015) Interaction analysis for CO_2 geological storage and underground coal mining in Ordos basin, China. Eng Geol 196:194–209. doi:10.1016/j.enggeo.2015.07.017
71. Stenhouse M, Zhou W, Savage D, Benbow S (2005) Framework methodology for long-term assessment of the fate of CO_2 in the Weyburn field. In: Benson SM (ed) Carbon dioxide capture for storage in deep geologic formations – results from the CO_2 capture project, vol 2. Elsevier, Oxford, UK
72. Walke R, Metcalfe R, Limer L, Maul P, Paulley A, Savage D (2011) Experience of the application of a database of generic features, events and processes (FEPs) targeted at geological storage of CO_2. Energy Procedia 4:4059–4066. doi:10.1016/j.egypro.2011.02.348
73. Stenhouse MJ, Zhou W, Arthur R (2006) Assessment of the long-term fate of CO_2 injected into the Weyburn field – system-level modeling of CO_2 migration and potential impacts. In: Lombardi S, Altunina LK, Beaubien SE (eds) Advances in the geological storage of carbon dioxide: international approaches to reduce anthropogenic greenhouse gas emissions, vol 65, NATO science series iv earth and environmental sciences. Springer, Dordrecht, the Netherlands, pp 231–242
74. LeNeveu DM (2008) CQUESTRA, a risk and performance assessment code for geological sequestration of carbon dioxide. Energy Convers Manag 49:32–46
75. Dodds K, Waston M, Wright I (2011) Evaluation of risk assessment methodologies using the In Salah CO_2 storage project as a case history. Energy Procedia 4:4162–4169. doi:10.1016/j.egypro.2011.02.361
76. Li Q, Liu GZ, Zhang J, Jia L, Liu H (2013) Status and suggestion of environmental monitoring for CO_2 geological storage. Adv Earth Sci 28:718–727 (in Chinese)
77. Liu L-C, Leamon G, Li Q, Cai B (2014) Developments towards environmental regulation of CCUS projects in China. Energy Procedia 63:6903–6911. doi:10.1016/j.egypro.2014.11.724
78. Jenkins C, Chadwick A, Hovorka SD (2015) The state of the art in monitoring and verification—ten years on. Int J Greenhouse Gas Control 40:312–349. doi:10.1016/j.ijggc.2015.05.009
79. Administrative Center for China's Agenda 21, Center for Hydrogeology and Environmental Geology (2012) Research on the guideline for site selection of CO_2 geological storage in China. Geological Publishing House, Beijing (in Chinese)
80. Mathieson A, Midgely J, Wright I, Saoula N, Ringrose P (2011) In Salah CO_2 storage JIP: CO_2 sequestration monitoring and verification technologies applied at Krechba, Algeria. Energy Procedia 4:3596–3603. doi:10.1016/j.egypro.2011.02.289

81. Cai B, Leamon G, Liu L-C (2013) Geological storage of carbon dioxide and environmental monitoring. Chemical Industry Press, Beijing
82. IEA Greenhouse Gas R&D Programme (IEA GHG) (2009) Safety in carbon dioxide capture, transport and storage. IEA GHG, Cheltenham, UK
83. Environmental Protection Agency (2014) Attachment F: emergency and remedial response plan for Archer Daniels Midland, CCS#1 Well. http://www.epa.gov/r5water/uic/adm/pdf/adm-ccs1-attachment-f-err-plan-final.pdf
84. Environmental Protection Agency (2014) Attachment F: emergency and remedial response plan for FutureGen 2.0 Morgan County CO_2 storage site. http://www.epa.gov/region5//water/uic/futuregen/pdfs/notice/well1/attachment-f.pdf
85. Sacuta N, Gauvreau L, Greenberg SE (2013) Emergency response planning: an example of international collaboration in CCS community outreach and project development. Energy Procedia 37:7388–7394. doi:10.1016/j.egypro.2013.06.680
86. Benson S, Hepple R (2005) Detection and options for remediation of leakage from underground CO_2 storage projects. In: Wilson M, Morris T, Gale J, Thambimuthu K (eds) Greenhouse gas control technologies, vol II. Elsevier, New York, USA. pp 1329–1335
87. Intergovenmental Panel on Climate Change (IPCC) (2005) Carbon dioxide capture and storage – Working Group III of Intergovernmental Panel on Climate Change. IPCC, New York, USA
88. IEA Greenhouse Gas R&D Programme (IEA GHG) (2007) Remediation of leakage from CO_2 storage reservoirs. IEA GHG, Cheltenham, UK
89. Esposito A, Benson SM (2011) Remediation of possible leakage from geologic CO_2 storage reservoirs into groundwater aquifers. Energy Procedia 4:3216–3223. doi:10.1016/j.egypro.2011.02.238
90. Esposito AMM (2010) Remediation of possible leakage from geologic CO_2 storage reservoirs into groundwater aquifers. Stanford University, Stanford, CA, USA
91. He M, Luis S, Rita S, Ana G, Eurpedes VJ, Zhang N (2011) Risk assessment of CO injection processes and storage in carboniferous formations: a review. Journal of Rock Mechanics and Geotechnical Engineering 3:39–56. doi:10.3724/SP.J.1235.2011.00039
92. Hnottavange-Telleen K (2013) Common themes in risk evaluation among eight geosequestration projects. Energy Procedia 37:2794–2801. doi:10.1016/j.egypro.2013.06.164

Numerical Modelling of CO_2 Gas Injection with Hydrate Formation: A Case Study in the Laboratory-Scale Sand Sediment

Takuya Nakashima and Toru Sato

Abstract Carbon capture and storage (CCS) is a potentially effective countermeasure against global warming. While CO_2 aquifer storage is currently considered as a mainstream CCS technology, further CCS options will increase the capacity of CO_2 storage. This study focuses on CO_2 storage in the form of a gas hydrate. In this method, the CO_2 is injected into sub-seabed sand sediments under high pressure and low temperature, allowing CO_2 to form hydrate. A large amount of CO_2 is sequestered as hydrate in the sediments by reactions with pore water. However, the hydrate formation itself can easily reduce permeability, leading to gas flow blockage. To maximize sequestration space, it is important that the injected gas expands over a wide area while maintaining sufficient permeability. This study models a gas-water two-phase flow with hydrate formation in sand sediment to reveal the mechanism of blockage due to hydrate formation, and simulates a laboratory-scale hydrate formation experiment in sand sediment.

1 Introduction

Carbon capture and storage (CCS), in which CO_2 is stored in geological formations such as depleted oil or gas fields or underground aquifers, is a potential method for mitigating global warming. The depth of storage aquifers can be thousands of meters below the seafloor in a continental shelf area, which is a couple of hundreds of meters below the sea surface. At such storage sites, CO_2 is in the form of a gas or a buoyant supercritical fluid. This means that there is a risk of CO_2 leakage through

T. Nakashima
Department of Ocean Technology, Policy, and Environment, University of Tokyo, 5-1-5 Kashiwanoha, Kashiwa 277-8563, Japan

Current Address: Mitsubishi Research Institute, Inc, 2-10-3 Nagatacho, Chiyoda-Ku, Tokyo 100-8141, Japan

T. Sato (✉)
Department of Ocean Technology, Policy, and Environment, University of Tokyo, 5-1-5 Kashiwanoha, Kashiwa 277-8563, Japan
e-mail: sato-t@k.u-tokyo.ac.jp

V. Vishal, T.N. Singh (eds.), *Geologic Carbon Sequestration*,
DOI 10.1007/978-3-319-27019-7_14

a network of undetected faults, abandoned bore holes, or, through direct faults formed by a big earthquake or other large diastrophism, although such events are rare [1]. This may impact marine organisms near the leakage site [2], and may re-release any non-dissolved CO_2 back into the atmosphere, thereby increasing the energy penalty of this option.

As an alternate option, Inui [3], Inui and Sato [4], and Inui and Sato [5] proposed CO_2 storage in sub-seabed sand sediments in the form of a gas hydrate. Since gas hydrates are stable under high-pressure and low-temperature conditions, the risk of leakage is greatly reduced and therefore long-term storage should be possible, as in the case of methane hydrates in sub-seabed sediments. Hydrates formed in the deep sea where water depth is more than about 300 m, resulting in important advantages compared with conventional storage methods, such as increased CO_2 storage capacity and reduced public concern.

One technical concern regarding this geological storage method in the deep sea is that the CO_2 hydrate formation blocks gas-water two-phase flow in the sand sediment during CO_2 injection, preventing further injection of meaningfully large CO_2 volumes [6]. To avoid this, it was proposed to use N_2 gas, which can inhibit the quick formation of CO_2 hydrate and the liquefaction of CO_2 at a depth of about 1000 m (Fig. 1) [3–5].

In this study, we modified an existing numerical computer program, TOUGH + HYDRATE [7], for simulation of three-dimensional (3D) gas-water two-phase flow in sand sediment, adding necessary mathematical models such as a newly-developed kinetic model for CO_2 hydrate formation. Takahashi et al. [6] conducted numerical simulations with a CO_2-hydrate formation model in sand sediment without flow. In their model, the gas-water two-phase interface is divided

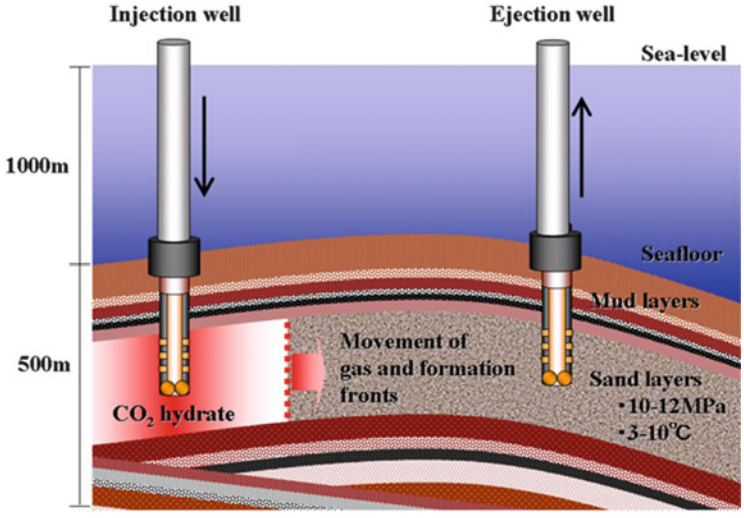

Fig. 1 Schematic image of the concept of CO_2 storage in the form of gas hydrate

into two types: fresh reaction interfaces and areas covered with CO_2 hydrate. This study is the successor of the study by Takahashi et al [6], considering hydrate formation in a two-phase flow.

Inui [3] conducted a series of experiments to measure cumulative CO_2 gas consumption due to CO_2 hydrate formation and the temperature at the centre of a high-pressure cell initially filled with three phases, gas-water-sand, and CO_2 hydrate formed by an abrupt increase of pressure. We determined unknown model parameters through history-matching of the results of the simulations and the experimental data of Inui [3].

A similar study with the same objectives was conducted by Nakashima et al. [8], which applied the hydrate formation model of Takahashi et al. [6] to hydrate rupturing in sand sediment. However, the model of Takahashi et al. [6] is valid only under no-flow conditions. We therefore developed a new hydrate formation model for gas-water two-phase flow, in which formed hydrate films rupture in the flow.

2 Numerical Methods

2.1 Theoretical

An existing gas-water two-phase flow simulator, TOUGH+ HYDRATE v1.0 [7] was modified to create the new 3D simulator. The governing equations of the original program are the equations of water mass balance in the aqueous phase, CO_2 mass balance in the gaseous phase, hydrate mass balance, and heat balance in the both phases, as follows.

$$\frac{\partial}{\partial t}\left[\varphi\left(S_G\rho_G X_G^{H_2O} + S_A\rho_A X_A^{H_2O}\right)\right] = \mathbf{F}_G X_G^{H_2O} + \mathbf{F}_A X_A^{H_2O} - Q_H X_H^{H_2O} \tag{1}$$

$$\frac{\partial}{\partial t}\left[\varphi\left(S_G\rho_G X_G^{CO_2} + S_A\rho_A X_A^{CO_2}\right)\right] = \mathbf{F}_G X_G^{CO_2} + \mathbf{F}_A X_A^{CO_2} + \mathbf{J}_G^{CO_2} + \mathbf{J}_A^{CO_2} - Q_H X_H^{CO_2} + Q_G^{CO_2} \tag{2}$$

$$\frac{\partial}{\partial t}(\varphi S_H\rho_H) = Q_H \tag{3}$$

$$\frac{\partial}{\partial t}\left[(1-\varphi)\rho_R C_R T + \sum_{\beta\equiv A,G,H}\varphi S_\beta\rho_\beta U_\beta\right] = -\lambda_m\nabla T + \sum_{\beta\equiv A,G} h_\beta\left(\mathbf{F}_\beta + \mathbf{J}_\beta + Q_\beta\right) - Q_{dis}^{CO_2}H_{dis}^{CO_2} + Q_H H_H \tag{4}$$

Here, φ is the porosity, S is the saturation, ρ is the density in kg m^{-3}, X is the mass fraction, $\mathbf{F}$ is the convection term, $\mathbf{J}$ is the diffusion term, Q is the source term in kg

$m^{-3}s^{-1}$, C is the specific heat in J $kg^{-1}K^{-1}$, T is the temperature in K, h is the enthalpy in J kg^{-1}, U is the internal energy in J kg^{-1}, λ_m is the thermal conductivity in W $m^{-1}K^{-1}$, and H is the enthalpy change in J kg^{-1}. The subscripts G, A, H, and *dis* respectively indicate the gaseous, aqueous, and hydrate phases, and the phase change due to gas dissolution into the aqueous phase. The superscripts CO_2, H_2O, and *hyd* respectively indicate carbon dioxide, water, and CO_2-hydrate. The mass fraction of CO_2 in the hydrate phase $X_H^{CO_2}$ is calculated from the chemical formula, CO_2 $5.75H_2O$. The original TOUGH + HYDRATE implicitly solves the four governing equations above.

The convection terms are given, following Darcy's law, as

$$\mathbf{F_G} = -k_s \frac{k_{rG}\rho_G}{\mu_G}(\nabla P_G - \rho_G \mathbf{g})\varphi S_G \tag{5}$$

$$\mathbf{F_A} = -k_s \frac{k_{rA}\rho_A}{\mu_A}(\nabla P_A - \rho_A \mathbf{g})\varphi S_A \tag{6}$$

where k_s is the absolute permeability in m^2, k_r is the relative permeability, μ is the viscosity in Pa· s, and P is the pressure in Pa. The difference in pressure between the gaseous and aqueous phases is the capillary pressure.

$$P_c = P_A - P_G \tag{7}$$

which is modelled later in this section.

In the original TOUGH + HYDRATE, the mass fraction of CO_2 in the aqueous phase is not involved in the implicit matrix solver, but is instead set as the equilibrium concentration on the basis of the total mass of CO_2 in each computational cell, as long as it is less than the solubility. However, it is important to consider the dissolution rate of CO_2 into the aqueous phase, namely, the kinetic dissolution, in the present study. We therefore added the CO_2 mass balance equation in the aqueous phase to the original code, as follows:

$$\frac{\partial}{\partial t}\left(\varphi S_A \rho_A X_A^{CO_2}\right) = \mathbf{F}_A X_A^{CO_2} + \mathbf{J}_A^{CO_2} + Q_{dis}^{CO_2} - Q_H X_H^{CO_2} \tag{8}$$

Also necessary is the N_2 gaseous phase mass balance equation, as follows:

$$\frac{\partial}{\partial t}\left(\varphi S_G \rho_G X_G^{N_2}\right) = \mathbf{F}_G X_G^{N_2} + \mathbf{J}_A^{N_2} + Q_G^{N_2} \tag{9}$$

The mass balance equation of CO_2 in the aqueous phase and that of N_2 in the gaseous phase increases the number of matrix rows in the Newton method solver from four to six. It is thus now possible to consider kinetic CO_2 gas dissolution into the aqueous phase, and the injection of a gas mixture of CO_2 and N_2 into the porous media.

An extension of the Brooks and Corey model [9] was used for the relative permeability of each phase, as follows:

$$k_{rG} = (1 - S_e)^{n_{kG}}\left(1 - {S_e}^2\right) \tag{10}$$

$$k_{rA} = {S_e}^4 \tag{11}$$

$$S_e = \left(S_A - S_A^{irr}\right)/\left(1 - S_A^{irr} - S_G^{res} - S_H\right) \tag{12}$$

Here, S_e is the effective saturation, S_A^{irr} is the irreducible water saturation (set to 0.39), and S_G^{res} is the residual gas saturation (set to 0.01). n_{kG} is an unknown parameter, and will be determined by history-matching between the present simulations and experiments.

The capillary pressure P_c is

$$P_c = -P_d(S_e)^{n_{Pc}} \tag{13}$$

where n_{Pc} is also an unknown parameter.

The model for the dissolution of CO_2 gas into the aqueous phase is

$$Q_{dis}^{CO_2} = k_t A_I\left(X_{A,eq}^{CO_2} - X_A^{CO_2}\right)\rho_A \tag{14}$$

where k_t is the mass transfer coefficient, which is also unknown. A_I is the specific interfacial area m^{-1} of Peng and Brusseau [10], given as

$$A_I = A_S[1 + (\alpha S_A)^n]^{-m} \tag{15}$$

$$\alpha = 14.3\ln(U) + 3.72 \tag{16}$$

$$n = 1/(2 - m) \tag{17}$$

$$m = \begin{cases} -0.098U_f + 1.53 & U_f \le 3.5 \\ 1.2 & U_f \ge 3.5 \end{cases} \tag{18}$$

$$A_S = \sqrt{\varphi^3/(5k_s)} \tag{19}$$

Where A_S is the specific surface area of sand in m^{-1} and U_f is a uniformity coefficient, for which we used the value of 1.33 for Toyoura sand [11].

Jin et al. [12] observed that hydrate films collapse when water enters the gas phase from the cracks in the film, causing the edges of the cracks to change to cement-like hydrate. Takahashi et al. [6] also suggested the rupture of hydrate films and the emergence of new gas-water interfaces in their numerical models, and thereby proposed the rupture ratio x, the areal ratio of the fresh gas-water interface to the whole interface. Firstly, hydrate forms on gas-water interfaces, which consist of the advancing gas front and the surface of the immobile water surrounding or bridging sand grains. Two-phase flow moves the hydrate film formed on the gas front, which hangs on downward sand grains and breaks into small splinters that can be trapped in the pore mouth of the grains. This hydrate film rupture continuously

produces wide fresh gas-water interfaces. Hydrate film formed on the immobile water surface may stay and break due to the volume expansion within the limited space between grains. Takahashi et al. [6] modelled the latter type of hydrate rupture without a flow effect, and Nakashima et al. [8] used the model of Takahashi et al. [6]. In two-phase flow, however, the rupture of moving hydrate film at the gas front and consequent hydrate formation may be significant in volume, compared to formation at the immobile water surface, and needs to be newly modelled.

We assume that the movement of the hydrate film is influenced by the two-phase flow driven by gas injection, and is therefore directly affected by the kinetic pressure of the gas flow. We also assume that larger the mobility of the water, the larger the area of the emerging fresh gas-water interface. Therefore, x is modelled as

$$x = \chi M_A p_G \tag{20}$$

$$M_A = k_s k_A / \mu_A \tag{21}$$

$$p_G = \frac{1}{2}\rho_G {u_G}^2 \tag{22}$$

where M_A is the mobility of the aqueous phase in m Pa^{-1} s^{-1}, p_G is the kinetic pressure of the gaseous phase in Pa, $u_G$is the velocity of the gaseous phase, and χ is an unknown constant in s m^{-1}.

Using x, the present hydrate formation model is given as

$$Q_H = k_f (xA_I)\left(f_G^{CO_2} - f_{eq}^{CO_2}\right) + (1-x)A_I \frac{\left(f_G^{CO_2} - f_{eq}^{CO_2}\right)}{\left(\frac{h}{D_H}\right) + \left(\frac{1}{k_f}\right)} + k_f A_S \left(f_A^{CO_2} - f_{eq}^{CO_2}\right) \tag{23}$$

$$h = \varphi S_H / A_I \tag{24}$$

where h is the thickness of the hydrate film; k_f is the kinetic rate constant of hydrate formation on the gas-water interface in mol m^{-2} $Pa^{-1}s^{-1}$; D_H is the diffusion coefficient of CO_2 in the hydrate film, following Takahashi et al. [6] and k_l is the kinetic constant of hydrate formation in the aqueous phase, set to be 4.82×10^{-9} mol $m^{-1}Pa^{-1}s^{-1}$, as obtained by Clarke and Bishnoi [13]. Three kinds of hydrate formation are assumed in Eq. 14; the first, second, and third terms on the right side indicate the formation at the gas-water interface, growth of the hydrate film formed at the interface, and formation on the sand surfaces in the aqueous phase, respectively.

Hydrate formation and dissociation in the sand sediment will change the mobility of gas and water. We used the model for the decrease of absolute permeability of sand sediment from Masuda et al. [14]:

$$k_s = k_{s,0}(1 - S_H)^N \tag{25}$$

where N is an unknown parameter.

As a result, we have five unknowns that require the determination through the history-matching to the experimental data: they are n_{kG} in Eq. 10, n_{Pc} in Eq. 13, k_t in Eq. 14, χ in Eq. 20, and N in Eq. 25.

2.2 Computational Conditions

To set conditions in the numerical simulations, we referred to experiments conducted by Inui [3] consisting of a cylindrical pressure vessel made of stainless steel, a gas plunger pump, and a cooling unit. Figure 2 shows the experimental setup. The vessel has diameter and length of 50 mm and 200 mm, respectively, and was filled with Toyoura sand saturated with pure water. The porosity was 0.39. CO_2 gas was injected at a constant rate with the mass flow controller. Pressure gauges were set on the upper and lower sides of the vessel. Seven thermo couples were set in the vessel at 2 cm intervals.

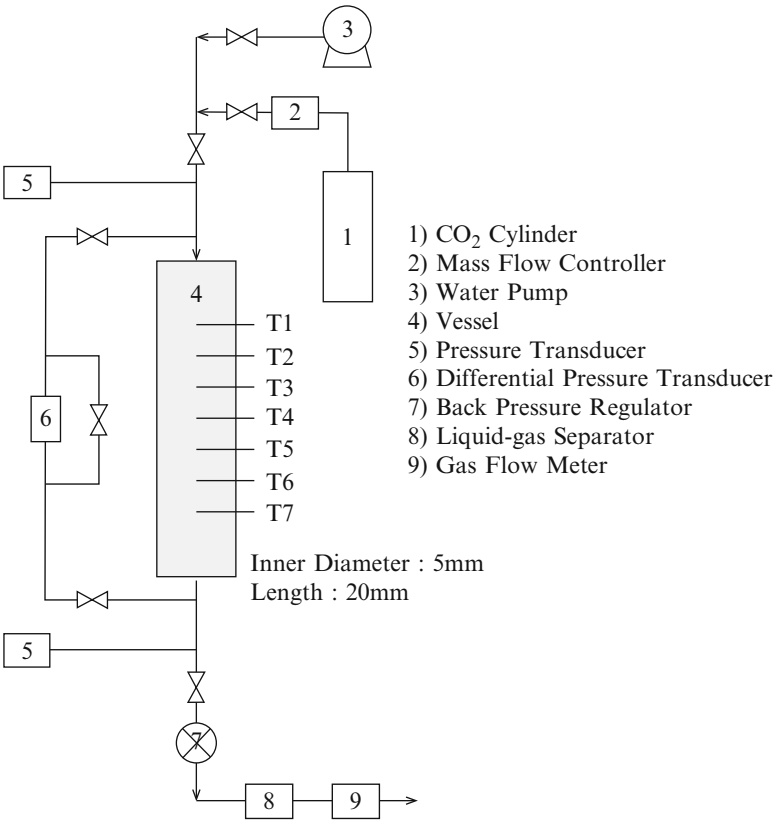

Fig. 2 Experimental setup

Table 1 Experimental conditions for CO_2 hydrate formation in sand sediment

	Case 1	Case 2	Case 3
Temperature [K]	275.15	278.15	275.15
Pressure [MPa]	3.1	3.1	4.0
Injection Rate [Nml min^{-1}]	300	300	105
Injected Gas	CO_2	CO_2	CO_2 and N_2

Table 2 Physical properties for each medium

	Toyoura sand	CO_2 hydrate	Stainless steel
Density [kg m^{-3}]	1.6×10^3	1.1×10^3	7.9×10^3
Heat conductivity [W m^{-1} K^{-1}]	7.0	0.49	15.0
Specific heat [kJ kg^{-1} K^{-1}]	1.8	2.1	0.48

The computational domain is the pressure vessel interior. To represent the stainless steel vessel, a thin layer of computational cells with no permeability was set around the sand sediment domain.

Table 1 shows the experimental conditions of Cases 1, 2, and 3. The physical properties for the Toyoura sand, CO_2 hydrate, and stainless steel are listed in Table 2, taken from Ikegawa [15], Inui [3], and a handbook published by the National Astronomical Observatory [16], respectively. Cases 1 and 2 were used to determine the unknown parameters, and Case 3 was used to validate the model with the obtained parameters.

3 Results and Discussion

We divided the fitting parameters into two types: n_{kG}, n_{Pc}, and k_t are parameters related to the gas-water two-phase flow; χ and N are related to hydrate formation. First, we defined the three flow parameters by history-matching the differential pressure, using the experimental data measured during the induction time period, before the formation of the hydrate. As a result, we set n_{kG}, n_{Pc}, and k_t to be 7.0, 0.1, and 2.0×10^{-6} m s^{-1}, respectively.

We then tried to simulate hydrate formation in Cases 1 and 2. Figures 3 and 4 compare the measured and calculated temporal changes in temperatures monitored at points where even thermocouples (T1 to T7) are set, in (a) and (b), respectively, and the differential pressure in (c) in Cases 1 and 2, respectively, with χ set to 1.23×10^{15} s m^{-1} and N set to 20. The pressure rise is seen in Fig. 3c and not in Fig. 4c. This suggests the permeability damage and consequent flow blockage caused by hydrate formation in Case 1.

Figure 5 shows the calculated temperatures and differential pressure, which are compared well with the measurement, in Case 3. Cases 1 and 2 are used to obtain

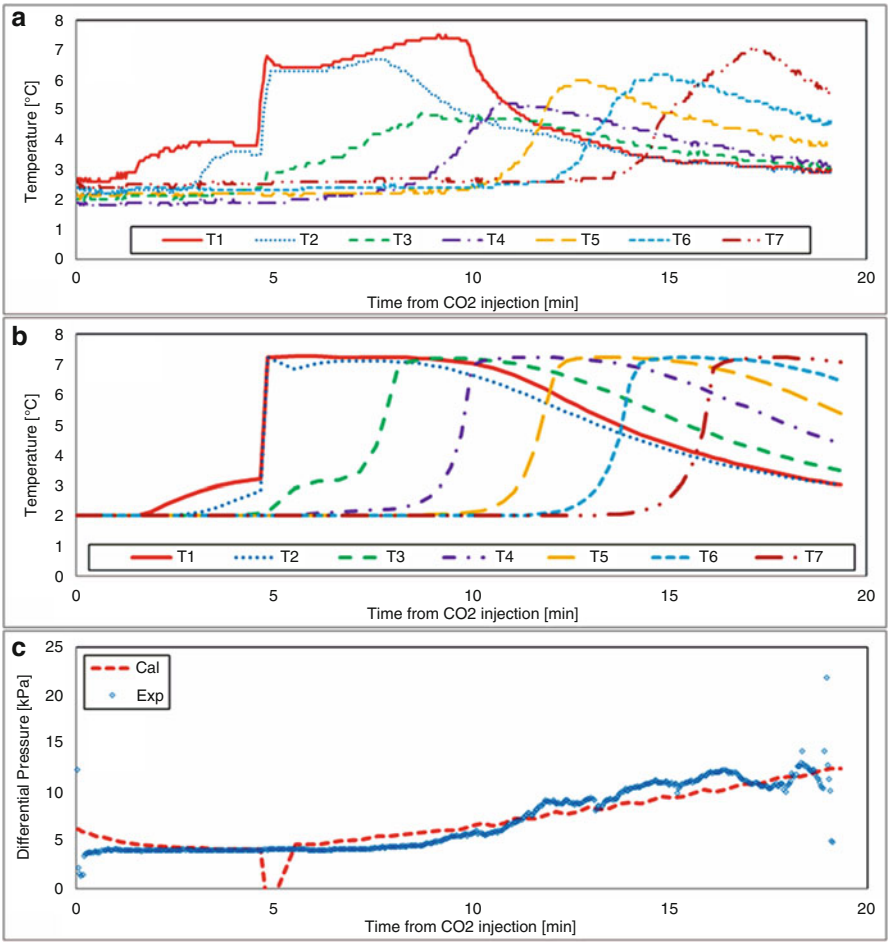

Fig. 3 Comparison of temporal changes between the present calculation and the experiment: (**a**) measured and (**b**) calculated temperatures monitored at the points at which seven thermocouples (T1 to T7) are set and (**c**) differential pressure in Case 1

values for the five unknown parameters by means of history-matching with the experimental data and these unknowns work properly in Case 3. This may support the validation of the present simulation method. It is observed in Fig. 5c that the pressure rise seen in Fig. 3c does not take place in Case 3.

Figures 6 and 7 show contour maps of the calculated hydrate formation rate Q_H and hydrate saturation S_H, respectively, in Case 1 at 5 min (a), 10 min (b), and 15 min (c). The left hand side of each figure is the centre line of the axisymmetric experimental vessel and the right is its temperature-controlled wall. The gas is injected from the upper end towards the lower end. Although Fig. 6 shows that hydrate formation takes place at the gas front, hydrate mainly exists near the wall-

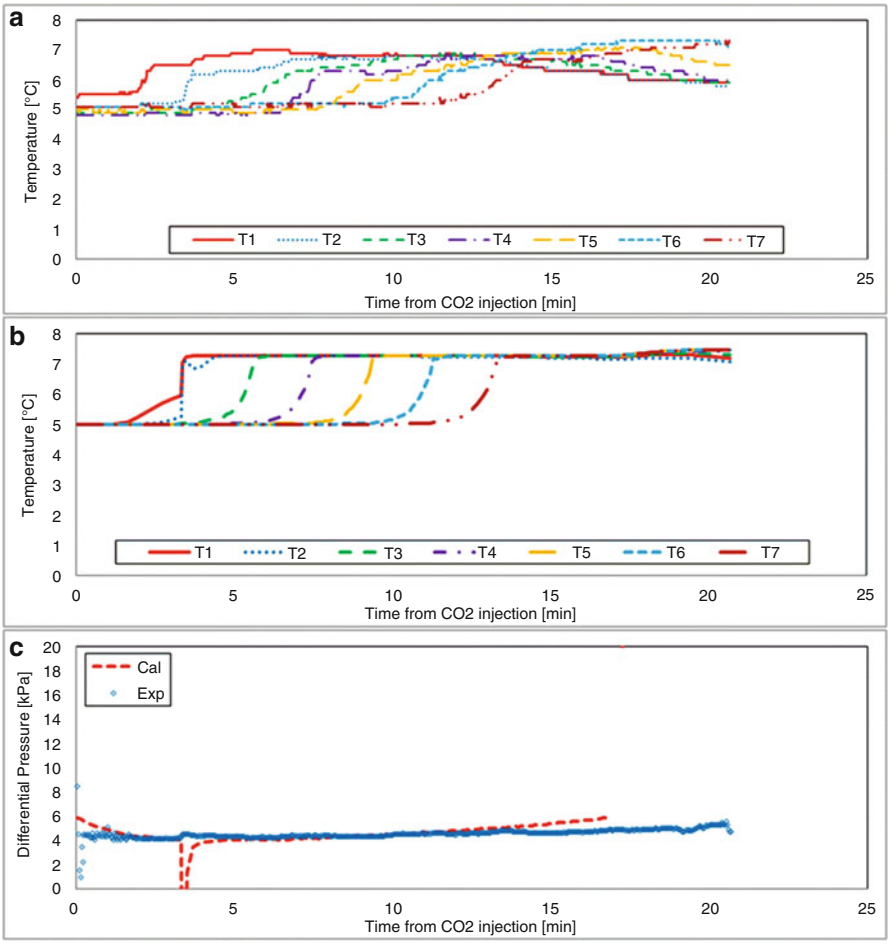

Fig. 4 Comparison of temporal changes between the present calculation and the experiment: (**a**) measured and (**b**) calculated temperatures monitored at the points at which seven thermocouples (T1 to T7) are set and (**c**) differential pressure in Case 2

side of the inlet, as seen in Fig. 7c. This may be because hydrate formation at the gas front, which does not stay at the same position, is accumulated behind the gas front. Figure 7 also explains the reason why hydrate formation is not homogeneous in the radial direction: temperature control at the wall cools down the sediment near the wall.

This hydrate saturation near the inlet should cause permeability damage, which was indicated by the large increase in differential pressure, shown in Fig. 4b. The hydrate saturation of about 0.17 at about $z = 0.005$ m and $z = 0.07$ m, the latter of which is the position of the first hydrate formation after an induction time, near the centre is considered obstructive enough to cause the flow blockage.

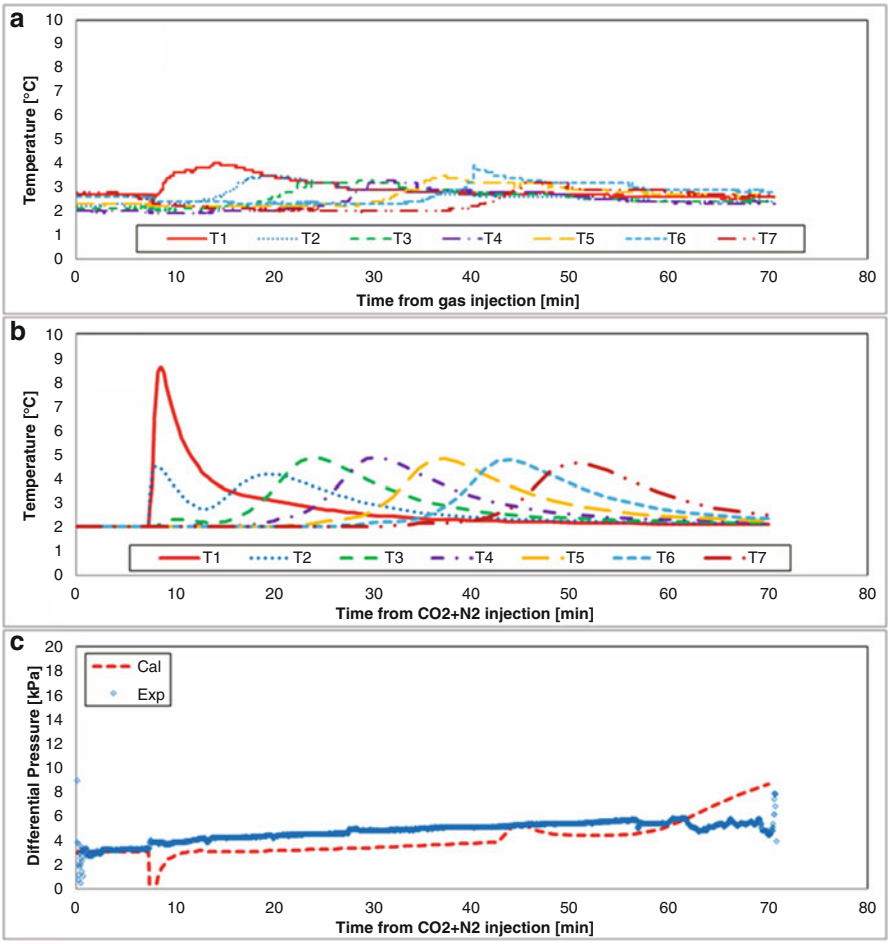

Fig. 5 Comparison of temporal changes between the present calculation and the experiment: (**a**) measured and (**b**) calculated temperatures monitored at the points at which seven thermocouples (T1 to T7) are set and (**c**) differential pressure in Case 3

Figures 8 and 9 show contour maps of QH and SH in Case 2 at 5 min (a), 10 min (b), and 14 min (c). It is seen that the hydrate forms near the wall more than it does near the centre, like Case 1. However, hydrate saturation at the first formation position, about z = 0.06 m, near the centre is about 0.06, lower than that in Case 1. It is, therefore, thought that this makes no flow blockage in Case 2.

Figures 10 and 11 show contour maps of Q_H and S_H, respectively, in Case 3 at 10 min (a), 20 min (b), 30 min (c), and 40 min (d). It seems that there are two gas fronts and instantaneous hydrate formation takes place at the second gas front more than that at the first front, as seen in Fig. 10. This may be because the concentration of CO_2 in the mixed gas gradually becomes small near the first gas front after used

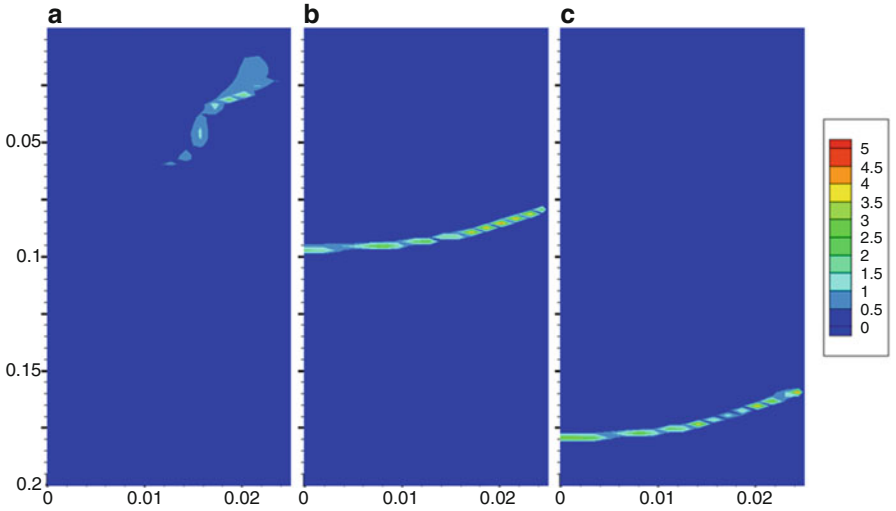

Fig. 6 Contour maps of the calculated hydrate formation rate in Case 1 at (**a**) 5 min, (**b**) 10 min, and (**c**) 15 min

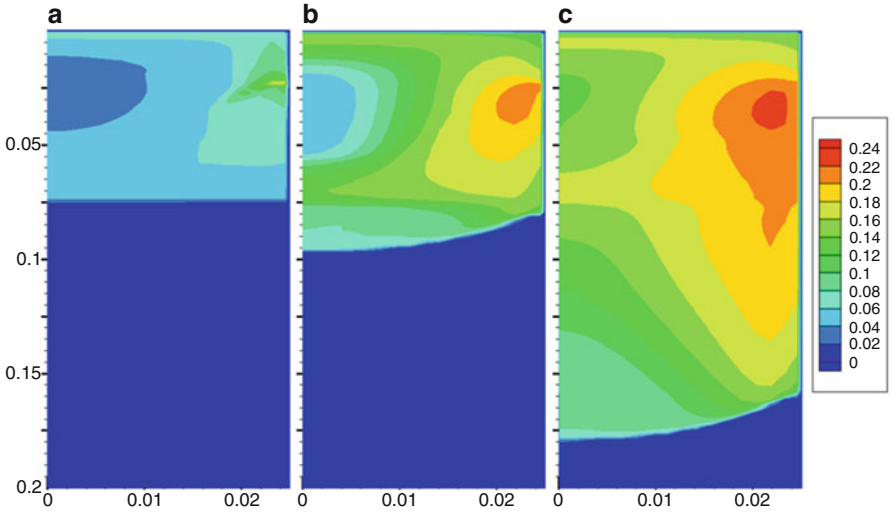

Fig. 7 Contour maps of the calculated saturation of hydrate phase in Case 1 at (**a**) 5 min, (**b**) 10 min, and (**c**) 15 min

for hydrate formation. The reason for avoiding flow blockage in Case 3 is that the hydrate saturation is not that large, up to 0.1, and not concentrated locally, as seen in Fig. 11. This should be because of the existence of N_2 gas: the hydrate formation at the two gas fronts is small, compared with those in Cases 1 and 2; the water left in the sediment changes to hydrate gradually after the gas front passes by because of

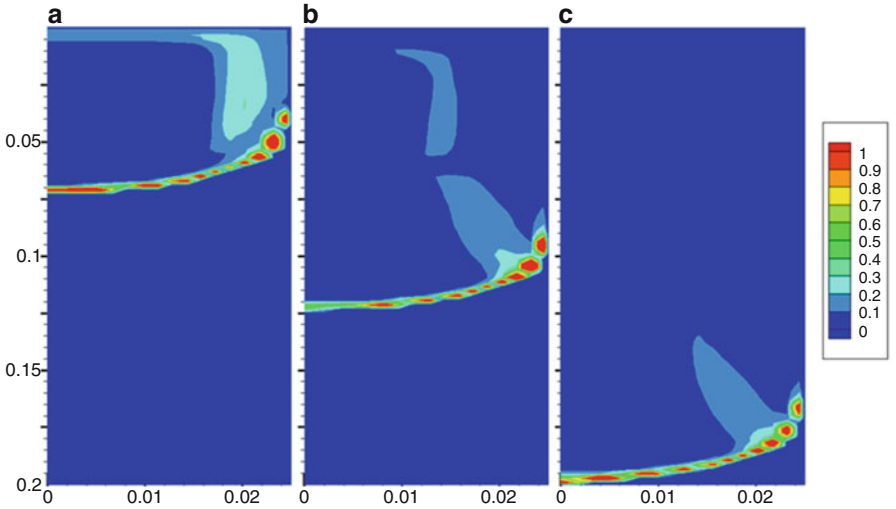

Fig. 8 Contour maps of the calculated hydrate formation rate in Case 2 at (**a**) 5 min, (**b**) 10 min, and (**c**) 15 min

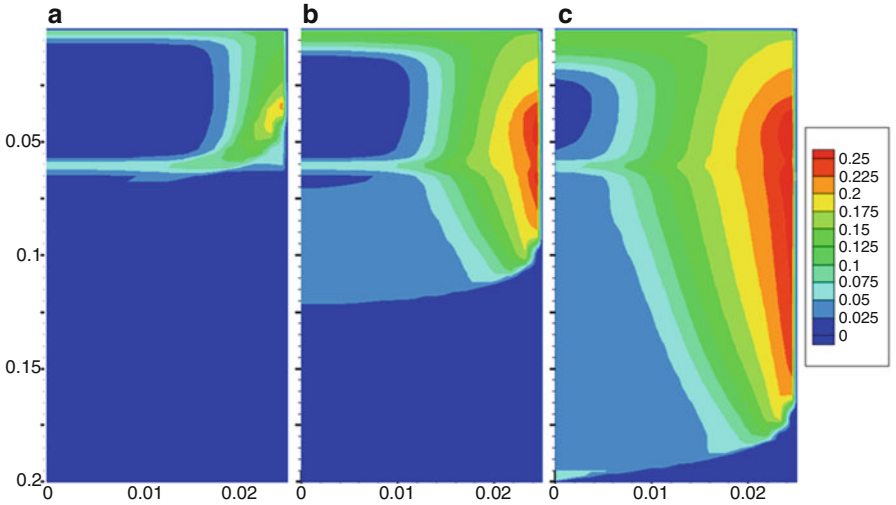

Fig. 9 Contour maps of the calculated saturation of hydrate phase in Case 2 at (**a**) 5 min, (**b**) 10 min, and (**c**) 15 min

the inhibitor effect of N_2; and therefore the hydrate saturation in Case 3 may not be the result of the accumulation of the hydrate formation at the gas front. This is very important for the concept of CO_2 storage in the form of gas hydrate: to avoid the flow blockage caused by hydrate formation, hydrate should be formed in the pore water remaining after the passage of the gas front, not right on the gas front.

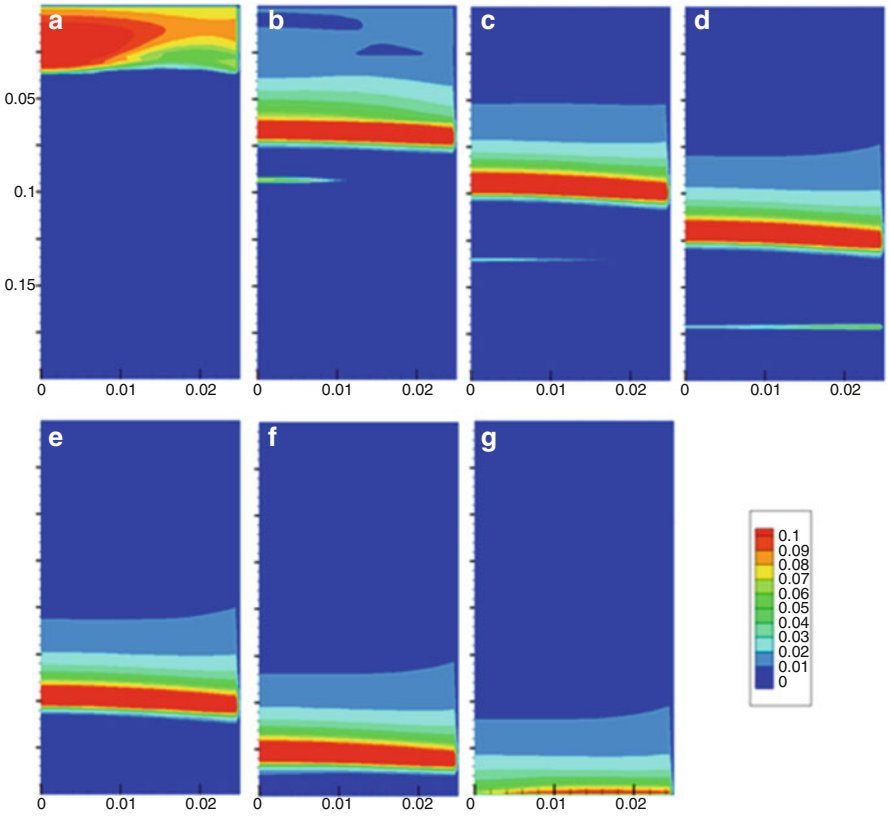

Fig. 10 Contour maps of the calculated hydrate formation rate in Case 3 at (**a**) 10 min, (**b**) 20 min, (**c**) 30 min, (**d**) 40 min, (**e**) 50 min, (**f**) 60 min, and (**g**) 70 min

4 Conclusion

We constructed a three-dimensional two-phase flow simulator in sand sediment with hydrate formation. We modified TOUGH + HYDRATE, enabling it to take CO_2 dissolution, mixed gas injection, and kinetic hydrate formation with hydrate film rupture into account. We also made a new rupture ratio model as a function of the gas pressure and water mobility.

From the comparison between the calculation and the experimental data, we verified the values of several unknown parameters: 7.0 for n_{kG}, 0.1 for n_{Pc}, 2.0×10^{-6} for k_t, and 1.23×10^{15} for χ and 20 for N. The basic behaviour of the temperatures at each measuring point was simulated moderately.

The numerical simulations demonstrated 2 case studies: laboratory-scale experiments with and without flow blockage due to hydrate formation. The hydrate forms mainly at the gas front, but it is temporary. Massive hydrate formation takes place in the sediment after the gas front passes by. Whether gas flow is blocked or not may depend on the saturation of the water left behind the gas front and on the formation rate

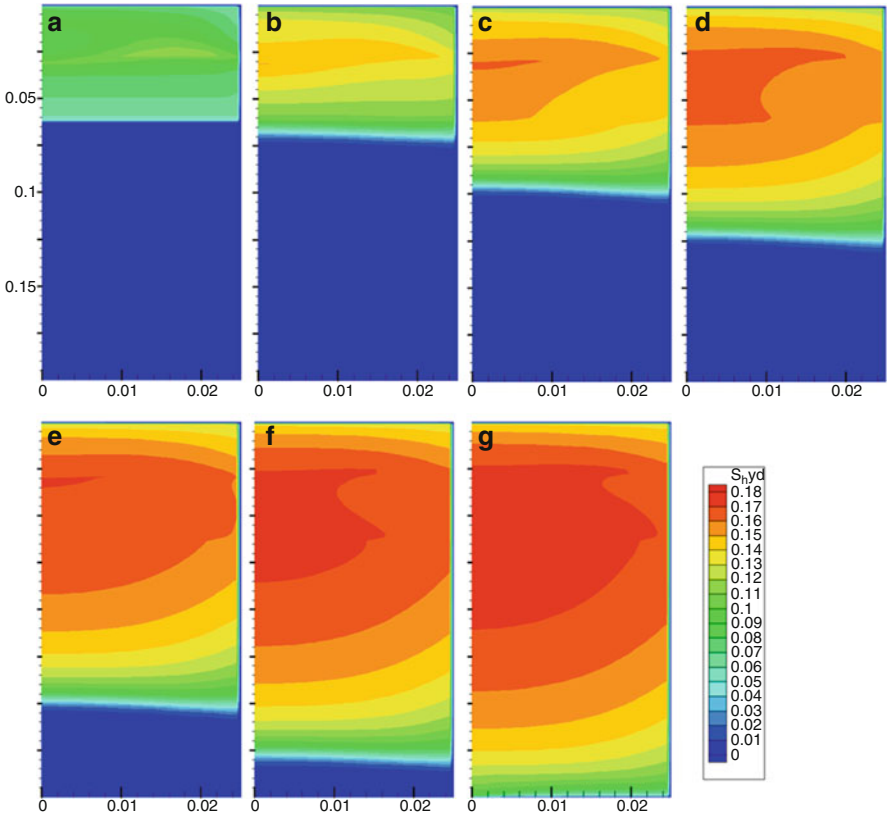

Fig. 11 Contour maps of the calculated saturation of the hydrate phase in Case 3 at (**a**) 10 min, (**b**) 20 min, (**c**) 30 min, (**d**) 40 min, (**e**) 50 min, (**f**) 60 min, and (**g**) 70 min

under the given temperature and pressure. Particularly, hydrate formation is concentrated near the temperature-controlled wall of the experimental vessel. Therefore, it is fair to say that the flow blockage is difficult to control if pure CO_2 is injected.

In the case of mixing of inhibitor, which is N_2 gas in this study, avoiding hydrate formation at the gas front was successful. Water is purged sufficiently before hydrate formation is completed using small-amount water and this assures the passage of gas through the porous media in the sediment. However, it is needless to say that further research is necessary: both experimental and numerical.

References

1. Kano Y, Sato T, Kita J, Hirabayashi S, Tabeta S (2010) Multi-scale modelling of CO_2 dispersion leaked from seafloor off Japanese coast. Mar Pollut Bull 60:215–224
2. Sato T, Watanabe Y, Toyota K, Ishizaka J (2005) Extended probit mortality model for zooplankton against transient change of pCO_2. Mar Pollut Bull 50:975–979

3. Inui M (2005) Master Thesis, University of Tokyo, Kashiwa (in Japanese)
4. Inui M, Sato T (2006) Economical feasibility study on CO_2 sequestration in the form of hydrate under seafloor. In: Proceedings of the 26th international conference on Offshore Mech and Arctic Eng OMAE06–92306
5. Inui M, Sato T (2011) Experiments and numerical simulations of hydrate formation in sand sediment simulating sub-seabed CO_2 storage in the form of gas hydrate. J MMIJ 127:194–201 (in Japanese)
6. Takahashi T, Sato T, Hirabayashi S, Brumby PE (2012) Modelling of CO_2-hydrate formation at gas-water interface in sand sediment. Chem Eng Technol 35:1751–1758
7. Moridis GJ, Kowalsky M, Pruess K (2009) TOUGH + HYDRATE v1.1 user's manual: a code for the simulation of system behavior in hydrate-bearing geologic media LBNL–0149E
8. Nakashima T, Sato T, Inui M (2013) Numerical modelling of hydrate formation in sand sediment simulating sub-seabed CO_2 storage in the form of gas hydrate. Energy Procedia 37:5986–5993
9. Byron RB, Warren ES, Edwin NL (2006) Transport phenomena, 2nd edn. Wiley, Hoboken
10. Peng S, Brusseau ML (2005) Impact of soil texture on air-water interfacial areas in unsaturated sandy porous media. Water Resour Res 41:W03021
11. Sakamoto Y, Komai T, Kawabe T, Tenma N, Yamaguchi T (2004) Formation and dissociation behavior of methane hydrate in porous media – estimation of permeability in methane hydrate reservoir, Part 1. J MMIJ 120:85–90 (in Japanese)
12. Jin Y, Konno Y, Nagao J (2012) Growth of methane clathrate hydrates in porous media. Energy Fuel 26:2242–2247
13. Clarke MA, Bishnoi RB (2005) Determination of the intrinsic kinetics of CO_2 gas hydrate formation using in situ particle size analysis. Chem Eng Sci 60:695–709
14. Masuda Y, Kurihara M, Ohuchi H, Sato T (2002) A field-scale simulation study on gas productivity of formations containing gas hydrates. In: Proceedings of the 4th international conference on gas hydrate, pp 40–46
15. Ikegawa Y (2007) Estimation by experiments and its analysis for thermal stimulation of methane hydrate using exothermic reaction of CO_2 hydrate formation. J Environ Syst Eng 63:206–215
16. National Astronomical Observatory (2006) Chronological scientific tables. Maruzen Co Ltd, Tokyo

Security Assessment on Geological Storage of CO_2: Application to Hontomin Site

Antonio Hurtado, Sonsoles Eguilior, and Fernando Recreo

Abstract The safety and risk assessment of CO_2 storage in geological formations requires a robust and iterative methodology based on an objective assessment, which shall provide an analysis and assessment of potential risks to health, safety and environment. The application of this methodology from the initial stages of the project will facilitate achieving its objectives. The results of the methodology should be twofold: the quality of the site from the point of view of the risks and the associated uncertainties. In the early stages of a project involving scarcely known natural systems, the methodology should take into account the unavoidable uncertainties in the available information and its impact on the risks, through a formalized quantification of those. In these phases the models used are mainly qualitative. As the project progresses and more information is available, the risk assessment methodology should allow gradual and continuous transition from qualitative data based models to quantitative ones.

Taking all these into account, in this work are presented the methodologies commonly used, based on those developed and fine-tuning for the past 20 or 30 years to the study of Deep Geological Repositories of high-level nuclear wastes, as well as the development carried out to estimate the risks of Hontomín Technological Development Plant, implemented under the formalism of Bayesian Networks (BNs).

1 Introduction

Two major challenges for engineering, applied to geology is the development of projects in a complex and uncertain environments. All projects in environments of significant complexity and uncertainty have a higher probability that a combination of variables that generates the materialisation of the risk occurs, defining risk as distribution functions of potential harm or loss associated with an activity

A. Hurtado • S. Eguilior (✉) • F. Recreo
CO2 Geological Storage Safety Analysis Unit, Department of Environment, CIEMAT, Avda. Complutense 40, Edif 20 P1.44, 28040 Madrid, Spain
e-mail: sonsoles.eguilior@ciemat.es

V. Vishal, T.N. Singh (eds.), *Geologic Carbon Sequestration*,
DOI 10.1007/978-3-319-27019-7_15

developed in an environment of uncertainty. It is always opposed to the achievement of the project goals.

Like the great majority of human activities, capture and geological storage of carbon dioxide (CCS) emissions is subject to risks. In fact this technology has a risk level similar to any other type of industrial activity and particularly those related to the oil and gas industry, for which there are specific regulatory frameworks. With regard to the CCS, the problem is reduced mainly to provide satisfactory answers to the questions concerning whether the CO_2 can leak and, if so, what would be the consequences for the environment, health and safety [1]. Stress should be laid on the importance of adequate response to these issues, among other reasons, for their influence on public acceptance of this technology, which being a key element for the implementation of CCS on a large scale [2]. The precise location of a safe storage site, able to sequester CO_2 for long time periods and with minimal risk is essential to gain public acceptance to the application of this technology.

The long-term safety and risk management associated with the Geological Storage of CO_2 should be considered as part of an ongoing and iterative process throughout the project lifecycle. Based on appropriate methodologies, it should establish a robust and reliable framework for identifying, assessing and managing the risks and uncertainties at each stages of the project, including: (i) the identification and initial selection of suitable geological formations; (ii) their characterization; (iii) project development activities; (iv) the operational period; (v) the closure operations in the preliminary stage of transferring facility control; and finally, (vi) the transfer of responsibilities. During all the stages risk management shall aim to improve the knowledge of the system and its risks to support achievement of the project objectives. As outlined in the Guide 1 for the implementation of the European CCS Directive [3, 4] the environmentally safe management of geological storage of CO_2 should be a key objective that must be present at all the stages. Today a broad range of methodologies and approaches are available. It will be necessary to reflect, learn and take into account the skills and limitations of each, so as to make the most of each approach at the different stages of project development [5].

The risk estimation takes into account the whole of the risk pathway from hazard identification to the unwanted consequences and will never be perfect or definitive. The intrinsic nature of the project prevents this to be an achievable goal. However this should not be considered as an obstacle, because, in reality, no risk assessment is perfect or definitive. The aim is not to achieve these levels of perfection but to provide a management support tool to reduce the chances of the emergence of circumstances that may cause the project does not meet the expectations previously established throughout the project development.

2 Geological Storage of CO_2 – Risk Assessment and Analysis

In the case of CCS projects, risks include first of all, those arising from the operation of surface facilities with associated impacts on safety, health and the environment during all phases of capture, pipeline transport (or others) and injection processes. They are similar to those associated with any other engineering project and its evaluation is a common practice in diverse industries such as oil and gas industries. Validated methods are available for quantitative risk assessment that are directly applicable and tools that have been used in other industrial processes. As estimates of probabilities and consequences are directly based on the experience, confidence in the assessment of these risks turns out to be high, but usually not free from bias. The reason for this is that such estimates introduce a type of "over confidence" bias known as "hindsight bias". This is manifested in the fact that, while reporting on the occurrence of an event, you tend to assign a higher posterior probability than the initially assigned to make the prediction. Thus, when reporting on a given fact it tends to be seen as inevitable, i.e., a joint influence of the observed data and previous theories is observed [6]. This means that, as a side effect, is obtained a reduction about the surprised results or events, which is especially important in the evaluation of scientific papers [7] taken as the basis for assigning events probabilities.

Along with the above, in the geological storage of CO_2 there are long-term risks associated with CO_2 leakage from storage or movements induced by it. These can be summarized as local risks associated with effects on the environment or health of the population, and global risks associated with the release of CO_2 into the atmosphere and the impact of such release in the processes of climate change that are trying to avoid the CCS [8].

In general, it is observed that the methodologies proposed for the evaluation of long-term risks arising from geological CO_2 storage (GCS) are based on those that have been developing and adjusting for the past 20 or 30 years during the study of deep geological repositories of high level nuclear waste. Geological storage of CO_2 shares with that field of knowledge the large periods of time and large spatial areas involved [9]. This brings implicit the high level of uncertainty, both associated with the natural environment and the future evolution. Both must be considered in risk analysis to be carried out.

The matters mentioned in the foregoing paragraphs require the identification of all the relevant issues from the point of view of safety in geological storage of CO_2, with the purpose to feed such projects in the future. This should include:

1. The risks identified that actually occurred and its causes;
2. Determine those that we will be able to describe as generic ones and therefore that could affect similar projects;
3. Identify those unique aspects;

4. The issue of risks that did not materialize also must be addressed, as well as the different reasons for that;
5. Determine which risk management measures were effective and determine those that were ineffective;
6. Determine all potential sources of bias and uncertainties.

3 Common Methodologies for Risk Analysis and Assessment

As stated earlier, a key activity in the risk analysis and assessment is to develop and/or adapt methodologies and tools to assess risks to health, safety and environment. That assessment would help to guide the development of monitoring tools that will enable in early detection and remediation. As geological storage of CO_2 is a relatively new research area, new methods are being proposed to perform risk analysis and assessments and there is no well – established method for this purpose [10].

The methodologies developed for CO_2 long-term storage risk assessments are essentially based on the determination of the storage formation potential for retaining CO_2 overtime and, therefore, attempt to determine the long term behaviour of CO_2 initially injected into the formation. These methodologies use systems analysis structured processes to organize and streamline the procedure leading to the definition of scenarios and reduce the role of subjective judgments in determine these. The development of a wide range of risks and the mechanisms that underlie them provides a good basis for a systematic assessment of the risks.

The Risk Analysis and Assessment Methodologies are generally classified into two groups: qualitative and quantitative. When there is a lack of data and/or specific knowledge, a qualitative risk assessment may be sufficiently effective. Among the most common qualitative methods are: Method of FEP (Features, Events and Processes) and scenarios [11], a systematic approach for identifying all relevant system elements from the point of view of its future evolution and subsequent identification of possible scenarios for the evolution thereof; Vulnerability Assessment Framework (VEF) [12], a regulatory and technical framework to systematically identify those conditions that could increase the potential for adverse impacts; and screening and ranking framework (SRF) developed to evaluate potential geologic carbon dioxide (CO_2) storage sites on the basis of health, safety and environmental (HSE) risks arising from possible CO_2 leakage [13].

Quantitative methods are used at a certain level of knowledge about the system under study, where the level of uncertainty is relatively low. Two main types of methods belong to this group: Deterministic Risk Assessment (DRA) [14] and Probabilistic Risk Assessment (PRA) [14, 15].

DRA provides an estimate of risk associated with a specific set of values of the parameters of the models. Therefore, it does not explicitly deal with uncertainty in parameter values. With respect to the values of the parameters used in the models,

the best estimate of each parameter has to be taken, performing a single or a few of execution of the model. Often conservative values of the parameters are used to lead to an overestimation of risks, but as the relationship between values and the risk does not have to be monotonous, this overestimation may not be valid or unusable from the point of view of risk management. DRA allows the use of more detailed calculation models. The calculation time may be longer because it does not require a very large number of executions. On the other hand, this also means that both temporal and spatial discretization can be thinner.

Deterministic assessments can also be applied only to a particular aspect of the system, using more sophisticated and detailed partial models. These aspects will be addressed throughout the entire process of assessment of CO_2 storage with more or less detailed models. Sometimes these studies are called Performance Assessment [16].

As mentioned above, uncertainties are not treated in the deterministic risk assessment. However, it is a useful approximation to determine trends and to learn about the behaviour of the system due to the individual variation of the parameters. When the input parameters are well known, DRA gives very precise and accurate results.

PRA provides a probability distribution of the risk connected with the uncertainty in all or some of the values of the parameters. Usually it is associated with the use of Monte Carlo methods where probability density functions are used to describe the possible range of variation in the parameters of the model describing the system. Multiple simulations are performed, each with a set of parameter values that are randomly selected from the probability distribution functions. The result is, in turn, a probability distribution function that evaluates the risk and the uncertainty of the model parameters. Lately alternative methodologies are being developed based on Bayesian [17, 18] or intervals [19] statistics.

Something important in assessing long-term risks of geological storage of CO_2 and related to uncertainty is the identification of the possible scenarios of system evolution. The methodology for developing scenarios is the procedure for identification and description of those that could influence the behaviour of the geological storage during the evaluation period. The need to perform a scenario development in behaviour and risk assessments arises from the fact that it is virtually impossible to accurately predict the evolution of the system over a long period. The scenario development phase aims to achieve a set of scenarios that describe the behaviour of the system overtime to provide a reasonably complete picture of the evolutionary paths of the system. These scenarios broadly define the context to perform the steps of modelling and the analysis of consequences. This is because the potential long-term behaviour in the geological environment should be assessed and the possible migration pathways and mechanisms should be defined. And all this depends on the scenario under consideration [20].

Among the systematic methodologies for developing scenarios, the scenario analysis approach, which includes analysis of FEP, can be mentioned. It was successfully applied in the field of radioactive waste disposal to assess the problem of long-term behaviour of radioactive waste in the geological environment [21]. In

addition it is the approach taken, for example, in the Weyburn Project in the part of performance evaluation and safety of the geological storage of CO_2 [22].

Each scenario may be considered a set of FEP and their interactions. The scenarios in turn are the starting points for the selection and development of physical–mathematical models. Details of the resolution of the various storage components of a model can vary significantly depending on the primary objectives of the evaluation, and the treatment of the uncertainties. The main disadvantages of this method are that it requires a lot of specific information of the site under consideration and that consumes a significant amount of resolution time.

A significant amount of information, much of it from the expert judgment (EJ) should be used. Therefore it is important that the methodology includes a plan of documentation designed to collect all the process and the justification for the performed scenarios selection, always looking for a maximization of traceability and transparency.

In this context, the generation of databases of international FEPs have proved a valuable asset in the field of radioactive waste storage as well as a useful tool for auditing lists of FEPs. In the framework of the European programs and in regard with the Weyburn research projects, QUINTESSA [23] developed a database of generic FEP for CCS, which includes the FEPs related to long-term safety and storage behaviour after CO_2 injection and sealing of injection wells. In this database the FEPs associated with the injection phase that may affect the long-term behaviour of the geological storage are included. This database was inspired on the FEP database NEA/OECD [24]. Currently it includes about 200 FEPs sorted into categories, with their description, references, links to other databases, etc., and has the potential to serve as a "knowledge base" for the geological storage of CO_2.

The most important applications of the FEPs analysis and scenarios are [24]:

- Encouraging extensive discussions among members of the evaluation team and independent experts during the identification of relevant FEPs.
- Providing a source of information that can be used for the development activities of scenarios and models.
- Providing a framework to store information about FEPs and whether or not they are included in the evaluation models.
- Operating as a tool to audit the models used in the evaluation to ensure that all relevant processes are included, or help in specifying the future needs in developing models or data acquisition.

The various options that have been presented above are not the only ones that have been used in the field of CO_2 capture and storage [10].

Therefore, quantitative techniques can be subsumed under the DRA or PRA headings, although they may differ in the simulation codes used and/or in the stochastic approach. In the same way, there is a wide range of qualitative techniques that systematize information from EJ and that focus on different aspects of risk management (stakeholder communication, conceptual framework for regulators, hazard identification, evaluation of alternatives in multiple objective, etc.). Thus, in the initial stages, where qualitative methods are most suitable, it will be necessary

to take into account the objectives pursued in the project to choose the methodology that best suits them.

4 Application of Methodologies to the Hontomín Technological Development Plant

One aspect to consider within the *Compostilla* (OXYCFB300) project was the construction of the facilities of a CO_2 storage pilot plant. For this, the first phase required the identification and initial selection of geological formations accomplishing certain requirements of suitability, among which highlights the fulfilment of the safety, health and environment criteria during the storage time [25].

The first step for evaluating the long-term safety related to the geological storage of CO_2 was conducted during the site selection process. Specific research [5] was required since no enough detailed information for the site to make an analysis of scenarios and assigning probabilities in order to perform a probabilistic analysis was available.

A method of selection and classification of formations (SCF) which evaluates the potential of possible geological storage of CO_2 was used for the first stage. The method is based on the analysis of risks to health, safety and environment (HSE) derived from potential CO_2 leaks [26].

The methodology is designed in such a way so that it can be applied at sites with limited data. The necessary data of general character are mainly based on the expert opinion and will be a function of the degree of characterization available for sites.

The methodology considers uncertainty as input and output values of the same, because of the fact that a lack of data is an expected condition in most processes of site selection, especially in the early stages. The overall uncertainty in this context is broadly defined and includes both uncertainty in the parameters (e.g., the degree of knowledge of a particular property) and variability (e.g., the degree of variability that has a certain property). The overall uncertainty reflects the confidence of the evaluator wherein the site characteristics are well known. Therefore, the methodology enables in comparing the sites, taking into account both the HSE risk expectation and the estimation of the level of knowledge of the risk.

4.1 Areas of Study and Results

The methodology described above was applied to three location areas as potential sites for the pilot plant named *Huérmeces*, *Huidobro* and *Leva*. These areas are located in the western part of the so-called "Cantabrian Basin" and the regional scheme of the study area can be seen in Fig. 1.

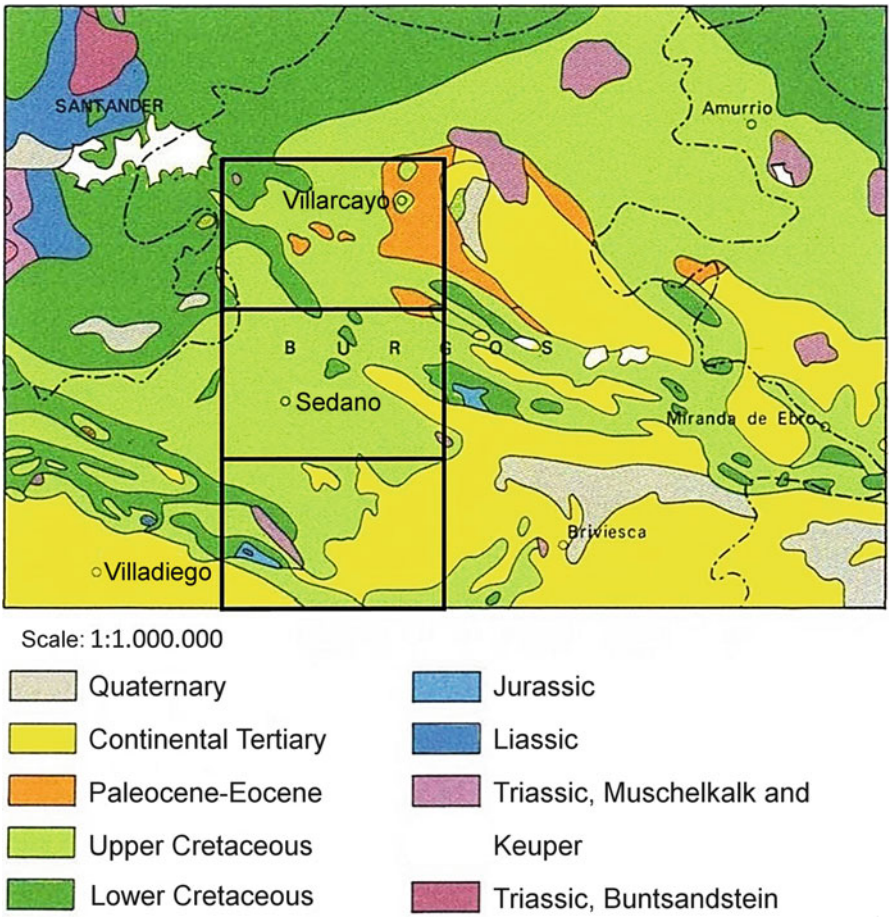

Fig. 1 Regional localization of the three areas studied (*Leva* (*up*), *Huidobro* (*middle*), *Huérmeces* (*down*) (Modified from Ref. [27])

The main benefit of the applied methodology is that it formally expresses knowledge and uncertainties associated with the assessment, which in future iterations could be reviewed and modified if new data becomes available. The system supports a wide degree of versatility, allowing the evaluator to assign different weights depending on the relative importance for the risk of the properties defined for evaluation. Since this would make the direct comparison among areas much more complex, therefore in the present work, weights assigned to the various properties were considered to be the same for all locations under study. However, the transparency of the system and its simplicity allows any reviewer to alter the assigned weights and further analyses to compare the effects of these changes on the response of the site.

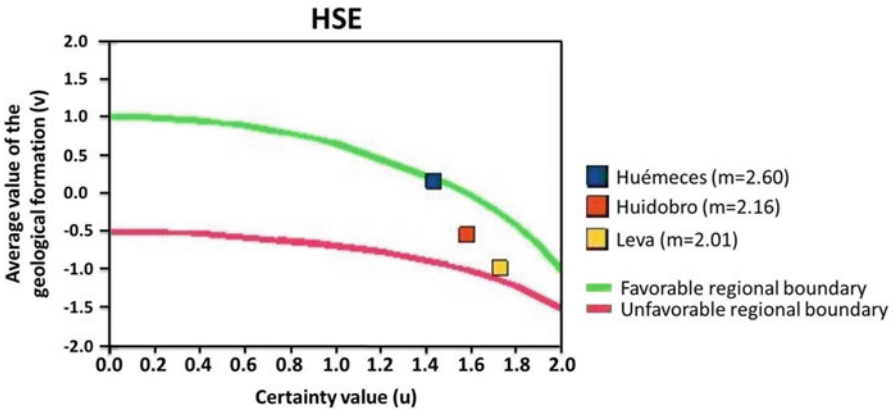

Fig. 2 Final evaluation of study areas

The methodology has allowed establishing an order that quantifies the relative suitability of a potential pilot site for CO_2 injection with respect to the other candidates. A summary of the results of the methodology applied to the locations is illustrated in Fig. 2. Of the three areas studied, *Huérmeces* is the one with the best results in the relative evaluation of the considered characteristics, with an average magnitude for the formation of 2.60 (the magnitude is the distance between the point and the origin), mainly associated with the certainty in the knowledge of the properties of the formation, since the magnitude of its "average value of the formation" evaluator index is only slightly positive (0.17). The other two formations share a high level of certainty, although mean values in both of them are negative ones (*Huidobro*,-0.54; *Leva*,-0.97) and therefore are at an evident disadvantage as compared to the former one as potential sites for an injection pilot plant. Table 1 shows the final assessment of the areas and the summary of the results is expressed.

The storage formation probably better qualified in the area of *Huérmeces* (*Hontomín* Anticline sector) is the Clastic Lias Unit, a limestone level inter bedded with limestone and dolomite levels, 114, 92 and 62 m thick at boreholes *Hontomín*-1, *Hontomín*-2 and *Hontomín*-3, respectively, to which is attributed a medium permeability value and constitutes a deep saline aquifer at hydrostatic pressure with a slow flux. In the borehole *Hontomín*-3, the storage formation is situated between 1238 and 1300 m depth, and the existence of a fault at a depth of 1259 m that causes total temporary loss of drilling fluid has been identified, which could compromise the tightness of it.

So, the finally selected site called *Hontomín* offers the following strong points:

- Primary containment: includes the storage level and the primary seal, expressing the target formation having a potential to contain CO_2 in the long term. An average attributes value of 0.67 in a range of 2.00 (excellent)/−2.00 (inadvisable) is obtained, which puts it above the "good performance" curve, with an

Table 1 Summary of the main results

	Prim. Cont.		Sec. Cont.		Atten. Pot.		Formation		
	Value	Cert.*	Value	Cert.*	Value	Cert.*	Value	Cert.*	Magnitude
Huermeces	0.67	1.84	0.18	1.12	−0.35	1.34	0.17	1.43	2.60
Huidobro	0.50	1.47	−2.00	2.00	−0.11	1.28	−0.54	1.58	2.16
Leva	−0.82	1.78	−2.00	2.00	−0.10	1.40	−0.97	1.73	2.01

*Cert. – certainty degree

average certainty degree of 1.84 out of a maximum 2.00, based on the borehole data at a reasonably well known level.

- Secondary containment: expresses the potential of an additional containment in case of leakage in the target formation. It is rated with an average of attributes of 0.18, slightly below the "good performance" curve, with an average certainty degree of 1.12.
- Potential of attenuation: expresses the ability of the site, including the overburden above the secondary seal, to mitigate or disperse any eventual leakage of CO_2 in the case of successive failure of the primary and secondary containment (multiple barrier concept). The resulting valuation is low, with an average value of -0.35, above the trace of the "unfavourable behaviour" curve, being -2.00 for an inadvisable site, and with a certainty degree of 1.34 on 2.00.

4.2 Risk Assessment Through a Methodology Based on Bayesian Networks

To advance in the risk assessment of the site selected in the previous phase, a methodology based on Bayesian networks (BN) has been developed [17]. The Bayesian point of view provides tools to cope with the resolution of problems in complex systems that require quantifying uncertainty by estimating a probability. It interprets probability as a measure of subjective belief as long as the axioms of probability are not violated and is accompanied by the Bayes Theorem as an updating rule of probability values as a function of new observations.

The Bayesian point of view allows a combination of quantitative probabilistic data from, for example, calculation models and/or databases, with qualitative estimates of probability coming from, for example, a EJ This allows a transition from some initial qualitative models to final quantitative models going through intermediate steps combining both types of probability estimates.

The development of models based on BNs for a description of these systems is not an easy task. However, it represents an attractive tool of making connections between different elements, because of the simplicity of its maintenance and because it allows taking decisions under uncertainty. Furthermore, this methodology given its conceptual development, allows the realization of fundamental activities in risk analysis of any CO_2 geological storage project, such as mathematical analysis (areas of maximum and minimum variation, zones of stability, etc.) or sensitivity analysis to estimate both the impact of different variables on the uncertainties of the system, and the level of uncertainty of different conceptual models, fundamental questions for the treatment of these uncertainties.

The application of this methodology for estimating the probability of risk of leakage in an GCS means modelling of a complex system, as illustrated in Fig. 3, where the global dependency graph between risk variables from an GCS are shown.

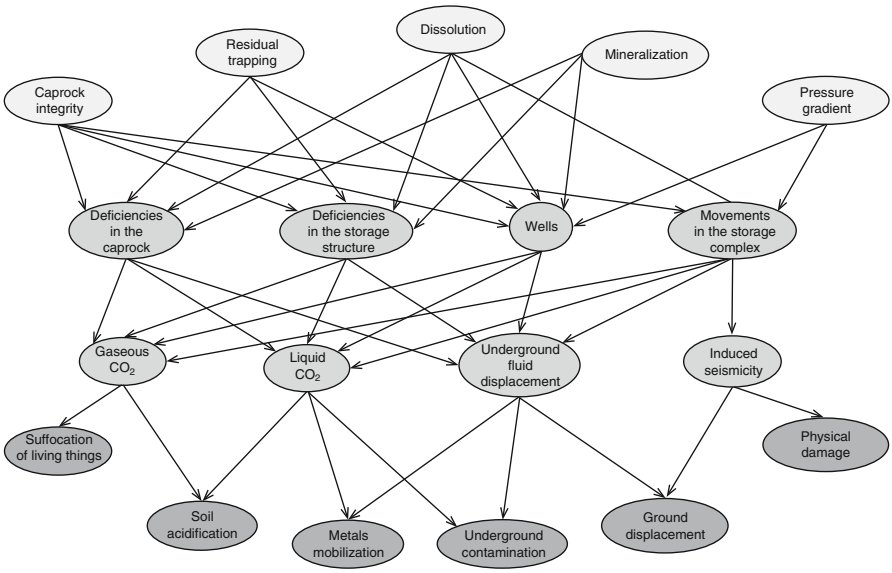

Fig. 3 Global dependency graph between risk variables derived from geological storage of CO_2

This BN model is oriented towards estimating the probability of system leakage. Its application in the early stages of the project implies that there will be a significant shortage of data. To overcome this situation, the model must be supplied with qualitative information, for example, from EJ to assess the initial conditions and offering the best answer.

This initial state of the assessment problem must be overcome gradually depending on the progress of the characterization studies and generation of modelling based on a gradual replacement of qualitative estimates by physical/chemical-mathematical models.

4.2.1 Implementation and Results

The model was applied to the *Huérmeces* area to be tested. Previously this area was the subject of an assessment of Selection and Classification of Formations (SCF) type, based on the analysis of possible CO_2 leakage resulting from the HSE methodology [26] and discussed above.

To this end, the proposed methodology applies the same criteria as in SCF. Thus the qualitative probability was coded on a scale from "0" (CO_2 leakage probability equal to 1) to "4" (no chance of leaking CO_2); and the degree of certainty was coded from "0" (weakly assumption based on objective data) to "2" (accurate measurement). This was because it is considered that including more levels only brings greater subjectivity to the evaluation given the level of information available. For

practical purposes, it was decided to decouple the edaphic capacity of attenuation of potential leakages from the other sub-systems due to the lack of information thereof.

The model identifies CO_2 leakage scenarios, prepared from [28–30]. Namely:

- CO_2 leakage through wells.
- CO_2 leakage due to the fracturing of the caprock by over-pressurization.
- CO_2 leakage through the pore system of the caprock, either by overpressure or by the presence of an undetected zone of high permeability.
- CO_2 leakage through a fault.
- Brine migration from the geological formation.

It should be noted that there are significant differences between the two methodologies. The SCF methodology provides relative comparisons between sites but does not include relations between parameters, simulations or assignment of probabilities. It makes impossible to carry out quantitative safety assessments.

Figure 4 shows an example of a BN from the probability model risk of leakage in geological storage of CO_2 applied to the *Huérmeces* study area. It was applied a colour code to display quickly the system information that is known and the influence of different variables (listed in the Table 2) on the estimated probability of the leakage risk value:

- Red indicates that the value of the probability of risk of leakage of the generic variable Vi is greater than 0.5. That is: $P(Vi) > 0.5$. The value of this variable may have been initially provided by the method of EJ in the case of a "root" variable, or it may have been derived from the application of the BN inference rules for the variables other than the root ones.
- In a similar way, the green colour indicates that $P(Vi) < 0.5$
- Finally, the blue colour indicates that $P(Vi) = 0.5$. This value is justified by the lack of information on this root node generic variable Vi. In the event that a variable Vi satisfies exactly that $P(Vi) = 0.5$, either derived from the application of EJ or by applying the BN rules of inference, the chosen colour was red.

Given the colour code it is easy to distinguish the variables that provide information to the model. Since this methodology takes into account uncertainties, the value of the estimation is given as a range of values, between an upper and a lower one. An approximate figure of 80 % is achieved in the BN that determines the upper range. And about two thirds of them provide information for CO_2 leakage. Such information should be supplemented by sensitivity analyses that indicate the relative importance of each of the variables in the contribution to the total uncertainty of the system, which is influenced by both the value itself as the network position of the variable and its associated dependencies.

For the study area, the estimated qualitative probability range of leakage risk is between 0.33 and 0.66, expressed in arbitrary units (au), with an associated dispersion value of the results of $d = 0.65$ (see Fig. 5). Given the conditions set out above, after eliminating the influence of the model variables related to the edaphic capacity

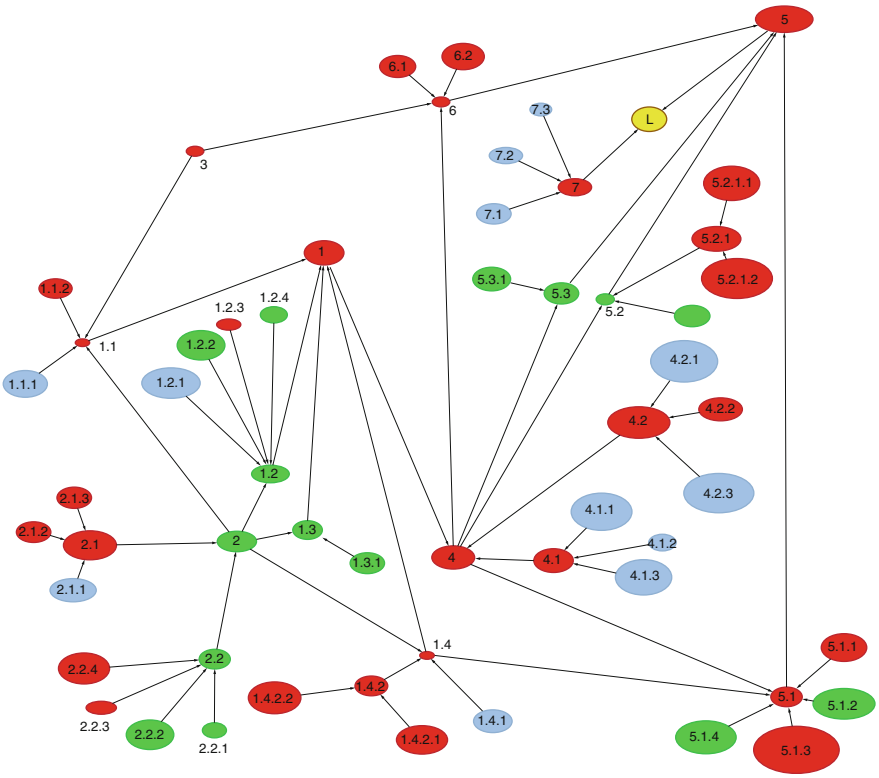

Fig. 4 Example of a Bayesian network from the leakage probability model risk in CO_2 geological storage applied to the Huérmeces study area

of attenuation of potential leakages, the probability range obtained is p∈ [0.41 − 0056] au, with a value of d = 0.31.

Comparing these results with those obtained in the evaluation of the same area using the methodology SCF [31] is consistent. Both methodologies conclude that the study area is qualified as an intermediate level of goodness for the geological storage of CO_2. Also similar resulting values are obtained in regard to the estimation of uncertainties.

To introduce statistical calculations, the model has been implemented in GoldSim [32] high-level programming language for the resolution of complex dynamic systems. This implementation allows to obtain the qualitative functions of probability (density or cumulative) of the storage subsystem (or primary), its convolution with the secondary containment subsystem (or secondary), and the probability function of the edaphic dispersion subsystem decoupled from previous ones. From these functions the estimation of the qualitative probability of global leakage risk is obtained. This is shown in Fig. 6.

Table 2 List of Fig. 4 codes

1 – Leakage in the primary containment system	1.1 – Geological fault in primary containment	1.1.1 – Presence of tectonic fault	
		1.1.2 – Permeability of the geological fault	
	1.2 – Caprock	1.2.1 – Injectivity of the storage geological formation	
		1.2.2 – Demonstrated sealing	
		1.2.3 – Thickness	
		1.2.4 – Permeability	
	1.3 – Structural leakage	1.3.1 – Lateral continuity	
	1.4 – Wells	1.4.1 – Number of active wells	
		1.4.2 – Abandoned wells	1.4.2.1 – Number of Abandoned wells
			1.4.2.2 – Permeability
2 – Extent of the CO_2 plume	2.1 – Geological environment conditions	2.1.1 – Geothermal gradient	
		2.1.2 – Hydrology	
		2.1.3 – Pressure gradient	
	2.2 – Storage geological formation	2.2.1 – Depth	
		2.2.2 – Porosity	
		2.2.3 – Pore fluid	
		2.2.4 – Permeability	
3 – Tectonics			
4 – Extent of the CO_2 plume in the secondary containment	4.1 – Permeable geological formations	4.1.1 – Permeability	
		4.1.2 – Pore fluid	
		4.1.3 – Porosity	
	4.2 – conditions of the geological environment	4.2.1 – Geothermal gradient	
		4.2.2 – Pressure gradient	
		4.2.3 – Hydrology	
5 – Leakage in secondary containment	5.1 – Seal geological formation	5.1.1 – Thickness	
		5.1.2 – Depth	

(continued)

Table 2 (continued)

		5.1.3 – Demonstrated sealing	
		5.1.4 – Permeability	
	5.2 – Wells	5.2.1 – Abandoned shallow wells	5.2.1.1 – Number of abandoned shallow wells
			5.2.1.2 – Permeability
		5.2.2 – Number of active wells	
	5.3 – Structural cause leakage	5.3.1 – Lateral continuity	
6 – Secondary containment fault	6.1 – Permeability		
	6.2 – Tectonic fault		
7 – Soil dispersion	7.1 – Permeability		
	7.2 – Thickness		
	7.3 – Landuse		
L-Leakage			

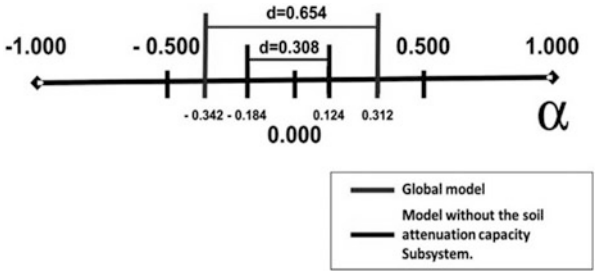

Fig. 5 Graphical representation of the results (range and dispersion) of qualitative probability estimation of risk of leakage of CO_2 in the *Huérmeces* study area for geological storage of CO_2, applied to the global system as well as the storage and secondary containment subsystems

The simplified results of the partial sensitivity analysis developed are reflected in Fig. 7. This is a partial analysis given that the influence of edaphic dispersion subsystem is not taken into account. Comparing the importance of the input parameters on the results leads to the conclusion in a clear manner about the domain of the secondary subsystem in contributing to the system uncertainty. This in turn leads to the conclusion about the importance of improving knowledge of this part of the system in order to reduce the uncertainties associated with these estimates.

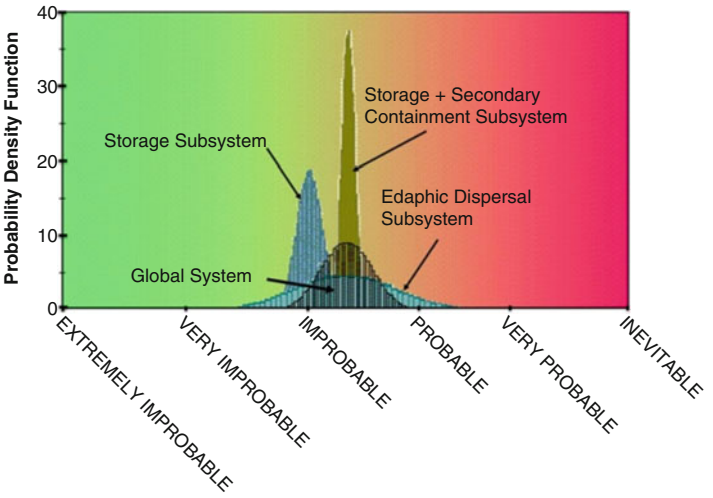

Fig. 6 Qualitative density probability functions from the stochastic model of leakage risk by applying to the Huérmeces study site

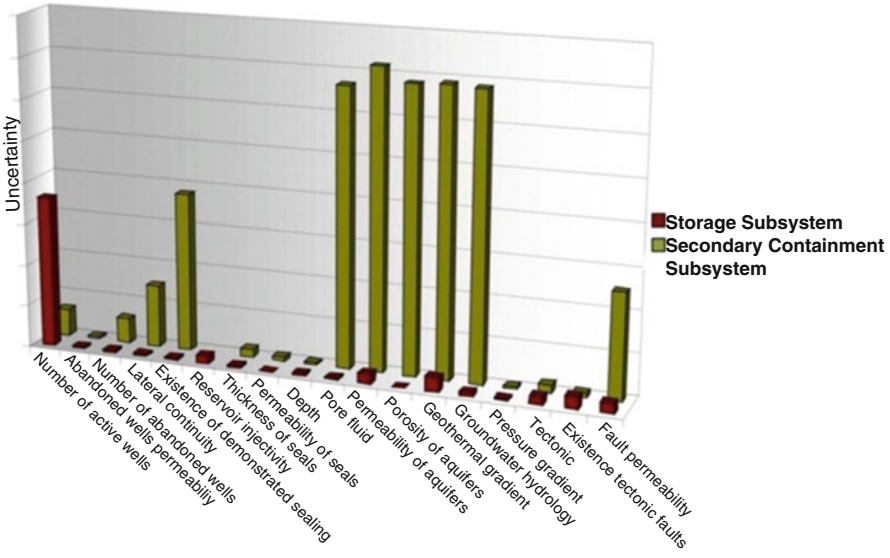

Fig. 7 Partial sensitivity analysis from the qualitative probability of leakage risk applied to the Huérmeces study site

5 Conclusions

The intention of this paper has been to show that it is possible to provide new information with a dimension of risk management from existing data, by selecting and developing appropriate methodologies, from the early stages of the project and under the current terms offered by this technology of CO_2 geological storage.

The safety analysis and risk assessment, based on appropriate methodologies should be able to assess the risk associated with geological storage of CO_2. All the approaches provide valuable elements. The choice of the appropriate methodology depends on the state of the project, the available data and objectives. Taking into account the above, it has been necessary to reflect, learn and consider the positive aspects of each approach and its limitations to get the best part out of the various approaches to the task of risk control. In our opinion a key issue in the development of such projects is that whatever the main risk assessment methodology is applied, it is necessary to include an assessment of the uncertainties associated with the process in order to facilitate the subsequent decision making.

One of the major constraints to overcome to the development of the studies, as we have reported here, is that there is currently no standardized method or combination of methods to assess the risk for these projects. This is in spite of the fact that since the capture and storage of CO_2 was proposed as a mitigation option to reduce anthropogenic emissions of CO_2 there have been many attempts to study potential long-term risks of CO_2 storage in geological formations and various projects worldwide have tried different industrial-like methods adapted to the geological storage of CO_2.

The lacks of data, especially in the early stages, and the level of uncertainty associated with project development have made it impossible for us the application or adaptation of quantitative risk assessment methods from industrial methods. It can be concluded that these methodological approaches are not a convenient starting point in the current development of these projects. Therefore it has been necessary to develop both a specific framework and a qualitative method that allows for a gradual introduction of quantitative methods from qualitative data as the most appropriate methodological approach suitable for ongoing projects.

References

1. Bachu S (2008) CO_2 storage in geological media: role means, status and barriers to deployment. Prog Energy Combust Sci 34:254–273
2. AIST Japan (2007) Building confidence in geological storage of carbon dioxide, s.l.: IEA Greenhouse Gas R&D Programme
3. European Communities (2011) Implementation of directive 2009/31/EC on the geological storage of carbon dioxide. Guidance document 1: CO_2 storage life cycle risk management framework. ISBN-13978-92-79-19833-5. s.l.:s.n
4. Commission for the European Communities (2009) Directive of the European parliament and of the council on the geological storage of carbon dioxide and amending Council Directive

85/337/EEC, Directives 2000/60/EC, 2001/80/EC, 2004/35/EC, 2006/12/EC, 2008/1/EC and Regulation (EC) No 1013/2006. s.l.:s.n
5. van Egmond B (2006) Developing a method to screen and rank geological CO_2 storage sites on the risk of leakage, s.l.: Copernicus Institute, Department of Science, Technology and Society. NWS-E-2006-108
6. Pérez M (1988) Razonamiento probabilístico y correlacional: influencia de teorías previas y de datos. s.l.:Tesis doctoral. Dpto. de Psicología Básica, Social y Metodología. Facultad de Psicología. Universidad Autónoma de Madrid
7. Slovic P, Fischhoff B (1977) On the psychology of experimental surprises. J Exp Psychol Hum Percept Perform 3(4):544–551
8. Intergovernmental Panel on Climate Change (IPCC) (2005) IPCC special report on carbon dioxide capture and storage, s.l. Cambridge University Press, New York
9. IEA Greenhouse Gas R&D Programme (IEA GHG) (2009) A review of the international state of the art in risk assessment guidelines and proposed terminology for use in CO_2 geological storage, Report Number: 2009/TR7, s.l.: IEA Environmental Projects Ltd. (IEA Greenhouse Gas R&D Programme)
10. Condor J, Unatrakarn D, Wilson M, Asghari K (2011) A comparative analysis of risk assessment methodologies for the geologic storage of carbon dioxide. Energy Procedia 4:4036–4043
11. Wildenborg AFB et al (2005) Risk assessment methodology for CO2 storage: the scenario approach. In: Benson SM (ed) Carbon dioxide capture for storage in deep geologic formations. Elsevier, London, pp 1293–1316. ISBN 9780080445700
12. U.S. Environmental Protection Agency (2008) Vulnerability evaluation framework for geologic sequestration of carbon dioxide, s.l.: Technical Support Document EPA430-R-08-009
13. Oldenburg C (2008) Screening and ranking framework for geologic CO_2 storage site selection on the basis of health, safety, and environmental risk. Environ Geol 54(8):1687–1694
14. Walton F, Tait J, LeNeveu D, Sheppard M (2004) Geological storage of CO_2: a statistical approach to assessing performance and risk. In: E.S.Rubin, D.W.Keith and C.F.Gilboy (Eds.) Proceedings of 7th international conference on Greenhouse gas control technologies, vol 1: peer-reviewed papers and plenary presentations. s.l.:IEA Greenhouse Gas Programme, Cheltenham, UK
15. Deel D et al (2007) Risk assessment and management for long-term storage of CO_2 in geologic formations – United States Department of Energy R&D. Syst Cybern inform 5(1):79–84
16. Metcalfe R et al (2009) A unified approach to Performance Assessment (PA) of geological CO_2 storage. Energy Procedia 1(1):2503–2510
17. Hurtado A, Eguilior S, Recreo F (2014) Methodological development of a probabilistic model for CO_2 geological storage safety assessment. Int J Energy Environ Eng 5:84
18. Gerstenberger M, Christophersen A, Buxton R, Nicol A (2015) Bi-directional risk assessment in carbon capture and storage with Bayesian Networks. Int J Greenhouse Gas Control 35:150–159
19. Rozell D, Reaven S (2012) Water pollution risk associated with natural gas extraction from the Marcellus Shale. Risk Anal 32(8):1382–1393
20. Bouc O et al (2010) CO_2 geological storage safety assessment: methodological development. In: 10th international probabilistic safety assessment & management conference, Seattle
21. SKI (1996) SKI Site-94: deep repository performance assessment project, s.l.: Swedish Nuclear Power Inspectorate, Stockholm, Sweden. SKI Report SKI 96:36
22. Stenhouse M (2001) Application of systems analysis to the long-term storage of CO_2 in the Weyburn reservoir. Monitor Scientific Report MSCI-2025-1, Denver, Colorado, USA: Monitor Scientific LLC
23. Savage D, Maul R, Benbow S, Walke R (2004) A generic FEP database for the assessment of long-term performance and safety of the geological storage of CO_2. QRS-1060A, s.l.: Quintessa

24. NEA/OECD (2000) Features, Events and Processes (FEPs) for geologic disposal of radioactive waste – an international database, NEA-OECD Report NEA 02549. Nuclear Energy Agency – Organization for Economic Cooperation and Development, Paris
25. Chadwick A et al (2007) Best practice for the storage of CO_2 in saline aquifers – observations and guidelines from the SACS and CO2STORE projects. British Geological Survey, Nottingham
26. Oldenburg C (2005) Health, safety, and environmental screening and ranking framework for geologic CO_2 storage site selection". LBNL 58873, s.l.: s.n
27. del Olmo Zamora P et al (1979) Mapa y Memoria explicativa de la Hoja 109 (Villarcayo) del Mapa Geológico de España a escala 1:50.000 (Segunda serie), Primera edición, Madrid, Spain: IGME
28. Bouc O, Fabriol H (2007) Towards a methodology to define safety criteria for CO_2 geological storage. Pittsburgh, Pennsylvania, sixth annual conference on carbon capture & sequestration
29. Bouc O et al (2009) Determining safety criteria for CO_2 geological storage. Energy Procedia 1 (1)
30. Stauffer P et al (2006) CO2-PENS: a CO_2 sequestration system model supporting risk-based decisión. CMWR XVI, Copenhagen
31. Hurtado A et al (2010) Aplicación de una evaluación preliminar de la seguridad y de los riesgos HSE a las potenciales ubicaciones de una planta piloto de almacenamiento geológico de CO_2. Fundacion CONAMA, Madrid
32. GoldSim Technology Group (2015) GoldSim: Monte Carlo Simulation Software. [Online] Available at: http://www.goldsim.com/

Biography of Editors and Authors

Editors

V. Vishal is an Assistant Professor in the Department of Earth Sciences, Indian Institute of Technology (IIT) Bombay, Mumbai, India. He worked in the Department of Earth Sciences, IIT Roorkee as DST Inspire Faculty and in the Department of Energy Resources Engineering, Stanford University (USA) as a Fulbright-Nehru Postdoctoral fellow during 2013–15. He obtained a Ph.D. degree jointly from IIT Bombay and Monash University (Australia). He is a recipient of the National Geosciences Award in the Young Researcher category by the Government of India, the Young Scientist Award by the Indian Science Congress Association, and Dr. Coggin Brown Memorial Award by the Mining, Geological and Metallurgical Institute of India. He holds to his credit a total of 42 publications on different domains of carbon sequestration, engineering geology, geomechanics, and unconventional petrophysics in various journals, book chapters and conference proceedings of repute. He is investigating three research projects funded by the Ministry of Science and Technology of the Govt. of India.

T.N. Singh is the Institute Geoscience Chair Professor in the Department of Earth Sciences, IIT Bombay, Mumbai, and is an expert in the field of rock mechanics, mining geology, and clean energy. He received his Ph.D. degree from the Institute of Technology BHU, Varanasi, in 1991 and subsequently served the institute until 2003. He is a recipient of many prestigious awards such as the National Mineral Award, the first P. N. Bose Mineral Award, the SEAGATE Excellence Award for Geo-Engineering, and the GSI Sesquicentennial Commemorative Award. He has nearly 28 years of experience in research and teaching with 16 doctoral theses completed under his supervision and has authored more than 350 publications in various journals and conferences of national and international repute. He is currently leading projects of immense scientific and industrial importance related to

V. Vishal, T.N. Singh (eds.), *Geologic Carbon Sequestration*,
DOI 10.1007/978-3-319-27019-7

coalbed methane, carbon sequestration, shale gas, nuclear waste repositories, and mine slope stability, to name a few. He is on the governing and advisory councils of several national institutes and universities.

Authors

Mario Anselmi graduated in earth sciences at the University of Rome "La Sapienza" in 2004. He completed a Ph.D. in earth sciences at the University of Rome "La Sapienza" in 2008. Currently he is a temporary Researcher at the INGV and his research focuses on i) seismic imaging of crust and active faults by P-waves tomography, ii) earthquake location (absolute and relative techniques), iii) seismic signal analysis of the crustal natural and induced seismicity, and iv) design and development of passive seismic experiments.

M.A. Atmanand is currently the Director of ESSO-NIOT and Project Director of Integrated Coastal and Marine Area Management, and has done pioneering work in the area of deep-sea technologies in India. An instrumentation and control engineer by profession, he obtained his Ph.D. from Indian Institute of Technology, Madras. His areas of interest include development of underwater vehicles with specific reference to their control, development of components for deep-sea applications, and development of test protocols for testing of deep-sea devices and project management. It was under his supervision that the design of electrical, instrumentation, and control system of the India's first remotely operable vehicle was done. He has also guided various indigenization programs for ocean observation and under water systems. He has published 65 papers in international journals, international conference, national conferences, and others. He received the National Geoscience Award 2010 from the Ministry of Mines and the International Society for Offshore and Polar Engineers (ISOPE) Ocean Mining Symposium Award in the year 2009. He is a Member of various professional bodies and has served in various capacities in professional organizations and research institutes.

Per E.S. Bergmo (M.Sc.) is presently a Research Scientist at SINTEF Petroleum Research. His main fields of competence are laboratory and field scale reservoir simulations including EOR/IOR, history matching, field development planning, and CO_2 injection/deposition. He has been involved in numerous CO_2 storage-related projects, including the EU projects: SACS (Saline Aquifer CO_2 Storage), CO2Store, CO_2ReMoVe, ECCO, and SiteChar doing field-scale model building and simulations. He is an experienced Reservoir Engineer and has laboratory experience including swelling of oil with CO_2 and CO_2-rich gases.

Antonio Hurtado Bezos has a Ph.D. in mining engineering and is a Scientist at the CIEMAT and has over 15 years of experience in risk management and assessment in both the industrial sector and scientific research in the area of the geological environment altered by human activity. He is currently working on the development

of methodologies for risk assessment of geological sites for both CO_2 geological storage and unconventional hydrocarbon exploitation and previously in the selection, characterization, capacity estimation, and determination of uncertainties associated with geological storage of CO_2.

Mauro Buttinelli completed a Ph.D. in 2012 with a thesis in 3D modeling of geological structures applied to CO_2 storage and seismological analysis via receiver functions. He has largely experienced in management and 2D/3D interpretation of underground data (seismic profiles, well logs), deployment of seismological stations networks, and related data analysis. His field of interest include oil and gas exploration, induced seismicity, fluids extraction and injection, geothermics, tectonophysics, seismotectonics, seismic hazard, impact of human activities to the underground resource exploitation in the light of environment protection, and geoethics. He is the author of more than ten scientific publications and 25 meeting contributions on these topics.

Barbara Cantucci is a permanent Researcher at INGV since 2010. She has completed her Ph.D. in 2007 at the University of Florence. Her research activity is focused on 1) fluid geochemistry and geochemical modeling of water-rock interaction, 2) reactive transport simulations related to CO_2 geological storage, and 3) multidisciplinary analysis for the characterization of geological reservoirs suitable for gas (CO_2 and CH_4) geological storage. She is the author of several scientific publications related to the fluid geochemistry, fluid geological storage, and energy use planning. She is the Reviewer for several international journals such as Geology, Energy Conversion and Management, and Applied Geochemistry.

Pablo García del Real is currently (or will be a Ph.D. in a few months) a student in the Department of Geological Sciences at Stanford University. He focuses his studies on the genesis of massive magnesite deposits and hydrous magnesium carbonates in serpentinized peridotite rocks in California. He applies thermodynamics, isotope geochemistry, and structural geology to study these natural analogues of mineral carbonation in ultramafic rocks. He completed his BSc. in geological and environmental sciences also at Stanford University in 2009.

G. Dharani has a Ph.D. in zoology from the University of Madras, Chennai, India, and is currently working as a Scientist E in Marine Biotechnology Department of ESSO-NIOT. He is a PADI-Certified Instructor for diving operations. His research interests are mariculture, marine ecology, and biochemistry. He has publications in national and international journals and conferences.

S. Eguilior has a Ph.D. in physics. She is a Scientist working in the CIEMAT, with more than 15 years of experience, where has worked in the areas of safety and risk assessment and the development of transport models in an inhomogeneous medium under advective-diffusive processes. Currently her main line of work is the

development of global models for the evaluation of risks associated with the geological storage of CO_2 and uncertainty treatment associated with long-term risks.

Javier Elío works in the research areas of geochemistry and environmental risk assessment, with a particular focus on carbon capture and storage. His Ph.D. thesis was oriented to detect and quantify possible CO_2 leakages to the atmosphere. Alongside the experimental measurements, the methodology for soil-gas monitoring at the Technological Development Plant for CO_2 injection at Hontomín (Spain) was proposed. Since 2009 he has published seven peer-reviewed journal articles (three as a first author) and 23 works at international and national conferences, including AGU, EGU, EAGE, IGC, and Goldschmidt.

Benjamin U. Emmel holds a position as a Researcher at SINTEF Petroleum Research. He has a diploma in geology/paleontology and a doctoral degree from the University of Bremen (Germany). He was employed as a Postdoctoral Researcher at the universities in Bremen and Bergen (Norway). His major expertise are geodynamics, tectonics, structural geology, and basin modeling.

Amin Ettehadtavakkol is an Assistant Professor at Bob L. Herd Department of Petroleum Engineering at Texas Tech University. His main research interests are unconventional reservoir modeling, oil field development optimization, CO_2-EOR and storage, reservoir simulation, and uncertainty analysis. He holds two BS degrees in petroleum engineering and industrial engineering from Sharif University, Tehran, Iran, and MS and PhD degrees in petroleum engineering from the University of Texas at Austin.

Wojciech Franus is a graduate of geology at the Faculty of Geology, Geophysics and Environmental Protection AGH–University of Science and Technology, with specialization in applied mineralogy. He works as a Professor at the Faculty of Civil Engineering and Architecture, Lublin University of Technology, Department of Geotechnics. His research scope is related to natural and synthetic zeolites in terms of their use in environment protection. He also investigated changes in reservoir and caprocks as a result of CO_2 injection into saline aquifers. He is the author of numerous scientific papers and has led and implemented several research projects.

Maria Jesus García-Martíinez has 34 scientific publications in national and international journals in different scientific fields being the most prominent and interesting related to analytical chemistry, characterization and bioremediation of fuel polluted soils, photodegradation of fuel polluted waters, and biofuels. In addition she has over 38 contributions to national and international conferences.

Nikhil Jain is a pre-final year engineering student, enrolled in integrated dual degree course, studying mining engineering at IIT (BHU) Varanasi. He has been pursuing dedicated research works in the field of shale gas and hydro fracturing at IIT's and CSIR laboratories. He has won IIT BHU Publication Awards for two

consecutive years (2012–2013) for record number of publication in undergraduate category from IIT BHU Global Alumni Association. He remained the N.C. Jain scholar during 2011–2015. He has authored or coauthored four conference papers, one book chapter, and one technical poster till date. His publications have been in varied fields of hydro fracturing, PEM fuel cells, and gas hydrates, but in recent his focus has been constant upon shale gas and fracture analysis in hydro fracturing.

Fernando Recreo Jiménez holds a degree in geology and hydrogeology. He has more than 30 years of experience in both nuclear safety of nuclear power stations sitting and nuclear waste repositories performance assessment. He is currently the Head of the Geological Storage Division of CIEMAT, Department of Environment, Member of Steering Committee of the EC projects PAGIS and EVEREST, and technical Leader for CIEMAT in EC projects BIOCLIM and PADAMOT.

Apoorv Jyoti completed his master thesis at the Department of Applied Geology, University of Göttingen, Germany, on modeling kinetic interface-sensitive tracers in CO_2-brine porous media systems.

Qi Li holds a BS in earth sciences with a diploma of minor program on computer science from Nanjing University, China (1995), and in 1998 he received an MS in hydrogeology and engineering geology from the same university. In 2004, he received a Ph.D. in civil engineering from Ibaraki University, Japan. Before joining the Institute of Rock and Soil Mechanics (IRSM), Chinese Academy of Sciences, he has been a Member of Geological Survey of Japan from 2005 to 2010. Dr. Li is now the Professor of CCUS and AGI research direction at IRSM.

Guizhen Liu graduated from China University of Geosciences and received a BE in environmental engineering in 2004 and an ME in groundwater science and engineering (2008). After graduating, Liu joined the IRSM, Chinese Academy of Sciences, and worked with Prof. Qi Li on risk assessment of CCUS.

Ane E. Lothe (PhD) is at present the Research Manager for the Basin Modelling Group at SINTEF Petroleum Research. Her background is from structural geology with special interest in deformation bands and faults in sedimentary basins. She is also interested in pressure modeling on basin scale for exploration and for drilling campaigns. For the last years she has been more involved in CO_2 storage-related projects like SACS, SiteChar, and NORDICCS with the main focus on the modeling part.

Luis F. Mazadiego has 90 scientific publications in national and international journals in different scientific fields being the most prominent and interest relating to the characterization of fractured media, measuring of radon activity in soil-gas (applied to petroleum exploration and hydrocarbon contamination in vadose zone), and, in recent years, characterization of sites for CO_2 storage including multi-criteria analysis of the viability of projects to capture and storage of CO_2. In

addition he has over 70 contributions to national and international conferences and courses or seminars for experts.

Gry Møl Mortensen has M.Sc. in geology from the University of Copenhagen, with special emphasis on sedimentology. Gry has a background in engineering geology, testing rocks for different characteristics in relation to crushing and screening processes. He is a Senior Geologist at the Geological Survey of Sweden since 2012 primarily working with CO_2 storage and the Swedish part of a Nordic storage atlas.

Sridhar Muddada holds a Ph.D. in Applied Mechanics from the Indian institute of Technology Madras and is currently working as a Scientist at the Ocean Structures Group of ESSO-NIOT. His research interests are active flow control, bluff body flows, and fluid structure interaction of intake pipes, wind turbine monopiles, etc.

K.N.V.V. Murthy received his master's degree in marine geology (2006–2008) from Andhra University, Visakhapatnam. He is currently working at ESSO-NIOT, Chennai, as a Project Scientist. His research interests include laboratory synthesis of gas hydrates, mineral carbonation of steel slag and fly ash, sedimentary environments, geomorphology, and heavy mineral estimation.

Takuya Nakashima graduated from the Dept. Systems Innovation (BEng) and Dept. Ocean Technol., Policy, and Environ. (M.Sc.), University of Tokyo. He is now working for Mitsubishi Research Institute, Inc. and carrying out researches mainly on climate change projection and adaptation process.

Barbara Nisi has experience in sampling and analytical techniques of fluid from different environments and in the management of different geochemical instrumentations such as kits for field analyses, chromatography, molecular and atomic absorption spectroscopy, mass spectrometry, and diffuse soil CO_2 measurements. Her research includes geochemical investigation in volcanic and geothermal fluids, monitoring protocols of pilot sites selected for CO_2 sequestration, and statistical treatments of diffuse soil gases. She is the author of about 60 scientific papers published in international and national journals and has attended more than 80 congress in Italy and abroad where oral and poster communications were presented.

Marcelo F. Ortega has experience in statistical simulation of environmental problems, in particular, the improvement of parameter estimation in both univariate and multivariate analyses as also in spatial statistical data analysis. He is the author of 13 scientific papers published in international journals indexed in Journal Citation Report and has attended more than 20 International congresses where oral and poster communications were presented.

Jack C. Pashin holds a Ph.D. in geology from the University of Kentucky. He worked at the Geological Survey of Alabama for 24 years, where he led the energy program. He joined the Faculty of Oklahoma State University in 2013. His research focuses on the characterization of hydrocarbon reservoirs and geologic carbon sinks. He has won many awards for his research on coal-bearing strata, including the Gilbert H. Cady Award of the Geological Society of America. Dr. Pashin serves on the editorial boards of the AAPG Bulletin and the International Journal of Coal Geology.

S.V.S. Phani Kumar has a Ph.D. in mechanical engineering from Tennessee Technological University, Cookeville, TN, USA. He is currently working as a Scientist-E in Ocean Structures Department of ESSO-NIOT. His research interests include fluid flow, heat transfer, desalination, and submarine riser systems. He has contributed to the system design, cold water pipe analysis, and process equipment for the island-based and barge-mounted low-temperature thermal desalination plants. He has published papers in international journals and national and international conferences.

Richa Shukla Potdar completed her Ph.D. in 2012 from Monash University, Australia. She is a specialist in geomechanics and carbon sequestration. She is currently employed in the role of Geotechnical Engineer at GHD Consultants - Melbourne and is an Hon. Research Associate with RMIT University, Australia. Dr. Richa is actively involved in carbon sequestration, mining, and tunneling research and has a proven record of accomplishment through industry and research projects and quality research publications in international journals.

Sarada Prasad Pradhan is an Assistant Professor in Indian Institute of Technology (IIT) Roorkee, India, in the Dept. of Earth Sciences. He obtained his M.Sc. (Applied Geology) and Ph.D. from IIT Bombay (India). He worked as a Reservoir Engineer in Oil and Natural Gas Corporation Ltd. (ONGC) for around five years where he was associated with many projects of national importance. He was awarded with the Young Scientist Award from CAFET INNOVA Technical Society and Asset Manager Award for his excellent performance in gas field development at ONGC Ltd. His research findings have been well received by the scientific community and published in leading national and international journals, book chapters, and conference proceedings. His major research interests are rock mechanics, engineering geology, reservoir geo-mechanics, petroleum geo-science, and carbon dioxide sequestration.

N. Thulasi Prasad received his bachelor degree in chemical engineering, S V University, Tirupati, and masters in petroleum exploration from Indian Institute of Technology Madras (IITM). He is currently working at ESSO-NIOT, Chennai, as a Project Scientist. His research interests are gas hydrates, reservoir modeling, and carbon sequestration studies.

Monia Procesi has completed her Ph.D. in 2010 at the University of Roma Tre. In 2012, she graduated at the Centre d– Hydrogéologie et de Géothermie at the University of Neuchatel (Switzerland), as part of the Course of Advanced Studies on Exploration & Development of Deep Geothermal Systems. Currently she is a temporary Researcher at the INGV and her research focus is on the characterization of potential areas suitable for fluids geological storage and geothermal energy. She is the author of several scientific publications related to the fluid geochemistry, geothermics, geological storage, and GIS mapping/modeling techniques.

S. Ramesh has a doctoral degree in marine geology from Madras University, Chennai, and is currently working as Scientist-E in Deepsea Technologies group of ESSO-NIOT. He has extensive experience in deep-sea mineral exploration, sedimentology, geochemistry, etc. His research interests are gas hydrates, carbon sequestration, geochemistry, mineral exploration with submersibles, etc. He has actively participated in several research cruises in Indian territorial waters and international waters. He has published many papers in national and international journals and conferences.

Sucheta Sadhu has a master's degree from IIEE, New Delhi, and M.Phil. from Jadavpur University, Kolkata, in environmental science and biotechnology. Currently she is a Project Assistant at ESSO-NIOT with experience in the area of microalgal biotechnology and environmental impact monitoring. She has been credited the award of "First Women Open Water Diver of NIOT" in 2011.

Toru Sato After graduating from UTokyo (BEng and MEng, Naval Architecture) and Imperial College London (PhD, Chem Eng), Prof. Toru Sato has been engaged in environmental impact assessment of CCS, development of dissociation and formation models of methane and CO_2 hydrates, and design and feasibility study of microalgae biofuel and has written a number of articles in international journals. He has also devoted himself as a Member of the Technical Committees on Ocean CCS of RITE, Environmental Impact Assessment for Sub-Seabed CCS of MOE, Antarctic Expedition Ship of MEXT, Ocean-Space Collaboration of JAXA, Editorial Board of Int J Greenhouse Gas Control, Director of JASNAOE, Chair of Division of Environmental Studies, UTokyo, etc.

Martin Sauter is a Professor of applied geology at the University of Göttingen, with the focus on the development of numerical tools for the quantification flow processes in the fractured-porous unsaturated zone as well as the characterization of the aquifer geometries and hydraulic parameters. He has further expertise in the area of water resource assessment in arid and semiarid areas and geothermal reservoirs.

Alessandra Sciarra is a Technologist (Geochemist) dealing with fluid geochemistry studies throughout geochemical surveys (i.e., study of the distribution of chemical and isotopic characteristics in soil gases concentration, fluxes

measurements, and dissolved gases in the water) and gas chromatographic analyses, applied to diffuse and natural degassing systems, geothermal resources, mitigation of environmental risk, and monitoring of volcanic and seismic areas. She has been scientific and technical project leader of three research studies applied to natural gas storage sites and WP leader in five research projects on environmental monitoring; moreover she has participated in 15 research projects related to fluid geochemistry.

Akash Srivastava is a final year B.Tech student, studying mining engineering at IIT BHU. He currently holds departmental rank 1 in academics. Besides academic excellence, he has shown a mettle in research works too in the field of mining engineering and hazards control in mines. He was a CPYLS (CSIR's Programme on Youth for Leadership in Science) Fellow in 2008 and an IOCL scholar from 2011 to 2015. He was also a Finalist Member of CIMA 2012 and 2013 in regional and national level. He also holds two papers that were presented at a national symposium in the year 2013.

Ashwin Sudhakaran is a graduate student at Clemson University, USA. He has an undergraduate degree in chemical engineering and has worked briefly in the area of CO_2 storage potential in Indian coal seams post graduating. His associations are predominantly with the CO_2 Sequestration Research Group at Indian Institute of Technology Bombay, Mumbai although he also worked at the Ground Stability Research Laboratory at Indian Institute of Technology Kharagpur. He intends to bring in a significant portion of earth sciences into his engineering proficiency and would like to further involve in CO_2 storage and related research in graduate school and beyond.

A. Syamsundar obtained his Ph.D. in reliability engineering in 2009 from the Indian Institute of Technology, Kharagpur, and is currently working as a Deputy General Manager (Research and Development) in charge in integrated steel works, RINL-VSP, Visakhapatnam. He has worked in various capacities in maintenance and operations of steel melting shops and later as a Technical Advisor to the Heads of Maintenance and Works and Director (Operations) of the integrated steel works. His research interests are in the fields of reliability and maintenance of industrial systems. He is the coauthor of a book and has published a number of papers in international journals and conferences on these issues.

Alexandru Bogdan Tatomir is a Postdoctoral Researcher at the University of Göttingen, Germany. He received his Ph.D. degree in 2012 at the University of Stuttgart on developing conceptual and numerical models for multiphase flow and transport in fractured porous media. His main research interests are on upscaling, code development, designing tracer tests for monitoring, and characterization for the fields of CO_2 storage, geothermal, unconventional shale gas, etc.

Ashwani Kumar Tiwari obtained his M.Sc. and M.Phil. degrees in the field of environmental sciences and worked as a Research Fellow more than one and half years at the Central Institute of Mining and Fuel Research (CIMFR), Dhanbad,

India. He was awarded the prestigious Erasmus Mundus Scholarship and he continued his research as exchange doctoral researcher in Politecnico di Torino, Italy, where he is also working at present after obtaining his PhD degree in Environmental Sciences at Indian School of Mines (ISM) Dhanbad. He has published a number of research papers in reputed international and national journals and contributed one book and four chapters in the edited research book volumes.

Orlando Vaselli works mainly in the areas of analytical methods in geochemistry and their applications. In 1999, he received the EUROPROBE-PANCARDI Award. Since 1998 he has been dealing with eruptive mechanisms and volcanic events and the application of the fluid geochemistry to geothermal and highly anthropogenic systems. Several geothermal and volcanic systems worldwide (America, Africa, Asia, and Europe) were studied in order to evaluate the geothermal potential and efficiency of geotracers and geoindicators in active volcanoes, respectively. More recently, he has addressed his studies to the impact of pollutants released from volcanic and geothermal systems and from anthropogenic sources. He has published more than 250 papers in international and national journals. He acts as reviewer for top-quality journals such as J. Geophys. Res., Chem. Geol., Appl. Geochem., Ophiolites, Sci. Tot. Environ., Geoderma, J. Geophys. Res, Eur. J. Min., and so forth.

M.B. Venkata Rao obtained his M.Tech in industrial metallurgy from Andhra University, Visakhapatnam. He is currently heading the Steel Making, Continuous Casting, Energy and Environment Group in Research and Development Department of Rashtriya Ispat Nigam Ltd. – Visakhapatnam Steel Plant (RINL-VSP). He has wide experience in the continuous casting of steels and also worked as an Advisor to the General Manager (Steel) and Head of Maintenance. He carried out R&D programs in steel making, continuous casting, energy, and environment and has published papers in international conferences.

Magdalena Wdowin is a graduate of geology at the Faculty of Geology, Geophysics and Environmental Protection AGH-University of Science and Technology, with specialization in mineralogy and applied geochemistry. He works as Assistant Professor in the Mineral and Energy Economy Research Institute of the Polish Academy of Sciences. Her research scope is related to the application of zeolites in purification of gaseous pollution as well as sequestration of CO_2, i.e., investigation of CO_2-brine-rock interaction and CO_2 capture by zeolites. She is the author of many publications at this scope. She also coordinates the international project: "CO_2 post-combustion capture using amine impregnated synthetic zeolites."

Index

V. Vishal, T.N. Singh (eds.), *Geologic Carbon Sequestration*,
DOI 10.1007/978-3-319-27019-7